

Dissertation zur Erlangung des Doktorgrades der Fakultät für Chemie  
und Pharmazie der Ludwig-Maximilians-Universität München

Biomimetic synthesis of (–)-PF-1018 and  
development of photoswitchable GABA<sub>A</sub>  
receptor potentiators

von

Hugo Quintela Varela

aus

A Coruña, Galizien, Spanien

2019

---

**Erklärung:**

Diese Dissertation wurde im Sinne von § 7 der Promotionsordnung vom 28. November 2011 von Herrn Prof. Dr. Dirk Trauner betreut.

**Eidesstattliche Versicherung**

Diese Dissertation wurde eigenständig und ohne unerlaubte Hilfsmittel erarbeitet.

A Coruña, Spanien, den 1. November 2019

.....

Hugo Quintela Varela

Dissertation eingereicht am: 11.10.2019

1. Gutachter Prof. Dr. Dirk Trauner

2. Gutachter: Prof. Dr. Klaus T. Wanner

Mündliche Prüfung am: 7.11.2019

For my family

“E ogallá que retorne de novo algún día, por  
estas mesmas augas, pra morrer onde nascín”



## ACKNOWLEDGMENTS

These recent years have been hard work and not without their sacrifices, notably being far from family and friends. Nevertheless they have been fulfilling years brimming with new experiences and learning. During this PhD I have not only greatly expanded my knowledge in chemistry, but also my professional skills and my world vision. The people who I have met on this journey have allowed me to learn much more about chemistry not to mention other ways of viewing life. Therefore, I would like to acknowledge the following people:

I would like to first thank Prof. Trauner for allowing me to be part of his group, for giving me freedom to develop my research and suggest new projects, as well as for his enthusiasm and generosity. I would also like to thank him for having brought me to New York, a truly exciting experience in itself. I also want to acknowledge all the Trauner staff, in München and New York: Luis de la Osa, Heike Traub, Alexandra Grilic, Dr. Martin Sumser, Carrie Louis, Mariia Palchyk and Danielle Nalband. Your work made our work possible. The same applies to the LMU and NYU staff, thanks to Dr. Peter Mayer and Chunhua Hu for their beautiful crystal structures, thanks to Ronald McLurkin and Chin Lin for keeping the analytic equipment in the best shape, to Irene Kiriazi and Aneleen Dizon for their administrative work and to Takeisha Benjamin, Rogelio Fuertez and Abayomi Elesho for maintaining the flow of chemicals and lab equipment. You have not only done your job with professionalism but also with incomparable kindness.

I would also like to express my gratitude to Prof. Dr. Klaus T. Wanner for being the second reviewer of this work and to Prof. Dr. Hendrik Zipse, Prof. Dr. Herbert Mayr, Dr. Oliver Thorn-Seshold and Dr. Henry Dube for being in the defence committee and to Frau Alessandra Wührer for her administrative work.

I am also very thankful to my interns, Felix Müller, Petr Tatarskiy and Janina Graf. It was a pleasure working with you, the time we shared was probably the best I had in the lab. Thank you for your tireless work on different projects.

To the members of the Trauner group: thanks for developing your work with professionalism and honesty, for your unconditional help and for the great lab atmosphere. When spending so much time at work these qualities become imperative. Among the Trauner lab members, I would like to especially thank Matt (probably my best "hoodmate" in New York) for cheering me up during difficult days and also revealing the force of selenium. To Bryan, thanks for the conversations on chemistry, more exotic topics, as well as his counselling. To Julius, for his advice, kindness and commitment with the HWE problem. Further thanks to Nynke, for her help on the hardest days in New York and to the proofreaders of this and other works: Peter Rühmann, Alex Novak, Belinda Hetzler, Bryan Matsuura, Julius Reyes, Anna Impastato, Matt DiCairano, Martin Reynders, Nynke Veprek, Christian Fischer, Andrii Shemet and to the external revisers Chris Hill and Fiona Harrison. My gratitude also goes to Martin Maier for hosting me at his place in München for a reasonable price, for his patience with guests, either mammal or arthropod and to Pauline for being a good friend. Also to Katharina Hüll for her help with the different steps of this bureaucracy and to Rob Webster and Boris Gaspar for their work on PF-1018.

I really want to thank my friends at the NYU, Brismar and Elsy, for getting me out of the lab once in a while, for feeding me on those hungry days and for taking me to see the Yankees; and the LMU friends, Luis de la Osa, Alicia Castelló, Ángel Puente, Malgorzata Borowiak and Yelena Wainman. Those lunch breaks were really mind-blowing and I really enjoyed singing with you.

I want to acknowledge my friends outside the lab, Orit, Fede, Juan, Andrea, Terry, Daniel and Trinity. I don't think they are aware of how much they helped keep my peace of mind; and to my friends in Galicia, because wherever I am, being with them is being at home.

All my gratitude goes to Prof. Josep Bonjoch and Roman Staiger for their faith in me and also to Dr. Ottmar Hütter for allowing me to start this journey.

Finally and most importantly, I am very grateful to my family for their love and support, for the values they imparted to me and the peace that fills me when we are all together.

**Parts of this thesis have been accepted by peer-reviewed journals:**

Quintela-Varela, H.; Jamieson, C. S.; Shao, Q.; Houk, K. N.; and Trauner, D. Bioinspired Synthesis of (–)-PF-1018, *Angewandte Chemie International Edition*.

**Parts of this thesis have been presented at scientific conferences:****Dechema 31. Irseer Naturstofftage**

“Total synthesis of (–)-PF-1018”, poster presentation.

Irsee, Germany, February 2019

**IX Jornada de Jóvenes Investigadores en el Extranjero**

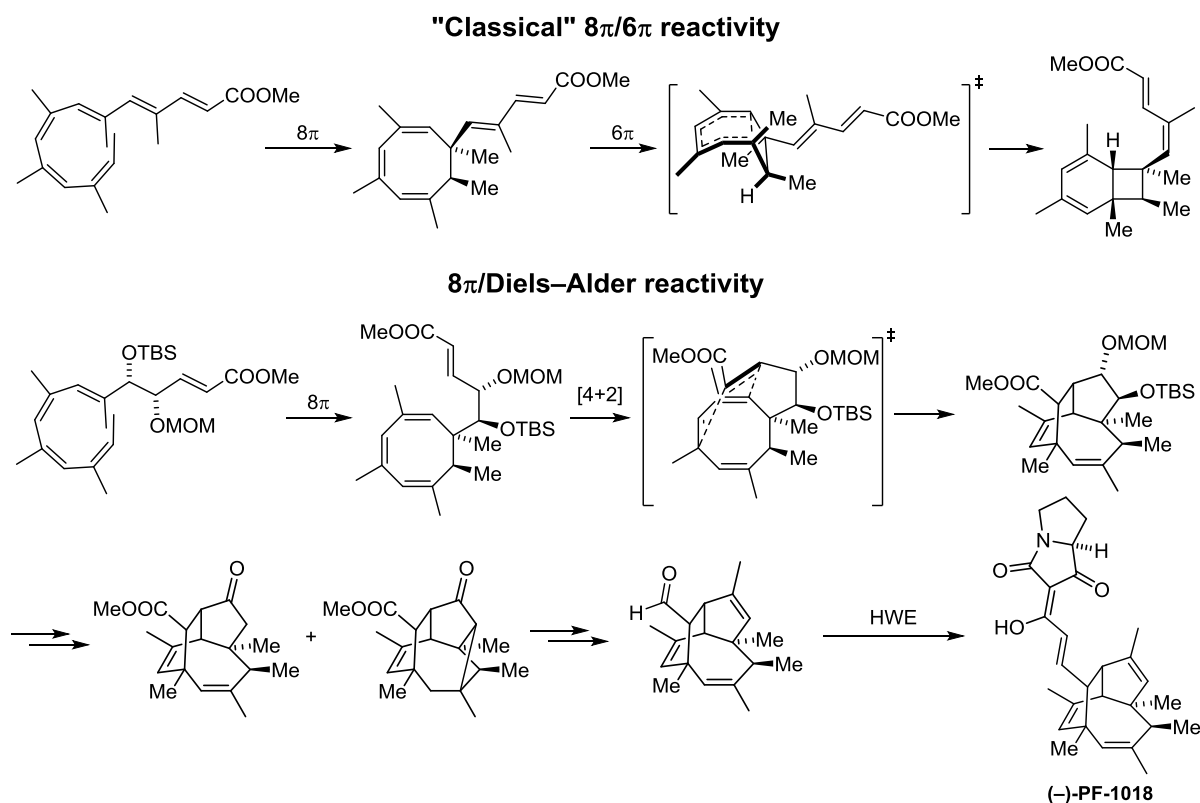
“Síntesis total de (-)-PF-1018 a través de un tándem de 8- $\pi$  electrociclación y Diels-Alder”

MUNCYT, A Coruña, Spain, December 2018

## ABSTRACT

### PART I - TOTAL SYNTHESIS OF (–)-PF-1018

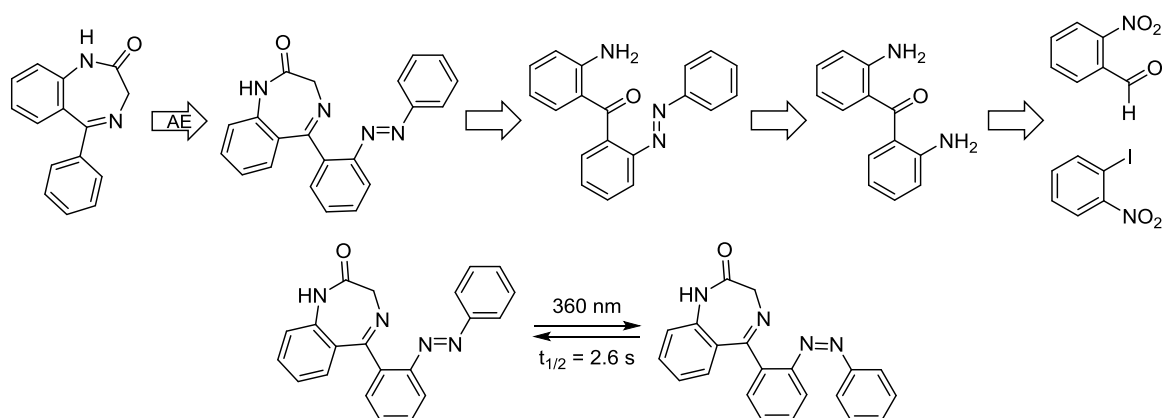
The family of polyketide natural products arising from 1,3,5-cyclooctatriene intermediates has grown significantly in the last decade. The oldest and most famous members of this family are the endiandric acids, and more recently natural products such as the elysiapyrones, kingianins and ocellapyrones have been isolated and synthesized. The reaction cascades that yield these compounds commence from conjugated *E,Z,E* tetraenes, which undergo an  $8\pi/6\pi$  electrocyclization sequence leading to bicyclo[4.2.0]octadienes. For some of these natural products, such as endiandric acid C, this cascade is followed by an intramolecular Diels–Alder reaction. (–)-PF-1018 can also be considered a member of this family, since this polyketide originates from a 1,3,5-cyclooctatriene precursor. However, (–)-PF-1018 is obtained through a variation of the  $8\pi/6\pi$ /Diels–Alder cascade: the cyclooctatriene intermediate is intercepted by a dienophile in an intramolecular [4+2] cycloaddition, bypassing the  $6\pi$  electrocyclization step. This unique reactivity defines the unprecedented structure of (–)-PF-1018, which comprises a tricyclic 8/6/5 ring system bearing 6 contiguous stereocentres. This core is linked to a bicyclic tetramic acid by an ethylene linker.



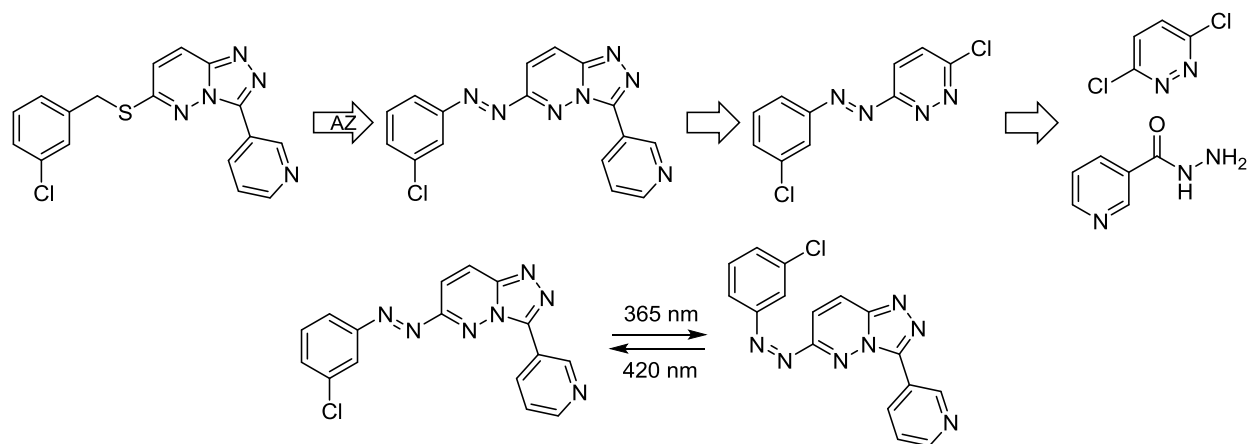
The first part of this thesis describes the total synthesis of (–)-PF-1018. The key cascade reaction started with a polyene bearing a doubly protected *syn*-diol responsible for the divergent reactivity that led to the [4+2] cycloaddition. In the absence of these hydroxy groups the corresponding polyene underwent the "classical"  $8\pi/6\pi$  electrocyclization cascade. The tricyclic core was further elaborated by means of a Barton–McCombie reaction which yielded the desired product together with an unexpected tetracycle. Both intermediates reconverged into an aldehyde which was transformed into (–)-PF-1018 *via* a Horner–Wasworth–Emmons reaction.

## PART II – DEVELOPMENT OF PHOTOSWITCHABLE GABA<sub>A</sub> RECEPTOR POTENTIATORS

GABA<sub>A</sub> receptors are ionotropic receptors ubiquitous in the central nervous system which are activated by gamma-aminobutyric acid (GABA). The binding of two molecules of GABA induces pore opening causing a flow of chloride anions into the cell which inhibits neurotransmission. The activity of these receptors can be modulated by different drugs, the most prevalent of which are benzodiazepines and Z-drugs. These compounds induce current potentiation by increasing the affinity of the GABA<sub>A</sub>R for the GABA neurotransmitter. Benzodiazepines and Z-drugs show low specificity for the different GABA<sub>A</sub>R subtypes, and therefore cause undesired side effects such as drowsiness, anterograde memory loss and ataxia. Although the binding site and binding modes of benzodiazepines have been recently elucidated, other binding pockets for these drugs exist. In the case of Z-drugs, it is known that they bind the benzodiazepine binding site, but their binding mode has yet to be described.



In the second part of this thesis we describe the principles of design and the synthesis of a photoswitchable benzodiazepine. The azo-extension approach on the benzodiazepine scaffold relied on the early introduction of the azobenzene moiety at the *ortho*-position of the pendant phenyl ring. This resulted in the isolation of new azobenzophenone intermediates as well as the envisioned azobenzodiazepine.



We also describe the design and synthesis of the first reported photoswitchable Z-drugs. The design was built on a lead compound found in a virtual screening campaign based on the benzodiazepine binding model. Given the high affinity of the parent compound for the GABA<sub>A</sub>R and the presence of an “azostere” in its structure, we decided to synthesize a series of photochromic ligands using an azologization approach. Again, the strategy relied on the early introduction of the azobenzene moiety, giving rise to new types of heterocyclic azobenzenes.

## GLOSSARY

Å	angstrom	CoA	coenzyme A
Ac	acetyl	Cp	cyclopentadienyl
acac	acetylacetone	cryo-EM	high resolution cryo-electron microscopy
ACP	acyl carrier protein	CSA	camphorsulfonic acid
AE	azo-extension	CTED	C-terminal extracellular domain
AIBN	azobisisobutyronitrile	Cy	cyclohexyl
AMPA	2-amino-3-(5-methyl-3-hydroxyisoxazol-4-yl)propanoic acid	Cys	cysteine
AP	action potential	$\delta$	chemical shift (NMR spectroscopy)
APCI	atmospheric-pressure chemical ionization	$\Delta$	heat
Ar	undefined aryl substituent	d	day(s)
Asn	asparagine	d	doublet (NMR spectroscopy)
ATR	attenuated total reflection	D	dexter “right”
AZ	azologization	DA	Diels–Alder reaction
BM	binding mode	dba	dibenzylideneacetone
Bn	benzyl	DBU	1,8-diazabicyclo[5.4.0]undec-7-ene
Boc	<i>tert</i> -butyloxycarbonyl	DCC	<i>N,N'</i> -dicyclohexylcarbodiimide
bpy	bipyridine	DCM	dichloromethane
BPO	benzoyl peroxide	DET	diethyl tartrate
br	broad (NMR and IR spectroscopy)	$\Delta G$	Gibbs free energy
Bu	butyl	DH	dehydratase
BZ	benzodiazepine	DIBAL	diisobutylaluminium hydride
cat.	catalytic/catalyst	DIPEA	<i>N,N</i> -diisopropylethylamine
CDI	carbonyldiimidazole	DMAP	<i>p</i> -dimethylaminopyridine
CM	cross-metathesis	DMF	<i>N,N</i> -dimethylformamide
CNS	central nervous system	DMP	Dess–Martin periodinane
		DMSO	dimethyl sulfoxide

dppf	1,1'-bis(diphenylphosphino)ferrocene	HOBt	hydroxybenzotriazole
d.r.	diastereomeric ratio	HOMO	highest-occupied molecular orbital
DTMP	2,6-di- <i>tert</i> -butyl-4-methylpyridine	HPLC	high performance liquid chromatography
<i>E</i>	opposite ( <i>trans</i> )	HP-LED	high-power light-emitting diode
EDC	<i>N</i> -(3-dimethylaminopropyl)- <i>N</i> '-ethylcarbodiimide	HWE	Horner–Wadsworth–Emmons reaction
<i>ee</i>	enantiomeric excess	Hz	hertz
eGABAR	extrasynaptic GABAR	<i>i</i> -Pr	isopropyl
equiv.	equivalent	IC <sub>50</sub>	half maximal inhibitory concentration
ESI	electron spray ionization	Im	imidazole
Et	ethyl	lpc	isopinocampheyl
EWG	electron withdrawing group	IR	infrared
G-II	second-generation Grubbs catalyst	<i>J</i>	coupling constant (NMR spectroscopy)
GABA	gamma-aminobutyric acid	KHMDS	potassium hexamethyldisilazane
GABA <sub>A</sub>	type A GABA receptor	KR	ketoreductase
GABA <sub>B</sub>	type B GABA receptor	KS	ketosynthase
GABAR	GABA receptor	λ	wavelength
GALiZA	GABA <sub>A</sub> R Light-dependent Z-drug Allosteric modulator	L	ligand
glu	glutamate	LCMS	liquid chromatography-mass spectroscopy
GluR	glutamate receptor	LDA	lithium diisopropylamide
GlyR	glycine receptor	LED	light emitting diode
GPCR	G protein-coupled receptor	LGIC	ligand-gated ion channel
h	hour(s)	LUMO	lowest unoccupied molecular orbital
HG-II	second-generation Hoveyda–Grubbs catalyst	lut	lutidine
His	histidine	μ	micro (10 <sup>-9</sup> )
HMDS	hexamethyldisilazane	m	medium (IR)
HMPA	hexamethylphosphoramide	<i>m</i>	<i>meta</i>
hν	irradiation		

m	multiplet (NMR spectroscopy)	PCC	pyridinium chlorochromate
M	molar	PDB	protein data bank
<i>m</i> -CPBA	<i>meta</i> -chloroperbenzoic acid	PG	protecting group
Me	methyl	Ph	phenyl
min	minutes	Phe	phenylalanine
MHz	megahertz	Pin	pinacol
mL	millilitre	Piv	pivaloyl
MOM	methoxymethyl	PKS	polyketide synthase
Mp	melting point	PMB	para-methoxybenzene
Ms	methanesulfonyl	PORTL	photoswitchable orthogonal remotely tethered ligand
MS	mass spectrometry	ppm	parts per million
MW	microwave	PS	pregnenolone sulfate
MV	methyl viologen	PTA	phenyltrimethylammonium
<i>n</i> -Bu	butyl (linear)	PTL	photoswitchable tethered ligand
<i>n</i> -Pr	propyl (linear)	PTSA	<i>p</i> -toluenesulfonic acid
nAChR	nicotinic acetylcholine receptors	Pyr	pyridine
NAM	negative allosteric modulator	q	quartet (NMR spectroscopy)
NBS	<i>N</i> -Bromosuccinimide	quant.	quantitative
nm	nanometer	R	unspecified substituent
NMO	<i>N</i> -methylmorpholine <i>N</i> -oxide	RCDA	radical cation Diels–Alder reaction
NMR	nuclear magnetic resonance	<i>R</i> <sub>F</sub>	retention factor
Np	neopentyl	rt	room temperature
NP	natural product	s	second(s)
NRPS	nonribosomal peptide synthetase	s	singlet (NMR spectroscopy)
NTED	N-terminal extracellular domain	s	strong (IR spectroscopy)
Nu	nucleophile	<i>s</i> -Bu	<i>sec</i> -butyl
<i>o</i>	<i>ortho</i>	Ser	serine
<i>p</i>	<i>para</i>	S <sub>N</sub> 2	bimolecular nucleophilic substitution
PAM	positive allosteric modulator		
PBS	phosphate-buffered saline		



S <sub>N</sub> Ar	nucleophilic aromatic substitution	TPMPA	1,2,5,6-Tetrahydropyridin-4-yl methylphosphinic acid
T	temperature	TRPV1	transient receptor potential vanilloid 1
T	transmembrane domain		
t	triplet (NMR spectroscopy)	Ts	<i>p</i> -toluenesulfonyl
t <sub>1/2</sub>	half life	TS	transition state
<i>t</i> -Bu	<i>tert</i> -butyl	TTMSS	tris(trimethylsilyl)silane
TASF	tris(dimethylamino)sulfonium difluorotrimethylsilicate	Tyr	tyrosine
		UV	ultraviolet
TBAF	tetrabutylammonium fluoride	v	volume
TBDPS	<i>tert</i> -butyldiphenylsilyl	Vis	visible
TBHP	<i>tert</i> -butyl hydroperoxide	w	(weak, IR spectroscopy)
TBS	<i>tert</i> -butyldimethylsilyl	wt%	weight percent
TBTH	tributyltin hydride	XPhos	2-Dicyclohexylphosphino-2',4',6'-triisopropylbiphenyl
TC	thiophene carboxylate	Z	together ( <i>cis</i> )
TCDI	thiocarbonyldiimidazole		
TES	triethylsilyl		
Tf	trifluoromethanesulfonyl		
TFA	trifluoroacetic acid		
TFP	tri(2-furyl)phosphine		
THF	tetrahydrofuran		
THIP	4,5,6,7-tetrahydroisoxazolo[5,4-c]pyridin-3-ol		
THPO	4,5,6,7-tetrahydroisoxazolo[4,5-c]pyridin-3-ol		
Thr	threonine		
TIPS	triisopropylsilane		
TLC	thin-layer chromatography		
TM	transmembrane		
TMS	trimethylsilyl		
TPAP	tetrapropylammonium perruthenate		

## TABLE OF CONTENTS

Acknowledgements.....	IV
Abstract.....	VII
Glossary.....	IX

### PART I - TOTAL SYNTHESIS OF (–)-PF-1018

1. Introduction.....	2
1.1 1,3,5-Cyclooctatriene: Thermal Electrocyclizations and Historical Perspective.....	2
1.2 Cyclooctatriene-Derived Natural Products .....	5
1.2.1 Endiandric acids .....	5
1.2.2 SNF4435.....	10
1.2.3 Elysiapyrones .....	17
1.2.4 Ocellapyrones.....	18
1.2.5 Shimalactones .....	18
1.2.6 Kingianins.....	20
1.2.7 Unified Synthesis of Kingianins and Endiandric acids .....	24
1.2.8 Hypnophilin, Coriolin and Ceratopicanol.....	26
2. Project Background.....	28
2.1 Isolation and Structure of (–)-PF-1018 .....	28
2.2 Proposed Biosynthesis of (–)-PF-1018.....	29
2.3 Biological Activity of (–)-PF-1018.....	30
2.4 Previous Efforts Towards (–)-PF-1018.....	31
2.5 Project Outline.....	32
3. Results and discussion .....	34
3.1 Evans Aldol Approach.....	34
3.2 Brown Allylation Approach.....	36
3.3 Bioinspired Synthesis of (–)-PF-1018.....	47
3.4 Unpublished Results.....	52
4. Summary and Outlook.....	58

### PART II – DEVELOPMENT OF PHOTOSWITCHABLE GABA<sub>A</sub> RECEPTOR POTENTIATORS

5. Introduction.....	61
5.1 GABA <sub>A</sub> Receptors .....	61
5.2 The GABA Binding Site, GABA <sub>A</sub> R Agonists and Antagonists.....	63
5.2.1 GABA <sub>A</sub> Receptor Agonists .....	64
5.2.1.1 Muscimol.....	64
5.2.1.2 THIP .....	64
5.2.2 GABA <sub>A</sub> Receptor Antagonists.....	65

5.2.2.1	Bicuculline, RU5135 and TPMPA .....	65
5.2.2.2	Picrotoxin .....	65
5.3	Elucidation of GABA <sub>A</sub> Receptor Binding Sites.....	66
5.4	GABA <sub>A</sub> R Allosteric Modulators.....	66
5.4.1	Neurosteroids .....	66
5.4.2	Anaesthetics.....	67
5.4.2.1	Propofol.....	67
5.4.2.2	Etomidate.....	67
5.4.2.3	Barbiturates .....	67
5.4.3	Ethanol.....	68
5.4.4	Benzodiazepines.....	68
5.4.4.1	General Aspects .....	68
5.4.4.2	Benzodiazepine Binding Sites.....	69
5.4.4.3	Benzodiazepine Binding Modes .....	71
5.4.5	Z-Drugs.....	73
5.5	Photopharmacology.....	74
5.6	Photoswitchable Ligands.....	76
5.6.1	Photoswitches Displaying Ring Opening/Closing Interconversion.....	76
5.6.1.1	Diarylethenes.....	76
5.6.1.2	Thiophenefulgides .....	76
5.6.1.3	Spiropyranes.....	76
5.6.2	Photoswitches Displaying <i>cis/trans</i> Isomerization .....	77
5.6.2.1	Hemithioindigos.....	77
5.6.2.2	Acylhydrazones.....	77
5.6.2.3	Stilbenes.....	77
5.6.2.4	Azobenzenes.....	77
5.6.2.5	Diazocines .....	79
5.7	Selected Examples of Photocontrolled LGICs.....	80
5.7.1	Photoregulation of Acetylcholine Receptors.....	80
5.7.2	Photocontrolled AMPA Receptors.....	81
5.7.3	Azo-Propofol .....	82
6.	Project Background and Aims .....	83
6.1	Synthesis of a Photoswitchable Benzodiazepine .....	83
6.1.1	Previous Work.....	83
6.1.2	Project Outline.....	84
6.1.3	Results and Discussion .....	85
6.2	Synthesis of GABA <sub>A</sub> R Light-Controlled Z-Drug Allosteric Modulators.....	92
6.2.1	Project Outline.....	92
6.2.2	Results and Discussion.....	93
7.	Summary and Outlook.....	104

## EXPERIMENTAL PART

<b>8. Experimental Section .....</b>	<b>107</b>
<b>8.1 General Experimental Details .....</b>	<b>107</b>
<b>8.2 Supporting Information for Chapter 3.1 .....</b>	<b>109</b>
<b>8.2.1 Experimental Procedures for Chapter 3.1 .....</b>	<b>109</b>
<b>8.3 Supporting Information for Chapter 3.2 .....</b>	<b>114</b>
<b>8.3.1 Experimental Procedures for Chapter 3.2 .....</b>	<b>114</b>
<b>8.4 Supporting Information for Chapter 3.3 .....</b>	<b>123</b>
<b>8.4.1 Experimental Procedures for Chapter 3.3 .....</b>	<b>123</b>
<b>8.4.2 Comparison of Natural and Synthetic (–)-PF-1018 and Pyreudione C.....</b>	<b>145</b>
<b>8.4.3 Potential Products from Cascade Reaction 16 to 18 .....</b>	<b>148</b>
<b>8.4.4 Crystallographic Data for Chapter 3.3 .....</b>	<b>149</b>
<b>8.4.4.1 Cascade Product 18 .....</b>	<b>149</b>
<b>8.4.4.2 Tricycle 22 .....</b>	<b>150</b>
<b>8.4.4.3 Tetracycle 30 .....</b>	<b>151</b>
<b>8.4.5 Computational Studies .....</b>	<b>152</b>
<b>8.4.5.1 Cartesian Coordinates of Calculated Structures.....</b>	<b>155</b>
<b>8.5 Supporting Information for Chapter 3.4 .....</b>	<b>173</b>
<b>8.5.1 Experimental Procedures for Chapter 3.4 .....</b>	<b>173</b>
<b>8.6 Supporting Information for Chapter 6.1 .....</b>	<b>175</b>
<b>8.6.1 Experimental Procedures for Chapter 6.1 .....</b>	<b>175</b>
<b>8.6.2 Crystallographic Data for Chapter 6.1.....</b>	<b>180</b>
<b>8.6.2.1 Azobenzophenone 6.23 .....</b>	<b>180</b>
<b>8.6.2.2 Azobenzodiazepine 6.13 .....</b>	<b>181</b>
<b>8.7 Supporting Information for Chapter 6.2 .....</b>	<b>183</b>
<b>8.7.1 Experimental Procedures for Chapter 6.2 .....</b>	<b>183</b>
<b>8.7.2 Crystallographic Data for Chapter 6.2 .....</b>	<b>192</b>
<b>8.7.2.1 Triazolopyridazine 6.40 .....</b>	<b>192</b>
<b>8.8 NMR Spectra .....</b>	<b>194</b>
<b>8.8.1 NMR Spectra for Chapter 3.1 .....</b>	<b>194</b>
<b>8.8.2 NMR Spectra for Chapter 3.2 .....</b>	<b>200</b>
<b>8.8.3 NMR Spectra for Chapter 3.3 .....</b>	<b>212</b>
<b>8.8.4 NMR Spectra for Chapter 3.4 .....</b>	<b>243</b>
<b>8.8.5 NMR Spectra for Chapter 6.1 .....</b>	<b>246</b>
<b>8.8.6 NMR Spectra for Chapter 6.2 .....</b>	<b>255</b>
<b>9. Bibliography.....</b>	<b>268</b>

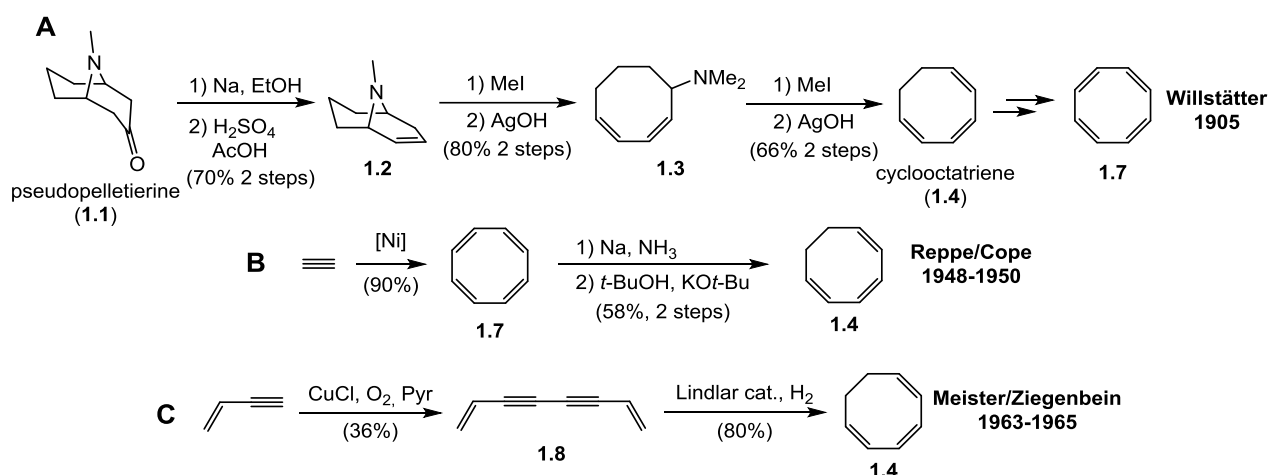
## **PART I - TOTAL SYNTHESIS OF (–)-PF-1018**

# 1. Introduction

## 1.1 1,3,5-Cyclooctatriene: Thermal Electrocyclizations and Historical Perspective

The first synthesis of 1,3,5-cyclooctatriene (**1.4** or simply cyclooctatriene) was reported by Richard Willstätter and Hans Veraguth in 1905 as an intermediate in the synthesis of cyclooctatetraene (**1.7**).<sup>[1]</sup> Starting from pseudopelletierine (**1.1**), a natural product present in the root-bark of the pomegranate tree, **1.4** could be obtained through ketone reduction and dehydration of the resulting alcohol followed by two consecutive Hofmann eliminations of the amino bridge present in **1.2** (Scheme 1.1, **A**). Three decades later, American chemists including Hurd, Drake, Horning, Goldwasser or Taylor, who could not reproduce these results argued that the product isolated by Willstätter could not be identified as cyclooctatetraene.<sup>[2–5]</sup> In 1947 however, Arthur C. Cope reproduced Willstätter's results and corroborated the structure of cyclooctatetraene (**1.7**) by comparison to a sample obtained by the method of Walter Reppe from BASF Ludwigshafen, who synthesized **1.7** from acetylene in the presence of a nickel catalyst at high pressures.<sup>[6,7]</sup> The previous laborious synthesis of 1,3,5-cyclooctatriene from pseudopelletierine did not allow for isolation of large quantities of **1.4**, but by Reppe's method significant amounts of cyclooctatetraene, a near precursor, could be readily prepared. This prompted Cope and others to develop a method in which **1.7** was transformed into a mixture of 1,3,5-cyclooctatriene and 1,3,6-cyclooctatriene under Birch conditions. Treatment of the mixture with potassium *tert*-butoxide yielded solely the conjugated isomer (Scheme 1.1, **B**).<sup>[7,8]</sup>

Years later, in 1965, coinciding with the publication of Woodward and Hoffman's article which established the rules for pericyclic reactions, the first synthesis of 1,3,5-cyclooctatriene from a linear precursor was developed by Ziegenbein using a method by Meister, which consisted of partial hydrogenation of diyne **1.8**, obtained by Glaser coupling of vinylacetylene, (Scheme 1, **C**) followed by an 8 $\pi$  electrocyclization.<sup>[9,10]</sup> This sequence was later used in the synthesis of endiandric acids by Nicolaou, as described in Chapter 1.2.1.

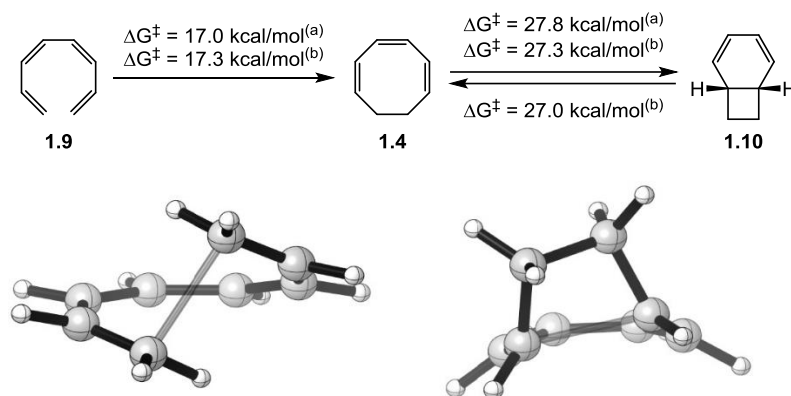


**Scheme 1.1.** Overview of the different synthetic routes towards cyclooctatriene in chronological order.

In 1950, Cope was intrigued by the slight variations found in the refractive indices of different samples of 1,3,5-cyclooctatrienes. Upon distillation of **1.4** at unusually high temperatures (80 °C instead of 40 °C), which

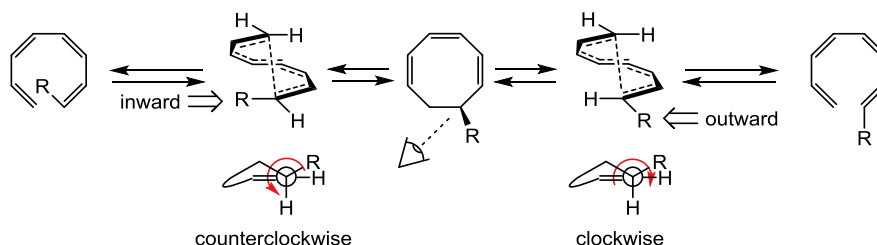
presumably triggered a  $6\pi$  electrocyclization, and treatment of the fractions with the lowest refractive index with silver nitrate, bicyclo[4.2.0]octa-2,4-diene (**1.10**) was isolated.<sup>[11]</sup> Its structure was confirmed by hydrogenation to bicyclo[4.2.0]octane and by separate Diels–Alder reaction with succinic anhydride. Cope recognized that the  $6\pi$  electrocyclization was a reversible reaction since upon heating **1.10** various amounts of cyclooctatriene were obtained.

After the first description of the valence isomerization of cyclooctatriene by Cope and given its now easy access, many chemists studied the  $8\pi/6\pi$  reaction cascade of octatetranes,<sup>[12,13]</sup> with Huisgen being the most prolific for several years.



**Scheme 1.2 and Figure 1.1. Top.** Activation energies for  $8\pi$  and  $6\pi$  electrocyclizations of **1.9** and **1.4** obtained by Huisgen experimentally<sup>(a)</sup> and calculated by Houk.<sup>(b)</sup> **Bottom.** Transition states for both transformations calculated by Houk (included with his permission).<sup>[20]</sup>

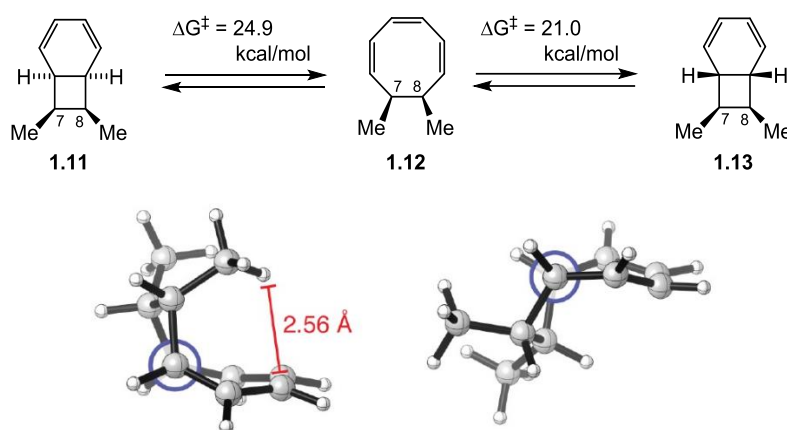
Huisgen focused on the kinetics and thermodynamics of these electrocyclizations providing the first activation energy values, (**1.9**→**1.4** = 17.0 kcal/mol and **1.4**→**1.10** = 27.8 kcal/mol, Scheme 1.2), reaction constants, distribution of the different species at different temperatures and substituent effects on the electrocyclization processes.<sup>[14–17]</sup> In the case of 2,4,6,8-decatetraene for example, he described that the (*E,Z,Z,E*)-isomer cyclized fastest, followed by the (*E,Z,Z,Z*)-isomer and the all *cis* (*Z,Z,Z,Z*)-isomer, which was the slowest.<sup>[18]</sup> He also noted that the processes were conrotatory for the  $8\pi$  electrocyclization and disrotatory for the  $6\pi$ , in agreement with the Woodward–Hoffman rules. At high temperatures (>140 °C), however, “forbidden” processes occurred to some extent.<sup>[19]</sup>



**Scheme 1.3.** Torquoselectivity in cyclooctatriene ring opening. The lowest energy transition state is the one in which the biggest substituent points out of the ring (outward), which in this case involves a clockwise rotation along the C–C axis next to the breaking sigma bond. Note that for ring closure, the positioning of the substituent in the transition state is predefined by the *Z*- or *E*- configuration of the terminal double bond.

Major contributions based on computational chemistry were later made by Kendall N. Houk. He reported the structures for transition states and made systematic studies on the influence of terminal substituents in the outcome of the cyclization cascade.<sup>[20–23]</sup> The torquoselectivity of the retro  $8\pi$  electrocyclization was one of the main subjects of study in these articles. This concept coined by Houk is defined as the preference of the terminal substituents to occupy an inward or an outward position during the transition state (Scheme 1.3).<sup>[24,25]</sup>

Unlike for cyclobutene, the electronic influence of the terminal substituents is not relevant in  $8\pi$  electrocyclizations given the low orbital overlap in the transition state.<sup>[21,25–27]</sup> Steric bulk, however, plays an important role in determining the direction of rotation of the side chains, with the outward preferred in a vast majority of cases. Interestingly, Houk also provided an explanation as to why no natural products with a disubstituted *endo-syn* pattern at C7 and C8 in bicyclo[4.2.0]octadienes have been found. The transition state for such compounds is too high in energy due to the steric clash of the substituents with the hexadiene ring and with each other (Scheme 1.4 and Figure 1.2).



**Scheme 1.4 and Figure 1.2.** Activation energies for the  $6\pi$  electrocyclization of triene **1.12** and calculated structures of the transition states by Houk (included with his permission).<sup>[20]</sup> The energy difference of 4 kcal/mol can explain why no disubstituted *endo*-C7,C8-*syn* natural products have been found.

Regarding other electrocyclizations of cyclooctatriene, the relative energies of the transition states for  $6\pi$  and  $4\pi$  thermal electrocyclizations are respectively 18 and 32 kcal/mol higher than the activation energy for the  $8\pi$  process.<sup>[27]</sup> This explains why such reactivities are scarcely observed (Scheme 1.5, Top).<sup>[28]</sup> The photochemical  $8\pi$  electrocyclization is outcompeted by [4+2] cycloaddition, yielding vinyl bicyclo[3.1.0]hexene.<sup>[28–31]</sup>

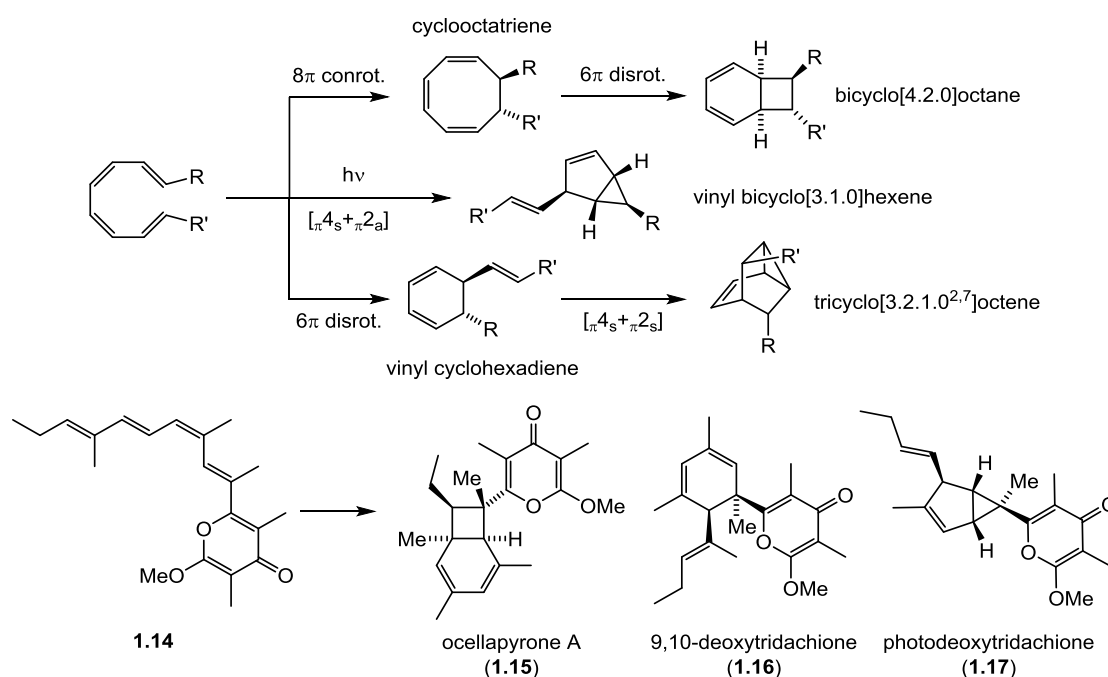
As a closing remark on Houk's studies on the  $8\pi/6\pi$  electrocyclization cascade, substitution at the octatetraene termini strongly influences the outcome of the cyclization process (Scheme 1.3). When  $R \neq H$ , the activation energy for the  $8\pi$  electrocyclization increases, especially for terminal (*Z*)-configured tetraenes. The presence of substituents at terminal positions also increases the instability of the resulting cyclooctatriene intermediates, (especially if they are *syn*-configured, such as **1.12**, Scheme 1.4) lowering the activation energy for the  $6\pi$  electrocyclization. Therefore, the equilibrium of the  $8\pi/6\pi$  electrocyclization cascade is generally shifted towards the bicyclo[4.2.0]octadienes (**1.13** in Scheme 1.4), except for unsubstituted cyclooctatriene (**1.4**, Scheme 1.2), isolable at room temperature.



## 1.2 Cyclooctatriene-Derived Natural Products

As shown in Chapter 1.1, cyclooctatrienes arise from octatetraenes upon  $8\pi$  electrocyclization, but this is not the only reactivity available to octatetraenes, since photochemically induced intramolecular Diels–Alder reactions and  $6\pi$  disrotatory electrocyclizations can also take place. These reactivities have been exploited for the synthesis of different natural products (NPs), many of which are thought to share common precursors. For example, ocellapyrone A (**1.15**), photodeoxytridachione (**1.16**) and 9,10-deoxytridachione (**1.17**) can be traced back to the same precursor **1.14** (Scheme 1.5, bottom).<sup>[31–33]</sup> In some occasions this reactivity has led to undesired side products or frustrated synthetic approaches, as later discussed with regard to Trauner's early attempts towards SNF4435.<sup>[34]</sup> Moreover, these reaction pathways can be responsible for the relatively low yields in many of the  $8\pi/6\pi$  cyclization cascades which follow.

In this chapter we will provide an overview on the total syntheses of most members of the Cyclooctatriene-Derived natural product family. The polyketide nature of these NPs together with the ubiquitous presence of cyclooctatriene derivatives as key intermediates in their total syntheses (and presumably also in the corresponding biosyntheses), justifies in our opinion the inclusion of these NPs, together with PF-1018 in the aforementioned family. We also include the syntheses of three sesquiterpene natural products which do not belong to this family but entail a cyclooctatriene key intermediate.

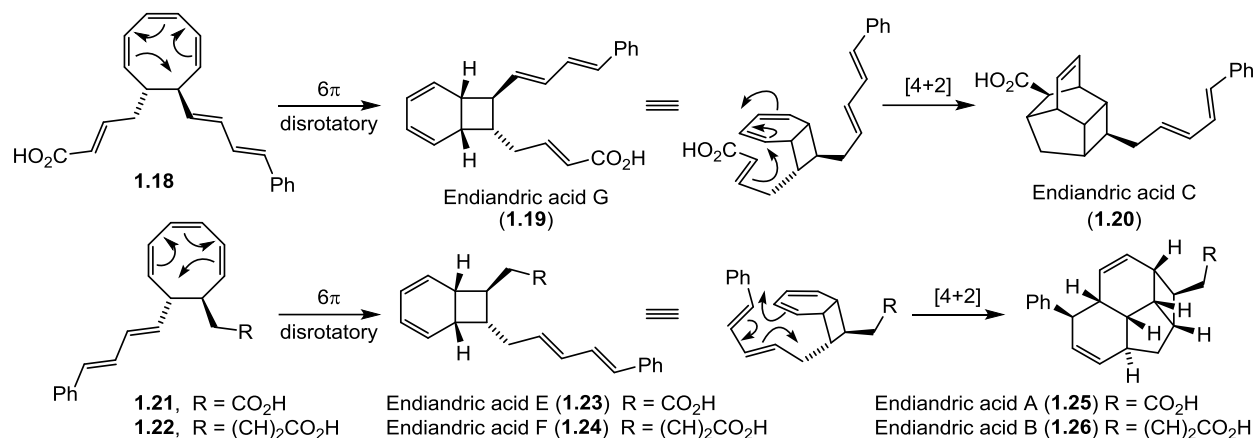


**Scheme 1.5.** *Top.* Octatetraene and its different pericyclic reactions. *Bottom.* Natural products which originate from the linear precursor **1.14** as a result of the processes shown above.<sup>[31–33]</sup>

### 1.2.1 Endiandric acids

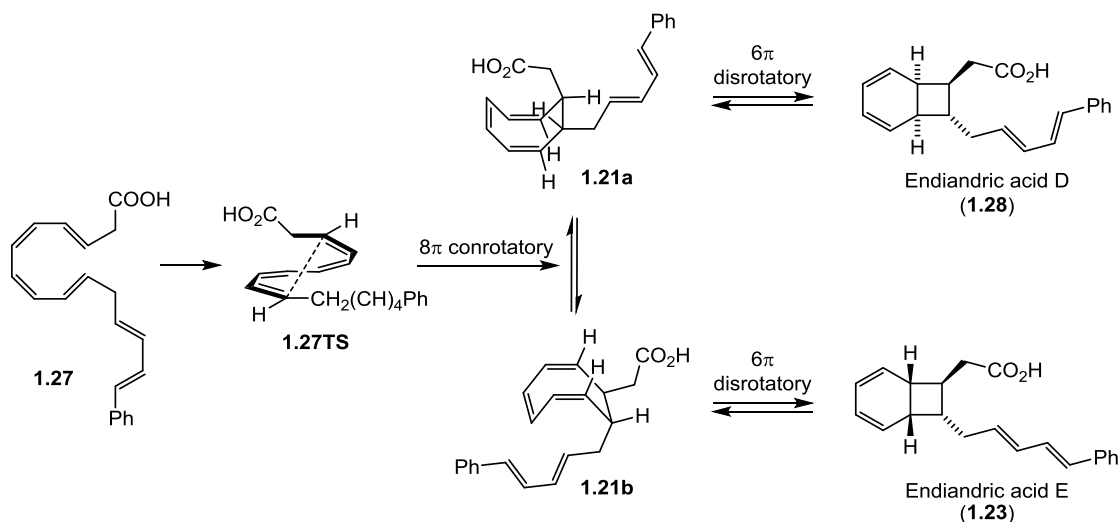
Until recent years, cyclooctatrienes had only been scarcely used as intermediates in total synthesis. The first and most remarkable use of cyclooctatrienes in natural product synthesis was reported by Nicolaou in his biomimetic synthesis of various endiandric acids.<sup>[35]</sup> This work was inspired by Black's brilliant 1980 biosynthetic proposal, in which he hypothesized that the endiandric acids A, B and C, isolated from

*Endiandra introrsa* (Lauraceae) were formed from linear polyenes. He posited that these polyenes underwent an  $8\pi$  electrocyclization to deliver functionalized cyclooctatrienes (Scheme 1.6),<sup>[36]</sup> which was followed by a  $6\pi$  thermal disrotatory electrocyclization to yield bicyclo[4.2.0]octadienes, known as endiandric acids E-G (Scheme 1.6).<sup>[36–38]</sup> Finally, upon intramolecular Diels–Alder reactions, the intricate structures of endiandric acids A, B, and C, bearing 8 stereocentres could be obtained. Black observed that these natural products were all racemic, and therefore suggested that no enzymes took part in the cyclization steps.



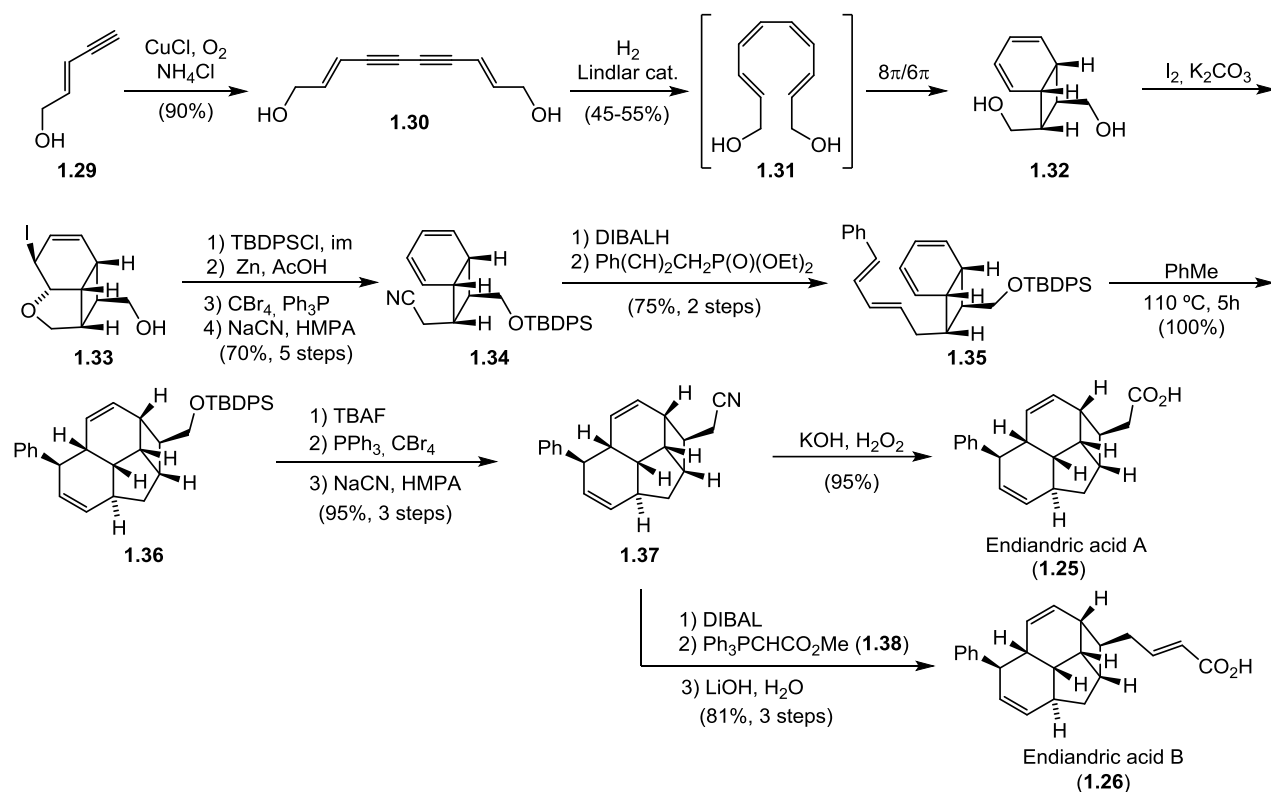
**Scheme 1.6.** Biosynthesis of endiandric acids A-C as proposed by D. St. C. Black.

As mentioned in Chapter 1.1, linear polyenes such as **1.27** (Scheme 1.7) bearing 1,3,5,7-tetraene entities (where C3-C4 and C5-C6 olefins must be *Z*) undergo  $8\pi$  thermal conrotatory electrocyclization *via* transition state **1.27TS** delivering cyclooctatriene **1.21**. This compound exist as a mixture of two conformers, **1.21a** and **1.21b**, which interconvert by a ring flip with an energy barrier of 4-7 kcal/mol (Scheme 1.7).<sup>[39]</sup> Each conformer, **1.21a** or **1.21b**, yields a different diastereomer upon  $6\pi$  electrocyclization, which in the case depicted in Scheme 1.7 are endiandric acids D and E.



**Scheme 1.7.** Biosynthesis of endiandric acids D-E as proposed by D. St. C. Black showing one of the two possible transition states for the  $8\pi$  electrocyclization and the two conformers of the resulting cyclooctatriene.

Following Black's reasoning, Nicolaou envisioned a biomimetic synthesis of endiandric acids using simpler substrates for the  $8\pi/6\pi$  cascade, which would be further functionalized prior to the Diels–Alder reaction.<sup>[40]</sup> Thus, starting from symmetric diyne **1.30** obtained through Glaser alkyne coupling of enyne **1.29**, partial reduction with Lindlar's catalyst presumably led to the non-isolable octatetraene **1.31**, which after the  $8\pi/6\pi$  cascade yielded bicyclo[4.2.0]octadiene **1.32** (Scheme 1.8). Selective protection of the *exo*-alcohol was achieved by regiospecific iodoetherification of the *endo*-alcohol followed by TBDPS protection of the remaining primary alcohol and reversal of the etherification by treatment with Zn dust and acetic acid. Appel reaction followed by nucleophilic substitution of the resulting bromide by sodium cyanide in HMPA allowed for isolation of the key intermediate **1.34**, which could be further elaborated affording endiandric acids A–G (Schemes 1.8 and 1.9). Subsequent DIBAL reduction of **1.34** and condensation of the resulting aldehyde with diethyl *trans*-cinnamylphosphonate yielded the Diels–Alder precursor **1.35**. The desired [4+2] cycloaddition was achieved in refluxing toluene, which smoothly yielded the core structure **1.36**. This was elaborated into the common precursor of endiandric acids A and B, **1.37** by TBAF deprotection, Appel reaction and one-carbon homologation *via* nucleophilic attack of sodium cyanide. **1.37** was finally converted into endiandric acids A and B by simple cyanide hydrolysis for endiandric acid A (**1.25**) and Wittig olefination with phosphonium salt **1.38** and ester hydrolysis for endiandric acid B (**1.26**).



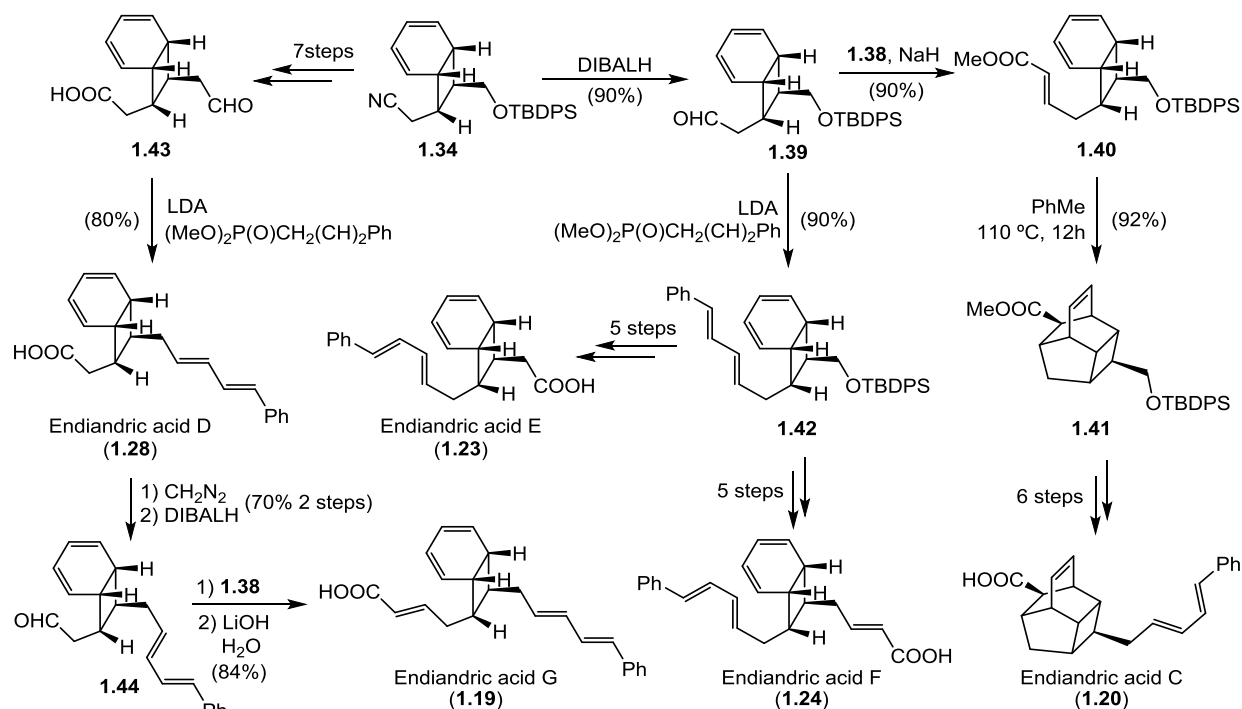
**Scheme 1.8.** Total synthesis of endiandric acids A and B by Nicolaou.

Starting from the key intermediate **1.34**, Nicolaou also accomplished the synthesis of endiandric acids C–G (Scheme 1.9). At the time, only endiandric acids C and D had been found in nature.<sup>[41]</sup>

Bicyclo[4.2.0]octadiene **1.43** was prepared from **1.34** in 7 steps and was condensed with dimethyl *E*-cinnamylphosphonate to yield endiandric acid D. Endiandric acid D was then transformed into its corresponding methyl ester by treatment with diazomethane, and was further reduced to give aldehyde **1.44**, which was coupled with phosphonate **1.38** and hydrolysed to yield endiandric acid G. Aldehyde **1.39**

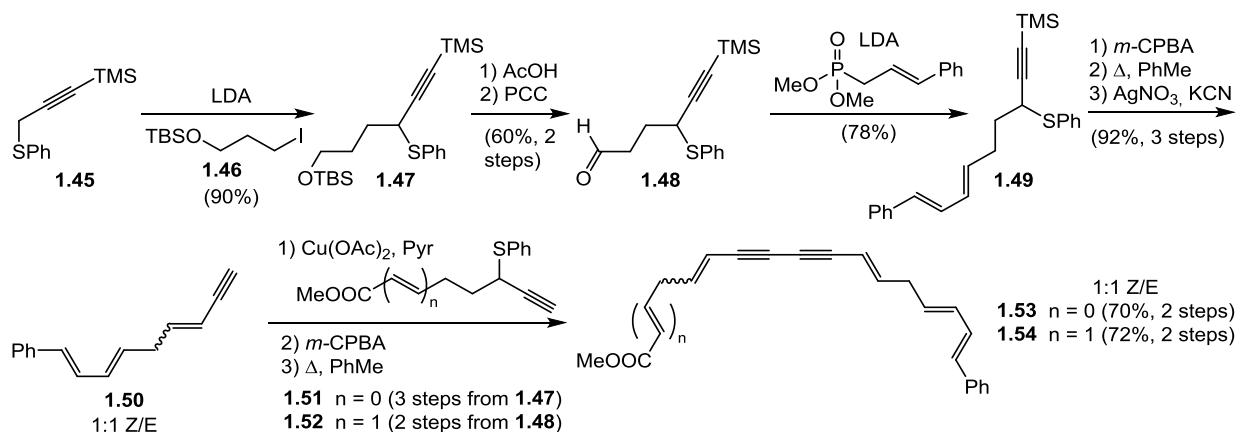
was obtained from the key intermediate **1.34** by DIBAL reduction and was submitted to a HWE reaction which yielded tetraene **1.42**, from which endiandric acids E and F were obtained in 5 steps each.

Aldehyde **1.39** was also an intermediate in the synthesis of endiandric acid C. After condensation with phosphonate ester **1.38**, an intramolecular Diels–Alder reaction took place in excellent yield by refluxing triene **1.40** in toluene for 12 hours. The resulting tetracycle **1.41** was converted into endiandric acid C in 6 steps using similar chemistry as previously described.



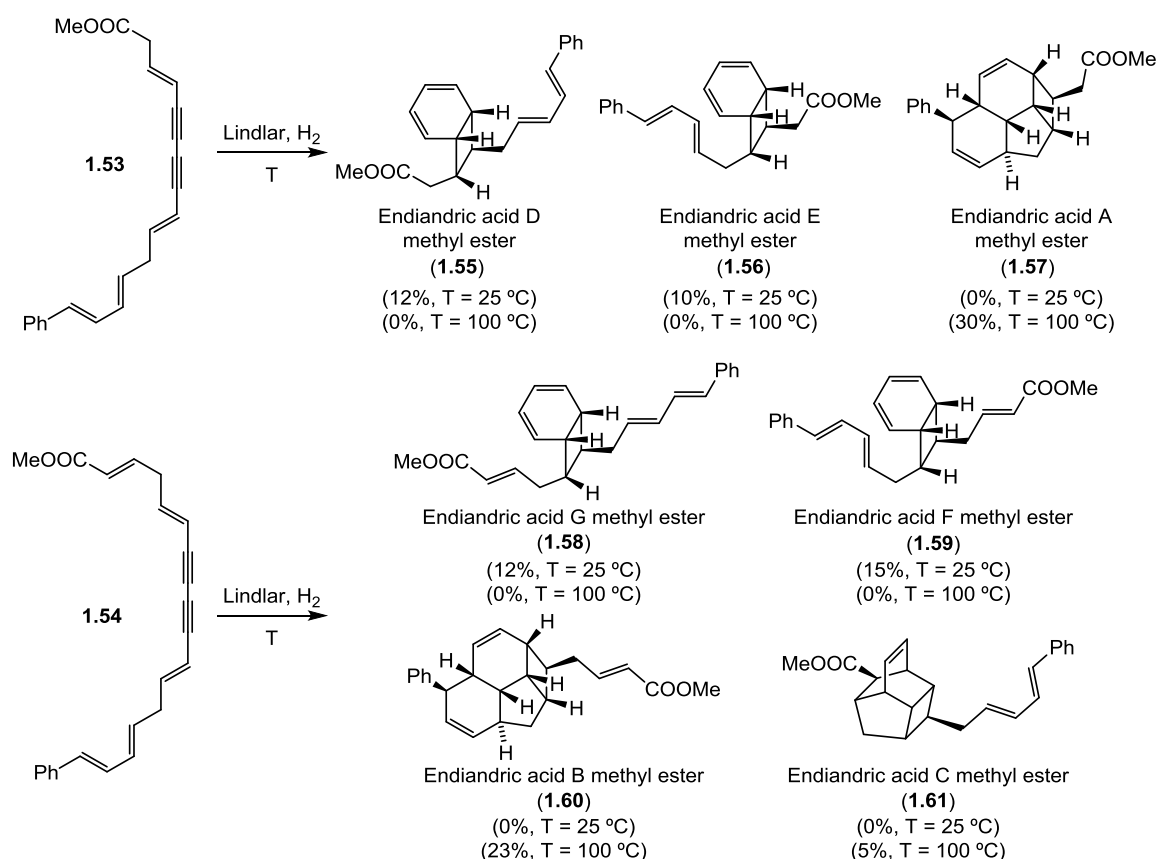
**Scheme 1.9.** Total synthesis of endiandric acids C-G by Nicolaou.

Having achieved the first total syntheses of endiandric acids A-G, Nicolaou provided another approach towards these natural products in a strictly biomimetic fashion.<sup>[42]</sup> Now the main goal was to give evidence to corroborate Black's hypotheses. Based on their previous experience, two initial considerations were taken as guidelines: 1) The central (Z,Z)-diene should be masked until a late stage to avoid undesired 8 $\pi$  electrocyclicization. 2) For practical reasons, the carboxylic acid groups would be exchanged by methyl esters.



**Scheme 1.10.** Preparation of the building blocks for the biomimetic syntheses of endiandric acid methyl esters A-G.

As depicted in Scheme 1.10, alkylation of deprotonated thioether **1.45** with alkyl iodide **1.46** led to silyl ether **1.47**, which was subsequently deprotected and oxidized to deliver aldehyde **1.48**. Condensation of **1.48** with dimethyl *trans*-cinnamylphosphonate yielded thioether **1.49**, which was converted to the corresponding sulfoxide by treatment with *m*-CPBA. Thermally induced elimination and TMS deprotection with silver nitrate and potassium cyanide then provided triene **1.50** as a 1:1 mixture of *E/Z* isomers. Upon purification, the *E*-isomer was independently submitted to two Glaser couplings with alkynes **1.51** and **1.52**, both derived from thioether **1.47**. A further oxidation/elimination sequence led to diynes **1.53** and **1.54**, which could be separated by flash chromatography.



**Scheme 1.11.** Biomimetic synthesis of the methyl ester derivatives of endiandric acids A-G.

Finally, the linear endiandric acid precursors **1.53** and **1.54** were successfully submitted to semi-reductive conditions with Lindlar's catalyst in the presence of hydrogen affording the desired endiandric acid methyl esters.<sup>[43]</sup> Thus, when **1.53** was stirred for few hours at room temperature under these conditions, the semi-reduction of the diyne was followed by an  $8\pi/6\pi$  electrocyclization sequence delivering endiandric acid analogues D and E (**1.55**, **1.56**) in low yields without any trace of the Diels–Alder product **1.57**. However, if the mixture was heated up to 100 °C for a few minutes under the previously described conditions, the  $8\pi$  electrocyclization was followed by a [4+2] cycloaddition resulting in the isolation of endiandric acid A methyl ester (**1.57**) as the single product.

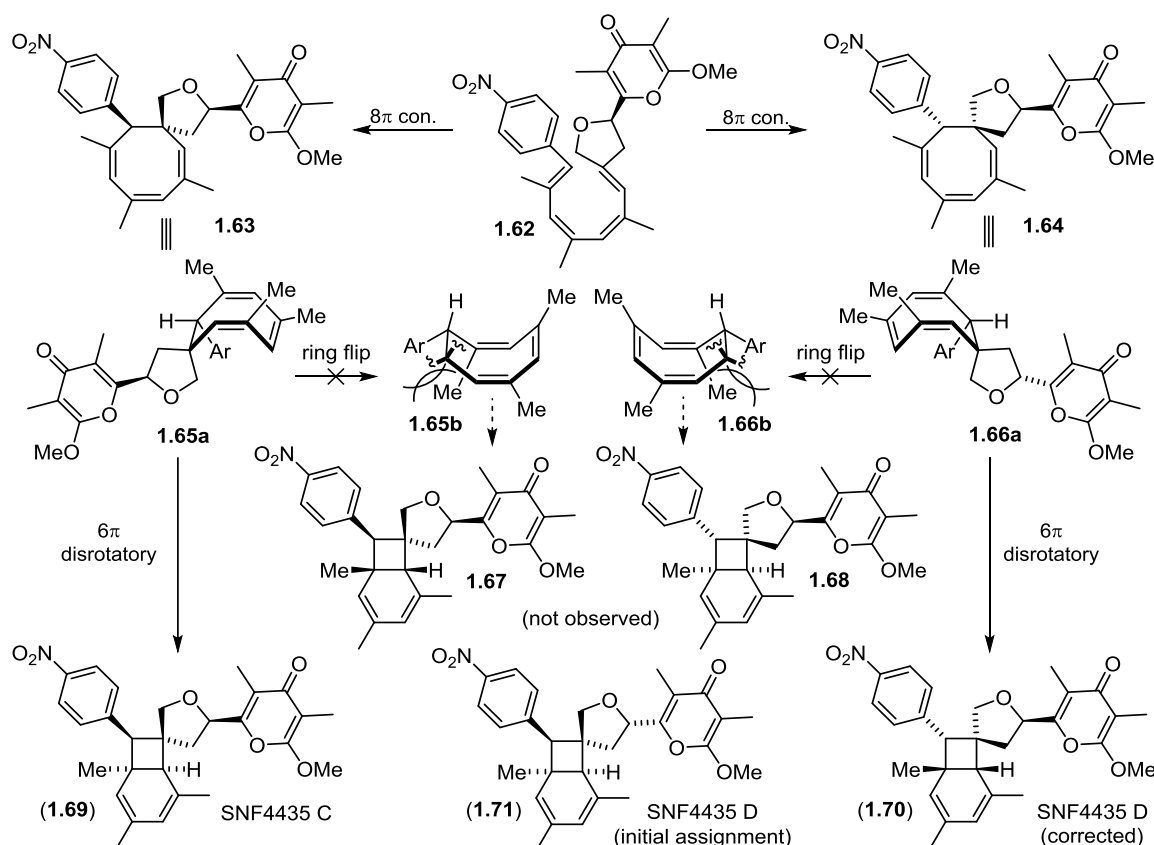
In the case of polyene **1.54**, the same reaction at room temperature led to the isolation of the respective methyl esters of endiandric acids F and G (**1.58**, **1.59**). When the reaction mixture was heated up for few minutes at 100 °C, the previous sequence was followed by a Diels–Alder reaction, which delivered endiandric acid methyl esters B and C (**1.60**, **1.61**).

Finally, a NMR study of the thermal conversion of these compounds was performed at 70 °C. The equilibrium between endiandric acid methyl esters E and D and the transformation of the former into endiandric acid A was monitored showing a half-life of 1.3 hours for **1.56**, with **1.57** being the major component after 6 hours. When pure endiandric acid F methyl ester was submitted to the same conditions, build-up of G took place quickly in the first 2 hours and then slowly decayed. Unlike the latter, endiandric acid B methyl ester slowly enriched the mixture and turned into the major isomer after 6 hours. Finally, endiandric acid C methyl ester slowly built-up and only represented 10% of the mixture after 14 hours.

This extensive work by Nicolaou proved Black's hypothesis for the biosynthesis of endiandric acids and described an elegant and high yielding synthesis of these complex natural products. It also established a new type of cascade that would be used in the future for the synthesis of other intricate natural products such as the kingianins and the elysiapyrones. The question of how the Diels–Alder reaction takes place in nature without the assistance of enzymes would remain an intriguing question until a possible explanation was provided with the total synthesis of kingianin A.<sup>[44]</sup>

### 1.2.2 SNF4435

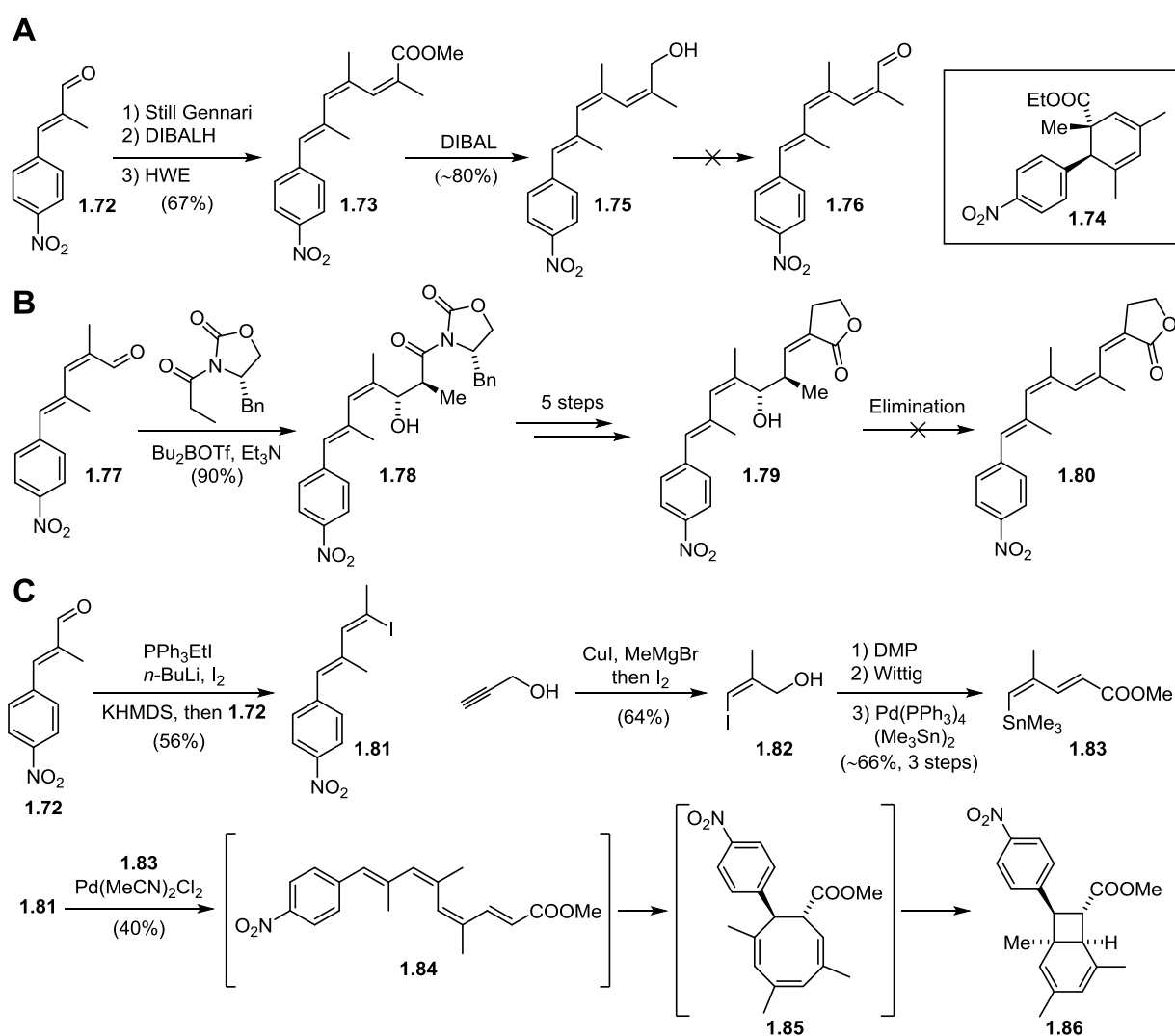
A remarkable case of a total synthesis race took place with the immunosuppressant natural products SNF4435C and SNF4435D.<sup>[45–47]</sup> Unlike the endiandric acids, these pyrones, isolated by Kurosawa from *Streptomyces spectabilis* were found as single enantiomers.



**Scheme 1.12.** Proposed biosynthesis of SNF4435 C and D. **1.67** and **1.68** represent a pair of isomers not found in nature, presumably due to the torsional strain between the contiguous nitrobenzene and methyl groups (the tetrahydrofuran ring was omitted for clarity). **1.71** represents the misassigned structure of SNF4435 D by Kurosawa and **1.70** the real structure as corrected by Trauner.

SNF4435C and SNF4435D showed unprecedented potent selective immunosuppressive activity towards B-cell proliferation without affecting T-cell production, suggesting a new mode of action. This interesting bioactivity together with their attractive bicyclo[4.2.0]octadiene core prompted several research groups to pursue their total synthesis, reviving a cascade sequence which had not been utilized for 20 years. The main participants in this race were Christopher M. Beaudry and Dirk Trauner from UC Berkeley; Jack E. Baldwin, John E. Moses, Robert M. Adlington, Mikkel F. Jacobsen and Rodolfo Márquez for Oxford University; and Kathlyn A. Parker and Yeon-Hee Lim from Stony Brook University, New York.

The first article was released in April 2002 from the Trauner group<sup>[34]</sup> and included synthetic studies, a proposed biosynthesis and a corrected structure for SNF4435D based on the logic of the  $8\pi/6\pi$  cascade. The synthesis portion consisted of two linear routes which failed to provide a cascade precursor and one elegant and simple modular approach which yielded a bicyclo[4.2.0]octadiene with a methyl ester handle for further functionalization (Scheme 1.13).



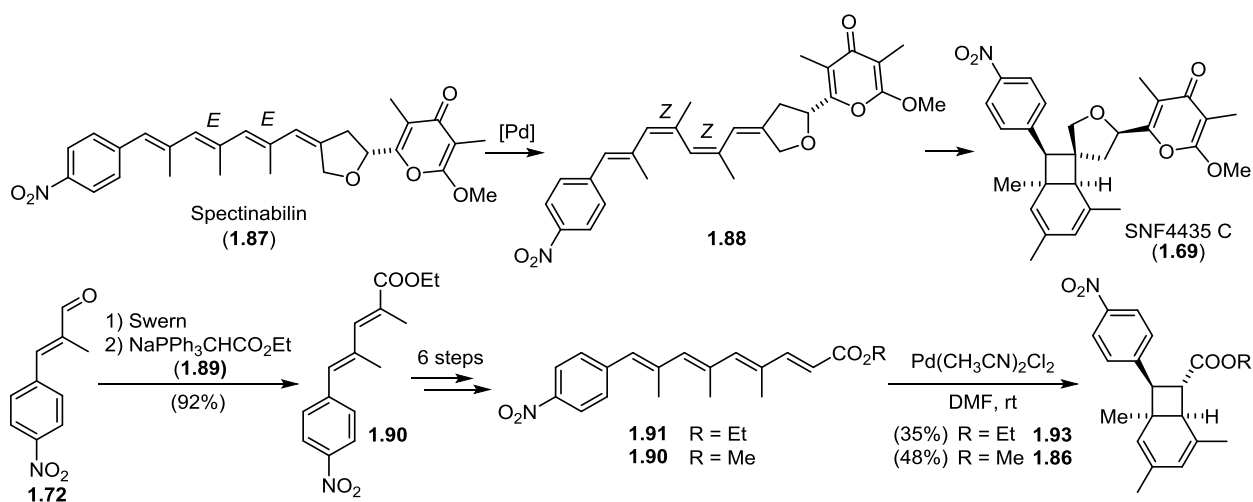
**Scheme 1.13.** Synthetic approaches towards SNF4435 by Trauner. **A**, **B**. failed attempts towards the bicyclo[4.2.0]octadiene core. **C**. Successful approach towards bicyclic precursor **1.86** via  $8\pi/6\pi$  electrocyclic cascade.

The first explored route started with aldehyde **1.72**, which was elongated *via* Still–Gennari olefination followed by DIBAL reduction and HWE reaction to install the ethyl ester handle. Although the labile ester **1.73** underwent spontaneous  $6\pi$  electrocyclization yielding undesired cyclohexadiene **1.74**, it could be reduced to alcohol **1.75** upon treatment with DIBAL. However, **1.75** was also unstable and could not be further oxidized to aldehyde **1.76**.

A second-generation approach was inspired by biogenetic considerations. Since the biosynthesis of polyenes is achieved by a series of reduction and dehydration steps,<sup>[48]</sup> this strategy was translated to the synthesis by the hydration of one of the double bonds in search for increased stability. Thus, starting with aldehyde **1.77**, an intermediate in the previous route, an Evans aldol reaction afforded oxazolidinone **1.78**, which was transformed into advanced intermediate **1.79** in 5 steps. Unfortunately, all attempts to dehydrate this compound led to decomposition.

The final approach relied on a late-stage Stille coupling of vinyl iodide **1.81** with stannane **1.83**. The former was synthesized by a Stork–Zhao olefination of aldehyde **1.72**, and the stannane was obtained by a carbocurpation of propargyl alcohol followed by trapping of the metalated species with iodine to give the branched product **1.82**. Oxidation of the alcohol followed by Wittig olefination and metalation with hexamethylditin yielded **1.83**. The tandem Stille coupling between **1.81** and **1.83** followed by the  $8\pi/6\pi$  cascade took place at room temperature in the presence of  $\text{Pd}(\text{MeCN})\text{Cl}_2$  yielding exclusively bicyclo[4.2.0]octadiene **1.86**. The high stereoselectivity could be assigned to the torsional strain between the adjacent aromatic and methyl groups, analogous to the repulsion present in **1.65b** and **1.66b** (Scheme 1.12).

Four months later Moses and Baldwin published their studies on the biomimetic synthesis of SNF4435 C.<sup>[49]</sup> Starting with the same aldehyde as Trauner, **1.72**, Moses and Baldwin aimed for the total synthesis of the natural product spectinabilin,<sup>[50]</sup> thought to be natural precursor of **1.69** and **1.70** *via* double bond isomerization and  $8\pi/6\pi$  electrocyclization cascade<sup>[34,49]</sup> (Scheme 1.14).



**Scheme 1.14. Top.** Biomimetic strategy followed by Moses and Baldwin for the synthesis of SNF4435 C from spectinabilin. A double olefin isomerization of spectinabilin would give the right stereochemistry to induce the  $8\pi/6\pi$  cascade. **Bottom.** Proof of principle with a simplified system using esters **1.90** and **1.91**.

Chain extension of aldehyde **1.72** was performed by a series of *E*-selective Wittig olefinations with stabilized ylide **1.89**. Once the conjugated tetraene was obtained, Pd(II)-induced *E/Z* isomerization at room



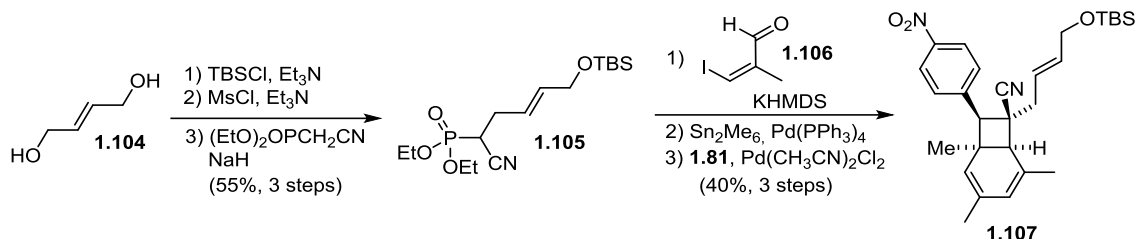
temperature triggered the electrocyclization process yielding the desired bicyclo[4.2.0]octadiene core in 35% and 48% yield for the ethyl (**1.93**) and methyl ester analogues (**1.86**), respectively. Interestingly, all thermal and photochemical attempts to convert the all-*E* tetraene **1.91** into hexadiene **1.93** failed, suggesting that the isomerization requires metal catalysis.

Parker's approach was published one year later.<sup>[51]</sup> Noting that the works by Trauner and Baldwin yielded only the diastereomer leading to SNF4435 C, she pursued a systematic study of the cascade. Using the successful domino Stille/ $8\pi/6\pi$  electrocyclization developed by Trauner, a series of vinyl stannanes with different substitution patterns were synthesized to evaluate whether they could give access to the skeleton of SNF4435 D (Scheme 1.15).

Entry	Diene	R <sub>Z</sub>	R <sub>E</sub>	Yield [%]	endo	Product	exo
1	<b>1.94</b>	CH <sub>2</sub> OTBS	Me	31	50	<b>1.99</b>	50
2	<b>1.83</b>	H	COOMe	62	100	<b>1.86</b>	0
3	<b>1.95</b>	COOEt	H	38	100	<b>1.100</b>	0
4	<b>1.96</b>	Me	COOEt	56	40	<b>1.101</b>	60
5	<b>1.97</b>	COOEt	Me	54	10	<b>1.102</b>	90
6	<b>1.98</b>	CN	Me	59	90	<b>1.103</b>	10

**Table 1.1.** Screening of different substituents at the terminal end of the vinyl stannane participating in the Stille coupling with vinyl iodide **1.81**.

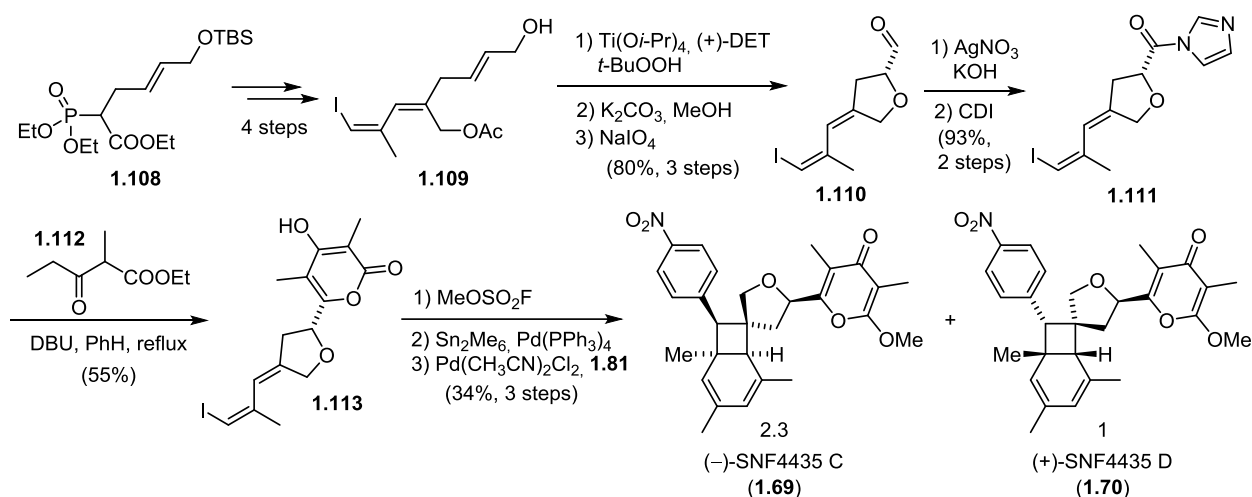
Parker was the first to explore the  $8\pi/6\pi$  cascade with two substituents, here called R<sub>E</sub> and R<sub>Z</sub>, present at one terminus of the tetraene. In contrast to the previous work by Trauner and Baldwin (Schemes 1.13 and 1.14, compound **1.86**) where only the endo product was obtained, when the reaction was run with diene **1.94** bearing a silyl ether (Table 1.1, Entry 1), a complete lack of selectivity for “endo” or “exo” products was observed. The torsional strain between the silyl ether chain and the cyclohexene ring presumably equals that of the aromatic ring with the adjacent methyl group, which previously governed the stereoselectivity of the  $6\pi$  electrocyclization. To compare with Trauner's and Baldwin's work, the reaction was run with stannane **1.83** (Entry 2), confirming the previous findings (exclusive *endo* selectivity) and increasing the yield from 48% (Baldwin) to 60%. When running the reaction with a terminal *Z* ethyl ester (Entry 3), *E/Z* isomerization occurred, affording product **1.100** with the same relative configuration found in entry 2 (100% endo). When replacing the hydrogen by a methyl group, the stereoselectivity gained in Entries 2 and 3 was lost once again (Entries 4 and 5). As for Entry 1, this could be explained by the steric clash between the R<sub>Z</sub> substituent and the cyclohexadiene ring, which destabilizes the *endo* transition state. Finally, when using the small linear cyano group, the mentioned torsional strain in the *endo* transition state was greatly diminished and a 9:1 *endo/exo* ratio was obtained. The nitrile was also a potential handle for future work in the installation of the tetrahydrofuran and the pyrone.



**Scheme 1.15.** Synthesis of the advanced intermediate **1.107** by Parker.

Thus, after having established the cyanide as suitable group, the advanced intermediate **1.107** was synthesized starting from diol **1.104**, which was monoprotected with TBS chloride followed by mesylation and  $S_N2$  displacement to install the required phosphonate ester. Horner–Wasworth–Emmons reaction of phosphonate **1.105** with aldehyde **1.106** followed by Stille coupling at room temperature yielded the stannane required for the cascade, which delivered bicyclo[4.2.0]octadiene **1.107** in 40% yield from **1.105**.

One year later, Parker published the first total synthesis of (–)-SNF4435 C and (+)-SNF4435.<sup>[44]</sup> The route took advantage of the previously developed Stille coupling and installed the enantiopure tetrahydrofuran-pyrone moiety prior to the cascade reaction (Scheme 1.16).

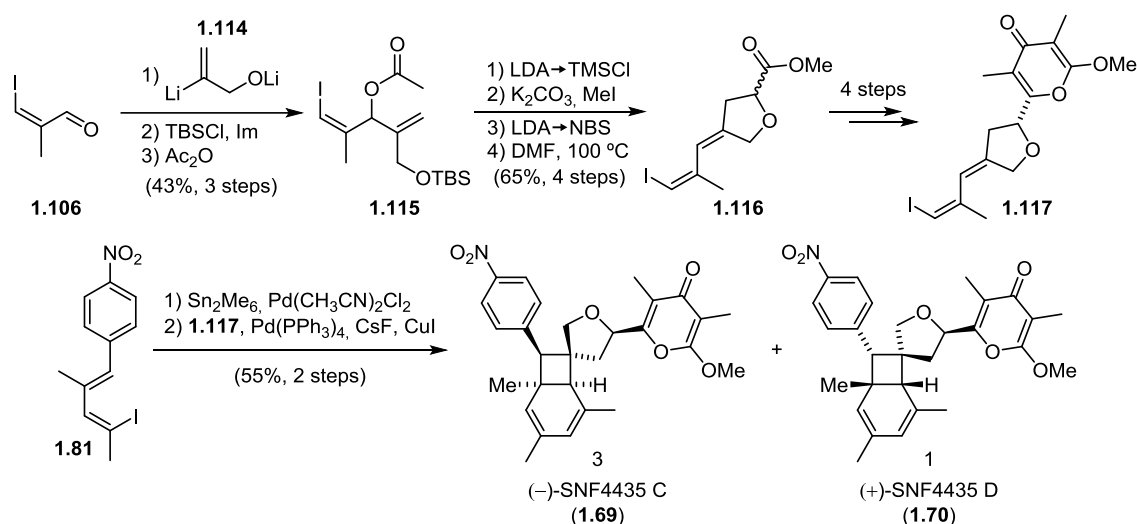


**Scheme 1.16.** Total synthesis of (–)-SNF4435 C and (+)-SNF4435 by Parker.

The synthesis started with the functionalized phosphonate ester **1.108**, analogous to **1.105** (Scheme 1.15), which was converted into vinyl iodide **1.109** in 4 steps (Scheme 1.16). Sharpless epoxidation of the allylic alcohol followed by ester hydrolysis triggered a 5-*exo-tet* cyclization, which was followed by oxidative cleavage of the resulting 1,2-diol by treatment with sodium periodate delivering aldehyde **1.110**. Oxidation of **1.110** by treatment with silver nitrate followed by activation of the acid with carbonyldiimidazole yielded acylimidazole **1.111**. This was condensed with **1.112** and heated to reflux in benzene to induce transesterification yielding 1,2-pyrone **1.113**. SNF4435 C and D were synthesized by the conversion of **1.113** into the desired 1,4-pyrone by treatment with methyl fluorosulfonate followed by Stille coupling, which yielded the required stannane for the reaction cascade. The Stille/ $8\pi$ / $6\pi$  sequence was performed with vinyl

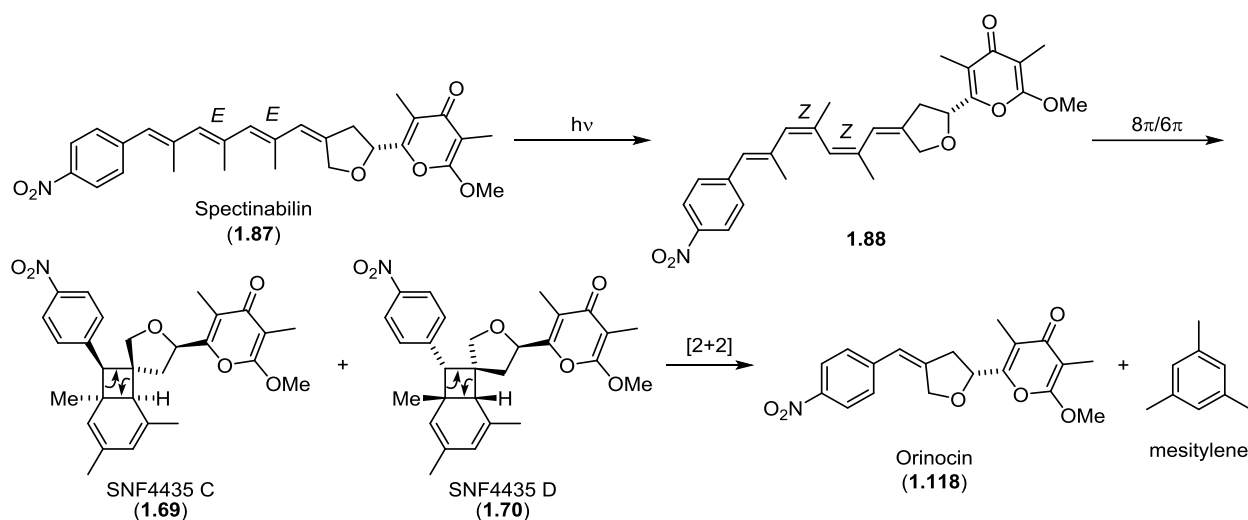
iodide **1.81** under palladium catalysis at room temperature, yielding (–)-SNF4435 C and (+)-SNF4435 D in a very similar ratio as in nature.

7 months later, Trauner and Beaudry published their total synthesis of these natural products featuring a biomimetic convergent synthesis which included a [3,3]-sigmatropic rearrangement and the tandem Stille coupling/ $8\pi/6\pi$  electrocyclization cascade (Scheme 1.17).<sup>[52]</sup> This approach started with vinyl iodide **1.106**, which instead of engaging in a Wittig olefination as for the previous synthesis (Scheme 1.15), was alkylated with dianion **1.114**. The resulting primary and secondary alcohols were protected with TBS chloride and acetic anhydride respectively. The resulting diene **1.115** underwent an Ireland–Claisen rearrangement upon treatment with LDA and TMSCl. The resulting acid was esterified, brominated at the  $\alpha$ -position and subjected to a transesterification after TBS deprotection, affording diene **1.116**. This route afforded pyrone **1.116** in 10 steps from commercially available starting materials vs 11 steps for Parker’s synthesis. Following the method developed by Parker, vinyl iodide **1.117** was prepared in 4 more steps and purified by chiral HPLC. Vinyl iodide **1.81** was stannylated with hexamethyl ditin under palladium catalysis and subsequently coupled to vinyl iodide **1.117** under Baldwin’s conditions<sup>[53]</sup> affording **1.69** and **1.70** in a remarkably high 89% combined yield. Again, the product ratio was similar to the mixture of isomers found in nature.



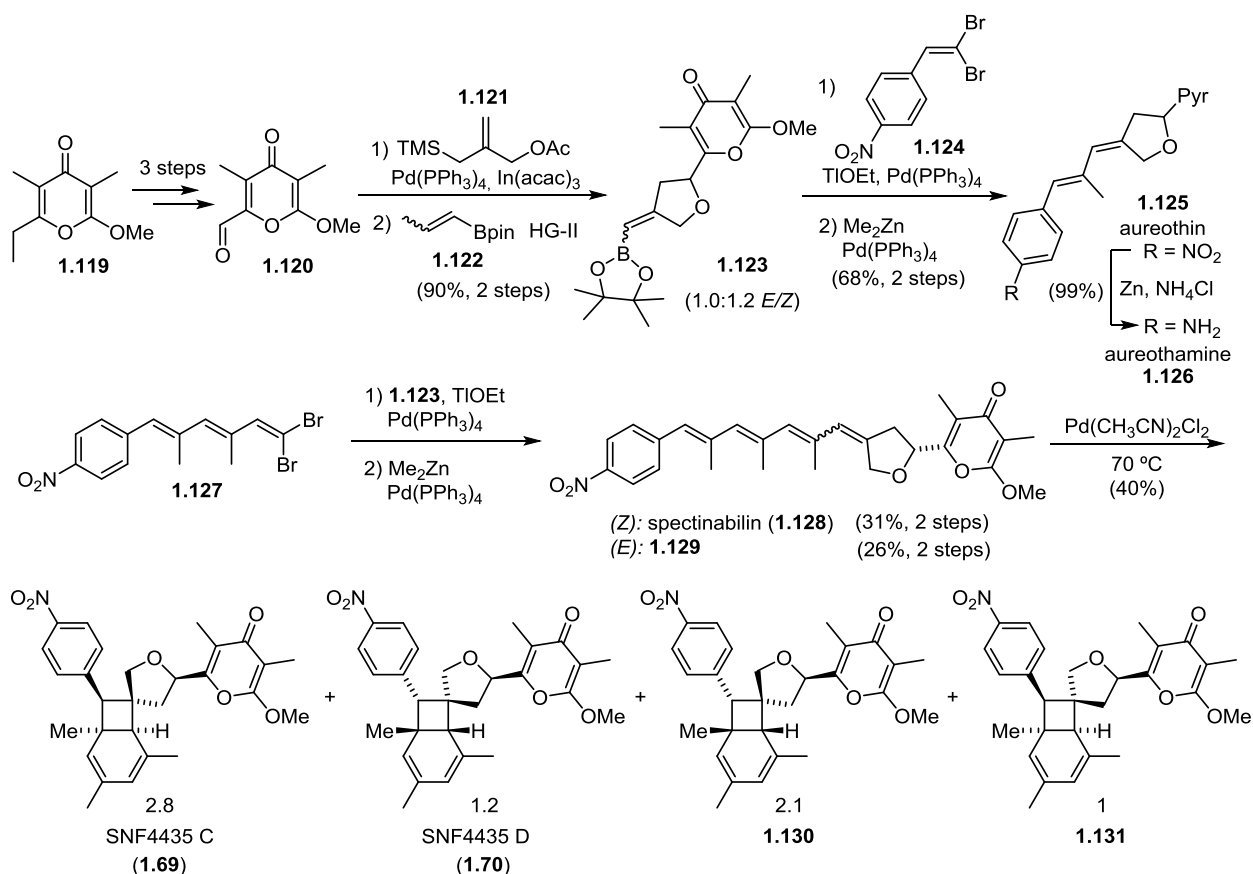
**Scheme 1.17.** Total synthesis of (–)-SNF4435 C and (+)-SNF4435 by Trauner.

Interestingly, a publication by Trauner and Hertweck published one year later showed that the  $8\pi/6\pi$  electrocyclization was not the end of the cascade. There was a consensus about the biosynthetic origin of **1.69** and **1.70**, thought to arise from spectinabilin after a double olefin isomerization and electrocyclic cascade (Scheme 1.18), which was proven by Baldwin’s later work.<sup>[54]</sup> Trauner and Hertweck studied the metabolic profile of *Streptomyces orinoci*, a bacteria known to produce spectinabilin under various growth conditions.<sup>[55]</sup> As expected, the bicyclo[4.2.0]octadienes were only produced under light exposure, which was necessary for the double olefin isomerization, but more interestingly, a new natural product named orinocin was found (Scheme 1.18). Orinocin was only produced in the presence of light and was detected together with isolated fractions of **1.69** and **1.70**, which suggested that **1.118** could originate from the SNF4435 natural products. This was proven by submitting SNF4435 C and D to fermentation conditions (28 °C, sunlight), under which **1.69** and **1.70** underwent a photochemical retro-[2+2] cycloaddition, releasing orinocin and mesitylene, the latter of which has been catalogued as a natural product. This process of extrusion of internal ketide units from a polyene backbone has been named “polyene splicing” by Trauner and Hertweck.<sup>[55]</sup>



**Scheme 1.18.** Biosynthetic origin of SNF4435 C and D as proven by Baldwin and further conversion into orinocin as proven by Trauner and Hertweck.

Baldwin and Moses later presented a unified synthesis of spectinabilin and SNF4435 C and D along with the related natural products aureothin and aureothamine.<sup>[54,56]</sup>



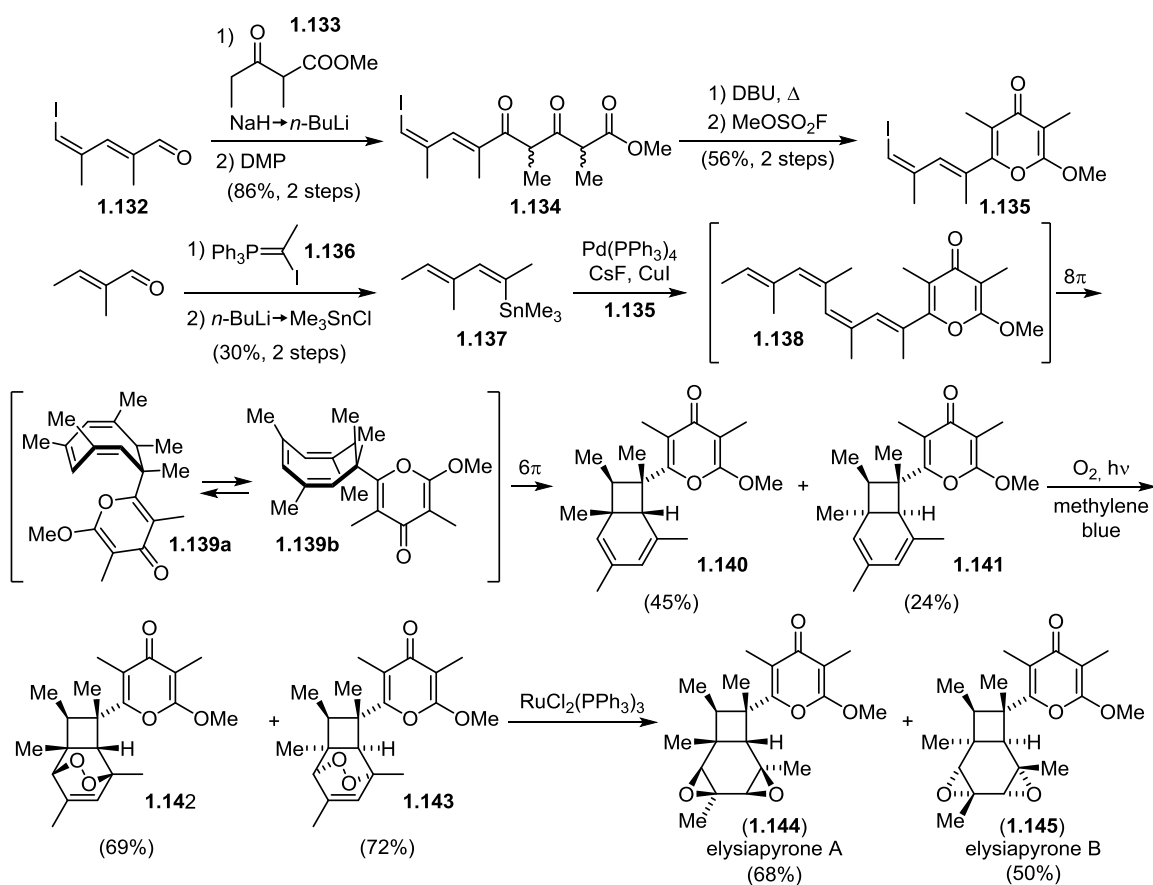
**Scheme 1.19.** Collective total synthesis of racemic SNF4435 C and D, spectinabilin, aureothin and aureothamine by Moses and Baldwin.

Their synthesis started with pyrone **1.120**, obtained from pyrone **1.119** in 3 steps. The aldehyde could be converted into alkenyl boronic ester **1.123** *via* a formal [3+2] cycloaddition with **1.121** under Tsuji–Trost conditions in the presence of an indium salt to promote 1,2-addition<sup>[57]</sup> followed by cross-metathesis with pinacol boronate **1.122** giving pyrone **1.123** as a mixture of *E/Z* isomers. Suzuki coupling of **1.123** with vinyl dibromide **1.124** in the presence of thallium ethoxide followed by Negishi coupling to install the olefinic methyl group yielded racemic aureothin (**1.125**), which was converted into aureothamine (**1.126**) by reduction of the nitro group with Zn/ammonium chloride.

Spectinabilin (**1.128**) was synthesized in a similar fashion as aureothin *via* Suzuki coupling of dibromotriene **1.127** with boronate **1.123** followed by Negishi coupling to install the olefinic methyl group. Treatment of spectinabilin with palladium(II) at 70 °C for 24 hours in the dark caused isomerization of the *E,E,E,Z*-tetraene to the required *E,Z,Z,Z* configuration, triggering the  $8\pi/6\pi$  electrocyclicization as previously seen. Racemic SNF4435 C and D were obtained together with isomers **1.130** and **1.131**, presumably consequence of the isomerization of **1.128** to the *E,Z,Z,E* tetraene. The yield of the final step was therefore quite modest.

### 1.2.3 Elysiapyrones

In 2005, Trauner published 3 papers on the synthesis of natural products originating from  $8\pi/6\pi$  electrocyclizations.<sup>[33,52,58]</sup> Elysiapyrones are natural products isolated from the sea slug *Elysia diomedea*,<sup>[59]</sup> one of the few animals capable of retaining ingested chloroplasts in its own tissues to perform photosynthesis.<sup>[60]</sup> These natural products contain a rare bis-epoxide pattern in the 6 membered ring of the bicyclo[4.2.0]octane (Scheme 1.20).



**Scheme 1.20.** Total synthesis of racemic elysiapyrones A and B by Trauner.

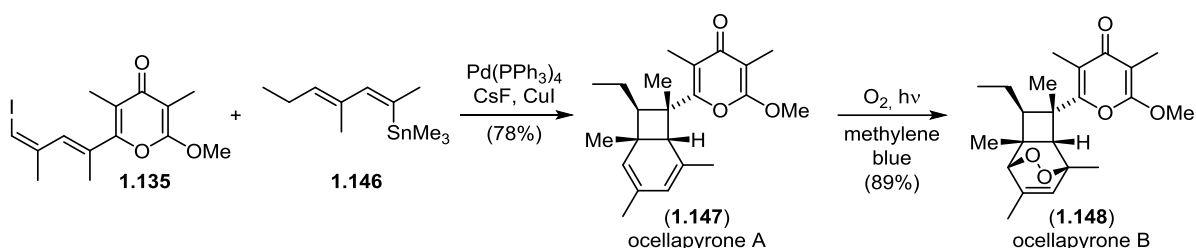
The synthesis started with dienal **1.132**, which was elongated by addition of ketoester **1.133** followed by DMP oxidation to yield tricarbonyl **1.134**. This species underwent a Dieckmann-type condensation upon heating in the presence of base and was later methylated with methyl fluorosulfonate affording 1,4-pyrone **1.135**. Synthesis of the stannane **1.137**, partner for the Stille coupling, was initiated by a Stork–Zhao<sup>[61]</sup> olefination of tiglic aldehyde with ylide **1.136** followed by lithiation/stannylation. Submission of vinyl iodide **1.135** and stannane **1.137** to Baldwin's Stille  $8\pi/6\pi$  electrocyclic conditions yielded a mixture of *endo* and *exo* isomers (**1.140** and **1.141**) which could be separated by column chromatography. The lower yield of the **1.141** is probably a consequence of the torsional strain between the pyrone and the  $\beta$ -methyl groups in the transition state of the  $6\pi$  electrocyclicization.

Now the core structure was set for the introduction of the bis-epoxide groups. This was accomplished by the Diels–Alder reaction of **1.140** and **1.141** with singlet oxygen generated upon light irradiation in the presence of a photosensitizer delivering *endo*-peroxides **1.142** and **1.143**. These adducts were isomerized using the Noyori protocol with  $\text{RuCl}_2(\text{PPh})_3$  yielding elysiapyrones A and B in good yield.<sup>[62]</sup>

## 1.2.4 Ocellapyrones

Ocellapyrones A and B were isolated from *Placobranchus ocellatus*, a mollusc found in shallow waters.<sup>[63]</sup> Ocellapyrone A, whose structure was corrected simultaneously by Baldwin and Trauner,<sup>[32,33]</sup> is an ethylated derivative of elysiapyrone A precursor **1.140** (Scheme 1.20) and ocellapyrone B the ethyl derivative of endoperoxide **1.142**, precursor of elysiapyrone A (Scheme 1.20). Trauner theorized that the ocellapyrones, photodeoxytridachione and 9,10-deoxytridachione could originate from the same tetraene precursor (Scheme 1.5). Since the biogenesis had been already established for photodeoxytridachione and 9,10-deoxytridachione,<sup>[31,32]</sup> the synthesis of **1.147** and **1.148** demonstrated the versatility of the tetraene scaffold.

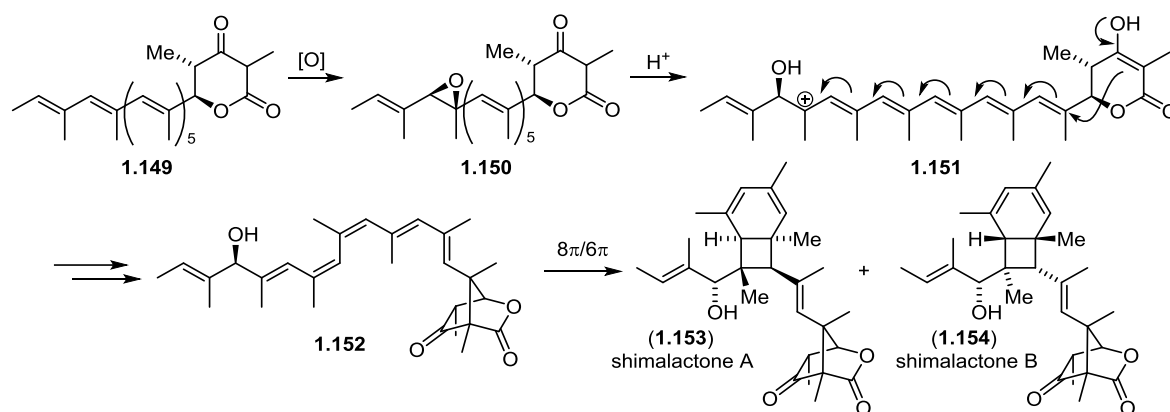
The synthesis followed the same pathway as for elysiapyrones and can be seen in Scheme 1.22.



**Scheme 1.22.** Total synthesis of ocellapyrones A and B by Trauner.

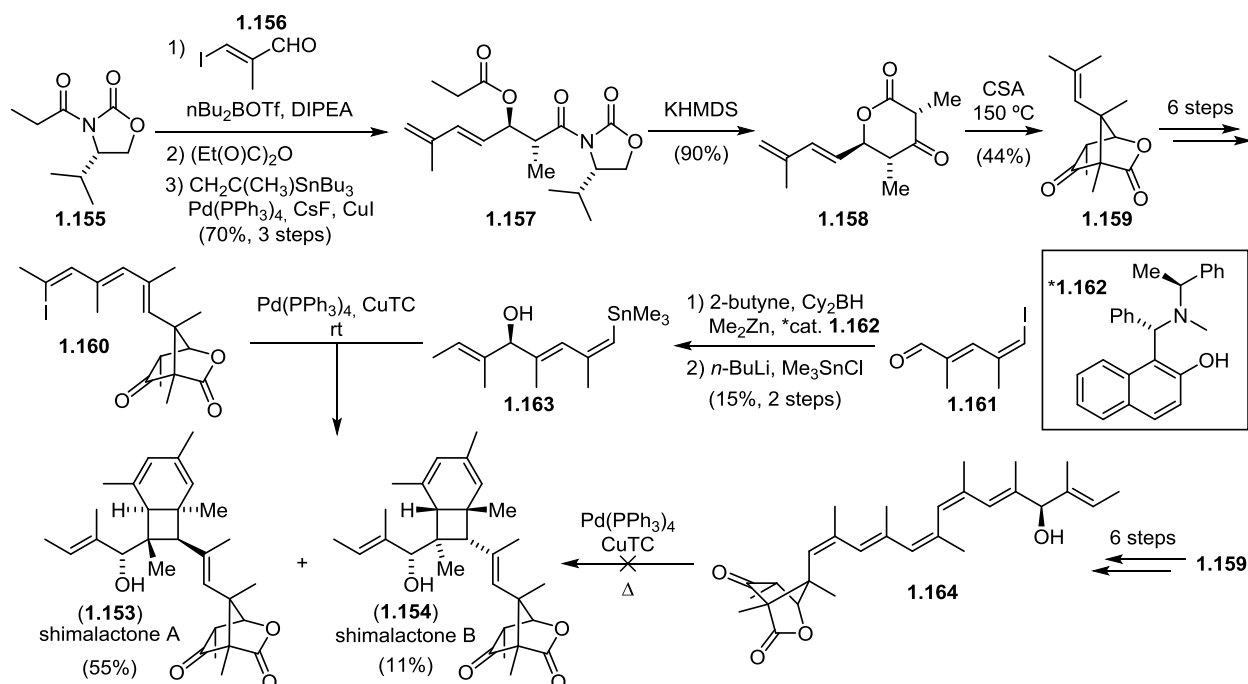
## 1.2.5 Shimalactones A and B

The shimalactones were isolated from the marine fungus *Emericella variecolor*.<sup>[64,65]</sup> They contain a unique oxabicyclo[2.2.1]heptane moiety linked to a bicyclo[4.2.0]octadiene core by a trisubstituted ethylene linker. Trauner proposed an interesting biosynthesis for these natural products in which the polyene chain of **1.149** (Scheme 1.23) would undergo oxidation to epoxide **1.150** followed by protonation yielding undecapentaheptenyl cation **1.151**. This species can now be intercepted by the enol present in the adjacent lactone, forming the bicyclic structure **1.152**. Finally, *E/Z* isomerization of the two central double bonds would trigger the  $8\pi/6\pi$  electrocyclicization.<sup>[66]</sup>



**Scheme 1.23.** Biosynthesis of shimalactones A and B as proposed by Trauner.

The bicyclic ketolactone moiety was prepared starting from oxazolidinone **1.155**, which was converted into diene **1.157** upon asymmetric *anti*-aldol reaction with aldehyde **1.156** followed by esterification of the secondary alcohol and a Stille coupling to introduce the terminal olefin. Then, a Dieckmann condensation of **1.157** afforded ketolactone **1.158**, which upon treatment with CSA at 150 °C cyclized to give the desired oxabicyclo[2.2.1]heptane **1.159**, which subsequently yielded vinyl iodide **1.160** in 6 further steps.



**Scheme 1.24.** Total synthesis shimalactones A and B by Trauner.

Stannane **1.163** was obtained from aldehyde **1.161** upon reaction with 2-butenyl methyl zinc in the presence of asymmetric ligand **1.162** followed by halogen-metal exchange. Finally, a Liebeskind-type Stille coupling between vinyl iodide **1.160** and stannane **1.163** at room temperature yielded both shimalactones in 66% overall yield. Interestingly, when the same reaction conditions were applied to polyene **1.164**, the equivalent *Z,E,Z,Z,E* isomer, the cascade did not take place even under forcing conditions and only **1.164**

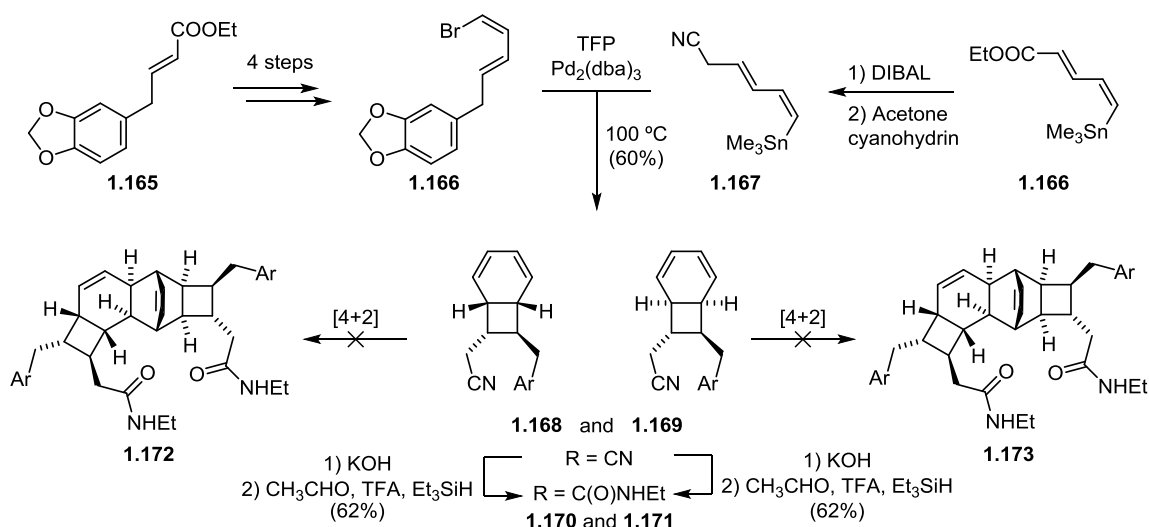
could be isolated. Presumably, the bulk of the bicyclic substituent which would be positioned in *endo* in the transition state does not allow for the  $8\pi$  electrocyclization to occur.

## 1.2.6 Kingianins

Once again, Parker and Moses worked in parallel on the same natural product and this time also Sherburn pursued the synthesis of Kingianin A (**1.175**). This natural product was found as a racemate in the bark of *Endiandra kingiana*, a tree collected in the rainforest of Malaysia.<sup>[67]</sup> The fact that Kingianin A is found as a racemic mixture again suggests that no enzymes take part in the  $8\pi/6\pi$  cascade.

The first synthetic approach was published by Moses, who tested the biosynthetic proposal suggested by Litaudon and co-workers, featuring an *endo*-Diels–Alder dimerization after the  $8\pi/6\pi$  electrocyclization.<sup>[67,68]</sup> This hypothesis was rather controversial, since a spontaneous intermolecular Diels–Alder reaction of unactivated dienes seemed unlikely without the assistance of enzymes.

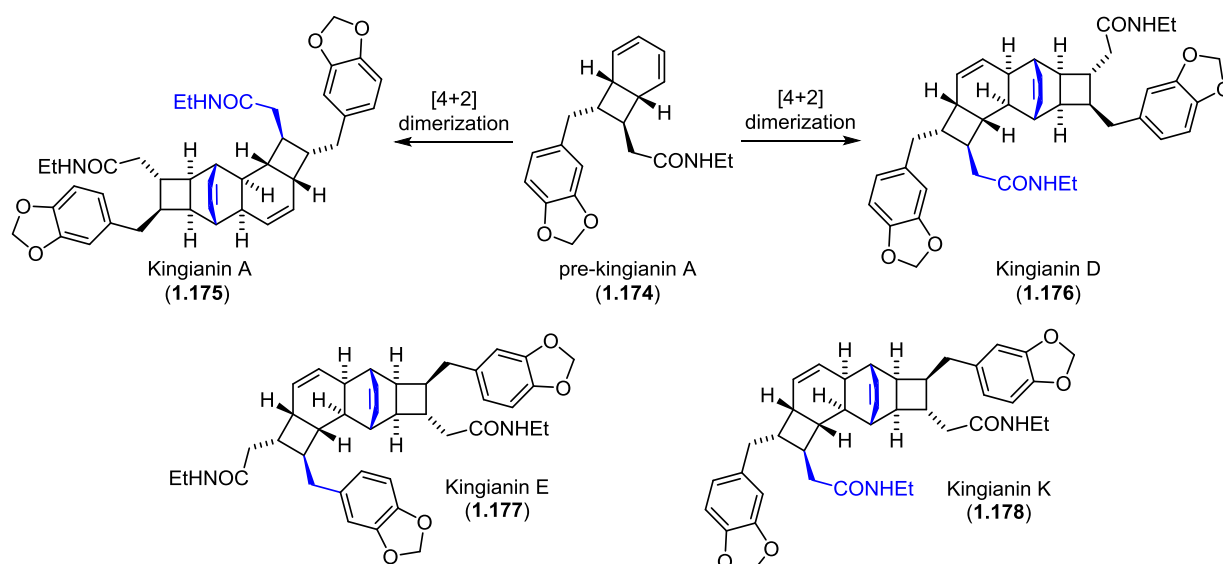
Thus, Moses synthesized prekingianins **1.168** and **1.169** starting from catechol acetal **1.165**, which was transformed into vinyl bromide **1.166** in four steps. The stannane partner for the Stille coupling was prepared by DIBAL reduction of ester **1.166** followed by treatment with acetone cyanohydrin, delivering vinyl stannane **1.167**. Stille coupling of **1.167** and **1.166** yielded the expected bicyclooctanes **1.168** and **1.169**, which were partially hydrolyzed to the respective amides and *N*-alkylated by reductive amidation affording **1.170** and **1.171**. All attempts to thermally induce the Diels–Alder dimerization of **1.170** and **1.171** failed, even at 195 °C or using Grieco's conditions in a 5M LiClO<sub>4</sub> ethereal solution.



**Scheme 1.25.** Moses' studies towards the synthesis of kingianin A.

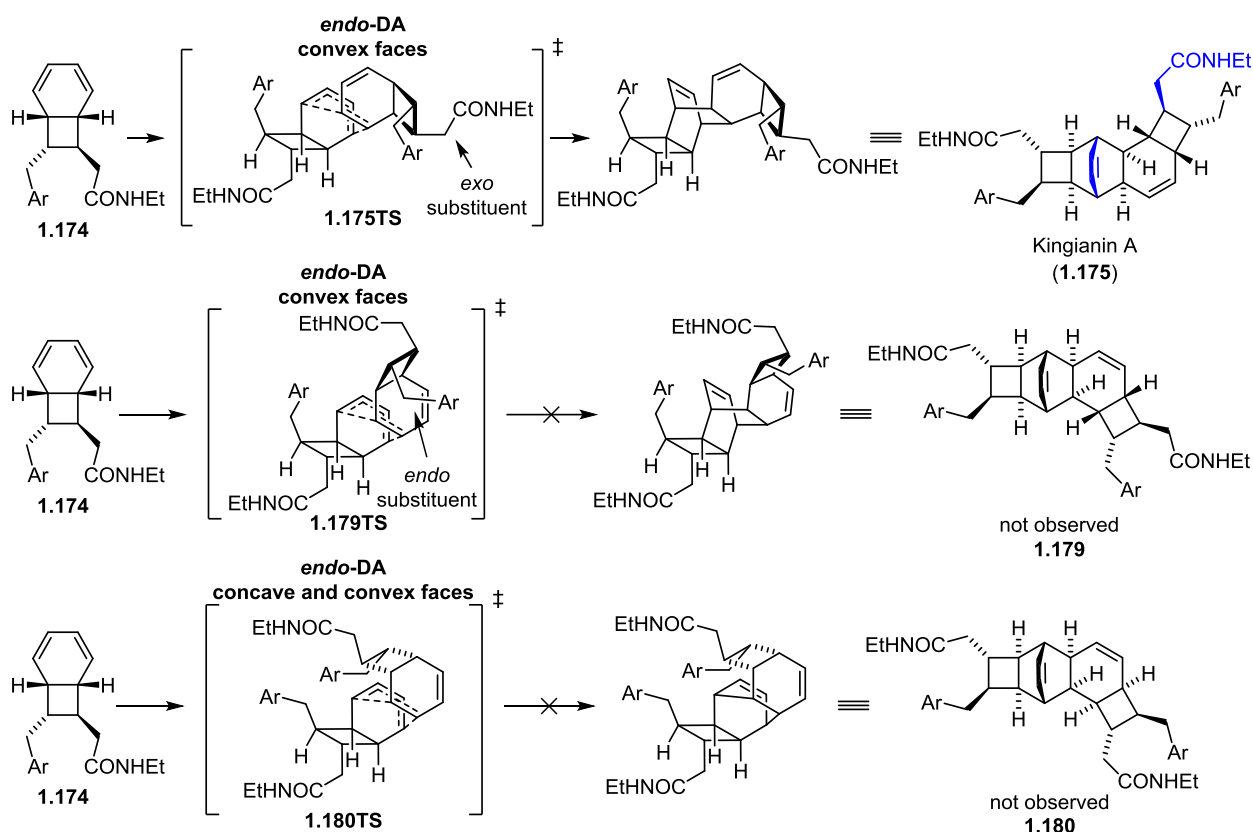
In parallel to this work, new kingianins were isolated<sup>[69]</sup> and tested for inhibition of Bcl-xL, an anti-apoptotic protein implicated in tumour growth, showing modest binding affinity (Scheme 1.26). All the kingianins isolated from *Endiandra kingiana* (A-N) share common patterns, since they derive from an *endo*-Diels–Alder reaction taking place on the less hindered convex face of both diene and dienophile ("open book effect") (**1.175TS**, Scheme 1.27). This arrangement leads to a transition state stabilized through secondary orbital interactions and avoids steric clashes between the cyclobutane ring of the dienophile and the hexadiene ring of the diene (Scheme 1.27).





**Scheme 1.26.** Structure of kingianins A, D, E and K. Kingianin A is the homodimer of one enantiomer of pre-kingianin A. Kingianin D is the heterodimer of both enantiomers of pre-kingianin A.

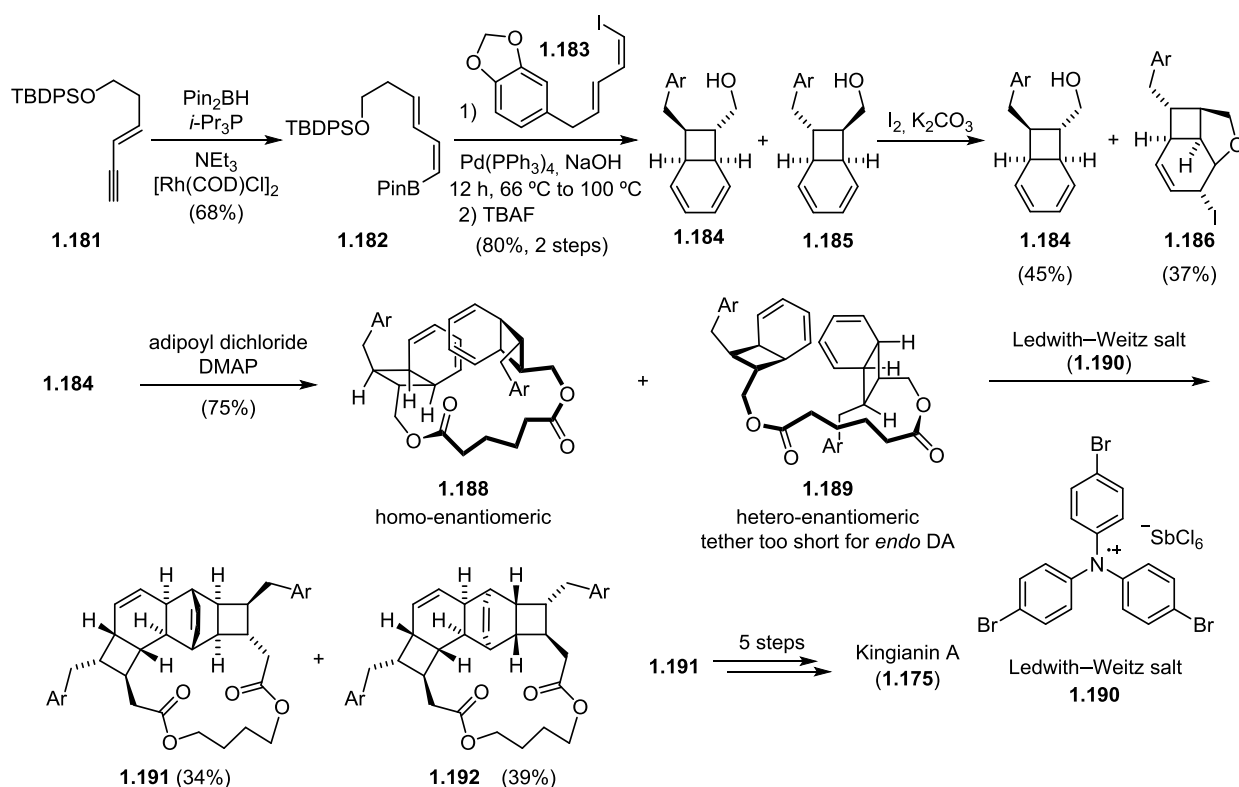
Moreover, of the two possible arrangements fulfilling the previous conditions, only the olefin closest to the *exo*-substituent engages as a dienophile in the [4+2] cycloaddition.



**Scheme 1.27.** Three possible regioisomers for the *endo*-[4+2] cycloaddition. **Top.** Favoured arrangement leading to kingianin A: reaction from both convex faces of diene and dienophile; dienophile olefin proximal to the *exo*-substituent. **Middle.** Unfavoured arrangement: dienophile olefin proximal to the *endo*-substituent. **Bottom.** Unfavoured arrangement: approach from the concave face of the dienophile, clash between the cyclobutane ring and the diene.

Therefore, the cyclohexene bridge formed upon the [4+2] cycloaddition is always located on the same face as the closest substituent on the cyclobutane ring of the former dienophile (marked in blue on Schemes 1.26 and 1.27).

Parker deduced that if the thermal Diels–Alder was not taking place and was not the result of enzymatic participation, the dimerization could occur *via* a radical cation Diels–Alder reaction (RCDA), maybe photoinduced in nature. Putting all this into context, kingianin A (homoenantiomeric, **1.175**) and kingianin D (heteroenantiomeric, **1.176**) would be obtained from racemic pre-kingianin A (**1.174**) by means of a RCDA reaction, whose stereochemistry would be defined by an *endo* transition state stabilized by secondary orbital interactions. The regiochemistry would in turn be dictated by the “open book effect” (i.e. reaction on both convex faces of diene and dienophile) and by the substituents at the cyclobutane ring of the dienophile. Given the difficulties experienced by Litaudon in separating kingianins A and D during the isolation process,<sup>[69]</sup> Parker opted to perform an intramolecular RCDA approach binding two molecules of **1.174** by a tether, reasoning that only the homoenantiomeric C2 symmetric dimer could adopt the conformation required for the *endo* transition state (**1.188**, Scheme 1.28). The disposition of the ester substituents in the heteroenantiomeric dimer would keep the diene and dienophile too far from each other to engage in the same reaction. Thus, this dimer was expected to remain unreacted and would be easily separated from the Diels–Alder product and recycled (**1.189**, Scheme 1.28).



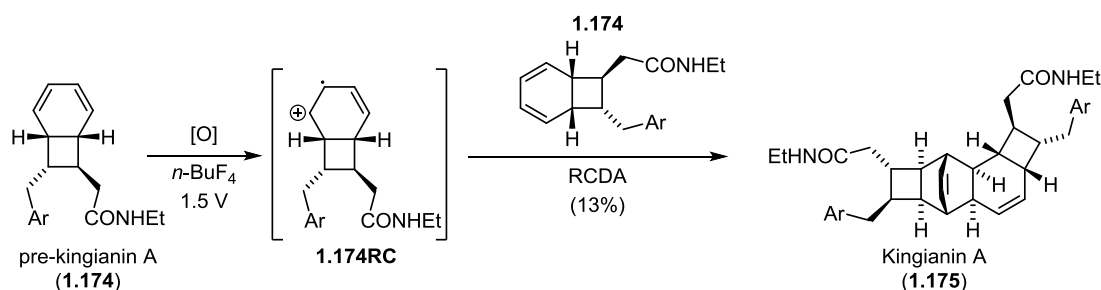
**Scheme 1.28.** Total synthesis of kingianin A by Parker.

Parker's synthesis began with *trans* hydroboration of enyne **1.181** under rhodium catalysis yielding *Z*-vinyl boronate **1.182** (Scheme 1.28). Suzuki coupling of **1.182** with vinyl iodide **1.183** followed by heating at 100 °C for several hours and TBAF deprotection delivered two diastereomeric analogues of pre-kingianin A, **1.184** and **1.185**, which were separated using Nicolaou's iodoetherification (Scheme 1.8).<sup>[40]</sup> The high yield of the Suzuki coupling is notable, and avoided the use of highly toxic organotin. Upon separation of the

reacted tricycle **1.186**, **1.184** was treated with adipoyl dichloride and DMAP yielding the expected 1:1 mixture of dimeric esters **1.188** and **1.189**.

As it was expected, only the homoenantiomeric dimer underwent the *endo*-Diels–Alder reaction upon treatment with Weitz' aminium salt (**1.190**). However, the heteroenantiomeric substrate **1.189** underwent an *exo*-Diels–Alder reaction, affording **1.192** in a slightly higher yield than the desired product **1.191**. Presumably, the presence of the tether induced a prearrangement favourable for this type of Diels–Alder. Upon isolation by column chromatography, the desired product **1.191** was converted into Kingianin A in 5 steps. In subsequent work, Kingianin A was prepared by the same means and in similar yields without the use of a tether, together with other members of the kingianin family.<sup>[70]</sup>

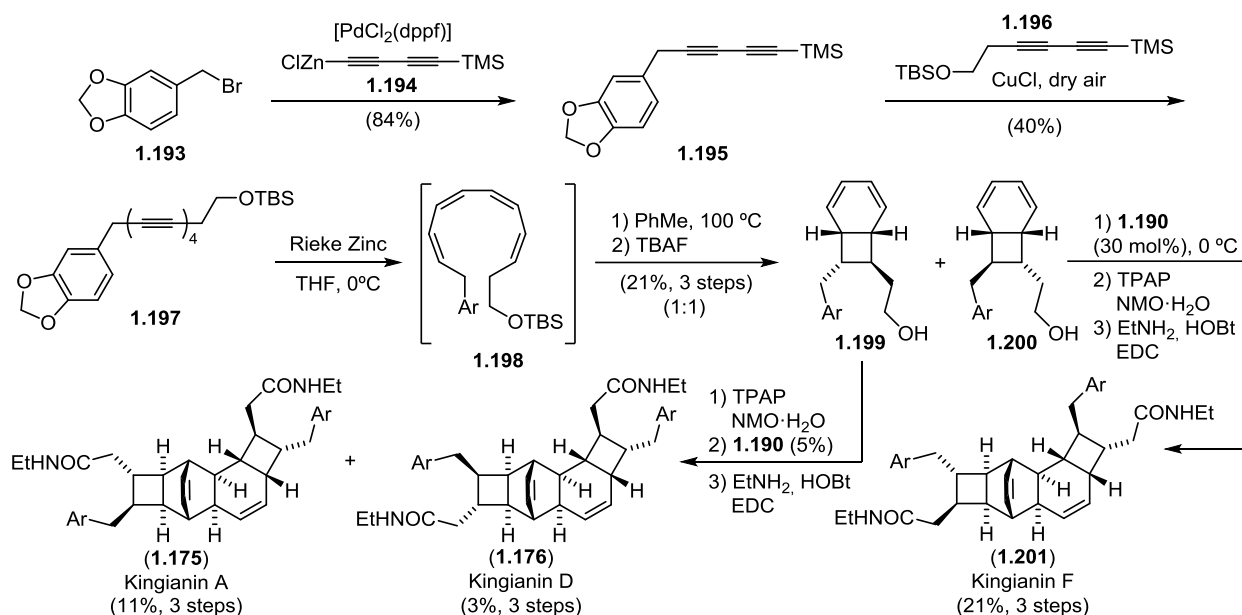
Moses, inspired by Nigenda et al., who performed an exhaustive study on the radical cation Diels–Alder reaction of cyclohexadiene,<sup>[71]</sup> later published on how the [4+2] cycloaddition could be performed by means of an electrochemically induced RCDA on pre-kingianin A. The reaction was triggered by electron transfer using a reticulated vitreous carbon electrode in a 0.4 M solution of *n*-Bu<sub>4</sub>NBF<sub>4</sub>.<sup>[72]</sup> The yield was however rather low (Scheme 1.29).



**Scheme 1.29.** Formal synthesis of kingianin A by Moses.

Michael S. Sherburn presented in a series of two articles the total synthesis of kingianin A by using a combination of the strategies developed by Nicolaou, featuring the semi-hydrogenation of polyynes, and Parker's intermolecular RCDA for the dimerization of pre-kingianins.<sup>[73,74]</sup> The synthesis featured an unprecedented semi-reduction of a tetrayne to an all-*Z* tetraene.

The starting point for the synthesis was a Negishi coupling between benzyl bromide **1.193** and alkynylzinc **1.194** affording TMS benzyl diyne **1.195**, which was then converted into tetrayne **1.197** by the first reported unsymmetric Mori–Hiyama coupling<sup>[75]</sup> (Scheme 1.30). In previous syntheses,<sup>[40,76]</sup> Lindlar reduction was ineffective due to the low reactivity of the catalyst, so after an extensive screening campaign, Rieke zinc in ethanol proved to be the best choice for semi-reduction of tetrayne **1.197**. The obtained tetraene **1.198** was immediately submitted to cyclization conditions (PhMe, 100 °C) followed by TBAF deprotection, delivering bicyclo[4.2.0]octadienes **1.199** and **1.200**. These were separated and submitted to a sequence of oxidation to carboxylic acid under Stark's conditions,<sup>[77]</sup> radical cation Diels–Alder reaction induced by Ledwith–Weitz's salt (**1.190**) and amidation to give Kingianins A, D and F.



**Scheme 1.30.** Total synthesis of kingianins A, D and F by Sherburn.

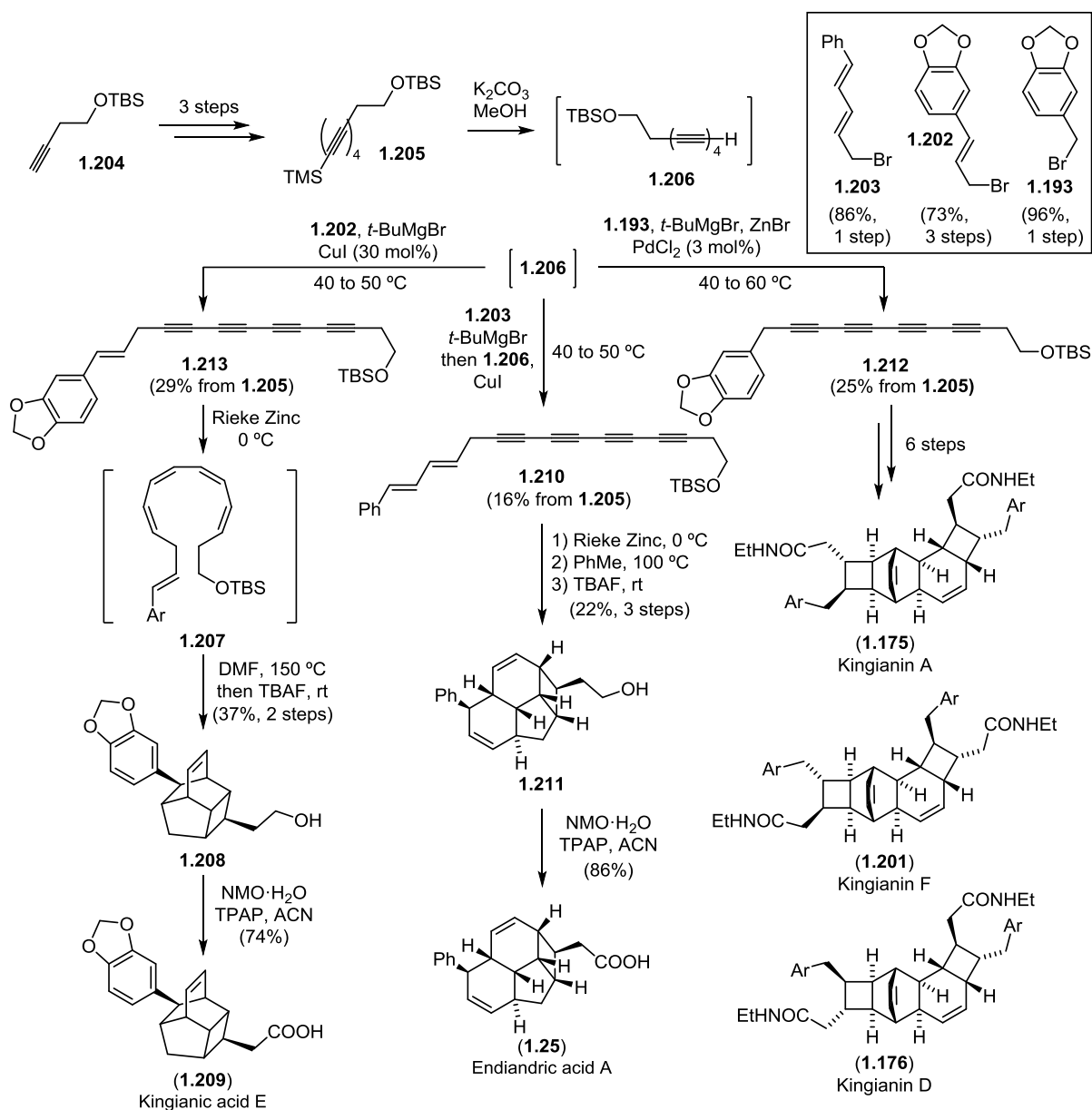
## 1.2.7 Unified Synthesis of Kingianins and Endiandric Acids

Finally, Sherburn developed a unified synthesis of endiandric acid A, kingianic acid E and kingianins A, D and F, achieving the highest step efficiency to date for these natural products.<sup>[74]</sup> The synthesis relied on the preparation of the versatile tetrayne intermediate **1.206**, which diverges into three different routes upon coupling with three different alkyl bromides (Scheme 1.31).

The preparation of the key building block **1.206** started with homopropargylic alcohol **1.204**, which was transformed into tetrayne **1.205** in 3 steps and deprotected by treatment with potassium carbonate in methanol to yield **1.206**, which was immediately submitted to three different reaction sequences.

For kingianic acid E, metalation of **1.206** with *tert*-butylmagnesium bromide was followed by alkylation with vinyl bromide **1.202** under copper catalysis. The resulting tetrayne **1.213** was submitted to reduction on Rieke zinc at 0 °C and subsequent thermal treatment at 150 °C, which triggered the  $8\pi/6\pi$ /Diels–Alder cascade yielding alcohol **1.208**. This alcohol was oxidized with TPAP/NMO·H<sub>2</sub>O under Stark's conditions<sup>[77]</sup> to yield racemic kingianic acid E.

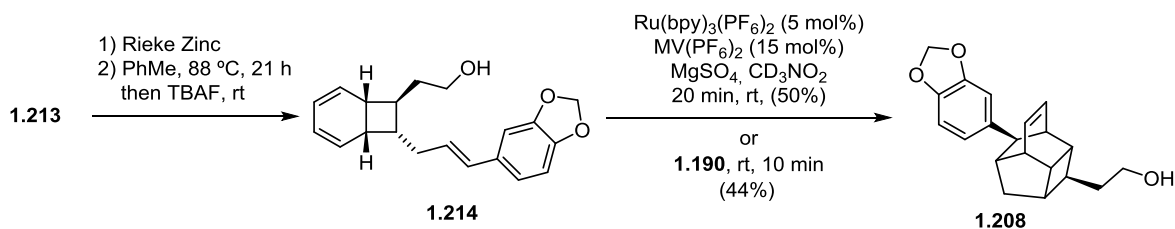
Endiandric acid A was synthesized in a similar manner as **1.209** by copper catalysed alkylation of **1.206** with allyl bromide **1.203**, semi-reduction on Rieke Zinc and  $8\pi/6\pi$ /Diels–Alder cascade sequence, delivering tetracycle **1.211**. Exhaustive oxidation of the primary alcohol of **1.211** afforded endiandric acid A in 9 total steps from commercial precursors.



**Scheme 1.31.** Unified total synthesis of endiandric acids and kingianins by Sherburn.

Tetrayne **1.206** failed to provide propargyl catechol **1.212** upon reaction with benzyl bromide **1.193** under the previous copper catalysed conditions. Therefore, **1.212** was accessed through Negishi cross-coupling and was further elaborated in 6 steps following the sequence shown in Scheme 1.30.

With this, Sherburn presented an elegant and step-economic synthesis of kingianins A, D and F, kingianic acid E and endiandric acid A with an approach that combines Nicolaou's alkyne reduction strategy,<sup>[40–43]</sup> extending it to more advanced tetrayne intermediates, and the intermolecular radical cation Diels–Alder reaction developed by Parker.<sup>[70]</sup> The low yields of the electrocyclization cascades are the major drawback of this otherwise brilliant work.



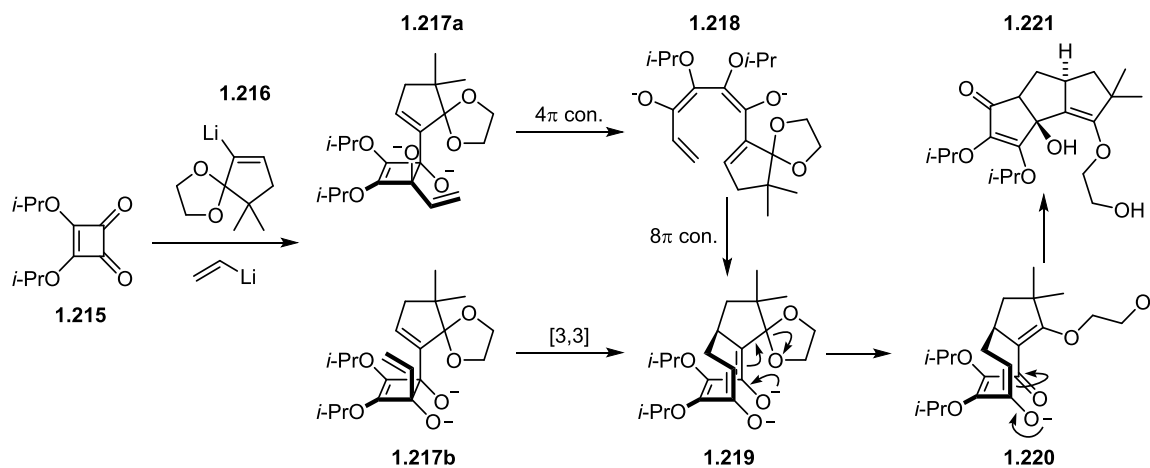
**Scheme 1.32.** Use of photoredox catalysis in the RCDA of **1.214** compared to the Ledwith–Weiz salt procedure.

Lastly, a new method for the generation of the radical cation intermediate was applied to bicyclo[4.2.0]octadiene **1.214**. Photoredox catalysis under Yoon’s conditions<sup>[78]</sup> yielded tetracycle **1.208** in slightly higher yields than Parker’s, who generated the radical cation with Ledwith-Weitz salt.<sup>[70]</sup>

## 1.2.8 Hypnophilin, Coriolin and Ceratopicanol

Although they cannot be considered members of the Cyclooctatriene-Derived NP family given their sesquiterpene nature, the total synthesis of these natural products presented by Paquette features a rare  $8\pi$  electrocyclization/transannular aldol cascade.

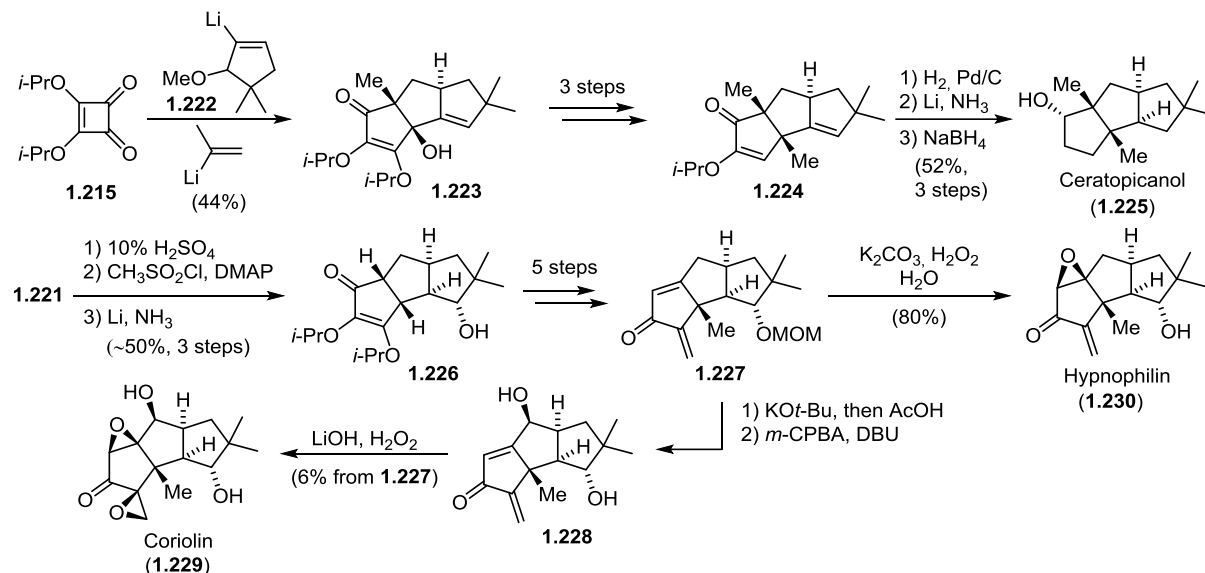
In 2002, Paquette et al. exploited the applications of his previously developed squarate ester cascade<sup>[79–81]</sup> for the step-economic total synthesis of hypnophilin, coriolin and ceratopicanol.<sup>[82,83]</sup> These compounds possess antibiotic and antitumor activity.<sup>[84–86]</sup>



**Scheme 1.33.** Squarate ester cascade developed by Paquette giving access to triquinane **1.221**.

The substrate for the cascade is obtained through selective 1,2-addition of a pair of alkenyl anions to squarate ester **1.215** resulting in *syn* or *anti* addition. The resulting *anti* cyclobutene undergoes a  $4\pi$  conrotatory ring opening followed by an  $8\pi$  electrocyclization leading to cyclooctatriene **1.219**. In the case of the *syn* product, the retro  $4\pi$  electrocyclization is outcompeted by a faster oxy-Cope rearrangement, which directly delivers the same cyclooctatriene **1.219**. Elimination of the  $\beta$ -acetal leads to intermediate **1.220**, which upon ring closing aldol reaction yields linear triquinane **1.221**.

This cascade was used for the synthesis of hypnophilin, coriolin and ceratopicanol (Scheme 1.34). For ceratopicanol, isolated from the fungus *Ceratocystis piceae*,<sup>[87]</sup> squarate ester **1.215** was treated with alkenyllithium **1.222** followed by isopropenyllithium, yielding triquinane **1.223** in 44% yield. Further elaboration of **1.223** afforded  $\alpha$ - $\beta$  unsaturated ketone **1.224** in 3 steps. Exhaustive reduction of **1.224** in 3 further steps delivered ceratopicanol (**1.225**).



**Scheme 1.34.** Total synthesis of racemic ceratopicanol, hypnophilin and coriolin by Paquette.

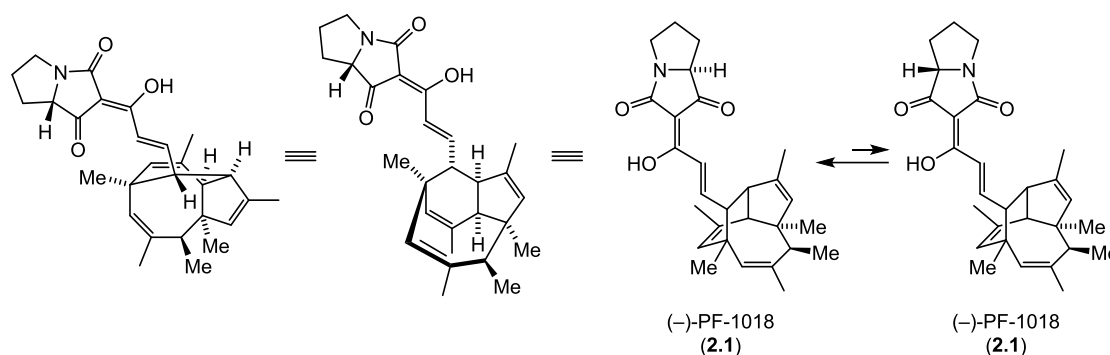
The cascade reaction shown in Scheme 1.33 delivered triquinane **1.221**, bearing an enol-ether handle. Hydrolysis of this ether with diluted aqueous sulfuric acid followed by chlorination of the tertiary hydroxylic carbon and Birch reductive cleavage of the resulting chloride led to alcohol **1.226** in good yield (Scheme 1.34). Further elaboration of **1.226** into **1.227** was accomplished in 5 steps after which one-pot epoxidation and MOM deprotection with basic hydrogen peroxide afforded hypnophilin (**1.230**). Intermediate **1.227** was also used for the synthesis of coriolin by means of a  $\text{KO}^t\text{-Bu}$ -induced double bond migration followed by monoepoxidation,  $\beta$ -elimination and bisepoxidation.

Starting from simple building blocks, this stereoselective cascade, featuring a non-isolable cyclooctatriene intermediate, delivered a tricyclic system bearing 4 stereocentres, which gave access to three different racemic natural products in few synthetic steps: 7 for ceratopicanol (vs 7 for Prof. Michel Chanon<sup>[88]</sup>), 10 for hypnophilin, shortening the previous shortest 14-step racemic synthesis by Curran<sup>[89]</sup> and 13 for coriolin, again shortening previous syntheses of 16-21 steps.<sup>[89–92]</sup>

## 2. Project Background

### 2.1 Isolation and Structure of (–)-PF-1018

In 1993, Koyama and co-workers, from the Meiji Seika Kaisha Pharmaceutical Research Center in Japan, performed a screening program in the search for novel insecticides of microbial origin. In this context, a fungal strain found in a soil sample from Ohmachi city, identified as *Humicola* sp. PF1018, produced a new polyketide which they called (–)-PF-1018 (**2.1**).<sup>[93]</sup>



**Scheme 2.1.** Different projections of (–)-PF-1018.

The structure of (–)-PF-1018 features two distinguishable parts. First, a tricyclic 8-6-5 ring system bearing six contiguous stereocentres, two of which are quaternary, and three trisubstituted double bonds containing methyl groups. This congested core is connected by an ethylene linker to a proline-derived tetramic acid bearing an additional stereocentre (Scheme 2.1).

<sup>1</sup>H and <sup>13</sup>C CDCl<sub>3</sub> NMR spectra of **2.1** showed a main set of signals accompanied by minor peaks, which upon the addition of water, coalesced into a single set of broad peaks. It was therefore concluded that PF-1018 existed as two interconverting isomeric forms, as it is known for other acyl tetramic acids.<sup>[94,95]</sup> 2D NMR studies provided the structure of **2.1**, which was later verified by X-ray analysis (Figure 2.1). The absolute configuration was confirmed by degradation with sodium hypochlorite followed by HCl, which afforded L-proline.

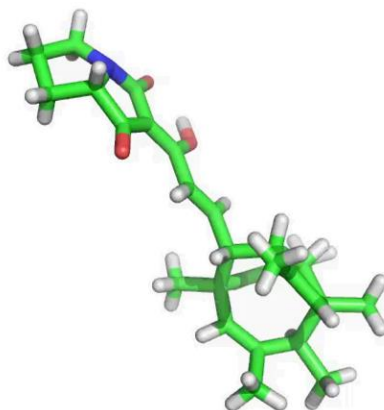
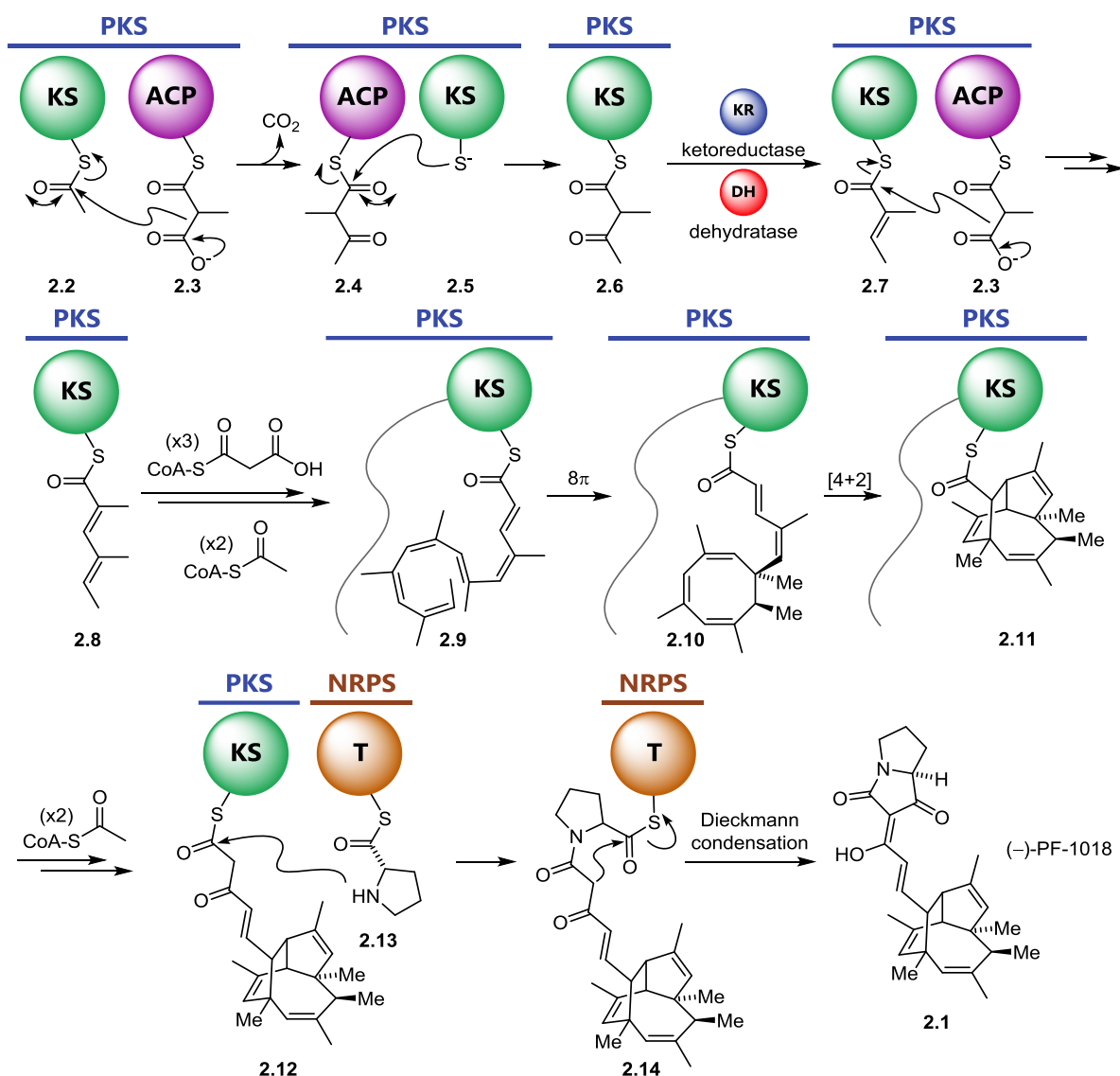


**Figure 2.1.** Crystal structure of (–)-PF-1018



## 2.2 Proposed Biosynthesis of (–)-PF-1018

As a polyketide, **2.1** originates from the assembly line within the polyketide synthase (PKS).<sup>[96,97]</sup> However, given the presence of a non-ribosomally-derived tetramic acid moiety, it is most likely that a hybrid of a PKS and a non-ribosomal peptide synthase (NRPS) is responsible for the biosynthesis of (–)-PF-1018.<sup>[98–102]</sup>



**Scheme 2.2.** Proposed biosynthesis of (–)-PF-1018.

Thus, the biosynthesis would start with a keto synthase domain (KS)-bound acetyl-CoA (**2.2**) which undergoes a Claisen condensation with a proximal methyl malonyl-CoA unit linked to the acetyl carrier protein (ACP) domain (**2.3**). Then KS-bound cysteinyl residue **2.5** binds covalently to the extended chain **2.4** forming complex **2.6**, which yields alkene **2.7** under the action of the ketoreductase (KR) and the dehydratase (DH) domains. Repetition of these Claisen condensation/decarboxylation/migration steps with a new methylmalonyl unit leads to diene **2.8**. The incorporation of three more units of methylmalonyl-CoA and 2 of acetyl CoA yields polyene **2.9**. We propose that the tricyclic core of **2.1** could be obtained from **2.9**

in a similar fashion as the natural products shown in Chapter 1.2, but with a key difference: After the  $8\pi$  electrocyclization, the resulting cyclooctatriene **2.10**, unlike for all the other cyclooctatriene-derived natural products, is intercepted by a dienophile engaging in a  $[4+2]$  cycloaddition instead of undergoing a  $6\pi$  electrocyclization. This reactivity leads to tricyclic intermediate **2.11**. We think that this sequence takes place early in the biosynthesis given the spontaneous nature of the  $8\pi/6\pi$  electrocyclization, but a latter cascade reaction cannot be ruled out.<sup>[103,104]</sup> To the best of our knowledge, this is an unprecedented reaction sequence, and consequently so is the structure of **2.1**. Given the fact that unlike the endiandric acids or the kingianins, PF-1018 has been isolated as a single enantiomer, it seems that the diastereo- and enantioselectivity of these steps could derive from the chiral environment within the enzyme.

After the pericyclic cascade, the chain is extended again with two units of acetyl-CoA leading to intermediate **2.12**. The transfer of proline takes place from the thiolation domain of the non-ribosomal peptide synthase (NRPS) **2.14** and the tetramic acid is formed upon Dieckmann condensation releasing **2.1** from the hybrid complex.

## 2.3 Biological Activity of (–)-PF-1018

As it has been mentioned in Chapter 2.1, PF-1018 was found in a screening campaign for new insecticides. **2.1** was tested against critical pests including *Thrips palmi* Kany, *Tetranychus cinnabarinus* Boisd., *Plutella xylostella* L. and *Musca domestica*.<sup>[105]</sup> Exposure of these insects to aqueous solutions of **2.1** at different concentrations led to high levels of mortality, especially for the diamondback moth (Table 2.1).<sup>[93,105]</sup> The mode of action has not been studied and is therefore unknown.

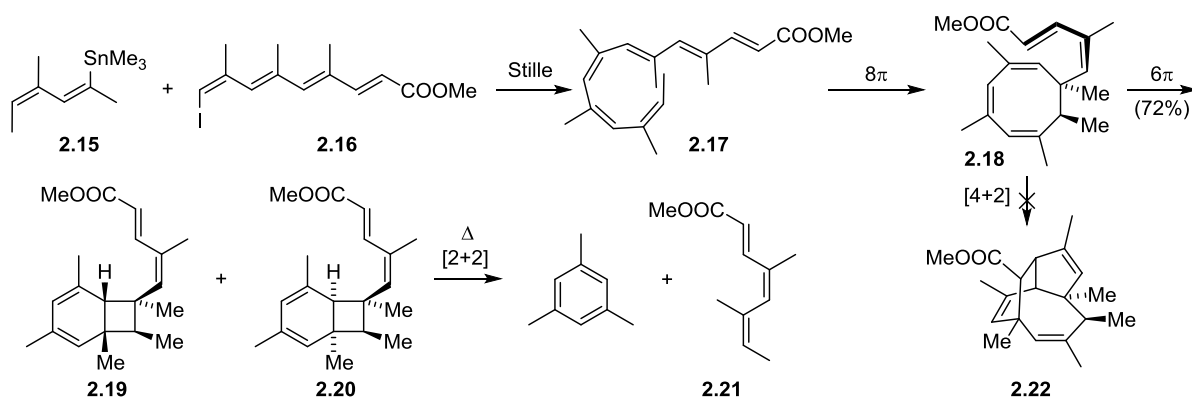
Species	Stage	Application	Concentration [ppm]	Mortality [%]
Plutella xylostella	Larvae	Larvae dipping	12.5	90
			25	100
Thrips palmi Kany	Larvae	Larvae leaf dipping	150	76
			300	96
Tetranychus cinnabarinus Boisd.	Adult	Foliar application	100	100

**Table 2.1.** Biological activity of **2.1** on critical pests. Test periods of 48 hours.

Of all the pests tested, the most problematic is *Plutella xylostella* or diamondback moth. This lepidoptera is a major destructive pest affecting the *Brassicaceus* vegetables (includes cabbage, brussels sprouts, cauliflower, broccoli, etc.) showing high adaptability to different environments, a fast reproductive cycle and high mutability, which results in quick development of insecticide resistance.<sup>[106–108]</sup> More specifically, the diamondback moth has developed resistance to virtually all insecticides, being the only species showing resistance against Bt toxin.<sup>[109]</sup> Moreover, *Plutella xylostella* has spread to the whole world affecting dramatically to the yields of *Brassicaceus* crops, lowering crop yields by nearly 70%.<sup>[108,110–112]</sup> Fighting this plague has an estimated cost of US\$ 5 billion per year,<sup>[113]</sup> therefore the development of new insecticides is essential to keep the damage under control.

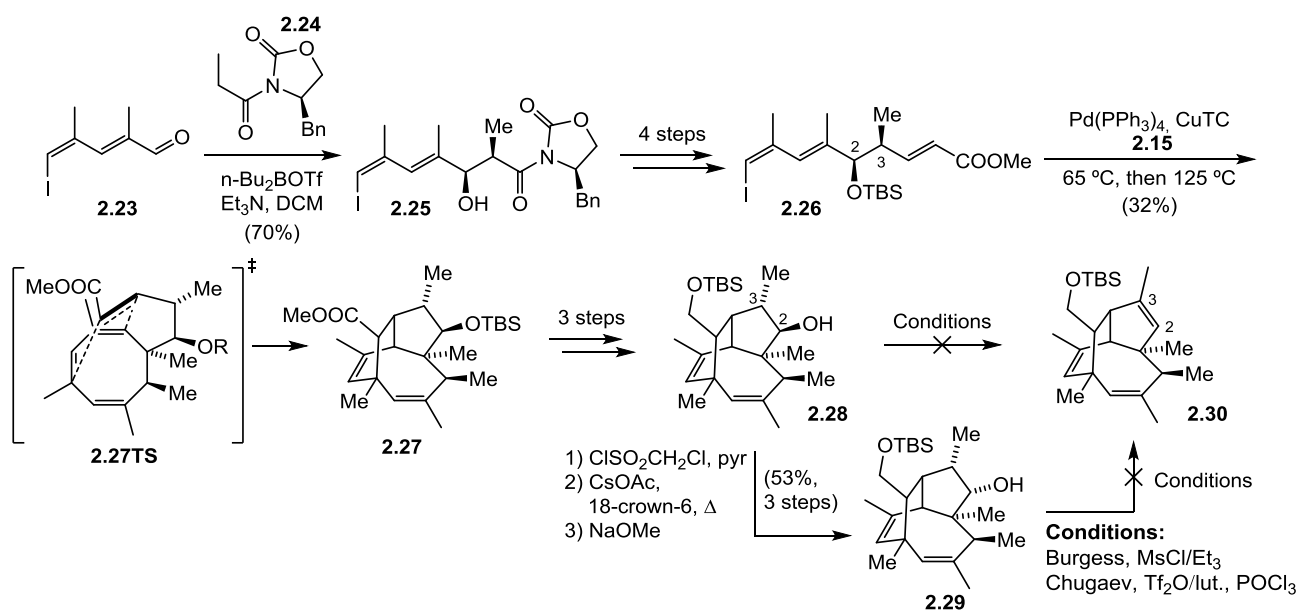
## 2.4 Previous Efforts Towards (–)-PF-1018

Initial studies at the Trauner group aimed for a straightforward synthesis of (–)-PF-1018 following the tandem Stille coupling/ $8\pi$  electrocyclization strategy analogous to the synthesis of ocellapyrones and elysiapyrones, which have been highlighted in Chapters 1.2.3 and 1.2.4. In this case, however, the desired reactivity involved intercepting the cyclooctatriene intermediate with an intramolecular dienophile inducing a Diels–Alder reaction. For this purpose, stannane **2.15** and vinyl iodide **2.16** were prepared (Scheme 2.3). Not surprisingly, the  $8\pi/6\pi$  electrocyclization reaction took place instead. Trying to reverse the  $6\pi$  electrocyclization by heating over  $150\text{ }^{\circ}\text{C}$  led to thermal retro-[2+2] cycloaddition, releasing triene **2.21** and mesitylene in a new case of “polyene splicing”, which was previously observed in the orinocin cascade (Scheme 1.18).



**Scheme 2.3.** Initial studies in the Trauner group towards (–)-PF-1018.

A new asymmetric approach started with aldehyde **2.23** (Scheme 2.4). Two stereogenic centres were introduced by means of an Evans aldol reaction in a “bioinspired” dehydration strategy in order to control the stereoelectronics of the polyene system.



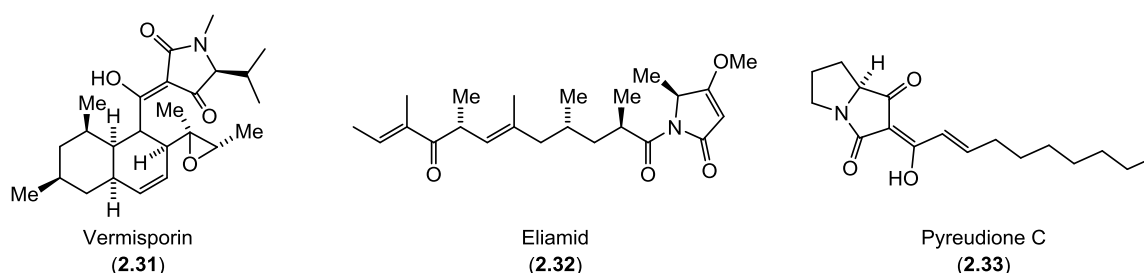
**Scheme 2.4.** Previous efforts towards (–)-PF-1018.

The resulting alcohol **2.25** was transformed in 4 steps into vinyl iodide **2.26**, which would serve as the reaction partner for the Stille coupling. The reaction cascade with stannane **2.15** gave **2.27** as the only isolable product in 32% yield.<sup>[114]</sup> Interestingly, the same reaction with the unprotected alcohol did not deliver the desired product, suggesting that the OTBS and the  $\beta$ -methyl group impart a torsional strain which avoids the  $6\pi$  electrocyclization (see Figure 1.1 for the  $6\pi$  transition state structure).

Further elaboration of cascade product **2.27** yielded alcohol **2.28** in 3 steps. A set of elimination conditions including Burgess and Chugaev was tried on **2.28**, but failed to afford the desired product **2.30** either by lack of reactivity or decomposition. Hoping that an *anti*-elimination would solve this problem, the configuration of the free alcohol was inverted by the formation of a chloromethyl sulfonate derivative followed by treatment with CsOAc, affording an acetate with net inversion of configuration. Methanolysis upon treatment with sodium methoxide in methanol yielded alcohol **2.29**. Unfortunately, all attempts for elimination failed again, frustrating this approach towards PF-1018.

## 2.5 Project Outline

The structure of (–)-PF-1018 is not only aesthetically attractive given the complexity of its tricyclic core, but also entails a challenge for synthetic chemists, since the ubiquitous  $8\pi/6\pi$  cascade must be intercepted at the cyclooctatriene intermediate with an intramolecular dienophile. This is a unique case in the Cyclooctatriene-Derived natural product family described in Chapter 1, and the synthesis of **2.1** will add new significant insights on how these secondary metabolites arise from cyclooctatrienes and what is the reason behind the fact that some are isolated as racemates or as single enantiomers.

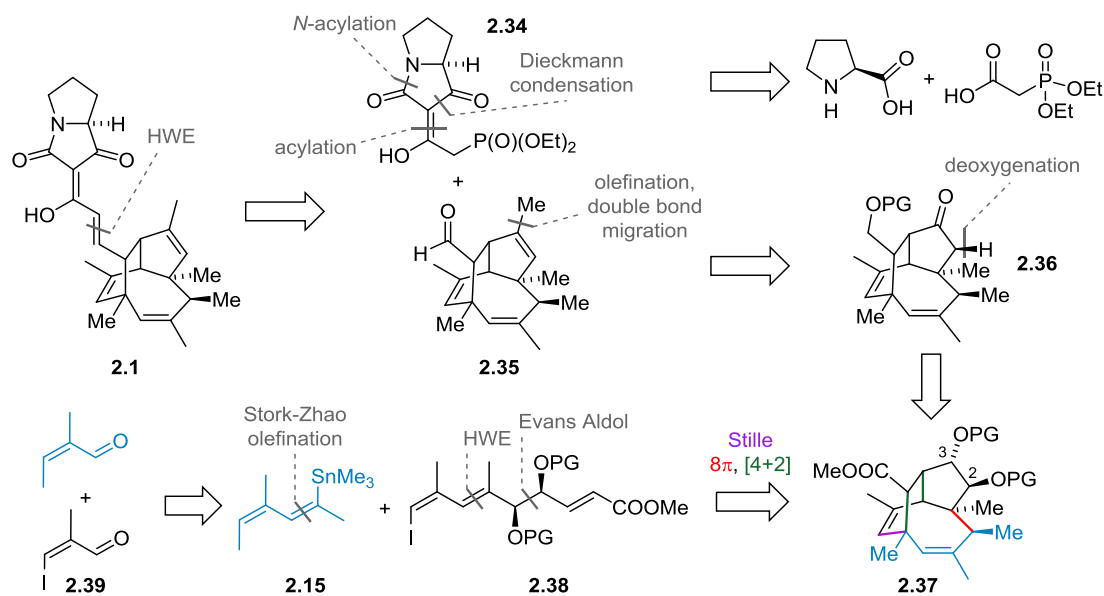


**Scheme 2.5.** Examples of tetramic acid natural products with relevant bioactivity.

Regarding the applications of synthetic **2.1** given its bioactivity, maybe the heavy economic losses in agriculture caused by the diamondback moth could justify the use of complex synthetic molecules such as (–)-PF-1018. Moreover, other natural products bearing tetramic acids have proven to entail a very broad range of interesting biological activities such as antibiotic<sup>[115]</sup>, antifungal<sup>[116]</sup>, cytotoxic<sup>[117]</sup>, antimoebal<sup>[98]</sup> and antiviral.<sup>[118–120]</sup> For example, vermisporin, produced by the fungus *Ophiobolus vermisporis* exhibits activity against *Bacteroides* spp, *Clostridium perfringens* (90% inhibition at 0.25–2  $\mu\text{g/mL}$ ), and *Staphylococcus aureus* (90% inhibition at 0.15–0.5  $\mu\text{g/mL}$ )<sup>[121]</sup> pyreudione C shows antimoebal activity ( $\text{IC}_{50}$  1  $\mu\text{g/mL}$ )<sup>[98]</sup> and eliamid cytostatic activity against human lymphoma cell line U-937 ( $\text{IC}_{50}$  0.5  $\text{ng/mL}$ ).<sup>[122]</sup> Hence, it is likely that **2.1** would also display potent bioactivity against some of these targets, which could be identified by means of a screening process. The material for this screening could be obtained through the total synthesis of (–)-PF-1018.

In our initial retrosynthesis, we envisioned that **2.1** could be obtained *via* Horner–Wasworth–Emmons reaction between aldehyde **2.35** and phosphonate ester **2.34** (Scheme 2.6). **2.34** could be accessed from L-

proline and diethyl phosphonacetic acid. Tricycle **2.35** could in turn be obtained from ketone **2.36** by olefination and double bond migration. Consequently, ketone **2.36** could be derived from diol **2.37** upon deprotection, oxidation and deoxygenation at C2. Diol **2.37** would in turn arise from the previously described Stille/ $8\pi$ /[4+2] cascade of stannane **2.15** and vinyl iodide **2.38**. By exchanging the methyl group at C3 (compound **2.26**, Scheme 2.4) by a protected alcohol (compound **2.38**, Scheme 2.6) we expected to overcome the elimination problem described above. Triene **2.38** would be synthesized in an analogous manner as **2.26** via Evans aldol reaction of conjugated aldehyde **2.23** (Scheme 2.4), itself arising from vinyl iodide **2.39**. Stannane **2.15** could be accessed from angelic aldehyde by means of a Stork–Zhao olefination.



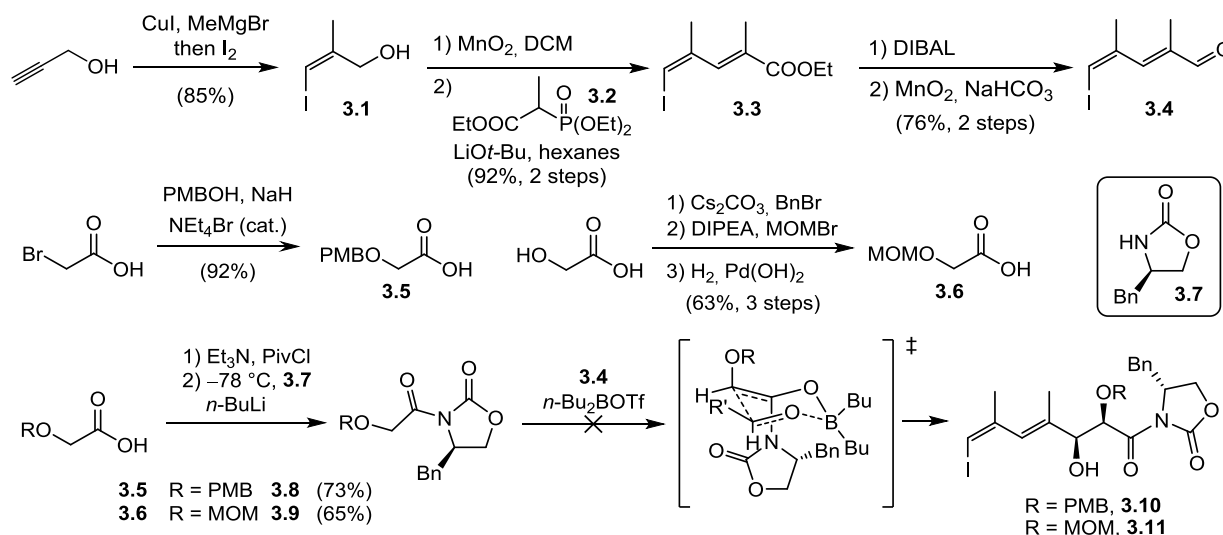
**Scheme 2.6.** Initial retrosynthetic analysis of (-)-PF-1018.

## 3. Results and Discussion

### 3.1 Evans Aldol Approach

This approach aimed for the asymmetric installation of the *syn*-diol *via* Evans aldol reaction of aldehyde **3.4** with oxazolidinones **3.8** and **3.9** (Scheme 3.1), chosen for their different bulk and stability towards deprotection. As it has been mentioned Chapter 2.4, it seemed that the substituent size at C2 and C3 strongly influence the outcome of the cascade reaction.

Thus, the preparation of aldehyde **3.4** started with propargyl alcohol, which underwent a carbocupration followed by iodine quench to deliver *Z*-vinyl iodide **3.1**.<sup>[123,124]</sup> Oxidation of the alcohol with manganese dioxide led to an unstable conjugated aldehyde which was immediately submitted to a Horner–Wadsworth–Emmons reaction with diethyl phosphonate **3.2**, leading to conjugated ester **3.3**. Aldehyde **3.4** was obtained by DIBAL reduction of **3.3** followed by allylic oxidation.



**Scheme 3.1.** Attempts for the preparation of *syn*-diols **3.10** and **3.11**.

Oxazolidinones **3.8** and **3.9** were synthesized by reaction of protected  $\alpha$ -hydroxy acids **3.5** and **3.6** with PivCl in the presence of a base and Evans auxiliary **3.7**. The Evans aldol reaction of aldehyde **3.4** and oxazolidinones **3.8** and **3.9** was initially performed using the same reaction conditions developed in previous work.<sup>[114]</sup> However, Evans glycolate aldol couplings with conjugated aldehydes are rare, and the reported yields are usually markedly lower than for non-conjugated or non-oxidized systems, occasionally displaying lower stereoselectivity.<sup>[125–128]</sup> Thus, these reaction conditions using dibutylboron triflate and triethylamine yielded only traces of **3.10** (Method A, Table 3.1, Entries 1, 2 and 7). The same reaction under Paterson's conditions (Method B, Entries 3–6 and 8) with different sources of dibutylboron triflate also failed to deliver the desired product.<sup>[129]</sup> We confirmed the validity of this method by testing it with the same substrate used by Paterson, noticing that freshly distilled dibutylboron triflate was required for the reaction to succeed (Table 3.2, Entry 3). An attempt lacking boron chelation also failed to provide the desired product (Table 3.1, Method C, Entry 9).<sup>[130,131]</sup>

$\text{R} = \text{PMB}, \mathbf{3.8}$   
 $\text{R} = \text{MOM}, \mathbf{3.9}$

$\text{R} = \text{PMB}, \mathbf{3.10}$   
 $\text{R} = \text{MOM}, \mathbf{3.11}$

Entry	R	Method	<i>n</i> -Bu <sub>2</sub> BOTf	[equiv.]	Result
1	PMB	A	1 M in DCM	1.15	complex mixture
2	PMB	A	1 M in DCM	1.15	trace
3	PMB	B	1 M in DCM	1.1	complex mixture
4	PMB	B	Neat	1.1	PMB deprotection
5	PMB	B	Freshly distilled	1.1	complex mixture
6	PMB	B	Freshly distilled	1.1	trace
7	MOM	A	1M in DCM	1.15	complex mixture
8	MOM	B	Freshly distilled	1.1	complex mixture
9	MOM	C	-	-	complex mixture

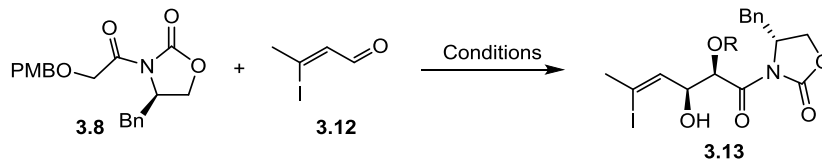
Experiments were run with 0.52 to 0.87 mmol of **3.8** or **3.9**

**A:** 1) **3.8/3.9**, DCM, 0 °C, *n*-Bu<sub>2</sub>BOTf, then Et<sub>3</sub>N (1.3 eq.). 2) -78 °C, **3.4** (1.2 eq.) in DCM, 3 h.

**B:** 1) **3.8/3.9**, PhMe, rt, Et<sub>3</sub>N (1.3 eq.), then -50 °C, *n*-Bu<sub>2</sub>BOTf 2) **3.4** (1.85 eq.) in PhMe, then -30 °C, 5 h.

**C:** 1) **3.8/3.9**, THF, -78 °C, LDA, (1.1 eq.) 15 min. 2) **3.4** (1.1 eq.), 1 h, then 0 °C, 1 h.

**Scheme 3.2 and Table 3.1.** Conditions screened for the Evans aldol reaction of aldehyde **3.4**.



Entry	<i>n</i> -Bu <sub>2</sub> BOTf	Result
1	1 M in DCM	complex mixture
2	Neat	trace
3	Freshly distilled	~55% yield

Experiments were run with 0.52 mmol of **3.8**

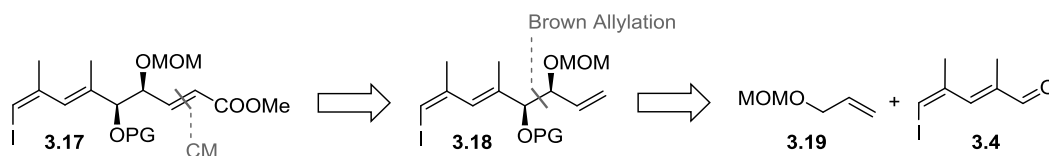
1) **3.8**, PhMe, rt, Et<sub>3</sub>N (1.3 eq.), then -50 °C, *n*-Bu<sub>2</sub>BOTf (1.1 eq.)

2) **3.12** (1.85 eq.) in PhMe, then -30 °C, 5 h.

**Scheme 3.3 and Table 3.2.** Reproduction of Paterson's Evans aldol reaction with different dibutylboron triflate sources.

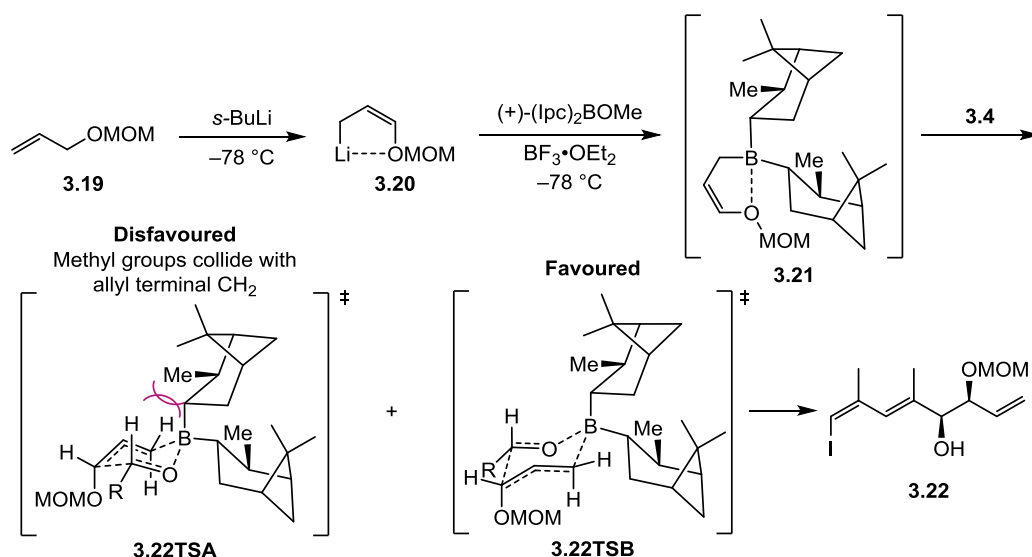
## 3.2 Brown Allylation Approach

Although many variations could still be applied to the Evans aldol reaction, we thought of a more straightforward approach towards 1,3-diol **3.17** which involved a cross-metathesis of triene **3.18** with methyl acrylate. In turn, **3.18** could be accessed from aldehyde **3.4** *via* Brown allylation with MOM protected allyl alcohol. This strategy would afford the desired triene **3.17** in three steps including alcohol protection, versus 4-5 steps for the Evans aldol route (Scheme 3.4).<sup>[132]</sup>



**Scheme 3.4.** New strategy towards **3.17** featuring a Brown allylation/cross-metathesis strategy.

In the Brown allylation, the allyllithium species **3.20** generated by treatment of allyl alcohol **3.19** with *sec*-butyllithium reacts with diisopinocampheylborane and boron trifluoride etherate to deliver allylboron intermediate **3.21**, whose *Z*-configuration is maintained at low temperature through boron-oxygen coordination (Scheme 3.5). This configuration will dictate the diastereoselectivity of the reaction upon addition of aldehyde **3.4**, yielding *syn*-diol **3.22** via transition state **3.22 TSB**. The isomer of  $\alpha$ -pinene employed is responsible for the enantioselectivity result of the steric repulsion between the methyl groups from pinene and the terminal allyl hydrogens (**3.22TSA**, Scheme 3.5).<sup>[132]</sup>



**Scheme 3.5.** Brown allylation mechanism.

Thus, the following conditions for Brown allylation were screened (Table 3.3).

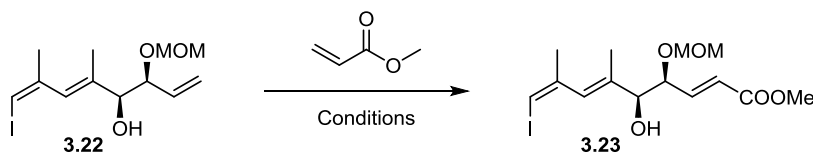


Entry	Equivalents				T [°C]	t [h]	Yield [%]	d.r.	e.e. [%]
	(+)-(lpc) <sub>2</sub> BOMe	allyl boronate ester	BF <sub>3</sub> ·OEt <sub>2</sub>	s-BuLi					
1	3.7	3.8	3.7	3.6	-70	3	55	6:1	-
2	3.1	3.1	2.9	2.9	-70	3	57	5:1	-
3	2.2	2.26	2.26	2.12	-78	4	53	>20:1	92
4	1.80	1.93	1.93	1.82	-78	3	60	>20:1	96

**Scheme 3.6 and Table 3.3.** Conditions screened for Brown allylation of **3.4**.

We first used the reaction conditions by Crimmins et al., who reported an excellent yield in the reaction of a conjugated aldehyde in the synthesis of Sorangicin A.<sup>[133]</sup> In our hands this method delivered the desired product in moderate yield (55%) and low diastereoselectivity (6:1 d.r.) for this kind of reaction (Table 3.3, Entry 1). Intrigued by the large excess of borane used by Crimmins, we decided to use less equivalents. This led to a slightly higher yield (57 %) but a decrease in stereoselectivity (5:1 d.r., Entry 2). Since the temperature is a key factor to control the stereoselectivity in the Brown allylation,<sup>[132,134]</sup> we decided to lower it to -78 °C while diminishing the equivalents of allyl borane (Entry 3). These changes led to a much higher diastereomeric rate (>20:1) and excellent enantioselectivity (92% e.e.). Finally, upon further modifications in concentration, reagent ratio and workup procedure, we obtained diol **3.22** in decent yield (60%) and excellent diastereo- and enantioselectivity (>20:1 d.r. and 94% e.e., Entry 4). The enantiomeric excess was calculated by Mosher ester analysis.<sup>[135]</sup>

Further chain elongation could be achieved by cross-metathesis of the terminal alkene of **3.22**. Both metathesis partners are considered type II olefins, therefore they are not expected to homodimerize at a significant rate.<sup>[136]</sup> Thus, the reaction was initially set with the second-generation Grubbs catalyst and an excess of methyl acrylate in refluxing toluene with phenol as a stabilizer,<sup>[137–139]</sup> and stirred for 45 minutes. The desired product **3.23** was obtained, although conversion was not complete (Table 3.4, Entries 1 and 2). We run again the reaction under the same conditions and then added more equivalents of catalyst and acrylate while extending the reaction time, but this did not lead to any relevant improvement (Entry 3). Thus, we exchanged the catalyst with the more stable second-generation Hoveyda-Grubbs and further extended the reaction time while decreasing the temperature. Unfortunately, these changes only led to lower starting material recovery or increased decomposition when the temperature was kept at 110 °C (Entries 4-5). Further improvement was observed when the reaction scale was increased from 100 to 700 mg and the temperature decreased to 80 °C (Entry 6). At this point it seemed clear that the catalyst turnover was low, and that the high temperatures were leading to decomposition. Therefore, addition of 10 mol% of the catalyst with a syringe pump over 19 hours to a refluxing toluene solution of **3.22** and methyl acrylate allowed for isolation of triene **3.23** in a 50% yield and no starting material recovery (Entry 7). When the addition was performed over 8 hours and at lower temperature (80 °C) the yields decreased again (Entry 8). Finally, given the inconvenience of injecting the material over so many hours, a solution of the catalyst was prepared, loaded into a syringe and connected to the system doing periodic injections of ~1% after each hour (Entries 9-17). The best reaction conditions involved the sequential addition of the catalyst solution over 12 hours to the reaction mixture at 50 °C, leading to a 66% yield (Entry 17).

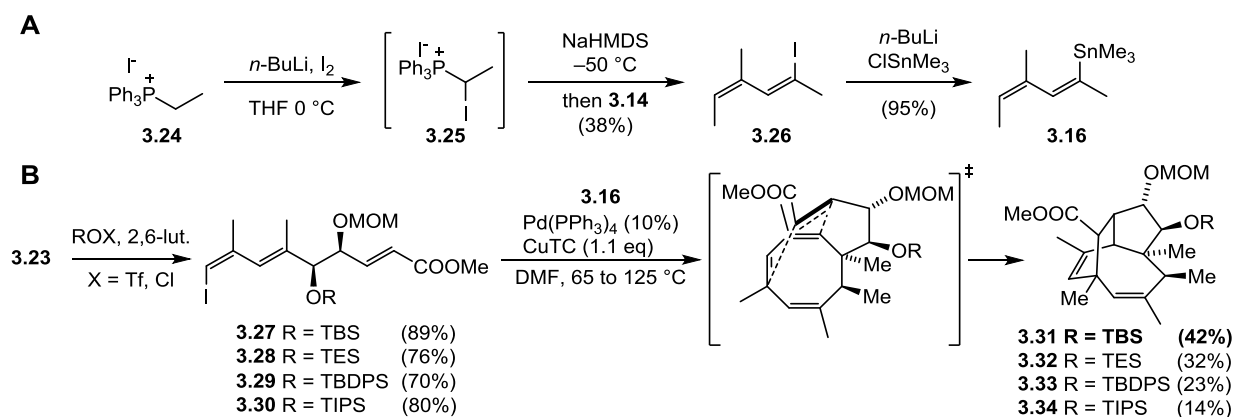


Entry	acrylate [eq.]	Catalyst	[mol%]	T [°C]	t [h]	Yield [%]	sm [%]	scale	Comment
1	5	G-II	2.5	110	0.75	29	58	100 mg	PhOH 0.5 eq
2	10	G-II	2.5	110	0.75	30	54	100 mg	PhOH 0.5 eq
3	10+5	G-II	2.5x2	110	1.5+18	36	59	60 mg	PhOH 0.5 eq
4	1.4x2	HG-II	2.5x2	110→85	10+48	36	22	60 mg	–
5	10	HG-II	2.5	110	10+48	16	8	60 mg	–
6	10	HG-II	2.5	80	4	37	61	700 mg	–
7	3	HG-II	10	110	19	50	trace	1.00 g	cat. over time
8	3	HG-II	10	75	9	33	28	2.00 g	cat. over time
9	3	HG-II	1.25x8	50	8+20	36	23	100 mg	cat. portions
10	3	HG-II	1.67x6	40	6+20	46	29	100 mg	cat. portions
11	3	HG-II	0.91x11	40	11+20	19	43	100 mg	cat. portions
12	3	HG-II	0.91x11	50	11+20	37	13	50 mg	cat. portions
13	3	HG-II	0.91x11	40	11+20	51	14	50 mg	cat. portions
14	3	HG-II	0.91x11	40	11+20	56	13	1.00 g	cat. portions
15	3	HG-II	0.91x11	50	11+20	54	14	1.00 g	cat. portions
16	3	HG-II	0.83x12	50	12+12	64	-	1.00 g	cat. portions
17	3	HG-II	0.83x12	50	12+18	66	-	1.00 g	cat. portions

**Scheme 3.7 and Table 3.4.** Reaction conditions screened for the cross-metathesis reaction.

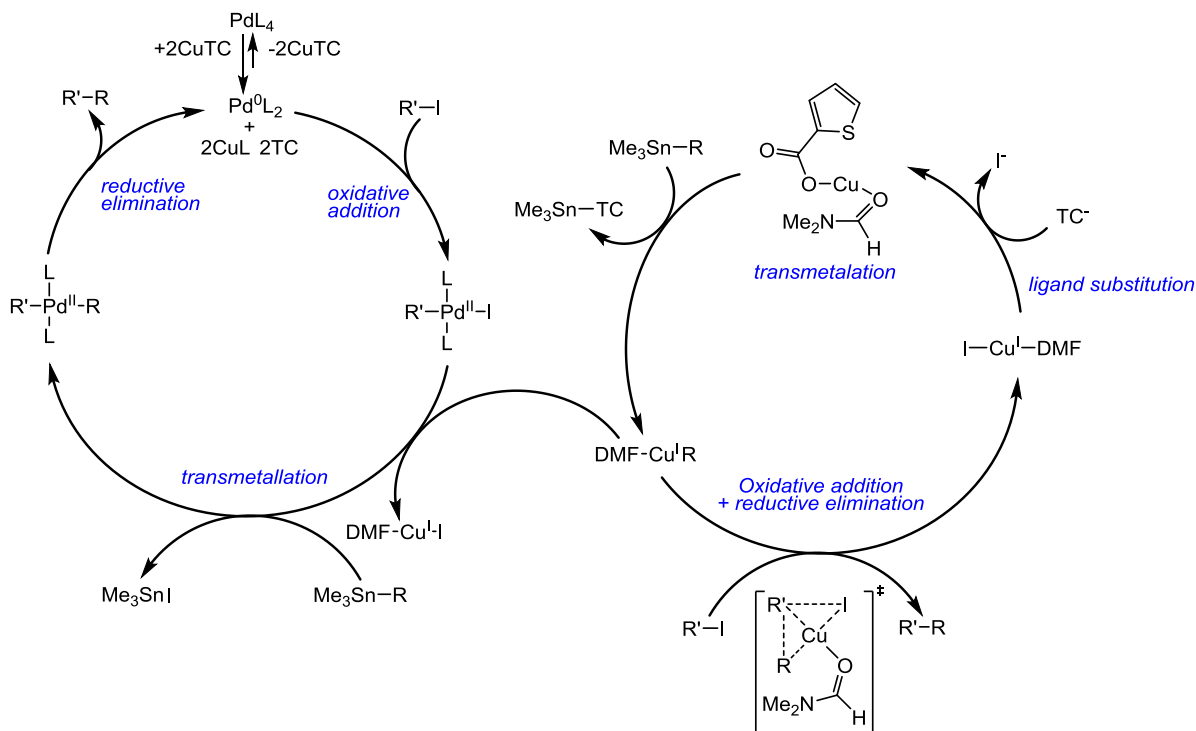
With vinyl iodide **3.23** in hand, the stannane partner was synthesized *via* Stork–Zhao olefination.<sup>[58,61]</sup> This one-pot procedure started with phosphonium salt **3.24** (Scheme 3.8, **A**), which was deprotonated with *n*-BuLi and trapped with iodine giving alkyl iodide **3.25**. This intermediate was subsequently deprotonated with a milder base and condensed with angelic aldehyde (**3.14**). The resulting vinyl iodide was then submitted to a lithium/halogen exchange with *n*-BuLi and transmetalated with trimethyltin chloride, affording the unstable stannane **3.16**.

As it has been mentioned in Chapters 2.4 and 3.1.1, the substitution pattern and stereochemistry of the hydroxy substituents in triene **3.23** proved to be essential for outcome of the cascade reaction, probably as a result of the existing steric strain between the OTBS and the  $\beta$ -methyl group, which disfavors the  $6\pi$  electrocycization. To further explore this effect, a series of silyl ethers was used to protect the free alcohol of triene **3.23** (Scheme 3.8, **B**).



**Scheme 3.8.** Synthesis of tricycles **3.31-3.34**.

Now the stage was set for the key step, a one-pot Liebeskind-type Stille coupling followed by an  $8\pi$  electrocyclozation and a Diels–Alder reaction.<sup>[140,141]</sup> The Liebeskind-type reaction takes advantage of the “copper effect”, which increases the reaction speed upon transmetalation from stannane **3.16** to copper and then to palladium. Copper also sequesters the free triphenylphosphine ligands which cause autoretardation and could also catalyse the cross-coupling by itself (Scheme 3.9).<sup>[53,142–144]</sup>



**Scheme 3.9.** Proposed mechanism for the Liebeskind-type Stille coupling.<sup>[143,144]</sup>

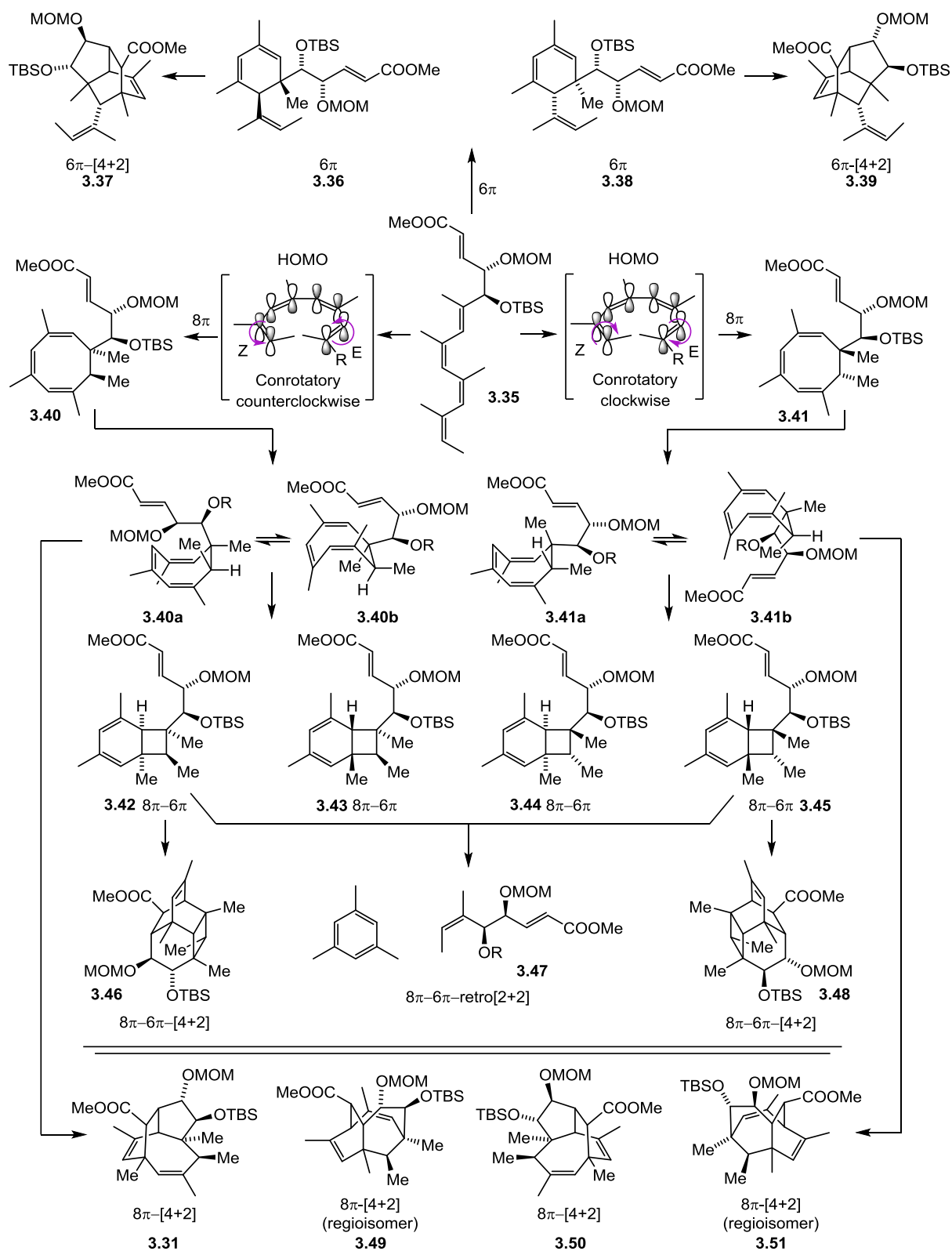
Thus, in parallel experiments performed in the dark to avoid undesired photochemical pathways (Scheme 1.5), stannane **3.16** and the different vinyl iodides **3.27-3.30** were heated in DMF together with  $\text{Pd}(\text{PPh}_3)_4$  and copper thiophene carboxylate. Under these conditions, the desired tricyclic product could be cleanly isolated for R = TBS (**3.31**) and TES (**3.32**) in 42 and 32% yield respectively (Scheme 3.8, B). The reactions with TIPS and TBDPS were more sluggish and **3.33** and **3.34** were obtained in lower purity and yield

(calculated by NMR). No other products could be isolated. Although computational studies later predicted that bulkier substituents at C2 would inhibit the  $6\pi$  electrocyclization while promoting the Diels–Alder reaction (Chapter 3.3), in our hands the introduction of TIPS and TBDPS silyl ethers led to decreased yields. These reactions were performed once, in parallel with the TBS and TES experiments and under optimized conditions. The fact that these were one-time reactions could explain the divergent results, but given our broad experience with this particular reaction, we think that other options should be considered: the introduction of these groups could have promoted unexplored reaction pathways, or, the presumably higher activation energies required for the  $8\pi$  electrocyclization in the presence of bulkier substituents may demand longer reaction times or higher temperatures.

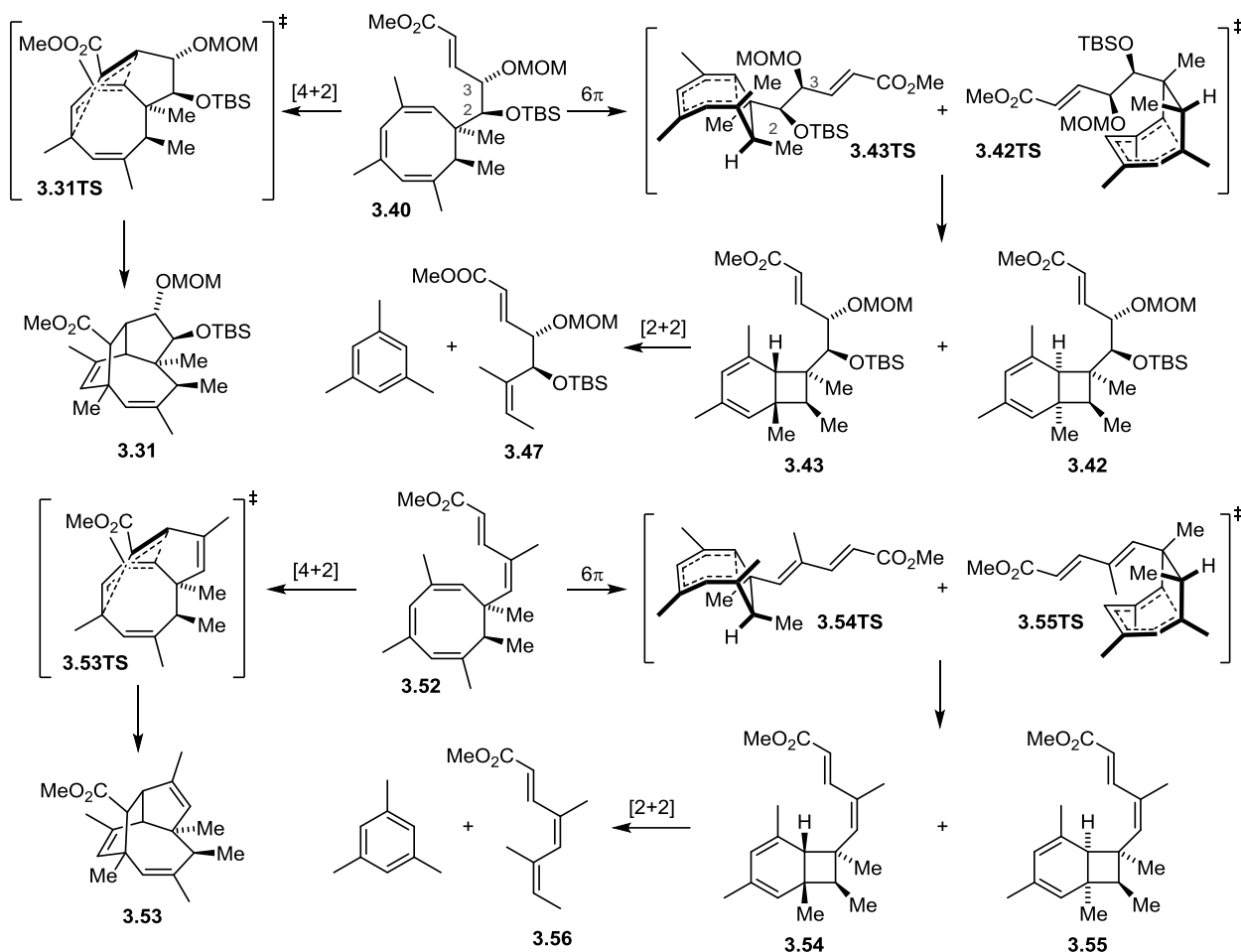
Taking a closer look to the cascade reaction, many potential products could arise from tetraene **3.35**. Discarding the photochemical pathway, polyene **3.35** could undergo a  $6\pi$  disrotatory electrocyclization yielding cyclohexadienes **3.36** and **3.38** depending on the reaction torquoselectivity (Scheme 3.10). Moreover, it would be theoretically possible for both to engage in a [4+2] cycloaddition affording tricycles **3.37** and **3.39**.

Given the lower activation energy required for  $8\pi$  electrocyclizations (in unsubstituted octatetraene 18 kcal/mol less than for the corresponding  $6\pi$ ), this is expected to be the major reaction pathway.<sup>[27]</sup> Depending on the torquoselectivity, the conrotatory electrocyclization could lead to cyclooctatrienes **3.40** and **3.41**, each of which exists as a mixture of two conformers that interconvert by ring flip with an activation energy of 4–7 kcal/mol.<sup>[39]</sup> These cyclooctatrienes would afford bicyclo[4.2.0]octadienes **3.42** to **3.45** upon  $6\pi$  electrocyclization, which in turn could undergo a retro-[2+2] cycloaddition extruding mesitylene and triene **3.47**, as earlier described for Orinocin (Scheme 1.18).<sup>[55]</sup> For *endo* bicycles **3.42** and **3.45**, a Diels–Alder reaction analogous to the one yielding endiandric acid C could take place affording tetracycles **3.46** and **3.48**.

Finally, the desired product **3.31** is obtained from **3.40** by the reaction sequence comprising a conrotatory counterclockwise  $8\pi$  electrocyclization followed by a [4+2] cycloaddition with the appropriate regioselectivity. If the other possible diene in cyclooctatriene precursor **3.40** would engage in the Diels–Alder reaction, tricycle **3.49** would be obtained instead. Evidently, the homologous compounds **3.50** and **3.51** would arise from the same process, starting with cyclooctatriene **3.41**, itself originating from clockwise  $8\pi$  electrocyclization of tetraene **3.35**.



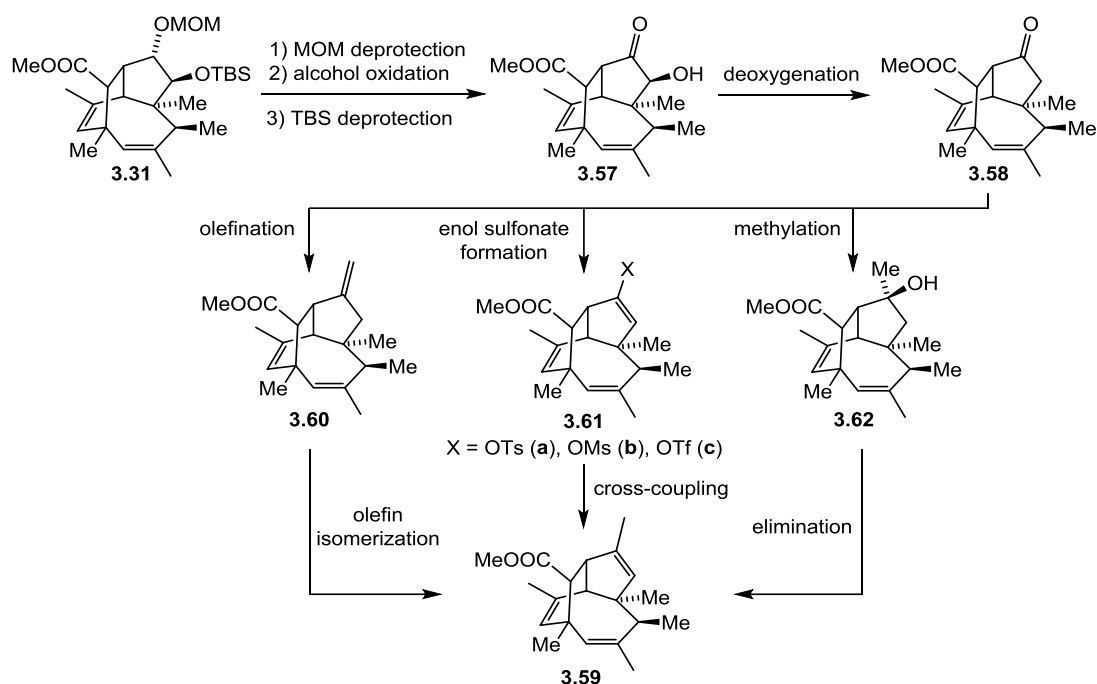
**Scheme 3.10.** Potential products that could arise from cascade reaction **3.35**  $\rightarrow$  **3.31**.



**Scheme 3.11.** Possible reaction pathways followed by **3.40** and **3.52** including transition states.

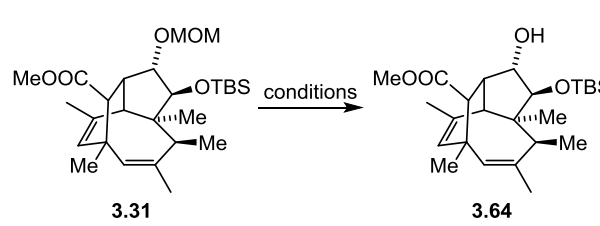
As it can be deduced from the experimental results, the right arrangement of substituents at C2 and C3 positions allowed for remarkable stereoselectivity, and consequently, a reaction which could yield at least 14 different products delivered the desired tricycle in 42% yield. The explanation for this phenomenon can be attributed to the steric strain between the side chain, increased by the presence of the OTBS group, and the  $\beta$ -methyl group present in transition states **3.43TS** and **3.42TS**, of which the latter is presumably higher in energy given the *endo* position of the alkyl chain (Scheme 3.11). Computational calculations in this regard can be seen in Chapter 3.3. This strain is not present (or is greatly minimized) in the transition states of the analogous tetraene (**3.54TS** and **3.55TS**), explaining why in previous work only the 6 $\pi$  products, bicyclo[4,2,0]octadienes **3.54** and **3.55** were isolated under similar reaction conditions. Moreover, attempts to thermally reverse this reaction only led to retro-[2+2] cycloaddition (Scheme 3.11).

With the core structure in hand, we aimed to install the olefinic methyl group in the cyclopentane ring. We envisioned that  $\alpha$ -hydroxyketone **3.57** (Scheme 3.12) obtained from tricycle **3.31** by MOM deprotection, oxidation and TBS deprotection could be deoxygenated with  $\text{SmI}_2$  yielding ketone **3.58**.<sup>[145,146]</sup> This versatile intermediate could potentially deliver cyclopentene **3.59** by 3 different approaches based on intermediates **3.60** to **3.62**. The first strategy would involve olefination of the ketone yielding *exo*-methylene **3.60**, which could be isomerized to the desired intermediate **3.59**.<sup>[147–150]</sup> Another option would be the synthesis of an enol sulfonate (**3.61a**, **b** or **c**) which could engage in a cross-coupling reaction to install the methyl group.<sup>[151,152]</sup> Finally, methylation of ketone **3.59** with a Grignard or an equivalent reagent would lead to tertiary alcohol **3.62**, which upon elimination would afford **3.59**.<sup>[153,154]</sup>



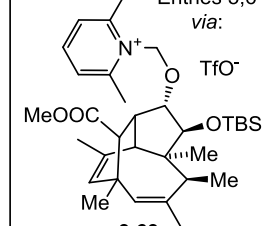
**Scheme 3.12.** Envisioned routes towards intermediate **3.59**.

For this purpose, we first proceeded to deprotect the MOM group of intermediate **3.31**. After trying different methods including the use of *B*-Bromo catecholborane, (Table 3.13, Entries 1-2),<sup>[155,156]</sup> zinc bromide (Entries 3-4)<sup>[157-159]</sup> and TES triflate and base (Entries 5, 7-8)<sup>[160]</sup> at different temperatures, either no conversion or decomposition was observed (Table 3.5, Entries 1-5). We then tried Fujioka's conditions, which consisted in the treatment of the acetal with TESOTf and 2,6-lutidine at 0 °C, forming a lutidinium salt intermediate which could be hydrolysed *in situ* yielding the desired alcohol.<sup>[161]</sup> For our hindered substrate, **3.31**, no conversion was observed under the mentioned conditions. This prompted us to apply more forcing conditions, switching the solvent to chloroform and heating up to reflux. After 5 hours the expected lutidinium salt **3.63** was observed by proton NMR, and further hydrolysis was achieved by keeping the sample in a biphasic mixture of chloroform and water at 65 °C for 48 h, obtaining alcohol **3.64** in 81% yield. In another publication by Fujioka,<sup>[162]</sup> the problem of lutidinium salt hydrolysis was addressed by the use of bipyridine, which yielded labile bipyridinium salts. However, when we applied this method, only decomposition was observed (Entries 7-8).<sup>[162]</sup>



**3.31** **3.64**

Entries 5,6  
via:



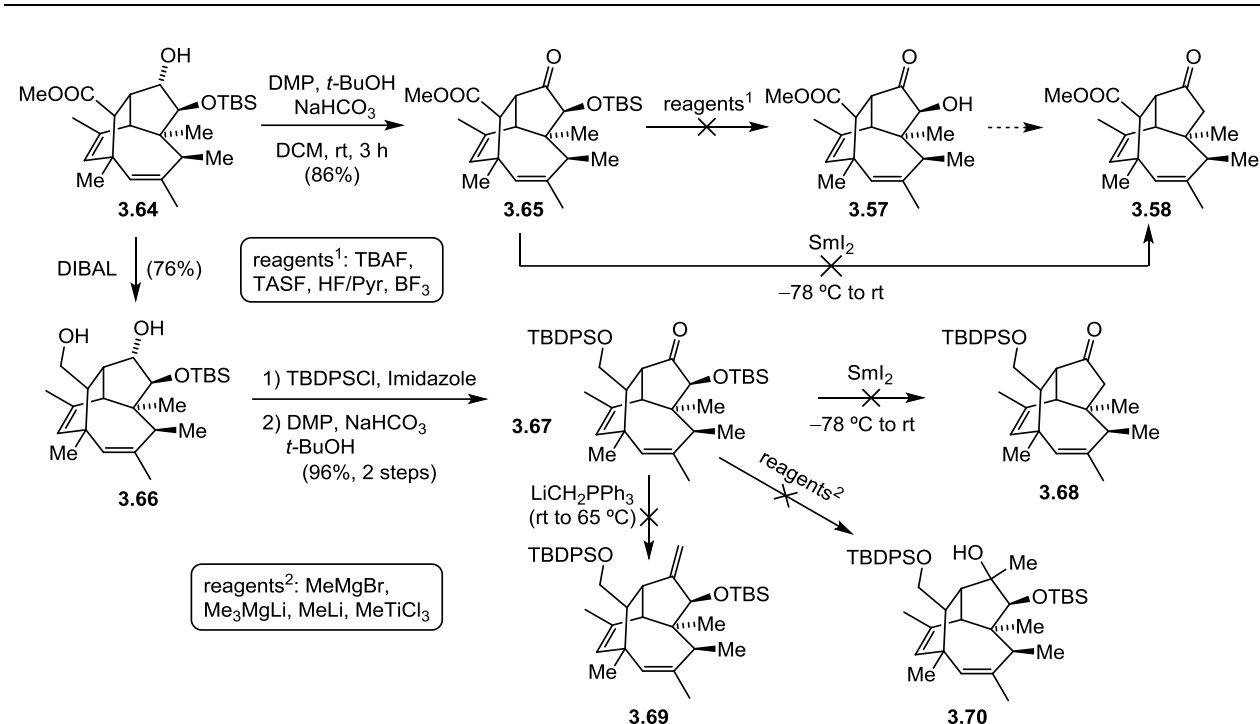
**3.63**

Entry	Reagents	Solvent	T [°C]	Time [h]	Outcome
1	<i>B</i> -Bromocatecholborane	DCM	−30 to −10	8	no conversion
2	<i>B</i> -Bromocatecholborane	DCM	0 to 23	2	decomposition
3	ZnBr <sub>2</sub> , <i>n</i> -PrSH	DCM	0	2	no conversion
4	ZnBr <sub>2</sub> , <i>n</i> -PrSH	DCM	23	2.5	decomposition
5	TESOTf, lut.	DCM	0 to 23	5	no conversion
6	TESOTf, lut.	CHCl <sub>3</sub>	61	5	81% yield
7	TESOTf, bipyridine	DCM	0 to 23	18	no conversion
8	TESOTf, bipyridine	DCE	62	6	decomposition

**Scheme 3.13 and Table 3.5.** Conditions screened for the deprotection of MOM alcohol **3.31**.

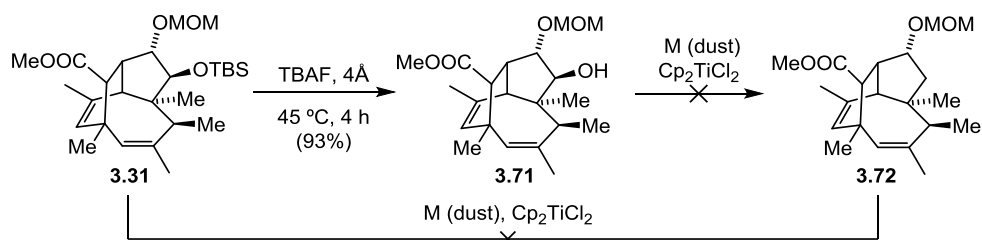
Alcohol **3.64** was oxidized with DMP yielding protected  $\alpha$ -hydroxy ketone **3.65**, which we were unable to deprotect by treatment with various fluoride sources including TBAF, TASF, HF/Pyridine and BF<sub>3</sub> due to decomposition (Scheme 3.13).<sup>[163–166]</sup> An attempt to directly deoxygenate silyl ether **3.65** with SmI<sub>2</sub> based on literature precedents also failed.<sup>[145,167]</sup> Thinking that the ester group could be playing a role in the decomposition of **3.65**, we opted to reduce it and protect the resulting alcohol. This was accomplished by treatment of **3.64** with DIBAL followed by primary alcohol protection with TBDPSCI and oxidation with DMP, which smoothly delivered ketone **3.67**. We attempted the SmI<sub>2</sub> mediated  $\alpha$ -hydroxy ketone deoxygenation on **3.67**,<sup>[163–166]</sup> but again no conversion was observed. Wittig olefination of **3.67** to obtain *exo*-methylene **3.69** and alkylation attempts with different organometallic reagents including methyl magnesium bromide, methyllithium, lithium trimethyl magnesiate and methyl titanium trichloride aiming to deliver tertiary alcohol **3.70** were also unsuccessful,<sup>[153,168–173]</sup> presumably due to the steric hindrance around the carbonyl group.





**Scheme 3.14.** Attempts to synthesize advanced intermediates **3.58** and **3.68** to **3.70**.

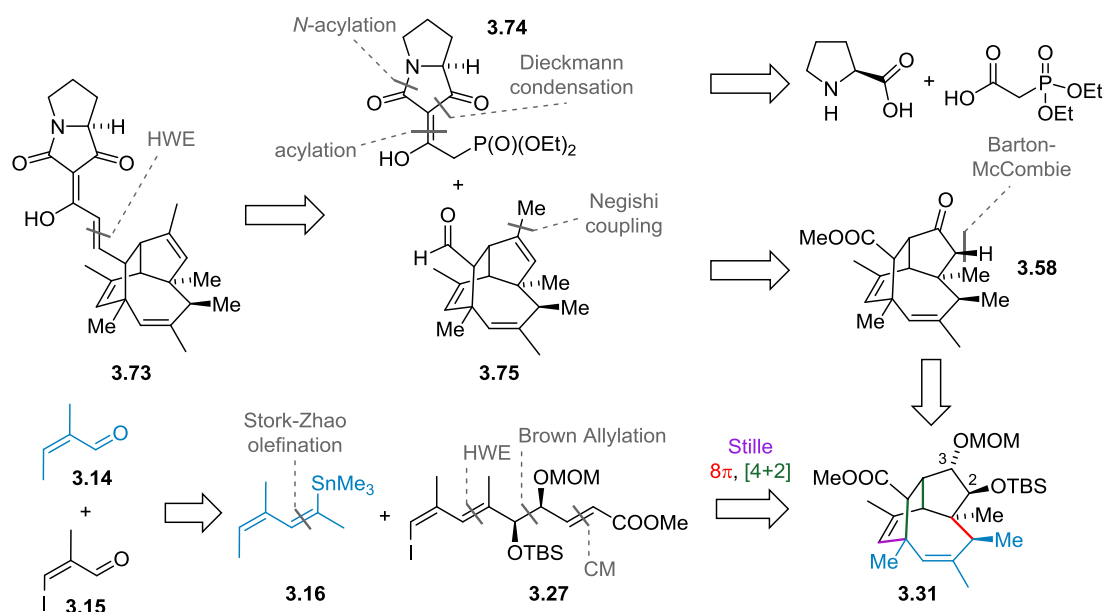
Since the deoxygenation attempts on  $\alpha$ -hydroxy ketones **3.65** and **3.67** were unsuccessful, we decided to first deprotect the TBS silyl ether and submit the resulting alcohol to deoxygenation with Nugent's reagent using Barrero's conditions (Scheme 3.15).<sup>[174]</sup> Unfortunately, when applied to alcohol **3.71** or silyl ether **3.31**, no conversion was observed. This prompted us to redesign our retrosynthesis for the last time (Scheme 3.16).



Sm	Metal	Solvent	Time [h]	T [°C]	Result
<b>3.31</b>	Mn	THF	5	66	No conversion
<b>3.31</b>	Zn	THF	6	66	No conversion
<b>3.31</b>	Zn	Dioxane	18	101	No conversion
<b>3.31</b>	Zn	PhMe	18	110	No conversion
<b>3.71</b>	Mn	THF	5	66	No conversion
<b>3.71</b>	Zn	PhMe	5	110	No conversion
<b>3.71</b>	Zn	Dioxane	18	101	No conversion

Reactions were carried out on a 21  $\mu$ mol run with 1.5 equiv. of **M** and 2.1 equiv. of  $\text{Cp}_2\text{TiCl}_2$ .

**Scheme 3.15 and Table 3.6.** Attempts to deoxygenate intermediates **3.31** and **3.71** with Nugent's reagent.



**Scheme 3.16.** Definitive retrosynthesis of (-)-PF-1018.

We envisioned a new way of obtaining tricycle **3.75** from diol **3.31**. The olefinic methyl group of **3.75** could be installed by means of Negishi coupling on an enol triflate derived from ketone **3.58**. **3.58** could in turn be obtained from **3.31** upon TBS deprotection, Barton–McCombie deoxygenation and oxidation of the alcohol at C3. This strategy together with the Brown allylation route towards **3.31** and the final HWE reaction define the retrosynthetic analysis that delivered (-)-PF-1018 (Scheme 3.16).

### 3.3 Bioinspired Synthesis of (–)-PF-1018

WILEY-VCH

#### COMMUNICATION

### Bioinspired Synthesis of (–)-PF-1018

Hugo Quintela-Varela,<sup>[a,b]</sup> Cooper S. Jamieson,<sup>[c]</sup> Qianzhen Shao,<sup>[c,d]</sup> K. N. Houk<sup>[c]</sup> and Dirk Trauner<sup>\*[b]</sup>

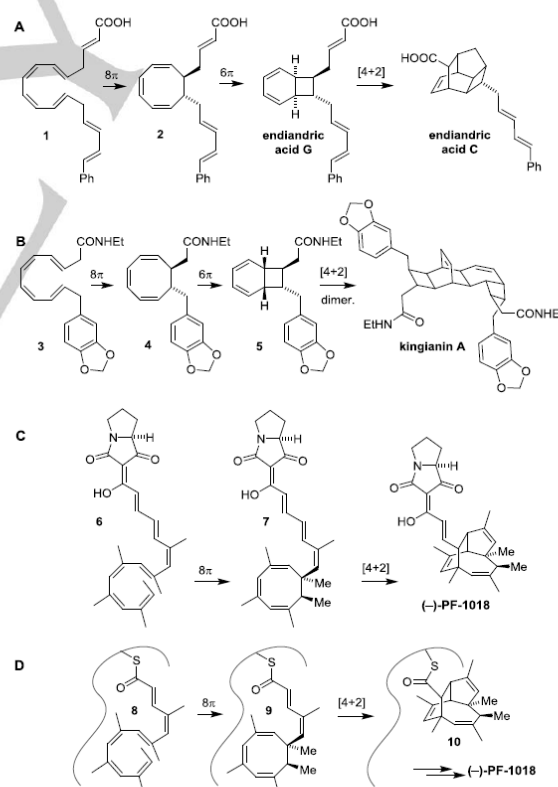
**Abstract:** The combination of electrocyclizations and cycloadditions accounts for the formation of a range of fascinating natural products. Cascades consisting of  $8\pi$  electrocyclizations, followed by  $6\pi$  electrocyclization, and a cycloaddition are relatively common. We now report the synthesis of the tetramic acid PF-1018 through an  $8\pi$  electrocyclization, the product of which is immediately intercepted by a Diels–Alder cycloaddition. The success of this pericyclic cascade was critically dependent on the substitution pattern of the starting polyene and could be rationalized through DFD calculations. The completion of the synthesis required the instalment of a trisubstituted double bond via radical deoxygenation. An unexpected byproduct formed through 4-*exo*-trig radical cyclization could be recycled through an unprecedented triflation/fragmentation.

The combination of an  $8\pi$ – $6\pi$ –electrocyclization cascade with a cycloaddition has been implicated in the biosynthesis of a range of natural products (Fig. 1). In the well-known endriandric acid family, for instance, conrotatory  $8\pi$  electrocyclization of **1** yields cyclooctatriene **2**, which then undergoes disrotatory  $6\pi$  electrocyclization to afford the bicyclo[4.2.0]octadiene endriandric acid **3**. This is followed by an intramolecular Diels–Alder reaction that leads to endriandric acid **C** (Fig. 1A).<sup>[1–3]</sup> In the case of kingianin A, the electrocyclization cascade yields cyclooctatriene **3** and then bicyclo[4.2.0]octadiene **5**, which engages in intermolecular Diels–Alder dimerization (Fig. 1B).<sup>[4,5]</sup> Other examples that have been validated by biomimetic or bioinspired synthesis include ocellapyrone A,<sup>[6]</sup> where the electrocyclizations are followed by an intramolecular hetero Diels–Alder reaction, and orinocin,<sup>[7]</sup> where they are followed by a *retro* [2+2]–cycloaddition, resulting in “polyene splicing”.

The unusual natural product PF-1018 appears to stem from a fascinating variation of this pericyclic chemistry (Fig. 1C). The anionic lipid was isolated from a fungal strain identified as *Humicola sp. 1018* in a screen against *Plutella xylostella*, the diamond back moth, which accounts for massive agricultural losses worldwide.<sup>[8,9]</sup> Its structure was established by NMR and X-ray analysis and was shown to feature a rare proline derived tetramic acid linked to a complex tricyclic hydrocarbon core. This core features six stereocenters, two of them quaternary, and three trisubstituted double bonds bearing methyl groups.

Biosynthetically, PF-1018 could originate, at least in principle, from the complex polyene **6** (Fig. 1C). A diastereoselective  $8\pi$  electrocyclization would generate the cyclooctatriene **7**. Unlike the cascades above, instead of a subsequent conrotatory  $6\pi$  electrocyclization to afford a bicyclo[4.2.0]octadiene, the cyclooctatriene engages in an intramolecular cycloaddition with one of the disubstituted alkenes to generate the tricyclic hydrocarbon core of the molecule.

It should be noted that the endriandric acids and kingianin A were isolated as racemates and spontaneously form from their achiral polyene precursors **1** and **3**.<sup>[1,4]</sup> By contrast, PF-1018 was isolated as a single enantiomer and diastereomer. It seems unlikely that the existing stereocenter in the hypothetical precursor **6** would govern the diastereoselectivity of the initial  $8\pi$  electrocyclization. This indicates that the pericyclic cascades could already occur on a shorter intermediate, such as **8**, within the chiral environment of a molecular assembly line (Fig. 1D).<sup>[10,11]</sup> The cyclization of an intermediate bound to a polyketide synthase–nonribosomal peptide synthetase (PKS–NRPS) via a thioester, could also explain why interception of the cyclooctadiene **9** via Diels–Alder reaction to afford **10** is favoured over a relatively fast  $6\pi$  electrocyclization, which is essentially irreversible at ambient temperatures.<sup>[12–15]</sup>

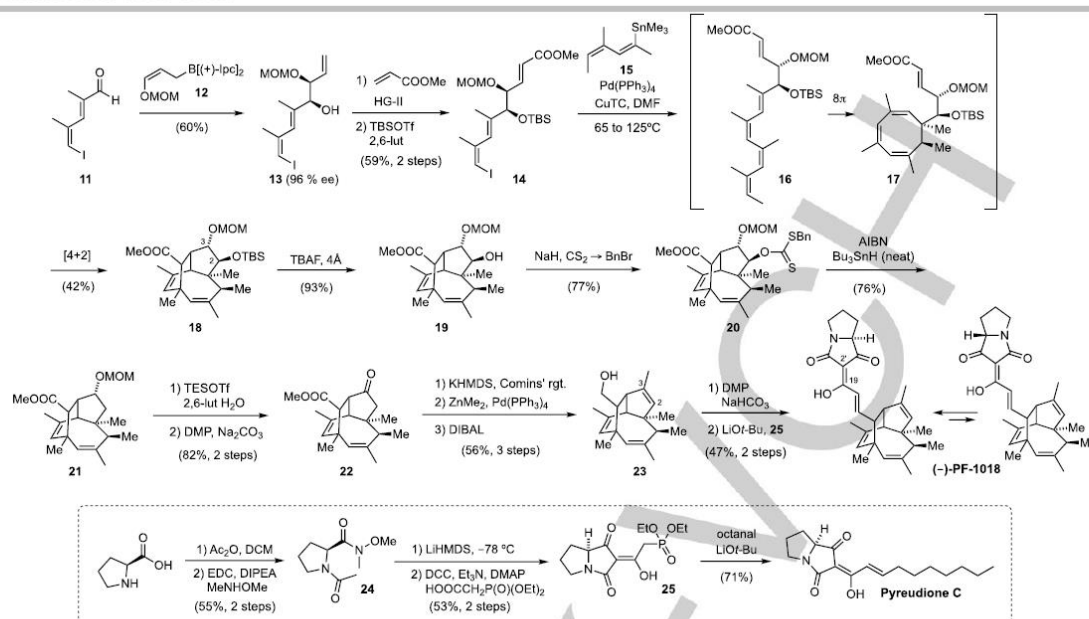


**Scheme 1.** Electrocyclization-Cycloaddition cascades in natural product chemistry.

- [a] H. Quintela-Varela  
Department of Chemistry  
Ludwig-Maximilians-Universität München  
Butenandtstrasse 5–13, 81377 München (Germany)
- [b] H. Quintela-Varela, Prof. Dr. D. Trauner  
Department of Chemistry  
New York University  
100 Washington Square East, New York, NY 10003 (USA)  
E-mail: [dirktrauner@nyu.edu](mailto:dirktrauner@nyu.edu)
- [c] C. S. Jamieson, Q. Shao, K. N. Houk  
Department of Chemistry and Biochemistry  
University of California, Los Angeles  
Los Angeles, CA 90095 (USA)
- [d] Q. Shao  
The College of Chemistry  
Nankai University  
Tianjin 300071 (China)

Supporting information for this article is given via a link at the end of the document.

## COMMUNICATION



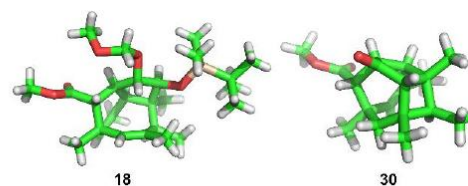
Scheme 2. Total synthesis of (–)-PF-1018 and Pyreudione C.

Given these considerations, a biomimetic laboratory synthesis of PF-1018 poses considerable challenges. We have previously developed an  $8\pi$  electrocyclization/Diels–Alder cascade that gave rise to the partially saturated tricyclic core of PF-1018.<sup>[16]</sup> However, our synthesis faltered because we were unable to install the remaining double bond in this highly hindered, caged intermediate. We now report the successful, asymmetric synthesis of PF-1018 that could overcome these issues through careful engineering of the cyclization substrate. It demonstrates that our strategy for the Diels–Alder interception of a cyclooctatriene is generalizable. It also features unusual and unexpected reactivity associated with the caged and congested tricyclic hydrocarbon core of our target.

Our synthesis started with the asymmetric addition of Brown's chiral allyl borane **12**<sup>[17]</sup> to the known aldehyde **11**. This gave the mono methoxymethyl (MOM)-protected diol **13** in decent yield and with excellent enantiomeric purity. Subsequent olefin cross-metathesis with methyl acrylate was achieved through sequential addition of the second-generation Hoveyda–Grubbs catalyst over several hours to overcome low conversion. This was followed by protection of the secondary alcohol as a silyl ether and afforded the unsaturated ester **14**. The stage was now set for the key step of the synthesis, which commenced with cross-coupling of **14** with the known vinyl stannane **15** under Stille–Liebeskind conditions. The initial cross-coupling product **16** was not isolated but was heated gradually in solution from 65 °C to 125 °C and then maintained for 20 hours at this temperature to promote the  $8\pi$  electrocyclization (**16** → **17**) and Diels–Alder interception (**17** → **18**). Under these conditions we could isolate the tricycle **18** in 42% yield. The X-ray structure of **18** is shown in Fig. 1 confirming the configuration and highly congested nature of this caged compound. With **18** in hand, our next task was to convert the doubly protected diol into the trisubstituted C2,C3 double bond of PF-1018 (original nomenclature). To this end, we first cleaved the silyl ether at C2 to afford the secondary alcohol **19** and then activated its hydroxy group as the benzyl xanthate **20**. Barton–McCombie deoxygenation under highly optimized conditions (see below) then gave MOM ether **21**. Cleavage of this ether using a modification of Fujioka's-

conditions,<sup>[18]</sup> followed by oxidation with Dess–Martin periodinane, yielded ketone **22**. Conversion to the enol triflate, followed by Negishi coupling, installed the required olefinic double bond. Subsequent reduction of the ester with DIBAL then gave the primary alcohol **23**.

In the final stage of our synthesis, **23** was oxidized to an unstable aldehyde, which was condensed with tetramic acid phosphonate **25**.<sup>[19]</sup> This gave (–)-PF-1018 as an inseparable 3.5:1 mixture of (*E*) and (*Z*) isomers with respect to the C19–C2' double bond. The analytical data of our synthetic samples were identical with those reported for the natural product, with the exception of the optical rotation, which is significantly lower in our case. However, we have confirmed the high optical purity of alcohol **19** by Mosher ester analysis (see Supporting Information) and it seems unlikely that the final steps of the synthesis result in partial racemization. The difference in optical rotation probably stems from variations of the (*E*)/(*Z*) ratio of the C19–C2' double bond (3.2:1 reported for the natural sample).<sup>[9]</sup>

Figure 1. X-ray crystal structure of compounds **18** and **30**.

The preparation of tetramic acid phosphonate **25** from proline through a modified route is shown in the lower portion of Fig. 2. Acetylation and conversion to the Weinreb amide gave **24**. A subsequent Dieckmann condensation then afforded an unstable pyrrolizidinedione,<sup>[20]</sup> which was coupled with diethyl phosphonoacetic acid to afford the tetramic acid phosphonate



## COMMUNICATION

25.<sup>[19,21]</sup> This building block was also condensed with octanal to afford the recently isolated anionic lipid pyreudione C.<sup>[20,22]</sup>

The key step of our synthesis warrants further analysis. Given the many possible isomers that can be formed, we consider this a remarkable result both in terms of selectivity and yield (see SI Fig. S1). In preliminary studies, we had established that the relative stereochemistry at C2 and C3, as well as the size of the silyl group at C2 are crucial to achieve high yields in the cascade.<sup>[16]</sup> Bicyclo[4.2.0]octadienes resulting from competing  $6\pi$  electrocyclization cascades were never observed but are likely destroyed *via* formal retro [2+2] cycloaddition under our optimized conditions.<sup>[7]</sup> Other isomers could not be isolated either.

To explain such reactivities and selectivities of the pericyclic cascade, density functional theory calculations were employed at the SMD(DMF)- $\omega$ B97X-D/def2-QZVPP//SMD(DMF)- $\omega$ B97X-D/6-311+G(d,p) level of theory (see SI for computational details).<sup>[23–33]</sup>

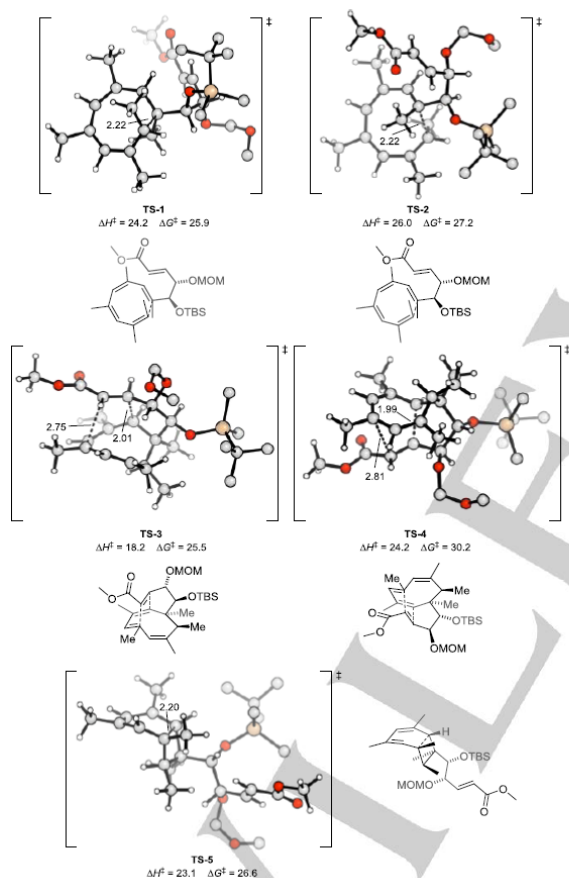


**Figure 2.** Density functional theory calculated transition state structures of pericyclic cascade. Hydrogens on protecting groups are omitted for clarity, silicon shown in wheat colour.

These calculations indicate that the polyene **16** can engage in two conrotatory  $8\pi$  electrocyclizations to form **17** and its diastereomer **17'** *via* TS-1 and TS-2, respectively (Fig. 2, S2). The cyclooctatrienes **17** and **17'** are nearly isoenergetic with their precursor **16** (Figure S3), resulting in an initial equilibrium between the species **16**, **17**, and **17'**. The subsequent intramolecular cycloaddition of **17**, forming **18** *via* TS-3, is 4.7 kcal mol<sup>-1</sup> lower in

Gibbs-free energy than the diastereomeric cycloaddition *via* TS-4. Consequently, the equilibrium mixture of **16**, **17**, and **17'** will funnel through TS-3 to selectively form the isolated product **18**. The Diels–Alder transition states TS-3 and TS-4 are both stabilized by favourable secondary orbital interactions between the diene and ester oxygen of the dienophile. The difference in Gibbs-free energy between TS-3 and TS-4 ( $\Delta\Delta G^\ddagger = 4.7$  kcal mol<sup>-1</sup>) is due to the MOM-ether being forced into a *pseudo*-axial position in TS-4. In TS-3, both the MOM-ether and silyl-ether groups on the emerging cyclopentane are in *pseudo*-equatorial positions. The silyl ether greatly affects the energy difference between the Diels–Alder cycloaddition *via* TS-3 and a competing  $6\pi$  electrocyclization *via* TS-5. Decreasing the size of this substituent would favour the  $6\pi$  electrocyclization according to our calculations (Fig. 2, S4, S5a). A substrate with the double bond in place at C2,3 will also predominantly form the  $6\pi$ -product, suggesting that an enzyme is necessary for the Diels–Alder reaction to occur in Nature (Fig. S5b).

A step in our synthesis that delivered unexpected but interesting results was the Barton–McCombie deoxygenation. (Scheme 3 and Table 1). Standard conditions involving the methyl xanthate **26** only gave a low yield of the desired product **21**. It was accompanied by substantial amounts of methyl ether **28** (byproduct previously reported in these reactions)<sup>[34–36]</sup> and, to our surprise, cyclobutane **29**. The latter results from a rare 4-*exo-trig* radical cyclization, which generates a secondary radical.<sup>[37]</sup> This unusual selectivity presumably results from the constrained nature of the caged precursor. Increasing the concentration of tributyl tin hydride suppressed this cyclization but also led to higher yields of the unwanted methyl ether **28**. This problem could be finally overcome by variation of the xanthate: use of the larger benzyl xanthate **20** to promote fragmentation gave a good yield of the desired intermediate **21**.<sup>[38]</sup>

Scheme 3 shows the Barton–McCombie deoxygenation reaction. The reaction involves a xanthate (26, 27, or 20) reacting with AIBN and HSnBu<sub>3</sub> to form products 21, 28, and 29. The structures of 21, 28, and 29 are shown with their respective R groups.

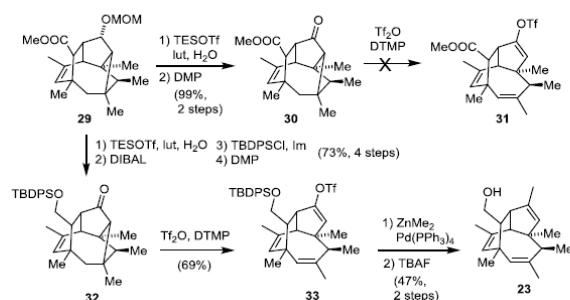
Entry	Xanthate	HSnBu <sub>3</sub> (equiv.)	Yield [%]:	21	28	29
1	26 R = Me	4.8		21	6	46
2	26 R = Me	50		41	29	10
3	27 R = Et	50		49	19	2
4	20 R = Bn	40		76	12	6

**Scheme 3 and Table 1:** Products of the Barton–McCombie deoxygenation.

Cyclobutane **29** was not a waste product but could be converted into a late-stage intermediate of our synthesis through an unusual fragmentation (Scheme 4). We reasoned that ketone **30** could fragment after electrophilic activation of the carbonyl compound with triflic anhydride to yield unsaturated vinyl triflate **31**.<sup>[39,40]</sup> Deprotection and oxidation of **29** with Dess–Martin periodinane gave cyclobutyl ketone **30**, the X-ray structure of which is shown in Fig 1 (right). It confirmed that the carbonyl group, the C,C-bond, and the requisite C-H bond are indeed stereoelectronically well aligned to allow for smooth formation of the two  $\pi$  bonds. Attempts to convert **30** into vinyl triflate **31** however, were unsuccessful and led to decomposition. We assigned this result to the interference of the methyl ester, which was accordingly reduced to afford primary alcohol **32**. Cleavage of the MOM-ether, DIBAL-reduction, selective protection of the primary alcohol with a bulky silyl group, and oxidation of the secondary alcohol then yielded cyclobutyl

## COMMUNICATION

ketone **32**. Treatment of this ketone with triflic anhydride in the presence of a sterically hindered pyridine base elicited the desired fragmentation and gave vinyl triflate **33**. Although the methyl group could also be deprotonated and is less hindered, only a small amount of the corresponding *exo*-methylene isomer was observed. To the best of our knowledge, a fragmentation of this type with concomitant enol triflate formation has only been reported once in the literature.<sup>[40]</sup> Negishi cross-coupling of **33** with dimethyl zinc and deprotection then afforded primary alcohol **23**, which could be used in the final steps of our total synthesis.



**Scheme 4:** Fragmentation of a cyclobutyl ketone and recycling of cyclobutane side product **29**.

In summary, we have achieved the first total synthesis of the unusual polyketide tetramic acid PF-1018. Our 15-step asymmetric synthesis is marked by a bioinspired cascade that combines an 8 $\pi$  electrocyclization with a Diels–Alder cycloaddition. Computational studies indicate that the size of substituent at C2 determines whether a 6 $\pi$  electrocyclization or Diels–Alder will be preferred, while the stereochemistry at C3 determines facial selectivity of the cycloaddition. This synthesis also rests on an unusual strategy to install a trisubstituted double bond. In the course this sequence, we observed a 4-*exo-trig* radical cyclization that generated an unexpected tetracycle. The product of this radical cyclization could be recycled by way on a stereoelectronically favourable fragmentation that simultaneously generated a trisubstituted double bond and a vinyl triflate. Future work will be directed towards exploring the biosynthesis, biological activity and structure activity-relationships of PF-1018 and other anionic lipids that feature proline-derived tetramic acids, such as talarotoxin<sup>[41]</sup> and the pyreudiones.<sup>[10,20,42]</sup>

## Acknowledgements

We thank Petr Tatarskiy for his synthesis work, Dr. Peter Mayer (LMU) and Prof. Chunhua Hu (NYU) for X-ray structure analysis and Dr. Chin Lin for assistance with NMR measurements. The TCI cryoprobe used for NMR acquisition was supported by the National Institutes of Health (OD016343). We would also like to thank the National Science Foundation (NSF CHE-1806581 to K.N.H.) for funding. All computational resources were provided by the Institute for Digital Research and Education. C.S.J. is supported by generous funding through the Saul Winstein Fellowship.

**Keywords:** Diels–Alder Cycloaddition • Electrocyclization • Total Synthesis • Biomimetic Synthesis • Tetramic Acids

- [1] W. M. Bandaranayake, J. E. Banfield, D. S. C. Black, *J. Chem. Soc., Chem. Commun.* **1980**, 902–903.
- [2] J. E. Banfield, D. S. C. Black, S. R. Johns, R. I. Willing, *Aust. J. Chem.* **1982**, *35*, 2247–2256.
- [3] K. C. Nicolaou, N. A. Petasis, J. Uenishi, R. E. Zipkin, *J. Am. Chem. Soc.* **1982**, *104*, 5557–5558.
- [4] A. Leverrier, M. E. T. H. Dau, P. Retailleau, K. Awang, F. Guéritte, M. Litaudon, *Org. Lett.* **2010**, *12*, 3638–3641.
- [5] H. N. Lim, K. A. Parker, *Org. Lett.* **2013**, *15*, 398–401.
- [6] A. K. Miller, D. Trauner, *Angewandte Chemie International Edition* **2005**, *44*, 4602–4606.
- [7] M. Müller, B. Kusebauch, G. Liang, C. M. Beaudry, D. Trauner, C. Hertweck, *Angewandte Chemie International Edition* **2006**, *45*, 7835–7838.
- [8] M. P. Zalucki, A. Shabbir, R. Silva, D. Adamson, L. Shu-Sheng, M. J. Furlong, *J. Econ. Entomol.* **2012**, *105*, 1115–1129.
- [9] S. Gomi, K.-I. Imamura, T. Yaguchi, Y. Kodama, N. Minowa, M. Koyama, *J. Antibiot.* **1994**, *47*, 571–580.
- [10] M. Klapper, D. Braga, G. Lackner, R. Herbst, P. Stallforth, *Cell Chem Biol.* **2018**, *25*, 659–665.e9.
- [11] K. Kasahara, T. Miyamoto, T. Fujimoto, H. Oguri, T. Tokiwano, H. Oikawa, Y. Ebizuka, I. Fujii, *ChemBioChem* **2010**, *11*, 1245–1252.
- [12] Rolf. Huisgen, Alexander. Dahmen, Helmut. Huber, *J. Am. Chem. Soc.* **1967**, *89*, 7130–7131.
- [13] R. Huisgen, A. Dahmen, H. Huber, *Tetrahedron Lett.* **1969**, *10*, 1461–1464.
- [14] B. E. Thomas, J. D. Evanseck, K. N. Houk, *Isr. J. Chem.* **1993**, *33*, 287–293.
- [15] A. Patel, K. N. Houk, *J. Org. Chem.* **2014**, *79*, 11370–11377.
- [16] R. Webster, B. Gaspar, P. Mayer, D. Trauner, *Org. Lett.* **2013**, *15*, 1866–1869.
- [17] H. C. Brown, P. K. Jadhav, K. S. Bhat, *J. Am. Chem. Soc.* **1988**, *110*, 1535–1538.
- [18] H. Fujioka, T. Okitsu, Y. Sawama, N. Murata, R. Li, Y. Kita, *J. Am. Chem. Soc.* **2006**, *128*, 5930–5938.
- [19] S. W. B. Tan, C. L. L. Chai, M. G. Moloney, *Org. Biomol. Chem.* **2014**, *12*, 1711–1716.
- [20] M. Klapper, S. Götz, R. Barnett, K. Willing, P. Stallforth, *Angewandte Chemie International Edition* **2016**, *55*, 8944–8947.
- [21] T. Rosen, P. B. Fernandes, M. A. Marovich, L. Shen, J. Mao, A. G. Pernet, *J. Med. Chem.* **1989**, *32*, 1062–1069.
- [22] M. Klapper, A. Paschold, S. Zhang, C. Weigel, H.-M. Dahse, S. Götz, S. Pace, S. König, Z. Rao, L. Reimer, et al., *ACS Chem. Biol.* **2019**, *14*, 1693–1697.
- [23] A. V. Marenich, C. J. Cramer, D. G. Truhlar, *J. Phys. Chem. B* **2009**, *113*, 6378–6396.
- [24] R. Krishnan, J. S. Binkley, R. Seeger, J. A. Pople, *J. Chem. Phys.* **1980**, *72*, 650–654.
- [25] V. A. Rassolov, J. A. Pople, M. A. Ratner, T. L. Windus, *J. Chem. Phys.* **1998**, *109*, 1223–1229.
- [26] M. M. Francl, W. J. Pietro, W. J. Hehre, J. S. Binkley, M. S. Gordon, D. J. DeFrees, J. A. Pople, *J. Chem. Phys.* **1982**, *77*, 3654–3665.
- [27] J. D. Dill, J. A. Pople, *J. Chem. Phys.* **1975**, *62*, 2921–2923.
- [28] W. J. Hehre, R. Ditchfield, J. A. Pople, *J. Chem. Phys.* **1972**, *56*, 2257–2261.
- [29] T. Clark, J. Chandrasekhar, G. W. Spitznagel, P. V. R. Schleyer, *Journal of Computational Chemistry* **1983**, *4*, 294–301.
- [30] J.-P. Blaudeau, M. P. McGrath, L. A. Curtiss, L. Radom, *J. Chem. Phys.* **1997**, *107*, 5016–5021.
- [31] A. Schäfer, C. Huber, R. Ahlrichs, *J. Chem. Phys.* **1994**, *100*, 5829–5835.

## COMMUNICATION

- [32] F. Weigend, R. Ahlrichs, *Phys. Chem. Chem. Phys.* **2005**, *7*, 3297–3305.
- [33] J.-D. Chai, M. Head-Gordon, *Phys. Chem. Chem. Phys.* **2008**, *10*, 6615–6620.
- [34] C. S. Bensasson, S. J. Comforth, M.-H. Du, J. R. Hanson, *Chem. Commun.* **1997**, 1509–1510.
- [35] S. J. Cristol, M. W. Klein, M. H. Hendewerk, R. D. Daussin, *J. Org. Chem.* **1981**, *46*, 4992–4998.
- [36] A. Srikrishna, S. J. Gharpure, *J. Org. Chem.* **2001**, *66*, 4379–4385.
- [37] G. Majetich, J. L. Grove, *Org. Lett.* **2009**, *11*, 2904–2907.
- [38] D. H. R. Barton, D. Crich, A. Löbberding, S. Z. Zard, *Tetrahedron* **1986**, *42*, 2329–2338.
- [39] M. Kato, M. Watanabe, B. Z. Awen, *J. Org. Chem.* **1993**, *58*, 5145–5152.
- [40] García Martínez, Herrera Fernández, A. Sánchez García, J. M., *An. Quim.* **1979**, *75*, 723.
- [41] K. Ishii, T. Itoh, K. Kobayashi, Y. Horie, Y. Ueno, *Appl. Environ. Microbiol.* **1995**, *61*, 941–943.
- [42] L. M. Petersen, J. C. Frisvad, P. B. Knudsen, M. Rohlfs, C. H. Gotfredsen, T. O. Larsen, *The Journal of Antibiotics* **2015**, *68*, 603–608.

## 3.4 Unpublished Results

The side reactions identified within the Barton–McCombie deoxygenation of methyl xanthate **3.76** are disclosed in Scheme 3.17.

**Pathway A** leading to desired product **3.72**.

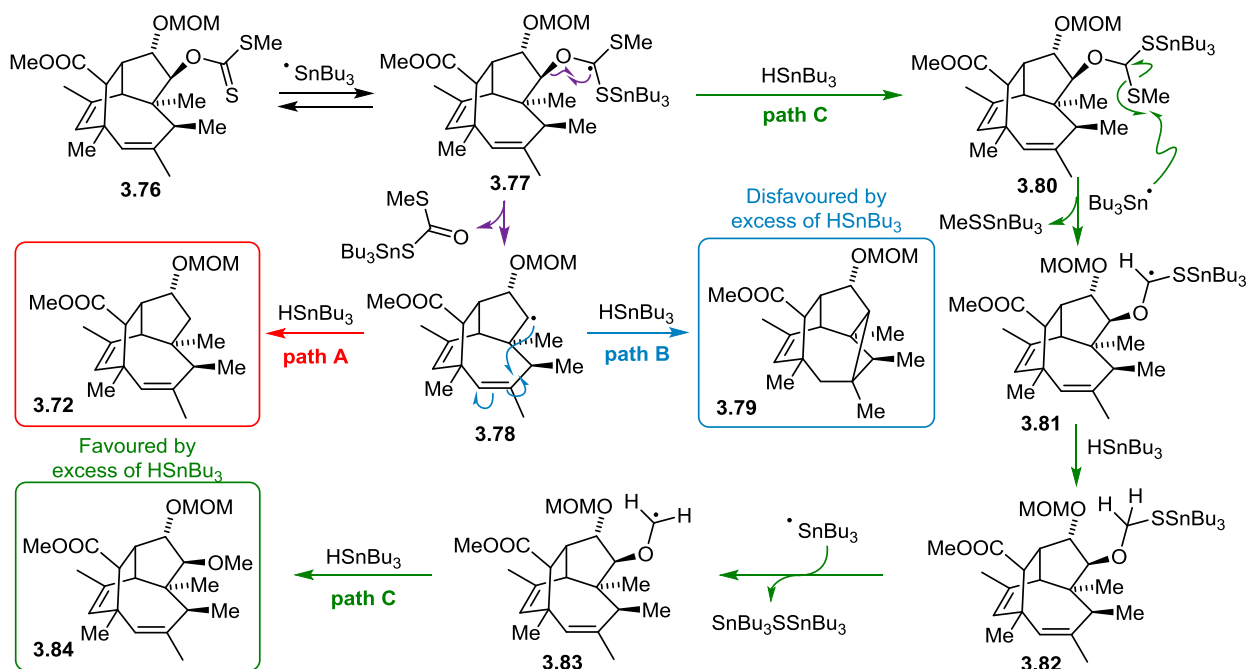
The stannyl radical derived from tributyltin hydride (TBHT) attacks the thiocarbonyl sulfur atom reversibly, originating xanthate-centred radical **3.77**, which undergoes homolytic cleavage of the adjacent C-O bond leading to the alkyl radical **3.78**. An extra equivalent of TBHT quenches radical **3.78** by hydrogen atom abstraction yielding the desired product **3.72**.<sup>[175,176]</sup>

**Pathway B** leading to tetracycle **3.79**.

Following the exact same route until intermediate **3.78**, the alkyl radical is not quenched by tin hydride and a 4-*exo-trig* radical cyclization takes place leading to tetracycle **3.79**. This pathway is inhibited by high loadings of TBTH, which would trap the alkyl radical before it undergoes cyclization to **3.79**.

**Pathway C** leading to methyl ether **3.84**.

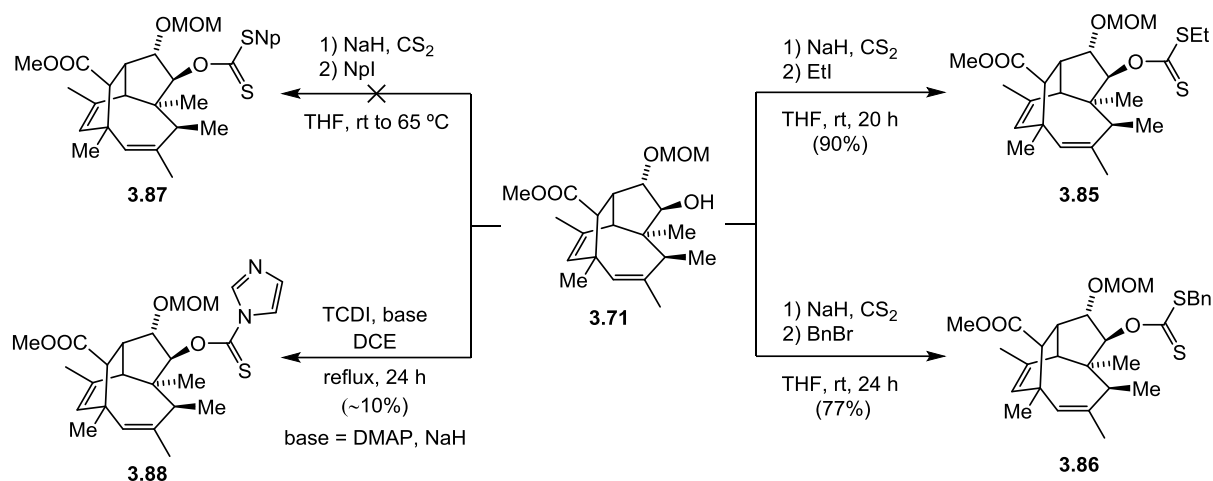
A different reaction course competes with the homolytic fragmentation of intermediate **3.77**. This radical can be quenched by TBHT generating intermediate **3.80**, which can be attacked again at the less hindered sulfur atom by a stannyl radical leading to mixed acetal **3.82**. Repetition of this process leads to methyl ether **3.84**.<sup>[177]</sup> Obviously, the greater the excess of the hydride source, the faster these reactions will occur and the higher the yields of **3.84**.



**Scheme 3.17.** Mechanism of the Barton–McCombie reaction of xanthate **3.76** leading to 3 different products.

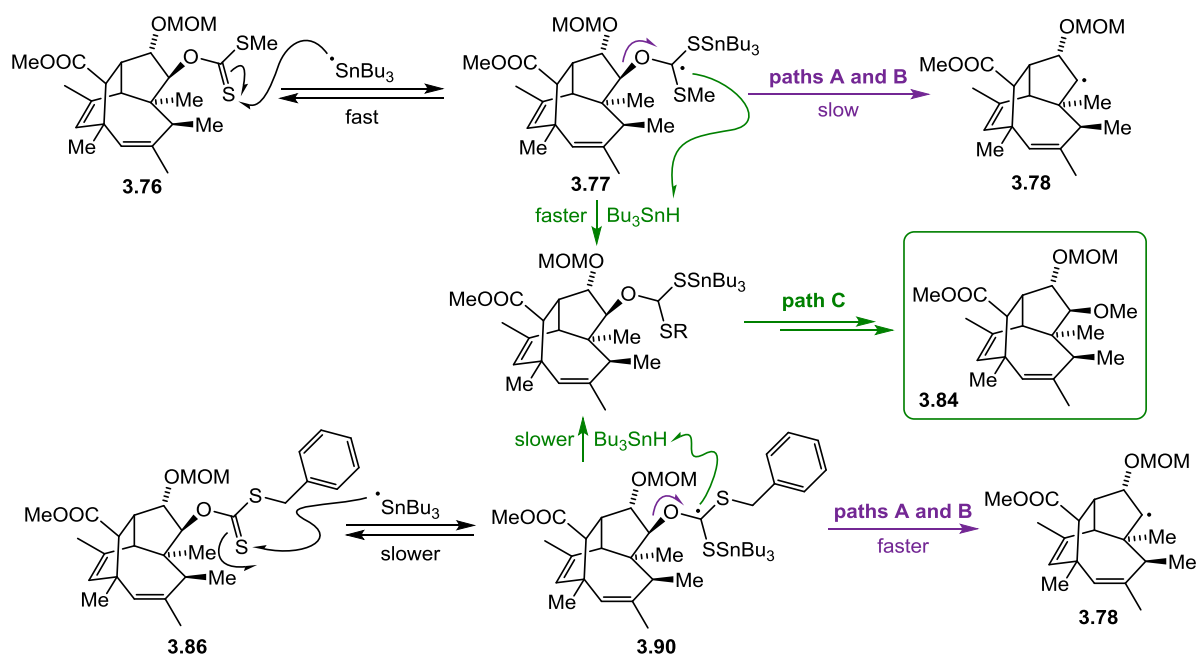


Hence, trying to inhibit pathway B by tuning the stoichiometry of TBHT will promote pathway C and *vice versa*. We therefore thought of two other methods to direct the reactivity of the Barton–McCombie reaction towards the desired product. The first consisted in the use of different hydride sources with a reductive potential capable of quenching radical **3.78** without encouraging pathway C.<sup>[178]</sup> The other method involved the employment of different xanthates more prone to undergo fragmentation in order to favour pathway A.<sup>[179]</sup>



**Scheme 3.18.** Preparation of different xanthates from alcohol **3.71**.

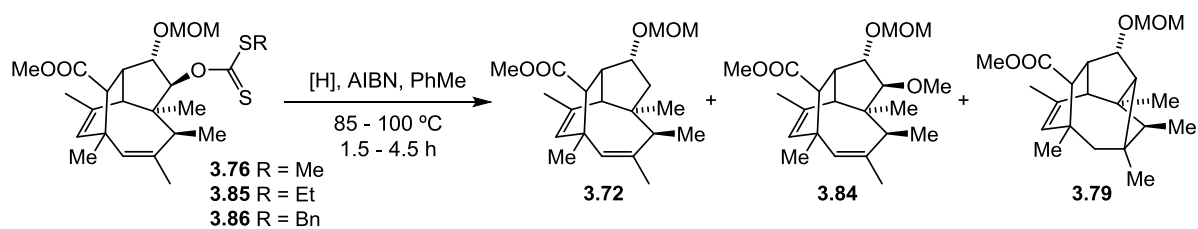
We therefore pursued the synthesis of xanthates **3.85** to **3.87** and succeeded in the isolation of ethyl xanthate **3.85** and benzyl xanthate **3.86**. We did not observe any conversion towards neopentyl xanthate **3.87** and could not surpass the 10% yield in the synthesis of the imidazole derivative **3.88**. With these increasingly hindered xanthates we hoped to obtain intermediate radical species more prone to undergo fragmentation as a consequence of a greater release of steric strain between the xanthate and alkyl moieties, as compared to methyl xanthate **3.76**.<sup>[179,180]</sup> Moreover, xanthate centred radical species such as **3.87** (Scheme 3.19), would more reluctant than **3.77** to be overreduced, since the environment around the radical is more congested.



**Scheme 3.19.** Comparison between the kinetics of xanthates **3.76** and **3.86** in the Barton–McCombie deoxygenation.

As it can be seen in Scheme 3.19, the first step consisting in addition of the stannyl radical to methyl xanthate **3.76** is fast and reversible. Once radical **3.77** is generated, the faster pathway C (if run in neat TBTH, see Table 3.7) leads to methyl ether **3.84**, and paths A and B, initiated by fragmentation are slightly slower in delivering radical **3.78**.<sup>[179,180]</sup> If xanthate **3.86** is submitted to the same process, the first addition of the radical will presumably be slowed down by the increased steric bulk around the sulfur atom, but this will still be the fastest step. The quench of radical intermediate **3.90** follows the same logic, occurring at a slower rate than for the methyl xanthate **3.77**. Finally, **3.90** will undergo fragmentation to deliver radical **3.78** at a faster rate than **3.77** given the greater steric strain between the alkyl and xanthate moieties.

The empirical proof for these claims can be seen in Table 3.7. While working with methyl xanthate **3.76**, we obtained a more favourable ratio of deoxygenated product **3.72** + tetracycle **3.79**, both arising from initial fragmentation, when the reaction was run with 1.5 equivalents of TBTH than when we used 50 (Entries 1 and 3). In the latter case the ratio of **3.84** increased almost fivefold. A larger scale attempt (400 mg of **3.76** versus 25 mg) followed this trend delivering large amounts of **3.79** (Entry 2).



Entry	sm	[H]	[H] equiv.	Yield (4.4)	3.72	3.84	3.79	Comment
1	3.76	HSnBu <sub>3</sub>	1.5	39%	1	0.23	0.65	–
2	3.76	HSnBu <sub>3</sub>	4.8	21%	1	0.28	2.23	400 mg of <b>3.76</b>
3	3.76	HSnBu <sub>3</sub>	50	41%	1	1.13	0.2	–
4	3.76	Et <sub>3</sub> SiH	5	0%	0	0	0	no conversion
5	3.76	TMS <sub>3</sub> SiH	3	–	–	–	–	unidentified products
6	3.85	HSnBu <sub>3</sub>	5	37%	1	0.04	0.66	–
7	3.85	HSnBu <sub>3</sub>	50	49%	1	0.80	trace	–
8	3.85	HSnPh <sub>3</sub>	40	43%	1	1.11	trace	–
9	3.85	HSnBu <sub>3</sub>	50	50%	1	0.35	0.09	–
10	3.85	HSnBu <sub>3</sub>	25	–	1	0.55	0.07	5 mg of <b>3.85</b> , calc. NMR
11	3.85	HSnBu <sub>3</sub> /PhSeH	25/0.2	–	1	0.53	0.09	5 mg of <b>3.85</b> , calc. NMR
12	3.86	HSnBu <sub>3</sub>	50	61%	1	0.20	trace	–
13	3.86	HSnBu <sub>3</sub>	50	68%	1	0.21	0	–
14	3.86	HSnBu <sub>3</sub>	50	60%	1	0.30	0	92 mg of <b>3.86</b>
15	3.86	HSnBu <sub>3</sub>	40	76%	1	0.13	0.08	–

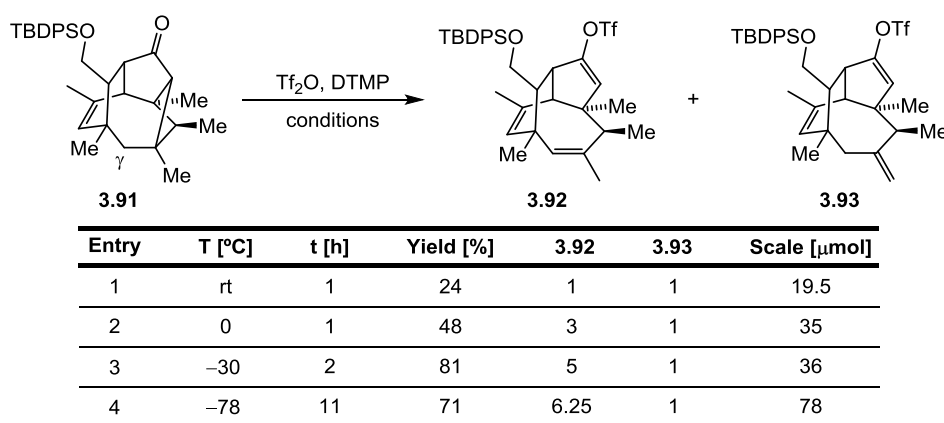
Reactions were performed with 10 to 25 mg of xanthate unless otherwise stated. Reactions with 40 or more equivalents of reductant were run without solvent.

**Scheme 3.20 and Table 3.7.** Conditions screened for the deoxygenation of **3.76**.

We also run the reaction with different hydride sources aiming for a faster quenching of radical **3.78** or a slowest overreduction of radical **3.77**. For the latter option, use of the milder reductant triethyl silane led to no observable reaction after 10 hours (in agreement with its hydrogen-atom abstraction rate constant, 3 orders of magnitude smaller than for TBHT)<sup>[178,181]</sup> and for tris(trimethylsilyl)silane, the reaction took 6 hours to reach completion, giving a mixture where none of the expected products could be identified (Entries 4 and 5).<sup>[178,182]</sup>

When using ethyl xanthate **3.85**, we observed the expected lower ratio of methyl ether **3.84** compared to the sum of **3.72** and **3.79**. Moreover, the yield of **3.72** increased to 50% (Entries 7 and 9). Using triphenyltin hydride as a more efficient hydrogen-atom donor did not lead to the expected increase in the yield of **3.72**, delivering instead **3.84** as the major product. The result was comparable to that of TBHT (Entries 7-8). Finally, we carried out the reaction in the presence of phenylselenol expecting that its electrophilic radical nature would induce an increase in reaction speed and an adjustment in product distribution,<sup>[183,184]</sup> but it did not induce any significant change in the product ratio (Entries 10 and 11).

For benzyl radical **3.86**, the differences in yield were more marked. If run in neat TBTH, the amount of overreduced product **3.84** dropped, and only traces of tetracycle **3.79** were found (Entries 12-15). Moreover, the yields for **3.72** increased up to 76% (Entry 15).



Reactions were run with 1.9 equiv. of  $\text{Tf}_2\text{O}$  and 2 equiv. of DTMP

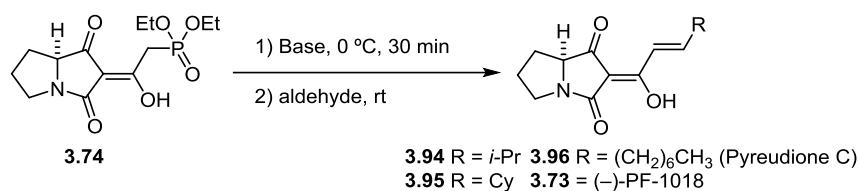
**Scheme 3.21 and Table 3.8.** Fragmentation of cyclobutene ring in tetracycle **3.91**.

As soon as we saw the crystal structure of **30** (see Chapter 3.3, Figure 1), we noticed that the hydrogen in the  $\gamma$  position relative to the carbonyl group was in an almost perfect antiperiplanar conformation with respect to the cyclobutane ring (see **3.91**, Scheme 3.21). We thought that we could use this in our advantage to recycle tetracycle **3.79** by means of a fragmentation reaction.<sup>[185]</sup> Since esters react with  $\text{Tf}_2\text{O}$  to yield unstable acyl triflates<sup>[186]</sup> we reacted instead alcohol derivative **3.91** with triflic anhydride in the presence of 2,6-di-*tert*-butyl-4-methylpyridine (DTMP) to provide enol triflate **3.92**, an intermediate that could be used to install the olefinic methyl group (Table 3.8).<sup>[187]</sup> When the reaction was run at room temperature the desired product **3.92** was obtained in 12% yield together with the same amount of *exo*-methylene product **3.93**, which results from elimination at the easily accessible methyl group (Entry 1). When the reaction temperature was lowered to 0 °C the yield improved to 24%, and the **3.92/3.93** ratio increased threefold (Entry 2). When performed at lower temperatures the reaction worked smoothly affording the desired product with increased yields and higher regioselectivity (Entries 3-4).

The last step of the synthesis was the Horner–Wasworth–Emmons reaction between phosphonate **3.74** and aldehyde **3.75** (Scheme 3.22). Given the high value of **3.75**, we decided to first run the reaction with simpler aliphatic aldehydes to find the most suitable reaction conditions. To the dianion of **3.74** generated by treatment with different *tert*-butoxide salts was added the corresponding aldehyde leading to the isolation of the different condensation products.

We first performed the reaction with isobutyraldehyde (**3.97**) using potassium, sodium and lithium *tert*-butoxide salts. Among these, the best yield was achieved with the latter. In addition, two different workups in combination with flash chromatography or HPLC were tested. The first method involved quenching with a saturated  $\text{NH}_4\text{Cl}$  solution followed by extraction (Table 3.9, Entry 1). In the second procedure, after quenching the reaction all solvents were evaporated under reduced pressure and the remaining residue was suspended in acetone, filtered and submitted to purification (no ext., Entries 2-3). The second method in combination with lithium *tert*-butoxide and HPLC purification gave **3.94** in excellent yield (97%, Entry 3). We confirmed the better performance of the lithium salt in the reaction with cyclohexanecarboxaldehyde (**3.98**), which delivered **3.95** in 75% yield, in contrast to the modest 52% for potassium *tert*-butoxide (Entries 4 and 5). The reaction with octanal (**3.99**) was completely unsuccessful upon extractive workup, but again the combination of lithium *tert*-butoxide with the alternative workup and HPLC purification delivered the natural product pyreudione C (**3.96**) in 71% yield (Entries 6 and 7).<sup>[98]</sup>

For aldehyde **3.75**, potassium *tert*-butoxide afforded the product in low yields and the combination of extractive workup with HPLC purification failed to provide (–)-PF-1018 (Entries 8-9). By using LiOt-Bu as base and after HPLC purification (–)-PF-1018 was obtained in 30% yield (Entry 10). Finally, we added additional equivalents of phosphonate **3.74** and LiOt-Bu and performed the extractive workup followed by flash chromatography. These conditions allowed for the isolation of (–)-PF-1018 in 47% yield (Entry 11). We assign the low yields to the unstable nature of aldehyde **3.75**, which decomposed slowly at room temperature. Not surprisingly, the reaction times varied notably depending on the starting aldehyde. The bulkier aldehyde **3.75**, required 26 hours to reach full conversion whereas with octanal the reaction was finished after 2.5 hours.



Entry	Aldehyde	μmol	Base	Base [eq.]	4.20 [eq.]	t [h]	Workup	Purif.	Yield [%]
1	<b>3.97</b>	35	KOt-Bu	3	1.5	22	ext.	Flash	37
2		17	NaOt-Bu	3	1.5	18	no ext.	HPLC	49
3		17	LiOt-Bu	3	1.5	18	no ext.	HPLC	97
4	<b>3.98</b>	17	KOt-Bu	3	1.5	4	no ext.	HPLC	52
5		17	LiOt-Bu	3	1.5	4	no ext.	HPLC	75
6		156	KOt-Bu	4	2	24	ext.	HPLC	trace
7		26	LiOt-Bu	3	1.5	2.5	no ext.	HPLC	71
8		7	KOt-Bu	6	3	24	ext.	Flash	20-30
9		7	KOt-Bu	6	3	20	ext.	HPLC	trace
10		8	LiOt-Bu	3	1.5	96	no ext.	HPLC	30
11		12	LiOt-Bu	5	2.5	26	ext.	Flash	47

ext.→ quench with NH<sub>4</sub>Cl, extraction, evaporation

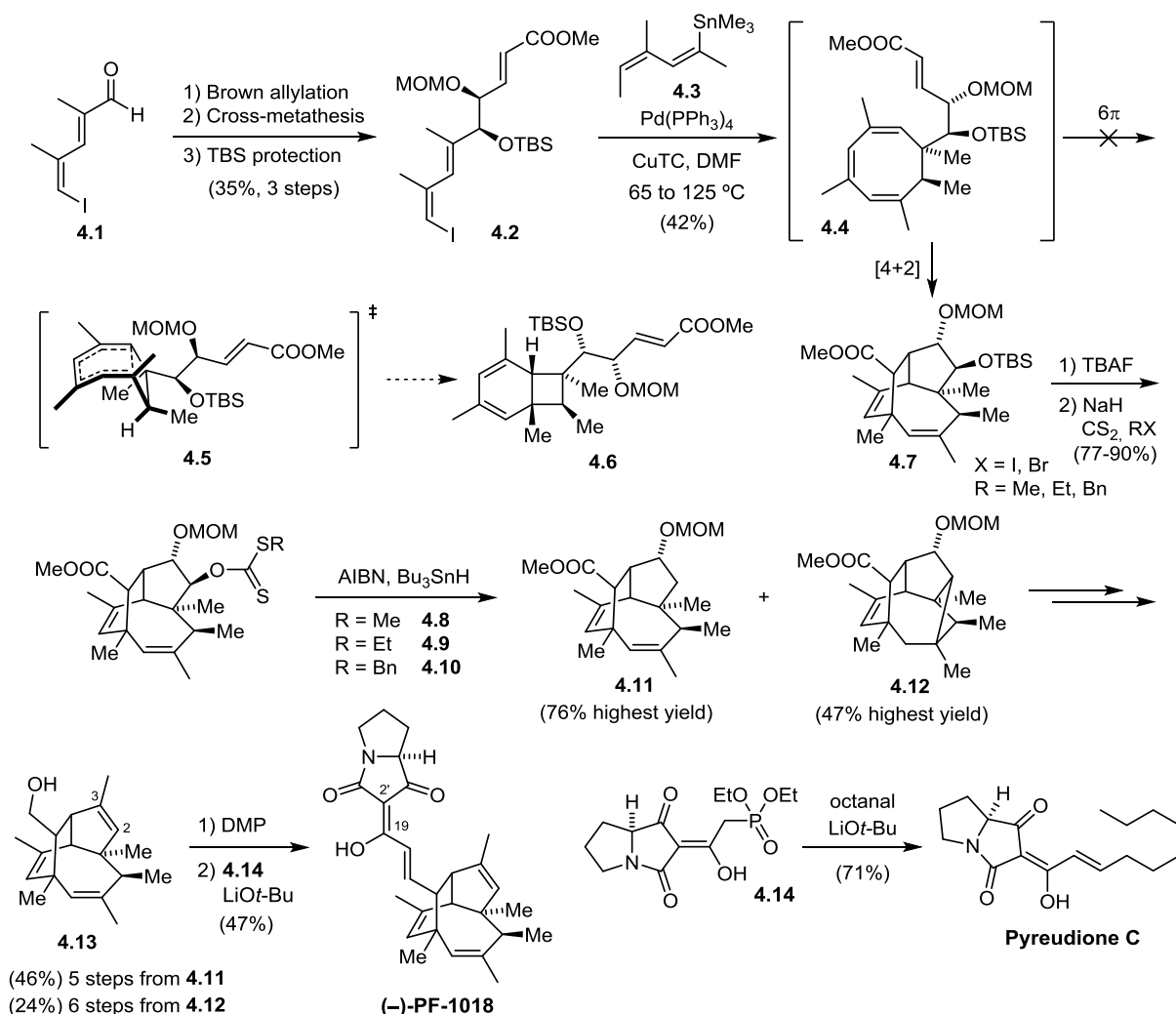
no ext.→ quench with NH<sub>4</sub>Cl, evaporation, suspension in acetone, filtration

**Scheme 3.22 and Table 3.9.** Reaction conditions screened for the HWE leading to (–)-PF-1018.

## 4. Summary and Outlook

The first total synthesis of (–)-PF-1018 was achieved using a biomimetic approach. The key step of the synthesis comprises an unprecedented Stille/ $8\pi$  electrocyclization/Diels–Alder cascade which is an exception to the ubiquitous  $8\pi/6\pi$  electrocyclization sequence which gives rise to all the other members of the Cyclooctatriene-Derived NP family, such as endiandric acids and the elysiapyrones. The regio- and diastereoselectivity of the key step was dictated by two protected hydroxy groups (**4.2**, Scheme 4.1), which promoted the  $8\pi$ /Diels–Alder pathway and inhibited the  $6\pi$  electrocyclization delivering the desired product in satisfactory yield. The synthesis of cascade precursor **4.2** was accomplished by means of a Brown allylation/cross-metathesis approach, which delivered the desired product with excellent enantiopurity and shortened a previous route by two steps.

The tricyclic core **4.7** obtained in the key step was deoxygenated by means of a highly optimized Barton–McCombie reaction using an uncommon benzyl xanthate (**4.10**). This reaction also gave variable amounts of a 4-*exo-trig* radical cyclization product (**4.12**) which could be recycled upon ring opening by means of a regioselective fragmentation triggered by triflic anhydride. Both routes reconverged into alcohol **4.13**, which was condensed with phosphonate ester **4.14** giving (–)-PF-1018. This phosphonate was also used to synthesize the natural product pyreudione C.



**Scheme 4.1.** Summarized synthesis of (–)-PF-1018.

With this synthesis we have shown how the introduction of substituents with a defined stereochemistry can modulate the reactivity of cyclooctatriene intermediates, proving that their chemistry goes beyond the classic  $8\pi/6\pi$  electrocyclization cascade. Moreover, given the interesting bioactivities displayed by other natural products bearing tetramic acids, our synthesis can be used to access (–)-PF-1018 to test its biological activity against new targets.

## **PART II – DEVELOPMENT OF PHOTOSWITCHABLE GABA<sub>A</sub> RECEPTOR POTENTIATORS**



## 5. Introduction

### 5.1 GABA<sub>A</sub> Receptors

GABA receptors (GABARs) are transmembrane protein assemblies that respond to gamma-aminobutyric acid or GABA. Once GABARs are activated, a sequence of events induces certain ions to flow through ion channels following concentration gradient and causing a repolarization of the membrane.<sup>[188]</sup>

Gamma aminobutyric acid is the most common inhibitory neurotransmitter found in the central nervous system (CNS) of mammals and is released by GABAergic neurons. GABA's main function is to keep the neuron's potential at or below the resting level (about  $-70$  mV), increasing the firing threshold and therefore reducing the chance of initiation of an action potential (AP).<sup>[188]</sup> GABA also influences brain development by regulating neuron proliferation and growth.<sup>[189–191]</sup>

The system formed by GABA and GABARs, together with other inhibitors of the nervous response, such as glycine receptors (GlyR),<sup>[192]</sup> act as a counterpart for the distinct excitatory systems of the CNS, the most prevalent of which in mammals are glutamate receptors (GluRs).<sup>[193]</sup> The balance between the excitatory and inhibitory neurotransmission generated by these mechanisms allows for the correct performance of the CNS. Decreased GABAR activity causes imbalances which provoke increased anxiety, fear, insomnia or seizures and disorders such as autism, epilepsy or depression.<sup>[194–196]</sup>

GABA receptors can be classified into two types, GABA<sub>A</sub> and GABA<sub>B</sub>.<sup>[197]</sup> The latter are metabotropic receptors mainly located at extrasynaptic sites which induce slow membrane polarization by efflux of potassium ions. GABA<sub>B</sub> receptors display a less marked effect on the inhibition of the AP and will not be further discussed here.<sup>[197]</sup>

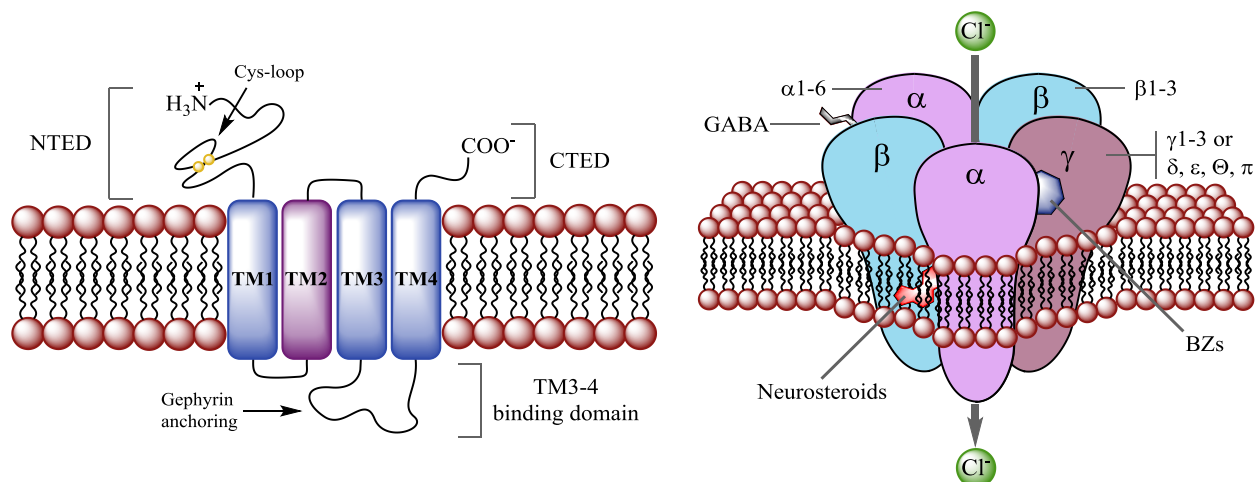


**Figure 5.1. Left.** Schematic representation of a GABA<sub>A</sub>R subunit comprising the N-terminal extracellular domain (NTED) with the cys-loop structure, 4 transmembrane domains (TM) connected by the corresponding amino acid chains, the TM3-4 binding domain where gephyrin binds and the C-terminal extracellular domain. **Right.** Schematic representation of a 2α2β1γ GABA<sub>A</sub>R assembly. The approximate binding sites of GABA, BZs and neurosteroids are indicated.

GABA<sub>A</sub>Rs are typically located in neuronal tissues but are also present in other organs. They belong to the Cys-loop super-family of the ligand-gated ion channels (LGIC), which also includes the nicotinic acetylcholine receptors, glycine receptors (GlyRs) and 5-HT<sub>3</sub> receptors.<sup>[198]</sup> All members of the family are formed by pentamers of analogous subunits, which contain an *N*-terminal extracellular domain (NTED) featuring a conserved 15-residue chain with a disulfide bridge forming the cysteine loop, 4 transmembrane (TM) domains, an intracellular TM3-4 binding domain, and an extracellular C-terminal domain (CTED). Five of these units assemble together to form a central ion channel. GABA<sub>A</sub>R and GlyR ion channels are anion selective due to the presence of several cationic residues on the pore surface.<sup>[192]</sup>

GABA<sub>A</sub>Rs are ionotropic receptors ubiquitous in CNS neurons which are activated by GABA and its isosteres (Figure 5.1). The binding of two molecules of GABA induces pore opening causing a flow of chloride anions into the cell making its potential more negative (polarization). As members of the Cys-loop superfamily, GABA<sub>A</sub>Rs are pentamers formed by limited combinations of 8 different subunit types with different variants: six types of  $\alpha$  subunit, three of  $\beta$ ,  $\gamma$ , and  $\rho$  and one known variant of  $\delta$ ,  $\epsilon$ ,  $\pi$ , and  $\theta$  subunits.<sup>[199]</sup> The sequence homology within one subtype is about 70%, whereas between classes it is only 30%.<sup>[200]</sup> The majority of the GABA<sub>A</sub>R subtypes contain two  $\alpha$ , two  $\beta$  and one  $\gamma$  unit, being  $\alpha 1\beta 2\gamma 2$  the most abundant and predominant in the mammalian brain, whereas the  $\rho$  containing subtypes are pseudo-homopentameric and prominently found in the retina.<sup>[201]</sup> The specific configuration of the GABA<sub>A</sub>Rs determines their channel and gating profile, pharmacokinetic properties as well as cell location and presence in different CNS regions. Table 5.1 shows the relative abundance and pharmacological roles of the different  $\alpha$  subunits.<sup>[202]</sup>

	$\alpha 1$	$\alpha 2$	$\alpha 3$	$\alpha 4$	$\alpha 5$
<b>Abundance</b>	60%	15-20%	10-15%	<5%	<5%
<b>Synaptic</b>	++	++	++	+	+
<b>Extrasynaptic</b>	+	–	+	++	++
<b>Functions</b>	Sedation, amnesia anticonvulsant Dependence	Anxiolysis Fear reduction Sensitivity to stress Myorelaxation Antihyperalgesia	Sensorimotor Myorelaxation Antihyperalgesia	Cognitive Alcohol intake	Anxiolysis Response to stress Sensorimotor Cognitive

**Table 5.1.** Location and function of the different GABA<sub>A</sub>R  $\alpha$  subunits.<sup>[202]</sup> + indicates that the minority of the receptors are located at the specified location. ++ indicates that the majority of receptors are located at the specified location. – indicates no presence of receptors at the specified location.  $\alpha 4$  is mostly extrasynaptic and present together with  $\delta$  subunits.  $\alpha 6$ , not shown here is mostly located at the cerebellum.

The majority of GABA<sub>A</sub>Rs cluster at the synaptic cleft of postsynaptic neurons anchored by proteins as gephyrin.<sup>[203]</sup> Gephyrin interacts with the loops of the TM3-4 intracellular binding chain, preferentially of GABA<sub>A</sub>R subtypes containing  $\alpha 1$ -3,  $\beta 2$ -3 and  $\gamma 2$  subunits<sup>[204,205]</sup> (Figure 5.1). The high local concentration of GABA at the synaptic cleft leads to fast receptor binding and chloride channel opening, mediating phasic inhibition that occurs within a few milliseconds. Other GABA<sub>A</sub>Rs are located at the extrasynaptic membrane causing tonic inhibition, which is constant (lasting for minutes or hours) and weaker given the low concentration of GABA in the extracellular medium.<sup>[202,206]</sup>

The affinity for GABA depends on the receptor subtypes. Generally, those responsible for keeping a tonic current and located outside of the synaptic cleft display much higher affinities given the lower concentration of GABA outside of the synapses. Thus, GABA<sub>A</sub>Rs expressed in *Xenopus* oocytes containing  $\alpha 4\beta 1\delta$   $\alpha 4\beta 3\delta$  subunits are activated by nanomolar concentrations of GABA, whereas  $\alpha 4\beta 2\delta$  is only activated at micromolar concentrations.<sup>[207]</sup>

## 5.2 The GABA Binding Site, GABA<sub>A</sub>R Agonists and Antagonists

The GABA binding site is located at the ECD of the  $\alpha/\beta$  subunit interface, and a large number of amino acids are implicated in its binding.<sup>[208]</sup> The exact location was corroborated by the works of Zhu and Aricescu, who unravel the structure of the  $\alpha 1\beta 2\gamma 2$  and  $\alpha 1\beta 3\gamma 2$  GABA<sub>A</sub>R complexes by means of high-resolution cryo-electron microscopy (cryo-EM)<sup>[208,209]</sup> (Figure 5.2). Thus, in subtypes containing two  $\alpha$ , two  $\beta$  and one  $\gamma$  units two binding sites for GABA exist, but the asymmetry of the heteropentameric complex given by the presence of the  $\gamma$  unit results in a three-fold higher affinity of GABA for one of the pockets. This affinity is reversed for the conformationally restricted analogues muscimol and tetrahydroisoxazolo-pyridinol (THIP).<sup>[210]</sup> When one GABA molecule binds to the receptor channel, opening occurs just to a small extent. When a second unit binds the open probability increases by more than 60-fold and chloride ions rush into the postsynaptic neuron.<sup>[210]</sup> The conformational change responsible for the channel opening induces closing of a large region of the receptor at the  $\alpha/\beta$  interface trapping the agonists inside the binding pockets<sup>[208,209,211]</sup> (Figure 5.2).

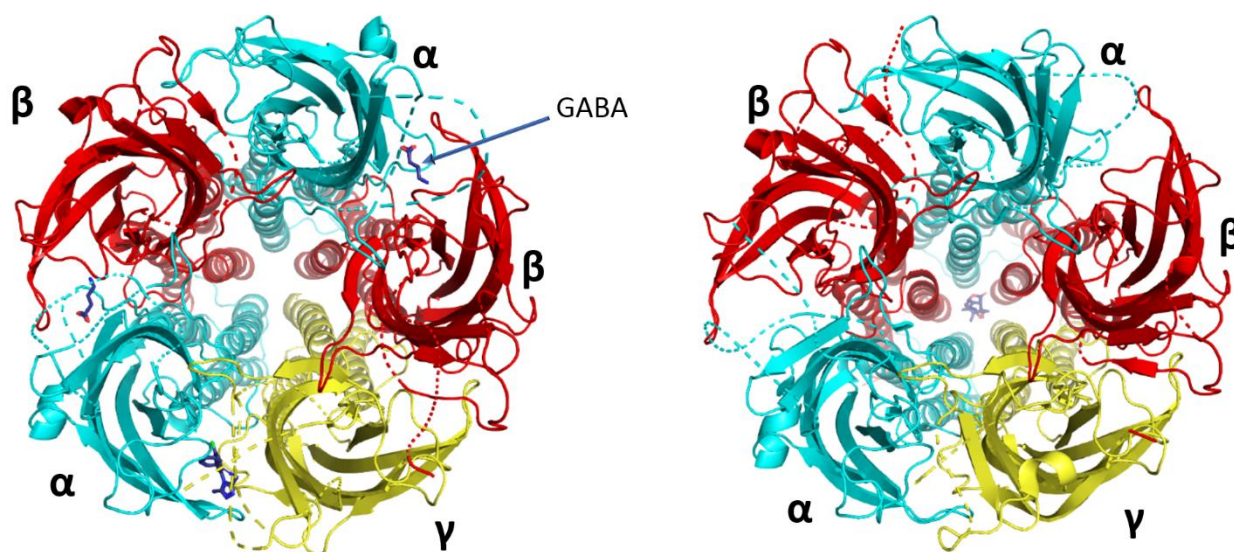


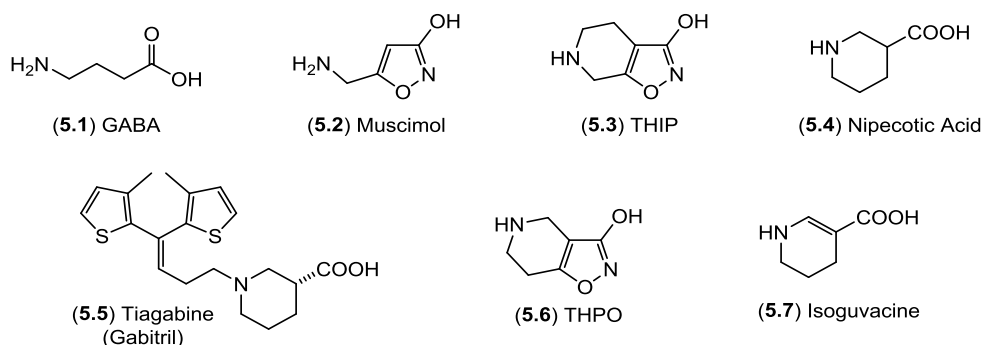
**Figure 5.2. Left.** Structure of a desensitized  $\alpha 1\beta 3\gamma 2$  subtype GABA<sub>A</sub>R bound to two units of GABA and alprazolam by Aricescu.<sup>[209]</sup> Binding sites for GABA can be found at the  $\alpha/\beta$  interfaces and alprazolam at the  $\alpha/\gamma$  interface. Comparison with the right structure highlights the free pore structure and the tight conformation of the  $\beta$  loops around the GABA neurotransmitters. **Right.** Structure of a picrotoxin-blocked  $\alpha 1\beta 3\gamma 2$  subtype GABA<sub>A</sub>R by Aricescu.<sup>[209]</sup> It can be observed how the red  $\beta$  loops are in an opened conformation in contrast with the left structure and how the constriction of the central TM2 units close the pore around picrotoxin. . Images from PDB database created with PyMOL.<sup>[212,213]</sup>

## 5.2.1 GABA<sub>A</sub> Receptor Agonists

GABA is the main endogenous agonist of GABA<sub>A</sub>Rs, although several molecules can replicate or antagonize its function by binding to the same or different pockets. Most GABA<sub>A</sub>R agonists are derived from GABA by restricting different conformations by means of ring incorporation (Scheme 5.1).

### 5.2.1.1 Muscimol

Muscimol, a constituent of the *Amanita muscaria* mushroom, is a potent agonist of the GABA<sub>A</sub>R and partial agonist of the  $\rho$  receptor subtype.<sup>[214]</sup> Its binding affinity and potency are higher for extrasynaptic receptors bearing  $\alpha 4\beta 3\delta$  subunits, on which it acts as a superagonist at high concentrations by reducing receptor desensitisation.<sup>[215]</sup> These and other properties make muscimol a hypnotic, depressant and inhibitor of memory retention by action on CNS GABA<sub>A</sub>Rs and an alleviator of airway constriction by action on peripheral GABA<sub>A</sub> receptors.<sup>[216,217]</sup> Muscimol has been used to study the pharmacology of GABA<sub>A</sub>Rs and as a lead compound for the development of related substances showing increased GABA<sub>A</sub>R affinity. Derivatives of muscimol such as THIP, THPO, nipecotic acid, isoguvacine or tiagabine, act as true inhibitors of GABA uptake and display anticonvulsant effects. Among these, tiagabine is an approved drug under the commercial name of Gabitril (Scheme 5.1).<sup>[214,215]</sup>



**Scheme 5.1.** Structure of gamma-aminobutyric acid and related agonists.

### 5.2.1.2 THIP

The GABA agonist THIP (tetrahydroisoxazolo-pyridinol, also known as gaboxadol) is a restricted analogue of muscimol which exhibits higher selectivity for certain GABA<sub>A</sub>R subtypes. Similar to muscimol, **5.3** binds preferentially and with high affinity to extrasynaptic GABA<sub>A</sub>Rs (eGABA<sub>A</sub>Rs) bearing  $\alpha 4\delta$  subunits, with channel activation taking place at nanomolar concentrations whereas lack of the  $\delta$  subunit causes a marked decrease in activity.<sup>[218]</sup> THIP also acts as a superagonist on the GABA<sub>A</sub>R  $\alpha 4\beta 3\delta$  subtype but in a different way than muscimol; instead of reducing desensitisation, **5.3** increases the duration and frequency of channel openings.<sup>[215]</sup> Unlike GABA or muscimol, THIP also works as an antagonist for GABA<sub>A</sub>  $\rho$  subtypes.<sup>[214]</sup> Given the unique performance of THIP at the molecular level it is not surprising that **5.3** also displays interesting pharmacological effects acting as a potent analgesic and hypnotic by mediating tonic inhibition at extrasynaptic sites, differently from other hypnotic drugs such as zolpidem and zaleplon which induce synaptic phasic inhibition. It was therefore considered as a candidate for the treatment of Huntington's disease, Alzheimer's disease and for the treatment of insomnia, but the studies were cancelled due to safety and efficacy concerns.<sup>[219,220]</sup>

## 5.2.2 GABA<sub>A</sub> Receptor antagonists

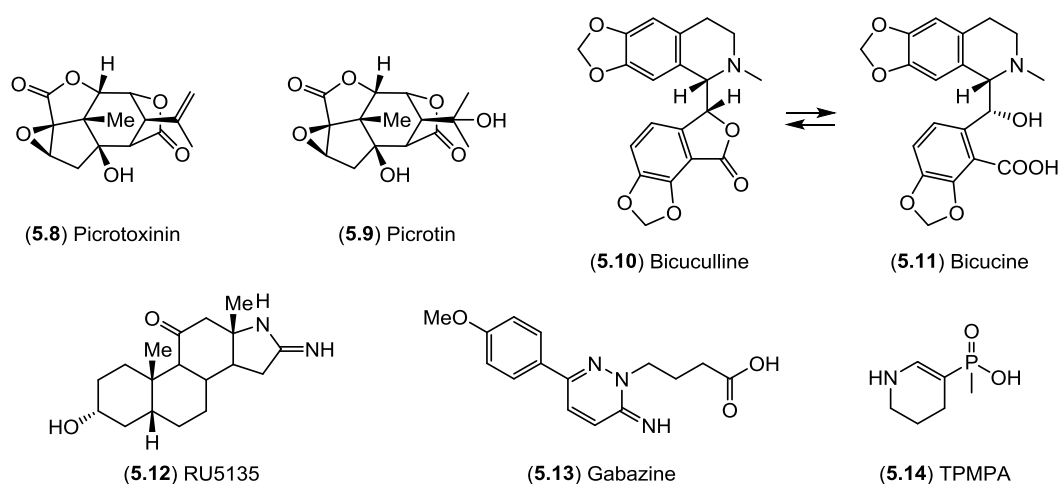
Unlike for GABA<sub>A</sub>R agonists, the activity of most antagonists is independent of the receptor-subunit composition and hence the potencies displayed on different subtypes are often very similar.

### 5.2.2.1 Bicuculline, RU5135 and TPMPA

Bicuculline's convulsant properties were first described in the 1960's.<sup>[221]</sup> Problems in reproducing the results revealed that bicuculline (**5.10**) is converted into the almost inactive bicucine (**5.11**) at physiological pH and that bicuculline can be recovered upon acidic treatment of **5.11**.<sup>[222,223]</sup> This problem could be overcome by using quaternary ammonium salts of **5.10**, but these exhibit off-target effects and do not cross the blood-brain barrier as easily as bicuculline, thus requiring injection.<sup>[224]</sup> **5.10** is a potent competitive antagonist of all kinds of GABA<sub>A</sub>Rs with the exception of  $\alpha 6$  subtypes (displaying milder effects) and  $\rho$  subtypes, which remain unaffected. Bicuculline prevents the open state by stabilizing  $\beta$  subunit rotation (Figure 5.2, right), encouraging the closed conformation of the GABA<sub>A</sub>R. Moreover, it has been found that **5.10** can also act as an allosteric inhibitor.<sup>[225]</sup> Gabazine, also a competitive GABA<sub>A</sub>R antagonists displays very similar properties.<sup>[226]</sup>

RU5135 is a steroid derivative. This competitive GABA<sub>A</sub>R antagonist is 500 times more potent than bicuculline but is not as specific and affects glycine receptors.<sup>[225]</sup>

Substitution of the acid group of GABA<sub>A</sub>R agonist isoguvacine by a methylphosphinic acid yields TPMPA (tetrahydropyridinyl methylphosphinic acid), which acts as a potent and selective  $\rho$  subtype GABA<sub>A</sub>R competitive antagonist, and only as a weak antagonist for other GABA<sub>A</sub>R subtypes. It shows 8-fold increased selectivity for human  $\rho 1$  over  $\rho 2$  GABA<sub>A</sub> subtype receptors. This selectivity for  $\rho$  subunits involves the lack of convulsant properties and makes of TPMPA a candidate in the treatment of myopia.<sup>[227]</sup>



**Scheme 5.2.** Structures of GABA<sub>A</sub>R antagonists.

### 5.2.2.2 Picrotoxin

Picrotoxin was the first non-competitive antagonist of GABA<sub>A</sub>Rs discovered. It was isolated from the fruit of *Anamirta cocculus* and can be accessed by total synthesis.<sup>[228,229]</sup> Picrotoxin is a 1:1 mixture of picrotoxinin (**5.8**) and picrotin (**5.9**) of which **5.8** is the more active species. Picrotoxin shows convulsant properties derived from induced stabilization of the closed form of the GABA<sub>A</sub>R and other Cys-loop superfamily

members, such as GlyRs and 5-HT<sub>3</sub> receptors, which occurs even in the presence of GABA.<sup>[209,230]</sup> The exact mechanism has been described by Ariescu by means of cryo-EM, showing how picrotoxin binds to the opened channel and subsequently stabilizes the closed state, explaining the previously observed properties as channel blocker and allosteric antagonist.<sup>[209]</sup>

## 5.3 Elucidation of GABA<sub>A</sub> Receptor Binding Sites

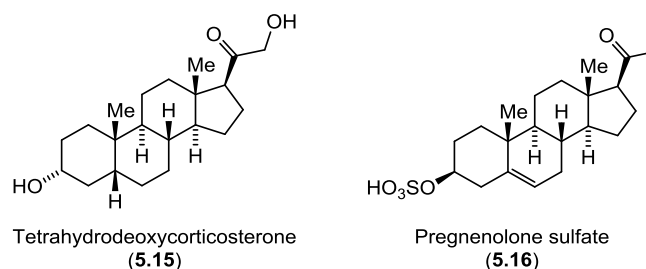
Multiple binding sites are present at GABA<sub>A</sub>R constructs as a result of the complexity of its assembly formed by limited combinations of 19 different subunits, the most ubiquitous of which comprises two  $\alpha$ 1, two  $\beta$ 2 and one  $\gamma$ 2 subunits (simply named  $\alpha$ 1 $\beta$ 2 $\gamma$ 2).<sup>[197]</sup>

Until recently, the architecture and binding sites within GABA<sub>A</sub>Rs had been mostly studied by means of radioligand binding, photolabeling, mutagenesis and homology models based on other members of the LGIC superfamily, as for example the *Torpedo marmorata* nicotinic acetylcholine receptor (nAChR), unveiled in 2005 by Unwin et al. or the high resolution structure of *Erwinia chrysanthemi*'s ligand-gated ion channel.<sup>[231,232]</sup> However, in the past few years major achievements on the knowledge of GABA<sub>A</sub>R structures and binding sites have been made. In 2014 the structure of a homopentameric  $\beta$ 3 GABA<sub>A</sub>R was solved by Miller and Aricescu.<sup>[233]</sup> In 2017 Duncan, Lavery and others presented the structure of a GABA<sub>A</sub>R  $\alpha$ 1 subunit chimera with NTED and TM3-4 binding region of a prokaryotic LGIC, helping to identify the binding sites of some neurosteroids.<sup>[234]</sup> In 2018, a cryo-EM structure of the  $\alpha$ 1 $\beta$ 2 $\gamma$ 2 GABA<sub>A</sub>R-Fab complex, the most predominant form in the human adult brain, was published, including bound flumazenil and GABA.<sup>[208]</sup> In 2019, Ariescu presented several cryo-EM structures of  $\alpha$ 1 $\beta$ 3 $\gamma$ 2 GABA<sub>A</sub>R bound to GABA, alprazolam, diazepam and picrotoxin, describing binding modes and mechanistic effects of these ligands (Figures 5.2 and 5.4).<sup>[209]</sup> The binding site of flumazenil at the  $\alpha$ / $\gamma$  interface was precisely defined giving a very high level of detail allowing for identification of binding poses and interactions.

## 5.4 GABA<sub>A</sub>R Allosteric Modulators

### 5.4.1 Neurosteroids

In addition to GABA, other endogenous ligands such as neurosteroids can bind to GABA<sub>A</sub>Rs. Neurosteroids are synthesized within the CNS by glial cells and neurons from cholesterol, but can also be exogenously administered.<sup>[235]</sup> Their main target are GABA<sub>A</sub>Rs, where they most often act as positive allosteric modulators (PAMs) influencing mood and behaviour through anxiolytic, analgesic, anticonvulsant, sedative, hypnotic and anaesthetic effects. Several binding sites have been identified but many of them do not exert allosteric effects.<sup>[236]</sup> In this regard, binding sites at the  $\alpha$ / $\beta$  interface on the inner edge of the TMD bind tetrahydrodeoxycorticosterone and similar steroids (with higher affinity for  $\beta$ 3 and  $\alpha$ 1 subunits) inducing positive allosteric modulation (Figure 1). Another allosteric binding site is present at the  $\alpha$  subunit TMD, where pregnenolone sulfate binds with high affinity acting as a negative allosteric modulator (NAM).<sup>[234]</sup>



**Scheme 5.3.** Structures of neurosteroids acting as PAM (5.15) and NAM (5.16) on GABA<sub>A</sub>Rs.

## 5.4.2 Anaesthetics

The clinical effect of anaesthetics involves a temporary loss of awareness or sensation. GABA<sub>A</sub> receptors are an important target for anaesthetic drugs, which entail substances such as barbiturates, propofol, etomidate or ketamine. Despite the fact that some of these drugs do not bind to the same binding site, the main pockets are thought to be close to each other at the TM2 of  $\beta$  subunits.<sup>[237]</sup>

### 5.4.2.1 Propofol

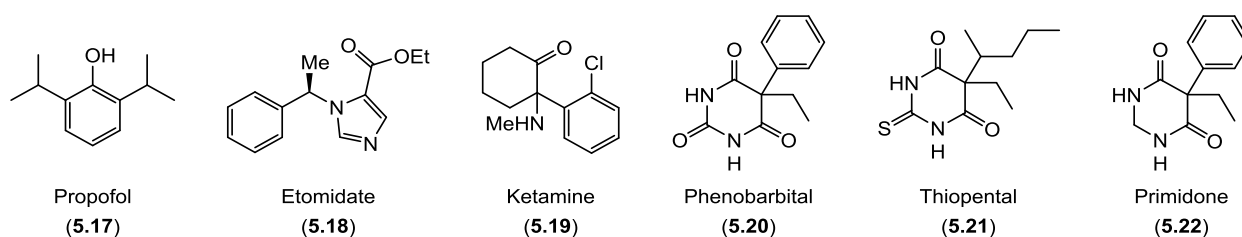
Propofol (5.17) is used for fast-acting general anaesthesia. 5.17 binds to the TMD2 of  $\beta$  subunits close to the etomidate binding pocket.<sup>[238,239]</sup> However, its affinity for GABA<sub>A</sub>Rs is affected by changes at  $\alpha$ ,  $\gamma$  and  $\delta$  subunits, suggesting that it binds to other sites depending on the receptor subtype. Propofol acts as a PAM at low concentrations and as a GABA agonist at high concentrations. The alcohol group is critical for its activity.<sup>[240]</sup>

### 5.4.2.2 Etomidate

Etomidate is used as a short-acting anaesthetic, sharing most of its properties with propofol. It is sensitive to  $\beta$ 2 and  $\beta$ 3 and insensitive to the  $\beta$ 1 subunit. The binding site is located at TM2, probably overlapping with the volatile anaesthetic binding site.<sup>[241]</sup> Mutation of key residues at  $\beta$ 2 and  $\beta$ 3 subunits suppressed its binding, with similar effects on propofol. These results suggested that they either share the same binding pocket or bind to proximal sites.<sup>[242]</sup>

### 5.4.2.3 Barbiturates

Barbiturates display anticonvulsant, anxiolytic, sedative and hypnotic effects, with a relatively narrow therapeutic window and high death risk in case of overdose. They also cause addiction, deep sedation and depression of the CNS activity including respiratory function. For these reasons they have been substituted by the safer benzodiazepines and Z-drugs. The barbiturates are still used for general anaesthesia (thiopental) and the treatment of epilepsy (phenobarbital, primidone).<sup>[243,244]</sup> Their structure features a pyrimidinetrione core with different substitution patterns at the  $sp^3$  carbon (Scheme 5.4).



**Scheme 5.4.** Anaesthetic compounds active on GABA<sub>A</sub>Rs.

Although barbiturates bind to GABA<sub>A</sub>Rs with lower affinity than other allosteric modulators, they act as potent GABA<sub>A</sub>R PAMs and enhance the binding affinity of the receptor to benzodiazepines while inhibiting the binding of some NAMs.<sup>[206]</sup>

Barbiturates act in three different ways depending on concentration. At low micromolar levels they act as PAMs. Above 50  $\mu$ M they behave as agonists, causing channel opening without need for GABA. When bound to  $\alpha 6$  subtype receptors the barbiturates cannot be displaced by competitive antagonists and cause more intense responses than GABA.<sup>[206]</sup> At high mM range, they block GABA induced current.<sup>[245]</sup> This behaviour can be explained by the presence of different binding sites with different pharmacological effects, two of which have been identified at the  $\alpha/\beta$  and the  $\gamma/\beta$  interfaces in the TMD.<sup>[246]</sup> Point mutations at  $\beta 1$  subunits blocked the allosteric function without affecting the agonistic or inhibitory effects of pentobarbital, supporting that these distinct action modes are mediated by different binding sites.<sup>[247]</sup> The selectivity of barbiturates for different GABA<sub>A</sub>R subtypes is rather low, but this is partially compensated by the variable potencies displayed on different receptor types.<sup>[245]</sup>

### 5.4.3 Ethanol

Ethanol acts as a PAM of tonic currents associated to extrasynaptic GABA<sub>A</sub>R bearing  $\delta$  subunits.<sup>[248]</sup> It has been reported that the potentiating effect of ethanol in tonic currents takes place at or below 30 mM concentration, and near to 10 mM for the more sensitive  $\alpha 4/6\beta 3\delta$  GABA<sub>A</sub>R subtype, although these experiments could not be reproduced.<sup>[206]</sup> The ethanol binding site is thought to overlap with the secondary imidazobenzodiazepine Ro15-4513 (Scheme 5.5) binding site at the  $\alpha 4,6+/\beta 3-$  interface, which is analogous to the classical  $\alpha/\gamma$  benzodiazepine binding site. This is in agreement with the fact that Ro15-4513 acts as an alcohol competitive antagonist in rats.<sup>[206]</sup> Moreover, the fact that flumazenil does not display these effects suggest that ethanol binds close to the azido-site of Ro15-4513's binding pocket.<sup>[248]</sup> Rats treated with ethanol show dramatic  $\delta$  subtype GABA<sub>A</sub>R downregulation.<sup>[188]</sup> It has been speculated that many of the effects induced by ethanol on GABA<sub>A</sub>R currents may be caused by its ability to increase neurosteroid levels, which favour GABA<sub>A</sub>R responses.<sup>[199]</sup> This is supported by the fact that these effects are inhibited by blockers of steroid synthesis.<sup>[249]</sup>

### 5.4.4 Benzodiazepines

#### 5.4.4.1 General Aspects

Benzodiazepines (BZs) have been used for treatment of anxiety, panic attacks, epilepsy, muscle relaxation and sleep disorders for more than 50 years.<sup>[250]</sup> Almost all clinically used benzodiazepines target GABA<sub>A</sub>R subtypes with low selectivity,<sup>[251]</sup> causing several side effects such as sleepiness, anterograde memory loss and ataxia, in addition to tolerance and physical and psychological dependence.<sup>[251,252]</sup>

BZs can act as positive allosteric modulators (PAMs, or potentiators), negative allosteric modulators (NAMs) or "benzodiazepine site antagonists". The classical BZ drugs (like diazepam, flunitrazepam or lorazepam) and most commercial drugs of this type are potentiators that increase the response generated by the GABA<sub>A</sub>R at a given GABA concentration. Hence, when BZs bind to the benzodiazepine binding site they induce conformational changes on the GABA<sub>A</sub>R increasing its affinity for GABA. This is followed by pore opening at lower neurotransmitter concentrations without increasing the maximal current.<sup>[253]</sup> These effects seem to be reciprocal, since GABA and its agonists stimulate BZ binding and inhibit binding of inverse agonists at benzodiazepine binding site.<sup>[206]</sup>



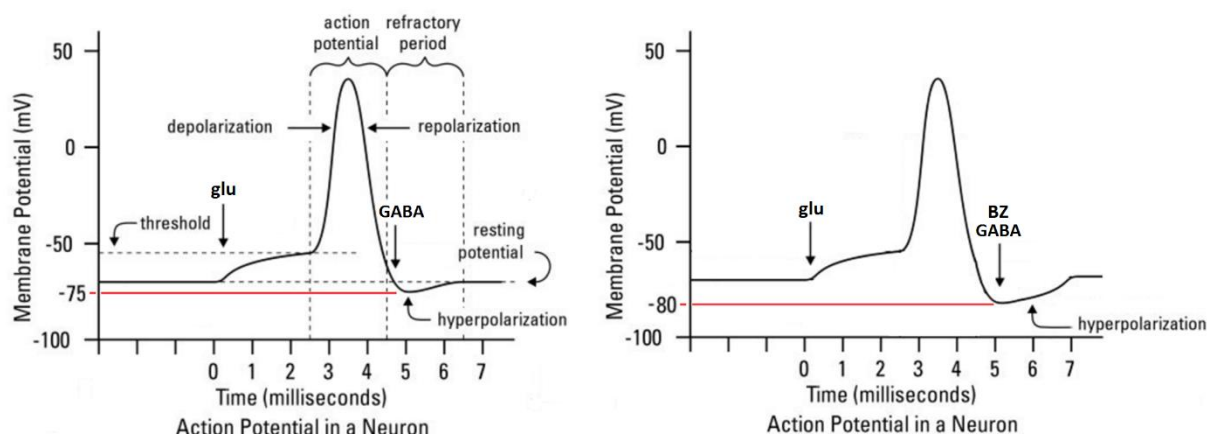


**Figure 5.3. Left.** Graphical representation of firing potential in neurons. Below time 0 the neuron is at resting state with an approx. potential of  $-70$  mV. When the glutamate receptors (glu) are activated, a flow of  $\text{Na}^+$  ions from the extracellular medium enters the cell and partially depolarizes the membrane. When a threshold of about  $-55$  mV is reached, additional sodium channels open starting an action potential which fully depolarizes the membrane. This is followed by a refractory period when the opening of  $\text{GABA}_A$ R channels causes hyperpolarization of the membrane at about  $-75$  mV. The hyperpolarization inhibits a new AP since the triggering threshold is harder to reach. **Right.** The same process in the presence of benzodiazepines. The higher affinity of  $\text{GABA}_A$ Rs for GABA induced by BZs causes a more marked hyperpolarization, which in this case reaches  $-80$  mV. The  $-55$  mV threshold is now further from the current membrane potential than in the absence of benzodiazepines.

NAMs display the opposite effect, lowering the affinity of  $\text{GABA}_A$ Rs for GABA, so that higher concentrations of the neurotransmitter are needed to induce channel opening.<sup>[254]</sup> Examples of these type of BZs are Sarmazenil or Ro15-4513 (Scheme 5.5). The “benzodiazepine site antagonists” used as benzodiazepine antidotes (flumazenil), displace ligands bound to the BZ binding site and recover the native activity of the  $\text{GABA}_A$ R.<sup>[255]</sup>

#### 5.4.4.2 Benzodiazepine Binding Sites

The BZ binding site is located at the  $\alpha/\gamma$  interface of the ECD and is chemically very similar to the GABA binding site, found at the  $\alpha/\beta$  junction. This explains why BZDs act as agonists at high concentrations although with low efficacy.<sup>[256]</sup>

Depending on the binding affinity of the BZ dictated by the different  $\alpha$  subunits, the receptors can be classified as diazepam-sensitive (containing  $\alpha 1,2,3,5$  subunits) or diazepam-insensitive (containing  $\alpha 4$  or  $\alpha 6$  subunits).<sup>[257]</sup> Diazepam is considered a “classical benzodiazepine”, meaning that it comprises a 5-phenyl-1,4-benzodiazepine structure, the same as flunitrazepam or lorazepam.<sup>[258]</sup> The diazepam-sensitive group can be further subdivided in 2 groups: type I BZ receptors, containing  $\alpha 1\beta\gamma 2$  subunits, which bind preferentially PAM benzodiazepines, and type II BZ receptors, containing  $\alpha 2,3,5\beta\gamma 2$  subunits and showing 10-fold decreased affinity for BZ PAMs.<sup>[206]</sup>

A specific histidine residue, H101 at the  $\alpha 1$  subunit, with homologous residues in  $\alpha 2,3$  and 5 is key for the high affinity of the receptor for BZs. When H101 is replaced by arginine the sensitivity for benzodiazepines decreases dramatically, explaining why classical BZs do not show any significant binding to  $\alpha 4,6$  containing receptors, which lack this residue. The cryo-EM structure of diazepam-bound  $\alpha 1\beta 3\gamma 2$   $\text{GABA}_A$ R confirmed these results.<sup>[209,259,260]</sup>

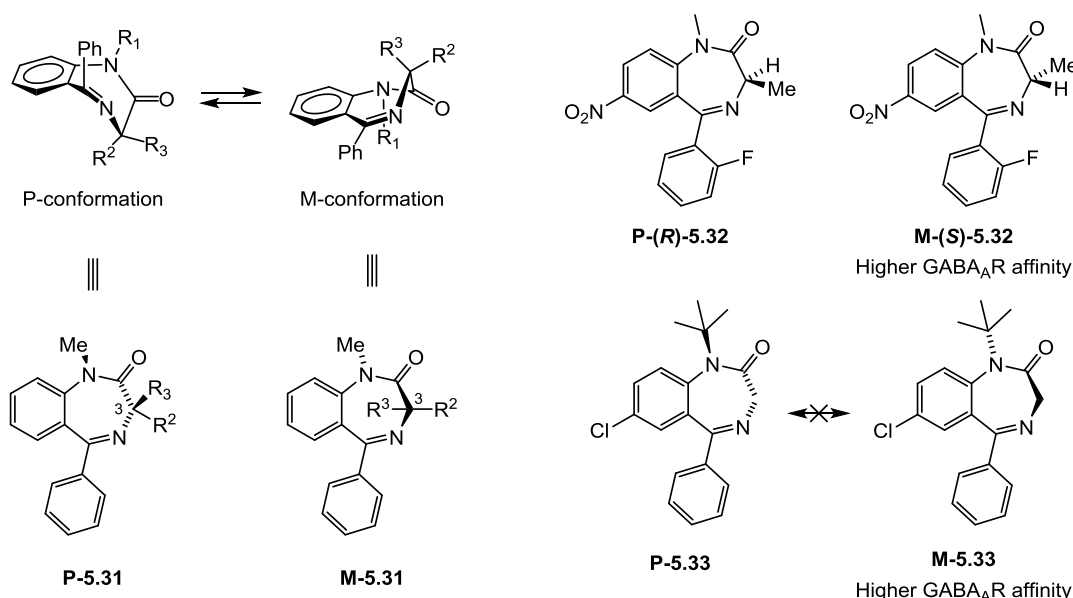


Effects of BZDs on memory are also attributed to the activity on tonic receptors bearing  $\alpha 5$  subunits (type II BZ receptors) mainly found at the hippocampus. This is based on the observation that deletion of this subunit in rats caused improved spatial learning.<sup>[263]</sup> New drugs based on the BZ scaffold are being developed in an effort to achieve higher selectivity for these receptor subtypes. For example, basmisanil (Scheme 5.5) has been designed trying to address disorders derived of schizophrenia or Down syndrome.<sup>[264,265]</sup>

Given the high similarities between type I and type II BZ receptors and the great abundance of high-affinity GABA<sub>A</sub>R subtypes containing  $\gamma 2$  subunits, which represent 75-90% of the GABA<sub>A</sub>Rs,<sup>[270]</sup> the design of BZs displaying selective GABA<sub>A</sub>R binding entails a major challenge. Alternative strategies include the design of ligands capable of exerting different degrees of potentiation on different receptor subtypes despite of binding non-selectively.<sup>[271]</sup> Another option would involve targeting the additional BZ binding sites, although the affinity for those is notably lower.<sup>[267]</sup> Finally, the use of photoswitchable benzodiazepine ligands could render the drug active only in specific areas of the brain at a given time, thus minimizing the side effects caused by BZ promiscuity.

### 5.4.4.3 Benzodiazepine Binding Modes

Benzodiazepines exist as an equilibrium of two conformers, P and M, in which the diazepine ring can flip to either face of the plane of the benzene ring (Scheme 5.6, left). When no substituents are present at C3, the interconversion of both forms occurs fast at room temperature yielding a racemic mixture with a calculated energy barrier of 12.3 kcal/mol for *N*-unsubstituted benzodiazepines.<sup>[272]</sup> When substituents other than H are present at C3, the conformation with the bulkiest substituent at a pseudo-equatorial position is favoured ( $R^3$  for P and  $R^2$  for M conformation, Scheme 5.6, left). Binding studies with 3-methylflunitrazepam (**5.32**), showed that the (*S*)-enantiomer, stabilized in M conformation, binds to GABA<sub>A</sub>Rs with 200 times more affinity than the (*R*)-isomer, most stable at the P conformation.<sup>[273]</sup> Further studies confirmed this binding preference with ethyl and *iso*-propyl C3 substituted BZs.<sup>[274]</sup> The energy barrier for ring flip can be increased upon introduction of bulky substituents at the amide nitrogen.<sup>[272]</sup> Hence, by introducing a *tert*-butyl substituent at  $R^1$ , Gilman and co-workers at Hoffmann-LaRoche could separate M and P isomers, confirming that the M conformers bind preferentially independently of the substitution pattern at C3.<sup>[272]</sup>



**Scheme 5.6.** Left. *P* and *M* atropisomers of a classical benzodiazepine. Right. Chiral benzodiazepines which confirmed the preference of the *M*-conformer for GABA<sub>A</sub>R binding. The *tert*-butyl group increases the energy barrier needed to interconvert both enantiomers allowing for individual testing of each atropisomer.

Years later, docking studies on species similar to **M-5.32** performed by Ernst, Sigel and others identified different BZ binding modes.<sup>[275]</sup> Three different BZ types were examined, all of them as C3-Me enantiomeric pairs leading to two possible binding modes named BM I and BM II (**5.34-5.36**, Scheme 5.7, A). The docking studies predicted that for all BZ types BM I was compatible with both (*R*) and (*S*) enantiomers, whereas BM II could only accommodate the (*S*) enantiomer given the steric clash caused by the C3-Me group of the (*R*) isomer with the receptor (Table 5.2). Hence, a similar affinity for GABA<sub>A</sub>Rs would be expected for both enantiomers of a BZ type if these would bind using BM I, whereas if using BM II, the (*S*) enantiomer would display a higher affinity for the receptor (Table 5.2). Indeed, when radioligand displacement experiments were performed on  $\alpha 5\beta 2\gamma 2$  GABA<sub>A</sub>R subtypes, only diazepam and triazolam derivatives **5.34** and **5.35** showed marked binding differences for (*R*) and (*S*) forms (>300 and >125 fold respectively), whereas (*R*) and (*S*) imidazobenzodiazepines **5.36** displayed similar affinities (Scheme 5.7, A; Table 5.2). The results strongly suggested that these BZs bind in different binding modes.<sup>[276]</sup>

**A**

	S	5.34	R	S	5.35	R	S	5.36	R
<b>BM I binding</b>	Y		Y	Y		Y	Y		Y
<b>BM II binding</b>	Y		N	Y		N	Y		N
<b>Binding Affinity</b>	31 nM		>10 $\mu$ M	80 nM		>10 $\mu$ M	17 nM		56 nM

**B**

**5.37**  
Ki = 11 nM

**5.38**  
Ki = 218 nM

**Scheme 5.7 and Table 5.2. A.** Studies on BZ binding modes by Sigel and Ernst. (*S*) enantiomers of benzodiazepines **5.34** and **5.35** bind with much higher affinity to  $\alpha 5\beta 2\gamma 2$  GABA<sub>A</sub>Rs than (*R*) enantiomers, as predicted by BM II. Both enantiomers of imidazobenzodiazepine **5.36** bind with similar affinity to  $\alpha 5\beta 2\gamma 2$  GABA<sub>A</sub>Rs as predicted by BM I. **B.** Two of the several ligands found in a virtual screening campaign using the docking parameters of BM II. **5.37** comprises a Z-drug structure and displayed a GABA<sub>A</sub>R affinity comparable to that of diazepam.

These results were in good agreement with previous studies based on radioligand displacement and covalent binding experiments that pointed flumazenil as a candidate for BM I and diazepam for BM II.<sup>[277,278]</sup> A virtual screening for new high-affinity binding partners based on BM II delivered 30 candidates with affinities below 20  $\mu$ M, of which **5.37** equalled diazepam.<sup>[277,278]</sup> **5.37** was later used by us as a lead compound for the development of photoswitchable Z-drugs (see Chapter 6.2).

Binding mode I was later confirmed by Zhu, who resolved the cryo-EM structure of  $\alpha 1\beta 3\gamma 2$  GABA<sub>A</sub>R subtype bound to flumazenil (Figure 5.4, Right).<sup>[208]</sup> Zhu argued that diazepam and other classical benzodiazepines would bind at the same pocket sharing the pose of flumazenil, claim which was contradicted by Sigel, who replied that diazepam would most likely bind using BM II.<sup>[279]</sup> Sigel's prediction was confirmed in 2019 by Aricescu, who published the structure of  $\alpha 1\beta 3\gamma 2$  GABA<sub>A</sub>R bound to diazepam in a strikingly similar pose as the one calculated by Sigel and Ernst (Figure 5.4, Left).<sup>[276]</sup>

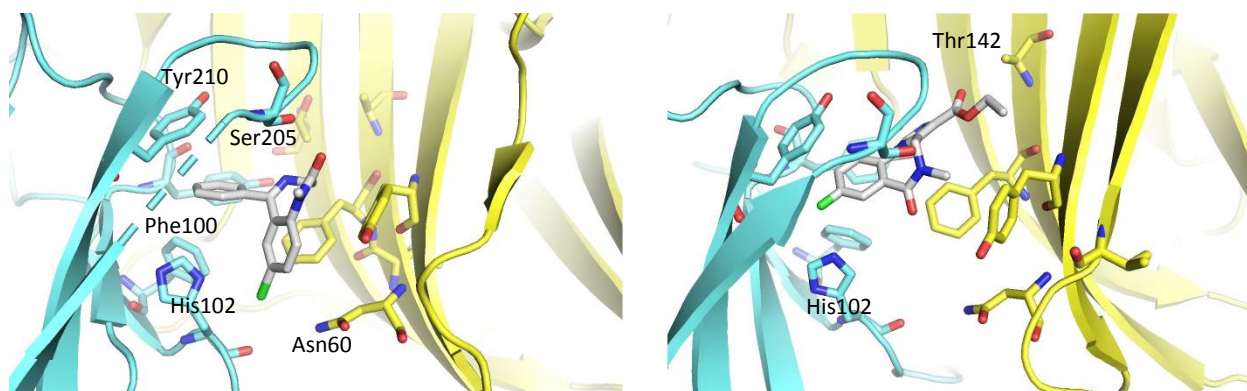
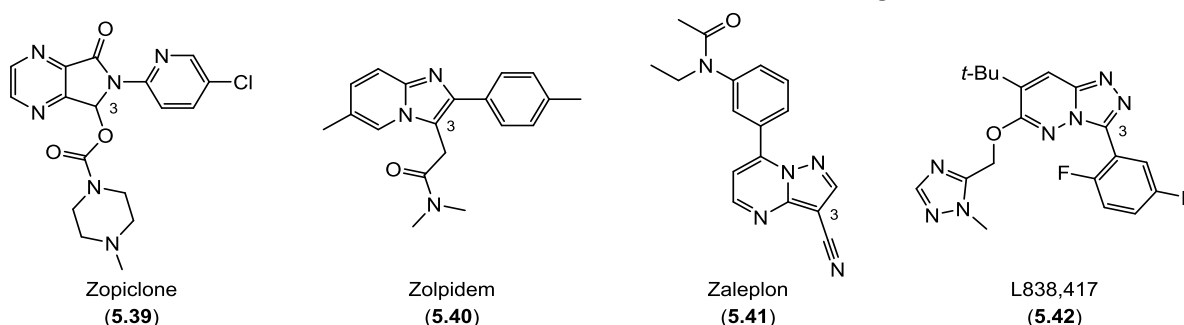


**Figure 5.4. Left.** Cryo-EM structure of  $\alpha 1 \beta 3 \gamma 2$  GABA<sub>A</sub> R BZ binding pocket by Aricescu<sup>[209]</sup> with the cyan and yellow chains respectively representing  $\alpha 1$  and  $\gamma 2$  subunits and bound diazepam displaying BM II. Note the M conformation of the diazepine ring and the interactions between the chloride atom and the residues Asn60 and  $\alpha$ His 102,  $\pi$  stacking between the pendant phenyl ring and Tyr210 and Phe100, and hydrogen bonding between the amide carbonyl and Ser205. **Right.** Cryo-EM structure of the same binding pocket by Zhu,<sup>[208]</sup> with bound flumazenil in BM I. It can be observed how flumazenil is located deeper and higher in the pocket than diazepam and how the ligand is anchored by interaction of the chloride atom with His102 and the ester carbonyl with Thr 142. Images from PDB database created with PyMOL.<sup>[212,213]</sup>

### 5.4.5 Z-Drugs

The binding sites of Z-drugs as well as their pharmacological performance are very similar to that of BZs, although their binding mode is still unknown. The structure of these compounds features an electron-deficient 6-5 fused ring system bearing at least two nitrogen atoms with different substitution patterns at C3 (Zolpidem numbering, Scheme 5.8). Most Z-drugs exhibit higher affinity for the  $\alpha 1$  receptor subtype, with some activity at  $\alpha 2$  and  $\alpha 3$  and very low affinity for  $\alpha 5$  subunits.<sup>[280]</sup> Hence, the effects of the majority of Z-drugs is related with sedation but not as much with anxiety, minimizing day drowsiness<sup>[281]</sup> and respiratory depression.<sup>[280]</sup> Moreover they display lower affinities for GABA<sub>A</sub>Rs, resulting into faster onset and clearance, with half-lives below 4 hours in most of cases, thus minimizing residual sedation.<sup>[281,282]</sup>



**Scheme 5.8.** Structure of selected Z-drugs. Zopiclone, zolpidem and zaleplon are commercially available for the treatment of insomnia. L838,417 is only used for research purposes. It binds to  $\alpha 1, 2, 3$  and 5 with  $K_i$  values of 0.67 to 2.25 nM. It is a non-sedative anxiolytic, anticonceptive and anti-inflammatory drug.<sup>[199]</sup>

With this, Z-drugs display slightly more benign side effects than BZs and a better pharmacological profile when used to treat sleep disorders. Finally, Z-drugs generally show milder withdrawal symptoms and lower tolerance according to studies performed on zopiclone, which proved to cause less receptor adaptation. Other drugs as zaleplon did not exhibit abuse potential on clinical studies.<sup>[283]</sup>

## 5.5 Photopharmacology

The field of photopharmacology aims to control biological function through the use of molecular tools sensitive to light, which is the unique stimulus capable of inducing controlled release or activation of a drug at the desired site with extremely high resolution and without inherent toxicity. As such, the development of photopharmacology is expected to overcome one of the major weaknesses of current pharmacology, which is the lack of control on the local action of the drug. Most current drug treatments involve the uptake of a substance followed by its distribution throughout the body causing several undesired interactions with multiple biological processes. Hence, each single drug exhibits a list of potentially serious side effects provoked by the perturbation of undesired targets in the patient's body. Off-target effects strongly influence the process of drug development and are the main factors to negatively influence the therapeutic window and the risk-benefit ratio. Examples of drugs with a narrow therapeutic window are the barbiturates, which if taken in excess can affect the respiratory function leading to death.<sup>[284]</sup> The suppression or drastic minimization of side effects by precisely controlling the activity of a drug in space and time would imply a huge improvement in the patient's life quality and bring out a medical revolution second only in significance to the discovery of antibiotics. Photopharmacology could in fact also help in fighting antibiotic resistance, given the possibility of deactivating the drug after interacting with its target.<sup>[285]</sup> It is hard to overstate how improvements in this field could boost the treatment of cancer or cognitive diseases, a fact which makes each attempt at advancing photopharmacology an exciting endeavour.

It can be considered that photopharmacology was born in 1969 with the work of Erlanger and colleagues, who were able to optically control the nicotinic acetylcholine receptors (nAChRs) of the electric cells (electroplax) of the *Electrophorus electricus*, or electric eel by using azobenzene based photoswitches.<sup>[286,287]</sup> This was followed by a long period with few publications until over the last 15 years a series of articles described the optical control of several biological processes, including ion channels, G-protein-coupled receptors, lipids, enzymes and others.<sup>[288–290]</sup>

There are different ways photopharmacology can precisely deliver a drug (Figure 5.5). First, it is possible to apply a photochromic ligand (PL) in an inactive form, followed by activation (irreversible or reversible) at the site of interest by a light-triggered structural change (Figure 5.5, A).

Another approach is known as photo-uncaging (Figure 5.5, B).<sup>[291]</sup> This consist in the application of a caged ligand, which is a biologically inactive pharmacophore formed by the drug covalently bound to a photolabile protecting group. Upon irradiation, the bond is broken in an irreversible process and the ligand is released at the desired site.

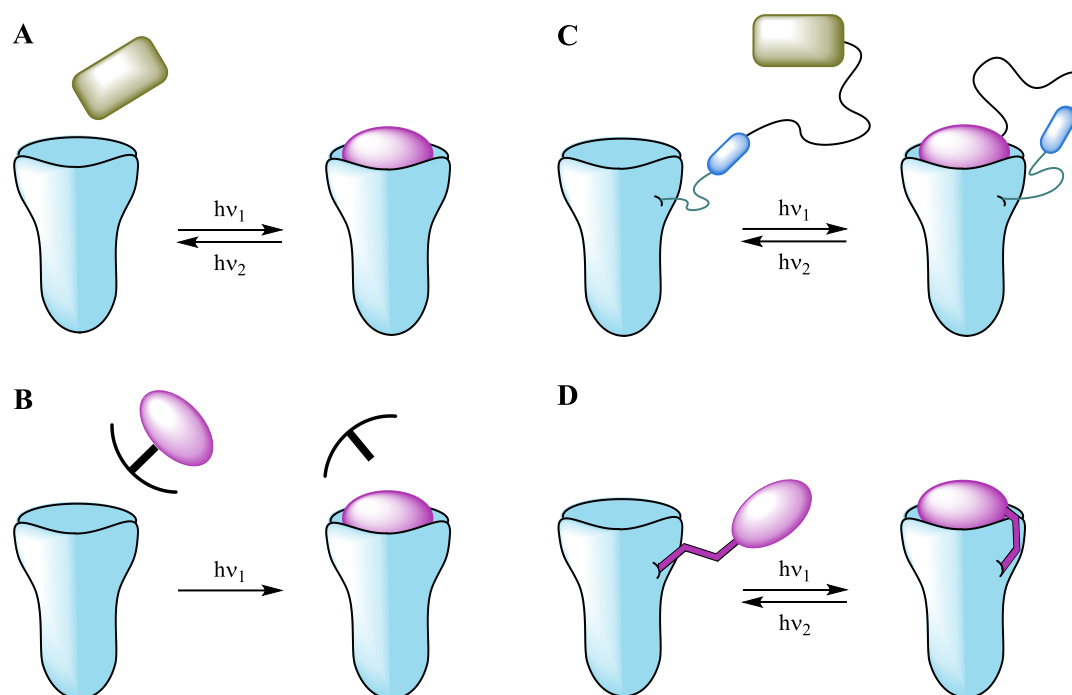


**Figure 5.5.** Four types of light-controlled drug delivery. **A)** Photoswitchable ligand, (PL). The initial form of the ligand does not bind the target, light irradiation induces a structural change in the ligand which allows binding to the receptor. This process can be either reversible or irreversible. **B)** Photo-uncaging. The drug is bound to a photochemically labile counterpart forming an inactive complex. Upon irradiation both parts split, releasing the active ligand in an irreversible process. **C)** Photoswitchable orthogonal remotely tethered ligand (PORTL). The same concept as for A regarding the structural change of the ligand, which in this case is bound to the target by a long linker. This results in constant ligand concentration and fast binding. **D)** Photoswitchable tethered ligand (PTL). Light irradiation induces a conformational change in the short tether that links the ligand to the receptor allowing for binding or pulling the ligand out of the pocket.

A third way known as PORTL (photoswitchable orthogonal remotely tethered ligand) involves tethering of the ligand to the wild type or engineered receptor with a long linker *via* any of the available tag techniques (SNAP, Halo, CLIP...).<sup>[292]</sup> Then, as for the free photoswitchable ligand (case A), light irradiation at the site of interest yields the active drug, which then binds to the target in a reversible manner. This approach keeps the concentration around the target constantly high, resulting in rapid binding (Figure 5.5, C).<sup>[292]</sup>

The last modality, which also involves tethered pharmacology, is known as PTL, photoswitchable tethered ligand. In this approach the linker itself contains the photoswitch. Thus, upon irradiation, the right configuration of the linker allows for the ligand to reach into the binding site in a reversible fashion.<sup>[292]</sup>

## 5.6 Photoswitchable Ligands

The basis of photopharmacology resides in the molecules that interact with light in a controlled manner, the photochromic ligands (PLs) or photoswitches. These entities undergo structural changes upon irradiation with light, triggering the desired biological response. The changes are based upon two principles: 1) Photoinduced ring closing/opening reactions 2) Photoinduced *cis/trans* isomerizations.

### 5.6.1 Photoswitches Displaying Ring Opening/Closing Interconversion

#### 5.6.1.1 Diarylethenes

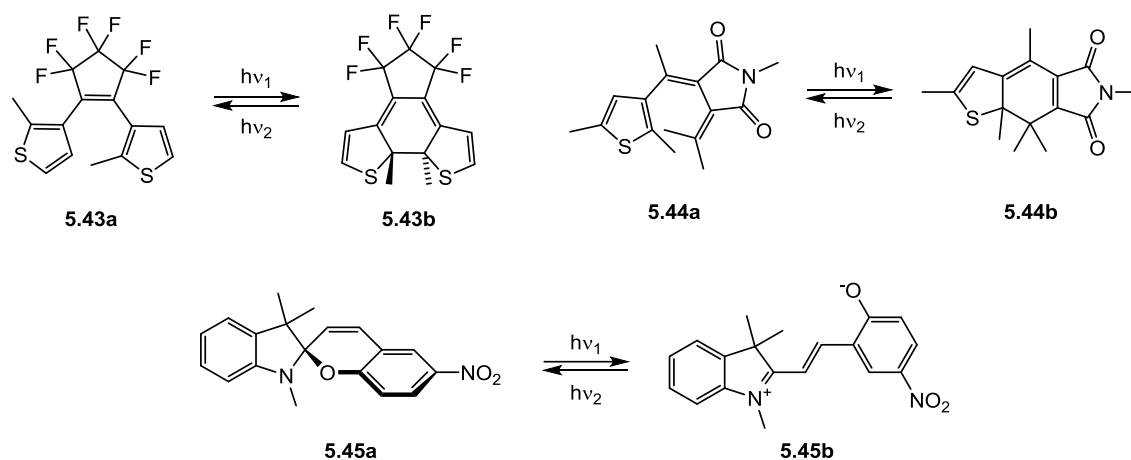
Diarylethenes (Scheme 5.9) are switched from the hexatriene opened state **5.43a** into a closed cyclohexadiene configuration **5.43b** by a photochemical  $6\pi$  electrocyclization with UV wavelengths strongly dependent on the substitution pattern, and can be re-opened by irradiation at  $>450$  nm.<sup>[293]</sup> These compounds are very resistant to fatigue, can undergo up to  $10^4$  switching cycles and cannot be switched thermally.

#### 5.6.1.2 Thiophenefulgides

Similarly to the diarylethenes, the thiophenefulgides (Scheme 5.9, **5.44**) also undergo photochemical  $6\pi$  electrocyclization to yield a tricyclic closed form. Simple substitution patterns strongly influence the absorption spectra, switching wavelengths and thermal reversibility.<sup>[288]</sup>

#### 5.6.1.3 Spiropyranes

Spiropyranes can be switched from their low polarity spiro-indoline (spiropyran) form **5.45a**, configured in two perpendicular planes, into planar zwitterion **5.45b** (merocyanine) upon irradiation with  $\sim 360$  nm light.<sup>[288]</sup> Switching back can in turn be achieved thermally or with visible light above 460 nm. The switching wavelengths are strongly influenced by the pH value. Other stimuli capable of isomerizing spiropyranes are solvents, metal ions, acids and bases, redox potential and mechanical force.<sup>[294]</sup> Spiropyranes have been incorporated into oligonucleotides and proteins, changing their polarity and conformations.<sup>[288,295]</sup>



**Scheme 5.9.** Different types of photochromic ligands undergoing reversible ring opening reactions.



## 5.6.2 Photoswitches Displaying *cis/trans* Isomerization

### 5.6.2.1 Hemithioindigos

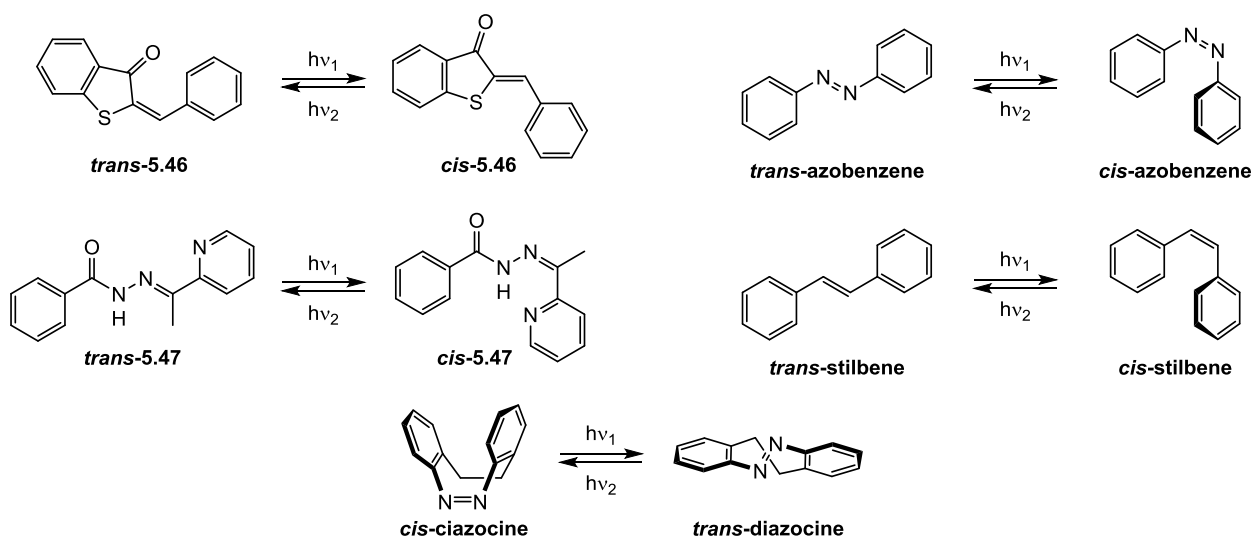
The *cis*→*trans* (or *E*→*Z*) isomerization of hemithioindigos is achieved upon irradiation at ~400 nm and the *trans*→*cis* at ~480 nm. The switching changes not only the geometry of the molecule but also its dipolar moment (Scheme 5.10, **5.46**). The thermal isomerization of the metastable *trans*-form takes place more slowly than for regular azobenzenes.<sup>[296]</sup> As a drawback, the quantum yield of the *trans* to *cis* isomerization is very low,  $\phi=0.05$ .<sup>[296]</sup>

### 5.6.2.2 Acylhydrazones

Acylhydrazones (Scheme 5.10, **5.47**) are the most versatile class of *cis/trans* photoswitches. They allow for functionalization at four different positions, permitting the tuning of several properties such as thermal stability, photostationary state (equilibrium composition during irradiation) or absorption spectrum.<sup>[297]</sup> Moreover, their synthesis is simple and often high yielding. As a drawback, the maximum absorption wavelength ( $\lambda_{\text{max}}$ ) for these photochromic ligands most often lies around ~320 nm.<sup>[297]</sup>

### 5.6.2.3 Stilbenes

Stilbenes are the simplest class of *cis/trans* photoswitches. Unlike for azobenzenes, the *trans*-isomer is metastable, with an energy barrier of ~40 kcal/mol. The *trans*→*cis* isomerization of stilbene occurs at about ~310 nm for unsubstituted stilbene.<sup>[288]</sup> The major disadvantage of these PLs is the lability of the *cis*-form, which tends to undergo irreversible 6 $\pi$  electrocyclizations.<sup>[298]</sup>

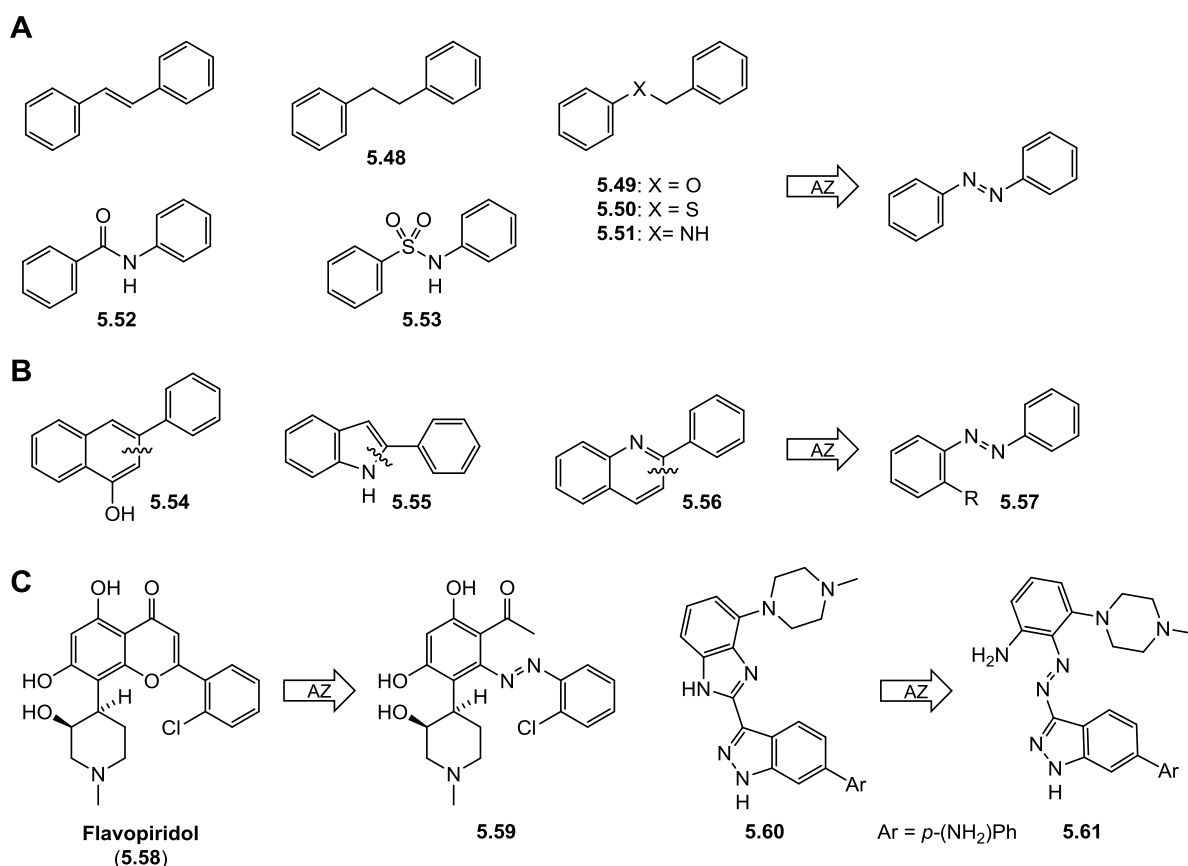


**Scheme 5.10.** Different types of photochromic ligands undergoing reversible *cis/trans* isomerization.

### 5.6.2.4 Azobenzenes

Azobenzenes have been known for more than 150 years and have the honour of being among the founders of the modern chemical industry. These compounds revolutionized the dye production thanks to their high affinity for different fabrics, their broad range of colours –easily tuned with simple structural modifications– and their simple chemistry, derived from inexpensive aniline.<sup>[299]</sup> Industries like Bayer or BASF (Badische Anilin & Soda Fabrik) owe their initial success to azobenzenes, which are still the most common base of

modern dyes.<sup>[300]</sup> In the field of photopharmacology, azobenzenes are the most widely used PLs given their relatively low size and molecular weight, simple synthesis, wide versatility towards functionalization, fast switching and favourable extinction coefficients and quantum yields. Azobenzenes usually show  $\lambda_{\text{max}} = 340\text{--}360\text{ nm}$  (*trans*→*cis*), with optimal switching at about 20 nm above the absorption maximum, and can be easily switched back upon irradiation at >440 nm. Photostationary states usually contain 50-90% of the *cis*-isomer, which is about 10 kcal/mol higher in energy than the *trans*-form. On the other hand, obtaining the pure *trans*-form is generally possible through the thermal relaxation of the *cis*-isomer, which occurs with half-lives ( $t_{1/2}$ ) varying from milliseconds to years depending on the substituent pattern.

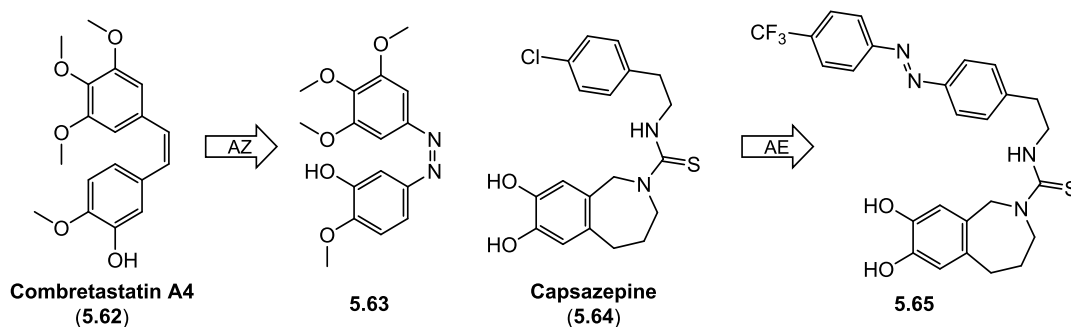


**Scheme 5.11.** **A)** Azologization (AZ inside of the arrows) motifs. **B)** Proposed new type of azosteres resulting from breaking planar rings. **C)** Two proposed bioactive molecules and azobenzene analogues which would arise upon application of the azologization principle depicted in B.

The incorporation of azobenzenes to the pharmacophore can be addressed by two different strategies. First, common patterns present in the original drug can be identified as potential analogues to the structure of azobenzene. These moieties known as “azosteres” can be stilbenes, diphenylethanes, benzyl phenyl (thio)ethers or amines, phenyl-benzamides and related compounds, where heterocycles can also be present (Figure 5.11, A).<sup>[301]</sup> The consideration of these groups as equivalent to the N=N moiety should be taken with care, since key interactions with the target protein may be established by the linkers, especially if they are amines or amides.<sup>[301]</sup> Additional azosteres could comprise some bicyclic systems such as naphthalene, indole or quinoline (5.55–5.57, Scheme 5.11), which would match the geometry of *trans*-azobenzenes. Upon azologization, the ring fragments excluded from the azo-linker would remain as *ortho* substituents in the azobenzene (R group, Scheme 5.11, 5.57). This kind of azologization has not yet been explored but could greatly increase the number of molecules available to turn into photoswitches. Two proposed examples for

this approach are flavopiridol, a CDK9 inhibitor tested for treatment of acute myeloid leukemia<sup>[302]</sup> which would yield azobenzene **5.59** or indazole **5.60**, a CDK2 inhibitor developed by Pfizer<sup>[303]</sup> which would render azobenzene **5.61**.

A successful example of classical azologization can be seen in Scheme 5.12, where azobenzene **5.63** was developed based on the structure of combretastatin A4, a potent inhibitor of tubulin polymerization, enabling optical control of cell division among other tubulin-dependent processes.<sup>[304]</sup>



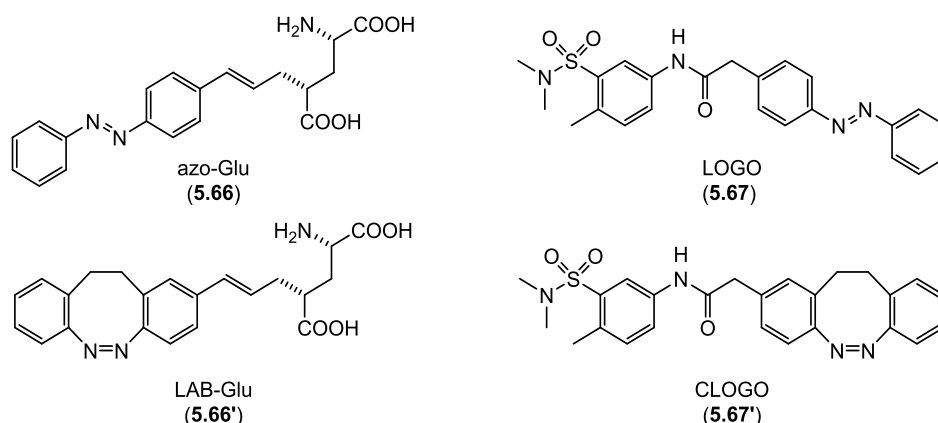
**Scheme 5.12.** Examples of successful azologization and azo-extension strategies on bioactive molecules. Azologization of combretastatin A4 (**5.62**) allowed for optical control of tubulin polymerization.<sup>[304]</sup> Azo-extension of capsazepine yielded a molecule whose inhibitory activity on TRPV1 (transient receptor potential vanilloid 1) could be regulated by light irradiation.<sup>[305]</sup>

A second approach for the introduction of azobenzene is the strategy known as “azo-extension”, which consists in the addition of an azobenzene group to the pre-existing drug structure. A successful azo-extension approach was performed on the structure of capsazepine (**5.64**, Scheme 5.12). This molecule is an antagonist of the transient receptor potential vanilloid 1 (TRPV1), an ion channel involved in pain and temperature sensation. The azo-extension strategy led to azobenzene **5.65**, which acted as a photoswitchable antagonist of the TRPV1 channels.<sup>[305]</sup> The azo-extension alternative involves a greater change in ligand shape, and requires empty regions in the binding pockets which can allocate the azo group.

This fertile azobenzene chemistry has been applied to several biological targets such as lipids, enzymes, GPCRs and LGICs, by means of tethered or untethered photopharmacology, allowing for optical control of processes like ion transport, cell adhesion and communication, metabolism or immunobiology.<sup>[288–290,306]</sup>

#### 5.6.2.5 Diazocines

Diazocines<sup>[307,308]</sup> are 8-membered heterocycles which result from the closure of an azobenzene by an ethylene or equivalent bridge (Scheme 5.13). Diazocines present some advantages compared to azobenzenes: they display a red-shifted absorption spectrum, with absorption maxima at about 400 nm for the *cis*-form and 490 nm for the *trans*-form, generally with less overlap than azobenzenes. This allows for the exclusion of UV radiation, harmful for living organisms.<sup>[308]</sup> Moreover, opposite to azobenzenes, *cis*-diazocines are thermodynamically stable isomers, resembling azobenzene's *cis*-configuration. This implies that many of the previously designed azobenzenes active in *trans*-state, which had to be deactivated with light irradiation, now can be turned into the corresponding diazocines and be activated *in situ*, a much more convenient scenario.<sup>[309]</sup> Diazocines have already been successfully used for the control of Shaker K<sup>+</sup>, GIRK and glutamate channels among others.<sup>[310,311]</sup>

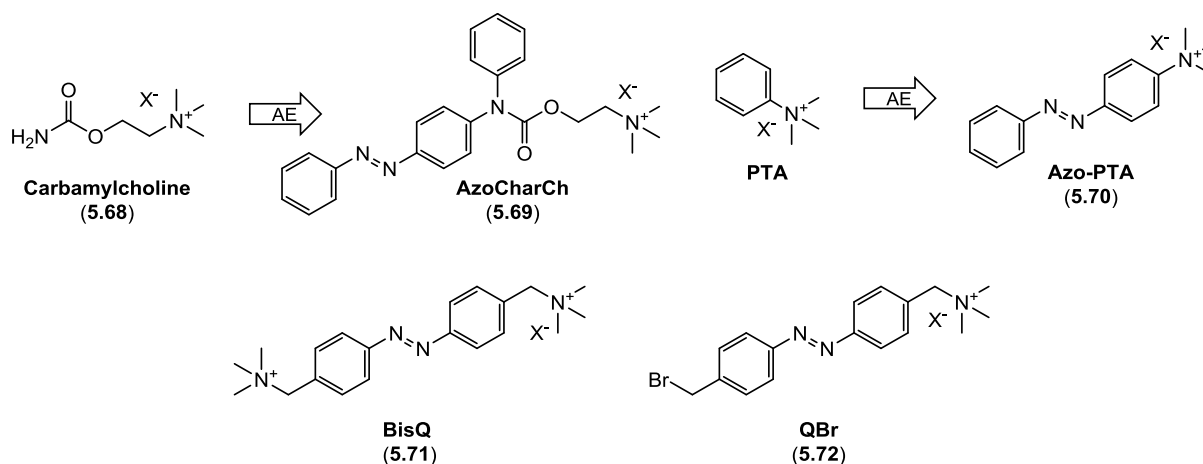


**Scheme 5.13.** Diazocines derived from analogous azobenzenes used for the control of Glutamate receptors (5.66) and GIRK channels (5.67).<sup>[310–313]</sup>

## 5.7 Selected Examples of Photocontrolled LGICs

### 5.7.1 Photoregulation of Acetylcholine Receptors

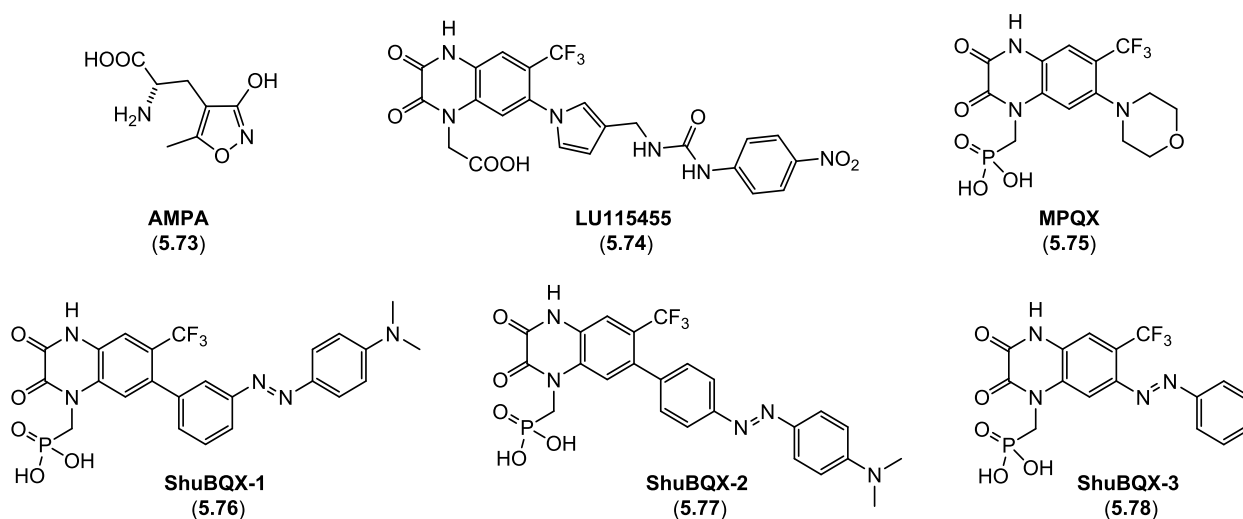
In 1969, Erlanger and co-workers inaugurated the field of photopharmacology by treating the electricity producing cells (electroplax) of electric eel (*Electrophorus electricus*) with a solution of azobenzene-derivatives of nAChR agonists. nAChRs, or nicotinic acetylcholine receptors, are ionotropic receptors that respond to acetylcholine, allowing sodium ions to rush into the cell propagating action potentials. The azobenzenes used were azo-extended versions of carbamylcholine (5.68) and PTA, named azo-CarCh (5.69) and azo-PTA (5.70, Scheme 5.14).<sup>[286]</sup> Once azo-CarCh was added to the nicotinic acetylcholine receptors in the presence of 5.68, the cell membrane repolarized (i.e. more negative potential inside the cell), meaning *trans*-5.69 displaced the native ligand and acted as a weaker agonist, discouraging channel opening and inhibiting the flow of sodium ions into the cell. When the same solution was irradiated with UV light (320 nm), inducing *trans*→*cis* isomerization of 5.69, the repolarization further increased, since *cis*-5.69 displayed a lower affinity for the receptor. This process could be reversed upon irradiation at 420 nm, thus leading to the first reported optical control of nAChR. The results obtained with PTA and 5.70 followed the same trend. Two years later, the first example of a photoswitchable tethered ligand (PTL) was presented by the same group.<sup>[287]</sup> Bis-Q (5.71) and QBr (5.72) proved to be potent agonists of nAChRs in their *trans*-form causing rapid depolarization whereas the *cis*-compound could be considered inactive. When electroplax cells were treated with pre-irradiated 5.71 (330 nm), a slight depolarization was observed given the presence of residual *trans*-5.71. When the mixture was illuminated with a photoflood lamp inducing *cis/trans* isomerization, strong depolarization occurred. Binding of 5.72 to cysteine residues yielded the first reported PTL, which gave similar results as the free ligands.<sup>[287]</sup>



**Scheme 5.14.** Structures of azobenzene photoswitches used by Erlanger for the optical control of *nAChRs*.<sup>[286,287]</sup>

## 5.7.2 Photocontrolled AMPA Receptors

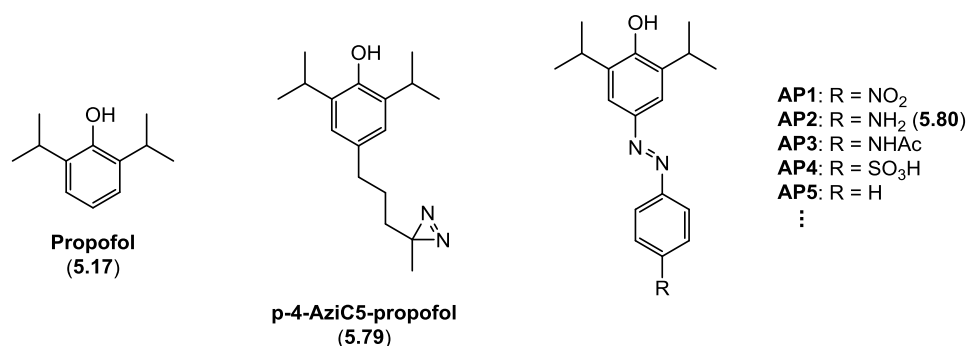
AMPA receptors are ligand-gated ion channels sensitive to glutamate which are specifically activated by AMPA (2-amino-3-(5-methyl-3-hydroxyisoxazol-4-yl)propanoic acid). Once the agonist binds, the channel opens and allows sodium ions to flow into the cell mediating synaptic transmission.<sup>[314]</sup> MPQX (**5.75**), a potent and selective AMPA receptor antagonist was derivatized to gain optical control over these receptors giving rise to azobenzenes **5.76-5.78**.<sup>[315]</sup> The design of these photoswitchable ligands was based on the following premises: The morpholino group was dispensable for the antagonistic activity, given its absence in potent antagonists such as **5.74** (Scheme 5.15). Moreover, LU115455 proved that bulky groups at the 6-position of the quinoxaline-dione were well tolerated. Thus, azo-extension was performed at the mentioned position leading to ShuBQX-1 to ShuBQX-3. Among these, ShuBQX-3 (**5.78**) displayed superior properties as a photochromic ligand, since in the *trans*-form and in the presence of glutamate (300  $\mu\text{M}$ ) it acted as a GluA1 (an AMPA receptor subtype) antagonist with an  $\text{IC}_{50}$  of 3.1  $\mu\text{M}$ .<sup>[315]</sup> Moreover, in the *cis*-form **5.78** displayed a much weaker antagonist character, allowing for reactivation of the GluA1 currents.<sup>[315]</sup> Thus, ShuBQX-3 was the first photoswitchable AMPA receptor antagonist.



**Scheme 5.15.** Structures of AMPA and antagonists used for the control of AMPA receptors.

### 5.7.3 Azo-propofol

In 2012, Sigel, Trauner and co-workers synthesized and studied a series of azo-extended propofol analogues (Scheme 5.16) aiming for the photocontrol of GABA<sub>A</sub> receptors.<sup>[316]</sup> Extension at the 4 position was performed based on the previous knowledge that relatively large groups were well tolerated (**5.79**, Scheme 5.16).<sup>[317]</sup> Of all the synthesized analogues, AP2 (**5.80**) proved to be the best-suited photoswitch. Inclusion of the amino group red shifted the maximum absorption of the *trans*-form to 400 nm and induced very fast thermal relaxation. Moreover, **5.80** exhibited higher affinity than propofol for the  $\alpha 1\beta 2\gamma 2$  GABA<sub>A</sub>R receptor subtype, albeit inducing half as much potentiation. When applied to HEK cells in patch-clamping experiments, *trans*-AP2 induced increased currents, which dramatically decreased when irradiated with 390-450 nm light. This indicated that the *cis*-isomer was inactive. *In vivo* experiments with *Xenopus* tadpoles in a 1.0  $\mu$ M solution of **5.80** showed deep anaesthesia in the dark and under green light. When the wavelength was switched to 360-370 nm, the specimens woke up and moved. Immediately after removing the light source the movement stopped again, due to the thermal relaxation of the *cis*-inactive form.



**Scheme 5.16.** Structures of GABA<sub>A</sub>R positive allosteric modulator propofol and derivatives thereof.

## 6. Project Background and Aims

As discussed in Chapter 5.4.4, benzodiazepines (BZs) and other GABA<sub>A</sub>R positive allosteric modulators (PAMs) generally lack specificity for different receptor subtypes, causing side effects that affect memory, wakefulness, movement and attention. The later development of Z-drugs, which share binding sites with BZs, slightly improved this situation, mostly because of their faster clearance. Further, the number of SAR studies on these drugs is strikingly scarce considering their extended use and economic impact.<sup>[318–320]</sup> Moreover, it has been only very recently that the BZ binding site has been elucidated, allowing for a deeper understanding of the binding mode of these drugs.<sup>[208,209]</sup>

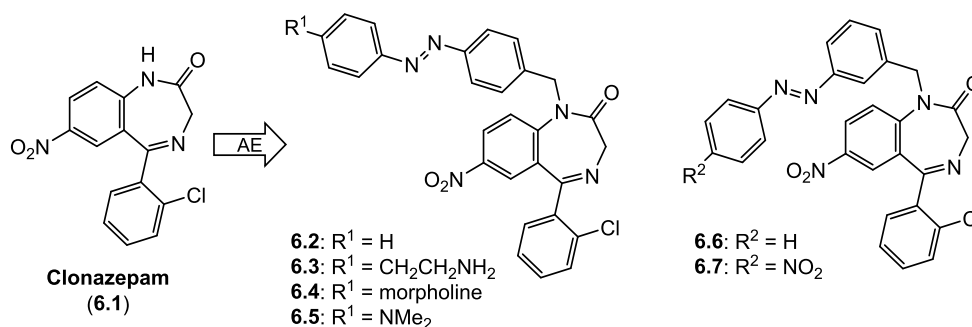
Therefore, the introduction of a photoswitchable benzodiazepine or Z-drug as a research tool could provide further insights into how these drugs bind to their target: influence of substituents, switching between binding modes, increase in subtype selectivity, secondary binding pockets, etc. It could be expected, for example, that a *cis*-state drug would more effectively bind to a specific receptor subtype, or that an *in situ* light-induced conformational change would provoke the exchange between binding modes within the binding pocket, or that the *cis*-form could bind with higher affinity to any of the secondary binding pockets allowing for better understanding of these new sites. All the potential knowledge that could arise from the transformation of a benzodiazepine into a photoswitchable ligand could help in the further development of these drugs by means of rational design.

These photochromic ligands could also be used to better understand the function of different GABA<sub>A</sub>Rs by selectively potentiating particular receptor subtypes, or receptor clusters within certain brain regions. In a longer timeframe, maybe photoswitchable benzodiazepines or Z-drugs could be the ultimate solution to the undesired side effects of sleeping drugs, including tolerance and addiction, since the PLs would not remain in the body in their active form.

### 6.1 Synthesis of a Photoswitchable Benzodiazepine

#### 6.1.1 Previous Work

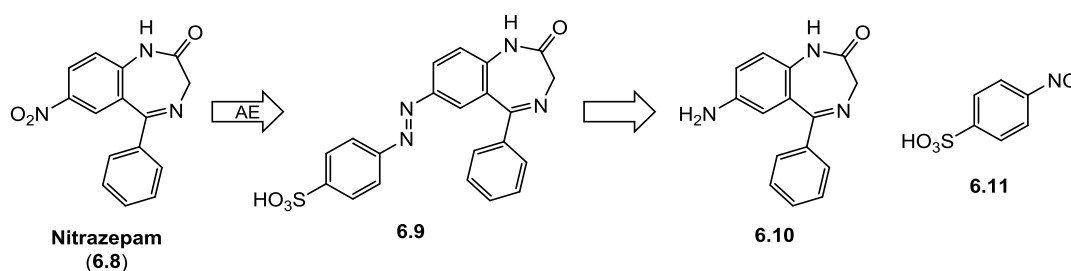
A previous collaboration with the Sigel group pursued the development of a photoswitchable benzodiazepine. Matthias Schönberger, a former Trauner group member synthesized 6 different azobenzodiazepines using the scaffold of clonazepam (Scheme 6.1). The azo-extension was performed at the amide nitrogen.



**Scheme 6.1.** Azo-extension approaches towards a photoswitchable BZ by Trauner and Sigel. Compounds **6.2** to **6.7** displayed low affinity for the GABA<sub>A</sub>R with only slight differences in *cis* and *trans* potentiation.

Unfortunately, the potentiation induced by these compounds was low compared to clonazepam (max. 154% potentiation at 10  $\mu$ M), suggesting that the extension negatively affected the receptor binding and modulation. Moreover, the difference in current potentiation induced by the *cis* and *trans*-forms was 29% in the best case, reason why they were not further investigated.

Gorostiza and co-workers recently published their own work on an azobenzodiazepine (Scheme 6.2). Their azo-extension approach was accomplished by reduction of the nitro group of nitrazepam followed by Baeyer–Mills coupling with aniline **6.11**. The presence of the sulfonate group aimed to increase solubility.<sup>[321]</sup> Interestingly, **6.9** did not behave as a PAM but as an inhibitor of the GABA<sub>A</sub>R currents. **6.9** displayed an IC<sub>50</sub> of 67  $\mu$ M for the GABA<sub>A</sub>  $\alpha$ 1 $\beta$ 2 $\gamma$ 2 receptor subtype and showed certain affinity for the GABA<sub>A</sub>  $\rho$ 2 subtype (IC<sub>50</sub> = 128  $\mu$ M) and for glycine channels. It was found that **6.9** works as a channel blocker which binds at the lowest end of the TM2 when the pore is opened. The *trans*-isomer blocked the flow of chloride ions more effectively since this conformation allowed the sulfonate group to reach deeper into the pore, stabilising hydrogen bonds with four serine residues.



**Scheme 6.2.** Photoswitchable BZ synthesized by Gorostiza *et al.* based on the structure of nitrazepam. **6.9** did not bind to the BZ binding site and acted as a channel blocker.<sup>[321]</sup>

## 6.1.2 Project Outline

We aimed to modify the structure of an unsubstituted classical benzodiazepine, leaving aside imidazo- and triazolo-BZs to obtain a simple lead compound. However, we presume that the chemistry described here would be compatible with a wide variety of substitution patterns and benzodiazepine subtypes.

We decided to perform the azo-extension at the *ortho*-position of the pendant benzene ring of **6.12** (Scheme 6.3) for the following reasons:

1. The presence of substituents at this position induces a ring twist out of the benzodiazepine ring plane which results in increased affinity for the receptor.<sup>[318]</sup> This twisted conformation was corroborated by a cryo-EM structure showing interactions of the pendant phenyl ring with Tyr210 and Phe100 residues (Figure 5.4, Left).<sup>[209]</sup>
2. Electron-withdrawing groups at this position increase bioactivity (known for F and Cl).<sup>[318]</sup>
3. Substitution of the pendant phenyl ring by naphthalene is well tolerated.<sup>[318,322]</sup>
4. Presence of a large hydrophobic pocket proximal to the non-fused phenyl ring that could accommodate the azobenzene moiety (both in predicted binding models and cryo-EM structure, Figure 6.1).<sup>[209,276]</sup>



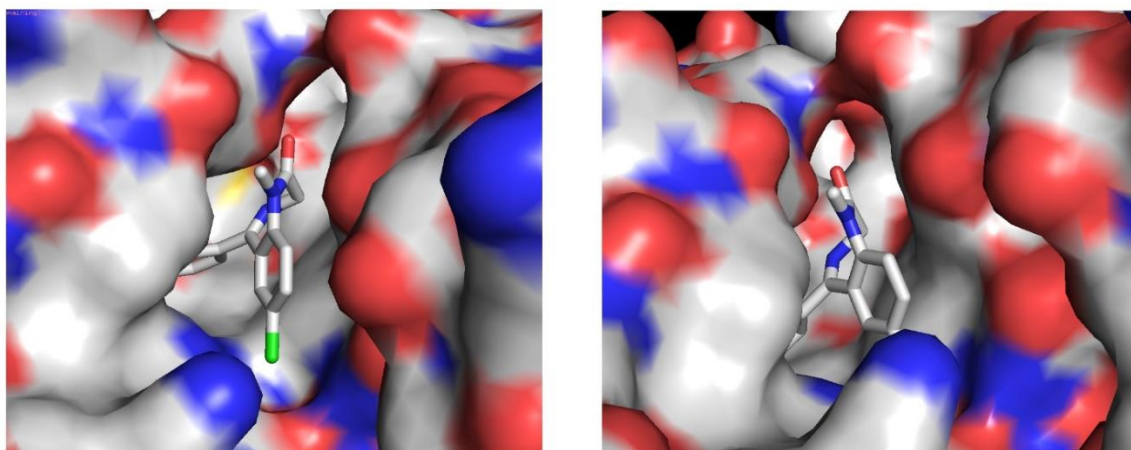
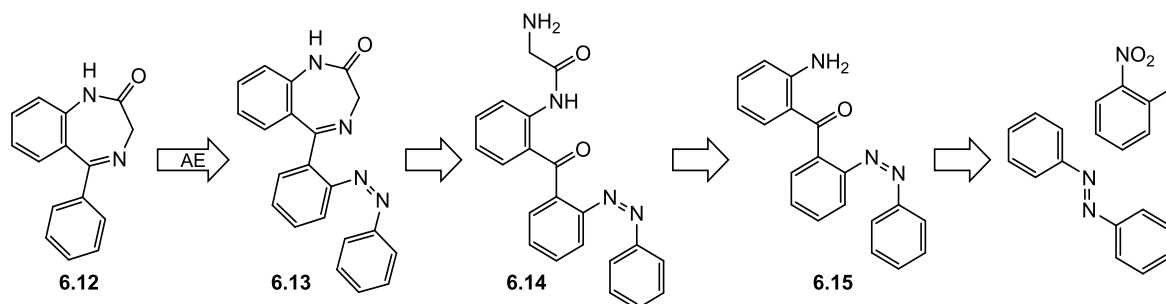


**Figure 6.1.** Cryo-EM structure of diazepam bound to GABA<sub>A</sub>R by Aricescu et al.<sup>[209]</sup> The large hydrophobic pocket present behind the ligand could allocate the azobenzene moiety. Images from PDB database created with PyMOL.<sup>[212,213]</sup>

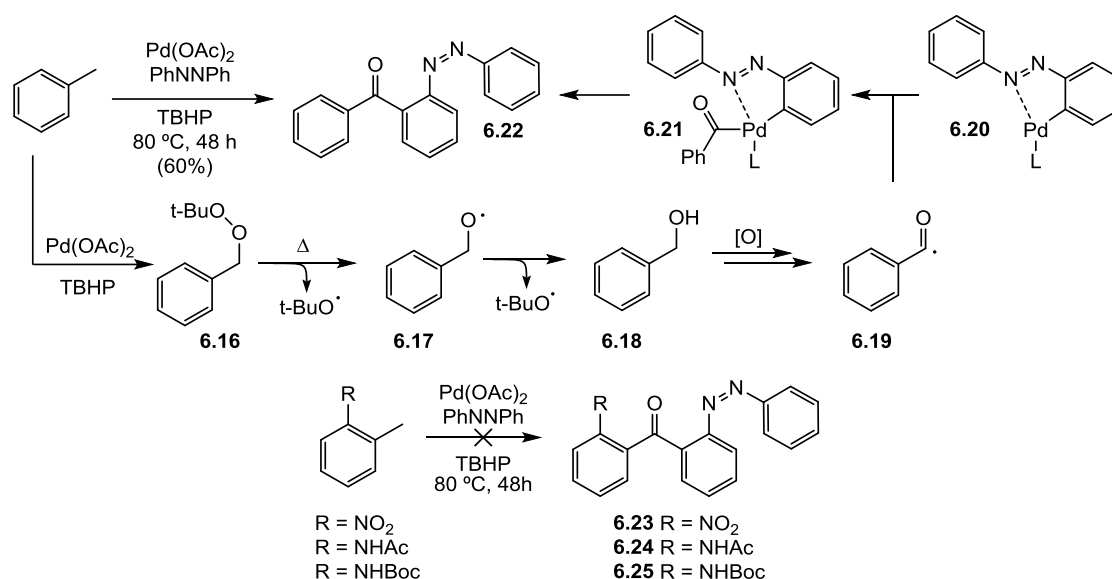
Our first retrosynthesis disconnected the imine of **6.13** at the C=N bond, which can be formed by means of Sternbach cyclization of intermediate **6.14**. This amide can be synthesized from aniline **6.15** via amidation with chloroacetyl chloride followed by Delepine reaction. **6.15** could in turn be obtained from the oxidative coupling of 2-nitrotoluene and azobenzene.



**Scheme 6.3.** Azo-extension of BZ **6.12** and first retrosynthetic analysis of the targeted photoswitchable benzodiazepine **6.13**.

### 6.1.3 Results and Discussion

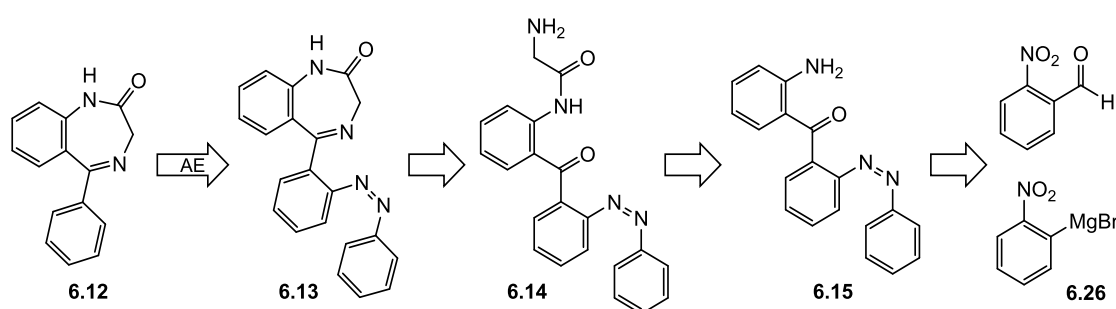
We initially aimed to synthesize benzophenones **6.23** to **6.25** using a method by Wu, which consisted in the one-pot reaction of the corresponding toluene derivative with azobenzene in the presence of palladium acetate and an excess of *tert*-butyl hydroperoxide (TBHP) at 80 °C.<sup>[323]</sup> Under these conditions toluene (present in large excess) undergoes a series of benzylic oxidations promoted by palladium acetate and TBHP, which generate acyl radical **6.19**. In parallel to this process, *ortho*-directed metalation of azobenzene takes place and the resulting palladium complex **6.20** incorporates acyl radical **6.19** and undergoes reductive elimination yielding the desired benzophenone **6.22**.



**Scheme 6.4. Top.** Reaction mechanism for the synthesis of azobenzophenone **6.22** by Wu reproduced by us.<sup>[323]</sup> **Bottom.** Attempts to synthesize azobenzophenones **6.23**–**6.25** using the method described above.

Although we could reproduce this reaction to obtain the known compound **6.22**, when we applied the same reaction conditions to deliver amino or nitro derivatives **6.23** to **6.25**, only complex product mixtures were obtained. In the case of aminobenzophenones **6.24** and **6.25** this could be due to the palladation of the starting toluidines leading to symmetrical benzophenones among other products.<sup>[324]</sup> For the case of nitrotoluene, presumably the system was too electron deficient to stabilize the benzyl radical intermediates, frustrating the generation of the corresponding acyl radical.

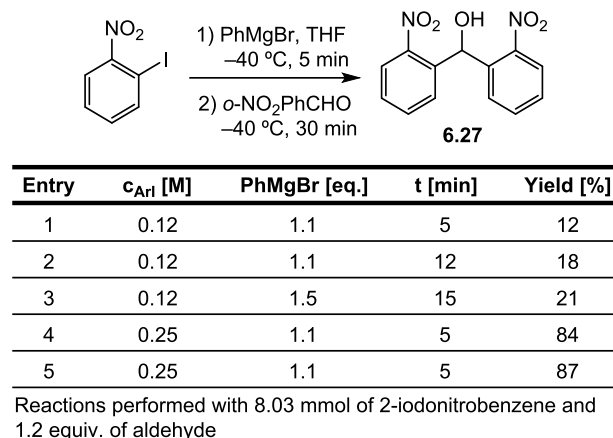
Given the difficulty of quickly accessing benzophenones **6.23** to **6.25** by means of Wu's procedure, we changed our strategy to obtain benzophenone **6.15**. We envisioned that this could be accomplished by the addition of Grignard reagent **6.26** to 2-nitrobenzaldehyde followed by alcohol oxidation and nitro group reduction followed by Baeyer–Mills coupling (Scheme 6.5).



**Scheme 6.5.** Second-generation retrosynthesis towards photoswitchable BZ **6.13**.

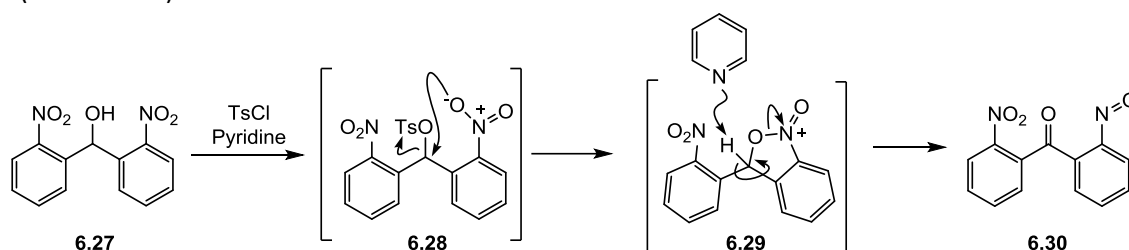
We proceeded to synthesize starting benzhydrol **6.27** using a method by Knochel, which consisted of metal-halogen exchange of 2-iodonitrobenzene to give a Grignard intermediate which would be trapped with 2-nitrobenzaldehyde (Scheme 6.6).<sup>[325]</sup> We started with a 0.12 M solution of 2-iodonitrobenzene obtaining the desired product in 12% yield and recovering unreacted 2-iodonitrobenzene (Table 6.1, Entry 1). We reasoned that the metal-halogen exchange had not been completed and therefore repeated the reaction

allowing the iodide and the phenylmagnesium bromide to react for a longer time period. This delivered **6.27** in 18% yield, which was still unsatisfactory (Entry 2). Addition of 0.4 more equivalents of the Grignard reagent together with a longer reaction time lifted the yield to 21% (Entry 3). We then opted to increase the speed of the first step by increasing the concentration of the reagents (Entries 4-5). This modification was crucial and delivered the desired product **6.27** in 87% yield.



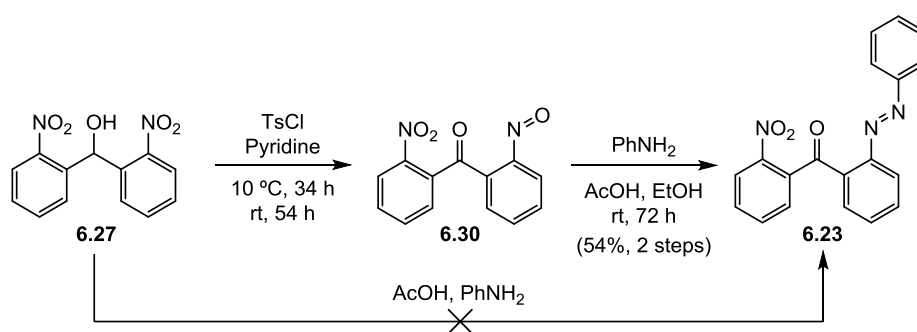
**Scheme 6.6 and Table 6.1.** Conditions screened for the synthesis of benzhydryl **6.27**.

In 1964, Dickinson described the transformation of 2-nitrobenzhydrol into 2-nitrosobenzophenone by reaction of the former with tosyl chloride in pyridine at low temperature.<sup>[326]</sup> The reaction mechanism is exemplified for substrate **6.27** in Scheme 6.7. The formation of adduct **6.28** is followed by an intramolecular S<sub>N</sub> displacement of the tosylate by the proximal nitro group. The subsequent heterocyclic intermediate **6.29** collapses into nitrosobenzophenone **6.30** upon deprotonation by pyridine resulting in the formal disproportionation of **6.27**. The key nitroso intermediate **6.30** could be used to access azobenzophenone **6.23** (Scheme 6.8).



**Scheme 6.7.** Reaction mechanism for the disproportionation of benzhydryl **6.27** into nitrosobenzophenone **6.30**.

Although Dickinson's method<sup>[326]</sup> was described only for mono-nitrobenzophenones, we were confident that the presence of an additional nitro group at the *ortho*-position would not be detrimental. Even though we could never isolate the nitroso intermediate, since it quickly decomposed at room temperature, we successfully ran the subsequent Baeyer–Mills reaction using the reaction crude. The azo-coupling delivered azobenzophenone **6.23** in good yield for this kind of transformation (Scheme 6.8). A crystal structure of **6.23** was obtained, showing a twisted conformation for the benzophenone rings and an almost planar conformation for the azobenzene moiety (Figure 6.2).



**Scheme 6.8.** Synthesis of azobenzophenone **6.23** from intermediate **6.27**.

We reasoned that this two-step procedure could be also triggered by acetic acid and aniline in a one-pot procedure, but no product was observed under these conditions.<sup>[327]</sup> However, when tosyl chloride was added to the mixture, traces of **6.23** were found.

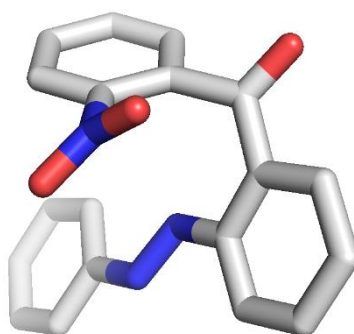
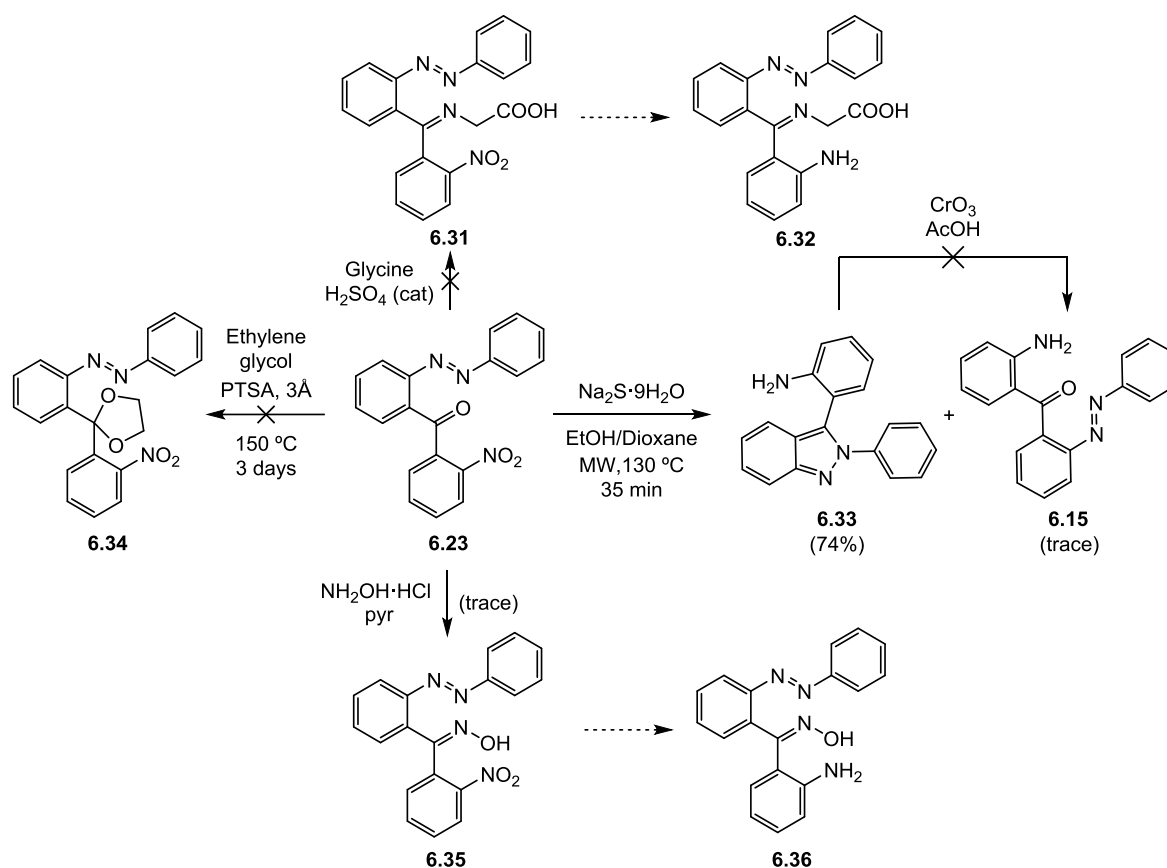


**Figure 6.2.** X-ray structure of azobenzophenone **6.23**.

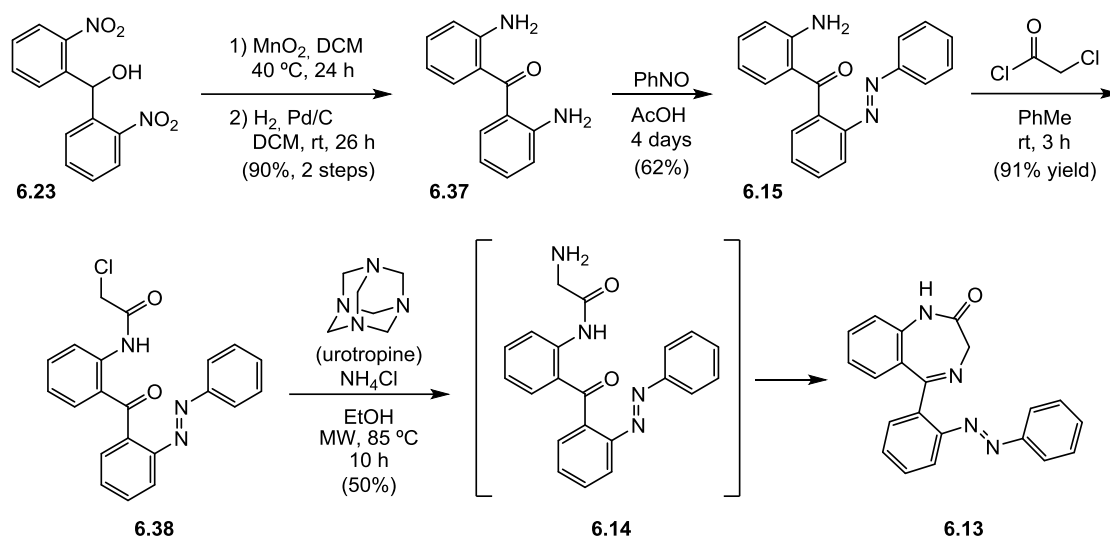
With the desired azobenzene **6.23** in hand, we proceeded to reduce the nitro group which would allow for installation of the amide needed for the subsequent Sternbach cyclization. The reduction of nitro groups in the presence of azobenzenes can be easily accomplished by treatment with sodium sulfide in refluxing ethanol.<sup>[328]</sup> In the case of nitrobenzophenone **6.23** however, these reaction conditions did not translate into any conversion (Scheme 6.9). Therefore, we exchanged the solvent for the less volatile dioxane, which also displayed better solubility, and allowed the mixture to react at 130 °C under microwave irradiation. Unfortunately, only traces of the desired product were obtained together with the major product, indazole **6.33**, which resulted from the condensation of the azobenzene nitrogen with the carbonyl group. This reaction had been previously reported under different reaction conditions.<sup>[329]</sup> We attempted an oxidative opening of **6.33** with Jones' reagent, but it failed to provide the desired product.<sup>[330]</sup>



**Scheme 6.9.** Attempts to synthesize azobenzodiazepine **6.13** from azobenzophenone **6.23**.

Moreover, attempts to avoid indazol formation by protecting the carbonyl group of intermediate **6.23** as an acetal,<sup>[331]</sup> an hydroxylamine<sup>[332]</sup> or an imine<sup>[333]</sup> were met with failure (Scheme 6.23).

Since the reduction of **6.23** to azobenzene **6.15** seemed unfeasible, we decided to change the order of events and first reduce both nitro groups prior to the Baeyer–Mills coupling with nitrosobenzene. This was accomplished by alcohol oxidation of dinitrobenzhydrol **6.27** with manganese dioxide followed by exhaustive nitro group reduction under hydrogen atmosphere catalyzed by palladium on charcoal (Scheme 6.10). The resulting diamine **6.37** was submitted to Baeyer–Mills conditions yielding azobenzophenone **6.15** in good yield, which was subsequently acylated by treatment with chloroacetylchloride delivering chloroacetamido intermediate **6.38**. Finally, **6.13** was obtained *via* Delépine reaction of **6.38** with urotropine and ammonium chloride in refluxing ethanol, yielding amine **6.14**, which underwent an *in situ* Sternbach cyclization.<sup>[334]</sup>



**Scheme 6.10.** Synthesis of photoswitchable benzodiazepine **6.13** from benzhydrol **6.23**.

We analysed the UV/Vis behaviour of the previously unreported azobenzophenone **6.15** (Figure 6.4). A 50  $\mu\text{M}$  DMSO solution of **6.15** was irradiated for 10 minutes at various wavelengths with the help of a monochromator and the resulting absorption spectra were measured. The absorption spectra of the *trans*-

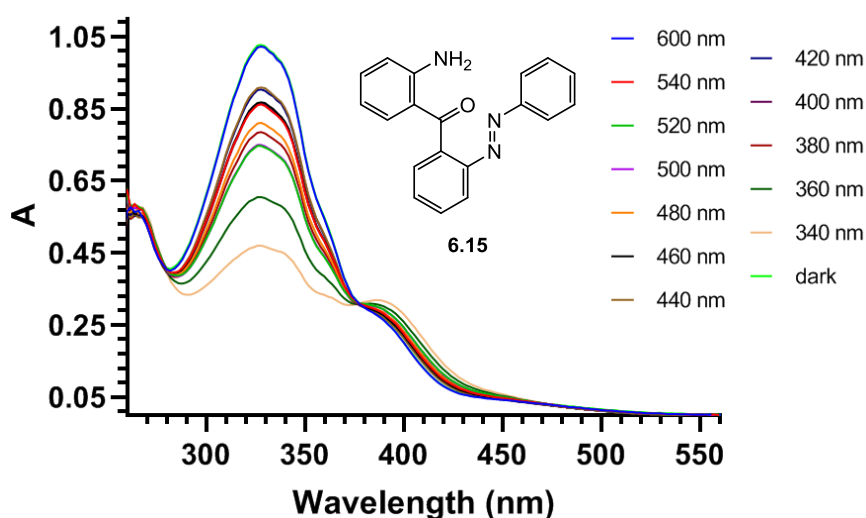


**Figure 6.3.** UV/Vis absorption spectrum of **6.15** in DMSO in the dark and upon light irradiation at the specified wavelengths.

form (blue) and the *cis*-form (orange) can be clearly distinguished in Figure 6.3, with absorption maxima at 328 nm and 389 nm, and an isosbestic point at 378 nm. The best wavelength to induce *trans*→*cis* isomerization was found at 340 nm.

The UV/Vis absorption spectra of azobenzodiazepine **6.13** are shown below (Figure 6.4, left). A 50  $\mu\text{M}$  solution of **6.13** in (20% v/v) DMSO/PBS mixture was irradiated at various wavelengths for 10 minutes with the help of a monochromator before the absorption spectra were measured. The maximum absorption was found at 327 nm. Switching between *cis*- and *trans*-forms is most effectively induced upon irradiation at

360 nm. The apparent weak switching between *cis*- and *trans*-isomers is owed to the fast thermal relaxation of **6.13**, with a *cis* half-life of 2.6 s (Figure 6.4, right).

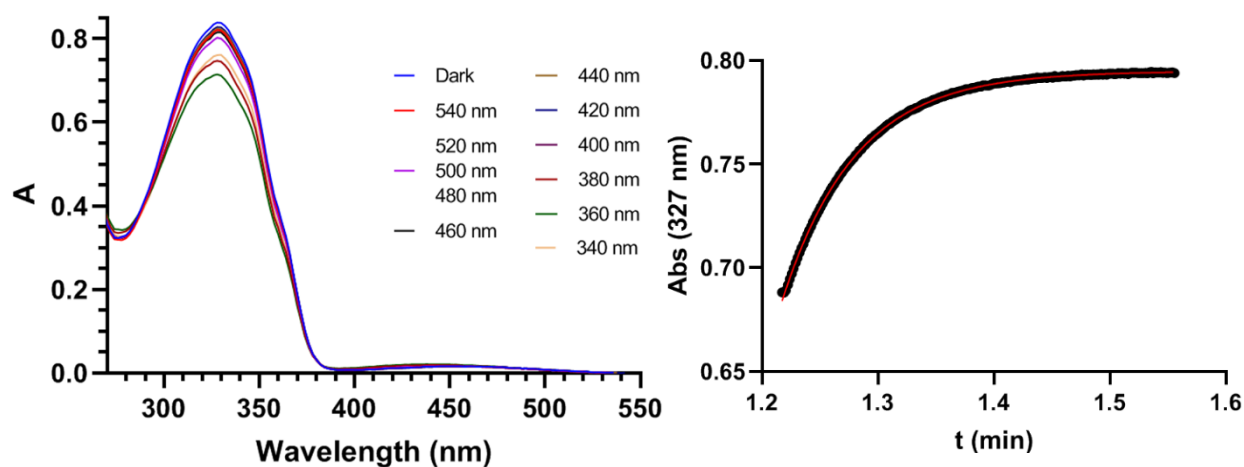


**Figure 6.4.** Left. UV/Vis absorption spectra of **6.13** in 20% DMSO/PBS buffer obtained in the dark and upon irradiation at the specified wavelengths. Right. Thermal relaxation of 50  $\mu$ M **6.13** in 20% DMSO/PBS buffer recorded at 327 nm from which *cis*  $t_{1/2}$  = 2.6 s was determined.

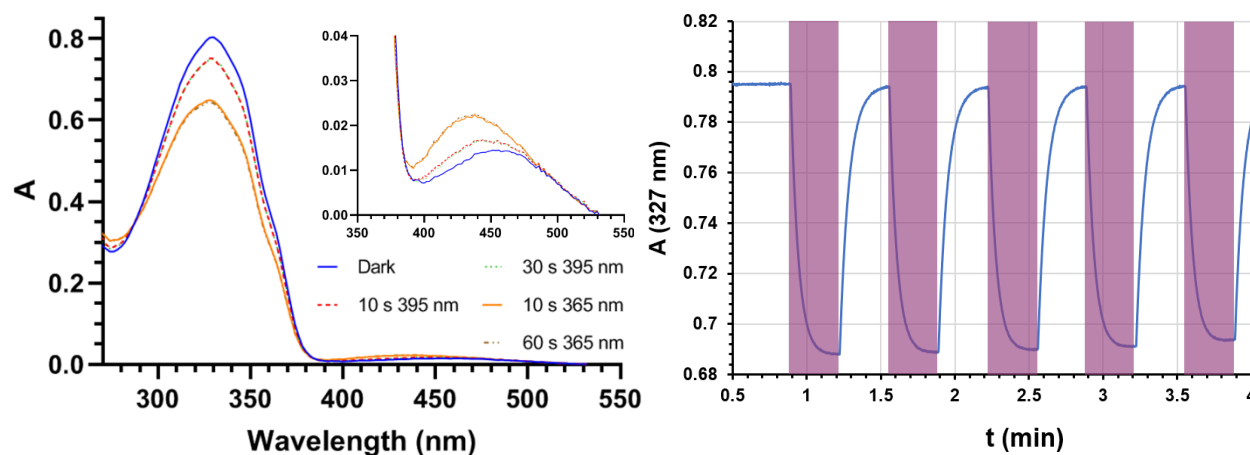


**Figure 6.5.** Left. UV/Vis absorption spectra of 50  $\mu$ M **6.13** in 20% DMSO/PBS buffer obtained in the dark and upon irradiation with HP-LEDs at the specified wavelengths for the given time periods. Note that there is almost no difference between the absorption spectrum after irradiation for 10 or 60 s, indicating that the photostationary state is quickly reached. Right. Photoswitching of **6.13** repeated over several cycles. The white columns represent no irradiation (dark, relaxation), and the purple columns irradiation with a 365 nm HP-LED inducing *cis*-isomerization.

Preliminary one pulse  $^1\text{H}$  NMR experiments in  $\text{CDCl}_3$  performed after 5 minutes of irradiation at 365 nm with HP-LED showed a *cis/trans* ratio of 33%. (See chapter 8.8.5). The fast thermal relaxation did not allow for precise calculation of the photostationary state (PSS).

We were able to obtain a crystal structure of azobenzodiazepine **6.13** (Figure 6.6). The X-ray structure shows how the *trans*-azobenzene moiety is oriented towards the benzodiazepine core, itself arranged in P conformation. As it has been discussed in Chapter 5.4.4.3, this conformation is not compatible with GABA<sub>A</sub> receptor binding. Therefore, if this arrangement is maintained in solution, **6.13** would be expected to be *trans*-inactive.

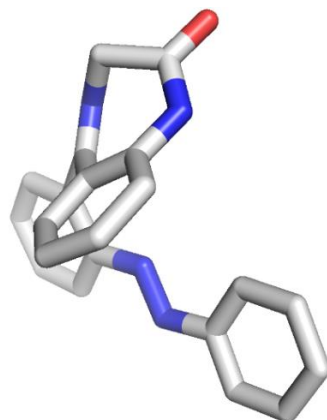


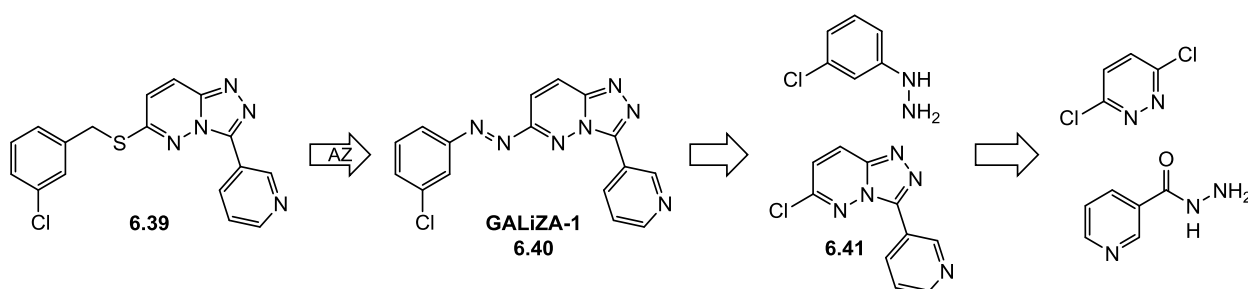
**Figure 6.6.** X-ray structure of azobenzodiazepine **6.13**.

## 6.2 Synthesis of GABA<sub>A</sub>R Light-Controlled Z-Drug Allosteric Modulators

### 6.2.1 Project Outline

As it has been discussed in Chapter 5.4.5, Z-drugs share a fused 6/5 heterocyclic aromatic scaffold bearing a variable number of nitrogen atoms and their binding mode to GABA<sub>A</sub>Rs is not known. In addition, in Chapter 5.4.4.3 it was explained that Sigel, Ernst and others used a combination of covalent binding experiments and docking studies to define BZ binding modes I and II, which were later used in a virtual screening campaign to find new high affinity ligands for the GABA<sub>A</sub>R.<sup>[277]</sup> The highest affinity was displayed by compound **6.39** ( $K_i = 11$  nM), comparable to that of diazepam.<sup>[318]</sup>

Given the high affinity displayed by **6.39** for the  $\alpha 1\beta 2\gamma 2$  GABA<sub>A</sub>R subtype and the presence of an “azostere” in its structure, we decided to pursue the azologization depicted in Scheme 6.11, which resulted in GABA<sub>A</sub>R Light-controlled Z-drug Allosteric modulator-1 (GALiZA-1, **6.40**). This azobenzene could be obtained by means of nucleophilic aromatic substitution of **6.41** with 3-chlorophenylhydrazine followed by hydrazine reduction. Triazolopyridazine **6.41** could in turn be obtained by condensation of nicotinic hydrazide and 2,6-dichloropyridazine (Scheme 6.11).

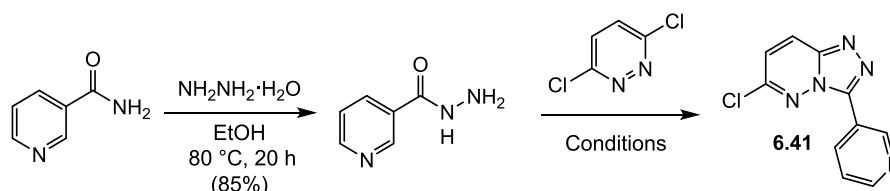


**Scheme 6.11.** Proposed azologization of **6.39** and retrosynthesis of GALiZA-1.



## 6.2.2 Results and Discussion

The synthesis started with nicotinamide, which was treated with hydrazine monohydrate in refluxing ethanol to yield nicotinic hydrazide.<sup>[335]</sup> The condensation of nicotinic hydrazide and 2,6-dichloropyridazine was attempted by following the method by Hernández et al., which consisted in the treatment of 2,6-dichloropyridazine derivatives with different aromatic hydrazides in a PTSA/Et<sub>3</sub>N buffered dioxane solution at high temperatures.<sup>[336]</sup> When we applied these reaction conditions to our system, no conversion was observed (Entry 1, Table 6.2). Heating at 135 °C led to some decomposition without any trace of product (Entry 2). We considered that the presence of water could be detrimental given the highly electrophilic nature of 2,6-dichloropyridazine, so we used anhydrous sulfonic acid instead of PTSA monohydrate under the same conditions, but again, the reaction failed to deliver the desired product (Entries 3 and 4). Since the exact role of the acid and the base was not clear, we decided to separately run the reaction under either basic or acidic conditions, but this only led to decomposition (Entries 5 and 6). Finally, the reaction was run in *n*-butanol, under microwave irradiation and in the absence of additives allowing for isolation of the desired product **6.41** in 86% yield (Entries 7 and 8).



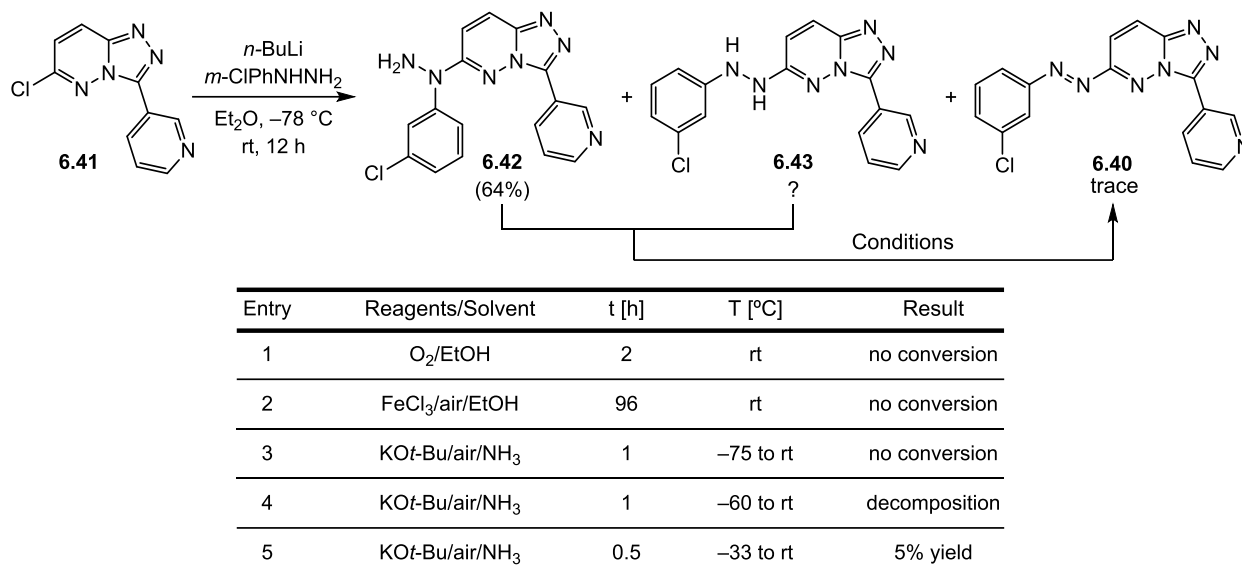
Entry	Solvent	Acid	Base	T [°C]	t [h]	Result
1	Dioxane	PTSA·H <sub>2</sub> O	Et <sub>3</sub> N	100	18	no conversion
2	Dioxane	PTSA·H <sub>2</sub> O	Et <sub>3</sub> N	135	18	partial decomposition
3	Dioxane	PhSO <sub>3</sub> H	Et <sub>3</sub> N	100	72	no conversion
4	Dioxane	PhSO <sub>3</sub> H	Et <sub>3</sub> N	135	18	partial decomposition
5	Dioxane	PhSO <sub>3</sub> H	–	100	20	partial decomposition
6	Dioxane	–	Et <sub>3</sub> N	100	20	partial decomposition
7	<i>n</i> -BuOH	–	–	120	1.1	71% yield
8	<i>n</i> -BuOH	–	–	125	1	86% yield

**Scheme 6.12 and Table 6.2.** Conditions screened for the synthesis of intermediate **6.41**.

With triazolopyridazine **6.41** in hand, we proceeded to introduce the 3-chlorophenylhydrazine at C5 *via* S<sub>N</sub>Ar. This reaction was unproductive when performed in refluxing toluene, and yielded only traces of hydrazine **6.43** when run at low temperature using *n*-BuLi as a base. The major product was instead *N,N*-disubstituted hydrazine **6.42**, and although we identified the desired product in the crude mixture, we were not able to isolate it. Moreover, traces of the final product **6.40** were also found in the crude mixture, suggesting that hydrazine **6.43** could spontaneously oxidize to the desired azobenzene when exposed to air.

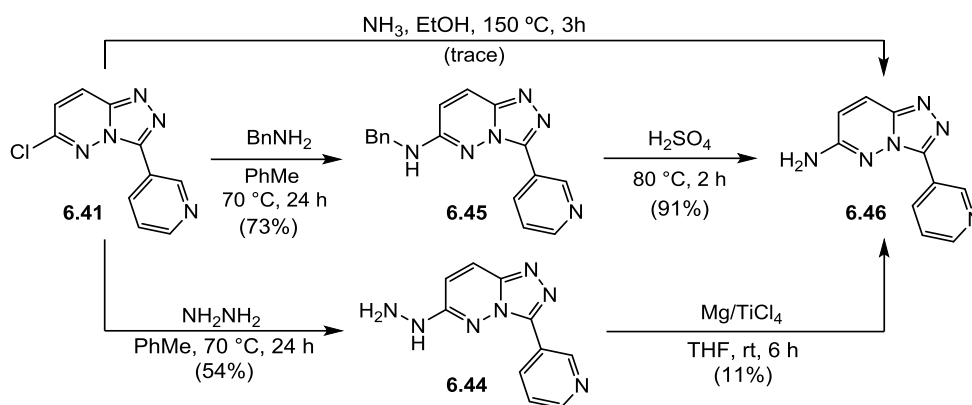
We therefore repeated the reaction and submitted the crude to different oxidation conditions reported to yield azobenzenes from *N,N'*-diaryl hydrazines.<sup>[337]</sup> The first approach consisted in bubbling oxygen through an ethanolic solution of the reaction crude containing **6.42** and **6.43**. However, after 2 hours no conversion was observed (Table 6.2, Entry 1). Stirring the mixture in EtOH under open air in the presence of excess

FeCl<sub>3</sub> over 96 hours led to the same result (Entry 2). In 2016, Hashidoko published an article on the dehydrogenation of a series of aromatic hydrazines mediated by potassium *tert*-butoxide in liquid ammonia at room temperature.<sup>[337]</sup> The reaction conditions described consisted in mixing liquid ammonia with the corresponding hydrazine, air and potassium *tert*-butoxide in a sealed tube, allowing the mixture to warm to room temperature and let react for a few minutes. Concerned about the handling of pressurized ammonia, we modified the reaction conditions letting the reaction stir at either –75 °C or –60 °C in an opened system for one hour and then allowed the solvent to evaporate slowly. Unfortunately, no product was found (Table 6.2, Entries 3 and 4). When the reaction mixture was stirred in the same manner at –33 °C for 30 minutes followed by rapid ammonia evaporation, **6.40** was found in the reaction crude and could be isolated by HPLC in 5% yield (Entry 5).



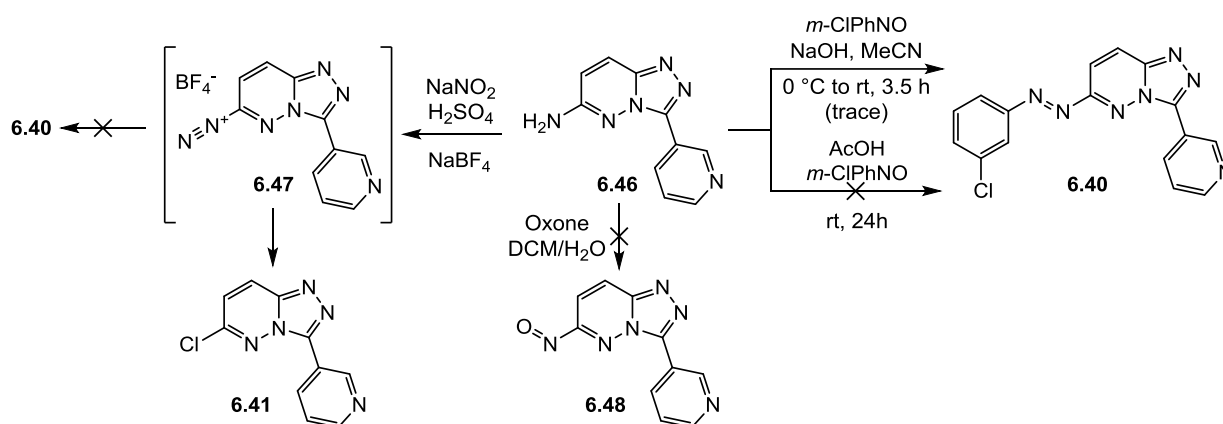
**Scheme 6.13 and Table 6.2.** Attempts to synthesize **6.40** from **6.41** and conditions screened.

We discarded the hydrazine method since it could not deliver substantial amounts of azobenzene **6.40** and opted to step back and introduce an amino group at the C2 position of **6.41**, which would allow for a subsequent Baeyer–Mills reaction. Since we only obtained traces of the desired amine **6.46** upon reaction of heteroaryl chloride **6.41** with ethanolic ammonia (Scheme 6.14) we decided to install the amine by S<sub>N</sub>Ar with benzylamine followed by deprotection with sulfuric acid. This strategy allowed us to obtain amine **6.46** in good yield, although the yield for the benzyl deprotection decreased dramatically when scaling up the reaction from 15 mg to 100 mg of benzylamine **6.45**. In parallel to this synthetic work we prepared unstable hydrazine **6.44** by reacting heteroaryl chloride **6.41** with hydrazine in toluene at 70 °C. The resulting product was immediately treated with a mixture of magnesium and titanium tetrachloride which induced radical cleavage of the terminal amine leading to the desired product **6.46** in low yield.<sup>[338]</sup>



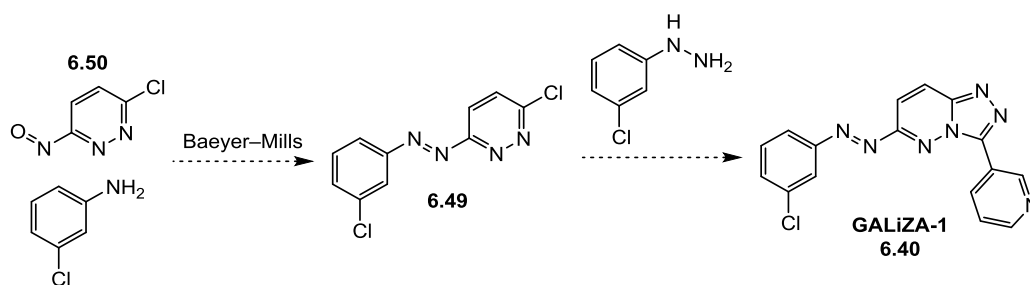
**Scheme 6.14.** Synthesis of amine **6.46** from intermediate **6.41**.

Now that we had established an efficient route to amine **6.46**, Baeyer–Mills coupling was performed with 3-chloronitrosobenzene under acidic and basic conditions, of which only the latter allowed us to obtain trace amounts of the desired product **6.40** (Scheme 6.15). We tried to transfer the nitroso functionality to the triazolopyridazine by treating heterocyclic amine **6.46** with Oxone in a biphasic system, but no product was obtained. Finally, since the Baeyer–Mills approach was unsatisfactory, we synthesized the diazonium salt of **6.46** by treatment with sodium nitrite in the presence of sulfuric acid and sodium tetrafluoroborate. However, we could not isolate or transform this salt with any substrate given the immediate conversion of **6.47** into heterocyclic chloride **6.41**, presumably upon uncatalyzed Sandmeyer reaction of the very reactive diazonium salt with trace amounts of chloride ions present in sulfuric acid.



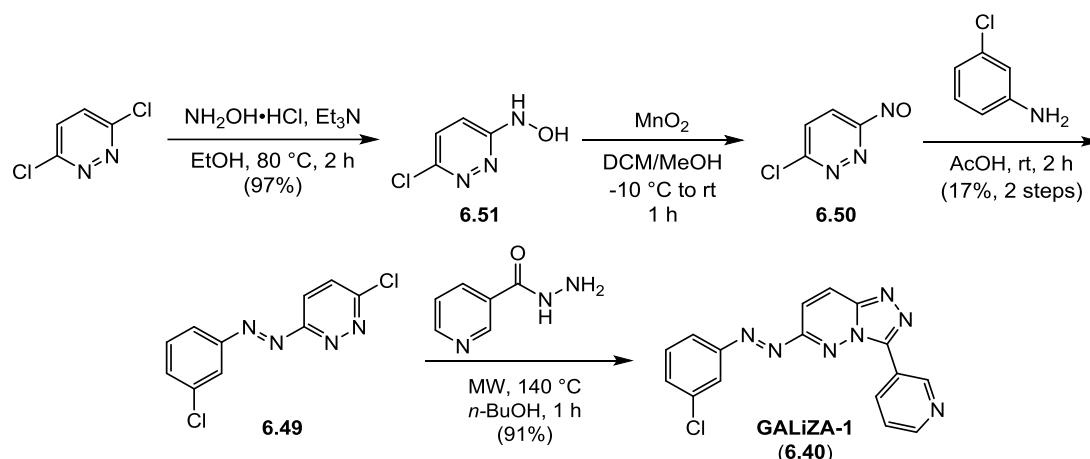
**Scheme 6.15.** Attempts to synthesize azobenzene **6.40** from amine **6.46**.

Given the unsatisfactory results, we decided to change the order of events and first perform an unprecedented Baeyer–Mills reaction with nitrosopyridazine **6.50**, which would yield azobenzene **6.49**, and condense the latter with 3-chlorophenylhydrazine to obtain GALiZA-1 (Scheme 6.16).



**Scheme 6.16.** New strategy followed for the synthesis GALiZA-1 starting from nitrosopyridazine **6.50**.

Hence, following a procedure by Yamamoto,<sup>[339]</sup> 2,6-dichloropyridazine was reacted with hydroxylamine in the presence of triethylamine in refluxing ethanol to yield hydroxylamine **6.51** (Scheme 6.17). **6.51** was subsequently oxidized with manganese dioxide at low temperature yielding unstable nitrosopyridazine **6.50**, which was immediately submitted to a Baeyer–Mills coupling with 3-chloroaniline, affording the desired azopyridazine **6.49**. Despite the low yield of the azo-coupling, given the low cost of the starting materials and the simplicity of the procedures, hundreds of milligrams of **6.49** could be easily obtained using this route. Finally, condensation of pyridazine **6.49** with nicotinic hydrazide under the previously examined conditions delivered GALiZA-1 in excellent yield (Scheme 6.17).



**Scheme 6.17.** Synthesis of GALiZA-1.

Given the unprecedented structure of **6.49**, we decided to record its UV/Vis absorption profile. Thus, a 50  $\mu\text{M}$  DMSO solution of **6.49** was irradiated for ten minutes at different wavelengths with help of a monochromator before the absorption spectra were measured (Figure 6.8). The spectra of **6.49** show a maximum absorption peak at 312 nm together with a small local maximum for the *cis*-form at 429 nm. These peaks are slightly blue-shifted compared to the homologous azobenzene (330 and 435 nm, solvent not reported)<sup>[340]</sup> The spectrum corresponding to the *trans*-form shows the highest absorption upon irradiation at 600 nm (top blue line), and the *cis*-enriched form the lowest (green line, 360 nm). The most efficient wavelength to induce *cis* isomerization was found at 360 nm whereas for *trans*-**6.49** was at 420 nm (Figure 6.8).

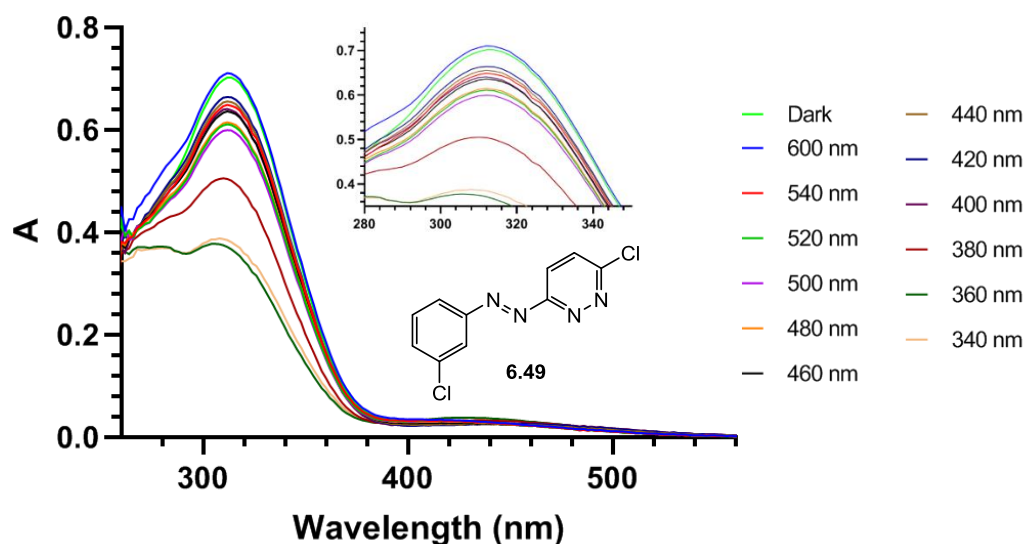


**Figure 6.8.** UV/Vis absorption spectra of a 50  $\mu\text{M}$  solution of **6.49** in DMSO. Each measurement was recorded after 10 minutes of irradiation at the specified wavelength.

The UV/Vis data of **GALiZA-1** was also collected, this time from a 50  $\mu\text{M}$  solution in 20% DMSO in PBS buffer. The spectra show clear switching and reveal 3 isosbestic points at 400, 279 and 263 nm, with maximum absorption at 312 nm and a *cis* local maximum at 438 nm. The best wavelength for *trans* to *cis* switching was 360 nm and from *cis* to *trans* 440 nm.

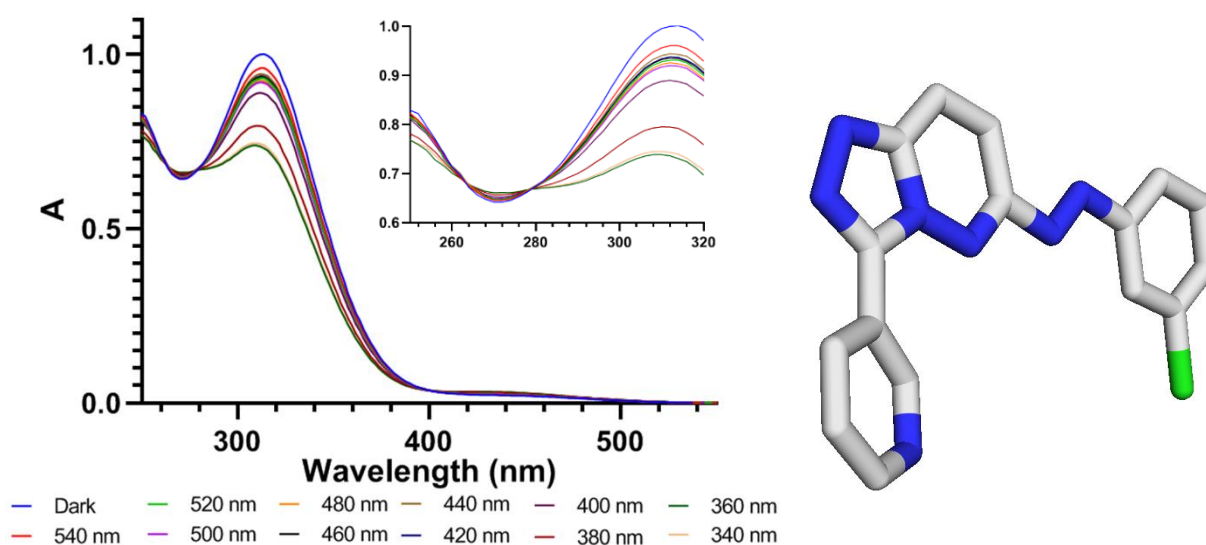


**Figure 6.9. Left.** UV/Vis absorption spectra of **GALiZA-1** in 20% DMSO/PBS buffer upon irradiation at the specified wavelengths for 10 minutes with help of a monochromator. **Right.** Crystal structure of **GALiZA-1**.

The crystal structure of GALiZA-1 revealed its high planarity, with a slightly twisted pyridine ring. The switching was repeated over several cycles without any significant loss in absorbance (Figure 6.10, left). The *cis*-form was allowed to thermally relax over several hours, allowing for the calculation of *cis*-**6.40** half-life,  $t_{1/2}$  = 40 minutes.

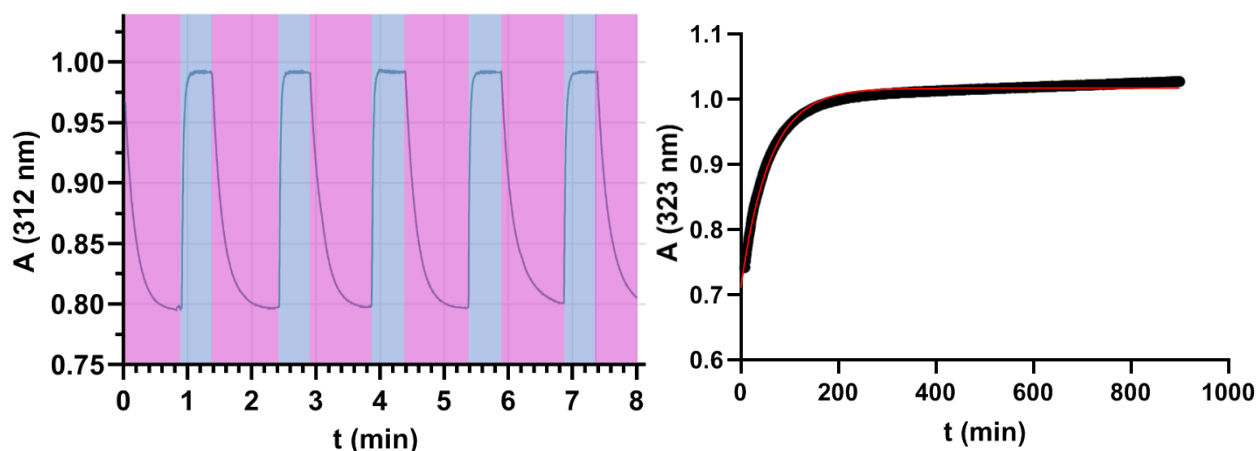
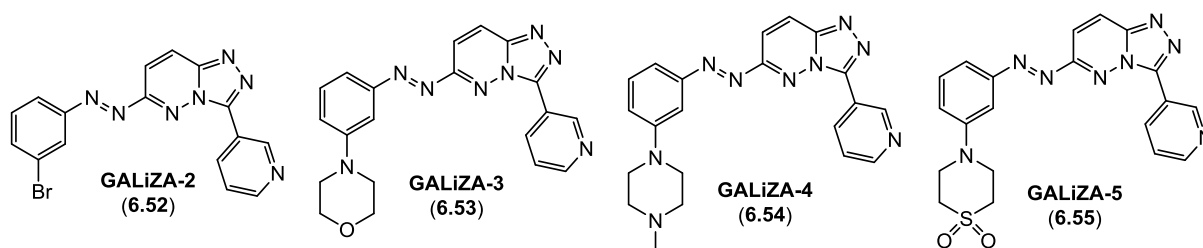


**Figure 6.10.** **Left.** Switching of a 50  $\mu$ M solution of **6.40** in 20% DMSO/PBS buffer induced by HP-LED at 365 nm (*trans* to *cis*, pink columns) and at 460 nm (*cis* to *trans*, blue columns). **Right.** Thermal relaxation of **6.40** recorded at 323 nm from which a  $t_{1/2}$  of 40 minutes was determined.

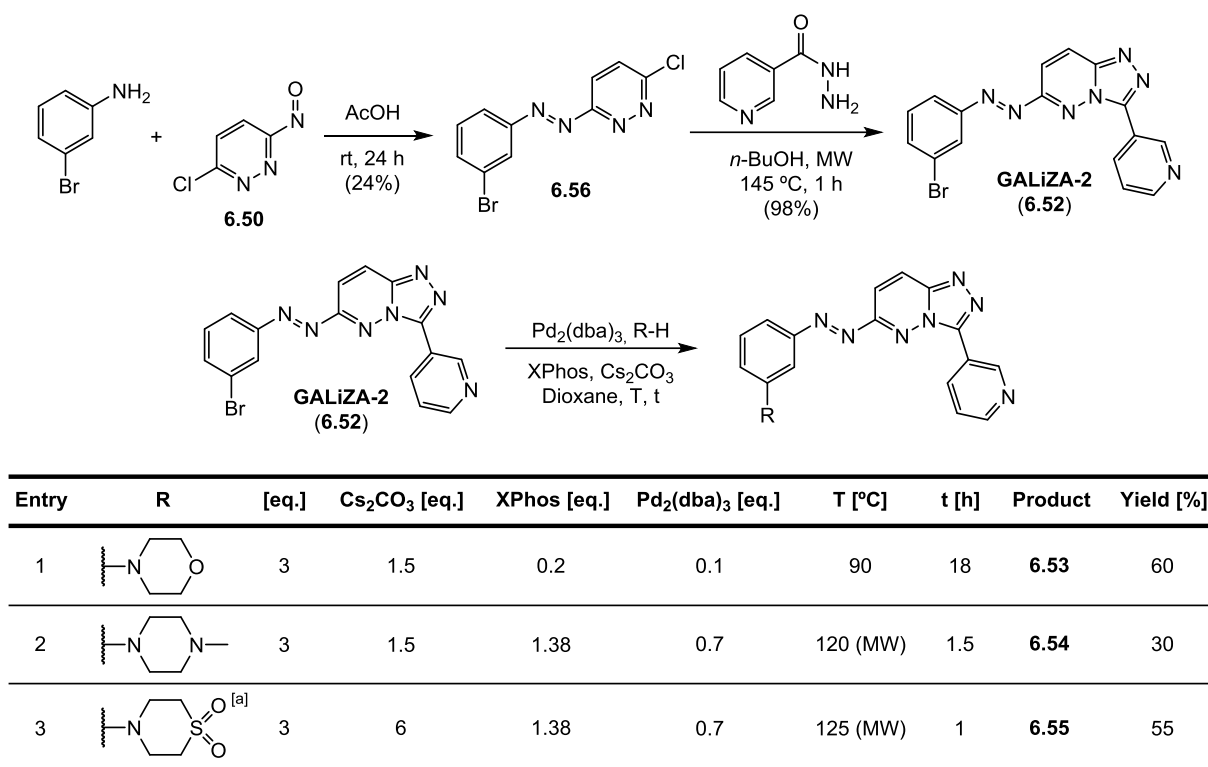
Preliminary  $^1\text{H}$  NMR measurements in  $\text{CDCl}_3$  were performed after irradiation at 365 nm for 5 minutes showing a *cis/trans* ratio of 25/75.

Given the successful synthesis of GALiZA-1, we decided to use this efficient route to obtain new derivatives with varying solubilities, steric bulk and maximum absorption wavelengths. Hence, we aimed to synthesize analogues GALiZA-2 to GALiZA-5 (Scheme 6.18).



**Scheme 6.18.** Structure of GALiZA-2 to 5.

The synthesis of GALiZA-2 was accomplished in the same way as GALiZA-1 and in higher yield (Scheme 6.19). Introduction of the 6-membered heterocyclic moieties was accomplished *via* Buchwald–Hartwig amination with variable amounts of catalyst and temperatures (Scheme 6.19).<sup>[341]</sup> The UV/Vis data for these compounds can be seen in Figures 6.11 to 6.19, together with the description.



<sup>[a]</sup>Used as TFA salt

**Scheme 6.19 and Table 6.3. Synthesis of GALiZA-2-5.**

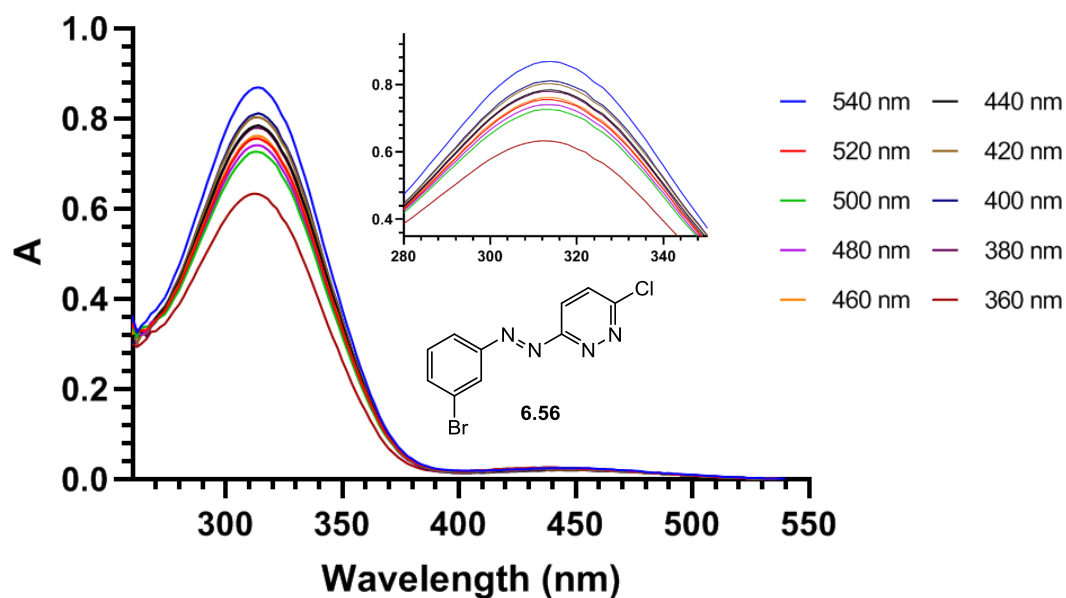


**Figure 6.11.** UV/Vis absorption spectra of a 50  $\mu$ M solution of 6.56 in DMSO upon 10 minutes of irradiation at the specified wavelengths with help of a monochromator. The maximum absorbance was found at 313 nm with a local maximum for the *cis*-form at 438 nm and no clear isosbestic points. The best *trans*→*cis* isomerization wavelength was found at 360 nm whereas for *cis*→*trans* was 400 or 420 nm.

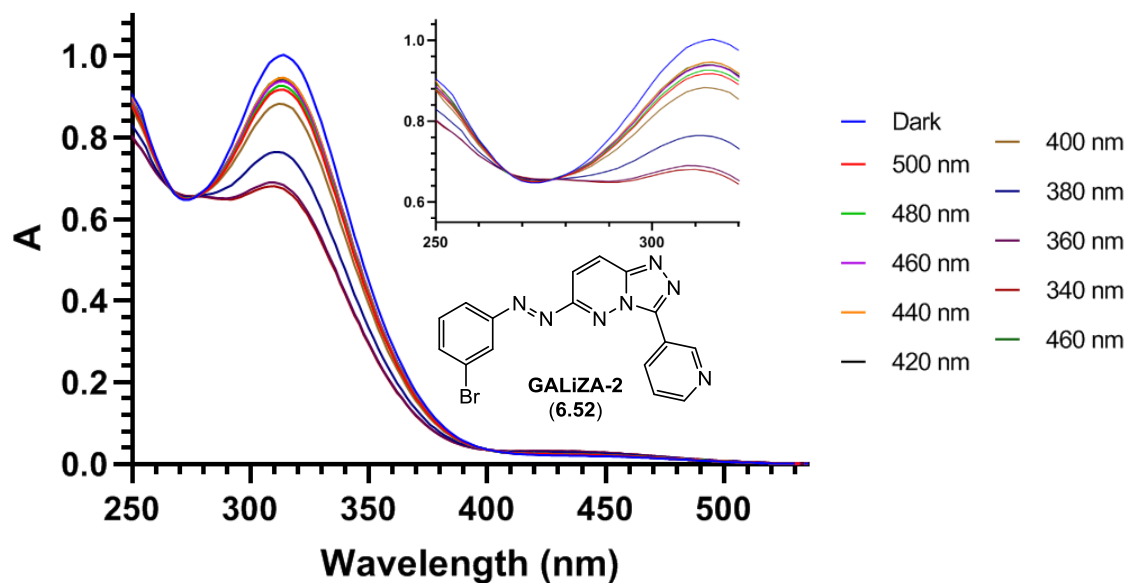


**Figure 6.12.** UV/Vis absorption spectra of a 50  $\mu\text{M}$  solution of **6.52** in 20% DMSO/PBS upon 10 minutes of irradiation at the specified wavelengths with help of a monochromator. The absorption maximum was found at 314 nm and 3 isosbestic points were found at 277, 266 and 401 nm. The best *trans*→*cis* isomerization wavelength was 340 nm whereas for *cis*→*trans* was 440 nm.

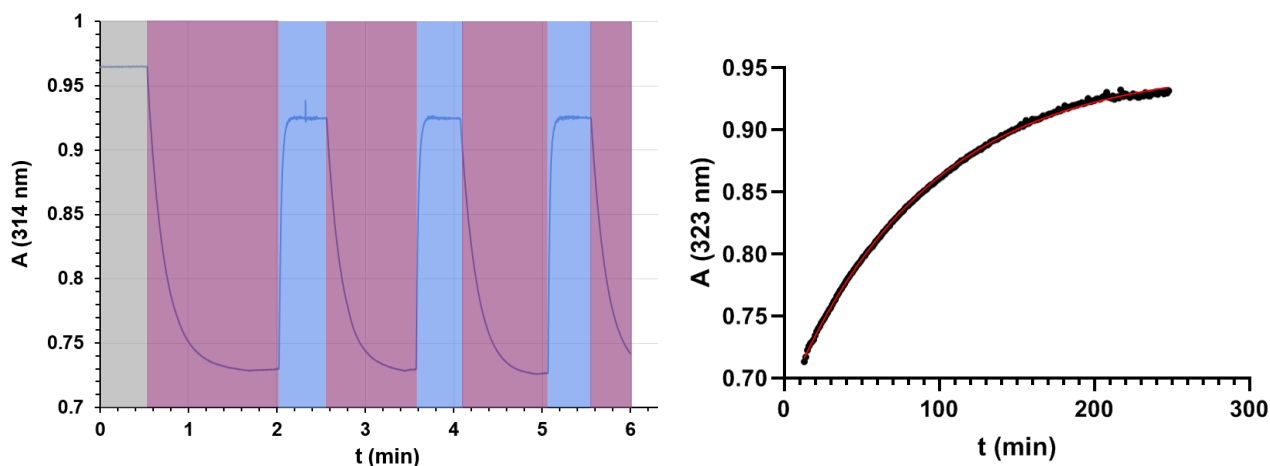


**Figure 6.13.** Left. Switching of a 50  $\mu\text{M}$  solution of **6.52** in 20% DMSO/PBS buffer induced by HP-LED. Starting in the dark (grey column) the solution was irradiated at 365 nm (*trans* to *cis* isomerization, purple columns) and then at 460 nm (*cis* to *trans* isomerization, blue columns). Right. Thermal relaxation of **6.52** recorded at 323 nm with a  $t_{1/2}$  of 40 minutes.



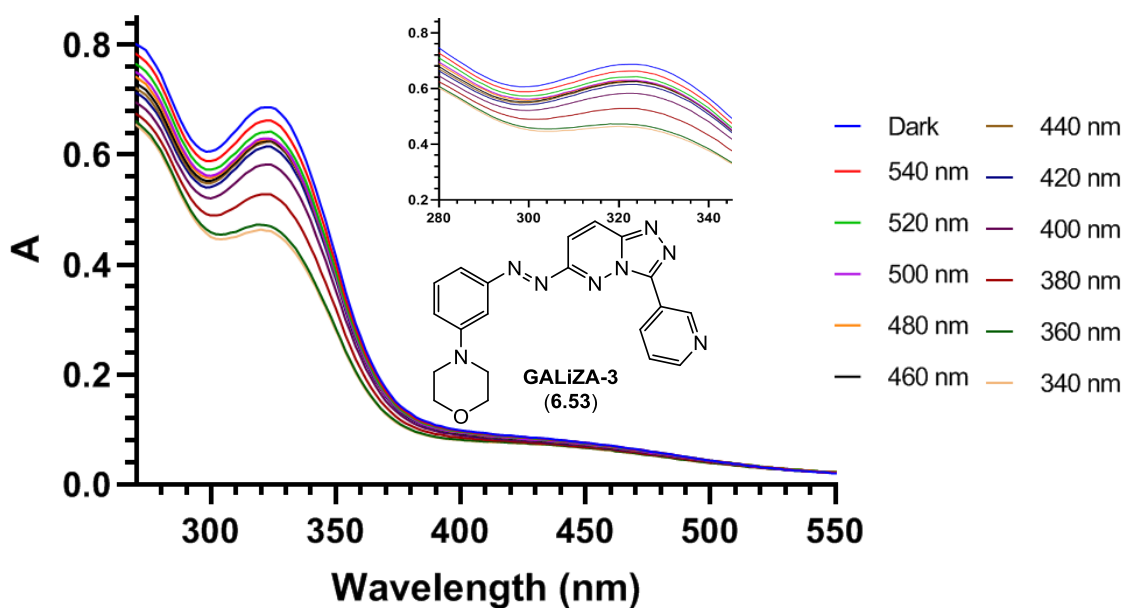


**Figure 6.14.** UV/Vis absorption spectra of a 50  $\mu$ M solution of **6.53** in 20% DMSO/PBS buffer upon 10 minutes of irradiation at the specified wavelengths with help of a monochromator. The absorption maximum was found at 324 nm and no isosbestic points were found. The best trans $\rightarrow$ cis isomerization wavelength was 340 nm whereas for cis $\rightarrow$ trans was 460 nm.

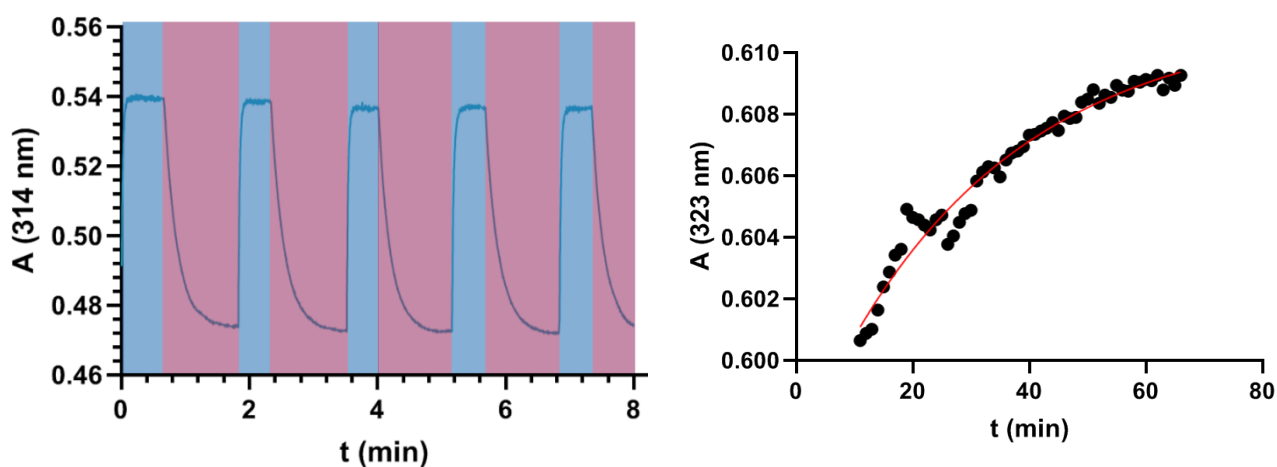


**Figure 6.15.** **Left.** Switching of a 50  $\mu$ M solution of **6.53** in 20% DMSO/PBS buffer induced by HP-LED upon irradiation at 365 nm (trans to cis isomerization, purple columns) and at 460 nm (cis to trans isomerization, blue columns). Preliminary  $^1\text{H}$  NMR measurements in  $\text{CDCl}_3$  were performed after irradiation at 365 nm for 5 minutes showing a cis/trans ratio of 17/83. **Right.** Thermal relaxation of **6.53** recorded at 323 nm with a  $t_{1/2}$  of 22 minutes. The fluctuation of data points could be consequence of the relatively small changes in absorption upon switching.

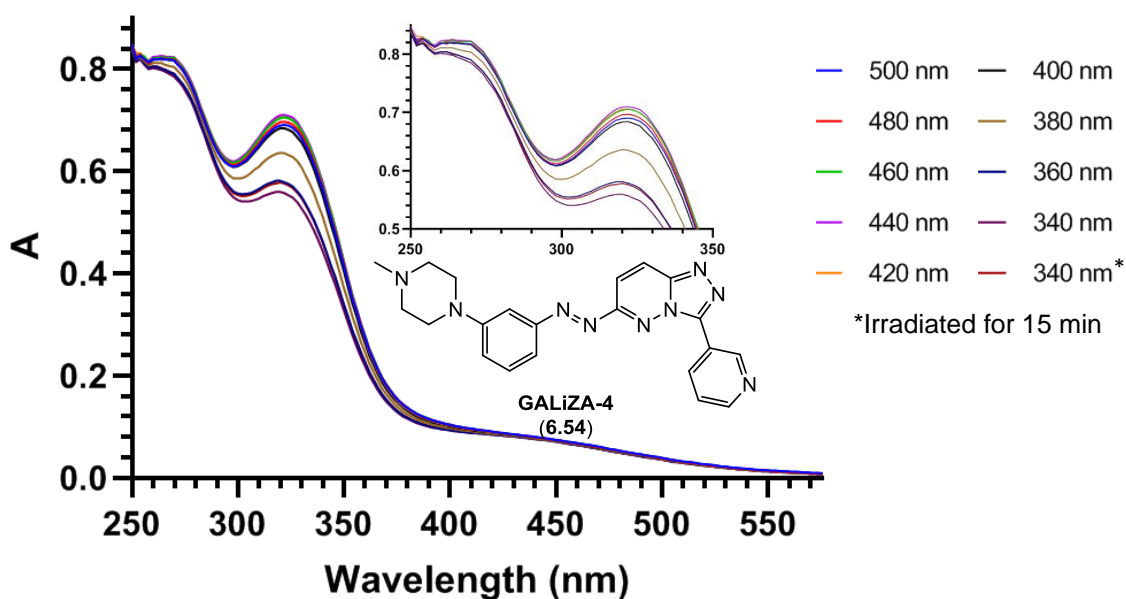


**Figure 6.16.** UV/Vis absorption spectra of a 50  $\mu\text{M}$  solution of **6.54** in 20% DMSO/PBS buffer upon 10 minutes of irradiation at the specified wavelengths with help of a monochromator. The absorption maximum was found at 322 nm with no isosbestic points. The best *trans*→*cis* isomerization wavelength was found at 340 nm whereas for *cis*→*trans* at 440 nm.

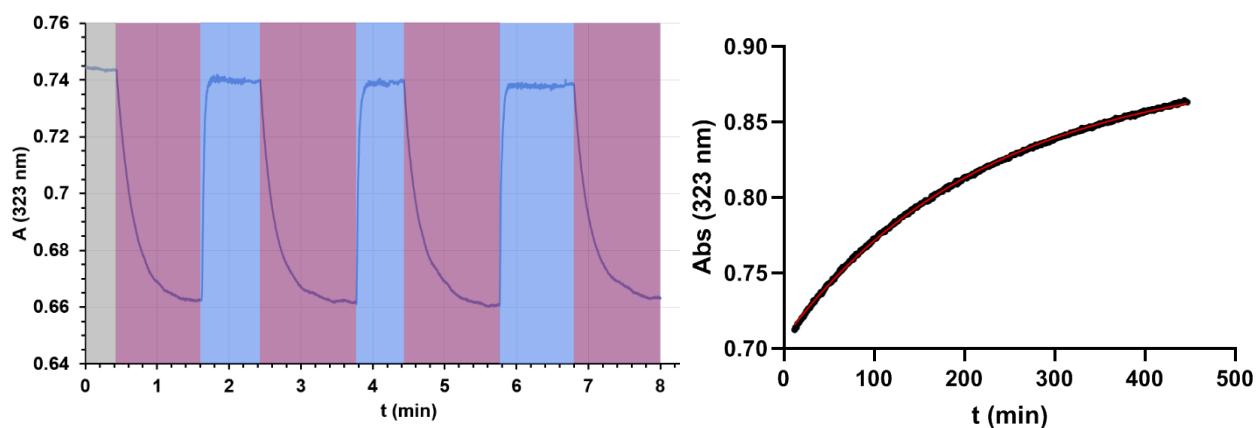


**Figure 6.17. Left.** Switching of a 50  $\mu\text{M}$  solution of **6.54** in 20% DMSO/PBS buffer induced by HP-LED at 365 nm (*trans* to *cis*, purple columns) and at 460 nm (*cis* to *trans*, blue columns). Preliminary  $^1\text{H}$  NMR measurements in  $\text{CDCl}_3$  were performed after irradiation at 365 nm for 5 minutes showing a *cis*/*trans* ratio of 13/87. **Right.** Thermal relaxation of **6.54** recorded at 323 nm with a  $t_{1/2}$  of 120 minutes.

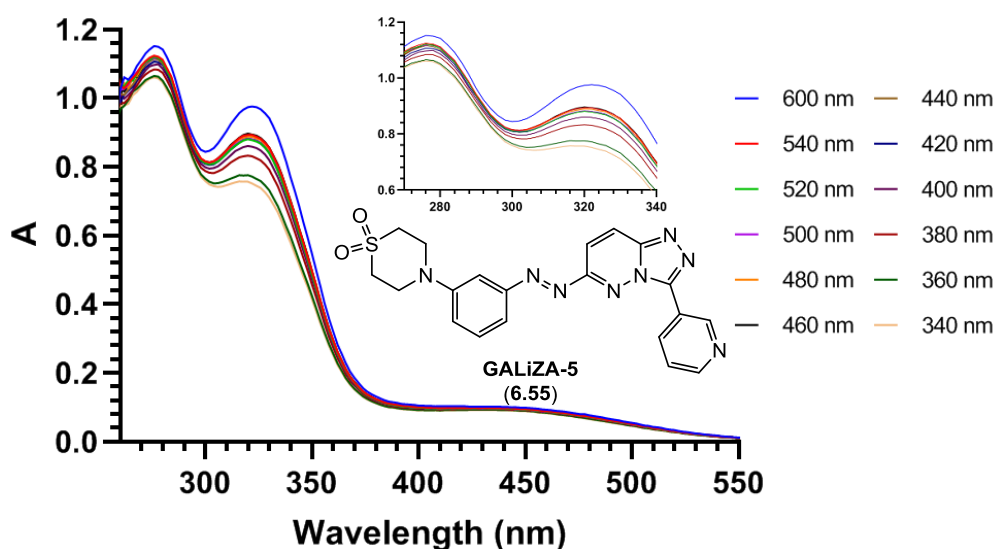


**Figure 6.18.** UV/Vis absorption spectra of a 50  $\mu\text{M}$  solution of **6.55** in 20% DMSO/PBS buffer upon 10 minutes of irradiation at the specified wavelengths with help of a monochromator. The absorption maximum was found at 322 nm with no isosbestic points. The best *trans*→*cis* isomerization wavelength was 340 nm whereas for *cis*→*trans* was 440 nm.

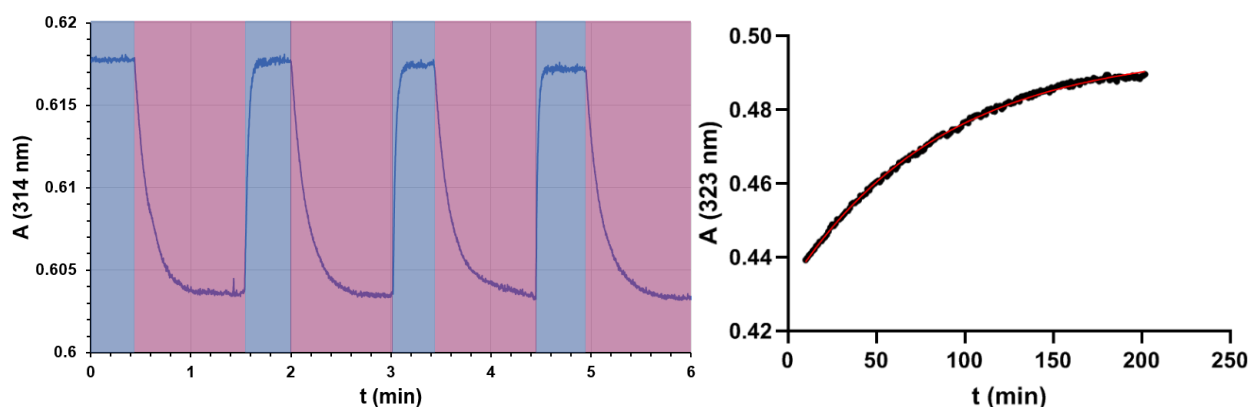
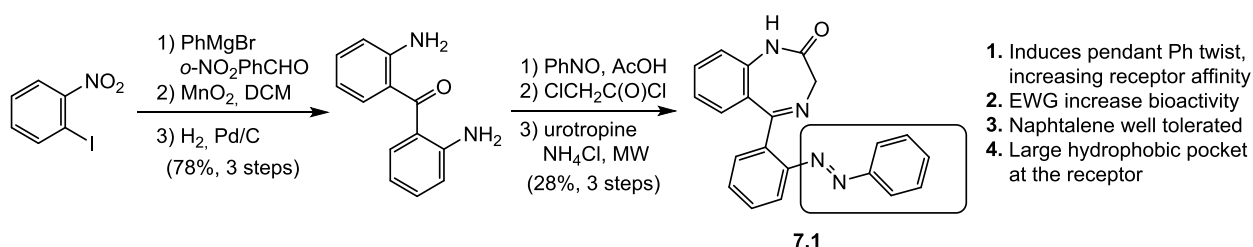


**Figure 6.19.** **Left.** Switching of a 50  $\mu\text{M}$  solution of **6.55** in 20% DMSO/PBS buffer induced by HP-LED at 365 nm (*trans* to *cis*, purple columns) and at 460 nm (*cis* to *trans*, blue columns). Preliminary  $^1\text{H}$  NMR measurements in DMSO- $d_6$  were performed after irradiation at 365 nm for 5 minutes showing a *cis*/*trans* ratio of 17/83. **Right.** Thermal relaxation of **6.54** recorded at 323 nm with a  $t_{1/2}$  of 59 minutes.

## 7. Summary and Outlook

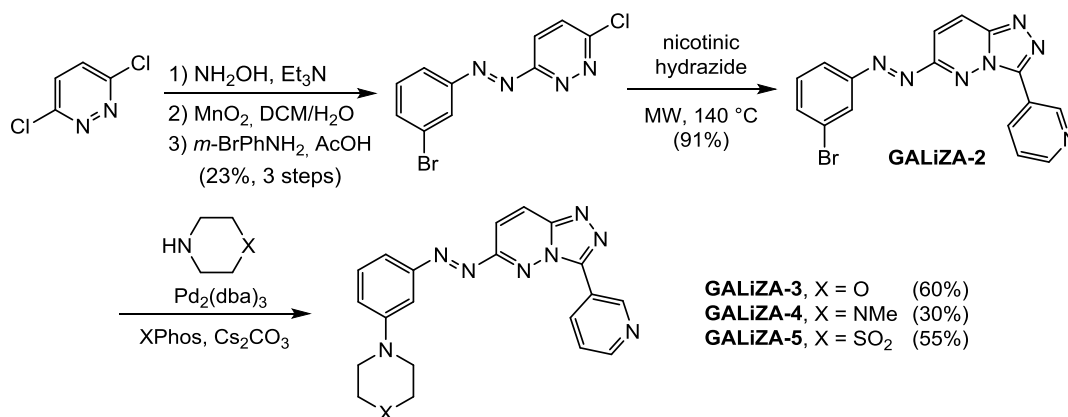
In the second part of the thesis we described the rational design and synthesis of a photoswitchable benzodiazepine bearing an azobenzene moiety. The design was based on four premises depicted in Scheme 7.1. Azobenzodiazepine **7.1** was synthesized in 6 steps from commercially available precursors and based on the unusual strategy of introducing the azobenzene moiety in initial stages, giving rise to rare azobenzophenone intermediates. Given the simplicity, low cost and robustness of this method, we presume that several other benzodiazepine derivatives could be synthesized along this route.

We have also acquired data on the UV/Vis properties of **7.1**, which presents an absorption maximum at 327 nm and half-life of 2.6 s for the *cis*-form. **7.1** has been isolated with high purity and is ready for biological testing, which will be performed in collaboration with Prof. Francisco Ciruela from University of Barcelona. We hope that this or other analogues will prove to be a useful tool to gain better understanding on BZ binding and GABA<sub>A</sub> receptors.



**Scheme 7.1.** Summarized synthesis of photoswitchable benzodiazepine **7.1** and premises which guided its design.

The synthesis of a small family of photoswitchable Z-drug derivatives based on the lead compound by Sigel was also described. These compounds entail a triazolo[4,3-b]pyridazine core, whose azologization led to an unprecedented class of heterocyclic azobenzenes. Again, an unusual strategy based on the early introduction of the azobenzene group allowed us to synthesize not only the desired GABA<sub>A</sub>R light-controlled Z-drug Allosteric modulators (GALiZA) but also previously unreported pyridazine azobenzenes. The synthetic route developed delivered the final products in 4-5 linear steps from inexpensive starting materials. We are again confident that this route could tolerate several modifications on the substitution pattern of any of the aromatic moieties.



**Scheme 7.1.** Summarized synthesis of photoswitchable Z-drugs.

The spectral properties of GALiZA 1-5 have also been defined, with  $\lambda_{\text{max}} \approx 324$  nm, and *cis* thermal relaxation half-lives between 22-120 minutes. Preliminary  $^1\text{H}$  NMR measurements showed photostationary states with low content of *cis*-isomer. These results could be improved by changing the solvent and diluting the samples. We hope that these compounds will provide new insights in the binding modes of Z-drugs upon testing on GABA<sub>A</sub>Rs by Ciruela's group.

## **EXPERIMENTAL PART**

## 8. Experimental section

### 8.1 General Experimental Details

Unless otherwise stated, reactions were carried out under nitrogen atmosphere utilizing standard Schlenk-technique using oven-dried glassware and stir bars (160 °C) or heat gun-dried (>550 °C) while under vacuum glassware and stir bars. Heating over room temperature was achieved with aluminium heating blocks or oil baths. Low temperature reactions were performed with acetone/dry ice baths (−78 °C, −50 °C, −30 °C) or ice baths (0 °C). Dry solvents were used from the following sources: tetrahydrofuran (THF), dichloromethane (DCM), benzene, hexane and diethyl ether (Et<sub>2</sub>O) were Fisher certified ACS reagents dried and degassed with an Innovative Technology PS-MD-6 solvent system. Chloroform (CHCl<sub>3</sub>), toluene (PhMe), pyridine, ethyl acetate, dioxane and *N,N*-dimethylformamide (DMF) were purchased as extra dry and stabilized from Acros Organics. Ethanol was purchased from Decon Labs with USP certified quality. *n*-Butanol 99% pure was purchased from Oakwood chemicals. Methanol >99.8% purity was acquired from VWR chemicals. The last three alcohols were independently stored in amber flasks under 3Å molsieves and septum.

*n*-Buthyllithium and *s*-Buthyllithium were purchased from Acros Organics and titrated using *N*-benzylbenzamide. All reagents used were purchased from commercial vendors and directly used unless otherwise stated.

Reactions were monitored by thin layer chromatography (TLC) on glass plates precoated with silica gel (0.25 mm, 60Å pore size, F254) from MilliporeSigma and visualized under UV light (254 nm) or stained with ceric ammonium molybdate. Flash column chromatography was performed either by hand or on Teledyne ISCO Combiflash Rf+ system with manually packed Universal RediSep cartridges using Geduran® Si 60 silicagel (40-60 µm particle size) from MilliporeSigma or when specifically stated with spherical 20-40 µm particle size silica from RediSep Rf. HPLC purifications were performed on an Agilent 1260 Infinity Prep Pump system with 1260 Infinity II Diode Array Detector WR connected to a Gemini 5 µm, C18, 110Å semipreparative column.

Microwave reactions were run in a Biotage Initiator+ with original equipment.

<sup>1</sup>H and <sup>13</sup>C spectra were measured with a Bruker Avance III HD 400 MHz spectrometer equipped with a CryoProbe™ operating at 400 MHz for <sup>1</sup>H and 100 MHz for <sup>13</sup>C spectra. Signals were calibrated from residual protium in NMR solvents (CHCl<sub>3</sub>: δ 7.26; DMSO-*d*<sub>6</sub>: δ 2.50) for <sup>1</sup>H and solvent resonance (CDCl<sub>3</sub>: δ 77.00; DMSO-*d*<sub>6</sub>: δ 39.53) for <sup>13</sup>C. NMR data are reported as: chemical shift (δ ppm), multiplicity expressed as: s = singlet, d = doublet, t = triplet, q = quartet, m = multiplet, br = broad, coupling constant (Hz), and integration. <sup>13</sup>C NMR shifts expressed with the exact same number are distinguishable as two peaks on the correspondent spectrum. All raw FID files were processed and the spectra analyzed using the program Mnova 11.0.3 from Mestrelab Research S. L.

High-resolution mass spectra (HRMS) were recorded on an Agilent Technologies 6224 time-of-flight (TOF) spectrometer with either atmospheric pressure chemical ionization (APCI) or electrospray ionization (ESI) sources. Infrared (IR) spectra were recorded on a ThermoScientific Nicolet-6700 Fourier Transform Infrared Spectrometer (FTIR) and reported as frequency of absorption (cm<sup>−1</sup>) with intensity of absorption (s = strong, m = medium, w = weak, br = broad). Optical rotations were measured on a Jasco P-2000 polarimeter using a 100 mm path-length Jasco CG3-100/10 Cylindrical Glass Cell at the Sodium D-line (589 nm) at the given temperature in (°C) and concentration expressed in g/100 mL. Melting points were measured on a Stanford

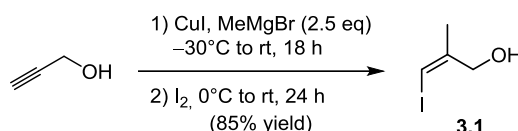
Research Systems OptiMelt MPA100 automated melting point system in open glass capillaries and are uncorrected.

The single-crystal X-ray analyses published here were performed by Dr. Peter Mayer (compound **18**) in the Analytic Department of the Faculty for Chemistry and Pharmacy of the Ludwig-Maximilians Universität Munich, and by Dr. Hu (rest of compounds) at the Department of Chemistry of New York University, with support from the X-ray facility from the Materials Research Science and Engineering Center (MRSEC) program of the National Science Foundation (NSF) under Award Numbers DMR-0820341 and DMR-1420073.



## 8.2 Supporting Information for Chapter 3.1

### 8.2.1 Experimental Procedures for Chapter 3.1



**Vinyl iodide 3.1** was synthesized following the procedure by Hiroya et al.<sup>[123]</sup>

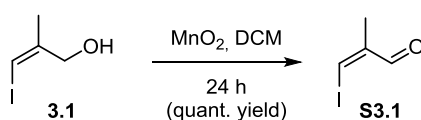
Propargyl alcohol (2.20 mL, 37.5 mmol, 1.00 equiv.) was added to a suspension of copper iodide (713 mg, 3.75 mmol, 0.10 equiv.) in anhydrous THF (83 mL) at 0 °C and stirred for 1 hour. Then a solution of MeMgBr (3.0 M in Et<sub>2</sub>O, 25 mL, 2.00 equiv.) was added to the reaction mixture over 10 minutes and the stirring was continued for 90 minutes at the same temperature. A solution of I<sub>2</sub> (14.4 g) in anhydrous Et<sub>2</sub>O (83 mL) was added to the reaction mixture over 10 min then stirred at room temperature for 90 min.

The reaction mixture was treated with a saturated aqueous NH<sub>4</sub>Cl (71 mL) solution and subsequently quenched with sat. Na<sub>2</sub>S<sub>2</sub>O<sub>3</sub> (30 mL). The aqueous layer was extracted three times with Et<sub>2</sub>O. The combined organic layers were washed with brine, dried over anhydrous MgSO<sub>4</sub> and concentrated under reduced pressure yielding a yellow oil.

The residue was purified by flash column chromatography on silica gel (EtOAc/Hexanes, 33%) yielded alcohol **3.1** as a yellow oil (5.76 g, 29.3 mmol, 76% yield).

<sup>1</sup>H NMR (400 MHz, CDCl<sub>3</sub>) δ 5.98 (s, 1H), 4.25 (s, 2H), 1.98 (s, 3H)

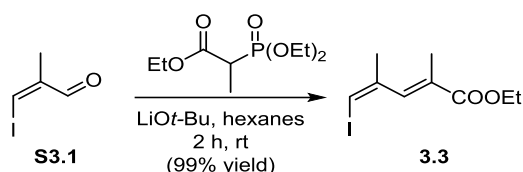
HRMS (+APCI): calc. for C<sub>4</sub>H<sub>6</sub>I [M-OH]<sup>+</sup> 180.9509, found 180.9509



**Aldehyde S3.1** was synthesized following the procedure by Baldwin and Moses.<sup>[342]</sup>

Alcohol **3.1** (5.67 g, 28.6 mmol, 1.00 equiv.) was dissolved in DCM (250 mL) and MnO<sub>2</sub> (49.74 g, 0.573 mol, 20.0 equiv.) was added in portions. The mixture was stirred at room temperature for 24 hours before it was filtered through a pad of Celite. The the solvent was evaporated at 28 °C and 350 mbar yielding a yellow liquid (5.60 g, 28.6 mmol, quant. yield) which was immediately used for the next step.

<sup>1</sup>H NMR (400 MHz, CDCl<sub>3</sub>) δ 5.98 (s, 1H), 4.25 (s, 2H), 1.98 (s, 3H)



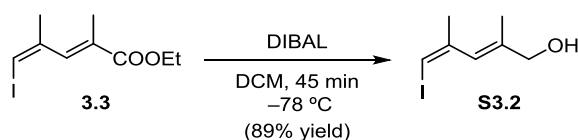
**Conjugated ester 3.3 was synthesized following the procedure by Parker et al.**<sup>[51]</sup>

To a solution of triethyl 2-phosphonopropionate (9.20 ml, 42.9 mmol, 1.5 equiv.) in dry hexane (77 mL) at room temperature was added a suspension of lithium *tert*-butoxyde (3.43 g, 42.9 mmol, 1.5 equiv.) in hexane (32 mL) which had been previously stirred for 10 minutes and sonicated for 2 minutes. The reaction mixture was stirred for 30 minutes after which aldehyde **S3.1** (5.60 g, 28.6 mmol, 1 equiv.) in hexane (30 mL) was added over 10 minutes *via* syringe. The reaction mixture was stirred for 1 hour.

Water was then added, the phases were separated and the organic phase was washed with water (4 x 100 mL), dried over anhydrous Na<sub>2</sub>SO<sub>4</sub> and concentrated under reduced pressure giving pure ester **3.3** an orange oil (7.94 g, 28.4 mmol, 99% yield), which was used for the next step without further purification.

**<sup>1</sup>H NMR** (400 MHz, CDCl<sub>3</sub>) δ 7.09 (s, 1H), 6.25 (br s, 1H), 4.24 (q, *J* = 7.1 Hz, 1H), 2.02 (s, 3H), 1.91 (s, 3H), 1.33 (t, *J* = 7.1 Hz, 1H)

**HRMS** (+APCI): calc. for C<sub>9</sub>H<sub>14</sub>IO<sub>2</sub> [M+H]<sup>+</sup> 281.0033 found 281.0031



**Allyl alcohol S3.2 was synthesized following the procedure by Trauner et al.**<sup>[58]</sup>

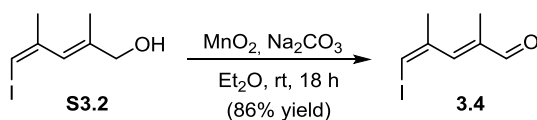
To a solution of **3.3** (13.5 g, 48.2 mmol, 1 equiv.) in DCM (400 mL) –78 °C was added dropwise a solution of DIBAL (1.2 M in PhMe, 101 mL, 2.52 equiv.).

After 45 minutes the reaction mixture was quenched with a half-saturated aqueous solution of Rochelle's salt (1065 mL), diluted with DCM (500 mL) and stirred vigorously for 30 min. The phases were separated and the aqueous phase was extracted with DCM (2 x 300 mL). The combined organic layers were dried over anhydrous Na<sub>2</sub>SO<sub>4</sub>, filtered and concentrated under reduced pressure yielding a yellow oil, 10.9 g.

Purification by flash column chromatography on silica gel (20% EtOAc in hexanes) delivered **S3.2** (10.2 g, 42.8 mmol, 89% yield) as a yellow oil.

**<sup>1</sup>H NMR** (400 MHz, CDCl<sub>3</sub>) δ 6.05 (s, 1H), 5.95 (br s, 1H), 4.10 (s, 2H), 2.01 (s, 3H), 1.73 (s, 3H)

**HRMS** (+ESI): calc. for C<sub>14</sub>H<sub>23</sub>I<sub>2</sub>O<sub>2</sub> [2M+H]<sup>+</sup> 476.9779 found 476.9782



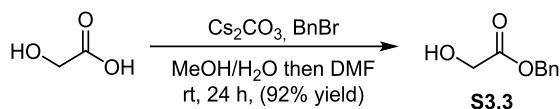
**Aldehyde 3.4 was synthesized following the procedure by Trauner et al.**<sup>[343]</sup>

To a solution of alcohol **S3.2** (2.45 g, 10.3 mmol, 1.00 equiv.) in Et<sub>2</sub>O (69 mL) was added Na<sub>2</sub>CO<sub>3</sub> (14.5 g, 137 mmol, 13.3 equiv.) followed by MnO<sub>2</sub> (12.2 g, 139 mmol, 13.6 equiv.). The suspension was stirred in the dark for 18 hours.

The reaction mixture was diluted with Et<sub>2</sub>O (75 mL), filtered through a pad of Celite and the solvent was evaporated under reduced pressure yielding a yellow oil (2.10 g, 8.90 mmol, 86% yield) which was directly used for the next step without further purification given its instability.

**<sup>1</sup>H NMR** (400 MHz, CDCl<sub>3</sub>) δ 9.56 (s, 1H), 6.93 (s, 1H), 6.50 (s, 1H), 2.17 (s, 3H), 1.90 (s, 3H)

**HRMS** (+APCI): calc. for C<sub>7</sub>H<sub>10</sub>IO [M+H]<sup>+</sup> 236.9771 found 236.9774



**α-hydroxy acid 3.6** was synthesized following the procedure by Hongwu et al.<sup>[344]</sup>

### α-hydroxy acid S3.3.

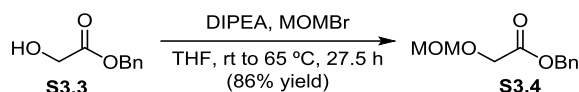
To a stirred solution of glycolic acid (4.56 g, 60.0 mmol, 1 equiv.) in MeOH (90 mL) and H<sub>2</sub>O (9.0 mL) was added a 20% m/v solution of Cs<sub>2</sub>CO<sub>3</sub> in H<sub>2</sub>O until pH 7 was reached (about 15 mL), and then the solvent was removed under reduced pressure (1 h, 64 °C, 14 mbar). The gummy residue was redissolved in DMF (60 mL) and after few minutes a white precipitate appeared. Then benzyl bromide (7.54 mL, 63.1 mmol, 1.05 equiv.) was added. The reaction mixture was stirred for 24 h at room temperature.

Brine was added to the solution, the phases were separated and the aqueous layer was extracted with EtOAc. The combined organic layers were washed with H<sub>2</sub>O and brine, dried over MgSO<sub>4</sub> and concentrated under reduced pressure yielding a colourless liquid.

The crude product was purified by flash column chromatography on silica gel (4:1 hexanes/EtOAc) to give product as a colourless oil (9.16 g, 55.1 mmol, 92% yield).

**<sup>1</sup>H NMR** (400 MHz, CDCl<sub>3</sub>) δ 7.37 (m, 5 H), 5.23 (s, 2 H), 4.20 (d, *J* = 4.6 Hz, 1H), 2.49 (t, *J* = 5.0 Hz, 1H)

**HRMS** (+APCI): calc. for C<sub>9</sub>H<sub>10</sub>NaO<sub>3</sub> [M+H]<sup>+</sup> 189.0522 found 189.0538



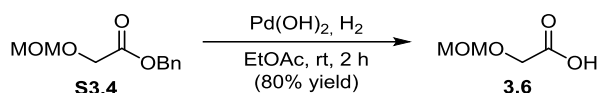
### MOM protected glycolate S3.4.

Benzyl glycolate **S3.3** (5.66 mL, 39.9 mmol, 1.00 equiv.) was dissolved in THF (35 mL) at room temperature and DIPEA (8.27 mL, 47.8 mmol, 1.20 equiv.) was added followed by MOMBr (7.48 mL, 59.8 mmol, 1.5 equiv.), resulting in fuming and exotherm. After stirring at room temperature for 3.5 hours the mixture was heated to reflux for 24 hours.

45 mL of an ice-cold aqueous saturated solution of K<sub>2</sub>CO<sub>3</sub> was added to the reaction mixture, which upon phase separation was extracted with EtOAc (3x45 mL). The combined extracts were washed with brine, dried over anhydrous MgSO<sub>4</sub>, filtered and concentrated under reduced pressure to give a brown gum which was purified by flash column chromatography on silica gel (EtOAc/Hexanes, gradient, 0 to 10%) yielding **S3.4** as a yellow liquid (7.25 g, 34.5 mmol, 86% yield).

**<sup>1</sup>H NMR** (400 MHz, CDCl<sub>3</sub>) δ 7.36 (m, 5 H), 5.20 (s, 2 H), 4.71 (s, 2H), 4.21 (s, 2H), 3.39 (s, 3H)

**HRMS** (+ESI): calc. for C<sub>11</sub>H<sub>15</sub>O<sub>4</sub> [M+H]<sup>+</sup> 211.0965 found 211.0951

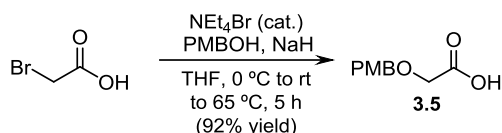


### $\alpha$ -hydroxy acid 3.6.

Ester **S3.4** (5.3 g, 25.2 mmol, 1 equiv.) was dissolved in EtOAc (65 mL). The flask was evacuated and flushed with  $\text{N}_2$  three times.  $\text{Pd(OH)}_2$  (582 mg) was added to the solution and the flask was evacuated and flushed with  $\text{H}_2$  (balloon pressure) three times. The suspension was stirred at room temperature for 2 hours, after which the mixture was filtered through a pad of Celite. The filtrate was evaporated under reduced pressure to give a yellow liquid which was purified by flash column chromatography on silica gel (EtOAc/hexanes, gradient, 0 to 60%) to deliver **3.6** as a yellow liquid, (2.43 g, 20.2 mmol, 80% yield).

$^1\text{H NMR}$  (400 MHz,  $\text{CDCl}_3$ )  $\delta$  8.89 (br s, 1 H), 4.72 (s, 2H), 4.22 (s, 2H), 3.40 (s, 3H)

**HRMS** (+ESI): calc. for  $\text{C}_4\text{H}_9\text{O}_4$   $[\text{M}+\text{H}]^+$  121.0495 found 121.0484



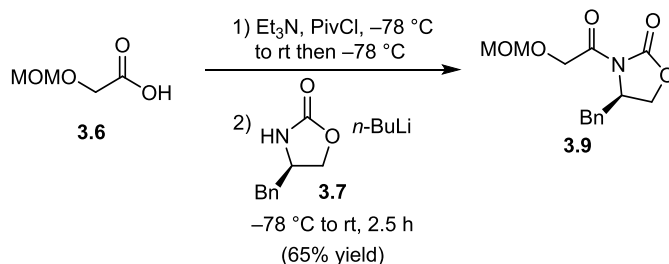
**Glycolic acid 3.5 was synthesized following a procedure by Solladié et al.**<sup>[345]</sup>

To a suspension of NaH (60 wt% in mineral oil, 1.50 g, 37.5 mmol, 2.5 equiv.) in THF (75 mL) was carefully added bromoacetic acid (2.08 g, 15.0 mmol, 1 equiv.) and the mixture was stirred at room temperature until the  $\text{H}_2$  evolution had ceased. After cooling to 0 °C, a solution of PMBOH (7.10 mL, 58.0 mmol, 1.05 equiv.) in THF (150 mL) was carefully added *via* cannula. The mixture was allowed to warm to room temperature and stirred for an additional 1 h at this temperature before adding  $\text{Bu}_4\text{NBr}$  (1.00 g, 3.00 mmol, 5.2 mol%) and heating the suspension to reflux for 4 h.

The reaction was cooled to 0 °C and EtOH (20 mL) was carefully added. The white precipitate was filtered off and dissolved in  $\text{H}_2\text{O}$  (50 mL). This solution was acidified with aqueous HCl (2N, 20 mL) to pH 1 precipitating a colourless solid. The aqueous phase was extracted with  $\text{Et}_2\text{O}$  (3 x 50 mL) and the combined organic layers were dried over  $\text{MgSO}_4$ . Evaporation of the solvent under reduced pressure yielded pure **3.5** (2.70 g, 13.8 mmol, 92% yield) as a slightly yellow solid. Was used for the next step without need for further purification.

$^1\text{H NMR}$  (400 MHz,  $\text{CDCl}_3$ )  $\delta$  7.26 (d,  $J$  = 8.6 Hz, 1H), 6.89 (d,  $J$  = 8.6 Hz, 1H), 4.58 (s, 2H), 4.11 (s, 2H), 3.81 (s, 3H)

**HRMS** (+ESI): calc. for  $\text{C}_{10}\text{H}_{12}\text{NaO}_4$   $[\text{M}+\text{Na}]^+$  219.0628 found 219.0627



**Oxazolidinones 3.8 and 3.9 were synthesized following the procedure by Askin et al.**<sup>[346]</sup>

### Oxazolidinone 3.9.

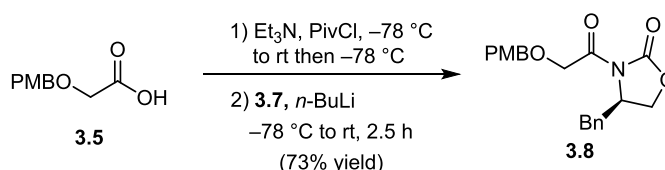
To a solution of **3.6** (84 mg, 0.700 mmol, 1.00 equiv.) in THF (2.5 mL) at  $-78\text{ }^{\circ}\text{C}$  was added triethylamine (122  $\mu\text{L}$ , 0.875 mmol, 1.25 equiv.) followed by pivaloyl chloride (95  $\mu\text{L}$ , 0.77 mmol, 1.1 equiv.). The resultant thick white precipitate was stirred 1 h at rt, then recooled to  $-78\text{ }^{\circ}\text{C}$ . Meanwhile, a separate solution of oxazolidinone **3.7** (123 mg, 0.700 mmol, 1.00 equiv.) in THF (2.0 mL) at  $-78\text{ }^{\circ}\text{C}$  was prepared. To this solution was added *n*-butyllithium (2.43 M in hexane, 0.331 mL, 0.805 mmol, 1.15 equiv.) and the resulting mixture was stirred for 25 min at the same temperature. The resulting orange solution was added by syringe (1 mL THF rinse) to the mixed anhydride solution. After being stirred for 20 min at  $-78\text{ }^{\circ}\text{C}$ , the mixture was allowed to warm to rt and was stirred 2 h before being quenched.

A saturated aqueous  $\text{NH}_4\text{Cl}$  was added. The bulk of the THF was removed under reduced pressure and the residue was poured onto DCM. After mixing, the layers were separated and the aqueous layer was extracted with DCM. The combined DCM layers were washed with saturated aqueous  $\text{NaHCO}_3$  and brine, dried over anhydrous  $\text{Na}_2\text{SO}_4$ , filtered and concentrated under reduced pressure. A yellow gum, 220 mg was obtained and purified by flash column chromatography on silica gel (EtOAc/hexanes, gradient, 0 to 50%) delivering **3.9** as a colourless oil (127 mg, 0.455 mmol, 65% yield).

$^1\text{H NMR}$  (400 MHz,  $\text{CDCl}_3$ )  $\delta$  7.38-7.16 (m, 5H), 4.77 (s, 4H), 4.73-4.65 (m, 1H), 4.33-4.20 (m, 2H), 3.43 (s, 3H), 3.32 (d,  $J = 13.4\text{ Hz}$ , 1H), 2.82 (dd,  $J = 13.4, 9.5\text{ Hz}$ , 1H)

**HRMS** (+APCI): calc. for  $\text{C}_{13}\text{H}_{14}\text{NO}_4$   $[\text{M}-\text{OMe}]^+$  248.0917 found 248.0913

$[\alpha]_D^{24}$   $-81.8^{\circ}$  ( $c$  0.93,  $\text{CHCl}_3$ )



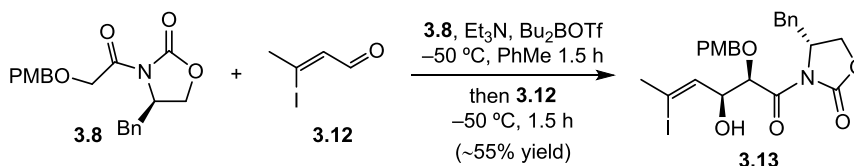
### Oxazolidinone 3.8.

The same procedure as for **3.9** was followed: **3.5** (4.67 g, 23.8 mmol, 1.00 equiv.),  $\text{Et}_3\text{N}$  (4.14 mL, 29.8 mmol, 1.25 equiv.), PivCl (3.22 mL, 26.2 mmol, 1.10 equiv.), **3.7** (4.22 g, 23.8 mmol, 1.00 equiv.), *n*-BuLi (2.33 M in hexane, 11.2 mL, 26.2 mmol, 1.10 equiv.). Purification by flash column chromatography on silica gel (EtOAc/hexanes, gradient, 0 to 30%) delivered **3.8** as a white solid (6.20 g, 17.4 mmol, 73% yield).

$^1\text{H NMR}$  (400 MHz,  $\text{CDCl}_3$ )  $\delta$  7.37-7.26 (m, 5H), 7.20 (d,  $J = 7.0\text{ Hz}$ , 2H), 4.73-4.60 (m, 5H), 4.31-4.20 (m, 2H), 3.81 (s, 3H), 3.43 (s, 3H), 3.33 (d,  $J = 13.4\text{ Hz}$ , 3.1 Hz, 1H), 2.81 (dd,  $J = 13.4, 9.5\text{ Hz}$ , 1H)

**HRMS** (+ESI): calc. for  $\text{C}_{20}\text{H}_{21}\text{NNaO}_5$   $[\text{M}+\text{Na}]^+$  378.1312 found 378.1294

$[\alpha]_D^{24}$   $+57.2^{\circ}$  ( $c$  0.4,  $\text{CHCl}_3$ )



**Oxazolidinone 3.13** was synthesized following the method by Paterson et al.<sup>[129]</sup>

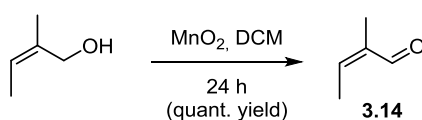
Et<sub>3</sub>N (52.2  $\mu$ L, 0.376 mmol, 1.3 equiv.) was added to a solution of **3.8** (103 mg, 0.289 mmol, 1.00 equiv.) in PhMe (0.38 mL) and cooled to  $-50$   $^\circ$ C prior to the careful addition of freshly distilled Bu<sub>2</sub>BOTf (87.1  $\mu$ L, 0.318 mmol, 1.1 equiv.) *via* syringe. The resulting yellow solution was stirred at  $-50$   $^\circ$ C for 1.5 h, during which time a light precipitate formed. Aldehyde **3.12** (104 mg, 0.532 mmol, 1.84 equiv.) in PhMe (0.38 mL) was added to the mixture *via* syringe and the system allowed to warm to  $-30$   $^\circ$ C and stirred for a further 1.5 h.

The solution was quenched by the addition of MeOH (0.24 mL), pH7 phosphate buffer (0.240 mL) and 30% v/v H<sub>2</sub>O<sub>2</sub> (0.24 mL) and stirred vigorously for 1 h at rt before separation of the organic phase and extraction of the aqueous layer (3  $\times$  0.5 mL Et<sub>2</sub>O). The combined organic phases were dried over MgSO<sub>4</sub> and concentrated under reduced pressure yielding the crude material a brown oil, 265 mg, which was purified by flash column chromatography on silica gel (EtOAc/hexanes, gradient, 0 to 40%) delivering **3.13** as a yellow oil (87.0 mg, 0.158 mmol, 55% yield).

<sup>1</sup>H NMR (400 MHz, CDCl<sub>3</sub>)  $\delta$  7.38-7.27 (m, 5H), 7.23-7.17 (d,  $J$  = 7.0 Hz, 2H), 6.90 (d,  $J$  = 8.7 Hz, 1H), 6.31 (dq,  $J$  = 8.9, 1.5 Hz, 1H), 5.18 (d,  $J$  = 4.2 Hz, 1H), 4.70-4.52 (m, 4H), 4.26 (dd,  $J$  = 8.6, 2.7 Hz, 1H), 4.19 (dd,  $J$  = 9.1, 2.2 Hz, 1H), 3.77 (s, 3H), 3.15 (dd,  $J$  = 13.5, 3.4 Hz, 1H), 2.65 (dd,  $J$  = 13.4, 9.7 Hz, 1H), 2.41 (d,  $J$  = 1.5 Hz, 3H)

## 8.3 Supporting Information for Chapter 3.2

### 8.3.1 Experimental Procedures for Chapter 3.2

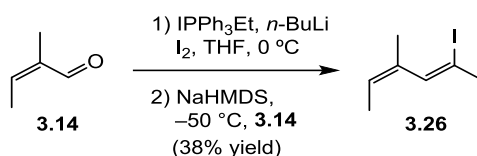


**Angelic aldehyde 3.14.**

Angelic alcohol (6.60 g, 76.6 mmol, 1.00 equiv.) was dissolved in THF (215 mL) and the flask was protected from light. Then MnO<sub>2</sub> (151 g, 1.53 mmol, 20 equiv.) was added in 5 portions over 2 hours. The reaction mixture was stirred at rt for 22 h.

The resulting suspension was filtered through celite and the solvent was removed under reduced pressure yielding pure angelic aldehyde as a yellow oil (6.50 g, 76.6 mmol, quant. Yield).

<sup>1</sup>H NMR (400 MHz, CDCl<sub>3</sub>)  $\delta$  10.19 (s, 1H), 6.60 (qq,  $J$  = 7.6, 1.4 Hz, 1H), 2.11 (dq,  $J$  = 7.6, 1.4 Hz, 3H), 1.76 (p,  $J$  = 1.4 Hz, 3H).

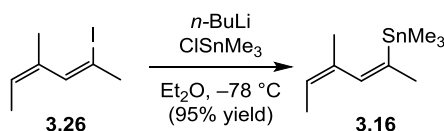


### Vinyl iodide **3.26**.<sup>[114]</sup>

To a suspension of ethyltriphenylphosphonium iodide (3.10 g, 7.40 mmol, 2.00 equiv) in THF (10 mL) was added *n*-BuLi (2.3 M in hexanes, 3.22 mL, 2.00 equiv.) at 0 °C. After 25 minutes, the red solution was slowly added to a vigorously stirred solution of I<sub>2</sub> (1.88 g, 7.40 mmol, 2.00 equiv.) in THF (20 mL) at –78 °C. A viscous yellow-brownish suspension resulted after addition of about 50% of the material, which turned into an homogeneous yellow suspension upon addition of the majority of the ylide. After 30 minutes of stirring the mixture was warmed to –50 °C. Then NaHMDS (1.0 M in THF, 3.33 mL, 3.33 mmol, 0.90 equiv.) and KHMDS (11% in toluene, 7.00 mL, 3.33 mmol, 0.90 equiv.) were added giving a red suspension which was stirred at –50 °C for 40 min. From this moment the reaction apparatus was kept in the dark. Angelic aldehyde (311 mg, 3.70 mmol, 1.00 equiv) in THF (50 mL) was added to the mixture, which was warmed to rt and stirred for an additional 40 minutes.

The reaction was quenched with sat NH<sub>4</sub>Cl (20.5 mL) and extracted with Et<sub>2</sub>O (2x26 mL). The organic layers were combined, washed with brine, dried over Na<sub>2</sub>SO<sub>4</sub> and filtered. About 95 % of the solvent was evaporated at 50 mbar at 28 °C and the residue was submitted to flash column chromatography over Basic Alumina (Brockman I) eluting with pure pentane. Vinyl iodide **3.26** was obtained as a colourless oil (312 mg, 1.40 mmol, 38% yield). Given its instability, **3.26** was directly submitted to the next step.

<sup>1</sup>H NMR (400 MHz, CDCl<sub>3</sub>) δ 6.11 (s, 1H), 5.40 (q, *J* = 6.8 Hz, 1H), 2.57 (d, *J* = 1.1 Hz, 3H), 1.76 (s, 3H), 1.58 (d, *J* = 6.8 Hz, 3H)

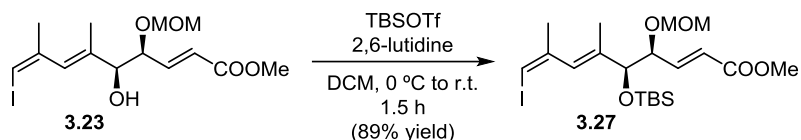


### Vinyl stannane **3.16**.<sup>[114]</sup>

Reaction performed in the dark. To a solution of vinyl iodide **3.26** (1.92 g, 7.78 mmol, 1 equiv.) in Et<sub>2</sub>O (55 mL) at –78 °C was added *n*-BuLi (2.49 M in hexanes, 2.60 mL, 1.04 equiv.) dropwise over 10 minutes. The resulting solution was stirred 5 additional minutes after which a solution of Me<sub>3</sub>SnCl (1.0 M in hexane, 8.80 mL, 8.80 mmol, 1.13 equiv.) was slowly added. The reaction mixture was stirred at –78 °C for 1.5 hours, after which it was quenched by addition of water (80 mL). After warming to room temperature, the mixture was extracted with Et<sub>2</sub>O (2 x 50 mL). The organic layers were combined, dried over anhydrous Na<sub>2</sub>SO<sub>4</sub>, filtered and concentrated under reduced pressure at 30 °C. The remaining liquid contained stannane **3.16** (1.92 g, 7.41 mmol, 95% yield) was kept in benzene (20 mL) at –20 °C, being stable for several weeks.

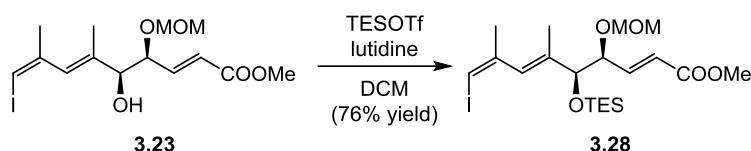
<sup>1</sup>H NMR (400 MHz, CDCl<sub>3</sub>) δ 6.54 (s, 1H), 5.27 (qt, *J* = 6.7, 1.4 Hz, 1H), 2.00 (d, *J* = 1.7 Hz, 3H), 1.73 (s, 3H), 1.59 (d, *J* = 6.8 Hz, 3H), 0.13 (s, 9H)

HRMS (+ESI): calc. for C<sub>9</sub>H<sub>17</sub>Sn [M-Me]<sup>+</sup> 245.0352 found 245.0357



### Silyl ether **3.27**.

See **Silyl ether 14** in Chapter 8.3.



### Silyl ether **3.28**.

To vinyl iodide **3.23** (250 mg, 0.631 mmol, 1.00 equiv.) in dry DCM (6.3 mL) was added 2,6-lutidine (0.21 mL, 1.8 mmol, 2.9 equiv.). The solution was cooled down to 0 °C and TESOTf (0.18 mL, 0.85 mmol, 1.3 equiv.) was added dropwise. The reaction mixture was allowed to warm up to room temperature and was stirred for 1.5 h.

An aqueous saturated NaHCO<sub>3</sub> solution was added and the layers were separated. The aqueous phase was extracted three times with DCM and the organic layers were combined, dried over MgSO<sub>4</sub>, filtered and concentrated under reduced pressure. The crude material (yellow oil, 365 mg) was purified by flash column chromatography on silica gel (EtOAc/hexanes, gradient, 0 to 10%) affording silyl ether **3.28** as a yellow oil (245 mg, 0.48 mmol, 76% yield).

**<sup>1</sup>H NMR** (400 MHz, CDCl<sub>3</sub>) δ 6.89 (dd, *J* = 15.9, 5.8 Hz, 1H), 6.06 (d, *J* = 15.0 Hz, 2H), 5.85 (s, 1H), 4.74 (d, *J* = 6.7 Hz, 1H), 4.65 (d, *J* = 6.8 Hz, 1H), 4.25 (t, *J* = 6.4 Hz, 1H), 4.10 (d, *J* = 6.8 Hz, 1H), 3.71 (s, 3H), 3.38 (s, 3H), 1.92 (s, 3H), 1.67 (s, 3H), 0.96 (t, *J* = 8.0 Hz, 9H), 0.63 (q, *J* = 8.0 Hz, 6H)

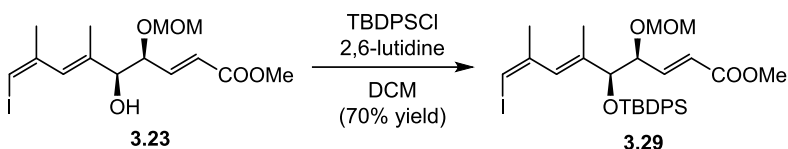
**<sup>13</sup>C NMR** (101 MHz, CDCl<sub>3</sub>) δ 166.52, 145.25, 144.29, 138.20, 129.82, 122.12, 95.78, 80.22, 78.28, 55.76, 51.56, 24.45, 14.18, 6.85, 4.84

**IR** (ATR): 2952 (m), 2912 (m), 2877 (m), 1728 (s), 1437 (m), 1436 (w), 1306 (w), 1275 (m), 1236 (w), 1167 (m), 1152 (m), 1098 (s), 1032 (s), 741 (m)

**HRMS** (+APCI): calc. for C<sub>20</sub>H<sub>36</sub>IO<sub>5</sub>Si [M+Na]<sup>+</sup> 511.1371, found 511.1387

[α]<sub>D</sub><sup>24</sup> +1.2° (c 0.36, CHCl<sub>3</sub>)

*R*<sub>F</sub> = 0.62 (20% EtOAc in hexanes)



### Silyl ether **3.29**.

**3.23** (42.0 mg, 0.106 mmol, 1.00 equiv.) was dissolved in chloroform (1.0 mL) and 2,6-lutidine (31.0 μL, 0.265 mmol, 2.50 equiv.) and imidazole (14.8 mg, 0.217 mmol, 2.05 equiv.) were added followed by TBDPSCI



(41.0  $\mu$ L, 0.159 mmol, 1.50 equiv.). The mixture was stirred under reflux for 24 hours before it was cooled down to room temperature. Then lutidine (31.0  $\mu$ L, 0.265 mmol, 2.50 equiv.) and TBDPSCI (41.0  $\mu$ L, 0.159 mmol, 1.50 equiv.) were added and the reflux was restarted and held for 48 hours. The solution was cooled down to room temperature and stirred for 1.5 hours after which an aqueous saturated solution of sodium bicarbonate was added. The layers were separated and the aqueous phase was extracted three times with DCM. The combined organic layers were combined, dried over anhydrous  $\text{MgSO}_4$  and concentrated under reduced pressure yielding a yellow oil, 142 mg. Purification by flash column chromatography on silica gel (AcOEt/Hexanes, gradient, 0 to 10%) led to the obtention of **3.29** as a yellow oil (48.0 mg, 75.6  $\mu$ mol, 70% yield).

**$^1\text{H}$  NMR** (400 MHz, Chloroform-*d*)  $\delta$  7.70 (dd,  $J$  = 21.7, 7.9 Hz, 4H), 7.45–7.36 (m, 6H), 6.95 (dd,  $J$  = 15.8, 5.7 Hz, 1H), 6.02 (d,  $J$  = 16.1 Hz, 1H), 5.98 (s, 1H), 5.78 (s, 1H), 4.47–4.42 (m, 2H), 4.27 (d,  $J$  = 6.0 Hz, 1H), 4.16 (t,  $J$  = 5.9 Hz, 1H), 3.71 (s, 3H), 3.20 (s, 3H), 1.76 (s, 3H), 1.59 (s, 3H), 1.11 (s, 9H)

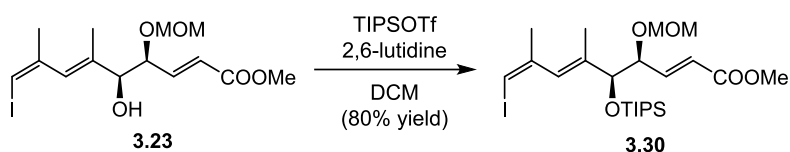
**$^{13}\text{C}$  NMR** (101 MHz,  $\text{CDCl}_3$ )  $\delta$  166.48, 145.09, 144.43, 137.35, 136.04, 135.98, 133.60, 133.35, 130.03, 129.78, 129.69, 127.61, 127.52, 122.32, 95.63, 79.29, 78.92, 55.74, 51.51, 27.10, 24.41, 19.35, 15.42

**IR** (ATR): 2931 (w), 2857 (w), 1724 (s), 1661 (w), 1427 (m), 1271 (m), 1167 (m), 1151 (m), 1104 (s), 1127 (s), 919 (m), 821 (m), 739 (m)

**HRMS** (+ESI): calc. for  $\text{C}_{30}\text{H}_{39}\text{IO}_5\text{NaSi}$   $[\text{M}+\text{Na}]^+$  657.1504, found 657.1528

$[\alpha]_D^{24} = +6.95$  (c 2.90,  $\text{CHCl}_3$ )

$R_F = 0.88$  (20% AcOEt in hexane)



### Silyl ether **3.30**.

The same procedure as for **3.28** was followed. **3.23** (250 mg, 0.63 mmol, 1.00 equiv.), lutidine (0.18 mL, 1.58 mmol, 2.50 equiv.), TIPSOTf (0.25 mL, 0.95 mmol, 1.30 equiv.). Stirred for 20 hours. Purification by flash column chromatography on silica gel (EtOAc/hexanes, gradient, 0 to 10%) yielded **3.30** as a yellow oil, (298 mg, 0.539 mmol, 80% yield).

**$^1\text{H}$  NMR** (400 MHz, Chloroform-*d*)  $\delta$  6.95 (dd,  $J$  = 15.7, 4.6 Hz, 1H), 6.09–5.85 (m, 3H), 4.72 (d,  $J$  = 6.6 Hz, 1H), 4.65 (d,  $J$  = 6.9 Hz, 1H), 4.33–4.28 (m, 2H), 3.71 (s, 3H), 3.38 (s, 3H), 1.92 (s, 3H), 1.69 (s, 3H), 1.15–1.07 (m, 3H), 1.08 (t,  $J$  = 6.0 Hz, 18H)

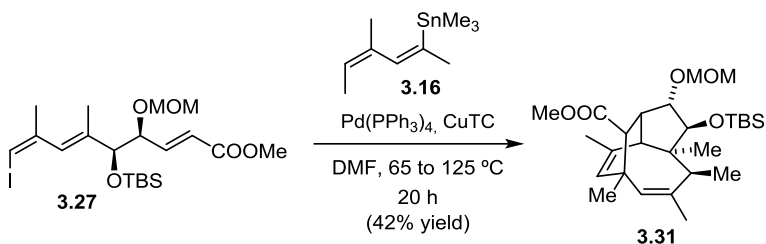
**$^{13}\text{C}$  NMR** (101 MHz,  $\text{CDCl}_3$ )  $\delta$  166.55, 145.28, 144.30, 138.19, 129.84, 122.10, 95.76, 79.67, 78.93, 55.81, 51.53, 24.53, 18.11, 18.09, 14.85, 12.46

**IR** (ATR): 2944(m), 2866 (m), 1726 (s), 1463 (w), 1435 (m), 1271 (m), 1151 (m), 1098 (s), 1028 (s), 919 (m), 882 (s), 771 (m)

**HRMS** (+ESI): calc. for  $\text{C}_{23}\text{H}_{41}\text{IO}_5\text{NaSi}$   $[\text{M}+\text{Na}]^+$  575.1660, found 575.1677

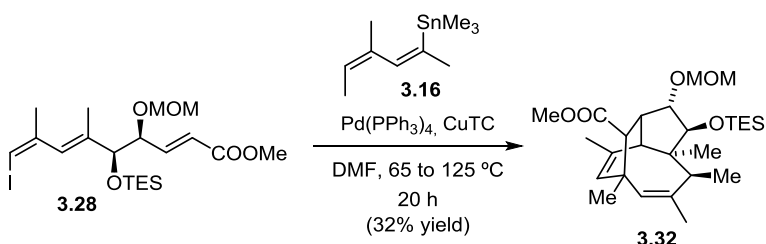
$[\alpha]_D^{24} = +2.8$  (c 3.83,  $\text{CHCl}_3$ )

$R_F = 0.70$  (20% EtOAc in hexanes)



### TBS cascade product 3.31.

See cascade product **18** in Chapter 3.3.



### TES cascade product 3.32.

The same procedure as for **18** (Chapter 3.3) was followed:

3.28 (102 mg, 0.200 mmol, 1.00 equiv), Pd(PPh<sub>3</sub>)<sub>4</sub> (23.0 mg, 0.020 mmol, 0.10 equiv.), CuTC (42.0 mg, 0.220 mmol, 2.20 equiv.), 3.16 (72.4 mg, 0.280 mmol, 1.4 equiv.). The crude material was purified by flash column chromatography on silica gel, (EtOAc/Hex, gradient, 0 to 3%) providing tricycle 3.32 as a white solid (31.0 mg, 64.8 μmol, 32% yield).

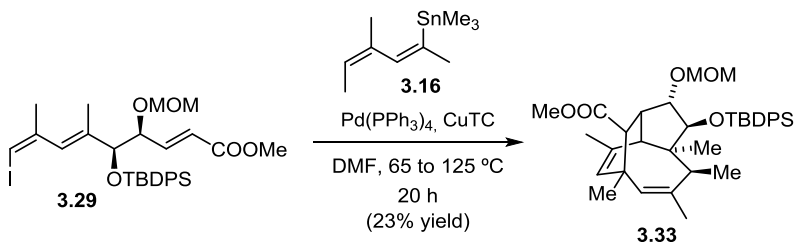
**<sup>1</sup>H NMR** (400 MHz, CDCl<sub>3</sub>) δ 5.33 (s, 1H), 4.99 (s, 1H), 4.62 (s, 2H), 3.87 (br s, 2H), 3.59 (s, 3H), 3.25 (s, 3H), 2.86 (q, *J* = 7.6 Hz, 1H), 2.70 (s, 1H), 2.65 (d, *J* = 11.3 Hz, 1H), 2.32 (dt, *J* = 10.1, 2.3 Hz, 1H), 1.85 (s, 3H), 1.81 (d, *J* = 1.8 Hz, 3H), 1.20 (s, 3H), 1.12 (s, 3H), 1.05 (d, *J* = 7.4 Hz, 3H), 0.96 (t, *J* = 7.9 Hz, 9H), 0.62 (q, *J* = 8.0 Hz, 6H)

**<sup>13</sup>C NMR** (101 MHz, CDCl<sub>3</sub>) δ 175.46, 140.81, 138.03, 132.98, 124.98, 97.84, 93.47, 87.74, 55.34, 54.09, 51.29, 50.92, 44.37, 40.51, 34.50, 29.40, 29.05, 24.95, 24.13, 15.67, 6.95, 5.08

**IR** (ATR): 2926 (s), 2854 (m), 1734 (s), 1463 (m), 1380 (w), 1251 (m), 1196 (m), 1107 (m), 1039 (s), 874 (m), 836 (s), 1032 (s), 776 (m)

**HRMS** (+APCI): calc. for C<sub>27</sub>H<sub>47</sub>O<sub>5</sub>Si [M+H]<sup>+</sup> 479.3187, found 479.3183

*R<sub>F</sub>* = 0.45 (10% EtOAc in hexanes)



### TBDPS cascade product 3.33.

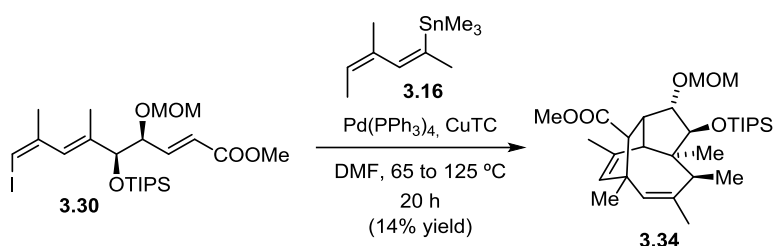
The same procedure as for **18** (Chapter 3.3) was followed:

**3.29** (117 mg, 0.200 mmol, 1.00 equiv), Pd(PPh<sub>3</sub>)<sub>4</sub> (23.0 mg, 0.020 mmol, 0.10 equiv.), CuTC (42.0 mg, 0.220 mmol, 2.20 equiv.), **3.16** (72.4 mg, 0.280 mmol, 1.4 equiv.). The crude material was purified by flash column chromatography on silica gel, (EtOAc/Hex, gradient, 0 to 3%) providing tricycle **3.33** as a white solid (27.7 mg, 46.0 μmol, 23% yield).

<sup>1</sup>H NMR (400 MHz, Chloroform-*d*) δ 7.79 (d, *J* = 7.2 Hz, 2H), 7.60 (d, *J* = 7.4 Hz, 2H), 7.41–7.33 (m, 6H), 5.30 (s, 1H), 5.09 (s, 1H), 3.98 (d, *J* = 7.4 Hz, 1H), 3.94 (dd, *J* = 8.3, 5.6 Hz, 1H), 3.79 (d, *J* = 8.5 Hz, 1H), 3.67 (d, *J* = 7.3 Hz, 1H), 3.53 (s, 3H), 2.96 (s, 3H), 2.94 (q, *J* = 7.5 Hz, 1H), 2.64 (s, 1H), 2.47 (d, *J* = 11.2 Hz, 1H), 2.12 (dd, *J* = 11.5, 5.6 Hz, 1H), 2.08 (s, 3H), 1.76 (s, 3H), 1.23 (d, 7.5 Hz, 3H), 1.15 (s, 3H), 1.12 (s, 3H), 1.08 (s, 9H)

HRMS (+APCI): calc. for C<sub>37</sub>H<sub>51</sub>O<sub>5</sub>Si [M+H]<sup>+</sup> 603.3500, found 603.3500

*R*<sub>F</sub> = 0.63 (15% EtOAc in hexanes)



#### TIPS cascade product **3.34**

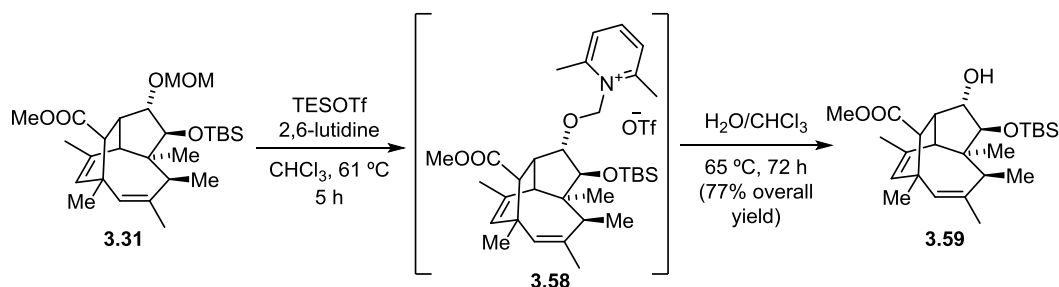
The same procedure as for **18** (chapter 3.3) was followed:

**3.30** (111 mg, 0.200 mmol, 1.00 equiv.), Pd(PPh<sub>3</sub>)<sub>4</sub> (23.0 mg, 0.020 mmol, 0.10 equiv.), CuTC (42.0 mg, 0.220 mmol, 2.20 equiv.), **3.16** (72.4 mg, 0.280 mmol, 1.4 equiv.). The crude material was purified by flash column chromatography on silica gel, (EtOAc/Hex, gradient, 0 to 3%) providing tricycle **3.34** in about 80% purity as a colourless oil, (15.0 mg, 28.8 μmol, 14% yield). Yield calculated by NMR standard (trimethoxybenzene).

<sup>1</sup>H NMR (400 MHz, Chloroform-*d*) δ 5.32 (s, 1H), 5.00 (s, 1H), 4.60 (s, 2H), 4.02 (d, *J* = 8.3 Hz, 1H), 3.93 (dd, *J* = 8.5, 5.5 Hz, 1H), 3.59 (s, 3H), 3.23 (s, 3H), 2.89 (q, *J* = 7.6 Hz, 1H), 2.70 (s, 1H), 2.66 (d, *J* = 11.3 Hz, 1H), 2.34 (dd, *J* = 11.4, 5.4 Hz, 1H), 1.88 (s, 3H), 1.82 (s, 3H), 1.13–0.99 (m, 30H)

HRMS (+APCI): calc. for C<sub>29</sub>H<sub>49</sub>O<sub>4</sub>Si [M-OMe]<sup>+</sup> 489.3395, found 489.3390

*R*<sub>F</sub> = 0.55 (15% EtOAc in hexanes)



#### Tricyclic alcohol **3.59**.

To a solution of acetal **3.31** (50.0 mg, 0.104 mmol, 1.00 equiv.) in dry chloroform (3.0 mL) were added 2,6-lutidine (73 μL, 0.63 mmol, 6.0 equiv.) and TESOTf (89 μL, 0.42 mmol, 4.0 equiv.). After stirring under reflux

for 5 h the solution was allowed to cool down and water (2.0 mL), hexanes (1.5 mL) and chloroform (1.0 mL) were added. The mixture was heated to 65 °C and stirred vigorously for 72 h.

The phases were separated and the aqueous layer was extracted three times with DCM. The organic layers were combined, dried over anhydrous  $\text{MgSO}_4$  and concentrated. The crude material was purified by flash column chromatography on silica gel (10% EtOAc/Hexanes) affording alcohol **3.59** (35.0 mg, 80.5  $\mu\text{mol}$ , 77% yield) as a white solid.

**$^1\text{H}$  NMR** (400 MHz,  $\text{CDCl}_3$ )  $\delta$  5.34 (s, 1H), 4.97 (s, 1H), 4.25 (br s, 1H), 3.77 (d,  $J$  = 8.2 Hz, 1H), 3.57 (s, 3H), 2.87 (q,  $J$  = 7.5 Hz, 1H), 2.64 (d,  $J$  = 11.2 Hz, 1H), 2.50 (s, 1H), 2.25 (dd,  $J$  = 11.3, 6.1 Hz, 1H), 1.85 (s, 3H), 1.81 (s, 3H), 1.65 (d,  $J$  = 4.1 Hz, 1H), 1.20 (s, 3H), 1.13 (s, 3H), 1.06 (d,  $J$  = 7.5 Hz, 3H), 0.93 (s, 9 H), 0.13 (d,  $J$  = 2.1 Hz, 6H)

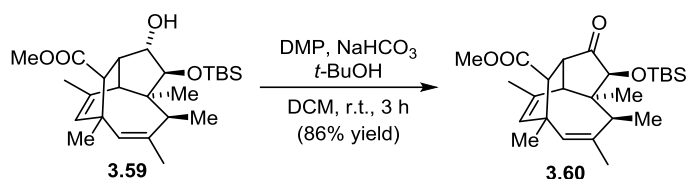
**$^{13}\text{C}$  NMR** (100 MHz,  $\text{CDCl}_3$ )  $\delta$  174.85, 141.23, 137.81, 132.63, 124.99, 89.95, 84.14, 56.49, 54.22, 51.09, 50.74, 45.93, 40.53, 34.54, 29.41, 29.02, 26.02, 25.22, 24.14, 18.25, 15.81, -4.06, -4.41

**IR** (ATR): 2956 (m), 2929 (m), 2855 (w), 2362 (w), 1719 (s), 1460 (w), 1435 (w), 1376 (w), 1250 (m), 1226 (m), 1098 (m), 876 (s), 835 (s), 753 (s)

**HRMS** (+ESI): calc. for  $\text{C}_{25}\text{H}_{43}\text{O}_4\text{Si}$   $[\text{M}+\text{H}]^+$  435.2925, found 435.2928

$[\alpha]_D^{25}$  +35.8° (c 0.66,  $\text{CHCl}_3$ )

$R_f$  = 0.39 (20% EtOAc in hexanes)



#### Ketone **3.60**.

Alcohol **3.59** (20.0 mg, 46.0  $\mu\text{mol}$ , 1.00 equiv.) was dissolved in DCM (0.55 mL) and  $\text{NaHCO}_3$  (11.6 mg, 0.138 mmol, 3.00 equiv.) was added followed by 1 small drop of *t*-BuOH. Dess-Martin periodinane (29.3 mg, 69.0  $\mu\text{mol}$ , 1.5 equiv.) was added and the reaction mixture was stirred at room temperature for 60 min before additional  $\text{NaHCO}_3$  (4.0 mg, 47.6  $\mu\text{mol}$ , 1.04 equiv.) followed by DMP (10.0 mg, 23.6  $\mu\text{mol}$ , 0.513 equiv.) were added. The reaction mixture was stirred for 2 hours.

A 1:1 solution of saturated aqueous  $\text{Na}_2\text{S}_2\text{O}_3/\text{NaHCO}_3$  (1.5 mL each) was added and the result was vigorously stirred for 15 min, after which the mixture was diluted with water and DCM. The phases were separated, and the aqueous layer was extracted three times with DCM. The organic layers were combined, dried over  $\text{Na}_2\text{SO}_4$  and concentrated under reduced pressure yielding a white solid, 20 mg.

Purification by flash column chromatography on silica gel ( $\text{Et}_2\text{O}$ /Hexanes, gradient, 0 to 15%) allowed for isolation of ketone **3.60** as a white solid (17.0 mg, 39.3  $\mu\text{mol}$ , 85% yield).

**$^1\text{H}$  NMR** (400 MHz,  $\text{CDCl}_3$ )  $\delta$  5.36 (s, 1H), 4.85 (s, 1H), 4.03 (d,  $J$  = 2.2 Hz, 1H), 3.60 (s, 3H), 3.07 (s, 1H), 3.01 (q,  $J$  = 7.3 Hz, 1H), 2.82 (d,  $J$  = 11.2 Hz, 1H), 2.72 (dd,  $J$  = 11.3, 2.2 Hz, 1H), 1.87 (d,  $J$  = 1.6 Hz, 3H), 1.69 (s, 3H), 1.37 (s, 3H), 1.16 (s, 3H), 1.06 (d,  $J$  = 7.5 Hz, 3H), 0.95 (s, 9H), 0.19 (s, 3H), 0.07 (s, 3H)

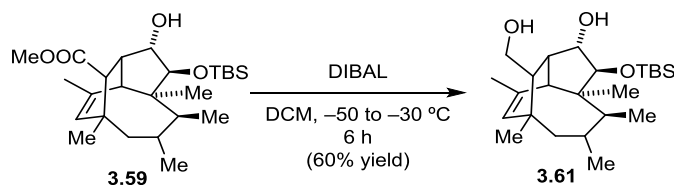
**$^{13}\text{C}$  NMR** (100 MHz,  $\text{CDCl}_3$ )  $\delta$  212.65, 173.23, 138.93, 136.89, 136.56, 125.45, 86.17, 53.47, 51.53, 51.31, 48.13, 44.11, 41.14, 34.05, 27.90, 27.78, 25.82, 24.51, 24.26, 18.47, 15.57, -4.34, -5.64.

**IR** (ATR): 2956 (s), 2928 (s), 2856 (m), 2361 (w), 1733 (s), 1461 (m), 1377 (w), 1252 (m), 1201 (s), 1174 (s), 1139 (s), 1092 (w), 1053 (m), 1020 (w), 949 (w), 876 (s), 838 (s), 779 (m)

**HRMS** (+ESI): calc. for  $C_{25}H_{41}O_4Si$   $[M+H]^+$  433.2769, found 433.2752

$[\alpha]_D^{24} +23.1^\circ$  (c 0.08,  $CHCl_3$ )

$R_F = 0.62$  (20% EtOAc in hexanes)



### Diol **3.61**.

To alcohol **3.59** (5.0 mg, 11  $\mu\text{mol}$ , 1.00 equiv.) dissolved in DCM (0.22 mL) at  $-50^\circ\text{C}$  was added dropwise a solution of DIBAL (1.5 M in toluene, 24  $\mu\text{L}$ , 46  $\mu\text{mol}$ , 4.0 equiv.). The mixture was stirred at the same temperature for 4 hours before additional DIBAL (1.5 M in toluene, 20  $\mu\text{L}$ , 38  $\mu\text{mol}$ , 3.3 equiv.) was added. The mixture was then warmed to  $-30^\circ\text{C}$  and stirred for 2 additional hours.

The reaction was quenched with saturated aqueous Rochelle's salt (0.40 mL), then warmed to room temperature and stirred for 30 min. The mixture was diluted with water/DCM and extracted three times with DCM. The combined organic layers were dried over  $Na_2SO_4$ , filtered and concentrated under reduced pressure to afford 6.2 mg of a colourless oil, which was purified by flash column chromatography on silica gel (EtOAc/hexanes, 10%, then 20%, then 32%) delivering diol **3.61** as a colourless solid (2.8 mg, 6.9  $\mu\text{mol}$ , 60% yield).

**$^1\text{H}$  NMR** (400 MHz,  $CDCl_3$ )  $\delta$  5.42 (s, 1H), 4.94 (s, 1H), 4.28 (t,  $J = 7.2$  Hz, 1H), 3.77 (d,  $J = 8.2$  Hz, 1H), 3.65 (dd,  $J = 10.7, 3.9$  Hz, 1H), 3.28 (t,  $J = 9.5$  Hz, 1H), 2.81 (q,  $J = 7.2$  Hz, 1H), 2.55 (d,  $J = 11.4$  Hz, 1H), 2.21 (dd,  $J = 11.4, 6.0$  Hz, 1H), 1.95 (br s, 1H), 1.85 (s, 3H), 1.74 (s, 3H), 1.60 (dd,  $J = 8.3, 4.1$  Hz, 2H), 1.19 (s, 3H), 1.12 (s, 3H), 1.07 (d,  $J = 7.5$  Hz, 3H), 0.94 (s, 9H), 0.14 (s, 6H)

**$^{13}\text{C}$  NMR** (100 MHz,  $CDCl_3$ )  $\delta$  139.12, 137.47, 133.99, 127.91, 90.11, 84.78, 63.64, 55.60, 51.90, 50.51, 44.49, 39.77, 34.42, 29.44, 28.18, 26.04, 25.22, 24.03, 18.28, 15.88, -4.03, -4.49.

**IR** (ATR): 3275 (m, br), 2955 (m), 2925 (s), 2854 (m), 1729 (w), 1461 (m), 1375 (w), 1251 (m), 1130 (m), 1105 (m), 1034 (m), 996 (m), 877 (s), 835 (s), 776 (s), 756 (s)

**HRMS** (+APCI): calc. for  $C_{24}H_{41}O_2Si$   $[M-OH]^+$  389.2870, found 389.2864

$[\alpha]_D^{24} +6.9^\circ$  (c 0.19,  $CHCl_3$ )

$R_F = 0.32$  (40% EtOAc in hexanes)



To a solution of diol **3.61** (2.0 mg, 4.9  $\mu$ mol, 1.00 equiv.) in DCM (0.16 mL) was added imidazole (0.7 mg, 10  $\mu$ mol, 2 equiv.) followed by TBDPSCI (1.4  $\mu$ L, 5.3  $\mu$ mol, 1.1 equiv.). The resulting mixture was stirred at room temperature for 6 h after which water (20  $\mu$ L) was added. The mixture was vigorously stirred for 5 min, after which the aqueous phase was separated and extracted three times with DCM. The organic layers were combined, dried over  $\text{MgSO}_4$  and concentrated under reduced pressure yielding a colourless oil.

**<sup>1</sup>H NMR** (400 MHz, CDCl<sub>3</sub>) δ 7.64 (ddd, *J* = 8.0, 5.4, 1.7 Hz, 4H), 7.43 – 7.35 (m, 6H), 5.23 (s, 1H), 4.89 (s, 1H), 4.26 (dt, *J* = 8.1, 5.4 Hz, 1H), 3.76 (d, *J* = 8.1 Hz, 1H), 3.68 (dd, *J* = 9.9, 4.5 Hz, 1H), 3.16 (t, *J* = 9.8 Hz, 1H), 2.79 (q, *J* = 7.3 Hz, 1H), 2.40 (d, *J* = 11.5 Hz, 1H), 2.30 (dd, *J* = 11.4, 5.7 Hz, 1H), 1.84 (s, 3H), 1.69 (dd, *J* = 9.6, 4.5 Hz, 1H), 1.64 (d, *J* = 1.5 Hz, 3H), 1.55 (s, 3H), 1.42 (d, *J* = 5.1 Hz, 1H), 1.16 (s, 3H), 1.04 (s, 9H), 0.94 (s, 9H), 0.93 (s, 3H), 0.16 (s, 3H), 0.14 (s, 3H)

**IR (ATR):** 2957 (s), 2929 (s), 2856 (m), 2361 (w), 1471 (w), 1428 (w), 11253 (w), 1112 (s), 1060 (m), 878 (m), 837 (m), 777 (w), 739 (w)

$$[\alpha]_D^{24} +13.41^{\circ} (c\ 0.14, \text{CHCl}_3)$$

**3.62**

Alcohol **S3.5** (5.0 mg, 7.8  $\mu$ mol, 1.00 equiv.) was dissolved in DCM (0.20 mL) and  $\text{NaHCO}_3$  (2.0 mg, 23  $\mu$ mol, 3.0 equiv.) was added followed by 1 small drop of *t*-BuOH. Dess–Martin periodinane (5.0 mg, 11.7  $\mu$ mol, 1.5 equiv.) was added and the reaction mixture was stirred at room temperature for 60 min before additional  $\text{NaHCO}_3$  (4.0 mg, 48  $\mu$ mol, 6.0 equiv.) followed by DMP (10.0 mg, 23.6  $\mu$ mol, 3.00 equiv.) were added. The reaction mixture was stirred for 2 hours.

A 1:1 solution of saturated aqueous  $\text{Na}_2\text{S}_2\text{O}_3/\text{NaHCO}_3$  (1.5 mL each) was added and the result was vigorously stirred for 15 min, after which the mixture was diluted with water and DCM. The phases were separated, and the aqueous layer was extracted three times with DCM. The organic layers were combined, dried over

Na<sub>2</sub>SO<sub>4</sub> and concentrated under reduced pressure yielding pure ketone **3.62** a colourless oil (4.8 mg, 7.5 μmol, 96% yield).

**<sup>1</sup>H NMR** (400 MHz, CDCl<sub>3</sub>) δ 7.62 (td, *J* = 8.7, 1.6 Hz, 4H), 7.39 (dd, *J* = 11.1, 6.5 Hz, 6H), 5.25 (s, 1H), 4.81 (s, 1H), 3.97 (d, *J* = 2.3 Hz, 1H), 3.71 (dd, *J* = 9.9, 4.8 Hz, 1H), 3.31 (t, *J* = 10.0 Hz, 1H), 2.93 (q, *J* = 7.4 Hz, 1H), 2.76 (d, *J* = 11.3 Hz, 1H), 2.46 (d, *J* = 11.3 Hz, 1H), 2.42 (dd, *J* = 10.0, 4.8 Hz, 1H), 1.70 (d, *J* = 1.4 Hz, 3H), 1.67 (s, 3H), 1.31 (s, 3H), 1.02 (s, 9H), 0.96 (s, 9H), 0.90 (s, 3H), 0.23 (s, 3H), 0.09 (s, 3H), 0.07 (s, 3H)

**<sup>13</sup>C NMR** (100 MHz, CDCl<sub>3</sub>) δ 214.24, 138.07, 136.83, 135.69, 135.56, 135.42, 134.18, 133.68, 129.60, 129.48, 127.75, 127.61, 86.29, 62.60, 51.86, 50.33, 47.66, 41.78, 40.05, 33.95, 31.94, 29.71, 26.90, 25.88, 24.44, 24.11, 22.71, 19.24, 18.52, 15.68, 14.14, 1.03, -4.22, -5.66

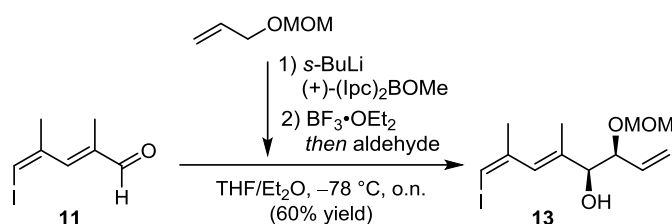
**IR** (ATR): 2958 (w), 2920 (s), 2850 (m), 2360 (s), 2341 (s), 1463 (w), 1261 (w), 1053 (m), 1034 (m), 1018 (w), 803 (w)

**HRMS**: No mass peak found

*R*<sub>F</sub> = 0.56 (5% Et<sub>2</sub>O in hexanes)

## 8.4 Supporting Information for Chapter 3.3

### 8.4.1 Experimental Procedures for Chapter 3.3



#### Vinyl iodide 13.

To a solution of allyl methoxymethyl ether (1.30 g, 12.7 mmol, 2.26 equiv.) in dry THF (12 mL) at -78 °C was added *s*-butyllithium (1.4 M in cyclohexane, 8.53 mL, 11.9 mmol, 2.12 equiv.) over 20 min. The reaction mixture was stirred at -78 °C for 30 min after which a solution of (+)-B-methoxydiisopinocampheylborane (3.74 g, 11.8 mmol, 2.10 equiv.) in dry diethyl ether (22 mL) was added over 20 min. The reaction was further stirred at -78 °C for 1 h before boron trifluoride diethyl etherate (1.61 mL, 12.7 mmol, 2.26 equiv.) was added dropwise, followed by immediate addition of a solution of aldehyde **11** (1.33 g, 5.63 mmol, 1.00 equiv.) in dry THF (30 mL) in the dark and in contact with the flask's inner wall to ensure pre-cooling. The reaction mixture was stirred for an additional 3 h at -78 °C, then slowly warmed to room temperature and stirred overnight.

The solvent was exchanged to diethyl ether (45 mL) and an aqueous solution of NaOH (2.5 M, 8 mL) was added followed by careful addition of H<sub>2</sub>O<sub>2</sub> in water (30% w/w, 23 mL) causing intense gas evolution. The mixture was stirred under reflux for 3 h or until no more gas evolution was observed at room temperature. The layers were separated, and the aqueous phase was extracted three times with diethyl ether. The combined organic layers were dried over MgSO<sub>4</sub>, filtered and concentrated under reduced pressure.

The crude residue was purified by flash column chromatography on silica gel, (EtOAc/Hex, gradient, 0 to 12%) yielding **13** as a colourless oil (1.14 g, 3.37 mmol, 60% yield, *d.r.* >20:1, 96% *ee*, Mosher's ester analysis, see below).

**<sup>1</sup>H NMR** (400 MHz, CDCl<sub>3</sub>) δ 6.05 (s, 1H), 5.94 (s, 1H), 5.74 (ddd, *J* = 17.5, 10.3, 7.3 Hz, 1H), 5.36–5.26 (m, 2H), 4.76 (d, *J* = 6.7 Hz, 1H), 4.64 (d, *J* = 6.7 Hz, 1H), 4.07 (t, *J* = 7.4 Hz, 1H), 4.01 (dd, *J* = 7.5, 2.1 Hz, 1H), 3.43 (s, 3H), 2.90 (d, *J* = 2.4 Hz, 1H), 1.97 (s, 3H), 1.71 (s, 3H)

**<sup>13</sup>C NMR** (100 MHz, CDCl<sub>3</sub>) δ 144.4, 137.2, 134.3, 130.5, 119.4, 94.5, 80.1, 79.4, 77.30, 55.9, 24.6, 14.1

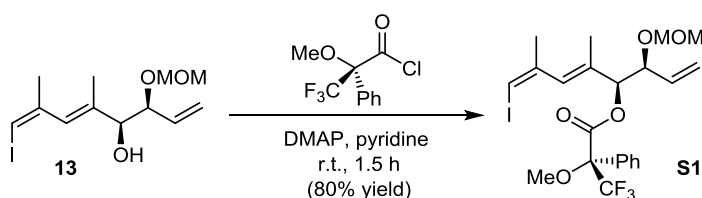
**IR** (ATR): 3465 (br), 2924 (s), 2851 (m), 2363 (w), 1261 (w), 1151 (m), 1081 (m), 1031 (s), 922 (m), 768 (w)

**HRMS** (+ESI): calc. for C<sub>12</sub>H<sub>19</sub>INaO<sub>3</sub> [M+Na]<sup>+</sup> 361.0271 found 361.0275

[α]<sub>D</sub><sup>23</sup> +70.6° (c 0.67, CHCl<sub>3</sub>)

*R<sub>F</sub>* = 0.42 (25% EtOAc in hexanes)

#### Procedure for Mosher's ester analysis



#### Mosher's ester **S1**.

To a solution of triene **13**, (5.0 mg, 15 μmol, 1.0 equiv.) and DMAP (6.4 mg, 52 μmol, 3.5 equiv.) in pyridine (0.50 mL) was added (*R*)-(-)-α-Methoxy-α-(trifluoromethyl)phenylacetyl chloride (Mosher's acyl chloride, 2.8 μL, 15 μmol, 1.0 equiv.). The reaction mixture was stirred for 1.5 h.

The solvent was evaporated and the residue was filtered through a pad of silica eluting with 30% EtOAc/hexanes affording ester **S1** as a colourless oil (6.6 mg, 12 μmol, 80% yield, *d.r.* 1:0.02).

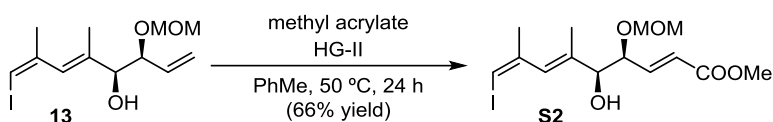
(*S*)-diastereomer:

**<sup>1</sup>H NMR** (400 MHz, CDCl<sub>3</sub>) δ 7.61–7.55 (m, 2H), 7.43–7.34 (m, 3H), 6.08 (br, 1H), 5.96 (s, 1H), 5.69 (ddd, *J* = 18.0, 10.3, 7.8 Hz, 1H), 5.41–5.31 (m, 3H), 4.69 (d, *J* = 6.7 Hz, 1H), 4.57 (d, *J* = 6.7 Hz, 1H), 4.27 (t, *J* = 8.2 Hz, 1H), 3.59–3.57 (br, 3H), 3.29 (s, 3H), 1.89 (s, 3H), 1.56 (d, *J* = 1.3 Hz, 3H)

(*R*)-diastereomer:

**<sup>1</sup>H NMR** (400 MHz, CDCl<sub>3</sub>) δ 7.59–7.50 (m, 2H), 7.42–7.34 (m, 3H), 6.10 (app quintet, *J* = 1.5 Hz, 1H), 6.03 (br, 1H), 5.66 (ddd, *J* = 17.2, 10.3, 7.7 Hz, 1H), 5.45 (d, *J* = 8.7 Hz, 1H), 5.37–5.27 (m, 2H), 4.50 (d, *J* = 6.8 Hz, 1H), 4.37 (d, *J* = 6.8 Hz, 1H), 4.22 (t, *J* = 8.1 Hz, 1H), 3.58 (d, *J* = 1.4 Hz, 3H), 3.10 (s, 3H), 1.90 (dd, *J* = 1.5, 0.7 Hz, 3H), 1.69 (d, *J* = 1.3 Hz, 3H)





### Conjugated ester **S2**.

A Schlenk tube was charged with vinyl iodide **13** (1.00 g, 2.96 mmol, 1.00 equiv.), methyl acrylate (0.80 mL, 8.9 mmol, 3.0 equiv.) and dry degassed toluene (freeze-pump-thaw, 3x10 min, 5.0 mL). A solution of 2<sup>nd</sup> generation Hoveyda–Grubbs catalyst (186 mg, 0.300 mmol, 0.10 equiv.) in dry degassed toluene (freeze-pump-thaw, 3x10 min, 6.6 mL) was loaded in a syringe. 0.55 mL of the solution were added in one portion every hour while the reaction mixture was stirred at 50 °C. After the addition was complete the suspension was stirred for an additional 12 h at the same temperature.

The solvents were evaporated at 28 °C and the crude product was submitted to flash column chromatography on silica gel (EtOAc/Hex, gradient, 0 to 30%) affording ester **S2** (776 mg, 1.96 mmol, 66% yield) as yellow oil.

**<sup>1</sup>H NMR** (400 MHz, CDCl<sub>3</sub>) δ 6.87 (dd, *J* = 15.8, 6.4 Hz, 1H), 6.10–6.04 (m, 2H), 5.91 (s, 1H), 4.70 (s, 2H), 4.24 (ddd, *J* = 7.4, 6.4, 1.3 Hz, 1H), 4.03 (dd, *J* = 7.4, 2.7 Hz, 1H), 3.72 (s, 3H), 3.43 (s, 3H), 2.96–2.94 (m, 1H), 1.94 (d, *J* = 1.3 Hz, 3H), 1.71 (d, *J* = 1.3 Hz, 3H)

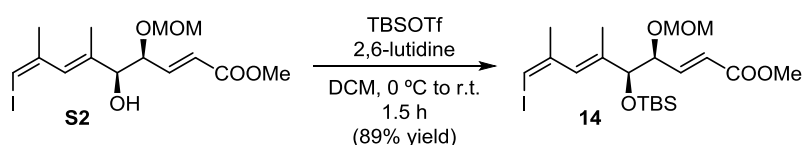
**<sup>13</sup>C NMR** (100 MHz, CDCl<sub>3</sub>) δ 166.2, 144.2, 144.0, 136.2, 131.0, 123.4, 95.5, 78.9, 78.5, 77.4, 56.1, 51.7, 24.6, 14.0

**IR** (ATR): 3560 (br), 2950 (m), 1721 (s), 1660 (w), 1436 (m), 1277 (s), 1150 (m), 1023 (s), 916 (s), 730 (s)

**HRMS** (+APCI): calc. for C<sub>14</sub>H<sub>20</sub>IO<sub>4</sub> [M–OH]<sup>+</sup> 379.0401, found 379.0434

[α]<sub>D</sub><sup>23</sup> +56.9° (c 0.93, CHCl<sub>3</sub>)

*R*<sub>F</sub> = 0.16 (20% EtOAc in hexanes)



### Silyl ether **14**.

To vinyl iodide **S2** (1.04 g, 2.63 mmol, 1.00 equiv.) in dry DCM (22 mL) was added 2,6-lutidine (0.76 mL, 6.6 mmol, 2.5 equiv.). The solution was cooled down to 0 °C and TBSOTf (0.91 mL, 3.9 mmol, 1.5 equiv.) was added dropwise. The reaction mixture was allowed to warm up to room temperature and was stirred for 1.5 h.

An aqueous saturated NaHCO<sub>3</sub> solution was added and the layers were separated. The aqueous phase was extracted three times with DCM and the organic layers were combined, dried over MgSO<sub>4</sub>, filtered and concentrated under reduced pressure. The crude material (yellow oil, 1.50 g) was purified by flash column chromatography on silica gel (EtOAc/hexanes, gradient, 0 to 15%) affording silyl ether **14** as a yellow oil (1.20 g, 2.35 mmol, 89% yield).

**$^1\text{H}$  NMR** (400 MHz,  $\text{CDCl}_3$ )  $\delta$  6.88 (dd,  $J$  = 15.7, 6.0 Hz, 1H), 6.09–6.03 (m, 2H), 5.82 (br s, 1H), 4.75 (d,  $J$  = 6.7 Hz, 1H), 4.65 (d,  $J$  = 6.7 Hz, 1H), 4.23 (ddd,  $J$  = 7.3, 6.0, 1.5 Hz, 1H), 4.08 (dd,  $J$  = 6.9, 0.9 Hz, 1H), 3.71 (s, 3H), 3.37 (s, 3H), 1.91 (dd,  $J$  = 1.5, 0.7 Hz, 3H), 1.66 (d,  $J$  = 1.3 Hz, 3H), 0.91 (s, 9H), 0.10 (s, 3H), 0.08 (s, 3H)

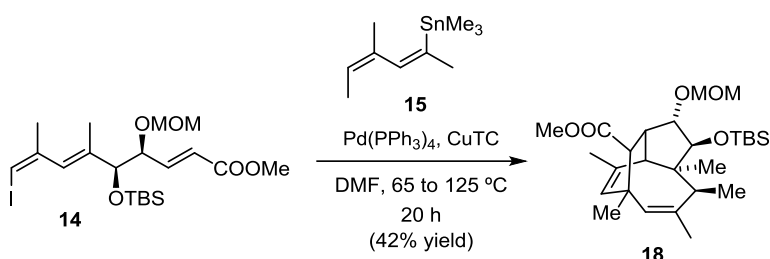
**$^{13}\text{C}$  NMR** (100 MHz,  $\text{CDCl}_3$ )  $\delta$  166.5, 145.2, 144.3, 138.0, 130.0, 122.1, 96.0, 80.4, 78.5, 77.1, 55.8, 51.5, 25.8, 24.4, 18.2, 14.2, –4.6, –4.9

**IR** (ATR): 2951 (m), 2928 (m), 2888 (w), 2856 (m), 2361 (w), 1726 (s), 1661 (w), 1435 (m), 1251 (m), 1152 (m), 1092 (s), 1028 (s), 912 (m), 872 (m), 837 (s), 775 (s)

**HRMS** (+APCI): calc. for  $\text{C}_{18}\text{H}_{30}\text{IO}_3\text{Si}$  [ $\text{M}-\text{OMOM}$ ] $^+$  449.1003, found 449.1009

$[\alpha]_D^{23}$  +1.5° (c 1.07,  $\text{CHCl}_3$ )

$R_f$  = 0.58 (20% EtOAc in hexanes)



#### Cascade product **18**.

$\text{Pd}(\text{PPh}_3)_4$  (25.8 mg, 22.3  $\mu\text{mol}$ , 0.100 equiv.) and copper(I) thiophene-2-carboxylate ( $\text{CuTC}$ , 46.8 mg, 0.246 mmol, 1.10 equiv.) were charged into a dried flask under  $\text{N}_2$  that was wrapped in aluminum foil to shield it from light. A solution of vinyl stannane **15** (81.0 mg, 0.313 mmol, 1.40 equiv.) in benzene (1.2 mL) and vinyl iodide **14** (114 mg, 0.223 mmol, 1.00 equiv.) were combined and concentrated (rotary evaporator bath temperature 30 °C, pressure 35 mbar, darkness) to azeotropically remove traces of water. The iodide/stannane mixture was redissolved in dry  $\text{DMF}$  (2.2 mL) and added to the  $\text{Pd}/\text{Cu}$  solid mixture avoiding light. The result was immediately heated to 65 °C (external aluminium block temperature) and stirred for 50 min. The temperature was then increased to 125 °C and the mixture further stirred in the dark for 20 h.

After cooling, the solvent was evaporated at 60 °C and 10 mbar. The resulting black gum was dissolved in a small amount of DCM and loaded on a pad of silica pre-equilibrated with hexanes. The DCM was evaporated under a flow of nitrogen and the remaining residue was eluted with 7:3 hexanes/ $\text{Et}_2\text{O}$  (4x3.8 mL) yielding 95 mg of a slightly yellow which was purified by flash column chromatography on silica gel, ( $\text{EtOAc}/\text{Hex}$ , gradient, 0 to 3%) providing tricycle **18** as a white crystalline solid (45.0 mg, 94.0  $\mu\text{mol}$ , 42% yield). The same procedure performed on 831 mg of vinyl iodide **14** afforded **18** (309 mg, 0.645 mmol, 40% yield).

**$^1\text{H}$  NMR** (400 MHz,  $\text{CDCl}_3$ )  $\delta$  5.34 (s, 1H), 5.00 (s, 1H), 4.63–4.57 (m, 2H), 3.93–3.84 (m, 2H), 3.59 (s, 3H), 3.25 (s, 3H), 2.88 (q,  $J$  = 7.6 Hz, 1H), 2.71 (s, 1H), 2.65 (d,  $J$  = 11.3 Hz, 1H), 2.32 (dd,  $J$  = 11.4, 4.9 Hz, 1H), 1.86 (s, 3H), 1.82 (s, 3H), 1.19 (s, 3H), 1.12 (s, 3H), 1.07 (d,  $J$  = 7.5 Hz, 3H), 0.91 (s, 9H), 0.11 (s, 3H), 0.06 (s, 3H)

**$^{13}\text{C}$  NMR** (100 MHz,  $\text{CDCl}_3$ )  $\delta$  175.4, 140.6, 138.0, 133.1, 125.0, 97.8, 92.9, 87.8, 55.3, 55.2, 53.9, 51.2, 50.9, 44.3, 40.5, 34.4, 29.3, 29.0, 26.0, 25.0, 24.2, 18.2, 15.8, –4.24, –4.39

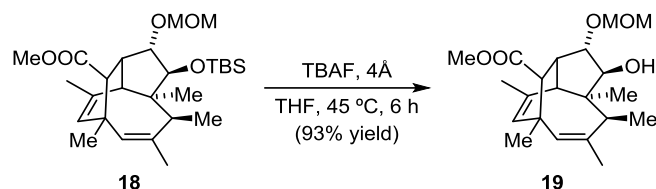
**IR** (ATR): 2929 (m), 2856 (w), 1731 (m), 1460 (m), 1252 (m), 1197 (m), 1173 (m), 1124 (s), 1109 (s), 1041 (s), 876 (s), 837 (s), 774 (s)

**HRMS** (+APCI): calc. for  $C_{27}H_{47}O_5Si$   $[M+H]^+$  479.3187, found 479.3191

$[\alpha]_D^{23} +15.1^\circ$  (c 2.33,  $CHCl_3$ )

$R_F = 0.29$  (12%  $Et_2O$  in hexanes), 0.36 (10%  $EtOAc$  in hexanes)

**Mp:** 84-86 °C



#### Alcohol **19**.

To a solution of silyl ether **18** (120 mg, 0.251 mmol, 1.00 equiv.) in dry THF (4.0 mL) at room temperature were added 4Å molecular sieves followed by a solution of TBAF (1.0 M in THF, 0.45 mL, 0.45 mmol, 1.8 equiv.). The mixture was stirred for 4 h at 45 °C after which additional TBAF (1.0 M, 0.10 mL, 0.10 mmol, 0.4 equiv.) was added, and the reaction was further stirred for 2 h.

The mixture was filtered over a plug of silica gel, eluting with 3:1 hexanes/ $EtOAc$ . Alcohol **19** was obtained as a colourless oil (85.0 mg, 0.233 mmol, 93% yield) which solidified upon standing and could be used for the next step without further purification.

**$^1H$  NMR** (400 MHz,  $CDCl_3$ )  $\delta$  5.34 (d,  $J = 1.2$  Hz 1H), 4.98 (s, 1H), 4.66 (q,  $J = 7.1$  Hz, 2H), 3.98 (dd,  $J = 7.9$ , 6.2 Hz, 1H), 3.79 (dd,  $J = 7.9$ , 1.5 Hz, 1H), 3.58 (s, 3H), 3.40 (s, 3H), 2.88 (q,  $J = 7.3$  Hz, 1H), 2.69 (d,  $J = 11.3$  Hz, 1H), 2.50 (s, 1H), 2.41 (dd,  $J = 11.3$ , 6.1 Hz, 1H), 1.88 (s, 3H), 1.82 (d,  $J = 1.5$  Hz, 3H), 1.28 (s, 3H), 1.13 (s, 3H), 1.10 (d,  $J = 7.5$  Hz, 3H)

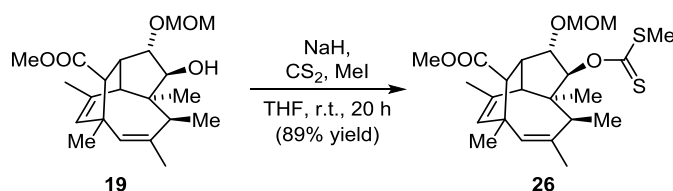
**$^{13}C$  NMR** (100 MHz,  $CDCl_3$ )  $\delta$  174.8, 141.5, 137.9, 132.7, 124.9, 97.9, 95.5, 87.4, 56.6, 55.6, 54.5, 51.4, 51.1, 44.1, 40.6, 34.7, 29.7, 29.0, 25.1, 24.1, 15.7

**IR** (ATR): 3473 (br), 2933 (m), 1731 (m), 1459 (m), 1376 (w), 1174 (m), 1148 (m), 1107 (s), 1039 (s), 912 (m)

**HRMS** (+ESI): calc. for  $C_{21}H_{33}O_5$   $[M+H]^+$  365.2323, found 365.2340

$[\alpha]_D^{23} +95.3^\circ$  (c 1.73,  $CHCl_3$ )

$R_F = 0.20$  (20%  $EtOAc$  in hexanes)



#### Methyl xanthate **26**.

To alcohol **19** (130 mg, 0.357 mmol, 1.00 equiv.) dissolved in dry THF (6.0 mL) was added NaH (60% w/w in paraffin oil, 42.8 mg, 1.07 mmol, 3.00 equiv.) followed by  $CS_2$  (64  $\mu$ L, 1.1 mmol, 3.0 equiv.). After vigorously stirring for 50 minutes, methyl iodide (68  $\mu$ L, 1.1 mmol, 3.0 equiv.) was added and the mixture was stirred for an additional 20 h.

The reaction was quenched by the addition of aqueous saturated  $\text{NH}_4\text{Cl}$ . The phases were separated and the aqueous layer was extracted three times with diethyl ether. The organic layers were combined, dried over  $\text{Na}_2\text{SO}_3$ , filtered and concentrated under reduced pressure. The crude material (168 mg) was purified by flash column chromatography on silica gel, (10% EtOAc/Hexanes). Methyl xanthate **26** was obtained as a dark yellow oil (145 mg, 0.319 mmol, 89% yield).

**$^1\text{H}$  NMR** (400 MHz,  $\text{CDCl}_3$ )  $\delta$  6.36 (d,  $J$  = 8.2 Hz, 1H), 5.39 (s, 1H), 5.12 (s, 1H), 4.56 (q,  $J$  = 6.9 Hz, 2H), 4.37 (dd,  $J$  = 8.1, 6.0 Hz, 1H), 3.60 (s, 3H), 3.26 (s, 3H), 2.96 (q,  $J$  = 7.4 Hz, 1H), 2.90 (d,  $J$  = 11.3 Hz, 1H), 2.66 (s, 1H), 2.62 (s, 3H), 2.51 (dd,  $J$  = 11.3, 5.8 Hz, 1H), 1.94 (s, 3H), 1.83 (s, 3H), 1.27 (s, 3H), 1.15 (s, 3H), 1.00 (d,  $J$  = 7.5 Hz, 3H)

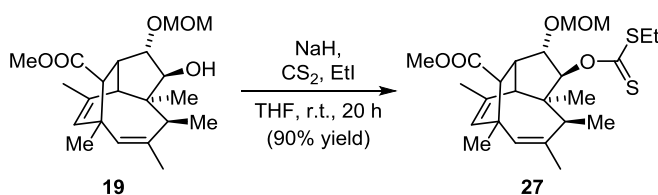
**$^{13}\text{C}$  NMR** (100 MHz,  $\text{CDCl}_3$ )  $\delta$  217.2, 174.7, 139.8, 137.2, 133.7, 125.7, 96.4, 94.6, 88.4, 57.1, 55.3, 54.0, 51.4, 51.1, 44.4, 40.5, 34.8, 29.3, 29.0, 25.1, 24.1, 19.7, 15.6

**IR** (ATR): 2919 (m), 2849 (w), 1731 (m), 1456 (m), 1380 (w), 1213 (s), 1106 (m), 1061 (s), 1036 (m), 914 (w), 754 (m)

**HRMS** (+ESI): calc. for  $\text{C}_{23}\text{H}_{34}\text{O}_5\text{S}_2\text{Na}$   $[\text{M}+\text{Na}]^+$  477.1740, found 477.1762

$[\alpha]_D^{23}$  +63.1° (c 2.14,  $\text{CHCl}_3$ )

$R_f$  = 0.59 (20% EtOAc in hexanes)



### Ethyl xanthate **27**.

The same procedure as for methyl xanthate **26** (see above) was followed changing the reagent ratio: **19**, (15.0 mg, 41.2  $\mu\text{mol}$ , 1.00 equiv.), NaH, (60% w/w in paraffin oil, 6.6 mg, 0.16 mmol, 4.0 equiv.),  $\text{CS}_2$ , (10  $\mu\text{L}$ , 0.16 mmol, 4.0 equiv.) and ethyl iodide, (20  $\mu\text{L}$ , 0.25 mmol, 6.0 equiv.). The crude material (20 mg) was purified by flash column chromatography on silica gel (10% EtOAc/Hexanes) yielding xanthate **27** as a dark yellow oil (17.3 mg, 0.369 mmol, 90% yield).

**$^1\text{H}$  NMR** (400 MHz,  $\text{CDCl}_3$ )  $\delta$  6.36 (d,  $J$  = 8.2 Hz, 1H), 5.39 (s, 1H), 5.11 (s, 1H), 4.56 (q,  $J$  = 6.9 Hz, 2H), 4.36 (dd,  $J$  = 8.3, 5.9 Hz, 1H), 3.60 (s, 3H), 3.26 (s, 3H), 3.20 (q,  $J$  = 7.4 Hz, 2H), 2.96 (q,  $J$  = 7.7 Hz, 1H), 2.90 (d,  $J$  = 11.3 Hz, 1H), 2.66 (s, 1H), 2.51 (dd,  $J$  = 11.3, 5.8 Hz, 1H), 1.94 (s, 3H), 1.83 (s, 3H), 1.36 (t,  $J$  = 7.4 Hz, 3H), 1.26 (s, 3H), 1.15 (s, 3H), 1.00 (d,  $J$  = 7.5 Hz, 3H)

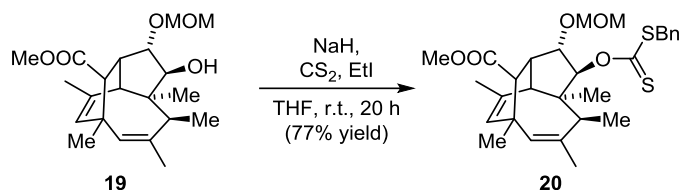
**$^{13}\text{C}$  NMR** (100 MHz,  $\text{CDCl}_3$ )  $\delta$  216.2, 174.7, 139.9, 137.2, 133.7, 125.7, 96.4, 94.1, 88.4, 57.1, 55.3, 54.1, 51.4, 51.1, 44.4, 40.5, 34.8, 31.0, 29.3, 29.0, 25.1, 24.1, 15.5, 13.0

**IR** (ATR): 2923 (m), 2851 (w), 1732 (m), 1457 (m), 1379 (w), 1211 (s), 1172 (m), 1107 (m), 1065 (s), 1032 (s), 915 (m)

**HRMS** (+ESI): calc. for  $\text{C}_{24}\text{H}_{36}\text{NaO}_5\text{S}_2$   $[\text{M}+\text{Na}]^+$  491.1896, found 491.1909

$[\alpha]_D^{23}$  +53.0° (c 0.4,  $\text{CHCl}_3$ )

$R_f$  = 0.59 (20% EtOAc in hexanes)



### Benzyl xanthate **20**.

The same procedure as for methyl xanthate **26** (see above) was followed changing the reagent ratio: **19** (40.0 mg, 0.110 mmol, 1.00 equiv.), NaH (60% w/w in paraffin oil, 17.6 mg, 0.439 mmol, 4.00 equiv.), CS<sub>2</sub> (26  $\mu$ L, 0.439 mmol, 4.00 equiv.) and freshly distilled BnBr, (65  $\mu$ L, 0.549 mmol, 5.00 equiv.).

The crude product (120 mg) was purified by flash column chromatography on silica gel, (Et<sub>2</sub>O/Hexanes, gradient, 0 to 10%) giving benzyl xanthate **20** as a yellow oil (45.0 mg, 84.8  $\mu$ mol, 77 % yield).

**<sup>1</sup>H NMR** (400 MHz, CDCl<sub>3</sub>)  $\delta$  7.39–7.27 (m, 5H), 6.36 (d,  $J$  = 8.2 Hz, 1H), 5.39 (s, 1H), 5.10 (s, 1H), 4.56 (dd,  $J$  = 9.6, 6.9, 2H), 4.46 (s, 2H), 4.36 (dd,  $J$  = 8.3, 5.9 Hz, 1H), 3.60 (s, 3H), 3.25 (s, 3H), 2.96 (q,  $J$  = 7.6 Hz, 1H), 2.90 (d,  $J$  = 11.2 Hz, 1H), 2.66 (s, 1H), 2.51 (dd,  $J$  = 11.4, 5.8 Hz, 1H), 1.91 (s, 3H), 1.83 (s, 3H), 1.28 (s, 3H), 1.15 (s, 3H), 1.00 (d,  $J$  = 7.5 Hz, 3H)

**<sup>13</sup>C NMR** (100 MHz, CDCl<sub>3</sub>)  $\delta$  215.5, 174.7, 139.8, 137.2, 135.0, 133.7, 129.2, 128.6, 127.7, 125.7, 96.5, 94.6, 88.5, 57.1, 55.3, 54.0, 51.4, 51.11, 44.4, 41.6, 40.5, 34.7, 29.3, 29.0, 25.1, 24.1, 15.6

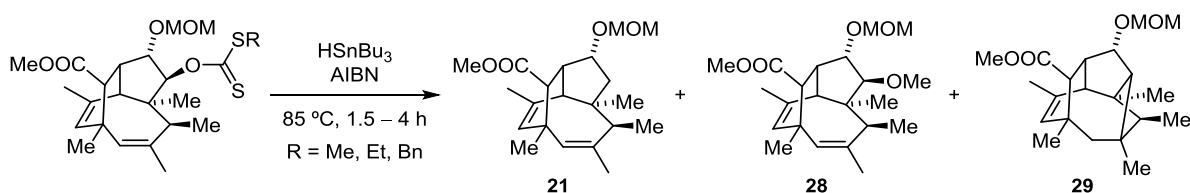
**IR** (ATR): 2924 (m), 2850 (w), 1730 (m), 1454 (m), 1380 (w), 1216 (s), 1107 (m), 1195 (m), 1058 (s), 1039 (s), 914 (w)

**HRMS** (+APCI): calc. for C<sub>27</sub>H<sub>33</sub>O<sub>3</sub>S<sub>2</sub> [M–OMOM]<sup>+</sup> 469.1866, found 469.1882

$[\alpha]_D^{23}$  +53.4° (c 0.20, CHCl<sub>3</sub>)

$R_F$  = 0.46 (15% EtOAc in hexanes)

### General procedure for Barton–McCombie Deoxygenation



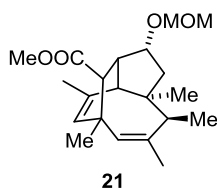
Entry	Xanthate	HSnBu <sub>3</sub> [eq.]	yield [%]
1*	<b>26</b> R = Me	4.8	21
2	<b>26</b> R = Me	50	41
3	<b>27</b> R = Et	50	49
4	<b>20</b> R = Bn	40	76

\* Reaction was run in PhMe (11.6 mL), with 580 mg of **27** and 97 mg of AIBN.

A vial was charged with the corresponding xanthate (45.0  $\mu$ mol, 1.00 equiv.) and AIBN (1.9 mg, 9.7  $\mu$ mol, 0.25 equiv.). The vial was evacuated and flushed with nitrogen three times and tributyltin hydride (0.59 ml, 2.2 mmol, 50 equiv., entries 2-3) or (0.47 ml, 2.8 mmol, 40 equiv., entry 4) was added. The mixture was stirred at 85 °C for 1.5 to 4 h (monitored by <sup>1</sup>H NMR).

The reaction mixture was then cooled down to room temperature and submitted to flash column chromatography on silica gel (Et<sub>2</sub>O/Hexanes, gradient, 0 to 12%).

Results for entry 4 are shown below.



#### Deoxygenated tricycle **21**.

Tricycle **21** was obtained together with methyl ether **28** as a white solid, 14 mg. NMR shows a **21** to **28** molar ratio of 1:0.15 (12.0 mg, 34.4  $\mu$ mol, 76% yield). Elution at 6% Et<sub>2</sub>O in hexanes.

An additional run using benzyl xanthate **20** (92 mg) allowed for isolation of fractions with clean tricycle **21** after a second separation on spherical 20-40  $\mu$ m particle size silica.

**<sup>1</sup>H NMR** (400 MHz, CDCl<sub>3</sub>)  $\delta$  5.31 (s, 1H), 5.01 (s, 1H), 4.61–4.56 (m, 2H), 4.05–3.96 (m, 1H), 3.58 (s, 3H), 3.29 (s, 2H), 2.82 (q,  $J$  = 7.0, 1H), 2.79 (d,  $J$  = 11.9, 1H), 2.59 (s, 1H), 2.57 (dd,  $J$  = 11.7, 4.9 Hz, 1H), 2.20 (dd,  $J$  = 13.7, 7.7 Hz, 1H), 1.83 (d,  $J$  = 1.3 Hz, 3H), 1.71 (s, 3H), 1.42 (dd,  $J$  = 13.7, 9 Hz, 1H), 1.41 (d,  $J$  = 13.5 Hz, 1H), 1.12 (s, 3H), 1.10 (s, 3H), 0.90 (d,  $J$  = 7.3 Hz, 3H)

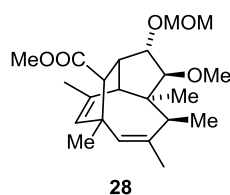
**<sup>13</sup>C NMR** (100 MHz, CDCl<sub>3</sub>)  $\delta$  174.9, 139.4, 138.3, 134.2, 124.3, 96.4, 88.2, 56.7, 56.4, 55.3, 55.0, 51.0, 50.0, 42.6, 40.8, 34.8, 30.7, 28.7, 25.4, 24.1, 14.7

**IR** (ATR): 2929 (s), 2851 (w), 1734 (s), 1461 (m), 1442 (m), 1378 (w), 1244 (w), 1195 (m), 1152 (s), 1102 (s), 1043 (s), 915 (w)

**HRMS** (+APCI): calc. for C<sub>21</sub>H<sub>33</sub>O<sub>4</sub> [M+H]<sup>+</sup> 349.2373, found 349.2372

$[\alpha]_D^{23}$  +26.0° (c 0.25, CHCl<sub>3</sub>)

$R_F$  = 0.28 (20% Et<sub>2</sub>O in hexanes)



#### Methyl ether **28**.

Methyl ether **28** was obtained together with tricycle **21** as a white solid, 14 mg. NMR shows a **21** to **28** molar ratio of 1:0.15 (2.0 mg, 5.3  $\mu$ mol, 12% yield). Elution at 6% Et<sub>2</sub>O in hexanes.

An additional run using benzyl xanthate **20** (92 mg) allowed for isolation of fractions with clean **28** after a second separation on spherical 20-40  $\mu$ m particle size silica.

**<sup>1</sup>H NMR** (400 MHz, CDCl<sub>3</sub>)  $\delta$  5.34 (s, 1H), 5.00 (s, 1H), 4.67 (dd,  $J$  = 18.1, 6.8 Hz, 2H), 4.06–4.01 (m, 1H), 3.59 (s, 3H), 3.52 (d,  $J$  = 7.9 Hz, 1H), 3.48 (s, 3H), 3.29 (s, 3H), 2.85 (q,  $J$  = 7.4 Hz, 1H), 2.71 (d,  $J$  = 11.3 Hz, 1H), 2.66 (s, 1H), 2.36 (dd,  $J$  = 11.3, 5.6 Hz, 1H), 1.82 (s, 3H), 1.81 (s, 3H), 1.27 (s, 3H), 1.12 (s, 3H), 1.04 (d,  $J$  = 7.4 Hz, 3H)

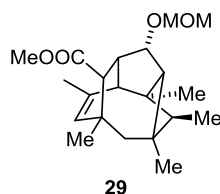
**$^{13}\text{C}$  NMR** (100 MHz,  $\text{CDCl}_3$ )  $\delta$  175.3, 140.8, 137.8, 132.8, 125.1, 96.7, 96.6, 91.5, 60.0, 55.7, 55.4, 54.6, 51.5, 51.0, 44.8, 40.5, 34.7, 29.9, 29.0, 24.9, 24.2, 15.6

**IR** (ATR): 2930 (s), 2851 (w), 2362 (w), 2337 (w), 1733 (s), 1460 (m), 1376 (w), 1198 (w), 1174 (m), 1124 (m), 1107 (s), 1142 (s), 977 (w), 917 (w)

**HRMS** (+APCI): calc. for  $\text{C}_{22}\text{H}_{35}\text{O}_5$   $[\text{M}+\text{H}]^+$  379.2479, found 379.2474

$[\alpha]_D^{23} +33.7^\circ$  (c 0.33,  $\text{CHCl}_3$ )

$R_F = 0.27$  (20%  $\text{Et}_2\text{O}$  in hexanes)



#### Tetracycle 29.

Tetracycle **29** was obtained as a colourless oil (1.0 mg, 2.9  $\mu\text{mol}$ , 6% yield). Elution at 5.5%  $\text{Et}_2\text{O}$  in hexanes.

**$^1\text{H}$  NMR** (400 MHz,  $\text{CDCl}_3$ )  $\delta$  5.33 (s, 1H), 4.62 (q,  $J = 6.7$  Hz, 2H), 3.74 (s, 1H), 3.59 (s, 3H), 3.34 (s, 3H), 2.86 (d,  $J = 9.3$  Hz, 1H), 2.68 (d,  $J = 9.3$  Hz, 1H), 2.21 (d,  $J = 8.9$  Hz, 2H), 2.01 (q,  $J = 7.5$  Hz, 1H), 1.60 (s, 3H), 1.20 (d,  $J = 14.7$  Hz, 1H), 1.13 (s, 3H), 1.13 (d,  $J = 14.8$  Hz, 1H), 1.01 (s, 3H), 0.95 (d,  $J = 7.6$  Hz, 3H), 0.87 (s, 3H)

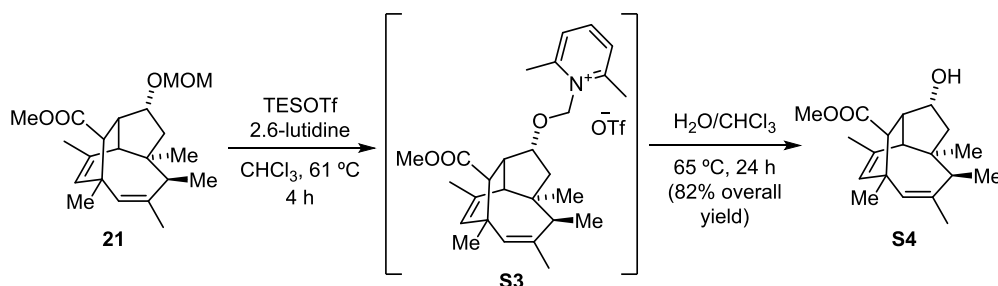
**$^{13}\text{C}$  NMR** (100 MHz,  $\text{CDCl}_3$ )  $\delta$  206.9, 175.3, 138.0, 125.7, 94.6, 87.6, 58.5, 55.5, 53.3, 51.7, 51.1, 50.9, 46.9, 38.18, 37.5, 30.9, 30.4, 26.5, 24.2, 23.5, 13.9

**IR** (ATR): 2956 (s), 2924 (s), 1739 (s), 1457 (m), 1374 (m), 1206 (w), 1150 (s), 1097 (m), 1038 (s), 922 (w)

**HRMS** (+APCI): calc. for  $\text{C}_{21}\text{H}_{33}\text{O}_4$   $[\text{M}+\text{H}]^+$  349.2373, found 349.2373

$[\alpha]_D^{23} +37.1^\circ$  (c 0.20,  $\text{CHCl}_3$ )

$R_F = 0.36$  (20%  $\text{Et}_2\text{O}$  in hexanes)



#### Tricyclic alcohol S4.

To a solution of acetal **21** (28.0 mg, 80.3  $\mu\text{mol}$ , 1.00 equiv.) in dry chloroform (0.62 mL) were added 2,6-lutidine (56  $\mu\text{L}$ , 0.48 mmol, 6.0 equiv.) and TESOTf (68  $\mu\text{L}$ , 0.32 mmol, 4.0 equiv.). After stirring under reflux for 4 h, the solution was allowed to cool down and water (0.67 mL) was added. The mixture was heated to 65  $^\circ\text{C}$  and stirred vigorously for 24 h.

The phases were separated and the aqueous layer was extracted three times with DCM. The organic layers were combined, dried over anhydrous  $\text{MgSO}_4$ , filtered and concentrated under reduced pressure. The crude material was purified by flash column chromatography on silica gel (35% EtOAc/Hexanes) affording alcohol **S4** (20.0 mg, 65.8  $\mu\text{mol}$ , 82% yield) as a white fluffy solid.

$^1\text{H}$  NMR (400 MHz,  $\text{CDCl}_3$ )  $\delta$  5.32 (s, 1H), 5.01 (s, 1H), 4.27 (ddd,  $J = 8.2, 5.1$  Hz, 1H), 3.59 (s, 3H), 2.84 (d,  $J = 11.4$  Hz, 1H), 2.82 (q,  $J = 7.3$  Hz, 1H), 2.56 (s, 1H), 2.47 (dd,  $J = 11.5, 4.9$  Hz, 1H), 2.23 (dd,  $J = 13.6, 7.6$  Hz, 1H), 1.83 (d,  $J = 1.5$  Hz, 3H), 1.71 (s, 3H), 1.37 (ddd,  $J = 13.6, 8.8, 1.1$  Hz, 1H), 1.14 (s, 3H), 1.12 (s, 3H), 0.92 (d,  $J = 7.4$  Hz, 3H)

$^{13}\text{C}$  NMR (100 MHz,  $\text{CDCl}_3$ )  $\delta$  174.7, 139.6, 138.3, 134.0, 124.3, 81.7, 57.3, 56.6, 55.2, 52.7, 51.1, 45.2, 40.8, 34.8, 30.8, 28.7, 25.5, 24.0, 14.7

IR (ATR): 3517 (m), 2923 (s), 2851 (w), 1709 (s), 1437 (m), 1373 (w), 1355 (w), 1238 (w), 1201 (m), 1178 (m), 1021 (w)

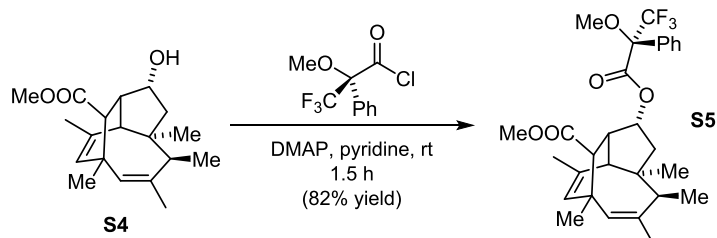
HRMS (+APCI): calc. for  $\text{C}_{19}\text{H}_{27}\text{O}_2$   $[\text{M}-\text{OH}]^+$  287.2006, found 287.2003

$[\alpha]_D^{23} +28.0^\circ$  (c 1.00,  $\text{CHCl}_3$ )

Mp: 158-160  $^\circ\text{C}$

$R_F = 0.20$  (30% EtOAc in hexanes)

#### Procedure for Mosher's ester analysis



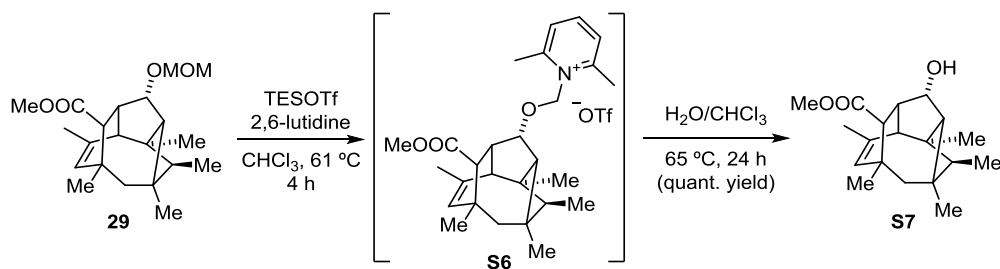
#### Mosher's ester **S5**.

To a solution of tricyclic **S4**, (3.5 mg, 12  $\mu\text{mol}$ , 1.0 equiv) and DMAP (4.9 mg, 40  $\mu\text{mol}$ , 3.5 equiv.) in pyridine (0.40 mL) was added (*R*)-(-)- $\alpha$ -methoxy- $\alpha$ -(trifluoromethyl)phenylacetyl chloride (Mosher's acyl chloride, 3.0  $\mu\text{L}$ , 12  $\mu\text{mol}$ , 1.0 equiv.). The reaction mixture was stirred for 1.5 h.

The solvent was evaporated, and the residue was filtered through a pad of silica eluting with 30% EtOAc/Hexanes. Ester **S5** was obtained as a colourless oil (4.9 mg, 9.4  $\mu\text{mol}$ , 82% yield, *d.r.* 1:0.02).

$^1\text{H}$  NMR (400 MHz,  $\text{CDCl}_3$ )  $\delta$  7.52–7.44 (m, 2H), 7.42–7.34 (m, 3H), 5.42 (td,  $J = 8.4, 4.9$  Hz, 1H), 5.36 (s, 1H), 5.15 (s, 1H), 3.58 (s, 3H), 3.55 (d,  $J = 0.8$  Hz, 3H), 2.89 (q,  $J = 7.3$  Hz, 1H), 2.85 (s, 1H), 2.79 (d,  $J = 11.6$  Hz, 1H), 2.53 (dd,  $J = 11.6, 4.8$  Hz, 1H), 2.33 (dd,  $J = 13.8, 7.9$  Hz, 1H), 1.82–1.77 (m, 6H), 1.56 (ddd,  $J = 13.8, 8.8, 1.0$  Hz, 1H), 1.15 (d,  $J = 2.7$  Hz, 6H), 0.94 (d,  $J = 7.4$  Hz, 3H)





#### Tetracyclic alcohol **7**.

The same procedure as for alcohol **4** was followed (see above). **29** (16.2 mg, 46.2  $\mu\text{mol}$ , 1.00 equiv.), TESOTf (40  $\mu\text{L}$ , 0.19 mmol, 4.0 equiv.), 2,6-lutidine (32  $\mu\text{L}$ , 0.28 mmol, 6.0 equiv.). Alcohol **7** was obtained as a white solid (14.1 mg, 46.3  $\mu\text{mol}$ , quantitative yield).

$^1\text{H NMR}$  (400 MHz,  $\text{CDCl}_3$ )  $\delta$  5.34 (s, 1H), 3.93 (s, 1H), 3.59 (s, 3H), 2.77 (s, 2H), 2.24 (s, 1H), 2.12 (s, 1H), 2.02 (q,  $J = 7.6$  Hz, 1H), 1.62 (s, 3H), 1.25 (br s, 1H), 1.20 (s, 3H), 1.17 (q,  $J = 14.7$  Hz, 2H), 1.02 (s, 3H), 0.96 (d,  $J = 7.6$  Hz, 3H), 0.88 (s, 3H)

$^{13}\text{C NMR}$  (100 MHz,  $\text{CDCl}_3$ )  $\delta$  175.2, 137.9, 125.8, 83.5, 61.5, 55.2, 54.0, 53.2, 51.6, 51.1, 47.0, 38.1, 37.7, 37.4, 30.4, 26.5, 24.9, 23.5, 13.8

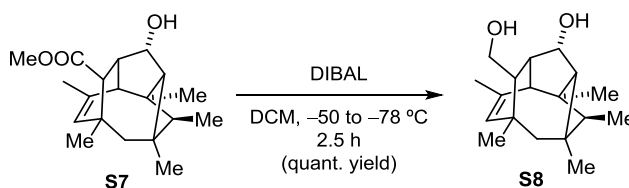
IR (ATR): 3418 (w, br), 2959 (s), 2922 (s), 2873 (m), 2358 (w), 1724 (s), 1457 (m), 1434 (m), 1374 (m), 1206 (m), 1158 (m), 1025 (m)

HRMS (+APCI): calc. for  $\text{C}_{19}\text{H}_{29}\text{O}_3$   $[\text{M}+\text{H}]^+$  305.2111, found 305.2108

$[\alpha]_D^{23} +19.1^\circ$  (c 0.42,  $\text{CHCl}_3$ )

Mp: 103-104  $^\circ\text{C}$

$R_F = 0.29$  (30% EtOAc in hexanes)



#### Tetracyclic diol **8**.

To alcohol **7** (49.2 mg, 0.162 mmol, 1.00 equiv.) dissolved in DCM (2.7 mL) at  $-78^\circ\text{C}$  was added dropwise a solution of DIBAL (1.5 M in toluene, 0.43 mL, 0.65 mmol, 4.0 equiv.). The mixture was warmed to  $-50^\circ\text{C}$  and stirred at the same temperature for 2.5 h.

The reaction was quenched with saturated aqueous Rochelle's salt (1.5 mL), then warmed to room temperature and stirred for 30 min. The mixture was diluted with water/diethyl ether and extracted three times with diethyl ether. The combined organic layers were dried over  $\text{Na}_2\text{SO}_4$ , filtered and concentrated under reduced pressure to afford pure diol **8** (44.8 mg, 0.162 mmol, quantitative yield) as a white fluffy solid. It was used for the next step without further purification.

$^1\text{H NMR}$  (400 MHz,  $\text{CDCl}_3$ )  $\delta$  5.42 (s, 1H), 3.95 (s, 1H), 3.68 (dt,  $J = 9.8, 4.6$  Hz, 1H), 3.47–3.38 (m, 1H), 2.74 (d,  $J = 9.3$  Hz, 1H), 2.68 (d,  $J = 9.3$  Hz, 1H), 2.13 (s, 1H), 1.93 (q,  $J = 7.5$  Hz, 1H), 1.56 (s, 3H), 1.45 (br s, 1H),

1.33 (dd,  $J = 7.1, 3.9$  Hz, 2H), 1.20 (s, 3H), 1.14 (d,  $J = 2.2$  Hz, 2H), 1.01 (s, 3H), 0.97 (d,  $J = 7.6$  Hz, 3H), 0.88 (s, 3H)

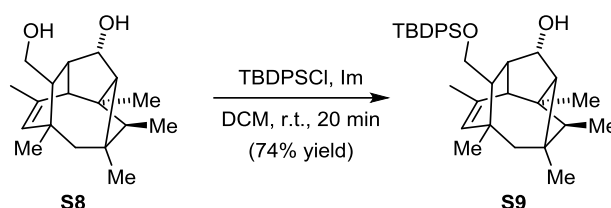
$^{13}\text{C}$  NMR (100 MHz,  $\text{CDCl}_3$ )  $\delta$  137.8, 128.6, 84.3, 65.0, 61.0, 53.1, 53.0, 52.7, 52.3, 47.6, 37.5, 37.4, 37.3, 29.6, 26.5, 24.9, 23.4, 13.9

IR (ATR): 3263 (m, br), 2957 (m), 2922 (s), 2868 (m), 1724 (w), 1453 (m), 1371 (w), 1022 (s), 981 (w), 814 (w)

HRMS (+APCI): calc. for  $\text{C}_{18}\text{H}_{29}\text{O}_2$   $[\text{M}+\text{H}]^+$  277.2162, found 277.2167

$[\alpha]_D^{23}$   $-14.1^\circ$  (c 1.00,  $\text{CHCl}_3$ )

$R_F = 0.10$  (40% EtOAc in hexanes)



#### TBDPS-protected alcohol **S9**.

To a solution of diol **S8** (45.0 mg, 0.163 mmol, 1.00 equiv.) in DCM (3.3 mL) was added imidazole (22.7 mg, 0.334 mmol, 2.05 equiv.) followed by TBDPSCI (63  $\mu\text{L}$ , 0.24 mmol, 1.5 equiv.). The resulting mixture was stirred at room temperature for 20 min after which an aqueous saturated  $\text{NaHCO}_3$  solution (4.0 mL) was added. The mixture was vigorously stirred for 5 min, after which the aqueous phase was separated and extracted three times with DCM. The organic layers were combined, dried over  $\text{MgSO}_4$  and concentrated under reduced pressure yielding a colourless oil, 113 mg.

Purification by flash column chromatography on silica gel (EtOAc/Hexanes, gradient, 0 to 20%) yielded 95 mg of a colourless oil containing alcohol **S9** (62.4 mg, 0.121 mmol, 74% yield). Despite our efforts, separation of product from TBDPSOH was not possible by either flash chromatography or HPLC.

$^1\text{H}$  NMR (400 MHz,  $\text{CDCl}_3$ )  $\delta$  7.69 (d,  $J = 6.9$  Hz, 4H), 7.47–7.34 (m, 6H), 5.21 (s, 1H), 3.87 (s, 1H), 3.73 (dd,  $J = 10.0, 4.2$  Hz, 1H), 3.29 (t,  $J = 9.8$  Hz, 1H), 2.80 (d,  $J = 9.3$  Hz, 1H), 2.47 (d,  $J = 9.3$  Hz, 1H), 1.89 (q,  $J = 7.6$  Hz, 1H), 1.43 (s, 3H), 1.37 (dd,  $J = 9.7, 4.3$  Hz, 1H), 1.16 (s, 3H), 1.10–1.00 (m, 12H), 0.93 (d,  $J = 7.6$  Hz, 3H), 0.85 (s, 3H), 0.78 (s, 3H)

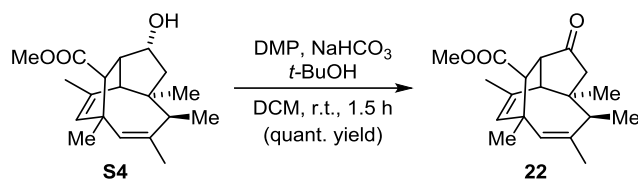
$^{13}\text{C}$  NMR (100 MHz,  $\text{CDCl}_3$ )  $\delta$  136.8, 135.7, 134.9, 134.2, 134.1, 129.5, 128.2, 127.6, 127.6, 84.5, 65.5, 61.0, 52.9, 52.7, 52.5, 52.2, 47.5, 37.4, 37.2, 29.5, 27.0, 26.6, 24.9, 23.3, 19.3, 13.9

IR (ATR): 3392 (w, br), 2958 (m), 2928 (m), 2857 (m), 2361 (s), 2340 (m), 1472 (w), 1428 (m), 1111 (s), 1061 (m), 822 (m), 739 (m)

HRMS (+ESI): calc. for  $\text{C}_{34}\text{H}_{47}\text{O}_2\text{Si}$   $[\text{M}+\text{H}]^+$  515.3340, found 515.3360

$[\alpha]_D^{23}$   $+6.9^\circ$  (c 1.00,  $\text{CHCl}_3$ )

$R_F = 0.29$  (10%  $\text{Et}_2\text{O}$  in hexanes)



### Tricyclic ketone **22**.

Alcohol **S4** (38.0 mg, 0.125 mmol, 1.00 equiv.) was dissolved in DCM (2.6 mL) and  $\text{NaHCO}_3$  (52.4 mg, 0.624 mmol, 5.00 equiv.) was added followed by 1 small drop of *t*-BuOH. Dess–Martin periodinane (132 mg, 0.312 mmol, 2.50 equiv.) was added and the reaction mixture was stirred at room temperature for 90 min.

A 1:1 solution of saturated aqueous  $\text{Na}_2\text{S}_2\text{O}_3/\text{NaHCO}_3$  (3.5 mL each) was added and the result was vigorously stirred for 15 min, after which the mixture was diluted with water and DCM. The phases were separated, and the aqueous layer was extracted three times with DCM. The organic layers were combined, dried over  $\text{Na}_2\text{SO}_4$  and concentrated under reduced pressure yielding a slightly yellow solid, 51 mg.

Purification by flash column chromatography on silica gel ( $\text{Et}_2\text{O}$ /Hexanes, gradient, 0 to 20%) allowed for isolation of ketone **22** as a white crystalline solid (37.8 mg, 0.125 mmol, quantitative yield).

**$^1\text{H}$  NMR** (400 MHz,  $\text{CDCl}_3$ )  $\delta$  5.37 (s, 1H), 4.92 (s, 1H), 3.60 (s, 3H), 3.07 (s, 1H), 3.04 (q,  $J = 7.3$  Hz, 1H), 2.97 (d,  $J = 11.8$  Hz, 1H), 2.82 (d,  $J = 11.8$  Hz, 1H), 2.36 (d,  $J = 17.2$  Hz, 1H), 2.08 (dd,  $J = 17.2, 0.9$  Hz, 1H), 1.88 (d,  $J = 1.5$  Hz, 3H), 1.58 (s, 3H), 1.26 (s, 3H), 1.17 (s, 3H), 0.91 (d,  $J = 7.4$  Hz, 3H)

**$^{13}\text{C}$  NMR** (100 MHz,  $\text{CDCl}_3$ )  $\delta$  216.4, 173.1, 137.7, 137.5, 124.9, 55.8, 52.7, 51.3, 50.0, 49.3, 48.0, 41.6, 34.4, 28.9, 27.7, 24.7, 24.2, 14.6

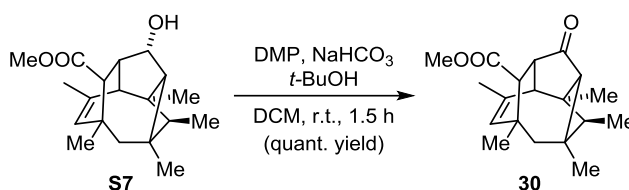
**IR** (ATR): 2923 (m), 2851 (w), 1733 (s), 1459 (m), 1234 (m), 1174 (m), 1019 (w)

**HRMS** (+APCI): calc. for  $\text{C}_{19}\text{H}_{27}\text{O}_3$   $[\text{M}+\text{H}]^+$  303.1955, found 303.1955

$[\alpha]_D^{23} +97.3^\circ$  (c 0.53,  $\text{CHCl}_3$ )

**Mp**: 110–112  $^\circ\text{C}$

$R_F = 0.40$  (20% EtOAc in hexanes)



### Tetracyclic ketone **30**.

The same procedure as for ketone **22** (see above) was followed: **S7** (11.9 mg, 39.1  $\mu\text{mol}$ , 1.00 equiv),  $\text{NaHCO}_3$  (16.4 mg, 0.195 mmol, 5.00 equiv.), Dess–Martin periodinane (41.4 mg, 98.5  $\mu\text{mol}$ , 2.50 equiv.). Ketone **30** was obtained as a white crystalline solid (11.8 mg, 39.0  $\mu\text{mol}$ , quantitative yield).

**$^1\text{H}$  NMR** (400 MHz,  $\text{CDCl}_3$ )  $\delta$  5.40 (s, 1H), 3.61 (s, 3H), 3.03 (dd,  $J = 10.1, 2.0$  Hz, 1H), 2.80 (d,  $J = 10.1$  Hz, 1H), 2.44 (s, 1H), 2.41 (s, 1H), 2.39 (q,  $J = 7.5$  Hz, 1H), 1.65 (s, 3H), 1.39 (d,  $J = 15.3$  Hz, 1H), 1.27 (d,  $J = 16.0$  Hz, 1H), 1.12 (s, 6H), 1.02 (d,  $J = 7.5$  Hz, 3H), 0.96 (s, 3H)

**$^{13}\text{C}$  NMR** (100 MHz,  $\text{CDCl}_3$ )  $\delta$  173.8, 137.6, 125.7, 62.2, 53.7, 53.1, 51.6, 51.5, 50.2, 40.6, 39.9, 38.7, 37.7, 30.2, 26.0, 23.9, 23.3, 14.0

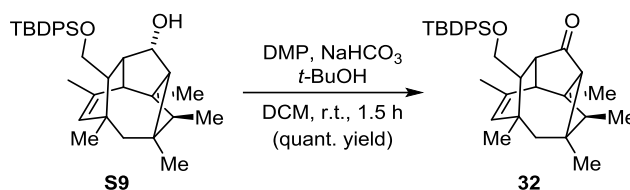
**IR** (ATR): 2960 (m), 2923 (m), 2851 (m), 2357 (W), 1743 (m), 1454 (w), 1376 (w), 1106 (s), 814 (m)

**HRMS** (+APCI): calc. for  $\text{C}_{19}\text{H}_{27}\text{O}_3$   $[\text{M}+\text{H}]^+$  303.1955, found 303.1947

$[\alpha]_D^{23}$  +76.7° (c 0.3,  $\text{CHCl}_3$ )

$R_f$  = (20%  $\text{Et}_2\text{O}$  in hexanes)

**Mp**: 147-150 °C



#### Tetracyclic ketone **32**.

The same procedure as for ketone **22** (see above) was followed. **59** (81.1 mg, 0.158 mmol, 1.00 equiv.),  $\text{NaHCO}_3$  (66.2 mg, 0.788 mmol, 5.00 equiv.), Dess–Martin periodinane (167 mg, 0.393 mmol, 2.50 equiv.). Purification by flash column chromatography on silica gel ( $\text{Et}_2\text{O}$ /Hexanes, gradient, 0 to 30%) yielded ketone **32** as a colourless oil (81.0 mg, 0.158 mmol, quantitative yield).

**$^1\text{H}$  NMR** (400 MHz,  $\text{CDCl}_3$ )  $\delta$  7.66 (td,  $J$  = 7.5, 1.8 Hz, 4H), 7.44–7.35 (m, 6H), 5.29 (s, 1H), 3.74 (dd,  $J$  = 9.9, 4.7 Hz, 1H), 3.35 (t,  $J$  = 9.8 Hz, 1H), 3.16 (dd,  $J$  = 10.2, 2.1 Hz, 1H), 2.45 (d,  $J$  = 10.2 Hz, 1H), 2.40 (br s, 1H), 2.26 (q,  $J$  = 7.5 Hz, 1H), 1.68 (dd,  $J$  = 9.8, 4.7 Hz, 1H), 1.48 (d,  $J$  = 1.5 Hz, 3H), 1.25 (d,  $J$  = 14.6 Hz, 1H), 1.19 (d,  $J$  = 14.3 Hz, 1H), 1.07 (s, 12H), 0.99 (d,  $J$  = 7.6 Hz, 3H), 0.94 (s, 3H), 0.82 (s, 3H)

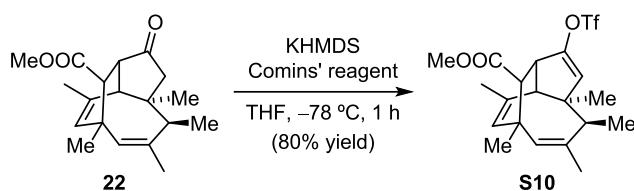
**$^{13}\text{C}$  NMR** (100 MHz,  $\text{CDCl}_3$ )  $\delta$  175.2, 136.1, 135.8, 135.6, 134.0, 133.8, 129.5, 129.5, 128.1, 127.6, 127.6, 64.0, 62.1, 52.3, 52.2, 50.8, 49.8, 40.4, 39.2, 37.7, 37.7, 29.1, 27.0, 26.1, 23.9, 23.1, 19.2, 14.1

**IR** (ATR): 2957 (m), 2928 (s), 2856 (m), 2360 (m), 2340 (w), 1724 (s), 1455 (m), 1428 (w), 1112 (s), 1087 (s), 823 (w)

**HRMS** (+APCI): calc. for  $\text{C}_{34}\text{H}_{45}\text{O}_2\text{Si}$   $[\text{M}+\text{H}]^+$  513.3183, found 513.3179

$[\alpha]_D^{23}$  +47.6° (c 0.6,  $\text{CHCl}_3$ )

$R_f$  = 0.36 (20%  $\text{Et}_2\text{O}$  in hexanes)



### Enol triflate S10.

A flame-dried vial charged with ketone **22** (15.0 mg, 49.6  $\mu\text{mol}$ , 1.00 equiv.) and dry THF (1.4 mL) was cooled to  $-78\text{ }^{\circ}\text{C}$ . To the stirred mixture was added a solution of KHMDS (1.2 M in toluene, 46  $\mu\text{L}$ , 55  $\mu\text{mol}$ , 1.1 equiv.) in a dropwise manner. The reaction was stirred at the same temperature for 35 min after which a solution of Comins' reagent (25.3 mg, 64.5  $\mu\text{mol}$ , 1.3 equiv.) in THF (0.40 mL) was added dropwise.

After stirring for 60 min at  $-78\text{ }^{\circ}\text{C}$ , diethyl ether (0.7 mL) was added to the reaction mixture followed by an aqueous saturated solution of  $\text{NH}_4\text{Cl}$  (1.2 mL). Upon warming to room temperature, the mixture was extracted three times with diethyl ether and the combined extracts were washed with brine, dried over  $\text{Na}_2\text{SO}_4$  and concentrated under reduced pressure yielding a yellow oil, 48 mg.

Purification by flash column chromatography on silica gel, (EtOAc/Hexanes, 0%, then 4%) afforded enol triflate **S10** as a colourless oil (12.0 mg, 39.7  $\mu\text{mol}$ , 80% yield).

**$^1\text{H}$  NMR** (400 MHz,  $\text{CDCl}_3$ )  $\delta$  5.38 (s, 2H), 5.06 (s, 1H), 3.61 (s, 3H), 3.19 (d,  $J = 9.8\text{ Hz}$ , 1H), 2.97 (q,  $J = 7.3\text{ Hz}$ , 1H), 2.81 (d,  $J = 9.8\text{ Hz}$ , 1H), 2.63 (s, 1H), 1.83 (s, 3H), 1.47 (s, 3H), 1.31 (s, 3H), 1.12 (s, 3H), 0.94 (d,  $J = 7.5\text{ Hz}$ , 3H)

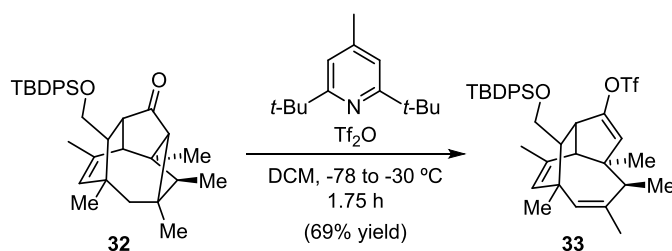
**$^{13}\text{C}$  NMR** (100 MHz,  $\text{CDCl}_3$ )  $\delta$  173.9, 149.5, 138.7, 137.1, 132.1, 125.5, 120.0, 118.4 (q,  $J = 320.2\text{ Hz}$ ), 57.3, 52.2, 51.5, 51.4, 46.4, 40.4, 37.3, 29.0, 27.5, 24.9, 24.1, 15.0

**IR** (ATR): 2925 (m), 2361 (m), 2340 (m), 1736 (m), 1423 (m), 1214 (s), 1142 (m), 827 (w)

**HRMS** (+APCI): calc. for  $\text{C}_{20}\text{H}_{26}\text{F}_3\text{O}_5\text{S}$   $[\text{M}+\text{H}]^+$  435.1448, found 435.1453

$[\alpha]_D^{23} +17.1^{\circ}$  (c 0.5,  $\text{CHCl}_3$ )

$R_f = 0.59$  (10%  $\text{Et}_2\text{O}$  in hexanes)



### Enol triflate 33.

To ketone **32** (18.5 mg, 36.1  $\mu\text{mol}$ , 1.00 equiv.) and 2,6-di-tertbutyl-4-methylpyridine (14.8 mg, 72.2  $\mu\text{mol}$ , 2.0 equiv.) dissolved in DCM (0.95 mL) at  $-78\text{ }^{\circ}\text{C}$  was added  $\text{Tf}_2\text{O}$  (11.5  $\mu\text{L}$ , 68.5  $\mu\text{mol}$ , 1.90 equiv.) and the mixture was stirred at  $-78\text{ }^{\circ}\text{C}$  for 45 min, then warmed to  $-30\text{ }^{\circ}\text{C}$  and stirred for 1 h.

A saturated aqueous solution of  $\text{NaHCO}_3$  was added and the cold solution was warmed to room temperature. The phases were separated, and the aqueous phase was extracted twice with diethyl ether. The organic layers were washed with brine, dried over  $\text{Na}_2\text{SO}_4$  and concentrated under reduced pressure. Crude product was a yellow oil, 39 mg.

Purification by flash column chromatography on silica gel (EtOAc/Hexanes, 0%, then 0.5%) allowed for isolation of enol triflate **33** as a colourless oil, (16.0 mg, 24.8  $\mu$ mol, 69% yield).

**$^1\text{H}$  NMR** (400 MHz,  $\text{CDCl}_3$ )  $\delta$  7.63 (ddd,  $J$  = 9.4, 7.8, 1.7 Hz, 4H), 7.40 (dd,  $J$  = 11.0, 7.0 Hz, 6H), 5.33 (d,  $J$  = 1.9 Hz, 1H), 5.27 (s, 1H), 4.99 (s, 1H), 3.66 (dd,  $J$  = 9.9, 4.6 Hz, 1H), 3.34 (d,  $J$  = 10.1 Hz, 1H), 3.19 (t,  $J$  = 9.9 Hz, 1H), 2.89 (q,  $J$  = 7.6 Hz, 1H), 2.55 (d,  $J$  = 10.1 Hz, 1H), 1.90 (dd,  $J$  = 10.1, 4.6 Hz, 1H), 1.67 (d,  $J$  = 1.7 Hz, 3H), 1.45 (s, 3H), 1.28 (s, 3H), 1.04 (s, 9H), 0.92 (d,  $J$  = 7.7 Hz, 3H), 0.91 (s, 3H)

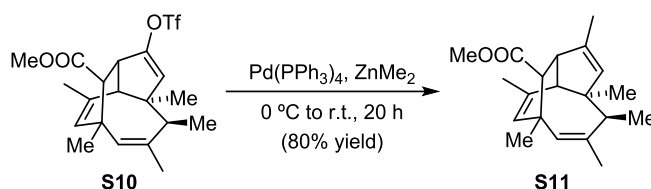
**$^{13}\text{C}$  NMR** (100 MHz,  $\text{CDCl}_3$ )  $\delta$  151.4, 136.8, 135.9, 135.6, 135.6, 133.9, 133.5, 129.6, 129.5, 127.9, 127.6, 116.6, 62.9, 56.6, 51.6, 49.0, 44.4, 39.6, 37.4, 34.7, 31.6, 26.8, 22.7, 19.1, 15.0, 14.1, 11.4

**IR** (ATR): 2956 (m), 2930 (m), 2856 (m), 2359 (w), 1565 (w), 1640 (s), 1423 (m), 1249 (w), 1432 (m), 1212 (s), 1143 (m), 1112 (m), 835 (m)

**HRMS** (+ESI): calc. for  $\text{C}_{35}\text{H}_{44}\text{F}_3\text{O}_4\text{SSi}$   $[\text{M}+\text{H}]^+$  645.2676, found 645.2670

$[\alpha]_D^{23}$  +8.6° (c 0.47,  $\text{CHCl}_3$ )

$R_F$  = 0.70 (5%  $\text{Et}_2\text{O}$  in hexanes)



#### Triene ester **S11**.

To a solution of triflate **S10** (4.0 mg, 8.3  $\mu$ mol, 1.0 equiv.) in THF (0.35 mL) at 0  $^\circ\text{C}$  was added  $\text{Pd(PPh}_3)_4$  (1.9 mg, 1.7  $\mu$ mol, 0.20 equiv.) and the mixture was stirred for 30 min at the same temperature. Then, a solution of dimethylzinc (1.2 M in toluene, 17.3  $\mu$ L, 20.7  $\mu$ mol, 2.50 equiv.) was added at 0  $^\circ\text{C}$ , and the reaction was stirred at room temperature for 20 h.

The reaction mixture was quenched with water (0.8 mL) and extracted four times with diethyl ether. The combined extracts were dried over  $\text{MgSO}_4$  yielding a brown residue, 5 mg, which was purified by flash column chromatography on silica gel ( $\text{Et}_2\text{O}$ /Hexanes, 0%, then 0.5%, then 1% then 2%) affording triene **S11** as a slightly yellow solid (2.0 mg, 6.7  $\mu$ mol, 80% yield).

**$^1\text{H}$  NMR** (400 MHz,  $\text{CDCl}_3$ )  $\delta$  5.35 (s, 1H), 5.04 (s, 1H), 4.91 (s, 1H), 3.59 (s, 3H), 2.86 (q,  $J$  = 7.4 Hz, 1H), 2.80 (d,  $J$  = 9.6 Hz, 1H), 2.69 (d,  $J$  = 9.6 Hz, 1H), 2.44 (s, 1H), 1.82 (d,  $J$  = 1.5 Hz, 3H), 1.70 (s, 3H), 1.42 (s, 3H), 1.22 (s, 3H), 1.08 (s, 3H), 0.91 (d,  $J$  = 7.5 Hz, 3H)

**$^{13}\text{C}$  NMR** (100 MHz,  $\text{CDCl}_3$ )  $\delta$  175.3, 141.0, 139.4, 139.0, 131.6, 129.0, 124.6, 60.8, 55.7, 53.2, 52.1, 51.0, 40.4, 37.3, 29.7, 29.1, 27.8, 24.9, 24.2, 15.3, 14.6

**IR** (ATR): 2961 (m), 2926 (s), 2854 (m), 2361 (s), 2340 (m), 1738 (s), 1434 (m), 1375 (w), 1170 (m), 1147 (s), 1015 (w), 841 (m)

**HRMS** (+APCI): calc. for  $\text{C}_{20}\text{H}_{29}\text{O}_2$   $[\text{M}+\text{H}]^+$  301.2162, found 301.2168

$[\alpha]_D^{23}$  +40.4° (c 0.2,  $\text{CHCl}_3$ )

$R_F$  = 0.53 (10%  $\text{Et}_2\text{O}$  in hexanes)



**<sup>1</sup>H NMR** (400 MHz, CDCl<sub>3</sub>) δ 7.70–7.60 (m, 4H), 7.44–7.34 (m, 6H), 5.20 (s, 1H), 4.99 (s, 1H), 4.84 (s, 1H), 3.69 (dd, *J* = 9.7, 4.5 Hz, 1H), 3.21 (t, *J* = 9.8 Hz, 1H), 3.01 (d, *J* = 9.8 Hz, 1H), 2.77 (q, *J* = 7.6 Hz, 1H), 2.49 (d, *J* = 9.9 Hz, 1H), 1.74 (s, 3H), 1.71 (dd, *J* = 10.2, 4.4 Hz, 1H), 1.66 (s, 3H), 1.40 (s, 3H), 1.20 (s, 3H), 1.05 (s, 9H), 0.92–0.87 (m, 6H)

**IR (ATR):** 2958 (m), 2927 (m), 2855 (m), 1428 (w), 1105 (s), 1055 (m), 821 (m), 777 (s), 757 (m)

**HRMS** (+ESI): calc. for  $C_{35}H_{46}OSi$   $[M+H]^+$  511.3391, found 511.3395

**$R_F = 0.26$  (1% Et<sub>2</sub>O in hexanes)**



The reaction was quenched with a saturated aqueous solution of Rochelle's salt (0.5 mL), then warmed to room temperature and stirred for 30 min. The mixture was diluted with water/DCM and extracted three times with DCM. The combined organic layers were dried over Na<sub>2</sub>SO<sub>4</sub>, filtered and concentrated under reduced pressure. Purification by flash column chromatography on silica gel (5% EtOAc/Hexanes) afforded alcohol **23** (4.0 mg, 15 μmol, 88% yield) as a white solid.

**<sup>1</sup>H NMR** (400 MHz, CDCl<sub>3</sub>) δ 5.45 (s, 1H), 5.00 (s, 1H), 4.87 (s, 1H), 3.62–3.49 (m, 2H), 2.84–2.74 (m, 1H), 2.64 (d, *J* = 9.7 Hz, 1H), 1.75 (s, 3H), 1.70 (s, 3H), 1.44 (br s, 1H), 1.40 (s, 3H), 1.25 (br s, 1H), 1.21 (s, 3H), 1.12 (s, 3H), 0.90 (d, *J* = 7.5 Hz, 3H)

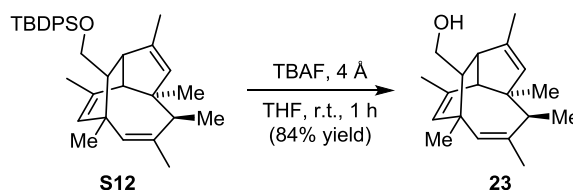
**$^{13}\text{C}$  NMR** (100 MHz,  $\text{CDCl}_3$ )  $\delta$  142.5, 140.1, 137.6, 132.8, 127.7, 127.5, 65.4, 60.0, 55.7, 51.4, 49.8, 39.7, 37.2, 28.5, 27.7, 24.9, 24.1, 15.3, 14.6

**IR** (ATR): 3286 (m, br), 2958 (s), 2919 (s), 2850 (m), 1728 (w, br), 1657 (w), 1455 (m), 1441 (m), 1033 (s), 1005 (s), 840 (s)

**HRMS** (+APCI): calc. for  $\text{C}_{19}\text{H}_{29}\text{O}$   $[\text{M}+\text{H}]^+$  273.2213, found 273.2219

$[\alpha]_D^{23} +8.5^\circ$  (c 0.30,  $\text{CHCl}_3$ )

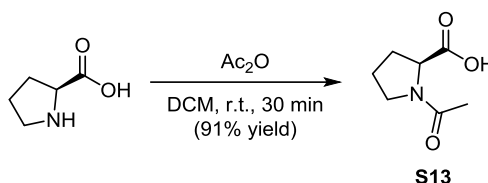
$R_f = 0.35$  (10%  $\text{Et}_2\text{O}$  in hexanes)



### Triene alcohol **23**.

To a solution of silyl ether **S12** (10.0 mg, 19.6  $\mu\text{mol}$ , 1.00 equiv.) in dry THF (0.76 mL) were added 4 Å molecular sieves followed by a solution of TBAF (1 M in THF, 35  $\mu\text{L}$ , 35  $\mu\text{mol}$  1.8 equiv.). The mixture was stirred at room temperature for 3 h, after which additional TBAF (1 M, 10  $\mu\text{L}$ , 10  $\mu\text{mol}$  0.50 equiv.) was added, and the reaction was further stirred for 1 h.

The mixture was filtered through a pad of silica, eluting with 25%  $\text{EtOAc}$  in hexanes. A colourless oil, 9 mg, was obtained and submitted to flash column chromatography on silica gel ( $\text{EtOAc/Hexanes}$ , 2%, then 3% then 3.75%) affording alcohol **23** as a colourless gum (4.5 mg, 16.5  $\mu\text{mol}$ , 85% yield).



**L-Proline was acylated following the procedure by Budiša et al.** <sup>[347]</sup>

### N-acetyl-L-proline (**13**).

L-Proline (500 mg, 4.34 mmol, 1.00 equiv.) was stirred in DCM (9.0 mL) and acetic anhydride (0.41 mL, 4.3 mmol, 1.0 equiv.) until a clear solution was obtained (30 min). DCM was removed under reduced pressure and the residue was dissolved in water (4.5 mL) and freeze-dried. The resulting solid contained approx. 1/10 of unreacted proline, therefore it was dissolved in water (5.6 mL) and filtered through a short ion-exchange column (Dowex® 50WX8, 50-100 mesh). Acidic fractions were collected and freeze-dried to give N-acetyl-L-proline (**S13**) as a white solid (620 mg, 3.95 mmol, 91% yield).

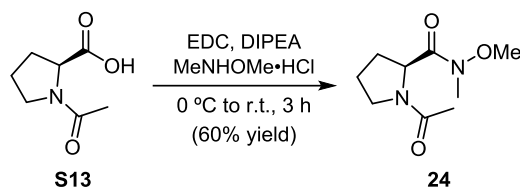
**$^1\text{H}$  NMR** (400 MHz,  $\text{CDCl}_3$ )  $\delta$  4.60 (dd,  $J = 8.0, 2.5$  Hz, 1H), 3.59 (ddd,  $J = 10.6, 7.4, 3.4$  Hz, 1H), 3.52–3.43 (m, 1H), 2.56–2.48 (m, 1H), 2.17 (s, 3H), 2.13–1.90 (m, 3H)

**$^{13}\text{C}$  NMR** (100 MHz,  $\text{CDCl}_3$ )  $\delta$  173.4, 171.2, 60.2, 48.8, 27.1, 24.8, 22.1

**HRMS** (+ESI): calc. for  $\text{C}_7\text{H}_{12}\text{NO}_3$   $[\text{M}+\text{H}]^+$  158.0812, found 158.0815

$[\alpha]_D^{27} -177.0^\circ$  (c 0.51,  $\text{CHCl}_3$ )





**Weinreb amide 24** was synthesized following the procedure by Stallforth et al.<sup>[98]</sup>

#### Weinreb amide 24.

*N*-acetyl proline (**S13**) (1.11 g, 7.09 mmol, 1.00 equiv.) was dissolved in DCM (20.6 mL) and cooled down to 0 °C. To the solution was added EDC (1.60 g, 8.36 mmol, 1.18 equiv.) followed by DIPEA (2.40 mL, 13.9 mmol, 1.96 equiv.). The mixture was stirred for 15 min at 0 °C and then *N*,*O*-dimethylhydroxylamine hydrochloride (691 mg, 7.09 mmol, 1.00 equiv.) was added. The resulting mixture was further stirred for 1 h at 0 °C and another 2 h at room temperature.

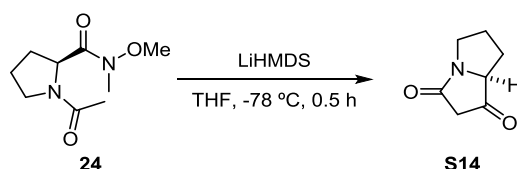
Water was added, the aqueous phase was extracted with DCM and the combined organic layers were dried over sodium  $\text{Na}_2\text{SO}_3$ . The solvent was evaporated, and the crude product purified by flash column chromatography on silica gel (5% MeOH/DCM) affording amide **24** as a slightly yellow oil (857 mg, 4.28 mmol, 60% yield).

**$^1\text{H}$  NMR** (400 MHz,  $\text{CDCl}_3$ )  $\delta$  4.96–4.86 (m, 1H), 3.83 (s, 3H), 3.70 (ddd,  $J$  = 9.9, 7.4, 4.9 Hz, 1H), 3.52 (dt,  $J$  = 9.7, 7.0 Hz, 1H), 3.20 (s, 3H), 2.21–2.11 (m, 2H), 2.09 (s, 3H), 2.02–1.86 (m, 2H)

**$^{13}\text{C}$  NMR** (100 MHz,  $\text{CDCl}_3$ )  $\delta$  172.5, 169.3, 61.2, 58.3, 56.1, 48.0, 29.1, 24.7, 22.3

**HRMS** (+ESI): calc. for  $\text{C}_9\text{H}_{17}\text{N}_2\text{O}_3$   $[\text{M}+\text{H}]^+$  201.1234, found 201.1237

$[\alpha]_D^{27}$   $-22.0^\circ$  ( $c$  0.43,  $\text{CHCl}_3$ )



**S14** was synthesized following the procedure by Stallforth et al.<sup>[98]</sup>

#### Pyrrolizidine dione S14.

A solution of LiHMDS (1 M in THF, 3.60 mmol, 3.60 mL, 2.00 equiv.) diluted in dry THF (17.7 mL) at  $-78\text{ }^{\circ}\text{C}$  was added over 0.5 h to a solution of **S14** (360 mg, 1.80 mmol) in THF (21 mL).

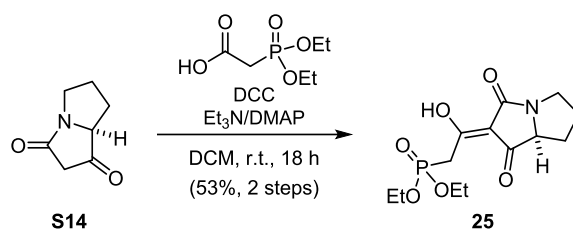
After 2 h the reaction was allowed to warm to  $-30\text{ }^{\circ}\text{C}$  and acidified with 1M HCl. The aqueous phase was extracted with DCM, dried over  $\text{Na}_2\text{SO}_4$  and concentrated under reduced pressure. A slightly yellow gum 230 mg containing **S14** was obtained.

Due to thermal instability it was directly used for the next step.

**$^1\text{H}$  NMR** (400 MHz,  $\text{CDCl}_3$ )  $\delta$  4.31–4.23 (m, 1H), 3.88 (dt,  $J$  = 11.6, 7.9 Hz, 1H), 3.45 (dd,  $J$  = 21.6, 2.0 Hz, 1H), 3.31–3.22 (m, 1H), 3.10 (dd,  $J$  = 21.6, 1.5 Hz, 1H), 2.20–2.05 (m, 3H), 1.72–1.62 (m, 1H)

**IR** (ATR): 2890 (w), 2579 (br), 1765 (m), 1688 (s), 1586 (s), 1369 (s), 1308 (s), 1258 (m), 1222 (m), 1074 (w), 809 (m), 750 (s)

$[\alpha]_D^{24}$   $-61.3^\circ$  ( $c$  0.1,  $\text{CHCl}_3$ )



The synthesis of phosphonate ester **25** was accomplished by a modification of the procedure by Yoshii et al.<sup>[348]</sup>

#### Phosphonate ester **25**.

To a solution of pyrrolizidinedione **S14** (230 mg, 1.65 mmol, 1.00 equiv.), DMAP (263 mg, 2.15 mmol, 1.30 equiv.) and DCC (375 mg, 1.82 equiv.) in DCM (11.3 mL) at room temperature was added dropwise diethyl phosphonacetic acid (292  $\mu$ L, 1.82 mmol, 1.10 equiv). The reaction mixture was stirred at room temperature for 18 h.

The suspension was filtered, and the solvents evaporated to yield a brown gum which was purified by flash column chromatography on silica gel (MeOH/DCM, gradient, 0 to 6%). The obtained fractions were washed with a saturated aqueous solution of  $\text{NH}_4\text{Cl}$  followed by a 1M aqueous solution of HCl. Phosphonate ester **25** was obtained as an orange gum (300 mg, 0.946 mmol, 53% yield from **24**), which turned solid upon standing for 2 days.

$^1\text{H}$  NMR spectrum showed broaden peaks, most likely caused by an increased isomer exchange rate in the presence of residual water. By using chloroform stored over 4Å mol. sieves, both isomers could be distinguished.

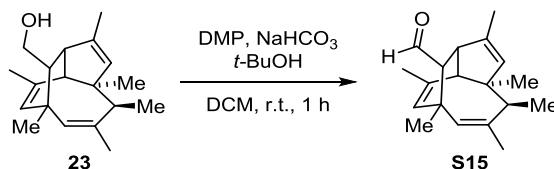
$^1\text{H}$  NMR (400 MHz,  $\text{CDCl}_3$ , \* denotes minor isomer)  $\delta$  4.17 (app quintet,  $J = 7.2$  Hz, 4H+4H\*), 3.99 (dd,  $J = 10.4$  Hz, 6.7 1H), 3.89 (dd,  $J = 23.0$  Hz, 13.6, 1H\*), 3.78–3.67 (m, 1H+1H\*), 3.61 (d,  $J = 23.4$  Hz, 1H\*), 3.57 (d,  $J = 23.8$  Hz, 1H), 3.51 (d,  $J = 23.4$ , 1H), 3.48 (d,  $J = 23.1$ , 1H\*), 3.29 (ddd,  $J = 11.9, 9.0, 3.8$  Hz, 1H), 3.21 (ddd,  $J = 8.4, 4.4, 3.7$  Hz, 1H\*), 2.25–2.02 (m, 3H+3H\*), 1.60–1.47 (m, 1H+1H\*), 1.32 (t,  $J = 7.1$  Hz, 6H+6H\*)

$^{13}\text{C}$  NMR (100 MHz,  $\text{CDCl}_3$ )  $\delta$  194.2, 177.7 (d,  $J = 9.4$  Hz), 176.0, 104.1 (d,  $J = 6.6$  Hz), 69.0, 62.8 (d,  $J = 6.2$  Hz), 62.8 (d,  $J = 6.1$  Hz), 42.8, 31.6 (d,  $J = 130.3$  Hz), 26.6 (d,  $J = 20.7$  Hz), 16.2 (d,  $J = 6.4$  Hz)

IR (ATR): 3399 (w, br), 2977 (w), 2926 (w), 1672 (m), 1609 (s), 1544 (m), 1441 (s), 1231 (s), 1033 (s), 968 (s), 753 (m)

HRMS (+APCI): calc. for  $\text{C}_{13}\text{H}_{21}\text{NO}_6\text{P}$   $[\text{M}+\text{H}]^+$  318.1101, found 318.1099

$[\alpha]_D^{23}$   $-19.5^\circ$  (c 0.53,  $\text{CHCl}_3$ )



#### Tricyclic aldehyde **S15**.

To alcohol **23** (4.0 mg, 15  $\mu$ mol, 1.0 equiv.) dissolved in DCM (1.6 mL) were added  $\text{NaHCO}_3$  (6.2 mg, 73  $\mu$ mol, 5.0 equiv.), 1 small drop of *t*-BuOH and Dess–Martin periodinane (15.6 mg, 37.0  $\mu$ mol, 2.50 equiv.). The mixture was stirred for 60 min at room temperature.

A 1:1 mixture of saturated aqueous  $\text{Na}_2\text{S}_2\text{O}_3/\text{NaHCO}_3$  (0.5 mL each) was added. The resulting mixture was stirred for 20 min at room temperature, the layers were separated and the aqueous phase was extracted three times with DCM. 3.2 mg of a colourless oil containing aldehyde **S15** were obtained. Given its instability it was immediately used for the next step.

**$^1\text{H}$  NMR** (400 MHz,  $\text{CDCl}_3$ )  $\delta$  9.49 (d,  $J$  = 4.5 Hz, 1H), 5.49 (s, 1H), 5.07 (s, 1H), 4.88 (s, 1H), 2.89–2.81 (m, 2H), 2.69 (d,  $J$  = 9.6 Hz, 1H), 2.22–2.17 (m, 1H), 1.80 (d,  $J$  = 1.5 Hz, 3H), 1.68 (s, 3H), 1.44 (d,  $J$  = 0.7 Hz, 3H), 1.23 (s, 3H), 1.18 (s, 3H), 0.92 (d,  $J$  = 7.5 Hz, 3H)

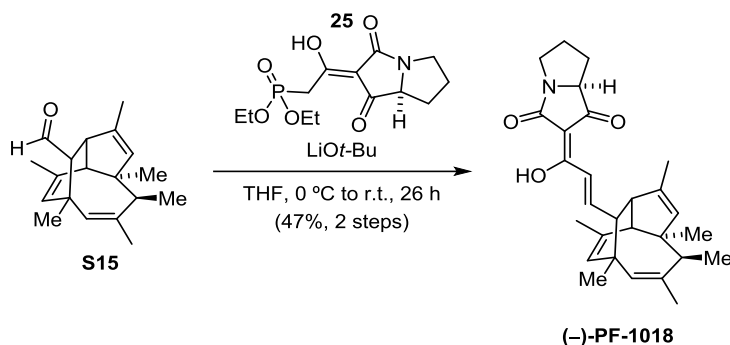
**$^{13}\text{C}$  NMR** (100 MHz,  $\text{CDCl}_3$ )  $\delta$  205.4, 140.2, 140.1, 139.7, 131.0, 129.1, 126.4, 61.0, 60.8, 55.5, 49.2, 39.6, 37.1, 28.4, 27.7, 24.8, 24.2, 15.3, 14.4

**IR** (ATR): 2957 (m), 2922 (s), 2851 (m), 2366 (w), 1719 (m), 1457 (w), 1019 (w)

**HRMS** (+APCI): calc. for  $\text{C}_{19}\text{H}_{27}\text{O}$   $[\text{M}+\text{H}]^+$  271.2056, found 271.2058

$[\alpha]_D^{23}$  +10.6° (c 0.26,  $\text{CHCl}_3$ )

$R_F$  = 0.68 (10%  $\text{Et}_2\text{O}$  in hexanes)



#### (–)-PF-1018.

To phosphonate **25** (9.4 mg, 30  $\mu$ mol, 2.5 equiv.) dissolved in THF (0.50 mL) at 0 °C was added  $\text{LiOt-Bu}$  (4.7 mg, 59  $\mu$ mol, 5.0 equiv.). The reaction was stirred at 0 °C for 30 min after which a solution of aldehyde **S15** (3.2 mg, 12  $\mu$ mol, 1.0 equiv.) in THF (0.16 mL) was added dropwise. The reaction mixture was allowed to warm to room temperature and stirred for 26 h.

To the resulting suspension was added an aqueous saturated solution of  $\text{NH}_4\text{Cl}$  followed by DCM. The phases were separated, and the aqueous layer was extracted five times with DCM. The organic layers were combined, dried over  $\text{Na}_2\text{SO}_4$ , filtered and concentrated under reduced pressure. The resulting yellow gum, 5.2 mg, was submitted to flash column chromatography on spherical 20–40  $\mu\text{m}$  particle size, 60Å pore size silica (MeOH/DCM, 0.1%, then 0.2% then 0.5%). (–)-PF-1018 was obtained as a slightly yellow solid, (2.4 mg, 5.5  $\mu$ mol, 47% yield from alcohol **23**).  $^1\text{H}$  NMR shows two isomers in ratio 4:1.

**$^1\text{H}$  NMR** (400 MHz,  $\text{CDCl}_3$ , \* denotes minor isomer)  $\delta$  13.72 (br, 1H+1H\*), 7.12 (d,  $J$  = 15.7 Hz, 1H\*), 7.04 (dd,  $J$  = 15.6, 10.1 Hz, 1H\*), 7.01–6.98 (m, 2H), 5.37 (s, 1H+1H\*), 5.03 (s, 1H+1H\*), 4.91 (s, 1H+1H\*), 4.05 (dd,  $J$  = 9.9, 6.9 Hz, 1H\*), 3.96 (dd,  $J$  = 10.0, 6.9 Hz, 1H), 3.78 (ddd,  $J$  = 11.6, 7.9, 7.9, 1H\*), 3.76 (ddd,  $J$  = 11.4, 7.9, 7.9, 1H), 3.27 (ddd,  $J$  = 11.2, 9.2, 3.8 Hz, 1H), 3.24–3.18 (m, 1H\*), 2.83 (q,  $J$  = 7.3 Hz, 1H+1H\*), 2.63 (d,  $J$  = 9.7 Hz, 1H+1H\*), 2.51 (d,  $J$  = 9.6 Hz, 1H+1H\*), 2.43 (d,  $J$  = 10.0 Hz, 1H\*), 2.43–2.38 (m, 1H), 2.00–2.23 (m, 3H +

$^1\text{H}$  NMR (400 MHz,  $\text{CDCl}_3$ , \* denotes minor isomer)  $\delta$  1.82 (br, s, 3H+3H\*), 1.73 (br, s, 3H+3H\*), 1.48-1.67 (m, 1H + 1H\*), 1.43 (br, s, 3H+3H\*), 1.22 (br, s, 3H+3H\*), 0.95 (br, s, 3H+3H\*), 0.92 (d,  $J = 7.5$  Hz, 3H+3H\*)

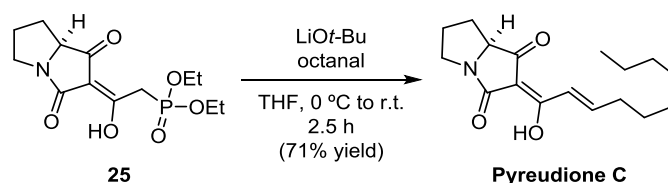
$^{13}\text{C}$  NMR (100 MHz,  $\text{CDCl}_3$ , \* denotes minor isomer)  $\delta$  203.8, 195.0, 177.6, 175.7\*, 174.3, 155.7\*, 154.7, 140.7, 140.7\*, 139.5\*, 139.4, 139.0, 139.0\*, 132.1, 132.0\*, 128.6, 126.4, 120.1, 119.6\*, 103.7\*, 101.3, 68.7, 66.4\*, 60.8\*, 60.8, 55.3, 55.3\*, 54.3, 54.2\*, 53.5\*, 53.3, 43.3\*, 43.1, 41.1, 37.4, 29.8 (q), 29.7\* (q), 27.7, 27.1\*, 27.0\*, 26.9, 24.8, 24.7\*, 24.2, 15.3, 14.6, 14.6\*

IR (ATR): 2959 (m), 2922 (s), 2852 (m), 1706 (m), 1640 (s), 1578 (s), 1432 (m)

HRMS (+APCI): calc. for  $\text{C}_{28}\text{H}_{36}\text{NO}_3$   $[\text{M}+\text{H}]^+$  434.2690, found 434.2686

$[\alpha]_D^{23} -76.6^\circ$  (c 0.04,  $\text{CHCl}_3$ )

$R_f = 0.30$  (4% MeOH in DCM)



### Pyreudione C.

To a solution of phosphonate **25** (12.4 mg, 39.0  $\mu\text{mol}$ , 1.50 equiv.) in THF (0.9 mL) at 0 °C was added LiOt-Bu (6.2 mg, 78  $\mu\text{mol}$ , 3.0 equiv.). The orange suspension was stirred at 0 °C for 30 min after which octanal (4.0  $\mu\text{L}$ , 26  $\mu\text{mol}$ , 1.0 equiv.) in THF (0.18 mL) was added dropwise. The reaction was stirred at room temperature for 2.5 h.

A saturated aqueous solution of  $\text{NH}_4\text{Cl}$  (0.5 mL) was added and all solvents were evaporated under reduced pressure. To the remaining residue was added acetone (1.0 mL) and the resulting suspension was stirred for 20 min at room temperature. The mixture was filtered through a pad of celite and the filtrate was concentrated under reduced pressure and submitted to HPLC purification ( $\text{H}_2\text{O}/\text{ACN}$ , gradient, 66 to 100%) yielding **pyreudione C** (5.4 mg, 18  $\mu\text{mol}$ , 71% yield) as yellow oil,  $^1\text{H}$  NMR shows two isomers in ratio 1:0.22.

$^1\text{H}$  NMR (400 MHz,  $\text{CDCl}_3$ , \* denotes minor isomer)  $\delta$  7.25–7.07 (m, 2H+2H\*), 4.06 (dd,  $J = 9.9, 6.8$  Hz, 1H\*), 3.96 (dd,  $J = 10.1, 6.8$  Hz, 1H), 3.75 (dt,  $J = 11.3, 8.2$  Hz, 1H+1H\*), 3.27 (ddd,  $J = 11.9, 8.8, 4.0$  Hz, 1H), 3.22 (ddd, 11.7, 8.6, 4.0 Hz, 1H\*), 2.32 (app. q,  $J = 7.1$  Hz, 2H+2H\*), 2.24–2.00 (m, 3H+3H\*), 1.60–1.44 (m, 3H+3H\*), 1.37–1.19 (m, 8H+8H\*), 0.88 (t,  $J = 6.7$  Hz, 3H+3H\*)

$^{13}\text{C}$  NMR (100 MHz,  $\text{CDCl}_3$ , \* denotes minor isomer)  $\delta$  203.9\*, 195.1, 177.5, 175.6\*, 174.3, 170.7\*, 152.1\*, 151.2, 121.3, 120.8\*, 103.6\*, 101.2, 68.7, 66.4\*, 43.4\*, 43.1, 33.5\*, 33.3, 31.7, 29.7\*, 29.2, 29.0, 28.2, 28.1\*, 27.1\*, 27.0\*, 26.9, 26.8, 22.6, 14.1

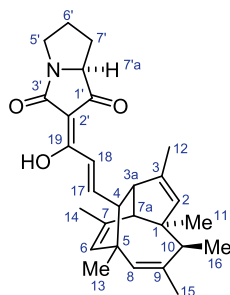
IR (ATR): 2925 (m), 2854 (w), 1704 (m), 1641 (s), 1575 (s), 1425 (m), 1532 (m), 1352 (m), 1242 (m), 1036 (w), 982 (w), 944 (w), 881 (w), 771 (w)

HRMS (+ESI): calc. for  $\text{C}_{17}\text{H}_{26}\text{NO}_3$   $[\text{M}+\text{H}]^+$  292.1907, found 292.1910

$[\alpha]_D^{27} -24.2^\circ$  (c 0.33,  $\text{CHCl}_3$ );  $[\alpha]_D^{24} -29.6^\circ$  (c 0.42, MeOH)

$R_f = 0.21$  (1% MeOH in DCM)

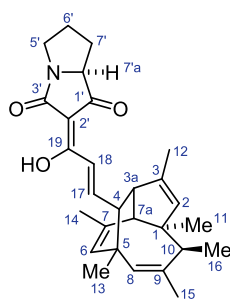
## 8.4.2 Comparison of Natural and Synthetic (–)-PF-1018 and Pyreudione C



(–)-PF-1018

Proton	Major Isomer		Minor Isomer	
	Natural	Synthetic	Natural	Synthetic
2	5.03 (br, s)	5.03 (br, s)	5.03 (br, s)	5.03 (br, s)
3a	2.50 (br, d, 9.7)	2.51 (br, d, 9.6)	2.50 (br, d, 9.7)	2.51 (br, d, 9.6)
4	2.41 (m)	2.38–2.43 (m)	2.43 (br, d, 10.1)	2.43 (br, d, 10.1)
6	5.37 (br, s)	5.37 (br, s)	5.37 (br, s)	5.37 (br, s)
7a	2.62 (d, 9.7)	2.63 (d, 9.7)	2.62 (d, 9.7)	2.63 (d, 9.7)
8	4.91 (br, s)	4.91 (br, s)	4.91 (br, s)	4.91 (br, s)
10	2.83 (br, q, 7.5)	2.83 (br, q, 7.3)	2.83 (br, q, 7.5)	2.83 (br, q, 7.3)
11	1.22 (br, s)	1.22 (br, s)	1.22 (br, s)	1.22 (br, s)
12	1.73 (br, s)	1.73 (br, s)	1.72 (br, s)	1.73 (br, s)
13	0.95 (br, s)	0.95 (br, s)	0.95 (br, s)	0.95 (br, s)
14	1.82 (br, d, 1.5)	1.82 (br, s)	1.83 (br, d, 1.5)	1.82 (br, s)
15	1.43 (br, d, 0.8)	1.44 (br, s)	1.43 (br, d, 0.8)	1.44 (br, s)
16	0.92 (d, 7.5)	0.92 (d, 7.5)	0.92 (d, 7.4)	0.92 (d, 7.5)
17	7.01 (m)	7.01–6.98 (m)	7.04 (dd, 15.6, 10.1)	7.04 (dd, 15.6, 10.1)
18	7.00 (m)	7.01–6.98 (m)	7.12 (d, 15.6)	7.12 (d, 15.7)
19-OH	12.35 (br)	13.72 (br)	12.35 (br)	13.72 (br)
5'	3.27(ddd, 11.5, 8.7, 3.8) 3.75 (ddd, 11.5, 7.8, 7.8)	3.27 (ddd, 11.2, 9.2, 3.8) 3.76 (ddd, 11.4, 7.9, 7.9)	3.22 (ddd, 11.5, 8.5, 4.1) 3.79 (ddd, 11.5, 8.0, 8.0)	3.24–3.18 (m) 3.78 (ddd, 11.6, 7.9, 7.9)
6'	2.04–2.22 (m)	2.00–2.23 (m)	2.04–2.22 (m)	2.00–2.23 (m)
7'	1.55 (dddd, 12.1, 10.3, 10.3, 8.2)	1.48–1.67 (m)	1.55 (dddd, 12.1, 10.3, 10.0, 8.2)	1.48–1.67 (m)
7'a	3.96 (dd, 10.3, 6.9)	3.96 (dd, 10.0, 6.9)	4.06 (dd, 10.0, 6.9)	4.05 (dd, 9.9, 6.9)

NMR signals from natural PF-1018.<sup>[93]</sup>

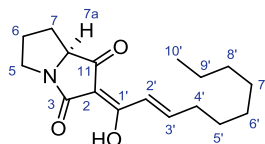


(-)-PF-1018

Carbon	Major Isomer		Minor Isomer	
	Natural	Synthetic	Natural	Synthetic
1	60.8	60.8	60.8	60.8
2	128.6	128.6	128.6	128.6
3	140.7	140.7	140.6	140.7
3a	54.4	54.3	54.3	54.2
4	53.3	53.3	53.5	53.5
5	41.1	41.1	41.1	41.1
6	126.4	126.4	126.4	126.4
7	138.9	139.0	138.9	138.9
7a	55.3	55.3	55.3	55.3
8	132.1	132.1	132.0	132.0
9	139.4	139.4	139.4	139.5
10	37.4	37.4	37.4	37.4
11	27.6	27.7	27.6	27.7
12	14.6	14.6	14.6	14.6
13	29.8	29.8	29.7	29.7
14	24.1	24.2	24.1	24.2
15	24.8	24.8	24.8	24.7
16	15.3	15.3	15.3	15.3
17	154.7	154.7	155.6	155.7
18	120.1	120.1	119.6	119.6
19	174.3	174.3	175.7	175.7
2'	101.3	101.3	103.7	103.7
3'	177.6	177.6	170.8	<sup>b</sup>
5'	43.1	43.1	43.3	43.3
6'	26.8 <sup>a</sup>	26.9	27.1 <sup>a</sup>	27.1
7'	26.8 <sup>a</sup>	26.9	27.0 <sup>a</sup>	27.0
7'a	68.7	68.7	66.4	66.4
1'	195.0	195.0	203.7	203.8

<sup>a</sup> Interchangeable according to the isolation paper <sup>b</sup> Indistinguishable from noise

NMR signals from natural PF-1018.<sup>[93]</sup>



Pyreudione C

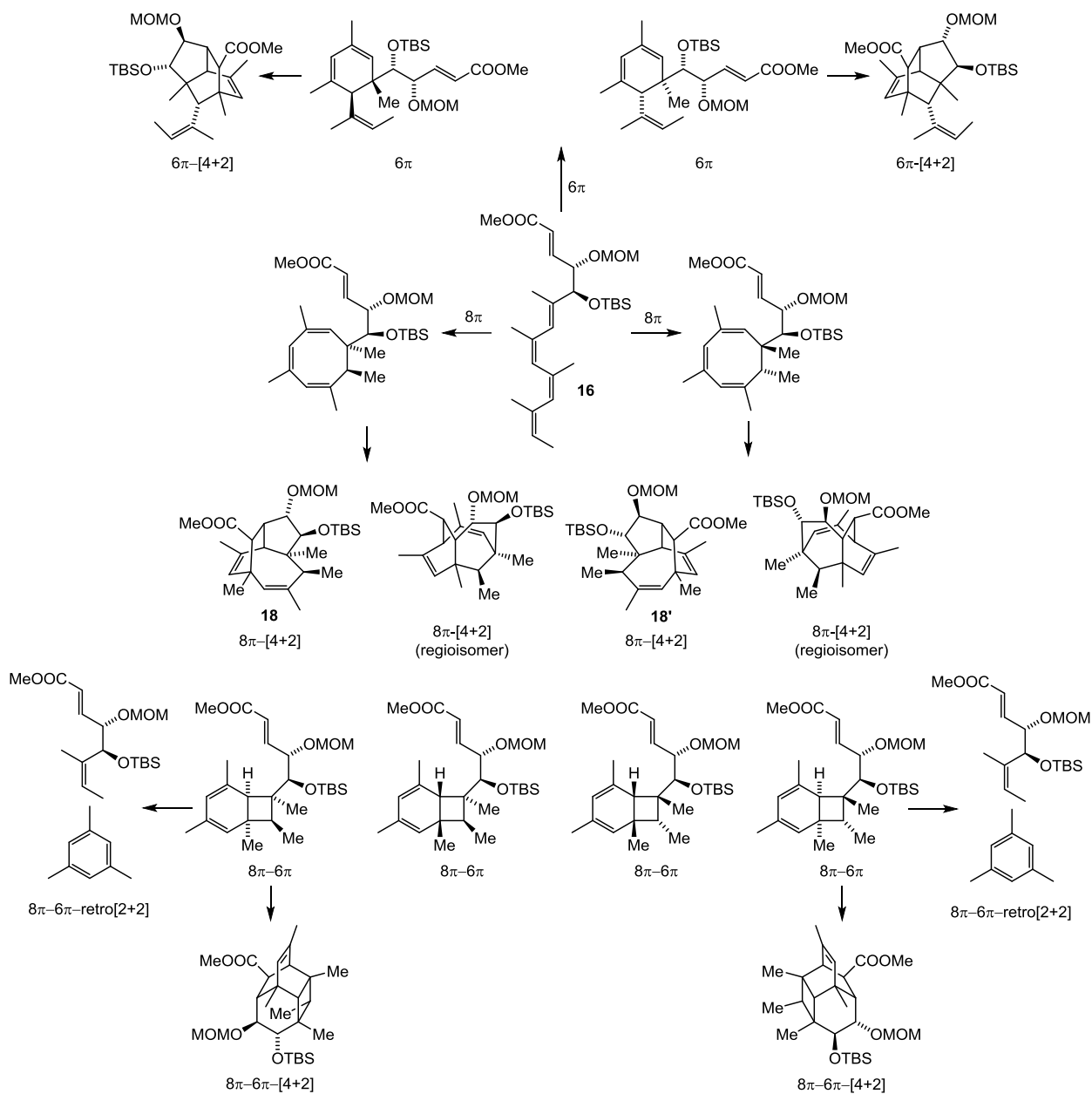
Proton	Major Isomer		Minor Isomer	
	Natural	Synthetic	Natural	Synthetic
5	3.25 (ddd, 11.5, 8.9, 4.0) 3.73 (dt, 11.5, 7.9)	3.27 (ddd, 11.9, 8.8, 4.0) 3.75 (dt, 11.3, 8.2)	3.20 (ddd, 11.6, 8.8, 4.2) 3.76 (dt, 11.4, 7.9)	3.22 (ddd, 11.7, 8.6, 4.0) 3.75 (dt, 11.3, 8.2)
6	2.05 (m), 2.14 (m)	2.24–2.00 (m) 1.60–1.44 (m)	2.05 (m), 2.14 (m)	2.24–2.00 (m) 1.60–1.44 (m)
7	1.52 (m), 2.14 (m)		1.52 (m), 2.14 (m)	
7a	3.94 (dd, 10.0, 6.9)	3.96 (dd, 10.1, 6.8)	4.04 (dd, 9.9, 7.0)	4.06 (dd, 9.9, 6.8)
2'	7.08 (dt, 15.7, 1.3)	7.25–7.07 (m)	7.19	7.25–7.07 (m)
3'	7.18 (dt, 15.8, 7.0)		7.20	
4'	2.30 (m)	2.32 (app q, 7.1)	2.30 (m)	2.32 (app q, 7.1)
5'	1.48 (m)	1.60–1.44 (m)	1.48 (m)	1.60–1.44 (m)
6'	1.30 (m)	1.37–1.19 (m)	1.30 (m)	1.37–1.19 (m)
7'	1.27 (m)		1.27 (m)	
8'	1.27 (m)		1.27 (m)	
9'	1.27 (m)		1.27 (m)	
10'	0.86 (t, 7.1)	0.88 (t, 6.7)	0.86 (t, 7.1)	0.88 (t, 6.7)

\*The 0.02 ppm deviation is owed to the different reference taken (Stallforth  $\delta$   $\text{CHCl}_3$  = 7.24, Trauner  $\delta$   $\text{CHCl}_3$  = 7.26)

Carbon	Major Isomer		Minor Isomer	
	Natural	Synthetic	Natural	Synthetic
1	195.1	195.1	203.8	203.9
2	101.2	101.2	101.2	103.6
3	177.5	177.5	170.7	170.7
5	43.1	43.1	43.4	43.4
6	26.9	26.9	27.1	27.1
7	26.8	26.8	27.0	27.0
7a	68.7	68.7	66.4	66.4
1'	174.3	174.3	175.6	175.6
2'	121.3	121.3	120.8	120.8
3'	151.1	151.2	152.1	152.1
4'	33.3	33.3	33.4	33.5
5'	28.2	28.2	28.1	28.1
6'	29.2	29.2	29.7	29.7
7'	29.0	29.0	29.0	29.0
8'	31.7	31.7	31.7	31.7
9'	22.6	22.6	22.6	22.6
10'	14.0	14.1	14.0	14.1

NMR signals from natural pyreudione C.<sup>[98]</sup>

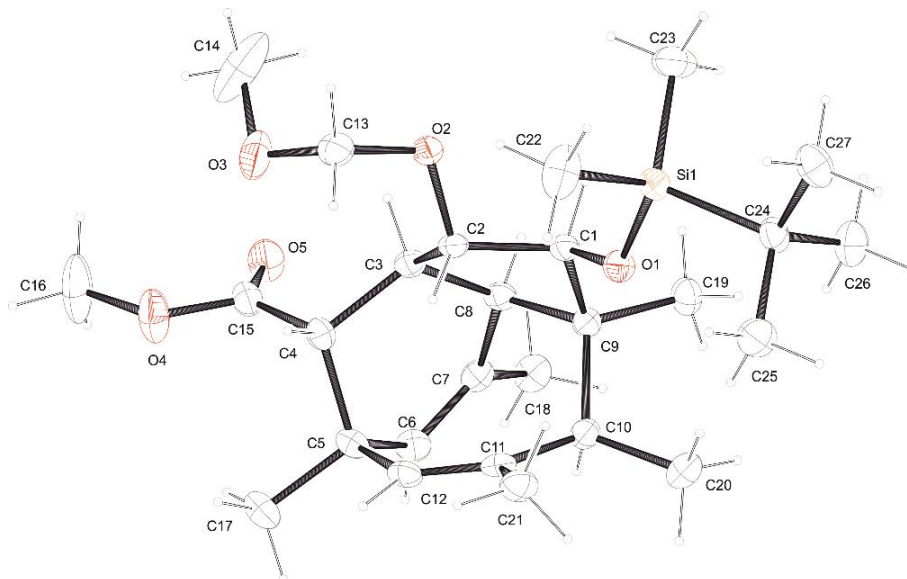
## 8.4.3 Potential Products from Cascade Reaction 16 to 18

Figure S1. Potential products that could arise from cascade reaction 16  $\rightarrow$  18.



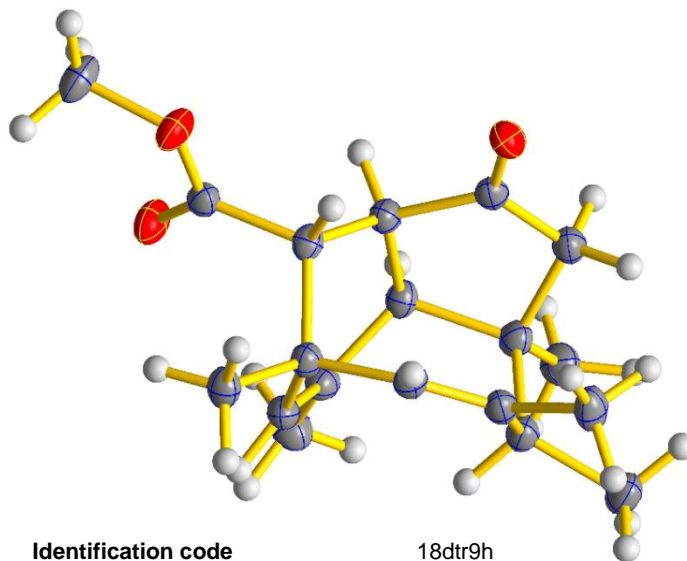
## 8.4.4 Crystallographic Data

### 8.4.4.1 Cascade Product 18



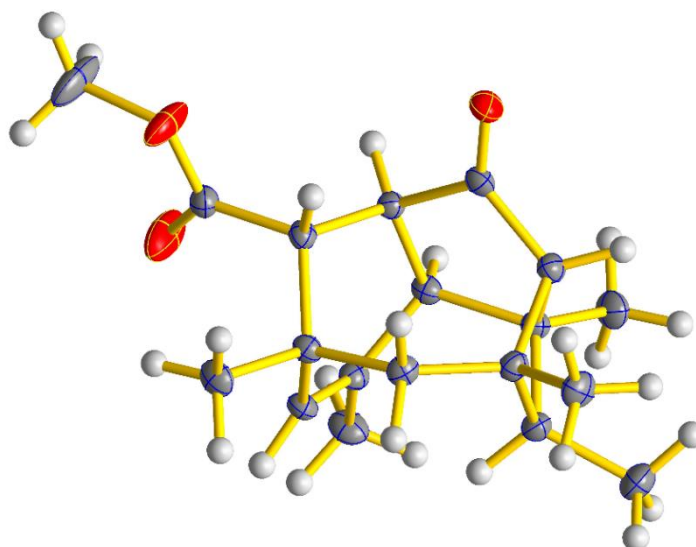
<b>net formula</b>	$C_{27}H_{46}O_5Si$
<b><i>M</i>/g mol<sup>-1</sup></b>	478.73
<b>crystal size/mm</b>	0.090 × 0.060 × 0.050
<b><i>T</i>/K</b>	100.(2)
<b>radiation</b>	MoKα
<b>diffractometer</b>	'Bruker D8 Venture TXS'
<b>crystal system</b>	monoclinic
<b>space group</b>	'P 1 21 1'
<b><i>a</i>/Å</b>	9.6241(3)
<b><i>b</i>/Å</b>	12.7646(4)
<b><i>c</i>/Å</b>	11.3130(4)
<b><i>α</i>/°</b>	90
<b><i>β</i>/°</b>	95.6180(10)
<b><i>γ</i>/°</b>	90
<b><i>V</i>/Å<sup>3</sup></b>	1383.10(8)
<b><i>Z</i></b>	2
<b>calc. density/g cm<sup>-3</sup></b>	1.150
<b><i>μ</i>/mm<sup>-1</sup></b>	0.117
<b>absorption correction</b>	Multi-Scan
<b>transmission factor range</b>	0.8915–0.9705
<b>refls. measured</b>	10273
<b><i>R</i><sub>int</sub></b>	0.0272
<b>mean <i>σ</i>(<i>I</i>)/<i>I</i></b>	0.0561
<b><i>θ</i> range</b>	3.192–27.472
<b>observed refls.</b>	5200
<b><i>x</i>, <i>y</i> (weighting scheme)</b>	0.0253, 0.4855
<b>hydrogen refinement</b>	constr
<b>Flack parameter</b>	0.12(7)
<b>refls in refinement</b>	6052
<b>parameters</b>	310
<b>restraints</b>	1
<b><i>R</i>(<i>F</i><sub>obs</sub>)</b>	0.0443
<b><i>R</i><sub>w</sub>(<i>F</i><sup>2</sup>)</b>	0.0916
<b><i>S</i></b>	1.055
<b>shift/error<sub>max</sub></b>	0.001
<b>max electron density/e Å<sup>-3</sup></b>	0.296
<b>min electron density/e Å<sup>-3</sup></b>	−0.280

## 8.4.4.2 Tricycle 22



Identification code	18dtr9h
Chemical formula	C <sub>19</sub> H <sub>26</sub> O <sub>3</sub>
Formula weight	302.40 g/mol
Temperature	100(2) K
Wavelength	0.71073 Å
Crystal size	0.160 x 0.190 x 0.530 mm
Crystal habit	colorless rod
Crystal system	monoclinic
Space group	P 1 21 1
Unit cell dimensions	a = 8.7775(10) Å b = 7.8110(9) Å c = 12.1927(14) Å α = 90° β = 99.3488(15)° γ = 90°
Volume	824.84(16) Å <sup>3</sup>
Z	2
Density (calculated)	1.218 g/cm <sup>3</sup>
Absorption coefficient	0.081 mm <sup>-1</sup>
F(000)	328
Diffractometer	Bruker APEX-II CCD
Radiation source	sealed tube, Mo
Theta range for data collection	1.69 to 28.28°
Index ranges	-11 ≤ h ≤ 11, -10 ≤ k ≤ 10, -16 ≤ l ≤ 16
Reflections collected	11424
Independent reflections	4102 [R(int) = 0.0245]
Cov. of independent reflections	99.8%
Absorption correction	multi-scan
Max. and min. transmission	0.7457 and 0.6166
Structure solution technique	direct methods
Structure solution program	SHELXT (Sheldrick 2015)
Refinement method	Full-matrix least-squares on F <sup>2</sup>
Refinement program	SHELXL-2018/3 (Sheldrick, 2018)
Function minimized	Σ w(Fo <sup>2</sup> - Fc <sup>2</sup> ) <sup>2</sup>
Data / restraints / parameters	4102 / 1 / 205
Goodness-of-fit on F <sup>2</sup>	1.061
Final R indices	3765 data; I > 2σ(I) R1 = 0.0412, wR2 = 0.1026 all data R1 = 0.0456, wR2 = 0.1054
Weighting scheme	w = 1/[σ <sup>2</sup> (Fo <sup>2</sup> ) + (0.0698P) <sup>2</sup> + 0.0163P] where P = (Fo <sup>2</sup> + 2Fc <sup>2</sup> )/3
Absolute structure parameter	0.6(4)
Largest diff. peak and hole	0.285 and -0.167 eÅ <sup>-3</sup>
R.M.S. deviation from mean	0.046 eÅ <sup>-3</sup>

## 8.4.4.3 Tetracycline 30



Identification code	18dtr10h
Chemical formula	C <sub>19</sub> H <sub>26</sub> O <sub>3</sub>
Formula weight	302.40 g/mol
Temperature	100(2) K
Wavelength	0.71073 Å
Crystal size	0.160 x 0.540 x 0.560 mm
Crystal habit	colorless plate
Crystal system	monoclinic
Space group	P 1 21 1
Unit cell dimensions	a = 8.7382(6) Å b = 8.1682(6) Å c = 11.6148(8) Å α = 90° β = 99.9432(10)° γ = 90°
Volume	816.56(10) Å <sup>3</sup>
Z	2
Density (calculated)	1.230 g/cm <sup>3</sup>
Absorption coefficient	0.081 mm <sup>-1</sup>
F(000)	328
Diffractometer	Bruker APEX-II CCD
Radiation source	sealed tube, Mo
Theta range for data collection	1.78 to 28.29°
Index ranges	-11 ≤ h ≤ 11, -10 ≤ k ≤ 10, -15 ≤ l ≤ 15
Reflections collected	12719
Independent reflections	4033 [R(int) = 0.0226]
Cov. of independent reflections	100.0%
Absorption correction	multi-scan
Max. and min. transmission	0.7457 and 0.6835
Structure solution technique	direct methods
Structure solution program	SHELXS-97 (Sheldrick 2008)
Refinement method	Full-matrix least-squares on F <sup>2</sup>
Refinement program	SHELXL-2014 (Sheldrick 2014)
Function minimized	Σ w(Fo <sup>2</sup> - Fc <sup>2</sup> ) <sup>2</sup>
Data / restraints / parameters	4033 / 1 / 205
Goodness-of-fit on F <sup>2</sup>	1.037
Final R indices	3883 data; I > 2σ(I) R1 = 0.0366, wR2 = 0.0958 all data R1 = 0.0380, wR2 = 0.0971
Weighting scheme	w = 1/[σ <sup>2</sup> (Fo <sup>2</sup> ) + (0.0631P) <sup>2</sup> + 0.0998P] where P = (Fo <sup>2</sup> + 2Fc <sup>2</sup> )/3
Absolute structure parameter	0.4(3)
Largest diff. peak and hole	0.259 and -0.183 eÅ <sup>-3</sup>
R.M.S. deviation from mean	0.041 eÅ <sup>-3</sup>

### 8.4.5 Computational Studies

Initial conformational searches were completed using the CREST conformer-rotamer ensemble sampling tool,<sup>[349,350]</sup> version 2.7.1 with xtb version 6.2 RC2 (SAW190805).<sup>[351–353]</sup> These initial conformer geometries were recalculated in Gaussian 16 Rev. A.03 (sse4)<sup>[354]</sup> with at the SMD(DMF)- $\omega$ B97X-D/6-311+G(d,p)<sup>[355–360]</sup> level of theory. This functional was chosen for its ability to reproduce CCSD geometries of asynchronous Diels–Alder reactions as well as its ability to accurately reproduce experimental reaction barriers.<sup>[361]</sup> Following Head-Gordon’s suggested basis set for energetics,<sup>[359]</sup> single point energies at the SMD(DMF)- $\omega$ B97X-D/def2-QZVPP level of theory were computed.<sup>[362–364]</sup> Thermochemistry was calculated using the program GoodVibes version 3.0.1,<sup>[365]</sup> using quasiharmonic approximations to entropy<sup>[366]</sup> and enthalpy<sup>[367]</sup> and corrected for 398.15 K. All reported energies are quasiharmonic corrected. All reported structures are stationary points on the energy surface and characterized as transition states or minima by frequency calculations.

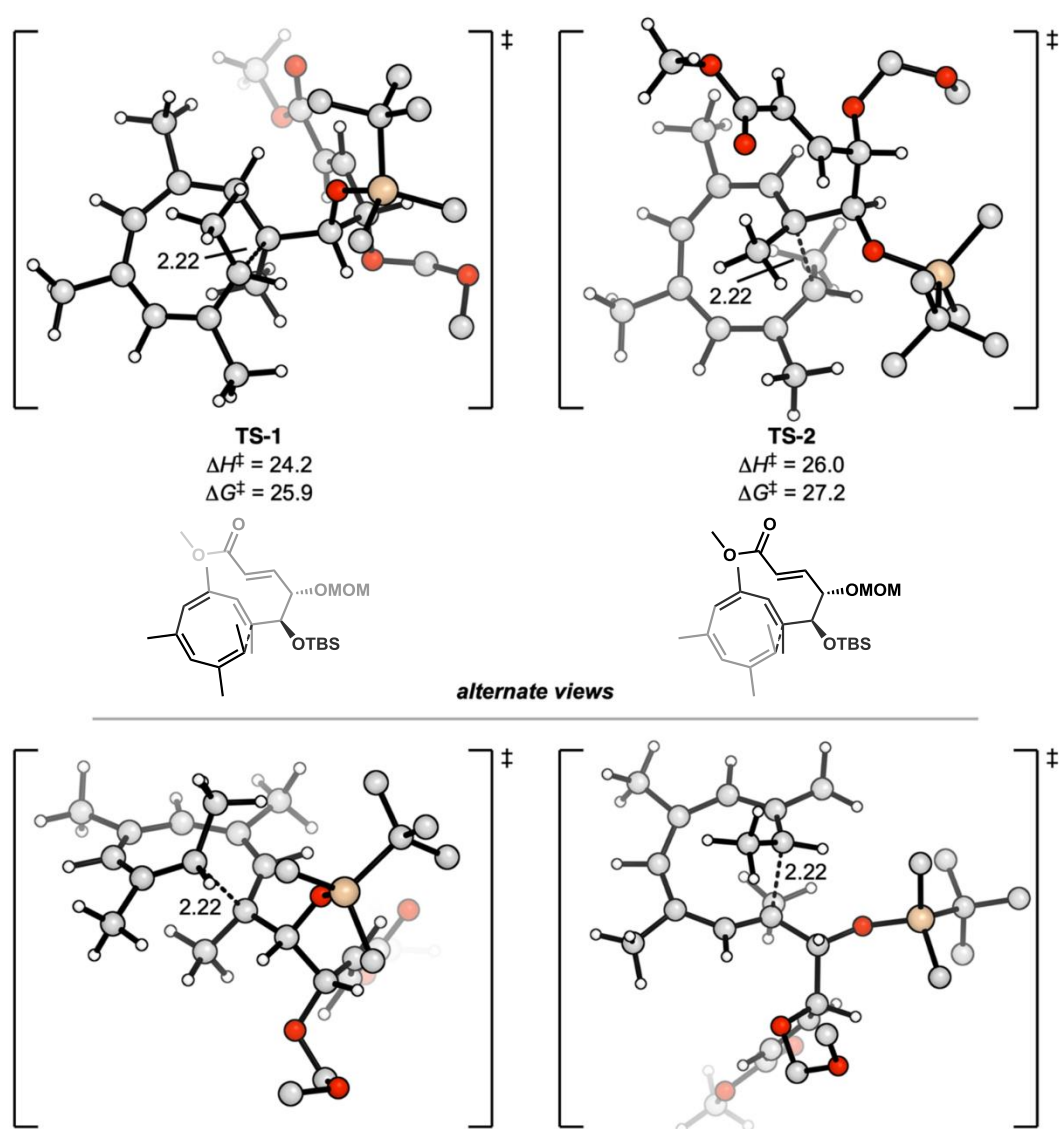


**Figure S2.** Calculated TS-1 and TS-2 shown in two alternate angles. Hs on protecting groups are omitted for clarity. Silicon is shown in wheat colour.

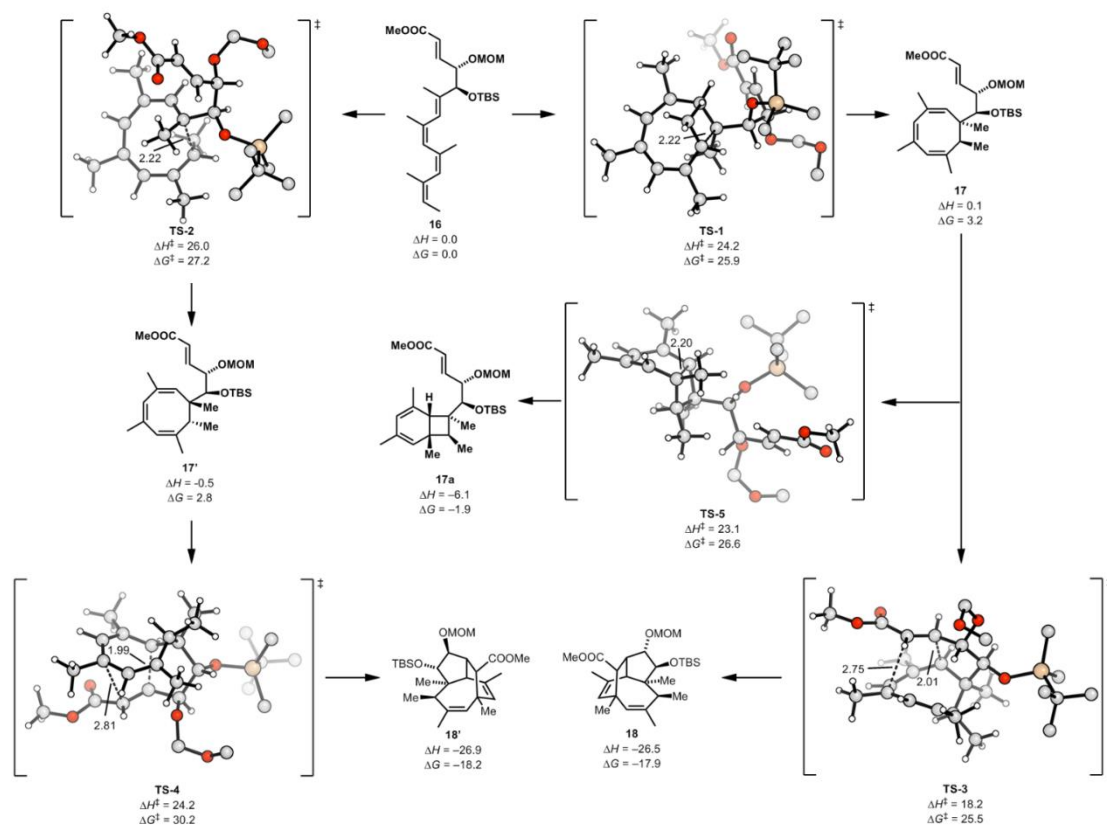


**Figure S3.** Calculated cascade energy surface starting from **16** and leading to **18**.

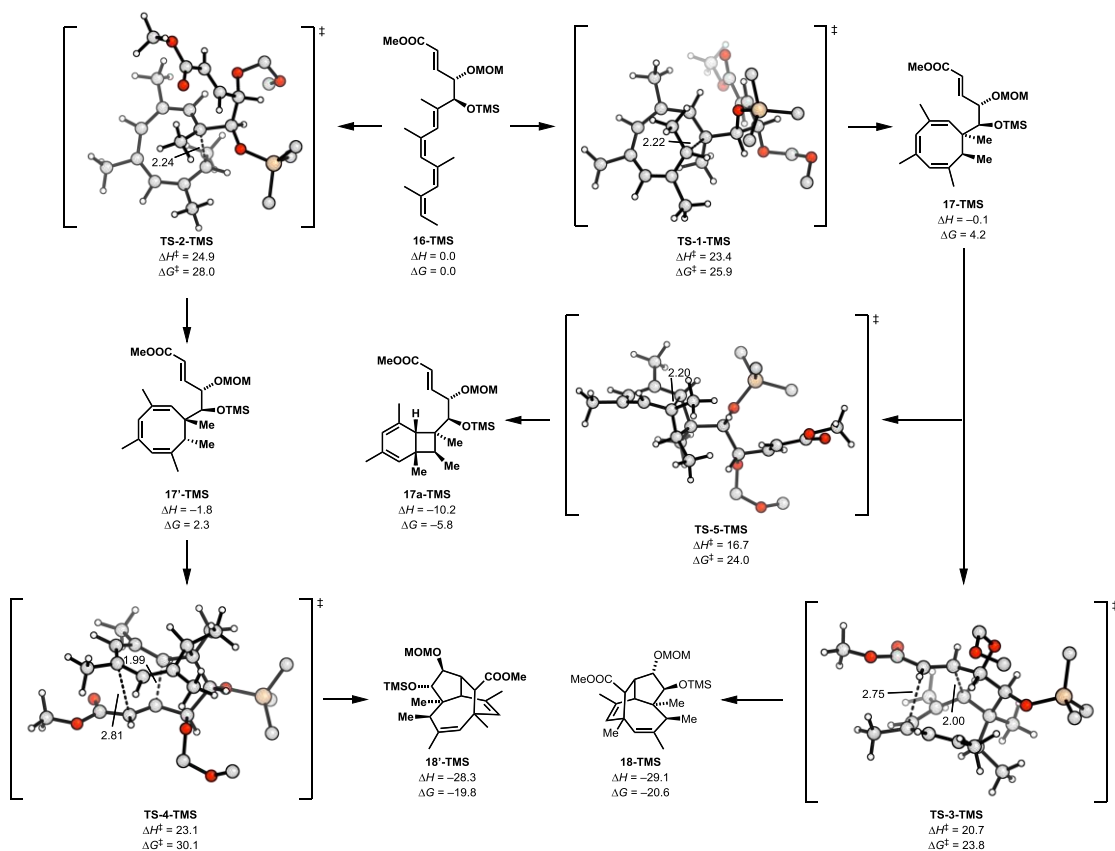
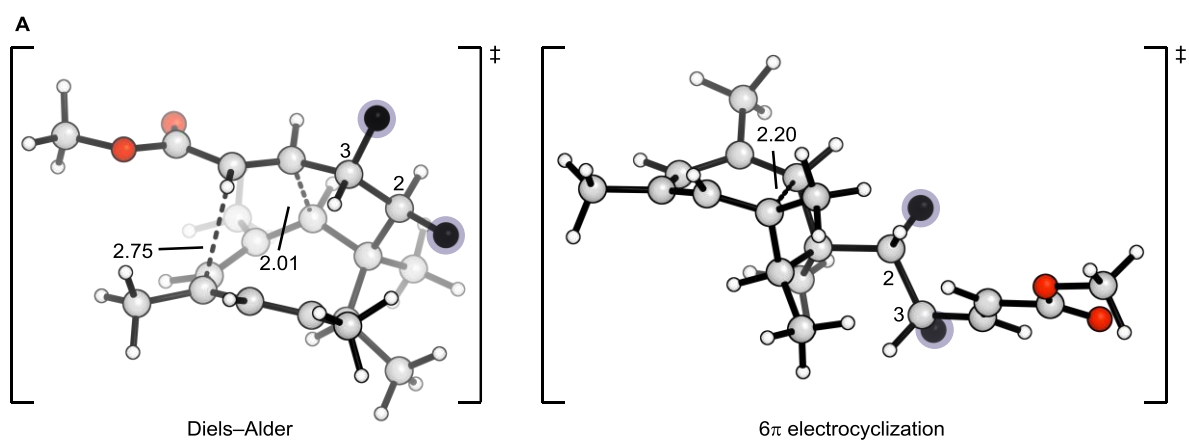


**Figure S4.** Calculated cascade energy surface starting from **16-TMS** and leading to **18-TMS**.



Barriers for Diels–Alder and  $6\pi$  electrocyclization transition states, reported as  $\Delta G^\ddagger$  relative to  $8\pi$ -cycloadduct

C2 substituent	C3 substituent	D.A. to <b>18</b>	D.A. to <b>18'</b>	6 $\pi$ electrocyclization
OTBS	OMOM	22.3	27.4	23.4
OTMS	OMOM	19.6	27.7	19.8
H	OMOM	28.1	–	23.5

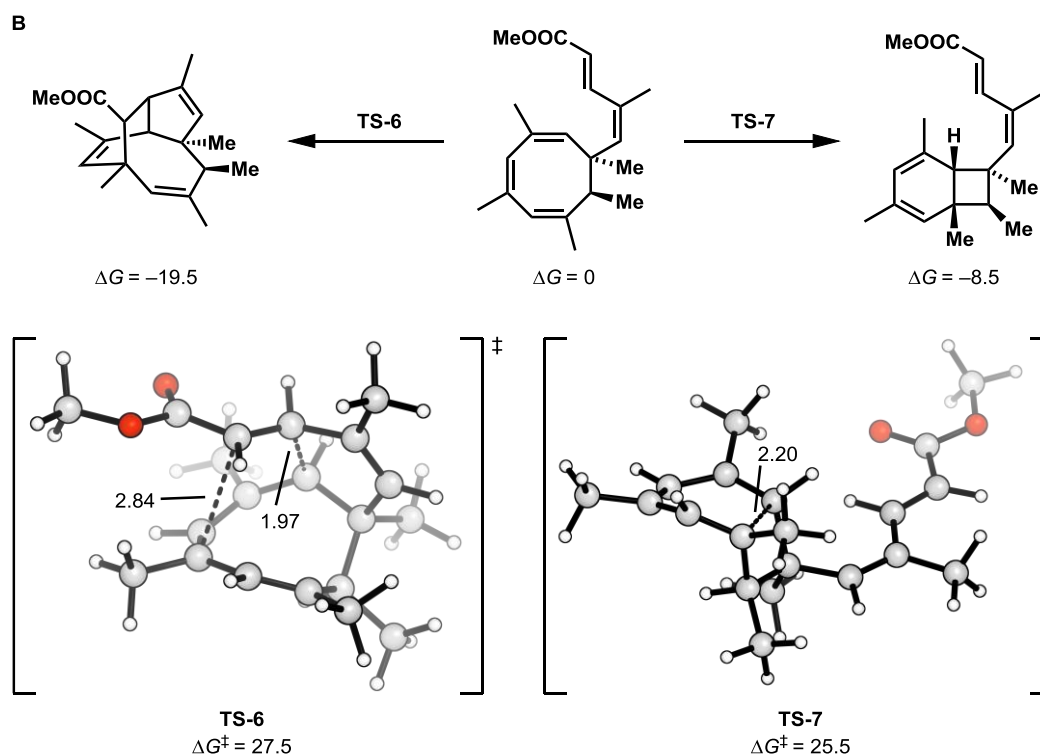


**Figure S5.** (A) barriers for Diels–Alder and 6- $\pi$  electrocyclization for OTBS, OTMS, and H substituent at the 2 position. (B) biomimetic reaction model for competing Diels–Alder and 6- $\pi$  electrocyclization.

### 8.4.5.1 Cartesian Coordinates of Calculated Structures

Energies reported below are at the  $\omega$ B97X-D/6-311+G(d,p) level of theory. Frequencies for transition states given as  $F$ .

Cartesian coordinates

16-TBS.out				H	-0.470189	-3.379819	-2.147738
ZPE	0.686264			H	0.858437	-3.970311	-1.089176
DE	0.728321			O	-0.959931	-4.040378	-0.257947
DH	0.729265			C	-2.293203	-3.563728	-0.368958
DG	0.610870			H	-2.354047	-2.497275	-0.136834
E	-1722.146990			H	-2.680554	-3.734209	-1.381290
H	-1721.417726			H	-2.896057	-4.128588	0.342828
G	-1721.536120			Si	1.271162	1.936697	0.935135
Cartesian coordinates				C	0.364395	2.484418	2.476616
C	-0.989261	0.190021	-2.866645	H	-0.695720	2.661035	2.271187
C	-4.482147	-1.181718	-1.787092	H	0.434445	1.720141	3.258049
C	-2.225246	-0.629351	-2.649815	H	0.795027	3.408247	2.876802
C	-3.324300	-0.236090	-1.992309	C	3.077765	1.636662	1.324258
C	-3.953464	3.010275	0.078977	H	3.195886	0.837932	2.063753
C	-3.443521	1.151854	-1.486073	H	3.640056	1.354859	0.429007
C	-3.851648	1.549610	-0.273446	H	3.531232	2.542556	1.740460
C	-3.949182	-1.066574	2.586948	C	1.059326	3.160364	-0.487565
C	-4.216451	0.623167	0.823026	C	1.705829	4.501333	-0.107503
C	-3.380637	-0.173462	1.515643	H	2.781330	4.399081	0.072327
C	-1.942279	-0.155939	1.215940	H	1.575534	5.226067	-0.921509
C	-0.994784	-2.059469	2.647323	H	1.252879	4.932814	0.791642
C	-0.934594	-0.910353	1.674514	C	1.740596	2.610532	-1.750042
C	0.468027	-0.650650	1.151193	H	2.817767	2.477925	-1.602712
C	0.994610	-1.843992	0.324550	H	1.321728	1.646237	-2.050039
C	2.381614	-1.527291	-0.146525	H	1.605599	3.309439	-2.585896
C	3.484866	-1.946533	0.467960	C	-0.437640	3.375179	-0.756995
C	4.841744	-1.492262	0.108111	H	-0.949761	2.433784	-0.971058
H	-0.440733	-0.154175	-3.747543	H	-0.936217	3.840965	0.099033
H	-1.208591	1.253762	-2.995335	H	-0.577660	4.037853	-1.621285
H	-0.325942	0.088523	-2.001174	16-TMS.out			
H	-5.421386	-0.723361	-2.113981	ZPE	0.600600		
H	-4.333902	-2.105077	-2.351937	DE	0.638975		
H	-4.605233	-1.444529	-0.732622	DH	0.639919		
H	-2.192102	-1.656002	-3.010052	DG	0.528669		
H	-4.963113	3.255311	0.427523	E	-1604.208888		
H	-3.267571	3.250252	0.899317	H	-1603.568969		
H	-3.714134	3.650212	-0.773574	G	-1603.680219		
H	-3.152132	1.934876	-2.185529	Cartesian coordinates			
H	-3.737262	-2.118603	2.374842	C	-0.840755	-0.327794	2.943558
H	-3.526519	-0.839248	3.569618	C	-4.156793	1.369473	1.768905
H	-5.032499	-0.944222	2.648220	C	-1.976304	0.607418	2.663217
H	-5.267490	0.635090	1.111602	C	-3.117432	0.305909	2.028301
H	-1.650991	0.593136	0.487634	C	-4.149145	-2.963822	0.164642
H	-0.003976	-2.253565	3.067780	C	-3.405171	-1.086040	1.606919
H	-1.670539	-1.871979	3.478884	C	-3.882539	-1.504266	0.426020
H	-1.317299	-2.978595	2.148086	C	-3.743141	0.945973	-2.579361
H	2.445287	-0.855772	-0.996865	C	-4.166373	-0.611588	-0.721588
H	3.441452	-2.605823	1.329018	C	-3.263429	0.069617	-1.452961
O	5.832210	-1.777081	0.747369	C	-1.837516	-0.057077	-1.130553
O	4.872941	-0.715977	-0.981217	C	-0.660626	1.542118	-2.751159
C	6.149057	-0.181093	-1.345483	C	-0.746470	0.520461	-1.649168
H	5.971995	0.417018	-2.236792	C	0.608478	0.151875	-1.064242
H	6.543047	0.446230	-0.544045	C	1.302232	1.363957	-0.408834
H	6.855410	-0.983255	-1.565088	C	2.655417	0.944008	0.082069
H	1.001096	-2.727582	0.970415	C	3.781812	1.137331	-0.599753
H	1.133559	-0.593270	2.027424	C	5.094603	0.606192	-0.184353
O	0.573450	0.512612	0.371292	H	-0.342893	-0.065533	3.881667
O	0.147250	-2.052582	-0.793628	H	-1.161932	-1.370612	3.005253
C	-0.071770	-3.394009	-1.126978				

H -0.102755 -0.257304 2.137104  
H -5.141064 1.044586 2.122359  
H -3.895718 2.298379 2.281424  
H -4.256968 1.586946 0.702119  
H -1.823058 1.644170 2.958490  
H -5.175877 -3.114861 -0.186854  
H -3.486080 -3.333498 -0.626105  
H -3.995581 -3.570526 1.060097  
H -3.191904 -1.856210 2.347315  
H -3.368505 0.601948 -3.547478  
H -4.834341 0.949265 -2.621986  
H -3.403269 1.977196 -2.445431  
H -5.213988 -0.552719 -1.016683  
H -1.636192 -0.742173 -0.315965  
H -1.393276 1.377613 -3.537907  
H -0.805081 2.552633 -2.354954  
H 0.330647 1.517653 -3.213669  
H 2.665910 0.402765 1.022595  
H 3.788890 1.668220 -1.546437  
O 6.097329 0.706967 -0.859235  
O 5.071957 -0.008224 1.003417  
C 6.305546 -0.582912 1.445839  
H 6.088960 -1.032983 2.412293  
H 6.646074 -1.345791 0.743801  
H 7.072411 0.185988 1.552678  
H 1.398162 2.151954 -1.162344  
H 1.257843 -0.135049 -1.907277  
O 0.540980 -0.874914 -0.111734  
O 0.523015 1.815081 0.688468  
C 0.427774 3.205619 0.817645  
H 0.081808 3.380694 1.842724  
H 1.397364 3.687651 0.655770  
O -0.450123 3.787507 -0.105307  
C -1.808323 3.442186 0.126826  
H -1.957620 2.361686 0.063249  
H -2.132703 3.794813 1.114273  
H -2.401639 3.939391 -0.641212  
Si 0.903429 -2.488532 -0.402455  
C 2.761725 -2.663858 -0.516564  
H 3.159575 -2.062099 -1.340914  
H 3.247051 -2.331286 0.406381  
H 3.047881 -3.705910 -0.695568  
C 0.182883 -3.389109 1.060069  
H -0.898383 -3.220096 1.111735  
H 0.354001 -4.467532 0.976732  
H 0.628875 -3.047323 1.998730  
C 0.093894 -3.031729 -1.997623  
H -0.996619 -2.978569 -1.920390  
H 0.406581 -2.403647 -2.838352  
H 0.368058 -4.065368 -2.234876

## 17-TBS.out

ZPE 0.689975  
DE 0.730508  
DH 0.731452  
DG 0.616971  
E -1722.151182  
H -1721.419730  
G -1721.534211

## Cartesian coordinates

C 1.611618 -3.174854 -0.393728  
C 1.822441 -1.285300 -2.677509  
C 2.358812 -1.853424 -0.163730  
C 2.754174 -1.216550 -1.493406  
C 6.364898 -1.174327 -1.030369  
C 3.979804 -0.702648 -1.668426  
C 5.027568 -0.600437 -0.644131

C 4.057413 2.149054 1.475919  
C 4.837295 -0.008148 0.544024  
C 3.665662 0.763228 1.005840  
C 2.376669 0.406992 1.071896  
C 1.655456 -1.579140 2.241275  
C 1.643622 -0.901788 0.850025  
C 0.182392 -0.581450 0.328220  
C -0.961541 -1.391704 0.972963  
C -2.199000 -1.193091 0.144213  
C -2.542669 -1.983567 -0.869965  
H 2.200615 -3.822202 -1.049540  
H 1.461191 -3.710307 0.545663  
H 0.634307 -3.038452 -0.863912  
H 0.905263 -0.711431 -2.520924  
H 1.517474 -2.313738 -2.890431  
H 2.308876 -0.884213 -3.569185  
H 3.298260 -2.117351 0.328638  
H 6.719160 -0.723120 -1.963787  
H 7.116964 -1.005256 -0.256641  
H 6.285931 -2.251956 -1.210353  
H 4.271279 -0.381538 -2.668555  
H 3.192732 2.712069 1.835473  
H 4.794711 2.093145 2.284893  
H 4.523618 2.715461 0.661747  
H 5.698386 0.055566 1.210443  
H 1.716870 1.164200 1.481904  
H 1.267848 -0.904584 3.005194  
H 1.062224 -2.495124 2.277445  
H 2.688176 -1.834153 2.497251  
H -2.777114 -0.300635 0.360545  
H -1.969523 -2.870417 -1.121793  
C -3.654764 -1.683147 -1.787639  
H -0.691665 -2.454247 0.978177  
H 0.157643 -0.869645 -0.724384  
O -0.171637 0.774757 0.445711  
Si -0.373617 1.923637 -0.755358  
C -1.166314 3.354836 0.191232  
C -0.192272 3.858625 1.267320  
H 0.074058 3.063221 1.970592  
H 0.733984 4.244850 0.829028  
H -0.650821 4.674195 1.841882  
C -1.499272 4.499822 -0.775888  
H -0.603631 4.883115 -1.276840  
H -2.208494 4.185071 -1.549035  
H -1.955485 5.336688 -0.231305  
C -2.454652 2.859016 0.866438  
H -2.248898 2.035734 1.557493  
H -2.922236 3.672975 1.435973  
H -3.188673 2.507390 0.133153  
C 1.270637 2.407558 -1.506569  
H 1.953830 2.820672 -0.759285  
H 1.760014 1.543109 -1.966740  
H 1.119646 3.161095 -2.287467  
C -1.496999 1.286661 -2.112413  
H -1.141613 0.331182 -2.511760  
H -2.523287 1.144255 -1.763380  
H -1.513900 2.003688 -2.940414  
O -1.155879 -0.934642 2.299437  
C -1.851478 -1.818906 3.128943  
H -1.476628 -2.841854 3.015149  
H -1.681030 -1.458515 4.150047  
O -3.224738 -1.882596 2.853254  
C -3.909807 -0.676009 3.142626  
H -3.791023 -0.403822 4.199335  
H -3.551742 0.152160 2.521856  
H -4.965606 -0.848626 2.933143  
O -3.860989 -2.294334 -2.815314  
O -4.411370 -0.652248 -1.388601  
C -5.451962 -0.243242 -2.280386



H -6.170230 -1.050499 -2.432634  
H -5.936202 0.602595 -1.796896  
H -5.034093 0.062464 -3.241290

## 17-biomimetic.out

ZPE 0.435464  
DE 0.459884  
DH 0.460828  
DG 0.382047  
E -929.329089  
H -928.868261  
G -928.947042

## Cartesian coordinates

C -2.909441 1.731959 -1.563751  
C -0.356961 0.685935 -2.517482  
C -2.243588 0.636939 -0.721111  
C -1.174827 -0.091263 -1.517665  
C -2.440038 -3.484931 -1.354368  
C -1.023582 -1.419811 -1.431598  
C -1.832320 -2.327266 -0.605998  
C -0.807925 -1.989007 2.854076  
C -2.026026 -2.180110 0.713203  
C -1.364782 -1.252713 1.653216  
C -1.203176 0.075096 1.585858  
C -2.940743 1.754908 1.445692  
C -1.742523 1.157091 0.667689  
C -0.739119 2.287456 0.491293  
C 1.351051 3.570754 0.190291  
C 0.601475 2.277595 0.379603  
C 1.377335 1.040411 0.348333  
C 2.692506 0.959021 0.105449  
H -3.797025 2.127029 -1.067120  
H -2.235021 2.567624 -1.768914  
H -3.231097 1.319310 -2.523699  
H -0.971532 0.966938 -3.379300  
H 0.480439 0.087491 -2.882252  
H 0.035880 1.613185 -2.096056  
H -3.018002 -0.096255 -0.477958  
H -1.659895 -4.058980 -1.866296  
H -2.984132 -4.157746 -0.688139  
H -3.128148 -3.126862 -2.127776  
H -0.310452 -1.903954 -2.098812  
H -0.333505 -1.307649 3.563250  
H -1.603374 -2.531966 3.376456  
H -0.068187 -2.733785 2.540576  
H -2.628878 -2.942132 1.207725  
H -0.667676 0.513785 2.427425  
H -2.634463 2.021306 2.461373  
H -3.326655 2.658724 0.968649  
H -3.748566 1.020884 1.513892  
H -1.207482 3.268083 0.429787  
H 2.123695 3.696410 0.955268  
H 1.854785 3.590009 -0.782101  
H 0.675369 4.425816 0.241694  
H 0.844828 0.108345 0.498571  
H 3.317637 1.825255 -0.075656  
C 3.346173 -0.359560 0.055526  
O 2.810494 -1.429711 0.250119  
O 4.651272 -0.240749 -0.245320  
C 5.394625 -1.460195 -0.331410  
H 4.986268 -2.105357 -1.111281  
H 6.412094 -1.167635 -0.582482  
H 5.380269 -1.988043 0.623700

## 17-TMS.out

ZPE 0.605684  
DE 0.641969

DH 0.642913  
DG 0.537815  
E -1604.214691  
H -1603.571778  
G -1603.676876

## Cartesian coordinates

C -1.086794 0.917664 -2.713454  
C -1.497498 -1.941638 -2.052262  
C -1.998001 0.587640 -1.522514  
C -2.450451 -0.868968 -1.585878  
C -6.040051 -0.315787 -1.818626  
C -3.730583 -1.198494 -1.363497  
C -4.800765 -0.275255 -0.964605  
C -4.256688 0.395498 2.529476  
C -4.712133 0.532311 0.102351  
C -3.665725 0.557521 1.144254  
C -2.340497 0.709050 1.025497  
C -1.398657 2.604941 -0.130506  
C -1.435188 1.058190 -0.139964  
C -0.012039 0.406757 0.099570  
C 1.196384 1.283029 -0.298012  
C 2.413354 0.407875 -0.398394  
C 2.779518 -0.212355 -1.517708  
H -1.592095 0.649003 -3.645454  
H -0.864666 1.985633 -2.758346  
H -0.138362 0.375327 -2.690902  
H -0.639341 -2.061090 -1.385660  
H -1.095314 -1.715790 -3.044083  
H -2.006496 -2.906397 -2.105865  
H -2.902857 1.184986 -1.659697  
H -6.435380 -1.336243 -1.870432  
H -6.822101 0.339213 -1.428559  
H -5.811571 -0.012883 -2.846225  
H -4.043878 -2.225413 -1.551513  
H -3.490399 0.454283 3.305563  
H -5.006146 1.170657 2.725603  
H -4.768532 -0.569255 2.620951  
H -5.583797 1.144774 0.335920  
H -1.797298 0.716082 1.964425  
H -1.087287 2.980815 0.845025  
H -0.722787 3.023328 -0.878866  
H -2.404793 2.980013 -0.339310  
H 2.957385 0.237938 0.525141  
H 2.238515 -0.071353 -2.448238  
C 3.871272 -1.198613 -1.584756  
H 0.998929 1.734628 -1.275500  
H 0.045566 -0.453445 -0.570269  
O 0.208320 -0.026441 1.425562  
Si 0.270523 -1.623627 1.944579  
C 0.791346 -1.501742 3.729643  
C -1.401465 -2.449246 1.794394  
H -2.150365 -1.963001 2.426373  
H -1.768678 -2.433096 0.763809  
H -1.321336 -3.496981 2.106304  
C 1.516918 -2.593673 0.939275  
H 1.280157 -2.576519 -0.129376  
H 2.533335 -2.210729 1.067011  
H 1.505704 -3.640344 1.263986  
O 1.383129 2.299973 0.671220  
C 1.998615 3.459597 0.186639  
H 1.529822 3.790785 -0.746305  
H 1.863611 4.211938 0.972182  
O 3.358191 3.294047 -0.110742  
C 4.163920 3.085485 1.036361  
H 4.071513 3.926154 1.735899  
H 3.896228 2.160256 1.556661  
H 5.196680 3.015676 0.694493

O	4.093173	-1.885626	-2.560025
O	4.590292	-1.278703	-0.458055
C	5.620122	-2.271069	-0.429949
H	6.362818	-2.078890	-1.205923
H	6.077561	-2.190952	0.553922
H	5.196140	-3.267400	-0.566847
H	0.066774	-0.922383	4.310447
H	0.862302	-2.498172	4.178351
H	1.768790	-1.018672	3.823500

## 17-MOM.out

ZPE	0.498443
DE	0.526626
DH	0.527570
DG	0.438802
E	-1120.286954
H	-1119.759384
G	-1119.848151

## Cartesian coordinates

C	1.368100	-2.211021	2.068964
C	1.513923	-3.206262	-0.709384
C	1.994389	-1.300150	1.004379
C	2.407481	-2.094342	-0.223659
C	5.997179	-1.506945	-0.188843
C	3.599303	-1.901022	-0.807143
C	4.617825	-0.932366	-0.381651
C	3.531289	2.390069	-1.333298
C	4.380195	0.374656	-0.188148
C	3.174094	1.158824	-0.523398
C	1.884516	0.950456	-0.218374
C	0.857254	0.720845	1.992352
C	1.148860	-0.030836	0.677219
C	-0.183041	-0.427804	-0.017661
C	-1.342611	0.566144	0.021500
C	-2.578964	-0.091336	-0.524757
C	-3.680125	-0.308736	0.189340
H	2.016508	-3.074167	2.244108
H	1.264475	-1.685171	3.019665
H	0.383847	-2.592968	1.786434
H	0.497393	-2.860134	-0.908746
H	1.433885	-3.997722	0.042560
H	1.910594	-3.650331	-1.624865
H	2.914648	-0.907751	1.445611
H	5.995235	-2.260567	0.606103
H	6.331413	-2.011698	-1.101990
H	6.726016	-0.734519	0.065699
H	3.897690	-2.571768	-1.613017
H	4.035150	2.113027	-2.265751
H	2.647084	2.981896	-1.579923
H	4.226529	3.027624	-0.775507
H	5.233580	0.989443	0.099654
H	1.198913	1.692197	-0.617494
H	0.451884	1.715816	1.794642
H	0.134530	0.185747	2.614652
H	1.781407	0.844159	2.564786
H	-2.540764	-0.400216	-1.567764
H	-3.752733	-0.005154	1.228456
C	-4.857252	-0.978482	-0.403465
H	-1.529336	0.886622	1.050613
H	0.011482	-0.681086	-1.064984
O	-4.946069	-1.381090	-1.541697
O	-5.847058	-1.088705	0.494730
C	-7.050285	-1.718081	0.039777
H	-6.850404	-2.742759	-0.277758
H	-7.724292	-1.714463	0.893665
H	-7.487164	-1.156316	-0.787493
H	-0.567606	-1.333092	0.459340

O	-1.036386	1.710428	-0.781902
C	-1.830111	2.836571	-0.504947
H	-1.699862	3.506247	-1.361763
H	-2.883239	2.560833	-0.395630
O	-1.472961	3.478087	0.687048
C	-0.255243	4.199172	0.597555
H	-0.086078	4.665971	1.568084
H	0.590653	3.544333	0.365386
H	-0.322297	4.980090	-0.170345

## 17a-TBS.out

ZPE	0.690780
DE	0.730685
DH	0.731629
DG	0.619380
E	-1722.161976
H	-1721.430347
G	-1721.542596

## Cartesian coordinates

C	0.988455	-2.515901	1.521120
C	-1.736008	-1.802194	2.453516
C	-0.130811	-2.417635	0.498644
C	-1.592880	-2.360314	1.038789
C	-3.828214	-5.283901	-0.235264
C	-2.311313	-3.671260	0.920198
C	-3.138765	-3.956729	-0.091239
C	-3.283162	-0.676824	-2.128282
C	-3.422312	-2.944092	-1.122677
C	-2.891990	-1.713709	-1.117817
C	-1.928561	-1.298730	-0.042458
C	-0.066229	-1.429360	-1.892043
C	-0.405094	-1.169122	-0.427109
C	0.143536	0.195733	0.057565
C	1.560004	0.547569	-0.439906
C	2.638709	-0.433767	-0.092081
C	3.399701	-1.053890	-0.990078
C	4.478338	-2.000568	-0.644605
H	-2.288989	-0.365126	0.390695
H	1.956770	-2.695577	1.051577
H	1.069846	-1.624732	2.148780
H	0.786623	-3.365193	2.182699
H	-1.349920	-2.501831	3.201722
H	-1.204718	-0.852795	2.569228
H	-2.793133	-1.620695	2.673086
H	-0.054132	-3.282338	-0.168164
H	-3.568942	-5.961237	0.581375
H	-4.916433	-5.158343	-0.248182
H	-3.553666	-5.762808	-1.181680
H	-2.110269	-4.415542	1.689646
H	-3.844006	-1.117453	-2.956116
H	-3.912840	0.086597	-1.659121
H	-2.410454	-0.154774	-2.527514
H	-4.129767	-3.216822	-1.903292
H	-0.261254	-0.554942	-2.518468
H	0.985554	-1.700667	-2.005566
H	-0.661116	-2.261011	-2.278885
H	2.821455	-0.573513	0.967672
H	3.249385	-0.911861	-2.055200
H	0.173894	0.195722	1.154316
H	1.510032	0.691720	-1.525608
O	5.145662	-2.581099	-1.473954
O	4.644085	-2.162268	0.672745
C	5.662847	-3.082505	1.078804
H	5.448365	-4.083108	0.700058
H	6.640572	-2.755766	0.721013
H	5.641910	-3.080649	2.166475
O	-0.726544	1.217620	-0.394836

O	1.897112	1.780778	0.190873
C	2.842020	2.524247	-0.524420
H	2.399891	2.897778	-1.463426
H	3.729538	1.915682	-0.762627
O	3.189657	3.587896	0.312261
C	3.966363	4.552043	-0.371241
H	3.405965	4.993987	-1.205332
H	4.214019	5.333341	0.346799
H	4.895623	4.116345	-0.760047
Si	-1.034951	2.701285	0.344804
C	-2.897365	3.055275	0.150459
C	-0.597434	2.596486	2.160932
H	-0.867755	3.527670	2.669521
H	-1.130126	1.778002	2.656370
H	0.476264	2.438660	2.288060
C	-0.101789	4.068930	-0.537057
H	0.058578	3.801949	-1.586512
H	-0.658696	5.010367	-0.517012
H	0.873684	4.241053	-0.076955
C	-3.219708	4.400504	0.825811
H	-2.650094	5.231917	0.400023
H	-4.284253	4.634246	0.694379
H	-3.022238	4.373615	1.902572
C	-3.761700	1.977282	0.818233
H	-3.498685	1.835341	1.872041
H	-4.820052	2.267897	0.779426
H	-3.672699	1.012489	0.317153
C	-3.253916	3.149150	-1.340729
H	-3.008389	2.226874	-1.874893
H	-4.329667	3.331541	-1.466065
H	-2.722478	3.972258	-1.830362

## 17a-TMS.out

ZPE	0.604816
DE	0.641030
DH	0.641975
DG	0.536792
E	-1604.229942
H	-1603.587967
G	-1603.693150

## Cartesian coordinates

C	0.594756	2.261582	1.489349
C	2.564870	0.291908	2.476927
C	1.488299	1.564734	0.477081
C	2.700869	0.748396	1.026125
C	6.136441	1.868625	-0.429322
C	4.012617	1.443570	0.812597
C	4.841521	1.143632	-0.193924
C	3.123252	-1.849020	-1.937040
C	4.513077	0.050041	-1.125334
C	3.392220	-0.678338	-1.040364
C	2.372481	-0.389070	0.022562
C	0.923169	0.693808	-1.887153
C	1.041021	0.339660	-0.408390
C	-0.168686	-0.488338	0.075945
C	-1.557825	-0.035442	-0.407664
C	-1.959502	1.368034	-0.074497
C	-2.260613	2.286095	-0.989638
C	-2.675253	3.666461	-0.670965
H	2.149311	-1.332478	0.529405
H	-0.135828	2.911254	1.004969
H	0.057226	1.563356	2.136019
H	1.214399	2.894530	2.133398
H	2.651828	1.132409	3.172846
H	1.602257	-0.198220	2.652467
H	3.354960	-0.427951	2.714023
H	1.872407	2.325325	-0.209774

H	6.300031	2.649946	0.316096
H	6.983507	1.174760	-0.394844
H	6.146610	2.331112	-1.422506
H	4.263826	2.243924	1.507492
H	3.836648	-1.894816	-2.763409
H	3.198098	-2.780486	-1.365321
H	2.107840	-1.817687	-2.339904
H	5.246387	-0.183193	-1.894752
H	0.628684	-0.168507	-2.490955
H	0.181459	1.482933	-2.035381
H	1.877837	1.064750	-2.269618
H	-2.048379	1.597131	0.981989
H	-2.195477	2.069223	-2.050740
H	-0.182238	-0.481999	1.172948
H	-1.595168	-0.191510	-1.491758
O	-2.935971	4.495558	-1.516488
O	-2.729298	3.917351	0.641699
C	-3.114948	5.242728	1.021479
H	-2.408775	5.975109	0.627227
H	-4.119242	5.468828	0.659580
H	-3.097309	5.252210	2.109168
O	-0.008254	-1.809069	-0.402676
O	-2.486740	-0.907069	0.236012
C	-3.602076	-1.194673	-0.557115
H	-3.302582	-1.804332	-1.426834
H	-4.083178	0.269019	-0.915351
O	-4.472240	-1.912276	0.267113
C	-5.537837	-2.478509	-0.470521
H	-5.167783	-3.195547	-1.214794
H	-6.179469	-2.999233	0.239781
H	-6.125594	-1.706694	-0.983636
Si	-0.275722	-3.236693	0.438492
C	1.232088	-4.300834	0.133422
C	-0.448406	-2.878913	2.265126
H	-0.560415	-3.818798	2.816698
H	0.435226	-2.365281	2.658697
H	-1.327310	-2.260594	2.467345
C	-1.782132	-4.121236	-0.225514
H	-1.775149	-4.138909	-1.320349
H	-1.786646	-5.160590	0.121970
H	-2.707432	-3.645493	0.108978
H	1.389039	-4.469106	-0.936688
H	2.136281	-3.838801	0.541518
H	1.107821	-5.279219	0.610814

## 17a-biomimetic.out

ZPE	0.435696
DE	0.459619
DH	0.460563
DG	0.383241
E	-929.344254
H	-928.883690
G	-928.961013

## Cartesian coordinates

C	0.135353	-0.388993	2.235216
C	-2.773943	-0.585569	2.560950
C	-0.662127	-0.652441	0.968395
C	-2.219343	-0.604404	1.138384
C	-4.558411	-2.486835	-1.352145
C	-2.936562	-1.678102	0.363648
C	-3.800697	-1.413573	-0.623481
C	-3.451734	2.408510	-1.108411
C	-4.024890	-0.025301	-1.066405
C	-3.298781	1.004407	-0.612529
C	-2.230703	0.758721	0.408750
C	-0.678008	0.027056	-1.527871
C	-0.757727	0.526686	-0.079653

C	0.124076	1.736038	0.094518
C	2.167585	3.135487	0.236806
C	1.466735	1.812835	0.074508
C	2.290674	0.619160	-0.097063
C	3.629865	0.604105	-0.148857
H	-2.233351	1.573092	1.142020
H	1.209964	-0.399167	2.039727
H	-0.109712	0.579149	2.680566
H	-0.070831	-1.164600	2.978638
H	-2.630730	-1.551647	3.056124
H	-2.299828	0.187147	3.171714
H	-3.848696	-0.378705	2.531810
H	-0.310727	-1.580839	0.504925
H	-4.325783	-3.479162	-0.959822
H	-5.638550	-2.325534	-1.266988
H	-4.319312	-2.472570	-2.421323
H	-2.772116	-2.705059	0.686589
H	-4.234220	2.491116	-1.866229
H	-3.688285	3.088659	-0.282681
H	-2.508680	2.760004	-1.544056
H	-4.790759	0.141806	-1.820824
H	-0.952371	0.822158	-2.227746
H	0.337633	-0.294677	-1.769456
H	-1.348042	-0.819124	-1.691624
H	-0.415268	2.673135	0.228459
H	2.827427	3.127519	1.110425
H	2.790389	3.361899	-0.634627
H	1.445790	3.944440	0.360133
H	1.784568	-0.337052	-0.186020
H	4.230737	1.502245	-0.070858
C	4.349868	-0.669335	-0.313834
O	3.845153	-1.767767	-0.408650
O	5.678750	-0.471331	-0.346656
C	6.489739	-1.640262	-0.499950
H	6.259481	-2.148086	-1.438051
H	7.518277	-1.285733	-0.508591
H	6.335959	-2.326776	0.334358

## 17'-TBS.out

ZPE	0.689667
DE	0.730075
DH	0.731020
DG	0.617626
E	-1722.152436
H	-1721.421417
G	-1721.534810

## Cartesian coordinates

C	1.524096	-1.411696	-2.558022
C	2.756948	-2.876649	-0.286563
C	2.325537	-0.585812	-1.541492
C	3.194334	-1.480709	-0.653838
C	6.347974	0.156967	-1.372478
C	4.430795	-1.088865	-0.316679
C	5.044596	0.215025	-0.621919
C	3.654731	2.243110	1.953768
C	4.512935	1.377285	-0.219711
C	3.331902	1.547088	0.652104
C	2.079953	1.155383	0.395622
C	1.414523	1.717436	-1.900757
C	1.479481	0.568477	-0.868142
H	2.202656	-2.053006	-3.127402
H	1.012905	-0.761961	-3.272249
H	0.773527	-2.057746	-2.096262
H	2.371793	-3.424038	-1.150643
H	3.600041	-3.439961	0.120173
H	1.975216	-2.880284	0.476923
H	3.056397	-0.031351	-2.134533

H	6.201596	-0.282889	-2.365065
H	7.065200	-0.482307	-0.845953
H	6.790122	1.148457	-1.493387
H	5.084226	-1.802072	0.186120
H	4.355419	1.645144	2.548041
H	2.756423	2.416760	2.550910
H	4.139847	3.208601	1.770378
H	5.068337	2.292060	-0.430713
H	1.341089	1.380322	1.157179
H	0.896977	2.582076	-1.486783
H	0.890958	1.409194	-2.811884
H	2.427606	2.025892	-2.171404
C	0.002330	0.155737	-0.586774
C	-0.203895	-0.989547	0.425706
O	-0.737334	1.272329	-0.150873
C	-1.603348	-1.521231	0.310718
H	0.496921	-1.788275	0.182360
O	0.034686	-0.505485	1.738741
Si	-2.138029	1.965430	-0.751887
C	-1.926521	-2.588777	-0.414843
H	-2.376019	-0.955847	0.821756
C	0.067256	-1.491916	2.732561
C	-3.013022	2.646490	0.783239
C	-1.718263	3.348512	-1.941287
C	-3.200901	0.708394	-1.646062
H	-1.172850	-3.173517	-0.933085
C	-3.315483	-3.035450	-0.634615
H	0.043868	-0.944580	3.681480
H	-0.794572	-2.163883	2.660588
O	1.197171	-2.314813	2.660333
C	-2.147338	3.738275	1.429538
C	-4.370464	3.242317	0.381079
C	-3.234275	1.515371	1.798038
H	-1.021738	4.067856	-1.501189
H	-1.266835	2.955350	-2.857453
H	-2.628802	3.888245	-2.223663
H	-3.700310	0.017668	-0.962006
H	-3.972585	1.235467	-2.217682
H	-2.612942	0.117917	-2.356465
O	-3.615300	-3.947223	-1.375708
O	-4.216844	-2.327330	0.055747
C	2.407677	-1.627331	2.941145
H	-1.164183	3.352528	1.717850
H	-1.992645	4.586841	0.755023
H	-2.634731	4.121491	2.335698
H	-4.261283	4.061512	-0.337672
H	-5.028965	2.488897	-0.064618
H	-4.882658	3.646121	1.264092
H	-3.727058	1.906331	2.698020
H	-3.875458	0.725026	1.391845
H	-2.285880	1.060337	2.100115
C	-5.591033	-2.671665	-0.146200
H	3.217549	-2.350481	2.842056
H	2.572411	-0.804535	2.239376
H	2.398459	-1.232995	3.965395
H	-5.778533	-3.702054	0.160073
H	-6.159024	-1.985610	0.478548
H	-5.868065	-2.543483	-1.193881
H	-0.404205	-0.212366	-1.534340

## 17'-TMS.out

ZPE	0.605174
DE	0.641625
DH	0.642569
DG	0.537132
E	-1604.217524
H	-1603.574955
G	-1603.680392

Cartesian coordinates				H	-3.315035	1.875403	2.452469
				H	-4.423647	2.712512	1.357295
				H	-4.065483	0.998625	1.104845
C	0.950051	-0.223766	-2.775762				
C	2.111334	-2.572778	-1.397627				
C	1.893463	0.053154	-1.596195	18-TBS.out			
C	2.695555	-1.194500	-1.222276	ZPE	0.695861		
C	5.985466	0.296794	-1.544434	DE	0.733707		
C	3.987229	-1.084578	-0.881984	DH	0.734651		
C	4.737785	0.170987	-0.711719	DG	0.628868		
C	3.746113	1.156643	2.567252	E	-1722.201046		
C	4.370627	1.122984	0.156814	H	-1721.466394		
C	3.268086	1.045246	1.137845	G	-1721.572178		
C	1.964746	0.898367	0.878965				
C	1.215520	2.369935	-0.936057	Cartesian coordinates			
C	1.221939	0.902290	-0.443529				
H	1.521560	-0.628345	-3.615723	C	-1.213997	-3.560059	0.159319
H	0.471183	0.696196	-3.119524	C	-0.565555	-2.529876	-2.395935
H	0.162637	-0.943368	-2.538365	C	-0.012162	-2.602954	0.137965
H	1.667077	-2.701301	-2.388202	C	0.448079	-2.313302	-1.294541
H	2.889106	-3.330226	-1.276607	C	4.101750	-1.549926	-1.712877
H	1.335331	-2.792231	-0.661001	C	1.654146	-1.854158	-1.654980
H	2.651198	0.736333	-1.986554	C	2.841968	-1.327268	-0.863390
H	5.737943	0.301068	-2.611583	C	2.592330	-2.169390	2.925118
H	6.646017	-0.560994	-1.376550	C	3.055941	-1.949672	0.495030
H	6.537330	1.210346	-1.311855	C	2.333910	-1.609336	1.558328
H	4.574422	-1.995750	-0.766095	C	1.183126	-0.657789	1.389842
H	4.409216	0.320963	2.819194	C	-0.866664	-1.777026	2.376250
H	2.911196	1.159147	3.271874	C	-0.191015	-1.349620	1.068088
H	4.325366	2.075330	2.714476	C	-0.970114	-0.160743	0.449328
H	5.021478	1.991775	0.263652	C	0.043184	0.622547	-0.386468
H	1.305590	0.880821	1.740101	C	1.400363	0.447376	0.315268
H	0.836481	3.037163	-0.162194	C	2.555097	0.205632	-0.670423
H	0.593895	2.492919	-1.829204	C	3.793949	0.952355	-0.228597
H	2.235234	2.679157	-1.179110	H	-1.400288	-3.925203	1.169679
C	-0.271690	0.525714	-0.206415	H	-2.129216	-3.094326	-0.208707
C	-0.575584	-0.884527	0.330841	H	-1.003856	-4.437602	-0.457293
O	-0.886769	1.468937	0.647137	H	-0.872303	-3.576321	-2.478556
C	-2.062098	-1.108444	0.268879	H	-0.163510	-2.219527	-3.362632
H	-0.077002	-1.607160	-0.317663	H	-1.465120	-1.943362	-2.187946
O	-0.112929	-1.010056	1.665344	H	0.801382	-3.159475	0.609369
Si	-2.204630	2.452523	0.306888	H	4.034122	-1.022025	-2.667540
C	-2.692878	-1.538793	-0.820995	H	5.001186	-1.205238	-1.194829
H	-2.623911	-0.832194	1.156028	H	4.221889	-2.617915	-1.917451
C	-0.156719	-2.312011	2.182718	H	1.795708	-1.693833	-2.724250
C	-1.696860	4.207884	0.694801	H	1.736208	-2.745508	3.289983
C	-2.687777	2.280788	-1.492158	H	3.469282	-2.821108	2.929281
H	-2.147642	-1.817451	-1.717557	H	2.756933	-1.359677	3.644660
C	-4.160816	-1.608984	-0.947059	H	3.870976	-2.663561	0.590482
H	-0.030084	-2.197727	3.265031	H	1.034368	-0.140968	2.342886
H	-1.112295	-2.799587	1.962008	H	-0.854865	-0.949268	3.091325
O	0.830541	-3.150517	1.653403	H	-1.906590	-2.061716	2.216248
H	-1.288247	4.282933	1.707745	H	-0.357977	-2.628730	2.835143
H	-0.938827	4.570997	-0.005459	H	1.634168	1.364101	0.850509
H	-2.561499	4.877540	0.633022	H	2.285435	0.610083	-1.649682
H	-3.033396	1.268171	-1.724281	O	4.166526	1.097339	0.912185
H	-3.508963	2.971413	-1.713554	O	4.458834	1.464163	-1.276041
H	-1.857288	2.523954	-2.162500	C	5.680623	2.145025	-0.976750
O	-4.729507	-1.934301	-1.967377	H	6.393351	1.464878	-0.506449
O	-4.806946	-1.262286	0.172080	H	6.068339	2.490116	-1.933051
C	2.144044	-2.773455	2.039004	H	5.496759	2.994674	-0.317067
C	-6.236787	-1.256898	0.111353	H	0.061521	0.179758	-1.379928
H	2.832411	-3.469658	1.559553	O	-0.351800	1.973286	-0.646484
H	2.378473	-1.755092	1.715602	C	-0.163386	2.910159	0.354905
H	2.260486	-2.842508	3.128261	H	-0.958457	3.660279	0.255978
H	-6.616120	-2.255454	-0.111141	H	-0.217849	2.462624	1.360483
H	-6.569847	-0.940414	1.097572	O	1.095131	3.527137	0.176375
H	-6.585268	-0.553440	-0.646613	C	1.439190	4.338639	1.280019
H	-0.751591	0.559064	-1.188199	H	2.400974	4.800681	1.056920
C	-3.632046	1.956537	1.407685	H	0.695401	5.128732	1.448934

H	1.532973	3.742953	2.198489
H	-1.288955	0.476059	1.288225
O	-2.077570	-0.536168	-0.331792
Si	-3.722288	-0.324549	-0.109492
C	-4.470457	-1.394018	-1.445201
H	-5.561653	-1.419828	-1.363859
H	-4.214521	-1.022579	-2.442239
H	-4.102827	-2.421664	-1.361256
C	-4.252493	-0.910866	1.587597
H	-4.127112	-1.993311	1.687512
H	-3.680032	-0.424780	2.383079
H	-5.310980	-0.679329	1.748555
C	-4.237218	1.490210	-0.333252
C	-3.802311	2.325724	0.880491
H	-2.723035	2.278747	1.049689
H	-4.064377	3.380963	0.726927
H	-4.298428	1.993259	1.798093
C	-5.768617	1.559588	-0.457043
H	-6.089977	2.606167	-0.539395
H	-6.128737	1.034579	-1.347622
H	-6.274224	1.130165	0.414828
C	-3.604058	2.067798	-1.606828
H	-2.512845	2.073356	-1.541015
H	-3.891747	1.496072	-2.496276
H	-3.942076	3.101943	-1.758879

## 18-TMS.out

ZPE	0.609918
DE	0.644122
DH	0.645067
DG	0.546177
E	-1604.266477
H	-1603.621411
G	-1603.720301

## Cartesian coordinates

C	-2.205980	-3.091403	0.187824
C	-1.286502	-2.331283	-2.375197
C	-0.857122	-2.354839	0.182296
C	-0.295576	-2.224280	-1.237643
C	3.448074	-2.075688	-1.513847
C	0.982411	-1.984975	-1.561537
C	2.206619	-1.607194	-0.741050
C	1.661214	-2.179795	3.066654
C	2.260735	-2.175874	0.655934
C	1.559796	-1.663372	1.662667
C	0.586935	-0.551780	1.389199
C	-1.666781	-1.268369	2.325132
C	-0.866021	-1.038039	1.037736
C	-1.412974	0.217536	0.322297
C	-0.263708	0.779051	-0.511909
C	1.019788	0.440990	0.267698
C	2.162049	-0.039130	-0.642743
C	3.486234	0.526521	-0.179510
H	-2.489903	-3.368659	1.203539
H	-3.010032	-2.489286	-0.238415
H	-2.128674	-4.020834	-0.381814
H	-1.757726	-3.316823	-2.425226
H	-0.800899	-2.140844	-3.334484
H	-2.085049	-1.596177	-2.236273
H	-0.170047	-3.011636	0.721295
H	3.505466	-1.601174	-2.496800
H	4.369030	-1.847253	-0.969960
H	3.403842	-3.159430	-1.656619
H	1.189705	-1.909595	-2.629543
H	0.705189	-2.584689	3.413307
H	2.415224	-2.966213	3.148969
H	1.927552	-1.368811	3.753562

H	2.942705	-3.005658	0.827340
H	0.484743	0.037154	2.305865
H	-1.535097	-0.420715	3.003935
H	-2.734010	-1.363665	2.116483
H	-1.348578	-2.173772	2.848251
H	1.370315	1.344062	0.762168
H	2.002130	0.343334	-1.654454
O	3.832577	0.676846	0.968859
O	4.264917	0.865379	-1.218915
C	5.568304	1.359495	-0.898059
H	6.142870	0.604067	-0.358571
H	6.043439	1.579735	-1.851875
H	5.499348	2.266120	-0.294528
H	-0.273874	0.278223	-1.477268
O	-0.441545	2.154142	-0.864920
C	-0.200470	3.106182	0.112123
H	-0.884841	3.944676	-0.067724
H	-0.373726	2.716412	1.127852
O	1.136327	3.551380	-0.000702
C	1.501491	4.378868	1.084003
H	2.527546	4.705302	0.913880
H	0.853902	5.263113	1.154332
H	1.453440	3.832451	2.036073
H	-1.640170	0.948061	1.114731
O	-2.555751	-0.017025	-0.464111
Si	-4.022532	0.776867	-0.309355
C	-4.993827	0.213845	-1.796763
H	-6.002618	0.639519	-1.791700
H	-4.502330	0.518678	-2.725770
H	-5.089057	-0.876764	-1.804290
C	-4.866461	0.263485	1.279406
H	-5.021657	-0.819414	1.315673
H	-4.275412	0.553403	2.154103
H	-5.845423	0.748497	1.363822
C	-3.752499	2.626600	-0.292757
H	-3.222477	2.958225	-1.189693
H	-4.712779	3.151584	-0.242244
H	-3.163207	2.927575	0.579623

## 18-biomimetic.out

ZPE	0.440461
DE	0.462326
DH	0.463270
DG	0.392605
E	-929.375010
H	-928.911740
G	-928.982405

## Cartesian coordinates

C	3.938487	0.037797	-0.889744
C	2.381380	-2.125059	-1.828777
C	2.426664	0.194518	-0.682586
C	1.629880	-0.874373	-1.434082
C	-1.874899	0.039772	-2.390388
C	0.316615	-0.846299	-1.694243
C	-0.800405	0.105243	-1.293674
C	0.674716	3.382801	0.189650
C	-0.382224	1.542264	-1.107105
C	0.240021	1.962541	-0.010438
C	0.612131	0.965601	1.047235
C	3.083277	1.033575	1.650425
C	2.021633	0.280717	0.837233
C	1.771771	-1.089029	1.418353
C	-0.095468	-2.642174	2.130728
C	0.484678	-1.366898	1.611448
C	-0.401853	-0.191694	1.253519
C	-1.356878	-0.458721	0.065141
H	4.470317	0.909211	-0.505537

H	4.344633	-0.848920	-0.394524
H	4.172788	-0.034076	-1.954469
H	3.199681	-1.920217	-2.524324
H	1.714225	-2.852755	-2.294781
H	2.827832	-2.593986	-0.944518
H	2.165763	1.162866	-1.114904
H	-2.273820	-0.972351	-2.495572
H	-2.708068	0.716221	-2.178009
H	-1.438924	0.338825	-3.348039
H	-0.081807	-1.724331	-2.203687
H	1.766483	3.446819	0.259888
H	0.346156	4.024148	-0.631665
H	0.274598	3.782309	1.127980
H	-0.620710	2.237730	-1.908664
H	0.685288	1.494582	2.001480
H	2.737742	1.159851	2.680241
H	4.029285	0.488028	1.684382
H	3.279805	2.026865	1.235303
H	2.584361	-1.785795	1.607398
H	-0.685671	-2.458978	3.035454
H	-0.772212	-3.095601	1.398451
H	0.685366	-3.368673	2.366530
H	-1.030223	0.046527	2.116878
H	-1.485244	-1.534565	-0.072516
C	-2.733469	0.099882	0.352413
O	-2.975799	1.165604	0.868818
O	-3.697715	-0.746789	-0.042641
C	-5.044162	-0.288449	0.111572
H	-5.211336	0.614159	-0.479323
H	-5.674845	-1.096533	-0.253494
H	-5.264714	-0.083968	1.160539

## 18'.out

ZPE	0.695653
DE	0.733442
DH	0.734386
DG	0.629042
E	-1722.201106
H	-1721.466720
G	-1721.572064

## Cartesian coordinates

C	1.345657	-3.607535	0.398089
C	0.744383	-2.739398	-2.214834
C	0.072521	-2.758438	0.288484
C	-0.313174	-2.475709	-1.166599
C	-3.861683	-1.471200	-1.841971
C	-1.467026	-1.939073	-1.585752
C	-2.687520	-1.396699	-0.850210
C	-2.685725	-2.866068	2.755091
C	-3.043040	-2.193392	0.380370
C	-2.414986	-2.031616	1.540756
C	-1.326472	-1.004409	1.636290
C	0.961178	-1.663983	2.429537
C	0.118857	-1.455277	1.166483
C	0.641329	-0.219339	0.373968
C	-0.264637	0.932832	0.784300
C	-1.656002	0.295458	0.883311
C	-2.361916	0.106094	-0.479955
C	-3.626466	0.938059	-0.502797
H	1.484585	-3.954291	1.422790
H	2.245846	-3.062320	0.105437
H	1.267983	-4.497546	-0.230232
H	0.995513	-3.801308	-2.289744
H	0.414467	-2.399545	-3.198325
H	1.672942	-2.213586	-1.967594
H	-0.722000	-3.376720	0.712116
H	-3.668211	-0.867973	-2.732745

H	-4.795227	-1.129502	-1.386247
H	-4.005732	-2.507860	-2.159014
H	-1.539867	-1.761887	-2.658823
H	-1.780625	-3.410200	3.050110
H	-3.483448	-3.591676	2.579759
H	-2.964760	-2.235265	3.606158
H	-3.815005	-2.951797	0.270003
H	-1.224065	-0.730015	2.689788
H	0.943210	-0.758930	3.042686
H	2.003923	-1.881262	2.200102
H	0.549002	-2.483713	3.026861
H	-2.307606	0.895955	1.518223
H	-1.727022	0.495020	-1.277493
O	-4.467013	0.970398	0.366339
O	-3.723626	1.656157	-1.630199
C	-4.911847	2.440401	-1.779821
H	-5.794532	1.798468	-1.787414
H	-4.810284	2.949906	-2.735711
H	-4.995745	3.169054	-0.971813
O	2.009536	0.024706	0.588130
Si	3.035328	0.902234	-0.408370
C	2.348771	0.979729	-2.147672
C	3.255289	2.621633	0.292295
C	4.684711	-0.035687	-0.378937
H	3.092736	1.413518	-2.824726
H	2.087387	-0.012303	-2.528225
H	1.452117	1.604509	-2.174927
H	2.278219	3.088868	0.448368
H	3.779231	2.593355	1.253543
H	3.836826	3.252119	-0.388650
C	5.045858	-0.410071	1.065634
C	5.790932	0.855117	-0.964991
C	4.574325	-1.316081	-1.218515
H	4.290929	-1.068134	1.506715
H	6.010118	-0.934948	1.092507
H	5.135091	0.474271	1.706164
H	6.741193	0.306193	-0.997990
H	5.561402	1.173487	-1.988147
H	5.950971	1.754448	-0.361634
H	3.775232	-1.969704	-0.855214
H	4.373686	-1.095561	-2.271996
H	5.512821	-1.884252	-1.171979
O	-0.137244	1.985283	-0.160084
C	-0.757157	3.171566	0.197115
H	-0.754668	3.809102	-0.695251
H	-1.797180	3.009004	0.524880
O	-0.033905	3.782058	1.240551
C	-0.688439	4.936512	1.725130
H	-0.066958	5.354176	2.517183
H	-0.812025	5.688839	0.935014
H	-1.676838	4.691919	2.136158
H	0.034757	1.294708	1.774403
H	0.468702	-0.377276	-0.694568

## 18'-TMS.out

ZPE	0.610070
DE	0.644291
DH	0.645235
DG	0.546095
E	-1604.265283
H	-1603.620048
G	-1603.719188

## Cartesian coordinates

C	1.656764	-3.707139	0.232921
C	0.913299	-2.858501	-2.335989
C	0.410355	-2.810601	0.209590
C	-0.042780	-2.493275	-1.221719

C -3.531912 -1.216660 -1.721813  
 C -1.171663 -1.865843 -1.579088  
 C -2.311238 -1.238739 -0.785130  
 C -2.244183 -2.756892 2.798190  
 C -2.665488 -2.025886 0.451468  
 C -1.972713 -1.926492 1.581191  
 C -0.812083 -0.978445 1.635468  
 C 1.443624 -1.814691 2.332611  
 C 0.574601 -1.527760 1.102922  
 C 1.154908 -0.326717 0.300764  
 C 0.353020 0.885993 0.748558  
 C -1.076689 0.351444 0.908673  
 C -1.859883 0.231620 -0.418919  
 C -3.061224 1.151970 -0.371391  
 H 1.836717 -4.082744 1.240702  
 H 2.558306 -3.182206 -0.094935  
 H 1.517209 -4.579222 -0.409107  
 H 1.036317 -3.941229 -2.432098  
 H 0.561779 -2.473247 -3.294747  
 H 1.908859 -2.444507 -2.148324  
 H -0.385258 -3.400555 0.672300  
 H -3.336332 -0.618211 -2.615282  
 H -4.416463 -0.814339 -1.220160  
 H -3.765209 -2.236470 -2.040382  
 H -1.289699 -1.688417 -2.648047  
 H -1.365101 -3.362608 3.047963  
 H -3.094756 -3.426570 2.651018  
 H -2.444335 -2.119925 3.666736  
 H -3.493346 -2.726695 0.368932  
 H -0.646015 -0.723564 2.685656  
 H 1.506361 -0.921332 2.959779  
 H 2.460857 -2.098025 2.066704  
 H 0.996126 -2.615073 2.930944  
 H -1.649914 0.992342 1.578787  
 H -1.238658 0.583340 -1.244068  
 O -3.848503 1.239293 0.542707  
 O -3.170280 1.879043 -1.491914  
 C -4.310594 2.740099 -1.578506  
 H -5.232538 2.156989 -1.541991  
 H -4.225157 3.246852 -2.537422  
 H -4.305393 3.468288 -0.765848  
 O 2.545276 -0.182648 0.462298  
 Si 3.595283 0.553782 -0.619090  
 C 2.831284 0.640553 -2.324104  
 C 4.013299 2.267364 -0.004130  
 H 3.550670 1.075148 -3.026993  
 H 2.553586 -0.348569 -2.700753  
 H 1.937759 1.270668 -2.316433  
 H 3.102961 2.865482 0.100475  
 H 4.506194 2.224123 0.972889  
 H 4.690197 2.777330 -0.698598  
 O 0.517335 1.926051 -0.203891  
 C 0.027727 3.161513 0.187197  
 H 0.015301 3.793919 -0.708731  
 H -0.993979 3.086884 0.593907  
 O 0.876249 3.713462 1.167120  
 C 0.357111 4.920109 1.687219  
 H 1.069343 5.289183 2.425115  
 H 0.235173 5.676465 0.900637  
 H -0.613609 4.759903 2.174910  
 H 0.720726 1.223841 1.723995  
 H 0.929324 -0.465482 -0.760684  
 C 5.121564 -0.524184 -0.633904  
 H 5.897264 -0.096046 -1.277979  
 H 5.540689 -0.626778 0.372309  
 H 4.886842 -1.526546 -1.006937

TS-1.out

ZPE 0.686447

DE 0.727508  
 DH 0.728452  
 DG 0.611182  
 E -1722.108355  
 H -1721.379903  
 G -1721.497172  
 F -501.214

Cartesian coordinates

C 1.471133 -3.180691 1.247136  
 C 0.488626 -2.752164 0.366650  
 C 2.845344 -3.299358 0.964773  
 C 3.710790 -2.705421 0.043241  
 C 0.844717 -0.568643 0.511289  
 C 1.352683 -0.399140 -0.770180  
 C 2.613038 -0.714110 -1.297246  
 C 3.578131 -1.637597 -0.881415  
 H -0.512612 -2.719192 0.787894  
 C 0.494145 -3.076948 -1.099820  
 H 1.491221 -3.064602 -1.537586  
 H -0.145016 -2.391693 -1.657835  
 H 0.087746 -4.088363 -1.224480  
 H 4.486378 -1.544999 -1.476124  
 H 3.365408 -3.930890 1.684718  
 H 0.653576 0.006579 -1.497433  
 C 1.734332 -0.406375 1.715004  
 H 2.674001 -0.944135 1.610078  
 H 1.237191 -0.734269 2.629794  
 H 1.965766 0.656378 1.833931  
 C 1.058819 -3.514348 2.666425  
 H 0.049920 -3.149975 2.874293  
 H 1.739378 -3.082731 3.405145  
 H 1.053340 -4.599848 2.818702  
 C 5.125842 -3.279553 0.046277  
 H 5.243719 -4.069750 0.789527  
 H 5.871604 -2.505716 0.251900  
 H 5.367316 -3.707902 -0.931960  
 C 2.916244 0.015957 -2.599042  
 H 2.268074 -0.353742 -3.401555  
 H 3.950323 -0.129798 -2.916566  
 H 2.734159 1.090455 -2.505046  
 C -0.591046 -0.093366 0.735508  
 H -0.993624 -0.613513 1.615191  
 C -0.710971 1.426651 1.060432  
 H -1.783509 1.642311 1.003243  
 O -1.361938 -0.334981 -0.411928  
 O -0.256866 1.664909 2.378518  
 Si -2.961654 -0.841445 -0.492323  
 C -4.019147 0.155899 0.685642  
 H -5.048813 -0.217082 0.669286  
 H -3.652757 0.065241 1.713734  
 H -4.040058 1.218099 0.426150  
 C -3.414556 -0.531177 -2.300350  
 C -2.458287 -1.310595 -3.215545  
 H -1.421594 -0.987935 -3.077713  
 H -2.503326 -2.389023 -3.030301  
 H -2.724315 -1.144185 -4.267578  
 C -4.857245 -0.992899 -2.555443  
 H -4.979507 -2.066082 -2.374780  
 H -5.574267 -0.460352 -1.921189  
 H -5.135639 -0.800958 -3.599584  
 C -3.295779 0.968844 -2.608747  
 H -3.533391 1.157781 -3.663642  
 H -3.986730 1.564820 -2.003495  
 H -2.281549 1.337427 -2.423902  
 C -3.093468 -2.650643 -0.038725  
 H -2.801605 -2.816361 1.003482  
 H -4.130375 -2.987232 -0.145188



H	-2.464507	-3.279026	-0.675437
C	-1.005158	2.630770	3.073297
H	-0.456504	2.801072	4.006055
H	-1.086509	3.559043	2.499434
O	-2.319458	2.225457	3.327946
C	-2.409229	1.079496	4.157789
H	-3.465951	0.925488	4.376085
H	-2.011911	0.188818	3.659762
H	-1.864761	1.233519	5.098130
C	-0.013607	2.262108	0.037073
H	-0.373635	2.143711	-0.981573
C	1.005508	3.082703	0.276449
H	1.406985	3.223782	1.273092
C	1.663071	3.792763	-0.836721
O	1.329506	3.756231	-2.000848
O	2.719174	4.497818	-0.400348
C	3.458076	5.212252	-1.396656
H	4.264513	5.711156	-0.863401
H	3.866978	4.523608	-2.138017
H	2.822662	5.948329	-1.892004

## TS-1-TMS.out

ZPE	0.601357
DE	0.638495
DH	0.639439
DG	0.531575
E	-1604.172479
H	-1603.533040
G	-1603.640904
F	-500.847

## Cartesian coordinates

C	-1.580302	-2.944468	-1.135382
C	-0.795386	-2.676757	-0.023759
C	-2.964488	-2.714956	-1.253746
C	-3.870446	-1.850413	-0.636530
C	-0.539907	-0.492925	-0.298638
C	-1.326289	-0.090980	0.772393
C	-2.721336	-0.048176	0.912633
C	-3.733123	-0.757394	0.258158
H	0.256378	-2.916210	-0.150570
C	-1.269383	-2.853964	1.390570
H	-2.300992	-2.537800	1.539996
H	-0.629851	-2.311103	2.088693
H	-1.207927	-3.920599	1.639536
H	-4.716553	-0.397930	0.559068
H	-3.410818	-3.276353	-2.074405
H	-0.780074	0.206594	1.663815
C	-0.987286	-0.241709	-1.714270
H	-2.022192	-0.534454	-1.877845
H	-0.352826	-0.761011	-2.434850
H	-0.904621	0.829768	-1.920272
C	-0.898114	-3.495079	-2.371319
H	0.188406	-3.422600	-2.281652
H	-1.204641	-2.969103	-3.279509
H	-1.146664	-4.554180	-2.505518
C	-5.327825	-2.077198	-1.032029
H	-5.432100	-2.887235	-1.755524
H	-5.769884	-1.175110	-1.465760
H	-5.926746	-2.339288	-0.153786
C	-3.179227	0.866010	2.041476
H	-4.265883	0.962688	2.074082
H	-2.748347	1.866648	1.941248
H	-2.852061	0.468634	3.008665
C	0.972670	-0.383778	-0.102176
H	1.461176	-1.061914	-0.814671
C	1.546348	1.030480	-0.422269
H	2.567565	1.018989	-0.026716

O	1.315040	-0.695394	1.226483
O	1.590703	1.206067	-1.825470
Si	2.662523	-1.578266	1.714079
C	2.609128	-3.300494	0.989860
H	1.741732	-3.862983	1.347942
H	2.581059	-3.279944	-0.104545
H	3.511040	-3.848159	1.285110
C	4.228456	-0.726885	1.149091
C	2.525190	-1.620939	3.569793
H	1.590597	-2.099310	3.878935
H	3.354645	-2.188036	4.004914
H	2.548417	-0.611555	3.991527
C	2.721787	1.905282	-2.280234
H	2.544185	2.070116	-3.348577
H	2.836992	2.859463	-1.756905
O	3.917502	1.210271	-2.069549
C	3.982657	-0.029330	-2.754865
H	4.994160	-0.413735	-2.623711
H	3.268033	-0.752536	-2.347771
H	3.782710	0.103343	-3.825725
C	0.787827	2.108911	0.280402
H	0.769413	2.034061	1.364236
C	0.128287	3.099280	-0.314089
H	0.107725	3.209246	-1.391918
C	-0.650416	4.060486	0.489296
O	-0.720556	4.086261	1.698500
O	-1.306799	4.925566	-0.300208
H	4.283906	-0.670898	0.056980
H	4.302987	0.290172	1.546417
H	5.102712	-1.288653	1.496258
C	-2.122043	5.896228	0.364791
H	-1.514046	6.528107	1.014369
H	-2.571914	6.493405	-0.425510
H	-2.898797	5.405645	0.953854

## TS-2.out

ZPE	0.686227
DE	0.727420
DH	0.728365
DG	0.610361
E	-1722.105340
H	-1721.376976
G	-1721.494979
F	-502.648

## Cartesian coordinates

C	0.876128	-3.323691	-0.507474
C	0.454404	-2.740493	0.678102
C	2.207302	-3.590395	-0.880630
C	3.450263	-3.063608	-0.524708
C	0.890882	-0.611710	0.203224
C	1.958330	-0.461063	1.081329
C	3.283760	-0.910561	0.993907
C	3.857244	-1.954373	0.259001
H	-0.620204	-2.608330	0.755236
C	1.109103	-2.985544	2.007140
H	2.195557	-3.035807	1.951840
H	0.831097	-2.217780	2.733731
H	0.748561	-3.946926	2.392797
H	4.942043	-1.949970	0.362179
H	2.272986	-4.310494	-1.696056
H	1.730305	0.063187	2.005655
C	1.113642	-0.612879	-1.286502
H	1.952891	-1.241850	-1.574809
H	0.220195	-0.935121	-1.820037
H	1.346168	0.407657	-1.608389
C	-0.173723	-3.677968	-1.540385
H	-1.152623	-3.292360	-1.253310

H 0.073988 -3.282093 -2.529388  
 H -0.259570 -4.766472 -1.636150  
 C 4.643817 -3.794734 -1.135001  
 H 4.332770 -4.637376 -1.754401  
 H 5.249449 -3.124489 -1.752634  
 H 5.297048 -4.185740 -0.348329  
 C 4.226632 -0.216585 1.968839  
 H 5.271481 -0.350681 1.681743  
 H 4.025876 0.855340 2.032675  
 H 4.107458 -0.633948 2.975322  
 C -0.434676 0.004723 0.664807  
 H -0.659588 -0.377226 1.669672  
 C -0.417005 1.555201 0.820107  
 O -1.452667 -0.321744 -0.246537  
 H -1.466448 1.829715 0.973295  
 O 0.325815 1.901540 1.973925  
 C 0.057553 2.261951 -0.405693  
 Si -3.068534 0.644574 0.088502  
 C -0.233596 2.950834 2.723964  
 H -0.495497 2.041986 -1.315406  
 C 1.083688 3.107811 -0.448190  
 C -3.780605 0.640120 1.248488  
 C -3.881452 -0.583207 -1.616199  
 C -3.249296 -2.321046 0.898467  
 H 0.521246 3.195351 3.479204  
 H -0.444488 3.820401 2.094017  
 O -1.451561 2.609087 3.320008  
 H 1.663168 3.348687 0.435041  
 C 1.486948 3.727293 -1.724154  
 H -4.816793 0.379917 1.490180  
 H -3.222980 0.676524 2.190328  
 H -3.777983 1.643900 0.814260  
 C -5.379401 -0.894864 -1.479051  
 C -3.703960 0.819150 -2.217450  
 C -3.227831 -1.616594 -2.545441  
 H -4.303176 -2.501970 1.136233  
 H -2.902496 -3.135565 0.256850  
 H -2.690025 -2.363706 1.839194  
 C -1.347362 1.552734 4.259891  
 O 0.955399 3.553284 -2.798910  
 O 2.551722 4.527586 -1.555102  
 H -5.550967 -1.896312 -1.070296  
 H -5.888343 -0.173958 -0.830207  
 H -5.864998 -0.852731 -2.462400  
 H -4.158880 0.862587 -3.215504  
 H -4.182884 1.589090 -1.603603  
 H -2.645968 1.080516 -2.320992  
 H -2.157922 -1.423859 -2.670516  
 H -3.343664 -2.637000 -2.165418  
 H -3.694978 -1.578562 -3.538211  
 H -2.321662 1.453881 4.738397  
 H -1.088029 0.605865 3.774748  
 H -0.591570 1.779688 5.022504  
 C 3.046731 5.180255 -2.728893  
 H 2.279239 5.822395 -3.164135  
 H 3.892803 5.778848 -2.397983  
 H 3.372101 4.446257 -3.468000

## TS-2-TMS.out

ZPE 0.601868  
 DE 0.638852  
 DH 0.639796  
 DG 0.532356  
 E -1604.170494  
 H -1603.530698  
 G -1603.638138  
 F -494.733

Cartesian coordinates

C -3.098976 -0.829442 -1.080238  
 C -2.715101 -0.030021 -0.015117  
 C -3.305470 -2.221976 -1.053874  
 C -2.848853 -3.266874 -0.248724  
 C -0.526371 -0.498996 -0.011817  
 C -0.509727 -1.240852 1.163184  
 C -0.942845 -2.548047 1.429852  
 C -1.871931 -3.362885 0.774627  
 H -2.596107 1.020847 -0.268305  
 C -3.151923 -0.243180 1.404510  
 H -3.187665 -1.292787 1.693214  
 H -2.500624 0.290817 2.101991  
 H -4.161418 0.170418 1.518888  
 H -1.888591 -4.360385 1.212524  
 H -3.887480 -2.572083 -1.905601  
 H -0.125155 -0.721102 2.036765  
 C -0.297137 -1.164630 -1.342846  
 H -0.878884 -2.077938 -1.448454  
 H -0.527582 -0.493232 -2.169197  
 H 0.759314 -1.442449 -1.420017  
 C -3.273717 -0.151684 -2.424690  
 H -2.572160 0.680064 -2.516825  
 H -3.100767 -0.836774 -3.257533  
 H -4.283941 0.260324 -2.529161  
 C -3.486332 -4.620968 -0.551518  
 H -4.222980 -4.554669 -1.353587  
 H -2.733976 -5.360898 -0.841201  
 H -3.996631 -5.010528 0.335206  
 C -0.392355 -3.112947 2.733090  
 H -0.551947 -4.190430 2.805748  
 H 0.677881 -2.918620 2.837319  
 H -0.893865 -2.647551 3.589333  
 C -0.020022 0.939225 0.116574  
 H -0.549371 1.400846 0.955766  
 C 1.493903 1.086506 0.471224  
 O -0.270364 1.647526 -1.073954  
 H 1.717750 2.151520 0.324745  
 O 1.739639 0.740172 1.820851  
 C 2.377482 0.317845 -0.450394  
 Si -0.664538 3.285050 -1.166990  
 C 1.957191 1.834599 2.675407  
 H 2.232969 0.517606 -1.508689  
 C 3.284938 -0.576396 -0.067396  
 C 0.888652 4.281207 -1.467205  
 C -1.830178 3.445726 -2.612409  
 C -1.472723 3.810646 0.434514  
 H 2.291846 1.399508 3.622915  
 H 2.724619 2.497035 2.263238  
 O 0.823530 2.631669 2.860087  
 H 3.452472 -0.805330 0.977559  
 C 4.079136 -1.308975 -1.071147  
 H 0.635785 5.327986 -1.668500  
 H 1.556292 4.261779 -0.599961  
 H 1.441021 3.897727 -2.331078  
 H -0.763159 3.775097 1.267092  
 H -1.834320 4.840693 0.343501  
 H -2.329610 3.175982 0.684331  
 C -0.185476 2.021275 3.648563  
 O 4.000538 -1.180951 -2.273420  
 O 4.923771 -2.169492 -0.480407  
 H 0.186627 1.807903 4.657919  
 H -1.013643 2.727269 3.711896  
 H -0.545903 1.090200 3.199071  
 C 5.745694 -2.951394 -1.353260  
 H 6.352553 -3.578006 -0.703019  
 H 5.130041 -3.572535 -2.006061  
 H 6.385556 -2.306767 -1.958212  
 H -2.799270 2.987035 -2.395443

H -2.001525 4.502697 -2.842898  
H -1.418679 2.970070 -3.508131

## TS-3.out

ZPE 0.690798  
DE 0.729355  
DH 0.730300  
DG 0.623980  
E -1722.125332  
H -1721.395033  
G -1721.501352  
F -450.791

## Cartesian coordinates

C 1.009276 -2.910385 1.411527  
C 0.553899 -0.350810 2.669415  
C -0.192499 -2.098040 0.910271  
C -0.552191 -0.996359 1.876155  
C -4.248678 -0.701467 2.369858  
C -1.813971 -0.576457 2.063960  
C -3.070807 -1.018068 1.478089  
C -3.472920 -2.459590 -2.033619  
C -3.343823 -1.774297 0.347289  
C -2.674027 -1.897624 -0.880900  
C -1.430861 -1.342667 -1.217365  
C 0.563857 -2.753255 -1.405880  
C -0.064779 -1.620777 -0.573679  
C 0.728090 -0.322211 -0.841854  
C -0.151327 0.886384 -0.534657  
C -1.580602 0.644833 -0.985154  
C -2.601841 1.130812 -0.166132  
C -3.962562 1.138743 -0.617656  
H 1.100602 -3.849734 0.864831  
H 1.944437 -2.361455 1.306360  
H 0.872442 -3.164304 2.466051  
H 0.971969 -1.048959 3.402042  
H 0.190123 0.527558 3.206833  
H 1.373157 -0.053019 2.010016  
H -1.041318 -2.789497 0.893057  
H -4.313291 0.380803 2.518021  
H -5.192969 -1.041054 1.942870  
H -4.120959 -1.157429 3.357650  
H -1.951937 0.208209 2.805774  
H -2.993307 -3.362205 -2.427364  
H -4.495708 -2.709061 -1.745646  
H -3.517170 -1.729292 -2.846580  
H -1.289974 -1.357764 -2.298869  
H 0.544764 -2.498267 -2.468914  
H 1.604209 -2.921563 -1.122777  
H 0.013655 -3.688888 -1.269175  
H -1.747540 0.738294 -2.056085  
H -2.387865 1.537599 0.811610  
H -0.144450 1.074289 0.539565  
H 0.901678 -0.294991 -1.929179  
O -4.373424 0.638685 -1.655772  
O -4.802935 1.748819 0.264571  
C -6.190885 1.655128 -0.032732  
H -6.510473 0.611099 -0.080719  
H -6.706118 2.160904 0.782791  
H -6.427723 2.145155 -0.979931  
O 1.956703 -0.252615 -0.156020  
Si 3.468264 -0.022766 -0.853921  
C 3.843154 -1.444183 -2.013915  
C 3.525548 1.572564 -1.827088  
C 4.695096 0.013760 0.591766  
H 3.920605 -2.397137 -1.482414  
H 3.059387 -1.541691 -2.772038  
H 4.788932 -1.267776 -2.536840

H 2.795388 1.551130 -2.640866  
H 3.297876 2.438801 -1.201692  
H 4.520199 1.708635 -2.265631  
C 4.453834 1.231916 1.495075  
C 6.115141 0.097863 0.005506  
C 4.578344 -1.258146 1.442956  
H 5.216116 1.268375 2.284445  
H 3.476612 1.180841 1.984545  
H 4.507191 2.174921 0.941098  
H 6.852273 0.138334 0.817487  
H 6.354502 -0.773765 -0.612422  
H 6.253638 0.994404 -0.608123  
H 3.615381 -1.302827 1.959135  
H 4.686585 -2.169595 0.845624  
H 5.364701 -1.270117 2.209126  
O 0.432760 2.000182 -1.200940  
C 0.009539 3.257050 -0.744600  
H 0.588473 3.977982 -1.334103  
H -1.063619 3.403342 -0.904363  
O 0.212842 3.453359 0.627762  
C 1.567127 3.305203 1.019768  
H 1.912822 2.282416 0.854350  
H 2.215890 3.996206 0.465476  
H 1.619729 3.537015 2.083926  
H -4.368974 -2.134151 0.310703

## TS-3-TMS.out

ZPE 0.605046  
DE 0.639972  
DH 0.640916  
DG 0.541575  
E -1604.189391  
H -1603.548474  
G -1603.647815  
F -448.263

## Cartesian coordinates

C 1.429985 -2.818008 1.662794  
C 0.835126 -0.258097 2.834156  
C 0.245325 -2.049378 1.057558  
C -0.199451 -0.931766 1.970243  
C -3.924604 -0.650591 2.194089  
C -1.475317 -0.521659 2.059546  
C -2.685306 -0.980470 1.395393  
C -2.831855 -2.489936 -2.106792  
C -2.875614 -1.759802 0.263193  
C -2.120580 -1.901166 -0.911273  
C -0.858444 -1.344323 -1.168523  
C 1.136725 -2.768636 -1.190278  
C 0.460504 -1.613616 -0.429571  
C 1.271330 -0.324920 -0.675218  
C 0.376817 0.887445 -0.443230  
C -1.017890 0.640793 -0.989791  
C -2.093572 1.144168 -0.252514  
C -3.419241 1.142732 -0.796757  
H 1.597411 -3.757851 1.135577  
H 2.353514 -2.237695 1.632722  
H 1.212742 -3.069291 2.704423  
H 1.195302 -0.935187 3.615596  
H 0.422707 0.629461 3.318474  
H 1.704174 0.031466 2.237939  
H -0.586455 -2.760513 1.005294  
H -4.005898 0.434701 2.308579  
H -4.834415 -1.008427 1.710947  
H -3.863771 -1.079564 3.200133  
H -1.670904 0.274566 2.775587  
H -2.320862 -3.397334 -2.446491  
H -3.871769 -2.739365 -1.888686

H	-2.819230	-1.776161	-2.935395
H	-3.894063	-2.126476	0.162108
H	-0.642203	-1.380840	-2.237014
H	1.180097	-2.544414	-2.259534
H	2.158393	-2.927825	-0.841977
H	0.579476	-3.701032	-1.059374
H	-1.109197	0.718155	-2.071119
H	-1.948972	1.564600	0.732229
H	0.308901	1.081741	0.627253
H	1.521606	-0.317186	-1.747915
O	-3.757870	0.623014	-1.851498
O	-4.318548	1.768118	0.014333
C	-5.683111	1.665155	-0.373618
H	-5.996903	0.619501	-0.425046
H	-6.252769	2.183012	0.396955
H	-5.857219	2.138471	-1.342707
O	2.441344	-0.240406	0.097821
Si	4.018163	-0.055696	-0.442708
C	4.147915	1.358959	-1.654877
C	4.969844	0.287350	1.123684
C	4.603309	-1.632844	-1.259443
H	5.189091	1.486399	-1.972091
H	3.544612	1.171454	-2.548036
H	3.801267	2.293957	-1.207492
H	4.816279	-0.513449	1.854166
H	4.648283	1.229742	1.578851
H	6.043817	0.358655	0.922384
O	1.011512	1.997206	-1.069017
C	0.629213	3.252025	-0.572700
H	1.224049	3.973765	-1.144886
H	-0.440554	3.433791	-0.719496
O	0.847246	3.403007	0.803272
C	2.200091	3.224339	1.189315
H	2.270503	3.506336	2.240255
H	2.509648	2.181895	1.074226
H	2.866799	3.865383	0.598115
H	4.007251	-1.865485	-2.147655
H	5.646978	-1.529527	-1.576740
H	4.541338	-2.483733	-0.573868

## TS-3-MOM.out

ZPE	0.499267
DE	0.525507
DH	0.526451
DG	0.445052
E	-1120.251677
H	-1119.725226
G	-1119.806625
F	-451.692

## Cartesian coordinates

C	2.451797	-3.104992	1.003365
C	2.245901	-0.580984	2.353742
C	1.230993	-2.244765	0.650348
C	1.030603	-1.143799	1.663171
C	-2.571861	-0.609938	2.518109
C	-0.173782	-0.642269	1.979443
C	-1.509330	-0.976108	1.508949
C	-2.322265	-2.219088	-2.006524
C	-1.940182	-1.652076	0.379018
C	-1.387089	-1.771853	-0.907694
C	-0.133823	-1.302120	-1.326491
C	1.707831	-2.867155	-1.749226
C	1.255910	-1.723276	-0.820915
C	2.151941	-0.502804	-1.074444
C	1.415022	0.777143	-0.706977
C	-0.071963	0.668635	-1.033577
C	-0.973005	1.220158	-0.119527

C	-2.362776	1.347461	-0.442018
H	3.394501	-2.581181	0.820348
H	2.422673	-3.385395	2.059162
H	2.460621	-4.028454	0.423724
H	3.019154	-0.296087	1.633596
H	2.700822	-1.317583	3.023066
H	1.987687	0.300290	2.943846
H	0.355459	-2.900575	0.705637
H	-2.569523	0.474240	2.669886
H	-3.569942	-0.902972	2.190377
H	-2.365797	-1.074408	3.488266
H	-0.183516	0.131632	2.745044
H	-1.953895	-3.140954	-2.469602
H	-3.335589	-2.396616	-1.641875
H	-2.370577	-1.455225	-2.787697
H	-2.990746	-1.928978	0.419487
H	-0.083002	-1.285360	-2.416023
H	1.585034	-2.573744	-2.795104
H	2.762409	-3.108995	-1.596678
H	1.117578	-3.772526	-1.577018
H	-0.320435	0.813283	-2.083369
H	-0.643876	1.565488	0.850141
H	1.513357	0.985021	0.359673
H	2.361623	-0.454636	-2.148978
O	-2.904668	0.917110	-1.451319
O	-3.070708	1.985531	0.533410
C	-4.483429	1.996189	0.369207
H	-4.879040	0.978155	0.326907
H	-4.882466	2.509945	1.242891
H	-4.773982	2.530394	-0.538347
H	3.115409	-0.574057	-0.563043
O	2.035964	1.842644	-1.428903
C	1.756231	3.127382	-0.937499
H	2.271918	3.811411	-1.621468
H	0.680760	3.329516	-0.930687
O	2.183202	3.325694	0.382619
C	3.580486	3.167659	0.555584
H	3.887964	2.124980	0.421240
H	3.813311	3.478846	1.574207
H	4.138513	3.796310	-0.150325

## TS-4.out

ZPE	0.691282
DE	0.729582
DH	0.730527
DG	0.624997
E	-1722.095035
H	-1721.364508
G	-1721.470038
F	-587.374

## Cartesian coordinates

C	4.587250	-2.473328	-0.341138
H	5.318398	-1.659834	-0.383861
H	4.583352	-2.979485	-1.308688
H	4.943762	-3.186570	0.408973
C	3.207260	-1.960573	0.017401
C	2.181670	-2.205914	-0.882652
C	3.180950	-0.994297	1.044946
C	0.869475	-1.751701	-0.732267
C	1.279866	0.417188	-0.754461
C	2.560906	0.734040	-0.302190
H	2.700988	1.395325	0.540149
H	1.201653	0.294140	-1.825731
C	3.679120	0.641389	-1.238890
O	3.643119	0.111888	-2.332064
O	4.804207	1.205938	-0.746502
C	5.960450	1.126418	-1.579434

H 6.228726 0.085907 -1.774960  
 H 5.793286 1.640587 -2.528110  
 H 6.758603 1.618007 -1.026040  
 C 0.004217 -1.801778 -1.977302  
 H -0.341806 -2.821240 -2.171975  
 H -0.876619 -1.167844 -1.874200  
 H 0.576945 -1.477230 -2.848907  
 C 0.214239 -2.109945 0.611408  
 H 0.987235 -2.622612 1.187424  
 C -0.221421 -0.940892 1.527319  
 C 0.963991 -0.421465 2.300038  
 H 0.658628 0.113438 3.197427  
 C 2.295314 -0.480920 2.125848  
 H 4.205343 -0.765366 1.338499  
 C 0.064420 1.080419 -0.111513  
 H -0.557274 1.463182 -0.925808  
 C -0.878394 0.224609 0.761146  
 H -1.257112 0.927353 1.513366  
 C -0.867884 -3.175144 0.366263  
 H -0.454782 -3.991357 -0.232656  
 H -1.201751 -3.606420 1.310946  
 H -1.734998 -2.766151 -0.150848  
 C -1.241661 -1.413673 2.581797  
 H -2.184395 -1.711841 2.120914  
 H -0.850181 -2.260098 3.153373  
 H -1.450845 -0.601412 3.284131  
 C 3.142518 0.225164 3.171583  
 H 2.534549 0.636824 3.978342  
 H 3.879432 -0.456725 3.608336  
 H 3.702687 1.048227 2.711876  
 O 0.445862 2.183757 0.717393  
 C 0.689688 3.373728 0.022966  
 H 1.170307 4.041619 0.747128  
 H 1.343859 3.212600 -0.839587  
 O -0.478089 3.958693 -0.488940  
 C -1.392378 4.352258 0.519894  
 H -2.212227 4.874039 0.025688  
 H -1.791380 3.487441 1.060505  
 H -0.914021 5.030433 1.238321  
 O -1.953328 -0.276938 -0.009049  
 Si -3.458524 0.450058 -0.163666  
 C -4.000902 1.109460 1.501906  
 C -3.371589 1.841464 -1.412230  
 C -4.607638 -0.925851 -0.770450  
 H -3.409369 1.979923 1.802161  
 H -5.049295 1.423155 1.459021  
 H -3.906445 0.347818 2.281633  
 H -3.126086 1.461432 -2.409150  
 H -4.330883 2.365674 -1.476570  
 H -2.608364 2.574880 -1.136063  
 C -4.019129 -1.593450 -2.022094  
 C -5.975534 -0.318313 -1.120859  
 C -4.791971 -1.980863 0.330314  
 H -3.059117 -2.072727 -1.811108  
 H -4.704481 -2.366511 -2.393801  
 H -3.864094 -0.874194 -2.833449  
 H -6.665604 -1.108304 -1.444014  
 H -6.433279 0.185524 -0.262499  
 H -5.901305 0.407590 -1.937148  
 H -3.839254 -2.432360 0.623339  
 H -5.252873 -1.554618 1.227495  
 H -5.446604 -2.787284 -0.025473  
 H 2.484867 -2.580628 -1.857875

## TS-4-TMS.out

ZPE 0.605029  
 DE 0.639922  
 DH 0.640866  
 DG 0.540483

E -1604.178638  
 H -1603.537772  
 G -1603.638154  
 F -451.557

## Cartesian coordinates

C -1.115201 -1.749933 2.992983  
 C -0.202679 0.949518 3.114161  
 C -0.032680 -1.369387 1.971520  
 C 0.604909 -0.047000 2.325326  
 C 4.296856 -0.013369 1.736481  
 C 1.873336 0.263258 2.014609  
 C 2.918022 -0.497948 1.351750  
 C 2.342361 -3.124877 -1.356400  
 C 2.869572 -1.626394 0.549825  
 C 1.889928 -2.105144 -0.338012  
 C 0.603232 -1.584536 -0.529584  
 C -1.306838 -2.808435 0.364532  
 C -0.532192 -1.480273 0.493388  
 C -1.417881 -0.294673 0.016095  
 C -0.550084 0.837477 -0.580060  
 C 0.771613 0.304301 -1.139218  
 C 1.957044 0.976382 -0.840692  
 C 3.158609 0.666518 -1.553695  
 H -1.385013 -2.802280 2.907830  
 H -2.026511 -1.156702 2.871702  
 H -0.745827 -1.594160 4.009050  
 H -0.338003 0.611999 4.147351  
 H 0.292277 1.921173 3.132252  
 H -1.197202 1.088566 2.685792  
 H 0.753451 -2.129213 2.047435  
 H 4.422903 1.021518 1.402807  
 H 5.086760 -0.612597 1.282058  
 H 4.425074 -0.022261 2.824066  
 H 2.219322 1.238784 2.350965  
 H 1.787986 -4.061392 -1.229199  
 H 3.409461 -3.342113 -1.283029  
 H 2.138151 -2.757490 -2.366014  
 H 3.843626 -2.083996 0.395633  
 H 0.167735 -1.986369 -1.444631  
 H -1.527940 -3.028601 -0.678941  
 H -2.254570 -2.780515 0.903834  
 H -0.703099 -3.625789 0.770745  
 H 0.702092 -0.053359 -2.163113  
 H 2.000653 1.728979 -0.068997  
 O 3.293208 -0.222460 -2.384695  
 O 4.204440 1.464803 -1.188512  
 C 5.473490 1.105894 -1.719638  
 H 5.750737 0.092046 -1.419078  
 H 6.184531 1.819468 -1.304867  
 H 5.480805 1.168888 -2.810326  
 O -2.282224 -0.735649 -1.019390  
 Si -3.945544 -0.510153 -0.989280  
 C -4.705150 -1.549647 0.368315  
 C -4.326538 1.289634 -0.657492  
 C -4.529828 -1.054142 -2.672197  
 H -5.778786 -1.345473 0.446602  
 H -4.577168 -2.619295 0.177664  
 H -4.251776 -1.319143 1.338521  
 H -3.748079 1.956046 -1.303673  
 H -5.391251 1.487814 -0.823009  
 H -4.100861 1.548348 0.381008  
 O -0.354683 1.855496 0.383502  
 C -0.367179 3.157674 -0.122081  
 H 0.141897 3.772700 0.629945  
 H 0.154629 3.222140 -1.081323  
 O -1.663698 3.637262 -0.353296  
 C -2.401193 3.811390 0.843485

H	-3.397371	4.154469	0.564218
H	-2.487249	2.873039	1.400771
H	-1.925612	4.564313	1.485783
H	-1.127753	1.250829	-1.412443
H	-1.998277	0.113936	0.851896
H	-4.249243	-2.093790	-2.867098
H	-5.619991	-0.981188	-2.742509
H	-4.098420	-0.430528	-3.461046

## TS-5.out

ZPE	0.687960
DE	0.728160
DH	0.729104
DG	0.615128
E	-1722.112161
H	-1721.383057
G	-1721.497034
F	-538.730

## Cartesian coordinates

C	4.989179	-1.428178	-0.347412
C	3.995440	-1.889077	-1.214156
C	4.835893	-0.218967	0.351342
C	3.787580	0.691301	0.157170
H	5.754296	0.184079	0.774257
C	2.457395	0.353222	-0.135732
C	2.632451	-1.643702	-1.033876
H	4.328458	-2.345730	-2.146528
C	2.062185	-1.891379	0.369976
C	1.549120	-0.501989	0.779734
H	1.913894	1.153043	-0.635987
H	2.926893	-2.075515	1.012769
C	1.775959	-0.205048	2.262728
H	1.423589	0.795489	2.523394
H	2.841198	-0.274248	2.497857
H	1.246364	-0.927252	2.890852
C	1.186786	-3.138340	0.462639
H	0.902887	-3.339017	1.499534
H	1.754766	-4.003501	0.106442
H	0.276747	-3.074169	-0.138195
C	1.733120	-1.871475	-2.230365
H	1.367780	-2.904312	-2.252800
H	0.856648	-1.221763	-2.230109
H	2.277997	-1.685646	-3.158564
C	6.352591	-2.072505	-0.382543
H	7.150970	-1.361974	-0.155655
H	6.548006	-2.516886	-1.362737
H	6.410204	-2.882479	0.352609
C	4.165267	2.157714	0.087155
H	5.246579	2.306486	0.120201
H	3.792072	2.592362	-0.846004
H	3.711706	2.728758	0.903773
C	0.076819	-0.221819	0.379277
H	-0.056506	-0.607074	-0.633847
C	-0.995378	-0.930089	1.248017
H	-0.619292	-1.914930	1.536677
O	-0.173457	1.164315	0.394641
O	-1.234440	-0.172367	2.421934
Si	-1.071658	2.061856	-0.700857
C	-2.909646	1.979190	-0.339023
H	-3.405779	2.869810	-0.740546
H	-3.382644	1.104206	-0.792014
H	-3.097492	1.949098	0.738648
C	-0.724064	1.424335	-2.426573
H	-1.271691	2.014267	-3.168813
H	0.341879	1.475228	-2.669574
H	-1.048881	0.383592	-2.530356
C	-0.470224	3.843398	-0.464291

C	1.061162	3.898736	-0.518052
H	1.452603	3.503715	-1.461949
H	1.408185	4.936470	-0.424791
H	1.505467	3.320511	0.295272
C	-0.943881	4.371489	0.898611
H	-0.570561	3.754268	1.722273
H	-0.576431	5.394088	1.056161
H	-2.036222	4.400191	0.967097
C	-1.047966	4.728538	-1.579749
H	-2.142909	4.706060	-1.600505
H	-0.686651	4.423637	-2.567404
H	-0.744715	5.772168	-1.425515
C	-1.518529	-0.937218	3.558168
H	-0.804758	-1.761673	3.663617
H	-1.435611	-0.247851	4.405823
O	-2.786723	-1.535537	3.529748
C	-3.846995	-0.605803	3.673704
H	-3.780088	-0.085253	4.637370
H	-3.847000	0.138902	2.870359
H	-4.778306	-1.170920	3.634983
C	-2.272945	-1.131463	0.474619
H	-3.177207	-0.731261	0.921642
C	-2.363322	-1.740412	-0.706743
H	-1.504087	-2.162115	-1.217366
C	-3.661182	-1.831403	-1.399692
O	-4.718010	-1.400285	-0.992988
O	-3.530842	-2.455069	-2.581671
C	-4.722746	-2.588766	-3.362982
H	-4.423177	-3.111262	-4.268983
H	-5.472559	-3.170258	-2.823990
H	-5.130029	-1.607528	-3.612398

## TS-5-TMS.out

ZPE	0.601972
DE	0.638614
DH	0.639558
DG	0.531368
E	-1604.177340
H	-1603.537782
G	-1603.645973
F	-540.738

## Cartesian coordinates

C	-4.957460	0.027121	-1.081900
C	-3.983953	-0.601339	-1.865655
C	-4.772905	0.208159	0.298436
C	-3.698209	-0.312670	1.033348
H	-5.678538	0.438968	0.856326
C	-2.383625	-0.431392	0.568336
C	-2.612812	-0.525626	-1.620968
H	-4.343042	-1.300051	-2.622129
C	-2.019113	0.863393	-1.349791
C	-1.502669	0.749287	0.094181
H	-1.820839	-1.195166	1.100953
H	-2.870660	1.547056	-1.296068
C	-1.765752	2.024540	0.897061
H	-1.400918	1.932219	1.922089
H	-2.839263	2.228768	0.923165
H	-1.270313	2.883171	0.436452
C	-1.125340	1.371421	-2.477581
H	-1.691088	1.376890	-3.414362
H	-0.238668	0.751111	-2.631616
H	-0.800430	2.397685	-2.284368
C	-1.736398	-1.557492	-2.296684
H	-1.528344	-1.265720	-3.332561
H	-0.773066	-1.680481	-1.800376
H	-2.229790	-2.531477	-2.313502
C	-6.335417	0.239135	-1.657971

H	-7.113962	0.194063	-0.892723
H	-6.555103	-0.508571	-2.425635
H	-6.399938	1.220299	-2.140524
C	-4.017300	-0.964253	2.364287
H	-5.085867	-0.941002	2.588613
H	-3.701430	-2.013541	2.344906
H	-3.478208	-0.485086	3.187648
C	-0.023495	0.291452	0.221881
H	0.125604	-0.509247	-0.508349
C	1.065613	1.337517	-0.106931
H	0.807425	1.831116	-1.046412
O	0.225898	-0.194365	1.523377
O	1.152326	2.305604	0.924544
Si	0.854037	-1.683609	1.973873
C	-0.180118	-2.235028	3.427729
H	0.184695	-3.187470	3.826672
H	-0.141931	-1.496791	4.235308
H	-1.227947	-2.366050	3.139318
C	2.641343	-1.503899	2.491820
H	2.968400	-2.407806	3.018223
H	3.306163	-1.357423	1.635118
H	2.769603	-0.656982	3.173756
C	0.711744	-2.890497	0.551121
C	1.484374	3.589906	0.480172
H	0.859489	3.881776	-0.370980
H	1.303655	4.253015	1.333622
O	2.808954	3.704196	0.034570
C	3.762175	3.635986	1.081472
H	3.605808	4.447438	1.803481
H	3.717639	2.678539	1.610523
H	4.747105	3.745508	0.627417
C	2.384430	0.631353	-0.271686
H	3.098543	0.744090	0.538648
C	2.685175	-0.156199	-1.301617
H	1.999986	-0.307728	-2.129742
C	3.954831	-0.903960	-1.327058
O	4.822803	-0.858994	-0.482504
O	4.036896	-1.677812	-2.420647
C	5.220889	-2.472703	-2.546611
H	5.305714	-3.169090	-1.710636
H	5.109716	-3.019894	-3.480252
H	6.107376	-1.837611	-2.585790
H	1.331972	-2.588264	-0.299025
H	1.054696	-3.878881	0.876446
H	-0.321833	-2.991138	0.205074

## TS-5-MOM.out

ZPE	0.495766
DE	0.523977
DH	0.524922
DG	0.434279
E	-1120.245916
H	-1119.720995
G	-1119.811638
F	-544.982

## Cartesian coordinates

C	4.330226	-0.984500	0.828102
C	4.216260	-0.592080	-0.508074
C	3.379525	-0.594315	1.788490
C	2.327213	0.298078	1.550765
H	3.700794	-0.704672	2.822619
C	1.617719	0.389964	0.345837
C	3.001948	-0.390099	-1.169129
H	5.138109	-0.292573	-1.008201
C	1.933451	-1.486121	-1.039514
C	0.813935	-0.767778	-0.282516
H	1.147395	1.365007	0.202649

H	2.345376	-2.233174	-0.355149
C	0.154748	-1.675691	0.759171
H	-0.535184	-1.126311	1.405492
H	0.911595	-2.137092	1.399102
H	-0.408641	-2.473946	0.263133
C	1.584081	-2.202618	-2.338744
H	0.823127	-2.966976	-2.153911
H	2.466783	-2.702108	-2.749135
H	1.198528	-1.522294	-3.102072
C	3.039836	0.420535	-2.444962
H	3.769746	1.229046	-2.367627
H	3.321481	-0.211694	-3.294951
H	2.071730	0.863437	-2.682867
C	5.634664	-1.570356	1.309377
H	5.843840	-1.313190	2.350499
H	6.467986	-1.227260	0.689481
H	5.610714	-2.662955	1.235787
C	2.035272	1.343791	2.606613
H	1.056921	1.176140	3.069929
H	2.790992	1.365948	3.394649
H	1.996128	2.335088	2.141314
C	-0.261450	-0.183355	-1.215298
H	-0.746994	-1.000823	-1.756806
C	-1.323146	0.668934	-0.503840
H	-0.981667	0.940699	0.499443
C	-2.649198	-0.027833	-0.408312
H	-3.104376	-0.313491	-1.353550
C	-3.266304	-0.286337	0.742474
H	-2.823637	-0.004676	1.692548
C	-4.569646	-0.970883	0.857474
O	-5.115798	-1.185488	1.918453
O	-5.092252	-1.331269	-0.320321
C	-6.359783	-1.995502	-0.276351
H	-6.613868	-2.210032	-1.312125
H	-6.287620	-2.923340	0.293345
H	-7.116760	-1.348791	0.170257
H	0.201427	0.461517	-1.964456
O	-1.497136	1.873339	-1.264573
C	-1.949685	2.963692	-0.503610
H	-2.225436	3.733626	-1.232514
H	-2.814294	2.692765	0.110520
O	-0.980984	3.441391	0.388886
C	0.139271	4.022946	-0.256183
H	0.657611	3.301178	-0.895829
H	-0.165946	4.882524	-0.866710
H	0.819870	4.361793	0.524941

## TS-6.out

ZPE	0.434588
DE	0.457718
DH	0.458662
DG	0.385032
E	-929.290232
H	-928.831569
G	-928.905200
F	-443.945

## Cartesian coordinates

C	-3.742929	-1.466312	0.195424
C	-2.304947	-1.370549	-2.291800
C	-2.270955	-1.043050	0.267898
C	-1.533032	-1.385576	-1.000844
C	1.906982	-2.685619	-0.356986
C	-0.221571	-1.666104	-1.039549
C	0.764877	-1.774388	0.024308
C	0.750706	0.295715	3.226010
C	0.773780	-1.288462	1.319966
C	0.179582	-0.154114	1.902325

C	-0.705104	0.746618	1.292177
C	-3.133132	0.913161	1.661021
C	-2.069909	0.470393	0.636163
C	-2.123960	1.390820	-0.555174
C	-0.853154	2.892759	-2.114968
C	-0.985419	1.952919	-0.953640
C	0.262194	1.601434	-0.192825
C	1.263150	0.876742	-0.849935
H	-4.216614	-1.399707	1.175605
H	-4.319070	-0.851296	-0.501463
H	-3.817794	-2.506329	-0.132736
H	-3.061789	-2.160712	-2.315315
H	-1.641692	-1.507668	-3.147842
H	-2.836613	-0.422087	-2.416775
H	-1.815914	-1.608175	1.087408
H	2.434443	-2.263249	-1.218295
H	2.625202	-2.809278	0.454337
H	1.534715	-3.671130	-0.656321
H	0.190493	-1.905016	-2.018176
H	-0.034782	0.347066	3.986974
H	1.539478	-0.367785	3.584288
H	1.172590	1.300369	3.122640
H	1.559309	-1.720141	1.934623
H	-0.818054	1.639139	1.907858
H	-2.941667	1.941997	1.977387
H	-4.137035	0.880570	1.232225
H	-3.115606	0.272506	2.548186
H	-3.071570	1.584577	-1.051303
H	-0.387608	3.833588	-1.802650
H	-0.209925	2.461036	-2.888617
H	-1.826963	3.115688	-2.556946
H	0.645443	2.382293	0.464059
H	1.080188	0.389365	-1.796624
C	2.569440	0.770640	-0.273816
O	2.904496	1.183690	0.829309
O	3.448457	0.113060	-1.085613
C	4.722197	-0.171668	-0.520483
H	4.623476	-0.784939	0.378825
H	5.271451	-0.722676	-1.283009
H	5.259526	0.745839	-0.269529

TS-7.out

ZPE	0.433075
DE	0.457376
DH	0.458320
DG	0.379735
E	-929.285916
H	-928.827596
G	-928.906181
F	-527.558

Cartesian coordinates

C	-3.670133	-1.584158	-0.103696
C	-3.673182	-0.445478	-0.917618
C	-2.471560	-2.119537	0.397137
C	-1.187429	-1.694950	0.022692
H	-2.550580	-3.130148	0.793031
C	-0.825606	-0.376262	-0.280431
C	-2.740251	0.582735	-0.803337
H	-4.357609	-0.446732	-1.766498
C	-2.416982	1.101076	0.600832
C	-0.917923	0.806997	0.715246
H	0.026876	-0.308876	-0.956133
H	-2.907971	0.421994	1.301926
C	-0.545317	0.434107	2.161346
H	0.498535	0.128750	2.258511
H	-1.177989	-0.386617	2.510945
H	-0.705900	1.295272	2.818435
C	-2.929210	2.504312	0.906261
H	-2.600330	2.816610	1.902418
H	-4.023010	2.514090	0.895564
H	-2.587057	3.253228	0.188466
C	-2.591562	1.554201	-1.949409
H	-3.373261	2.321426	-1.909919
H	-1.629895	2.071990	-1.915815
H	-2.668369	1.040162	-2.909507
C	-4.926350	-2.412671	0.000305
H	-4.710692	-3.469362	0.174377
H	-5.526805	-2.323510	-0.909698
H	-5.548583	-2.058636	0.829229
C	-0.155596	-2.767434	-0.263762
H	-0.556924	-3.773447	-0.123937
H	0.183545	-2.681829	-1.302623
H	0.731250	-2.652336	0.367777
C	-0.044938	1.962790	0.265144
H	-0.549218	2.920434	0.173636
C	1.275362	1.975056	0.002976
C	1.953668	3.250546	-0.425128
H	2.764423	3.516599	0.260652
H	2.396173	3.145804	-1.421107
H	1.243572	4.078530	-0.453904
C	2.105371	0.776595	0.117363
H	1.639422	-0.138209	0.467322
C	3.411807	0.707389	-0.173013
H	3.983215	1.554696	-0.532616
C	4.132365	-0.567870	-0.015314
O	3.656752	-1.611582	0.377424
O	5.421773	-0.440552	-0.371137
C	6.227242	-1.618724	-0.266358
H	5.841941	-2.406620	-0.915889
H	7.224019	-1.323059	-0.586967
H	6.254363	-1.975444	0.764614



A saturated aqueous solution of  $\text{NH}_4\text{Cl}$  (0.4 mL) was added and all solvents were evaporated under reduced pressure. To the remaining residue was added acetone (0.8 mL) and the resulting suspension was stirred for 20 min at room temperature. The mixture was filtered through a pad of celite and the filtrate was concentrated under reduced pressure and submitted to HPLC purification ( $\text{H}_2\text{O}/\text{ACN}$ , gradient, 40 to 90%) yielding **3.94** (3.8 mg, 16.2  $\mu\text{mol}$ , 97% yield) as yellow oil,  $^1\text{H}$  NMR shows two isomers in ratio 1:0.25.

**<sup>1</sup>H NMR** (400 MHz, CDCl<sub>3</sub>, \* denotes minor isomer) δ 7.24–7.07 (m, 2H+2H\*), 4.09 (dd, *J* = 9.9, 6.9 Hz, 1H\*), 3.99 (dd, *J* = 10.1, 6.9 Hz, 1H), 3.78 (dt, *J* = 11.4, 7.9 Hz, 1H+1H\*), 3.30 (ddd, *J* = 11.8, 8.9, 4.0 Hz, 1H), 3.25 (ddd, *J* = 11.9, 8.0, 4.0 Hz, 1H\*), 2.62 (dq, *J* = 13.4, 6.6 Hz, 1H+1H\*), 2.26 – 2.02 (m, 3H+3H\*), 1.56 (dt, *J* = 20.5, 10.1 Hz, 1H+1H\*), 1.14 (d, *J* = 6.8 Hz, 6H+6H\*)

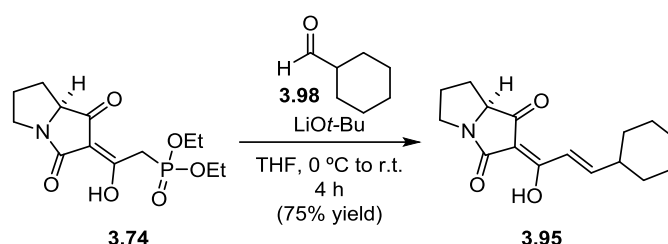
**<sup>13</sup>C NMR** (100 MHz, CDCl<sub>3</sub>, \* denotes minor isomer) δ 202.4\*, 195.1, 177.5, 176.0\*, 174.7, 175.6\*, 174.3, 170.7\*, 157.7\*, 156.8, 118.7, 118.3\*, 101.4, 68.8, 66.4\*, 43.4\*, 43.1, 32.2\*, 32.0, 27.2\*, 27.1\*, 26.9, 26.8, 21.3, 21.2\*

**IR** (ATR): 3350 (br w), 2962 (m), 2927 (m), 1700 (s), 1640 (s), 1582 (s), 1363 (m), 1244 (m), 1191 (m), 1025(w), 911 (s), 729 (s)

**HRMS** (+ESI): calc. for C<sub>13</sub>H<sub>17</sub>NNaO<sub>3</sub> [M+Na]<sup>+</sup> 258.1101 found 258.1110

[α]<sub>D</sub><sup>26</sup> –11.6° (c 0.17, CHCl<sub>3</sub>)

*R*<sub>F</sub> = 0.35 (1% MeOH in DCM)



#### Tetramic acid **3.95**.

To a solution of phosphonate **3.74** (8.24 mg, 26.0 μmol, 1.50 equiv.) in THF (0.6 mL) at 0 °C was added LiOt-Bu (4.2 mg, 52 μmol, 3.0 equiv.). The orange suspension was stirred at 0 °C for 30 min after which **3.98** (2.0 μL, 17 μmol, 1.0 equiv.) in THF (120 μL) was added. The reaction was stirred at room temperature for 4 h. A saturated aqueous solution of NH<sub>4</sub>Cl (0.4 mL) was added and all solvents were evaporated under reduced pressure. To the remaining residue was added acetone (0.6 mL) and the resulting suspension was stirred for 20 min at room temperature. The mixture was filtered through a pad of celite and the filtrate was concentrated under reduced pressure and submitted to HPLC purification (H<sub>2</sub>O/ACN, gradient, 40 to 90%) yielding **3.95** (3.6 mg, 13.1 μmol, 75% yield) as yellow oil, <sup>1</sup>H NMR shows two isomers in ratio 1:0.25.

**<sup>1</sup>H NMR** (400 MHz, CDCl<sub>3</sub>, \* denotes minor isomer) δ 13.66 (br s, 1H), 7.20–7.03 (m, 2H+2H\*), 4.06 (dd, *J* = 9.9, 6.9 Hz, 1H\*), 3.96 (dd, *J* = 10.1, 6.8 Hz, 1H), 3.75 (dt, *J* = 11.3, 7.9 Hz, 1H+1H\*), 3.27 (ddd, *J* = 11.4, 8.8, 4.0 Hz, 1H), 3.21 (ddd, *J* = 11.9, 8.0, 3.9 Hz, 1H\*), 2.37–2.2 (m, 1H+1H\*), 2.23–2.00 (3H+3H\*), 1.79 (td, *J* = 13.2, 3.2 Hz, 4H+4H\*), 1.69 (br d, *J* = 16.1, 1H+1H\*), 1.53 (dtd, *J* = 11.6, 10.1, 8.4 Hz, 1H+1H\*), 1.39–1.12 (5H+5H\*)

**<sup>13</sup>C NMR** (100 MHz, CDCl<sub>3</sub>, \* denotes minor isomer) δ 203.0\*, 195.12, 194.81\*, 177.49, 176.07\*, 174.73, 156.60\*, 155.68, 119.05\*, 116.1\*, 105.8\*, 101.36, 68.74, 66.42\*, 43.37\*, 43.11, 41.52, 31.69, 31.67, 31.61, 31.58\*, 27.14\*, 27.04\*, 26.88, 26.85, 25.86, 25.62, 25.60\*.

**IR** (ATR): 3320 (br w), 2924 (s), 2852 (m), 1702 (s), 1638 (s), 1575 (s), 1429 (s), 1352 (m), 1242 (m), 986(w), 945 (w), 731 (w)

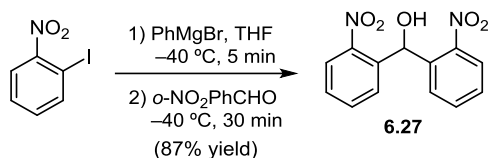
**HRMS** (+ESI): calc. for C<sub>13</sub>H<sub>17</sub>NNaO<sub>3</sub> [M+H]<sup>+</sup> 298.1414 found 298.1401

[α]<sub>D</sub><sup>26</sup> –35.08 (c 0.32, CHCl<sub>3</sub>)

*R*<sub>F</sub> = 0.38 (1% MeOH in DCM)

## 8.6 Supporting Information for Chapter 6.1

### 8.6.1 Experimental Procedures for Chapter 6.1



The synthesis of Benzhydrol **6.27** was accomplished by a modification of the procedure by Knochel et al.<sup>[325]</sup>

#### Benzhydrol **6.27**.

A dry flask was charged with 2-iodonitrobenzene (500 mg, 2.01 mmol, 1.00 equiv.). Dry THF (8.0 mL) was added and the mixture was cooled to  $-40\text{ }^{\circ}\text{C}$ . PhMgBr (0.74 mL, 2.21 mmol, 1.10 equiv., 3M in THF) was added dropwise. The I-Mg exchange was complete after 5 min. 2-nitrobenzaldehyde (364 mg, 2.41 mmol, 1.20 equiv.) was added to the Grignard. The reaction was stirred for 30 min at  $-40\text{ }^{\circ}\text{C}$ .

A saturated NH<sub>4</sub>Cl solution (2.0 mL) was added to the reaction mixture and the mixture was poured into water (25 mL). The aqueous phase was extracted five times with DCM and the combined organic layers were washed with brine, dried over Na<sub>2</sub>SO<sub>4</sub>, filtered and concentrated under reduced pressure. Purification of the crude material by flash column chromatography on silica gel (EtOAc/Hexanes 35%) afforded benzhydrol **6.27** as a brown solid, (480 mg, 1.75 mmol, 87% yield).

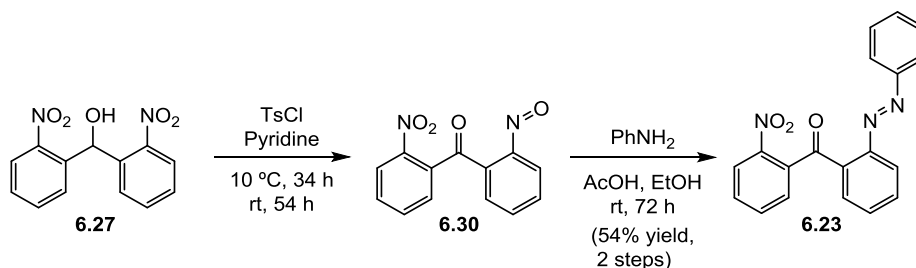
<sup>1</sup>H NMR (400 MHz, CDCl<sub>3</sub>)  $\delta$  8.05 (dd,  $J$  = 8.1, 1.1 Hz, 2H), 7.66–7.57 (m, 4H), 7.50 (ddd,  $J$  = 8.7, 7.2, 1.8 Hz, 2H), 6.93 (d,  $J$  = 4.2 Hz, 1H), 3.60 (d,  $J$  = 4.2 Hz, 1H)

<sup>13</sup>C NMR (100 MHz, CDCl<sub>3</sub>)  $\delta$  148.00, 136.97, 133.77, 128.89, 128.79, 125.06, 67.47

IR (ATR): 3525 (br w), 1750 (w), 1682 (w), 1608 (w), 1577 (w), 1520 (s), 1342 (s), 1297 (m), 1176 (m), 1078 (w), 1024 (m), 933 (w), 855 (m), 737 (s)

HRMS (+ESI): calc. for C<sub>13</sub>H<sub>9</sub>N<sub>2</sub>O<sub>4</sub> [M-OH]<sup>+</sup> 257.0557 found 257.0555

$R_f$  = 0.51 (40% EtOAc in hexanes)



#### Azobenzophenone **6.23**.

To a solution of benzhydrol **6.27** (100 mg, 0.365 mmol, 1.00 equiv.) in pyridine (3.7 mL) at  $10\text{ }^{\circ}\text{C}$  was added TsCl (139 mg, 0.729 mmol, 2.00 equiv.) and the mixture was stirred at the same temperature for 34 hours before it was warmed up to room temperature and stirred for 54 additional hours. The solvent was

evaporated under reduced pressure at 22 °C and the crude material containing **6.30** was immediately submitted to the following step.

The crude material was dissolved in acetic acid (2.2 mL) and aniline (40 µL, 0.422 mmol, 1.00 equiv.) was added. The reaction mixture was stirred at room temperature for 48 h, after which more aniline (40 µL, 0.422 mmol, 1.00 equiv.) was added and the reaction was stirred for additional 48 h.

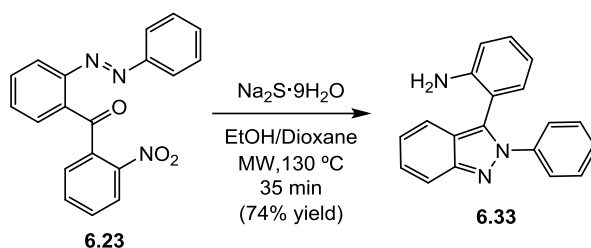
Water and DCM were added to the mixture. The phases were separated and the aqueous layer was extracted four times with DCM. The organic layers were combined, washed with saturated aqueous bicarbonate and brine, dried over anhydrous MgSO<sub>4</sub>, filtered and concentrated under reduced pressure to afford a red solid.

Purification of the crude material by flash column chromatography on silica gel (EtOAc/Hexanes 15%) afforded benzhydrol **6.27** as an intense red solid (74 mg, 0.223 mmol, 54% yield).

**<sup>1</sup>H NMR** (400 MHz, CDCl<sub>3</sub>) δ 8.08 (dd, *J* = 7.7, 1.5 Hz, 1H), 7.93 (dd, *J* = 8.2, 0.9 Hz, 1H), 7.70 – 7.55 (m, 4H), 7.51 (dd, *J* = 7.6, 1.4 Hz, 1H), 7.47 (ddd, *J* = 8.3, 7.5, 1.5 Hz, 1H), 7.43 – 7.38 (m, 1H), 7.36 – 7.27 (m, 4H)

**<sup>13</sup>C NMR** (100 MHz, CDCl<sub>3</sub>) 193.38, 152.19, 151.21, 146.75, 138.65, 133.97, 133.61, 133.45, 131.65, 130.69, 130.62, 130.05, 129.05, 128.79, 124.08, 123.09, 116.68

**HRMS** (+ESI): calc. for C<sub>19</sub>H<sub>14</sub>N<sub>3</sub>O<sub>3</sub> [M+H]<sup>+</sup> 332.1030 found 332.1031



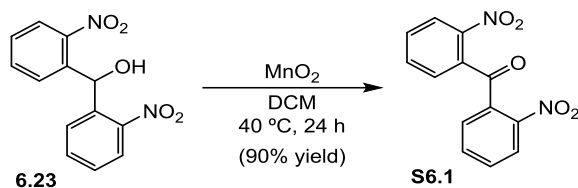
### Imidazole **6.33**.

To a solution of azobenzophenone **6.23** (47.0 mg, 0.142 mmol, 1.00 equiv.) in EtOH/Dioxane (1.2 mL each) at room temperature was added a solution of sodium sulfide nonahydrate (136 mg, 0.567 mmol, 4.00 equiv.) in water (0.47 mL) and the mixture was stirred in a microwave at 130 °C for 35 minutes.

After cooling to room temperature the mixture was partitioned between water and Et<sub>2</sub>O. The organic layer was separated and the aqueous phase was extracted twice with Et<sub>2</sub>O. The organic layers were combined, washed with saturated aqueous bicarbonate, water, dried over anhydrous MgSO<sub>4</sub>, filtered and concentrated under reduced pressure to afford a yellowish solid containing pure **6.33** (30 mg, 0.105 mmol, 74% yield).

**<sup>1</sup>H NMR** (400 MHz, CDCl<sub>3</sub>) δ 7.82 (d, *J* = 8.8 Hz, 1H), 7.56 (d, *J* = 8.5 Hz, 1H), 7.50 (d, *J* = 7.8 Hz, 2H), 7.36 (dt, *J* = 10.6, 7.1 Hz, 4H), 7.22 (t, *J* = 8.4 Hz, 1H), 7.16 – 7.07 (m, 1H), 6.99 (dd, *J* = 7.6, 1.1 Hz, 1H), 6.78 (d, *J* = 8.1 Hz, 1H), 6.73 (t, *J* = 7.5 Hz, 1H)

**HRMS** (+ESI): calc. for C<sub>19</sub>H<sub>19</sub>N<sub>4</sub> [M+NH<sub>4</sub>]<sup>+</sup> 303.1604 found 303.1583



### Benzophenone **S6.1**.

$\text{MnO}_2$  (8.350 g, 96.0 mmol, 10.3 equiv.) was added to a solution of **6.23** (2.56 g, 9.34 mmol, 1.00 equiv.) in DCM (44 mL) and the reaction mixture was refluxed for 22 h (40 °C) before more  $\text{MnO}_2$  (1.28 g, 14.8 mmol, 1.5 equiv.) was added and the suspension was stirred for an additional 2 h.

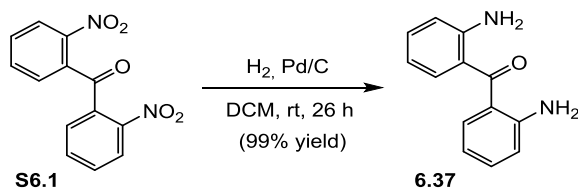
The suspension was filtered through a pad of celite and washed with DCM. The filtrate was concentrated under reduced pressure affording a white solid (2.30 g, 8.45 mmol, 91% yield).

$^1\text{H}$  NMR (400 MHz,  $\text{CDCl}_3$ )  $\delta$  7.97 (dd,  $J$  = 5.9, 3.5 Hz, 1H), 7.70 (dd,  $J$  = 6.0, 3.4 Hz, 2H), 7.61 (dd,  $J$  = 5.8, 3.4 Hz, 1H)

$^{13}\text{C}$  NMR (100 MHz,  $\text{CDCl}_3$ )  $\delta$  189.77, 148.24, 132.95, 132.72, 132.48, 130.51, 124.43

HRMS (+APCI): calc. for  $\text{C}_{13}\text{H}_9\text{N}_2\text{O}_5$   $[\text{M}+\text{H}]^+$  273.0506 found 273.0505

$R_f$  = 0.36 (40% EtOAc in hexanes)



### Diamine **6.37**.

To a stirred solution of **S6.1** (61 mg, 0.224 mmol, 1.00 equiv.) in DCM (9.8 mL) was added Pd/C (10% Pd on activated charcoal, 23.8 mg, 0.022 mmol, 0.10 equiv.) and the reaction vessel was backfilled three times with  $\text{H}_2$ . The mixture was stirred under  $\text{H}_2$  atmosphere for 20 h before it was filtered through a pad of Celite washing with DCM. The solvent was evaporated under reduced pressure and submitted to purification by flash column chromatography on silica gel (EtOAc/Hexanes 20%), which delivered diamine **6.37** as an intense yellow solid (47 mg, 0.221 mmol, 99% yield).

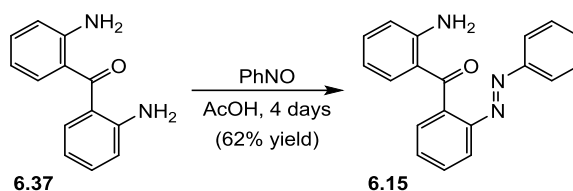
$^1\text{H}$  NMR (400 MHz,  $\text{CDCl}_3$ )  $\delta$  7.36 (dd,  $J$  = 7.9, 1.4 Hz, 2H), 7.26 (dd,  $J$  = 15.4, 1.5 Hz, 2H), 6.73 (dd,  $J$  = 8.2, 0.9 Hz, 2H), 6.69 – 6.60 (m, 2H), 5.45 (br s, 4H)

$^{13}\text{C}$  NMR (100 MHz,  $\text{CDCl}_3$ )  $\delta$  200.18, 149.28, 133.26, 133.05, 120.92, 116.88, 115.90

IR (ATR): 3469 (br m), 3355 (br m), 3026 (w), 2360 (w), 1604 (s), 1578 (s), 1542 (s), 1483 (s), 1450 (s), 1299 (s), 1237 (s), 1158 (s), 1029 (w), 929 (s), 749 (s)

HRMS (+APCI): calc. for  $\text{C}_{13}\text{H}_{13}\text{N}_2\text{O}$   $[\text{M}+\text{H}]^+$  213.1022 found 213.1024

$R_f$  = 0.28 (20% EtOAc in hexanes)



### Azobenzophenone 6.15.

**6.37** (550 mg, 2.59 mmol, 1.00 equiv.) and nitrosobenzene (278 mg, 2.59 mmol, 1.00 equiv.) were dissolved in acetic acid (18 mL). The reaction mixture was stirred at room temperature for 24 h before additional nitrosobenzene (55.6 mg, 0.518 mmol, 0.20 equiv.) were added. The mixture was further stirred for 24 hours, after which additional nitrosobenzene (139 mg, 1.30 mmol, 0.50 equiv.) was added. The reaction was stirred for an additional 48 h before the solvent was evaporated under reduced pressure. The brown residue was submitted to purification by flash column chromatography on silica gel (EtOAc/hexanes, gradient, 10 to 15%) affording azobenzophenone **6.15** as a red solid (630 mg, 1.61 mmol, 62% yield).

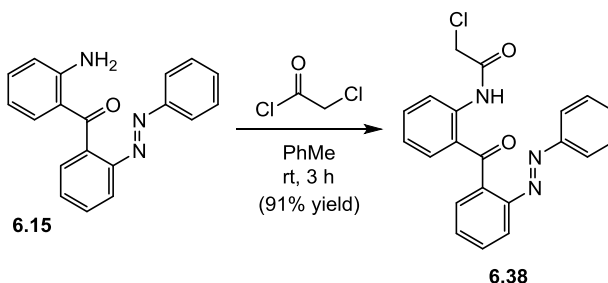
**<sup>1</sup>H NMR** (400 MHz, CDCl<sub>3</sub>) δ 7.93 (dd, *J* = 7.9, 1.1 Hz, 1H), 7.65 – 7.56 (m, 3H), 7.56 (td, *J* = 7.4, 1.5 Hz, 1H), 7.50 (dd, *J* = 7.4, 1.6 Hz, 1H), 7.37 (dd, *J* = 5.2, 1.7 Hz, 3H), 7.20 (ddd, *J* = 8.4, 7.1, 1.5 Hz, 1H), 7.14 (dd, *J* = 8.1, 1.4 Hz, 1H), 6.70 (d, *J* = 8.3 Hz, 1H), 6.43 (t, *J* = 8.1 Hz, 1H), 6.37 (br s, 2H)

**<sup>13</sup>C NMR** (100 MHz, CDCl<sub>3</sub>) δ 199.23, 152.17, 150.35, 149.66, 138.29, 134.42, 134.30, 131.17, 130.73, 129.97, 128.89, 128.11, 122.95, 119.71, 119.35, 116.64, 115.68

**IR** (ATR): 3475 (br m), 3345 (br m), 3060 (w), 2359 (w), 2342 (w), 1610 (s), 1583 (s), 1548 (s), 1479 (m), 1450 (m), 1302 (s), 1244 (s), 1159 (m), 933 (m), 774 (s), 751 (s)

**HRMS** (+ESI): calc. for C<sub>19</sub>H<sub>15</sub>N<sub>3</sub>NaO [M+Na]<sup>+</sup> 324.1107 found 324.1111

**R<sub>F</sub>** = 0.28 (15% EtOAc in hexanes)



### Azobenzophenone 6.38.

To a solution of **6.15** (271 mg, 0.896 mmol, 1.00 equiv.) in toluene (2.0 mL) at 10 °C was slowly added chloroacetyl chloride (76.0 μL, 0.953 mmol, 1.06 equiv.). The reaction mixture was stirred at room temperature for 3 h before the solvent was evaporated under reduced pressure.

To the crude residue was added 96% ethanol (0.87 mL) and the resulting mixture was stirred at room temperature for 20 hours. The suspension was filtered and the remaining solid was washed with 96% ethanol (3 x 0.2 mL). The solid was dried under high vacuum over 3 days yielding **6.38** as a red solid (308 mg, 0.815 mmol, 91% yield).

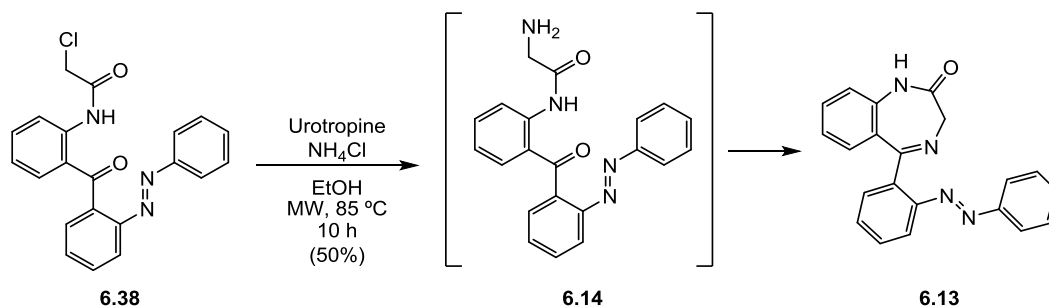
**<sup>1</sup>H NMR** (400 MHz, CDCl<sub>3</sub>) δ 12.35 (s, 1H), 8.71 (d, *J* = 8.5 Hz, 1H), 8.00 (dd, *J* = 7.8, 0.9 Hz, 1H), 7.69 (td, *J* = 7.6, 1.6 Hz, 1H), 7.61 (td, *J* = 7.4, 1.2 Hz, 1H), 7.56 (dd, *J* = 7.5, 1.4 Hz, 1H), 7.51–7.43 (m, 3H), 7.40–7.33 (m, 3H), 7.31 (dd, *J* = 7.9, 1.5 Hz, 1H), 6.95 (t, *J* = 8.2 Hz, 1H), 4.26 (s, 2H)

**$^{13}\text{C}$  NMR** (100 MHz,  $\text{CDCl}_3$ )  $\delta$  200.69, 165.71, 151.75, 150.08, 139.31, 135.78, 134.51, 133.29, 131.65, 131.05, 130.89, 129.04, 128.41, 124.47, 123.24, 122.74, 121.79, 120.55, 43.32

**IR** (ATR): 3201 (br w), 3060 (br w), 1685 (m), 1640 (m), 1582 (m), 1518 (s), 1446 (s), 1295 (m), 1275 (m), 1247 (s), 1159 (m), 963 (w), 927 (m), 753 (s)

**HRMS** (+ESI): calc. for  $\text{C}_{21}\text{H}_{17}\text{ClN}_3\text{O}_2$   $[\text{M}+\text{H}]^+$  378.1004 found 378.1008

$R_f$  = 0.52 (30% EtOAc in hexanes)



### Benzodiazepine 6.13.

To a suspension of ammonium chloride (39.6 mg, 0.741 mmol, 3.00 equiv.) and urotropine (79.2 mg, 0.565 mmol, 2.27 equiv.) in EtOH (950  $\mu\text{L}$ ) was added **6.38** (94.0 mg, 0.249 mmol, 1.00 equiv.) and the mixture was stirred in the microwave at 85  $^\circ\text{C}$  for 10 h.

The crude mixture was partitioned between water and ethyl acetate. The phases were separated and the aqueous phase was extracted twice with EtOAc. The organic layers were put together, dried over anhydrous  $\text{MgSO}_4$ , filtered and concentrated under reduced pressure affording an orange solid.

Purification by flash column chromatography on silica gel, (EtOAc/Hexanes, gradient 0 to 40%) afforded benzodiazepine **6.13** as an intense red crystalline solid (42.7 mg, 125  $\mu\text{mol}$ , 50% yield).

**$^1\text{H}$  NMR** (400 MHz,  $\text{CDCl}_3$ )  $\delta$  9.06 (s, 1H), 7.81–7.75 (m, 1H), 7.70–7.65 (m, 1H), 7.61–7.54 (m, 2H), 7.34–7.27 (m, 6H), 7.06 (dd,  $J$  = 16.4, 8.0 Hz, 2H), 6.94 (t,  $J$  = 7.6 Hz, 1H), 4.45 (s, 2H)

**$^{13}\text{C}$  NMR** (100 MHz,  $\text{CDCl}_3$ )  $\delta$  171.60, 171.48, 152.21, 150.30, 138.83, 136.98, 131.19, 131.16, 130.72, 130.46, 130.17, 130.00, 128.78, 123.65, 122.71, 120.55, 116.93, 56.66.

**IR** (ATR): 3063 (br w), 2969 (br w), 2922 (br w), 2359 (w), 1680 (s), 1611 (m), 1483 (m), 1370 (m), 1329 (w), 1235 (w), 1017 (w), 774 (m), 756 (m)

**HRMS** (+ESI): calc. for  $\text{C}_{21}\text{H}_{17}\text{N}_4\text{O}$   $[\text{M}+\text{H}]^+$  341.1397 found 341.1395

$R_f$  = 0.18 (50% EtOAc in hexanes)

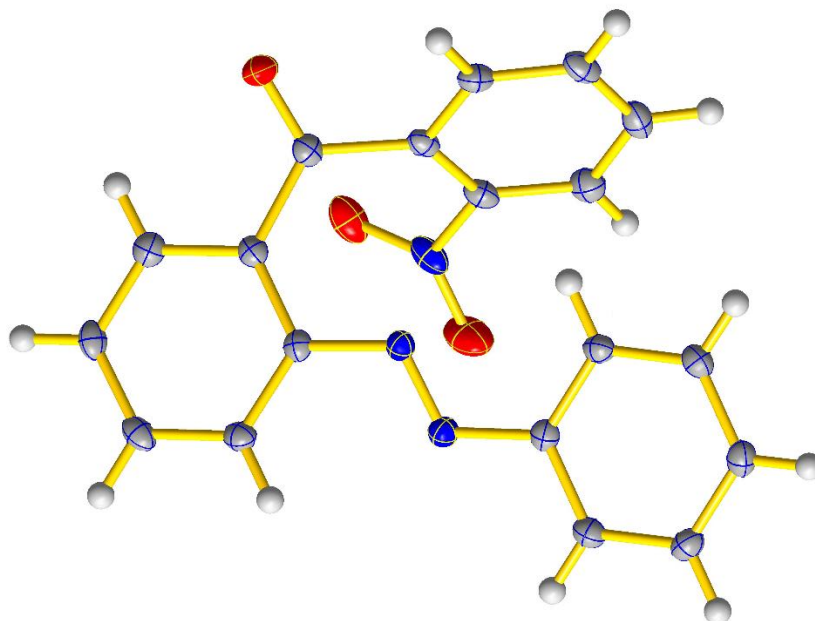
$\lambda_{\text{max}}$  = 325 nm

$t_{1/2}$  = 2.6 s

**PSS** (Z/E, 5 min 365 nm) >33/66 ( $^1\text{H}$  NMR spectroscopy in saturated  $\text{CDCl}_3$ ). The fast thermal relaxation greatly enriches the mixture with *E*-isomer.

## 8.6.2 Crystallographic Data for Chapter 6.1

### 8.6.2.1 Azobenzophenone 6.23

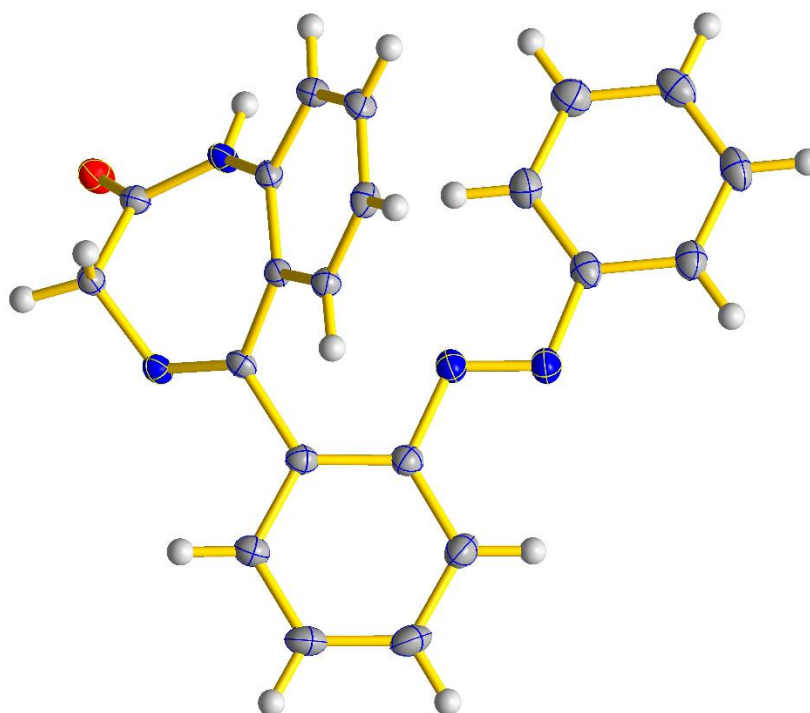


<b>Identification code</b>	18dtr5h
<b>Chemical formula</b>	C <sub>19</sub> H <sub>13</sub> N <sub>3</sub> O <sub>3</sub>
<b>Formula weight</b>	331.32 g/mol
<b>Temperature</b>	100(2) K
<b>Wavelength</b>	0.71073 Å
<b>Crystal size</b>	0.150 x 0.260 x 0.450 mm
<b>Crystal habit</b>	red block
<b>Crystal system</b>	orthorhombic
<b>Space group</b>	P 21 21 21
<b>Unit cell dimensions</b>	a = 7.1461(6) Å b = 13.1648(11) Å c = 16.4572(13) Å α = 90° β = 90° γ = 90°
<b>Volume</b>	1548.2(2) Å <sup>3</sup>
<b>Z</b>	4
<b>Density (calculated)</b>	1.421 g/cm <sup>3</sup>
<b>Absorption coefficient</b>	0.099 mm <sup>-1</sup>
<b>F(000)</b>	688
<b>Diffractometer</b>	Bruker APEX-II CCD
<b>Radiation source</b>	sealed tube, Mo
<b>Theta range for data collection</b>	1.98 to 28.28°
<b>Index ranges</b>	-9 ≤ h ≤ 9, -17 ≤ k ≤ 17, -21 ≤ l ≤ 21
<b>Reflections collected</b>	19353
<b>Independent reflections</b>	3838 [R(int) = 0.0349]
<b>Coverage of independent reflections</b>	100.0%
<b>Absorption correction</b>	multi-scan



Max. and min. transmission	0.7457 and 0.7046
Structure solution technique	direct methods
Structure solution program	SHELXT (Sheldrick 2014)
Refinement method	Full-matrix least-squares on F <sup>2</sup>
Refinement program	SHELXL-2018 (Sheldrick 2018)
Function minimized	$\sum w(F_o^2 - F_c^2)^2$
Data / restraints / parameters	3838 / 0 / 226
Goodness-of-fit on F <sup>2</sup>	1.080
Final R indices	3583 data; $I > 2\sigma(I)$ R1 = 0.0352, wR2 = 0.0918 all data R1 = 0.0381, wR2 = 0.0936
Weighting scheme	$w = 1/[\sigma^2(F_o^2) + (0.0580P)^2 + 0.0567P]$ where $P = (F_o^2 + 2F_c^2)/3$
Absolute structure parameter	-0.2(4)
Largest diff. peak and hole	0.324 and -0.203 eÅ <sup>-3</sup>
R.M.S. deviation from mean	0.042 eÅ <sup>-3</sup>

#### 8.6.2.2 Azobenzodiazepine 6.13

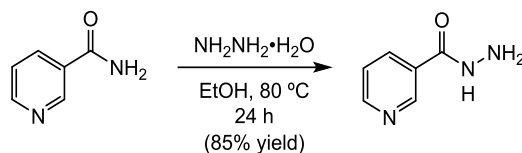


Identification code	19dtr4h
Chemical formula	C <sub>21</sub> H <sub>16</sub> N <sub>4</sub> O
Formula weight	340.38 g/mol
Temperature	100(2) K
Wavelength	0.71073 Å
Crystal size	0.350 x 0.450 x 0.560 mm
Crystal habit	red prism
Crystal system	monoclinic
Space group	P 1 21/c 1
Unit cell dimensions	a = 9.4667(6) Å

	b = 16.9844(10) Å
	c = 10.6023(6) Å
	$\alpha = 90^\circ$
	$\beta = 93.5402(9)^\circ$
	$\gamma = 90^\circ$
<b>Volume</b>	1701.45(18) Å <sup>3</sup>
<b>Z</b>	4
<b>Density (calculated)</b>	1.329 g/cm <sup>3</sup>
<b>Absorption coefficient</b>	0.085 mm <sup>-1</sup>
<b>F(000)</b>	712
<b>Diffractometer</b>	Bruker APEX-II CCD
<b>Radiation source</b>	sealed tube, MoK $\alpha$
<b>Theta range for data collection</b>	2.15 to 28.29°
<b>Index ranges</b>	-12 ≤ h ≤ 12, -22 ≤ k ≤ 22, -14 ≤ l ≤ 14
<b>Reflections collected</b>	32741
<b>Independent reflections</b>	4223 [R(int) = 0.0263]
<b>Coverage of independent reflections</b>	100.0%
<b>Absorption correction</b>	multi-scan
<b>Max. and min. transmission</b>	0.7457 and 0.7142
<b>Structure solution technique</b>	direct methods
<b>Structure solution program</b>	SHELXT (Sheldrick 2015)
<b>Refinement method</b>	Full-matrix least-squares on F <sup>2</sup>
<b>Refinement program</b>	SHELXL-2018/3 (Sheldrick, 2018)
<b>Function minimized</b>	$\sum w(F_o^2 - F_c^2)^2$
<b>Data / restraints / parameters</b>	4223 / 0 / 239
<b>Goodness-of-fit on F<sup>2</sup></b>	1.006
<b>Final R indices</b>	3772 data; R1 = 0.0397, wR2 = 0.1104 I > 2σ(I)
	all data R1 = 0.0440, wR2 = 0.1148
<b>Weighting scheme</b>	w = 1/[σ <sup>2</sup> (F <sub>o</sub> <sup>2</sup> ) + (0.0721P) <sup>2</sup> + 0.4791P] where P = (F <sub>o</sub> <sup>2</sup> + 2F <sub>c</sub> <sup>2</sup> )/3
<b>Largest diff. peak and hole</b>	0.412 and -0.181 eÅ <sup>-3</sup>
<b>R.M.S. deviation from mean</b>	0.046 eÅ <sup>-3</sup>

## 8.7 Supporting Information for Chapter 6.2

### 8.7.1 Experimental Procedures for Chapter 6.2



The synthesis Nicotinic hydrazide was accomplished by a modification of the procedure by Farag et al.<sup>[335]</sup>

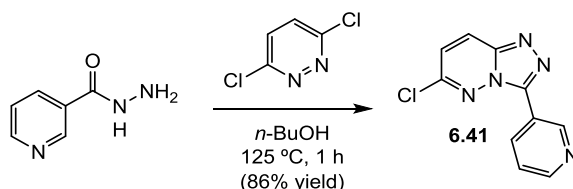
#### Nicotinic hydrazide.

Hydrazine monohydrate (0.40 mL, 8.2 mmol, 2.0 equiv.) was added to a solution of nicotinamide (500 mg, 4.09 mmol, 1.00 equiv.) in absolute ethanol (8.2 mL) and the resulting mixture was stirred at 80 °C for 24 h.

The mixture was allowed to cool down to room temperature and the solvent was removed under reduced pressure. The remaining solid was recrystallized from ethanol yielding nicotinic hydrazide (475 mg, 3.46 mmol, 85% yield) as colourless crystals.

**<sup>1</sup>H NMR** (400 MHz, DMSO-*d*<sub>6</sub>): δ 9.96 (s, 1H), 8.96 (d, *J* = 2.1 Hz, 1H), 8.69 (dd, *J* = 4.9, 1.5 Hz, 1H), 8.20–8.10 (m, 1H), 7.49 (dd, *J* = 8.0, 4.8 Hz, 1H), 4.56 (s, 2H)

**HRMS** (+ESI): calc. for C<sub>6</sub>H<sub>8</sub>N<sub>3</sub>O [M+H]<sup>+</sup> 138.0662 found 138.0666



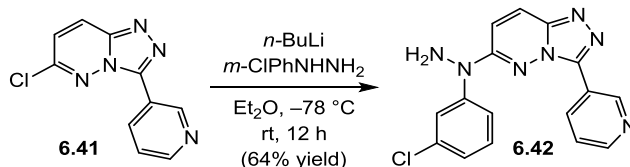
#### Triazolopyridazine 6.41.

A suspension of nicotinic hydrazide (500 mg, 3.65 mmol, 1.5 equiv.) and 2,6-dichloropyridazine (362 mg, 2.42 mmol, 1.00 equiv.) in *n*-BuOH (22 mL) was stirred in the microwave at 125 °C for 1 h.

The solvent was removed under reduced pressure and the remaining residue was purified by flash column chromatography on silica gel (MeOH/DCM, gradient 0 to 4%), which afforded **6.41** as a pale brown solid (484 mg, 2.09 mmol, 86% yield).

**<sup>1</sup>H NMR** (400 MHz, DMSO-*d*<sub>6</sub>) δ 9.44 (s, 1H), 8.78 (d, *J* = 4.8 Hz, 1H), 8.63 (d, *J* = 8.1 Hz, 1H), 8.60 (d, *J* = 9.7 Hz, 1H), 7.69 (t, *J* = 7.9, 4.9 Hz, 1H), 7.62 (d, *J* = 9.7 Hz, 1H).

**HRMS** (+ESI): calc. for C<sub>10</sub>H<sub>7</sub>ClN<sub>5</sub> [M+H]<sup>+</sup> 232.0384 found 232.0384



### Triazolopyridazine 6.42.

To a solution of **6.41** (65.0 mg, 0.280 mmol, 1.00 equiv.) and 3-chloro-phenylhydrazine (50.2 mg, 0.280 mmol, 1.00 equiv.) in Et<sub>2</sub>O (1.2 mL) at  $-78^\circ\text{C}$  was added *n*-BuLi (2.33 M in hexane, 0.48 mL, 4.0 equiv.) dropwise over 30 minutes. After stirring at room temperature for 12 hours, the reaction was quenched with MeOH and the solvent was removed under reduced pressure. The remaining residue was partitioned between water and DCM. The aqueous phase was extracted with DCM (3x10 mL) and the organic layers were combined, washed with brine (15 mL), dried over anhydrous MgSO<sub>4</sub>, filtered and concentrated under reduced pressure. The crude material was purified by flash column chromatography on silica gel (MeOH/DCM, gradient 0 to 3%), delivering **6.42** as a pale white solid (60.5 mg, 1.79 mmol, 64% yield).

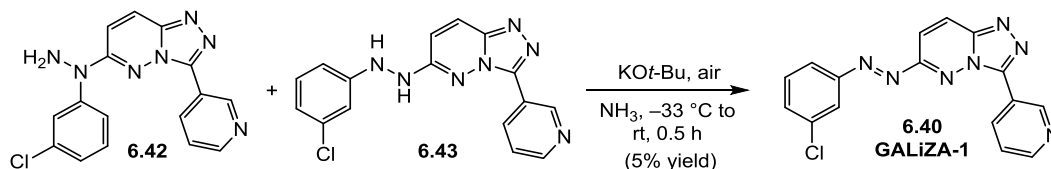
<sup>1</sup>H NMR (400 MHz, CDCl<sub>3</sub>)  $\delta$  9.73 (s, 1H), 8.76–8.68 (m, 2H), 7.93 (d,  $J$  = 10.1 Hz, 1H), 7.49–7.44 (m, 2H), 7.41 (t,  $J$  = 8.0 Hz, 1H), 7.31 (dddd,  $J$  = 7.9, 5.9, 2.2, 1.1 Hz, 2H), 7.18 (d,  $J$  = 10.1 Hz, 1H), 4.67 (br s, 2H)

<sup>13</sup>C NMR (100 MHz, CDCl<sub>3</sub>)  $\delta$  155.44, 150.60, 148.04, 144.92, 144.06, 135.29, 134.61, 132.85, 130.55, 127.15, 125.22, 124.89, 123.60, 122.76, 114.81, 113.91

IR (ATR): 3671 (br w), 2975 (m), 2939 (m), 2867 (w), 2191 (w), 1631 (w), 1592 (m), 1545 (m), 1477 (s), 1413 (m), 1382 (m), 1341 (m), 1246 (w), 1054 (s), 1034 (s), 994 (m), 962 (w), 810 (m), 759 (m), 705 (s)

HRMS (+ESI): calc. for C<sub>16</sub>H<sub>13</sub>ClN<sub>7</sub> [M+H]<sup>+</sup> 338.0915 found 338.0908

*R*<sub>F</sub> = 0.67 (4% MeOH in DCM)

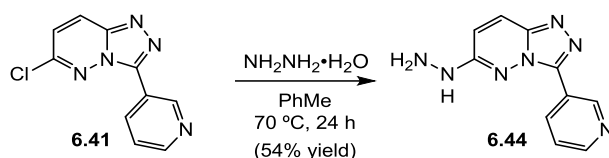


### GALiZA-1 (6.40).

The crude mixture containing an unknown proportion of hydrazines **6.42** and **6.43** (15.0 mg, 0.0445 mmol, 1.00 equiv.) and KOt-Bu (1.0 mg, 9.4  $\mu\text{mol}$ , 0.2 equiv.) was added to liquid ammonia (0.57 mL) at  $-33^\circ\text{C}$ . The mixture was stirred in an opened vial at  $-33^\circ\text{C}$  for 25 min and then the cooling bath was removed and the solvent was allowed to evaporate (about 5 min). The remaining residue was dissolved in Et<sub>2</sub>O, washed with water, brine, dried over MgSO<sub>4</sub>, filtered and concentrated under reduced pressure.

The crude material was submitted to HPLC purification (H<sub>2</sub>O/ACN, gradient, 20 to 80%) yielding **6.40** as an orange solid (0.8 mg, 18  $\mu\text{mol}$ , 5% yield).

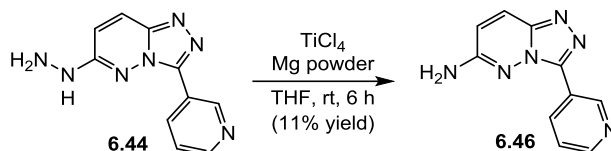
See below for full analytics.



#### Hydrazine 6.44.

To a suspension of triazolopyridazine **6.41** (300 mg, 1.29 mmol, 1.00 equiv.) in toluene (2.0 mL) was added hydrazine monohydrate (0.490 mL, 98%, 9.90 mmol, 7.60 eq.) and the resulting mixture was heated at 70 °C for 24 h. The volatile material was evaporated under reduced pressure and the remaining residue was recrystallized from MeOH. Hydrazine **6.44** (159 mg, 0.700 mmol, 54%) was obtained as a colourless solid.

**<sup>1</sup>H NMR** (400 MHz, DMSO-*d*<sub>6</sub>): δ 9.64 (d, *J* = 2.3 Hz, 1H), 8.89 (d, *J* = 7.9 Hz, 1H), 8.69 (d, *J* = 4.7 Hz, 1H), 8.59 (s, 1H), 8.02 (d, *J* = 9.9 Hz, 1H), 7.59 (dd, *J* = 8.1, 4.7 Hz, 1H), 6.87 (d, *J* = 9.9 Hz, 1H), 4.46 (br s, 2H)

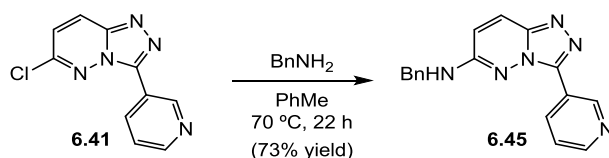


The synthesis Amine **6.45** was accomplished by following the procedure by Meiming et al.<sup>[338]</sup>

To a stirred suspension of Mg powder (5.4 mg, 0.22 mmol, 2.5 equiv.) in degassed THF (0.90 mL) at 0 °C was added TiCl<sub>4</sub> (3.9 μL, 35.2 mmol, 0.4 equiv.) dropwise. The resulting mixture was allowed to warm to room temperature and stirred for 2 hours. A solution of and hydrazine **6.44** (20.0 mg, 88 μmol, 1.00 equiv.) in THF (0.25 mL) was added and the mixture was stirred at room temperature for another 6 hours.

A saturated aqueous solution of NaHCO<sub>3</sub> was added and the resulting mixture was filtered through celite. The filtrate was extracted three times with DCM. The organic layers were combined, dried over MgSO<sub>4</sub>, filtered and concentrated under reduced pressure to yield a yellow crude which was purified by flash column chromatography on silica gel (MeOH/DCM, gradient, 0 to 15%) delivering **6.46** as a colourless solid (2.1 mg, 9.7 μmol, 11% yield).

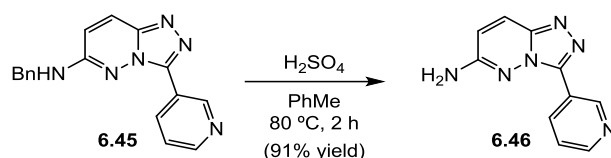
See below for analytics.



#### Benzylamine 6.45.

To a suspension of **6.41** (300 mg, 1.29 mmol, 1.00 equiv.) in toluene (2.0 mL) was added benzylamine (1.1 mL, 9.9 mmol, 7.6 equiv.) and the solution was heated at 70 °C for 22 h. The volatile material was removed under reduced pressure. The crude residue was recrystallized from MeOH, yielding **6.45** (284 mg, 0.939 mmol, 73%) as orange crystals.

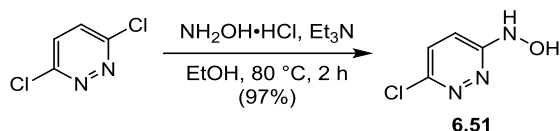
**<sup>1</sup>H NMR** (400 MHz, DMSO-*d*<sub>6</sub>): δ 9.47 (d, *J* = 2.1 Hz, 1H), 8.66 (dd, *J* = 4.9, 1.5 Hz, 1H), 8.57 (d, *J* = 8.1 Hz, 1H), 8.17 (t, *J* = 5.6 Hz, 1H), 8.06 (d, *J* = 9.8 Hz, 1H), 7.55 (dd, *J* = 8.1, 4.8 Hz, 1H), 7.43 (d, *J* = 7.6 Hz, 2H), 7.37 (t, *J* = 7.5 Hz, 2H), 7.26 (t, *J* = 7.3 Hz, 1H), 6.97 (d, *J* = 9.8 Hz, 1H), 4.51 (d, *J* = 5.4 Hz, 2H)



#### Amine 6.45.

A solution of benzylamine **6.45** (25.0 mg, 0.083 mmol, 1.00 equiv.) in concentrated sulfuric acid (0.23 mL, 98%) was heated at 80 °C for 2 h. The reaction mixture was poured into ice-water (10 mL) and basified with aq. ammonia (5 mL, 30%). The aqueous phase was extracted with DCM (4 x 5.0 mL), AcOEt (4 x 5.0 mL) and the combined organic layers were washed with water (5.0 mL) and brine (5.0 mL). After drying with MgSO<sub>4</sub>, the solvent was removed under reduced pressure to yield amine **6.46** (16.0 mg, 0.075 mmol, 91%) as a colourless solid.

<sup>1</sup>H NMR (400 MHz, DMSO-*d*<sub>6</sub>) δ 9.58 (d, *J* = 2.1 Hz, 1H), 8.72 (dd, *J* = 8.1, 2.1 Hz, 1H), 8.69 (dd, *J* = 4.8, 1.5 Hz, 1H), 8.06 (d, *J* = 9.8 Hz, 1H), 7.60 (dd, *J* = 8.0), 7.00 (s, 2H), 6.86 (d, *J* = 9.8 Hz, 1H)



The synthesis pyridazine **6.51** was accomplished following the method by Yamamoto et al.<sup>[339]</sup>

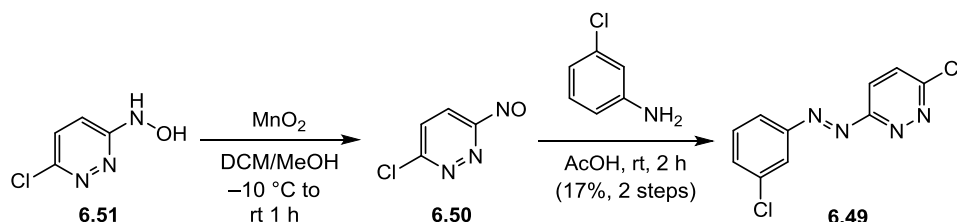
#### Pyridazine 6.51.

To a solution of 2,6-dichloropyridazine (998 mg, 6.70 mmol, 1.00 equiv.) and hydroxylamine hydrochloride (1.862 mg, 26.8 mmol, 4.00 equiv.) in EtOH (13.4 mL) was added Et<sub>3</sub>N (3.73 mL, 26.8 mmol, 4.0 equiv.). The reaction mixture was stirred at 80 °C for 2 h.

After cooling down to room temperature the solvent was evaporated under reduced pressure. The remaining residue was partitioned between water and EtOAc. The aqueous phase was separated and extracted three times with EtOAc and the organic layers were combined, dried over anhydrous MgSO<sub>4</sub>, filtered and concentrated under reduced pressure delivering **6.51** as a yellow solid (950 mg, 6.53 mmol, 97% yield).

<sup>1</sup>H NMR (400 MHz, CDCl<sub>3</sub>) δ 12.14 (br s, 1H), 10.53 (br s, 1H), 7.25 (d, *J* = 9.6 Hz, 2H), 6.96 (d, *J* = 9.8 Hz, 1H)

HRMS (+ESI): calc. for C<sub>4</sub>H<sub>5</sub>ClN<sub>3</sub>O [M+H]<sup>+</sup> 146.0116 found 146.0117



The synthesis nitrosopyridazine **6.51** was accomplished following the method by Yamamoto et al.<sup>[339]</sup>

#### Azobenzene 6.49.

To a round bottom flask charged with MnO<sub>2</sub> (2.06 g, 23.7 mmol, 20 equiv.) was added dry DCM (30 mL) and the suspension was stirred for 20 min at rt. Then, MeOH (0.30 mL) was added, the mixture was cooled to

–10°C and **6.51** (172 mg, 1.18 mmol, 1.00 equiv.) was added in two equal portions. The mixture was stirred at –10°C for 30 min and at rt for 30 min before it was filtered through a pad of Celite and washed with DCM. The resulting solution was evaporated under reduced pressure below 20 °C and immediately submitted to the next step.

To the crude material containing **6.50** was added 3-chloroaniline (125 µL, 1.184 mmol, 1.00 equiv.) followed by AcOH (4.9 mL) and the mixture was stirred at rt for 3 h before water and DCM were added. The aqueous phase was extracted three times with DCM and the organic layers were combined, washed with brine, 0.5 M aqueous HCl, water, dried over anhydrous Na<sub>2</sub>SO<sub>4</sub>, filtered and concentrated under reduced pressure yielding a brown solid.

Purification by flash column chromatography on silica gel (MeOH/DCM, gradient, 0 to 1%) delivered **6.49** as an orange solid (50.0 mg, 0.198 mmol, 17% yield for 2 steps).

<sup>1</sup>H NMR (400 MHz, CDCl<sub>3</sub>) δ 8.09 (s, 1H), 8.00 (d, *J* = 7.7 Hz, 1H), 7.94 (d, *J* = 9.0 Hz, 1H), 7.71 (d, *J* = 9.0 Hz, 1H), 7.60–7.49 (m, 2H)

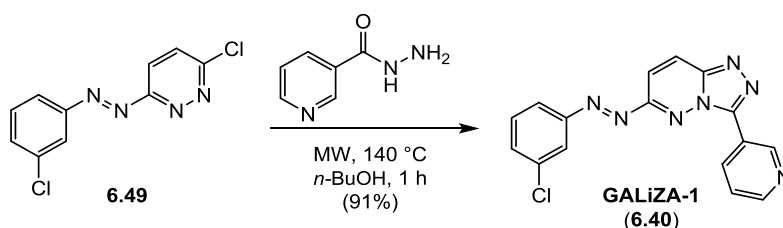
<sup>13</sup>C NMR (100 MHz, CDCl<sub>3</sub>) δ 164.88, 158.09, 152.73, 135.60, 133.13, 130.44, 130.37, 123.18, 123.15, 118.72

IR (ATR): 3061 (br w), 2924 (m), 2852 (w), 1560 (m), 1460 (m), 1391 (s), 1179 (s), 1163 (m), 1073 (m), 885 (m), 856 (m), 786 (m), 760 (m)

HRMS (+ESI): calc. for C<sub>10</sub>H<sub>6</sub>Cl<sub>2</sub>N<sub>4</sub>Na [M+Na]<sup>+</sup> 274.9862 found 274.9869

*R*<sub>F</sub> = 0.45 (1% MeOH in DCM)

λ<sub>max</sub> = 312 nm



#### GALiZA-1 (**6.40**).

A suspension of **6.49** (49.0 mg, 0.194 mmol, 1.00 equiv) and nicotinic hydrazide (39.8 mg, 0.290 mmol, 1.50 equiv.) in *n*-BuOH (1.7 mL) was stirred in the microwave at 140 °C for 1 h.

The solvent was evaporated under reduced pressure yielding a brown residue which was purified by flash column chromatography on silica gel ((MeOH + 2% Et<sub>3</sub>N)/DCM, gradient, 0 to 10%) delivering **GALiZA-1** as an orange solid (59.0 mg, 0.176 mmol, 91% yield).

<sup>1</sup>H NMR (400 MHz, CDCl<sub>3</sub>, *trans*) δ 9.87 (s, 1H), 8.92 (d, *J* = 7.7 Hz, 1H), 8.81 (d, *J* = 4.6 Hz, 1H), 8.33 (d, *J* = 9.9 Hz, 1H), 8.09 (s, 1H), 8.01 (d, *J* = 7.6 Hz, 1H), 7.86 (d, *J* = 9.9 Hz, 1H), 7.59 (dt, *J* = 14.9, 7.7 Hz, 3H)

<sup>1</sup>H NMR (400 MHz, CDCl<sub>3</sub>, *cis*) δ 9.37 (s, 1H), 8.74 (dd, *J* = 4.9, 1.6 Hz, 1H), 8.31 (dt, *J* = 8.0, 1.8 Hz, 1H), 8.25 (d, *J* = 9.6 Hz, 1H), 7.47–7.43 (m, 1H), 7.26–7.20 (m, 2H), 7.13 (t, *J* = 1.8 Hz, 1H), 7.07 (d, *J* = 9.6 Hz, 1H), 6.70 (dt, *J* = 7.0, 2.0 Hz, 1H)

<sup>13</sup>C NMR (100 MHz, CDCl<sub>3</sub>) δ 159.82, 152.56, 151.34, 148.79, 146.97, 145.26, 135.76, 134.89, 133.60, 130.59, 126.70, 123.64, 123.52, 123.00, 122.32, 112.18, 77.00

**IR** (ATR): 3428 (br w), 3.45 (br m), 2924 (w), 2853 (w), 2361 (w), 1576 (m), 1532 (m), 1471 (s), 1433 (s), 1417 (s), 1375 (s), 1334 (s), 1281 (w), 1186 (s), 1154 (m), 1067 (w), 986 (m), 827 (m), 786 (m), 732 (m)

**HRMS** (+ESI): calc. for  $C_{16}H_{11}ClN_7$   $[M+H]^+$  336.0759 found 336.0760

$R_F$  = 0.45 (5% MeOH in DCM)

$\lambda_{max}$  = 313 nm

$t_{1/2}$  = 40 min

**PSS** (Z/E, 5 min 365 nm) = 25/75 ( $^1H$  NMR spectroscopy in saturated  $CDCl_3$ )



#### Azobenzene **6.56**.

To the crude material containing **6.50** (run with 3.01 mmol of **6.51**) was added 3-chloroaniline (328  $\mu$ L, 3.01 mmol, 1.00 equiv.) followed by AcOH (12 mL) and the mixture was stirred at rt for 3 h before water and DCM were added. The aqueous phase was basified by addition of sodium carbonate and extracted four times with DCM. The organic layers were combined, washed with brine, dried over anhydrous  $Na_2SO_4$ , filtered and concentrated under reduced pressure yielding a brown solid.

Purification by flash column chromatography on silica gel (MeOH/DCM, gradient, 0 to 1%) delivered **6.56** as an orange solid (214 mg, 0.719 mmol, 24% yield for 2 steps).

$^1H$  NMR (400 MHz,  $CDCl_3$ )  $\delta$  8.25 (t,  $J$  = 1.7 Hz, 1H), 8.04 (d,  $J$  = 8.0 Hz, 1H), 7.93 (d,  $J$  = 9.0 Hz, 1H), 7.72 (d,  $J$  = 7.9 Hz, 1H), 7.71 (d,  $J$  = 9.0 Hz, 1H), 7.47 (t,  $J$  = 8.0 Hz, 1H)

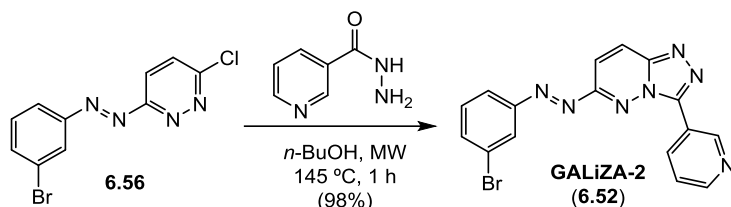
$^{13}C$  NMR (100 MHz,  $CDCl_3$ )  $\delta$  164.84, 158.09, 152.78, 136.02, 130.72, 130.37, 125.96, 123.75, 123.42, 118.70

**IR** (ATR): 3057 (br m), 1558 (m), 1457 (w), 1391 (s), 1177 (s), 1161 (m), 1140 (m), 1073 (w), 995 (w), 848 (m), 790 (m), 752 (w)

**HRMS** (+ESI): calc. for  $C_{10}H_6ClBrN_4Na$   $[M+Na]^+$  318.9357 found 318.9366

$R_F$  = 0.62 (1% MeOH in DCM)

$\lambda_{max}$  = 314 nm



#### **GALIZA-2 (6.52).**

A suspension of **6.56** (60.0 mg, 0.202 mmol, 1.00 equiv) and nicotinic hydrazide (41.5 mg, 0.302 mmol, 1.50 equiv.) in  $n$ -BuOH (2.4 mL) was stirred in the microwave at 145  $^{\circ}C$  for 1 h.



The solvent was evaporated under reduced pressure yielding a brown residue which was purified by flash column chromatography on silica gel ((MeOH+ 2% Et<sub>3</sub>N)/DCM, gradient, 0 to 10%) delivering **GALiZA-2** as an orange solid (75.0 mg, 0.197 mmol, 98% yield).

**<sup>1</sup>H NMR** (400 MHz, CDCl<sub>3</sub>) δ 9.87 (d, *J* = 1.6 Hz, 1H), 8.92 (dt, *J* = 8.0, 1.8 Hz, 1H), 8.81 (dd, *J* = 4.8, 1.5 Hz, 1H), 8.33 (d, *J* = 9.9 Hz, 1H), 8.25 (t, *J* = 1.7 Hz, 1H), 8.06 (d, *J* = 8.0 Hz, 1H), 7.86 (d, *J* = 9.9 Hz, 1H), 7.77 (d, *J* = 8.0 Hz, 1H), 7.57 (dd, *J* = 8.0, 4.9 Hz, 1H), 7.51 (t, *J* = 8.0 Hz, 1H)

**<sup>13</sup>C NMR** (100 MHz, CDCl<sub>3</sub>) δ 159.79, 152.64, 151.35, 148.81, 146.98, 145.26, 136.50, 134.89, 130.87, 126.71, 125.83, 124.10, 123.64, 123.59, 122.32, 112.16

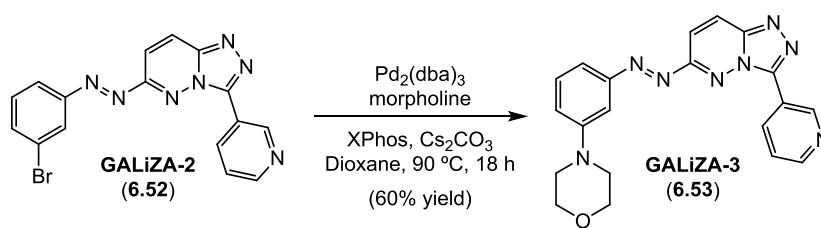
**IR** (ATR): 3043 (br m), 2960 (m), 1574 (m), 1531 (m), 1466 (s), 1432 (s), 1416 (s), 1374 (s), 1333 (s), 1281 (w), 1282 (s), 1153 (s), 1060 (m), 986 (s), 826 (m), 750 (s)

**HRMS** (+ESI): calc. for C<sub>16</sub>H<sub>11</sub>BrN<sub>7</sub> [M+H]<sup>+</sup> 380.0254 found 380.0249

**R<sub>F</sub>** = 0.45 (5% MeOH in DCM)

**λ<sub>max</sub>** = 314 nm

**t<sub>1/2</sub>** = 62 min



#### **GALiZA-3 (6.53).**

A pressure vial was charged with **6.52** (14.8 mg, 38.9 μmol, 1.00 equiv), morpholine (10.2 μL, 117 μmol, 3.00 equiv.), Cs<sub>2</sub>CO<sub>3</sub> (19.1 mg, 58.5 mmol, 1.50 equiv.), XPhos (3.6 mg, 7.6 μmol, 0.19 equiv.) and degassed dioxane (20 min N<sub>2</sub> sparging, 0.35 mL). The mixture was stirred at 95 °C for 18 hours.

Upon cooling down to room temperature the solvent was evaporated under reduced pressure and the remaining residue was partitioned between DCM and a half-saturated aqueous sodium carbonate solution. The phases were separated and the aqueous layer was extracted twice with DCM. The organic layers were combined, washed with brine, dried over anhydrous Na<sub>2</sub>SO<sub>4</sub>, filtered and concentrated under reduced pressure yielding a red solid which was purified by flash column chromatography on silica gel (MeOH/DCM, gradient, 0 to 10%) delivering **GALiZA-3** as red solid (9.0 mg, 23 μmol, 60% yield).

**<sup>1</sup>H NMR** (400 MHz, CDCl<sub>3</sub>, *trans*) δ 9.94 (s, 1H), 8.90 (d, *J* = 8.0 Hz, 1H), 8.80 (d, *J* = 4.7 Hz, 1H), 8.30 (d, *J* = 9.9 Hz, 1H), 7.89 (d, *J* = 9.9 Hz, 1H), 7.63 (d, *J* = 7.7 Hz, 1H), 7.59–7.54 (m, 2H), 7.51 (t, *J* = 8.0 Hz, 1H), 7.20 (d, *J* = 8.3 Hz, 1H), 3.92 (dd, *J* = 9.3, 4.5 Hz, 4H), 3.31 (dd, *J* = 9.3, 4.7 Hz, 4H)

**<sup>1</sup>H NMR** (400 MHz, CDCl<sub>3</sub>, *cis*) δ 9.43 (s, 1H), 8.74 (d, *J* = 4.8 Hz, 1H), 8.48 (d, *J* = 9.1 Hz, 1H), 8.14 (d, *J* = 9.6 Hz, 1H), 7.47–7.42 (m, 1H), 7.10 (t, *J* = 8.3 Hz, 1H), 6.86 (d, *J* = 9.2 Hz, 1H), 6.78 – 6.73 (m, 2H), 6.10 (d, *J* = 8.1 Hz, 1H), 3.82 (t, *J* = 4.8 Hz, 4H), 3.12 (t, *J* = 4.4 Hz, 4H)

**<sup>13</sup>C NMR** (100 MHz, CDCl<sub>3</sub>) δ 160.13, 152.83, 152.16, 151.24, 148.72, 146.87, 145.38, 135.04, 130.06, 126.43, 123.68, 122.48, 121.14, 118.60, 112.52, 107.42, 66.73, 48.82

**IR** (ATR): 2929 (br m), 2855 (m), 1595 (m), 1538 (w), 1485 (m), 1467 (m), 1449 (m), 1377 (s), 1333 (s), 1246 (s), 1230 (s), 1153 (m), 1121 (s), 987 (m), 907 (m), 817 (w), 731 (w)

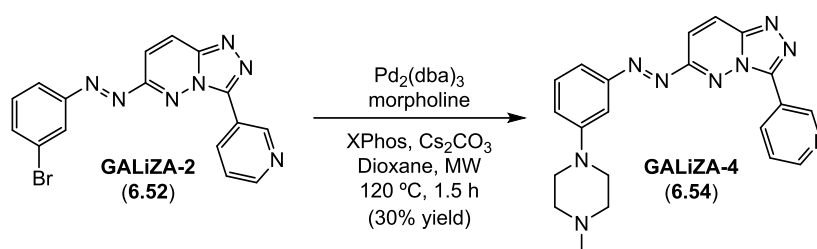
**HRMS** (+ESI): calc. for  $C_{20}H_{19}N_8O$   $[M+H]^+$  387.1676 found 387.1678

$R_F$  = 0.39 (5% MeOH in DCM)

$\lambda_{max}$  = 322 nm

$t_{1/2}$  = 22 min

**PSS** (Z/E, 5 min 365 nm) = 17/83 ( $^1H$  NMR spectroscopy in saturated  $CDCl_3$ )



#### **GALiZA-3 (6.54).**

A microwave vial was charged with **6.52** (24.0 mg, 63.1  $\mu$ mol, 1.00 equiv),  $Pd_2(dba)_3$  (40.5 mg, 44.2  $\mu$ mol, 0.70 equiv), *N*-methylpiperazine (21.0  $\mu$ L, 189  $\mu$ mol, 3.00 equiv.),  $Cs_2CO_3$  (30.9 mg, 94.8 mmol, 1.50 equiv.), XPhos (41.5 mg, 87.1  $\mu$ mol, 1.38 equiv.) and degassed dioxane (freeze-pump-thaw, 3x10 min, 1.5 mL). The mixture was stirred in the microwave at 120 °C for 1.5 hours.

The reaction mixture was directly submitted to flash column chromatography on Brockman type I alumina (MeOH/DCM, 0% then 12%). The dark orange fractions were combined, washed with saturated ammonium chloride, brine and saturated aqueous sodium carbonate, then dried over anhydrous  $Na_2SO_4$ , filtered and concentrated under reduced pressure yielding a red solid which was purified again by flash column chromatography on silica gel ((MeOH+2%  $Et_3N$ )/DCM, gradient, 0 to 10%) delivering **GALiZA-4** as an orange solid (7.6 mg, 19  $\mu$ mol, 30% yield).

**$^1H$  NMR** (400 MHz,  $CDCl_3$ , *trans*)  $\delta$  9.93 (dd,  $J$  = 2.1, 0.7 Hz, 1H), 8.91 (dt,  $J$  = 8.0, 1.9 Hz, 1H), 8.80 (dd,  $J$  = 4.8, 1.7 Hz, 1H), 8.30 (d,  $J$  = 9.9 Hz, 1H), 7.89 (d,  $J$  = 9.9 Hz, 1H), 7.62–7.58 (m, 2H), 7.56 (ddd,  $J$  = 8.0, 4.9, 0.8 Hz, 1H), 7.49 (t,  $J$  = 8.0 Hz, 1H), 7.22 (dd,  $J$  = 8.2, 2.8 Hz, 1H), 3.37 (dd,  $J$  = 10.0, 4.9 Hz, 4H), 2.64 (dd,  $J$  = 9.5, 4.8 Hz, 4H), 2.39 (s, 3H)

**$^1H$  NMR** (400 MHz,  $CDCl_3$ , *cis*)  $\delta$  9.49 (d,  $J$  = 2.2 Hz, 1H), 8.74 (dd,  $J$  = 4.8, 1.7 Hz, 1H), 8.47 (dt,  $J$  = 8.1, 2.0 Hz, 1H), 8.12 (d,  $J$  = 9.6 Hz, 1H), 7.46–7.43 (m, 1H), 7.08 (t,  $J$  = 7.9 Hz, 1H), 6.81 (d,  $J$  = 9.6 Hz, 1H), 6.79–6.75 (m, 2H), 6.10 (dd,  $J$  = 7.8, 2.2 Hz, 1H), 3.17 (t,  $J$  = 5.1 Hz, 4H), 2.51 (t,  $J$  = 5.1 Hz, 4H), 2.33 (s, 3H)

**$^{13}C$  NMR** (100 MHz,  $CDCl_3$ )  $\delta$  160.19, 152.86, 152.08, 151.22, 148.76, 146.87, 145.38, 135.01, 129.97, 126.39, 123.65, 122.49, 121.38, 117.81, 112.59, 108.02, 54.91, 48.54, 46.13

**IR** (ATR): 2924 (s), 2852 (m), 2361 (br w), 1729 (s), 1609 (s), 1465 (s), 1378 (m), 1333 (m), 1291 (w), 1251 (m), 1153 (m), 1116 (w), 1000 (w), 821 (m)

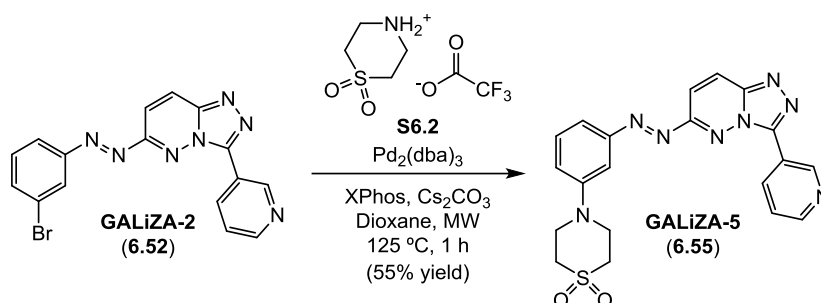
**HRMS** (+ESI): calc. for  $C_{21}H_{22}N$   $[M+H]^+$  400.1993 found 400.1997

$R_F$  = 0.36 (10% MeOH in DCM)

$\lambda_{\max} = 322 \text{ nm}$

$t_{1/2} = 155 \text{ min}$

**PSS** (Z/E, 5 min 365 nm) = 13/87 ( $^1\text{H}$  NMR spectroscopy in saturated  $\text{CDCl}_3$ )



### **GALiZA-3 (6.55).**

A microwave vial was charged with **6.52** (24.0 mg, 63.1  $\mu\text{mol}$ , 1.00 equiv),  $\text{Pd}_2(\text{dba})_3$  (40.5 mg, 44.2  $\mu\text{mol}$ , 0.70 equiv), **S6.2** (47 mg, 189  $\mu\text{mol}$ , 3.00 equiv.),  $\text{Cs}_2\text{CO}_3$  (123 mg, 379  $\mu\text{mol}$ , 6.00 equiv.), XPhos (41.5 mg, 87.1  $\mu\text{mol}$ , 1.38 equiv.) and degassed dioxane (freeze-pump-thaw, 3x10 min, 1.5 mL). The mixture was stirred in the microwave at 125  $^\circ\text{C}$  for 1 hour.

The reaction mixture was directly submitted to flash column chromatography on Brockman type I alumina (MeOH/DCM, 0% then 12%). The dark orange fractions were combined, washed with saturated ammonium chloride, brine and saturated aqueous sodium carbonate, then dried over anhydrous  $\text{Na}_2\text{SO}_4$ , filtered and concentrated under reduced pressure yielding a red solid which was purified again by flash column chromatography on silica gel ((MeOH+2%  $\text{Et}_3\text{N}$ )/DCM, gradient, 0 to 10%) delivering **GALiZA-5** as an orange solid (15.0 mg, 34.5  $\mu\text{mol}$ , 30% yield).

$^1\text{H}$  NMR (400 MHz,  $\text{DMSO}-d_6$ , *trans*)  $\delta$  9.95 (d,  $J = 1.6 \text{ Hz}$ , 1H), 8.89 (dt,  $J = 8.0, 1.9 \text{ Hz}$ , 1H), 8.82 (dd,  $J = 4.8, 1.6 \text{ Hz}$ , 1H), 8.32 (d,  $J = 9.9 \text{ Hz}$ , 1H), 7.89 (d,  $J = 9.9 \text{ Hz}$ , 1H), 7.71 (d,  $J = 8.0 \text{ Hz}$ , 1H), 7.61–7.54 (m, 3H), 7.21 (dd,  $J = 8.1, 2.3 \text{ Hz}$ , 1H), 4.01 (dd,  $J = 10.4, 5.2 \text{ Hz}$ , 4H), 3.19 (dd,  $J = 10.2, 5.3 \text{ Hz}$ , 4H)

$^1\text{H}$  NMR (400 MHz,  $\text{DMSO}-d_6$ , *cis*)  $\delta$  9.08 (s, 1H), 8.73 (d,  $J = 3.7 \text{ Hz}$ , 1H), 8.54 (d,  $J = 9.7 \text{ Hz}$ , 1H), 8.38 (d,  $J = 7.9 \text{ Hz}$ , 1H), 7.60 (dd,  $J = 8.0, 4.7 \text{ Hz}$ , 1H), 7.37 (d,  $J = 9.7 \text{ Hz}$ , 1H), 7.16–7.06 (m, 2H), 6.93 (dd,  $J = 8.2, 2.3 \text{ Hz}$ , 1H), 6.21 (d,  $J = 8.7 \text{ Hz}$ , 1H), 3.92 (t,  $J = 5.2 \text{ Hz}$ , 4H), 3.07 (t,  $J = 5.3, 4.6 \text{ Hz}$ , 4H)

$^{13}\text{C}$  NMR (100 MHz,  $\text{DMSO}-d_6$ )  $\delta$  159.80, 152.67, 151.14, 148.84, 148.05, 146.12, 145.38, 134.94, 130.67, 127.12, 124.12, 122.38, 121.03, 114.16, 112.98, 110.57, 49.95, 46.55, 29.05, 22.12

IR (ATR): 3409 (br s), 2924 (s), 2853 (m), 2362 (m), 1702 (s), 1596 (s), 1494 (s), 1468 (s), 1433 (m), 1417 (m), 1379 (s), 1334 (s), 1287 (w), 1220 (s), 1151 (w), 1054 (s), 1005 (s), 951 (m), 822 (w), 751 (s)

HRMS (+ESI): calc. for  $\text{C}_{20}\text{H}_{18}\text{N}_8\text{NaO}_2\text{S}$   $[\text{M}+\text{Na}]^+$  457.1166 found 457.1166

$R_f = 0.23$  (5% MeOH in DCM)

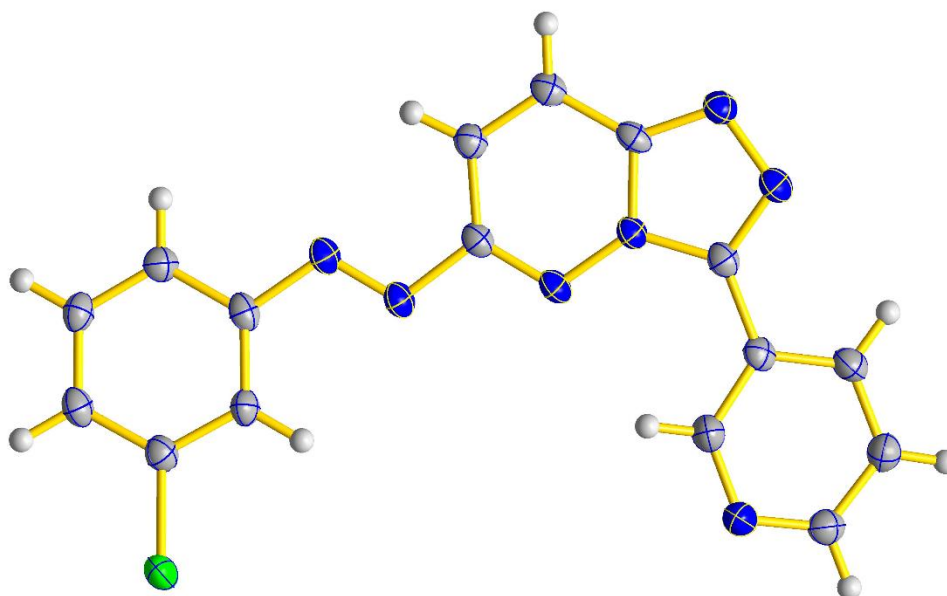
$\lambda_{\max} = 322 \text{ nm}$

$t_{1/2} = 59 \text{ min}$

**PSS** (Z/E, 5 min 365 nm) >17/83 ( $^1\text{H}$  NMR spectroscopy in saturated  $\text{DMSO}-d_6$ )

## 8.7.2 Crystallographic Data for Chapter 6.2

### Triazolopyridazine 6.40 (Chapter 6.2)



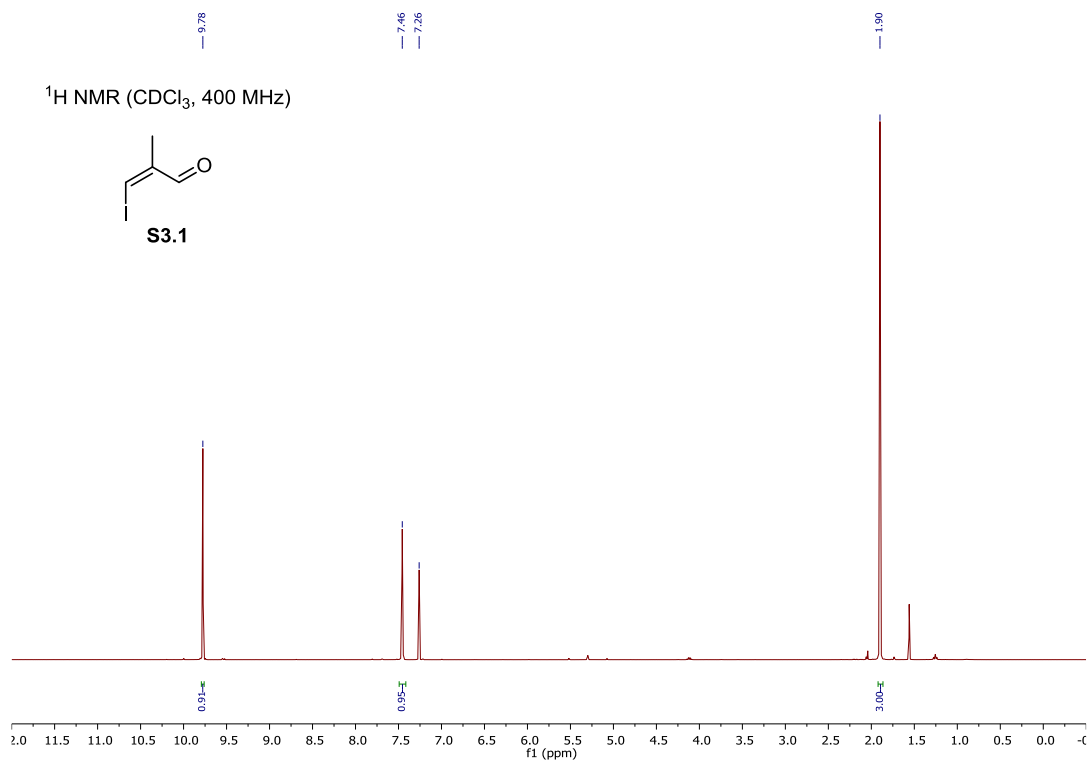
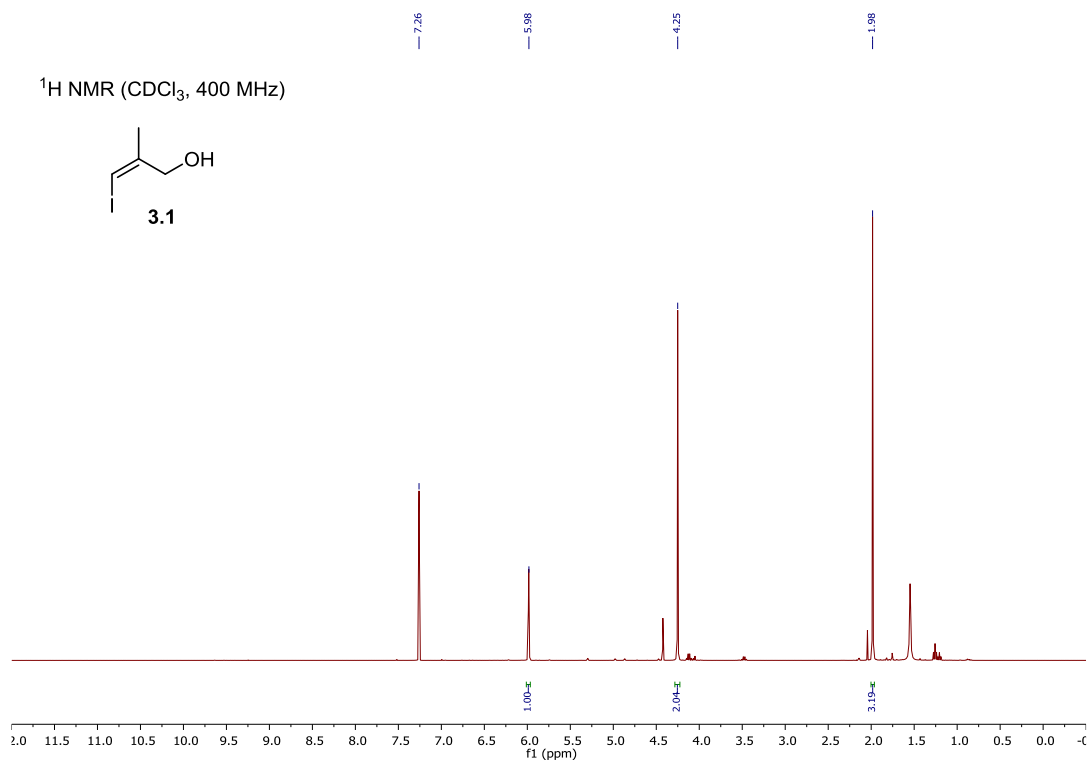
<b>Identification code</b>	19dtr6h
<b>Chemical formula</b>	C <sub>16</sub> H <sub>10</sub> ClN <sub>7</sub>
<b>Formula weight</b>	335.76 g/mol
<b>Temperature</b>	100(2) K
<b>Wavelength</b>	0.71073 Å
<b>Crystal size</b>	0.020 x 0.060 x 0.460 mm
<b>Crystal habit</b>	yellow needle
<b>Crystal system</b>	triclinic
<b>Space group</b>	P -1
<b>Unit cell dimensions</b>	a = 4.1940(15) Å b = 11.511(4) Å c = 15.759(6) Å  α = 106.587(5)° β = 95.933(5)° γ = 94.986(6)°
<b>Volume</b>	719.8(4) Å <sup>3</sup>
<b>Z</b>	2
<b>Density (calculated)</b>	1.549 g/cm <sup>3</sup>
<b>Absorption coefficient</b>	0.279 mm <sup>-1</sup>
<b>F(000)</b>	344
<b>Diffractometer</b>	Bruker APEX-II CCD
<b>Theta range for data collection</b>	1.36 to 28.30°
<b>Index ranges</b>	-5 ≤ h ≤ 5, -15 ≤ k ≤ 15, -20 ≤ l ≤ 20
<b>Reflections collected</b>	10872
<b>Independent reflections</b>	3572 [R(int) = 0.0562]
<b>Coverage of independent reflections</b>	99.5%
<b>Absorption correction</b>	multi-scan
<b>Max. and min. transmission</b>	0.7457 and 0.5649

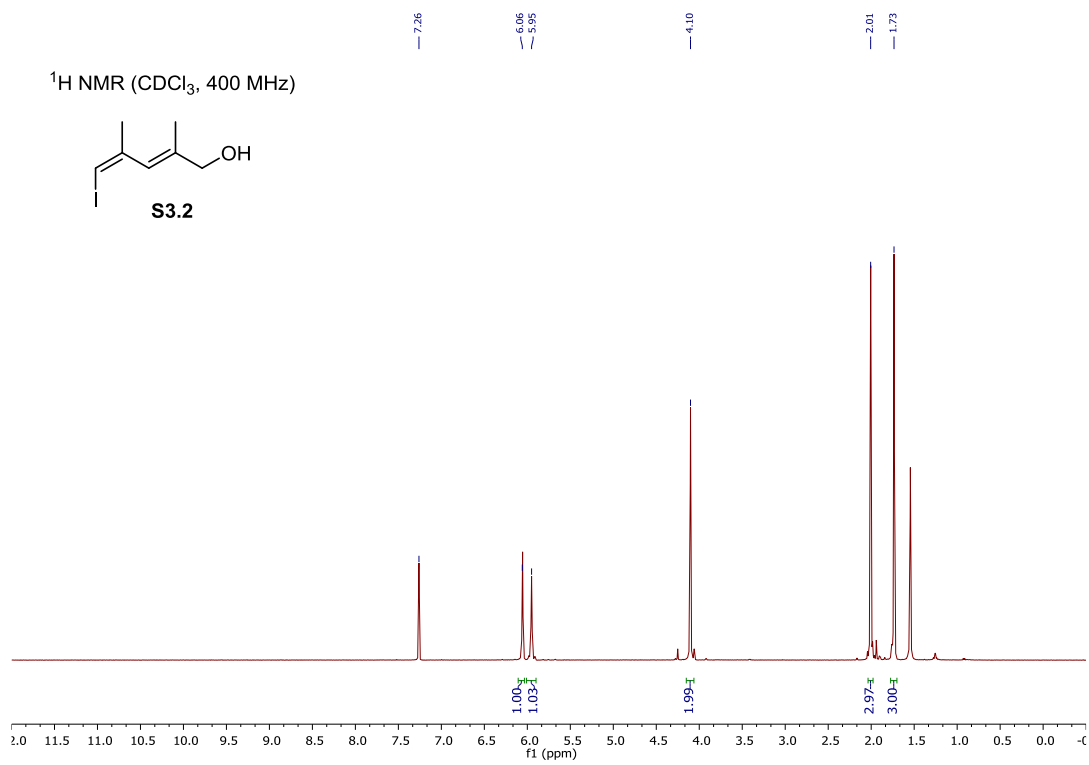
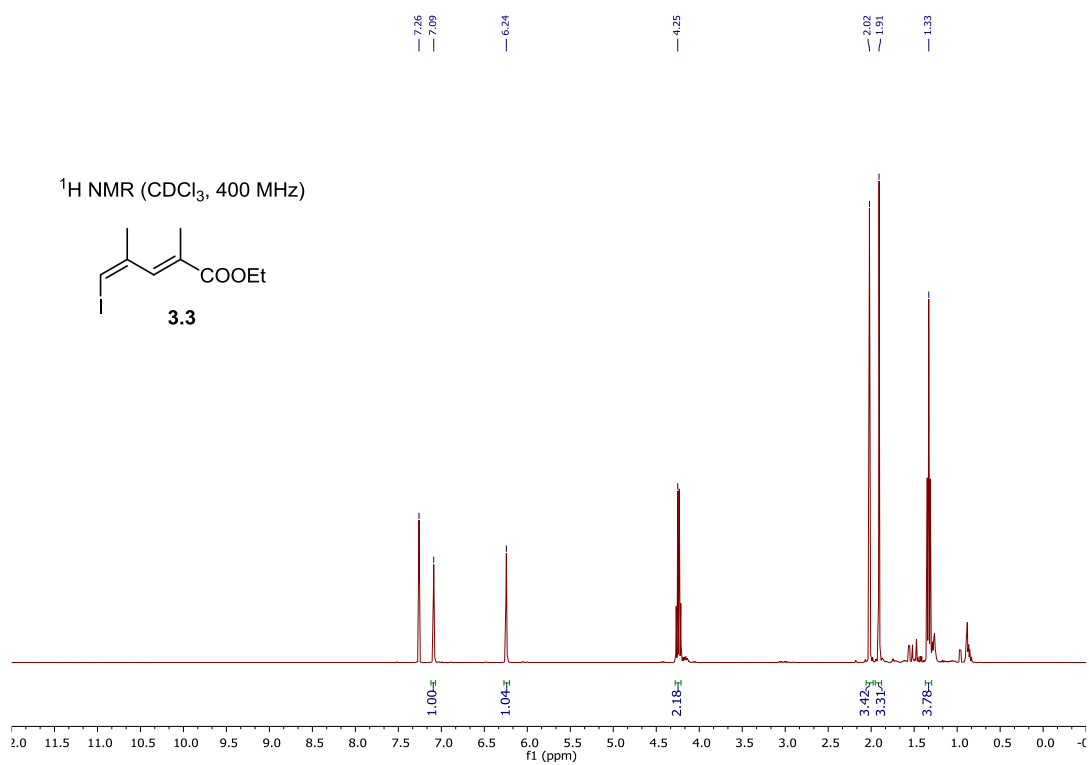
---

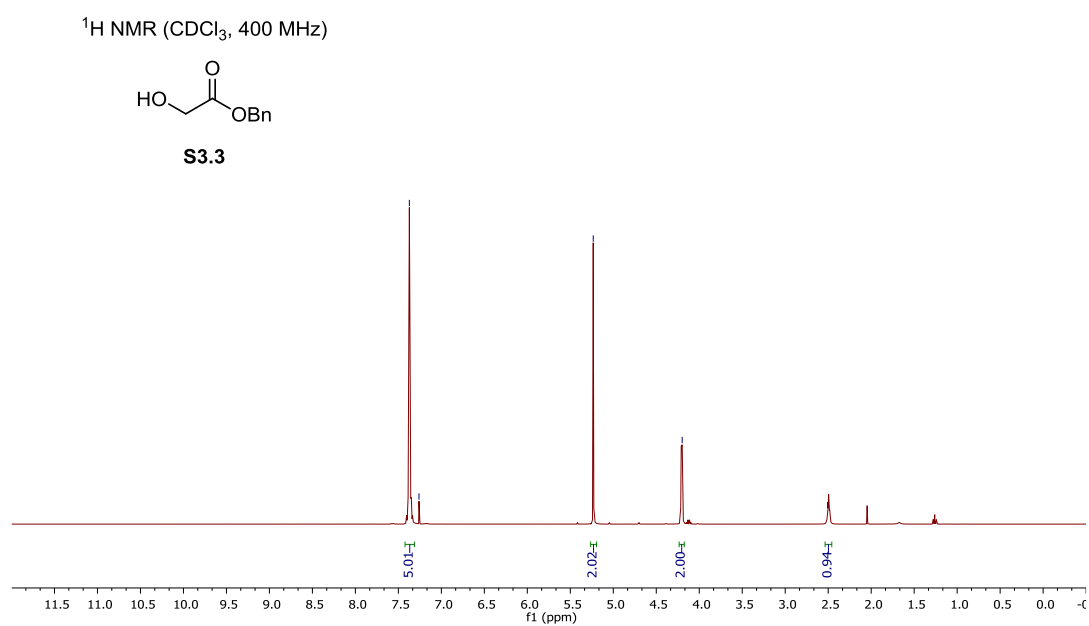
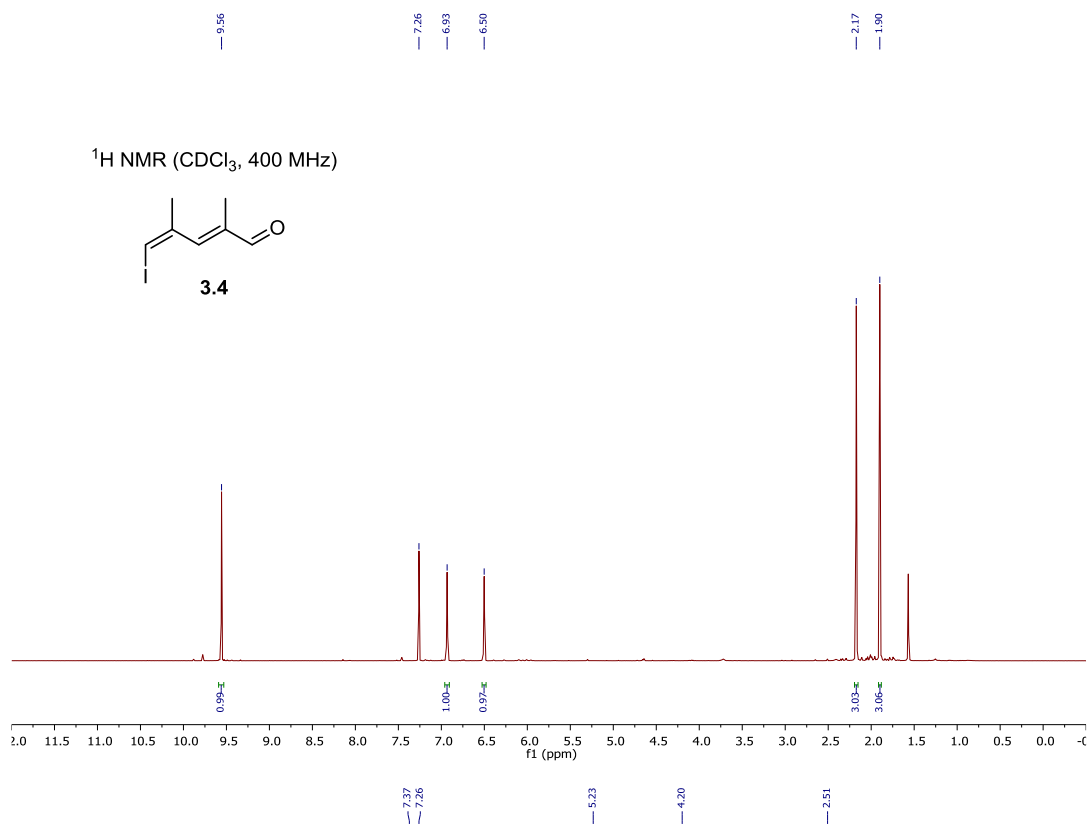
<b>Structure solution technique</b>	direct methods
<b>Structure solution program</b>	SHELXT (Sheldrick 2015)
<b>Refinement method</b>	Full-matrix least-squares on F <sup>2</sup>
<b>Refinement program</b>	SHELXL-2018/3 (Sheldrick, 2018)
<b>Function minimized</b>	$\Sigma w(F_o^2 - F_c^2)^2$
<b>Data / restraints / parameters</b>	3572 / 0 / 217
<b>Goodness-of-fit on F<sup>2</sup></b>	0.959
<b>Final R indices</b>	2452 data; $I > 2\sigma(I)$ R1 = 0.0543, wR2 = 0.1280 R1 = 0.0833, wR2 = 0.1418 all data
<b>Weighting scheme</b>	$w = 1/[\sigma^2(F_o^2) + (0.0786P)^2]$ where $P = (F_o^2 + 2F_c^2)/3$
<b>Largest diff. peak and hole</b>	0.408 and -0.439 eÅ <sup>-3</sup>
<b>R.M.S. deviation from mean</b>	0.074 eÅ <sup>-3</sup>

## 8.8 NMR Spectra

### 8.8.1 NMR Spectra for Chapter 3.1

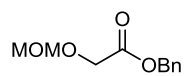




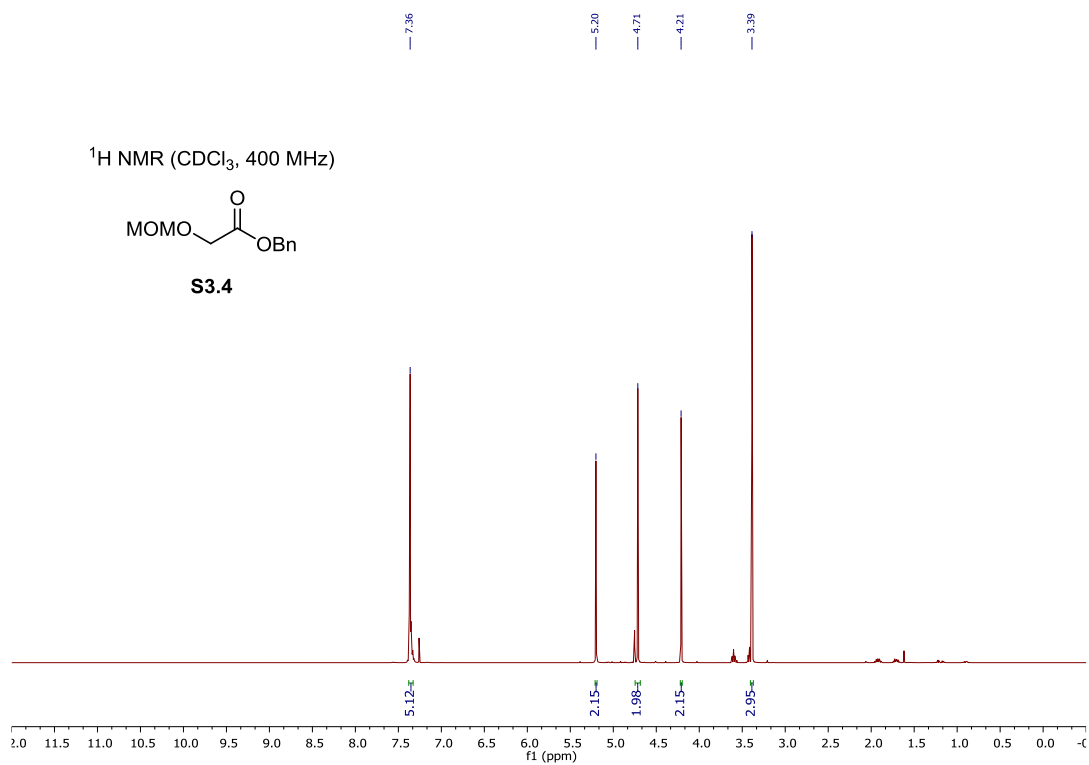




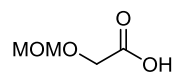
$^1\text{H}$  NMR ( $\text{CDCl}_3$ , 400 MHz)



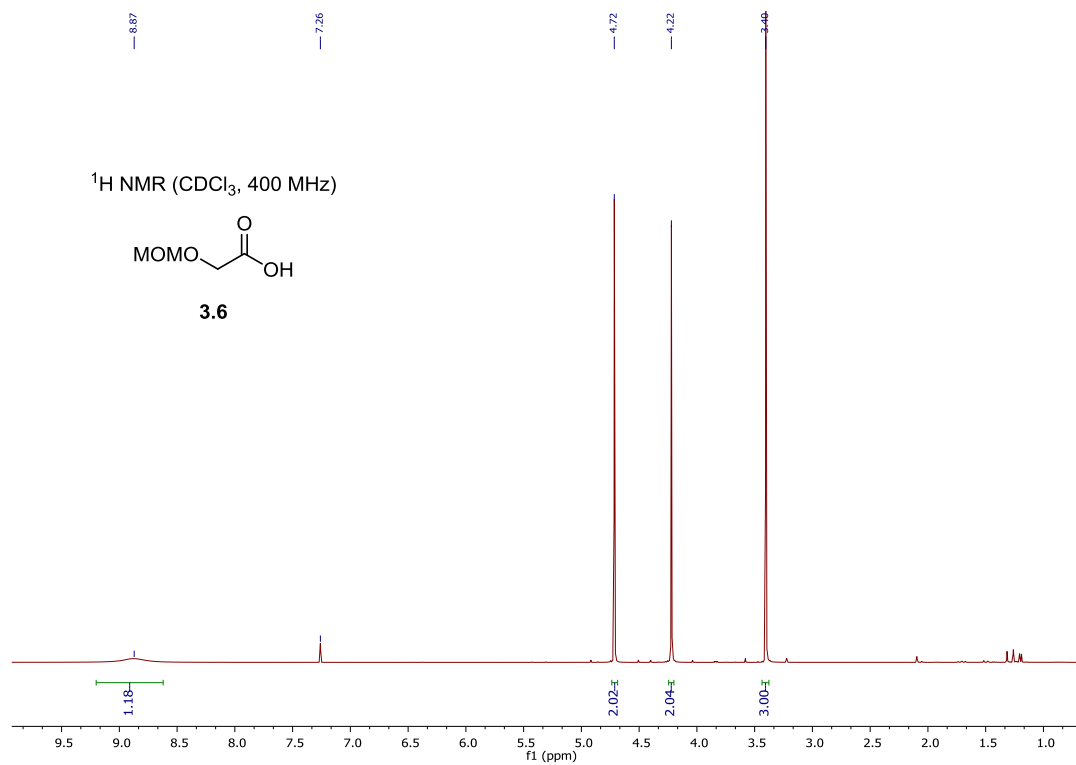
**S3.4**

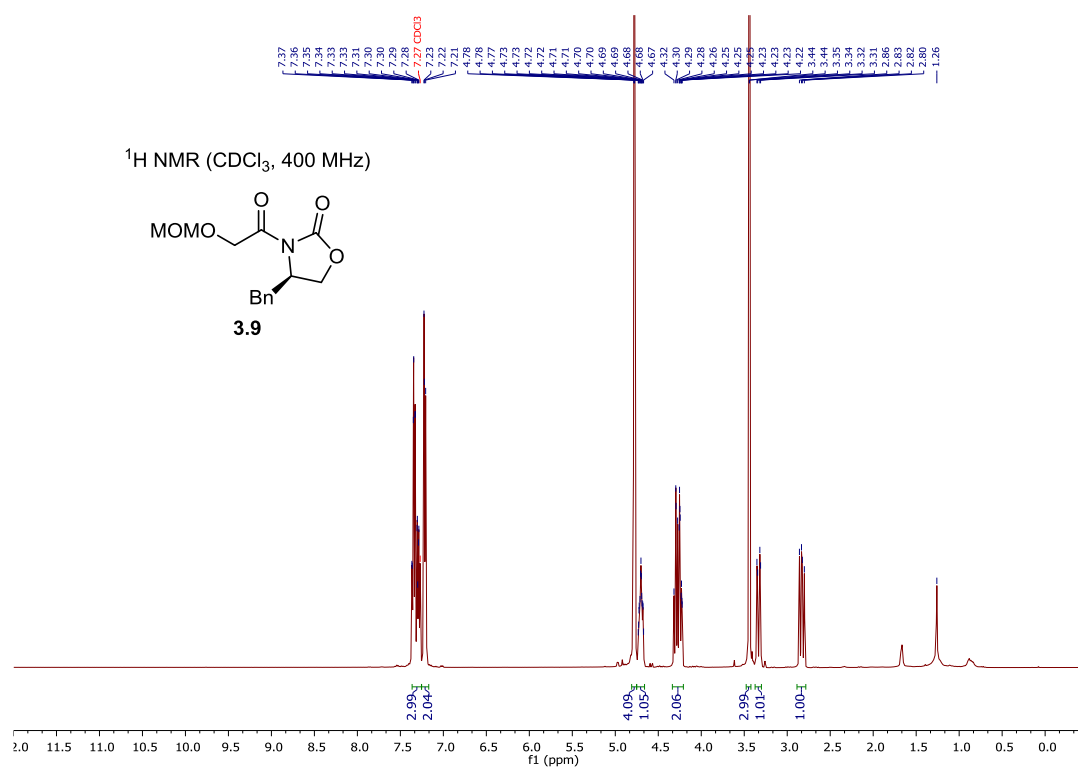
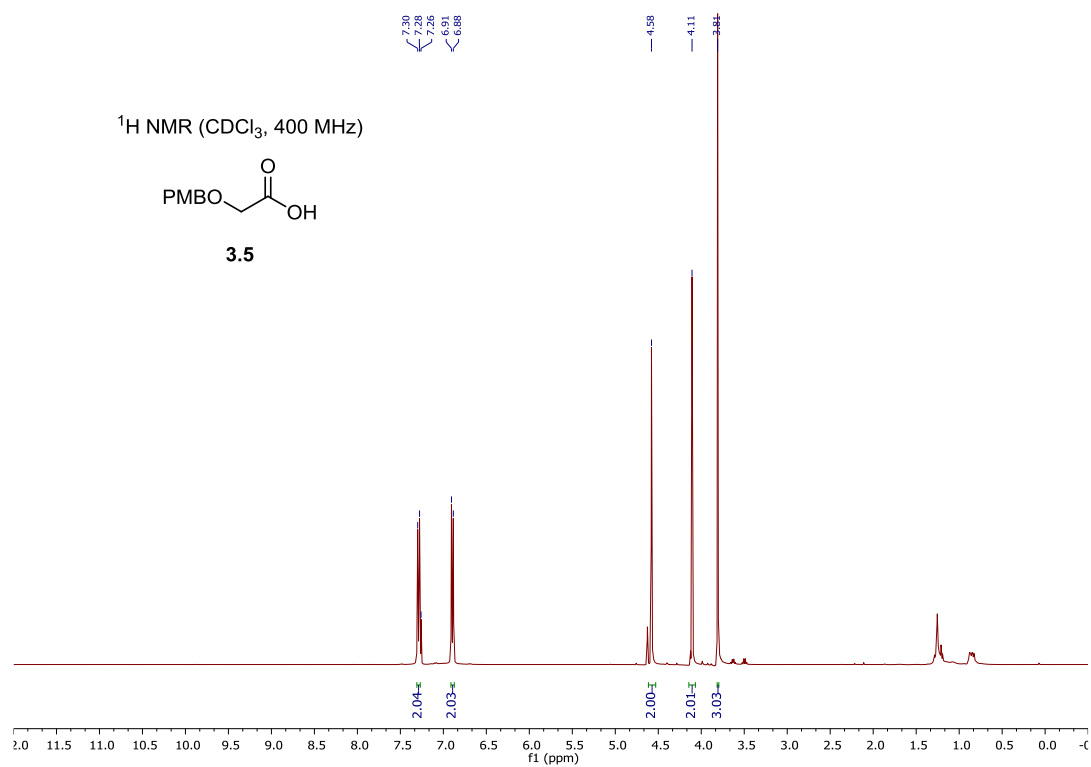


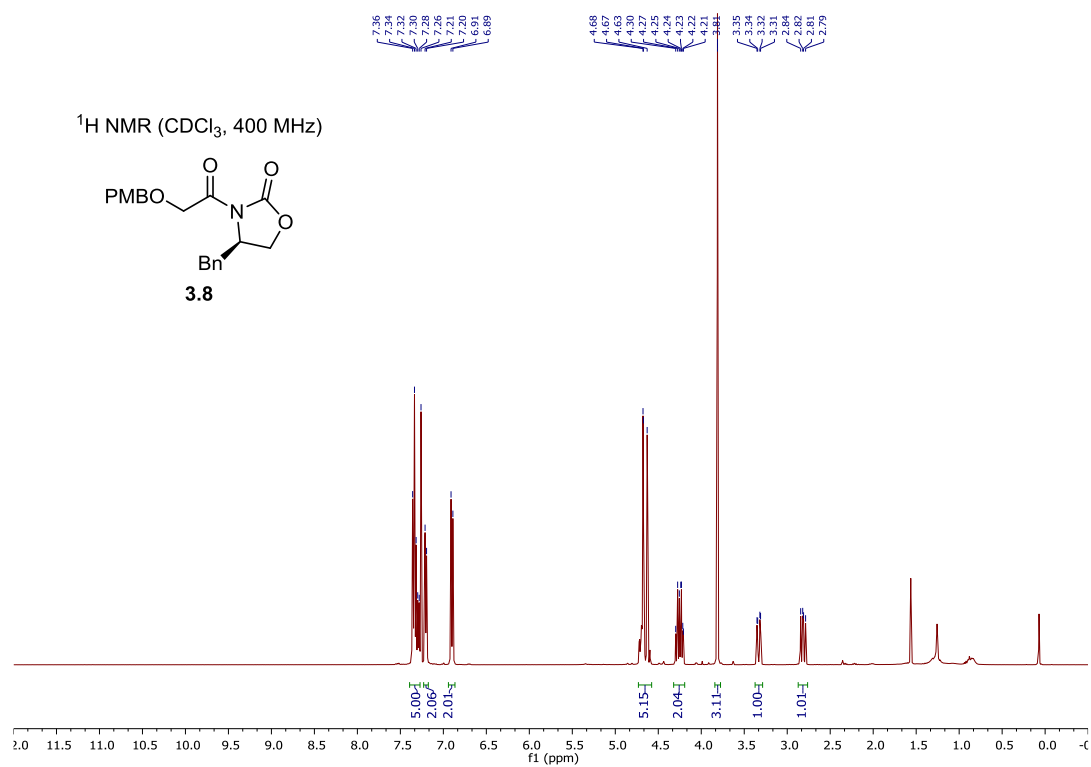
$^1\text{H}$  NMR ( $\text{CDCl}_3$ , 400 MHz)



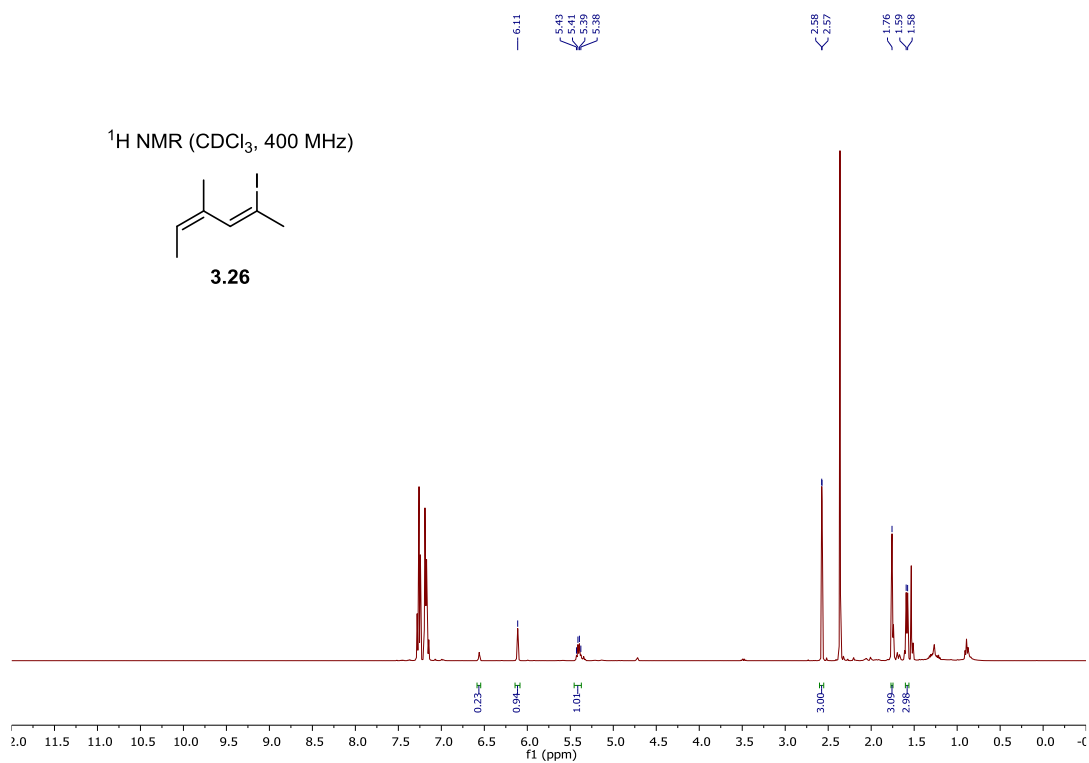
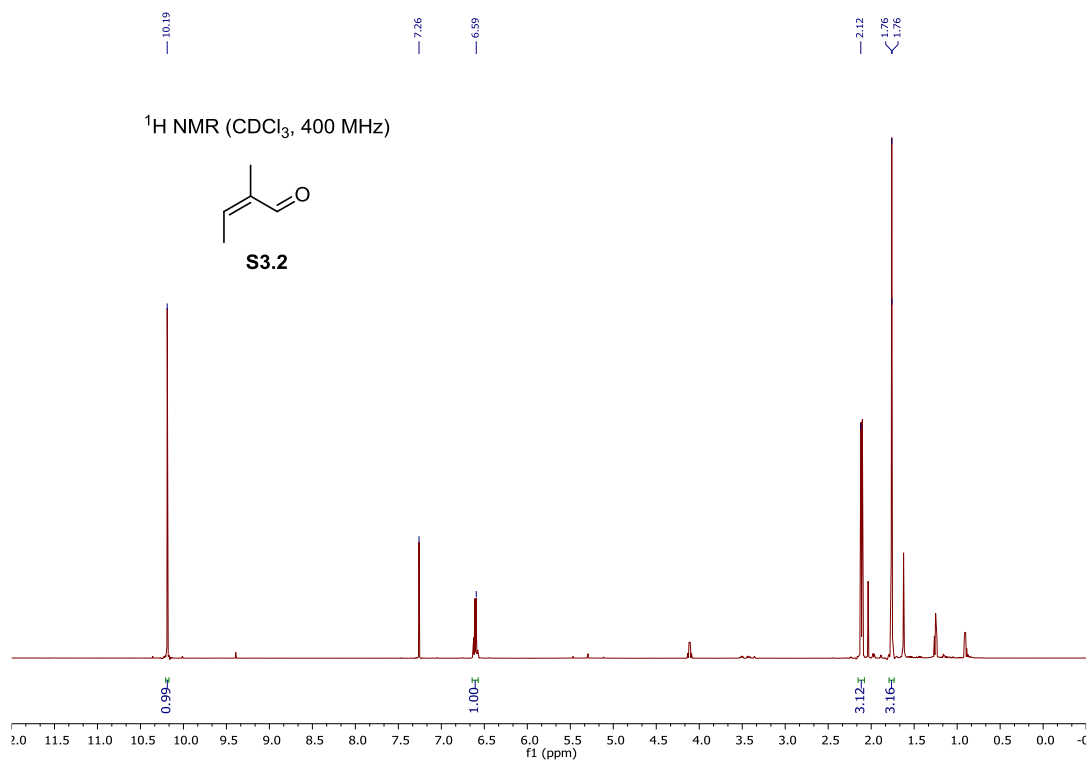
**3.6**

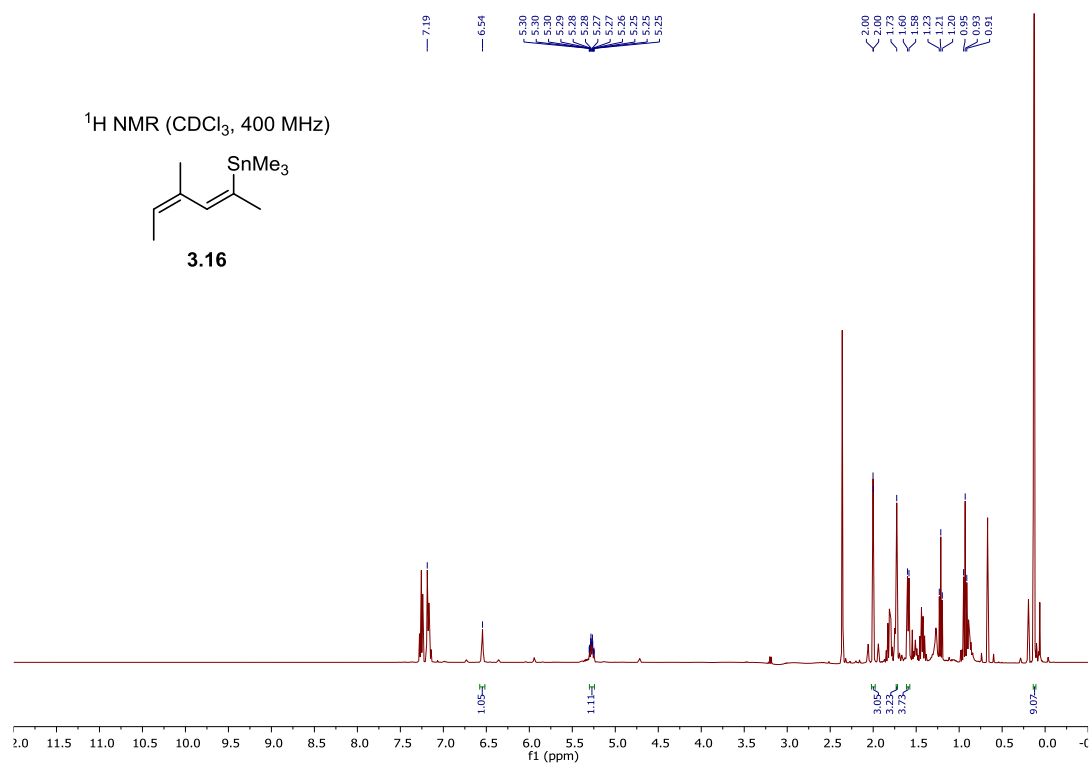


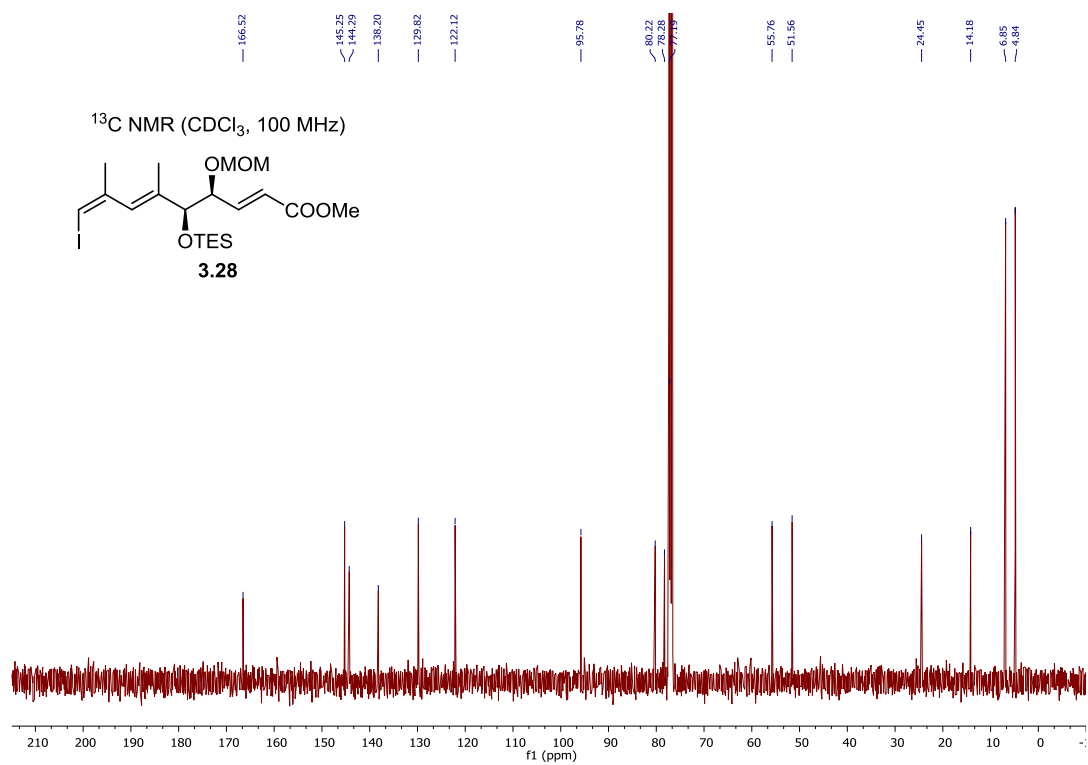
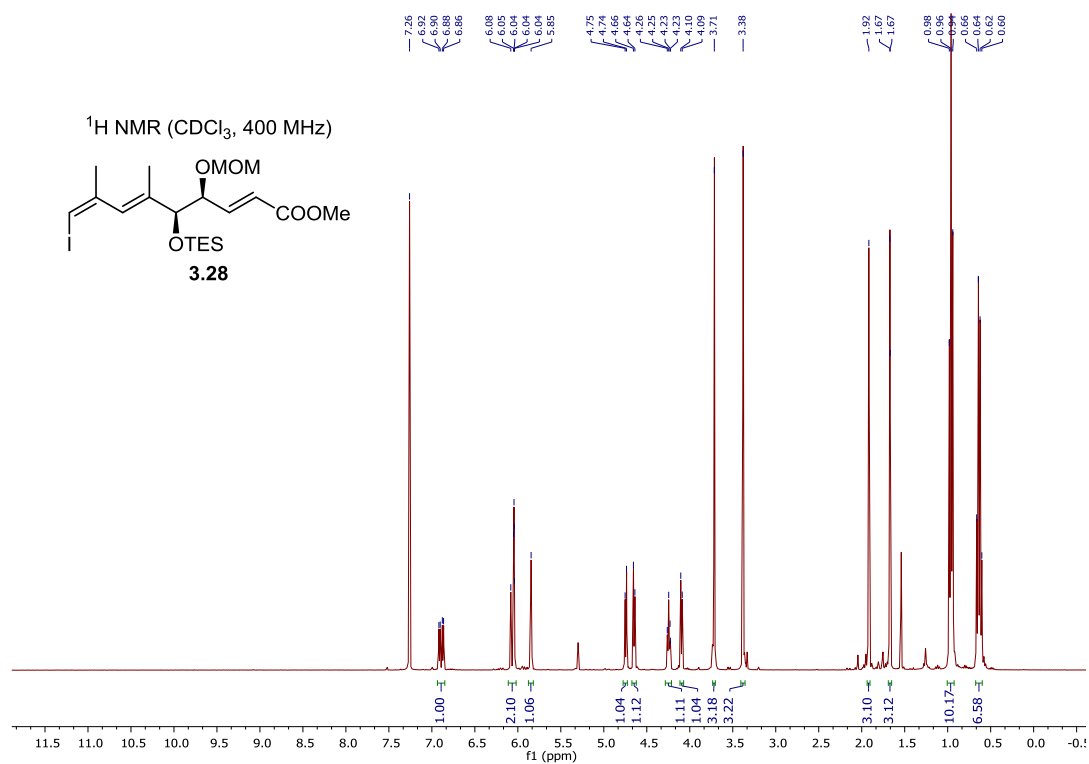


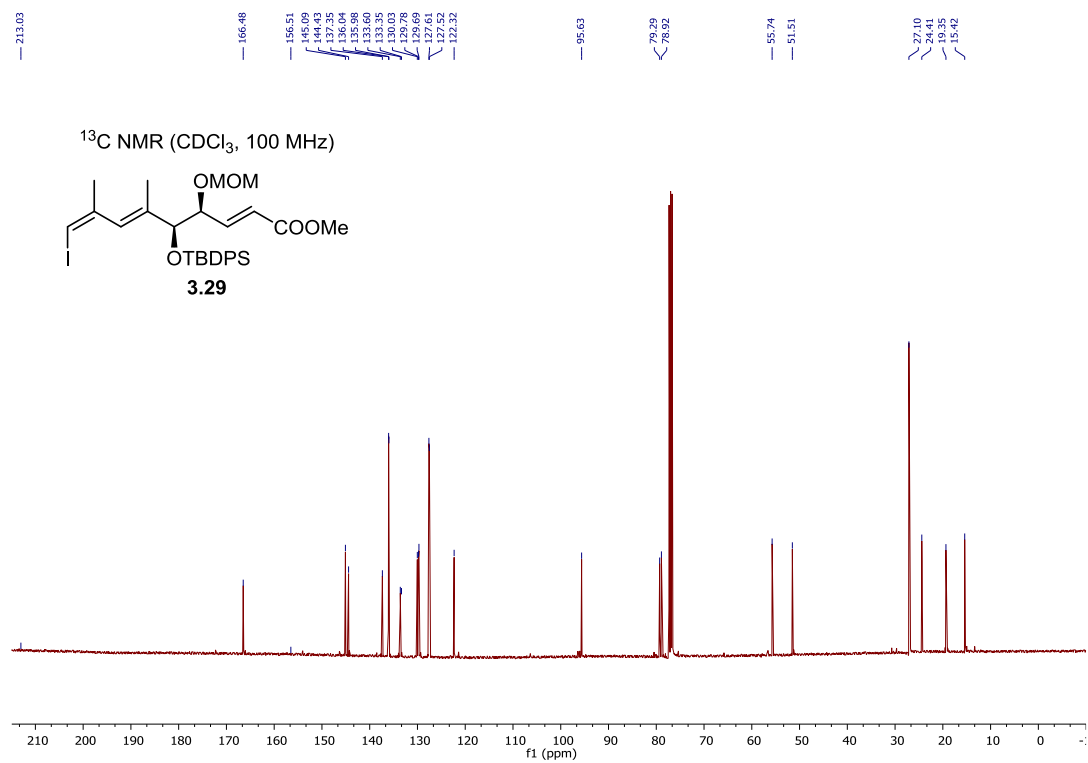
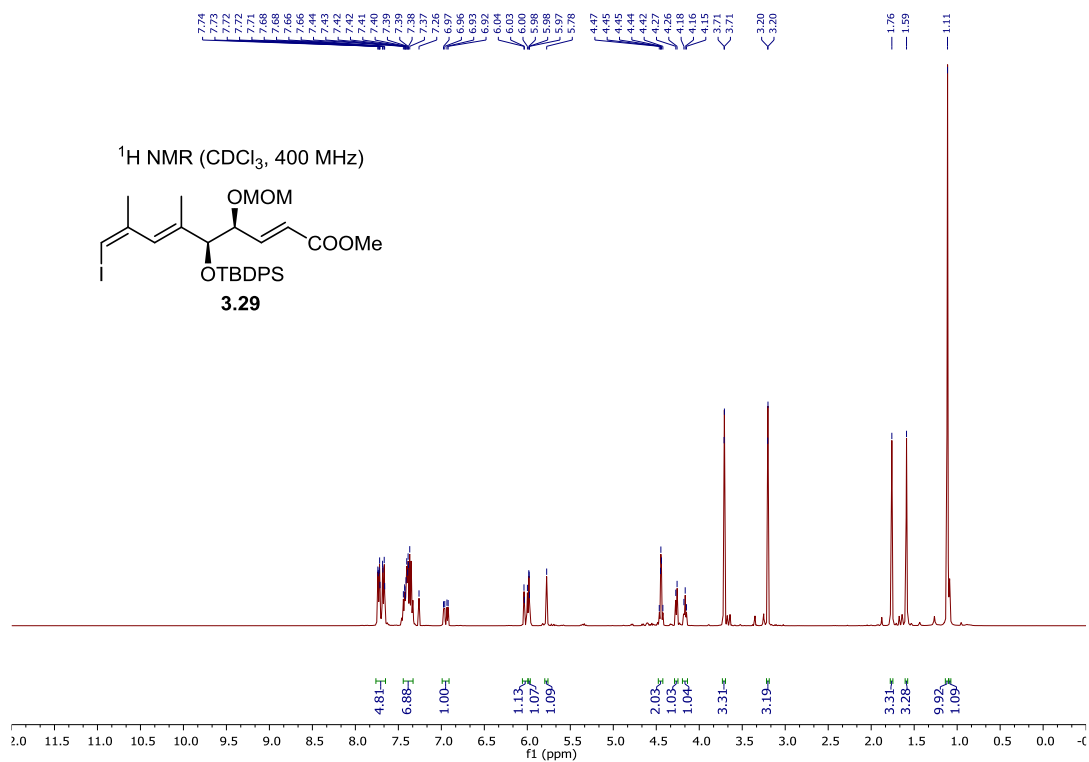


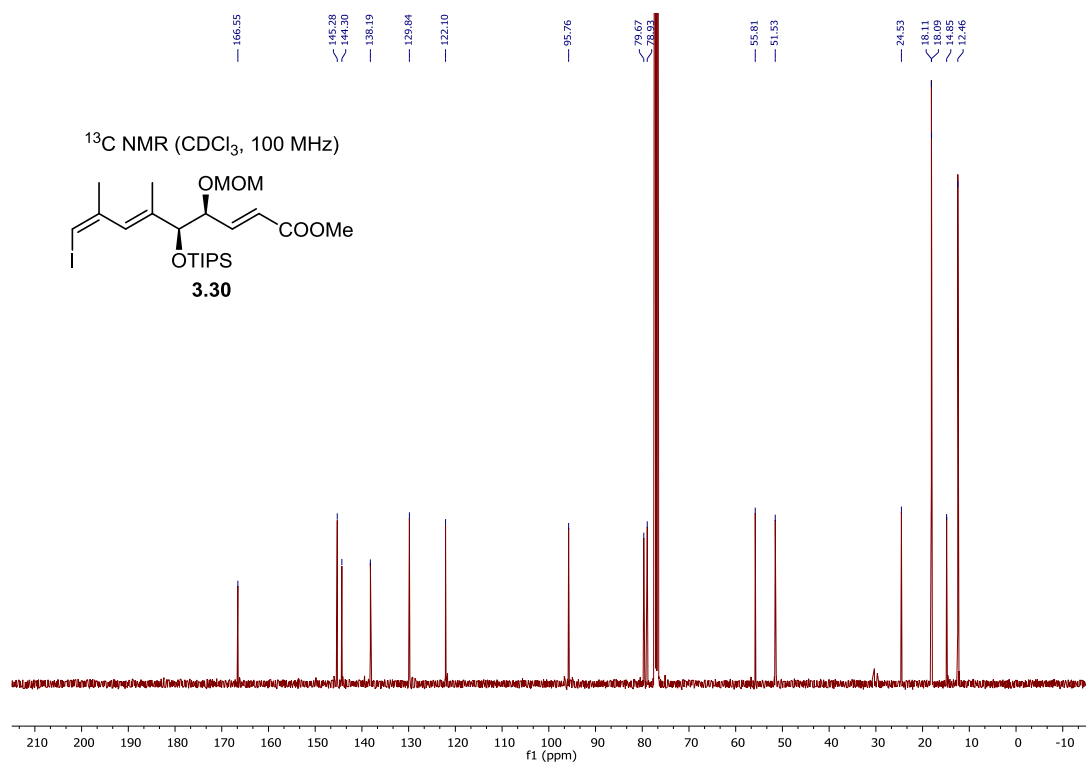
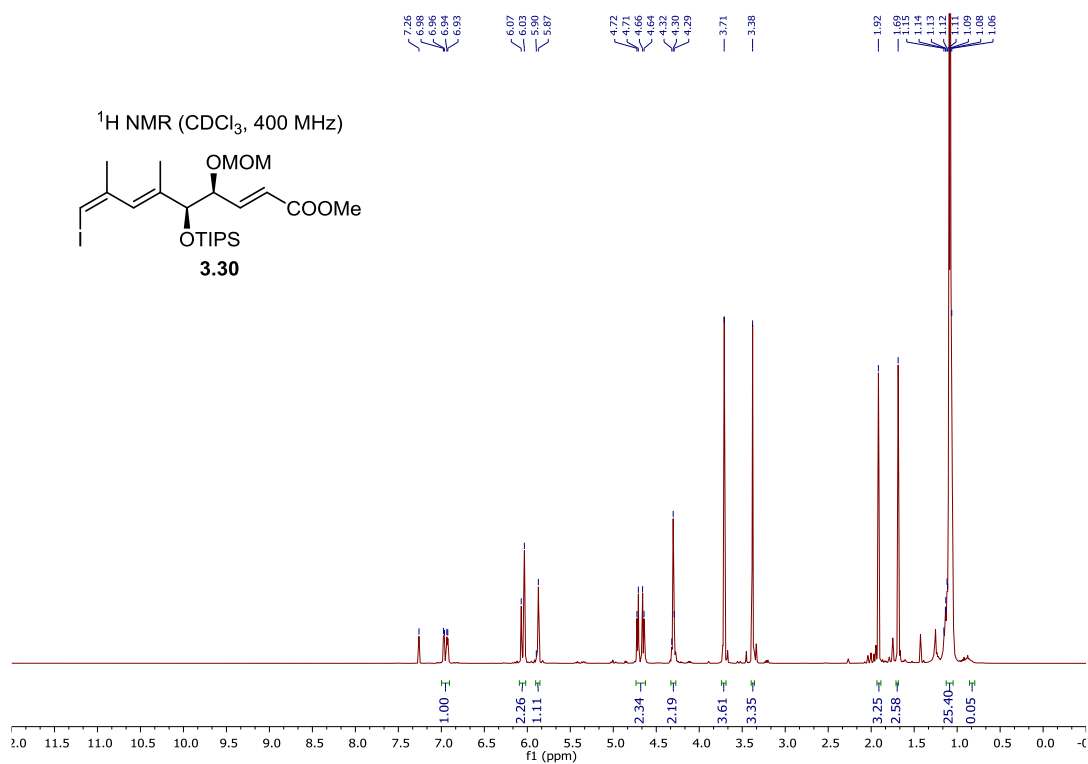
## 8.8.2 NMR Spectra for Chapter 3.2



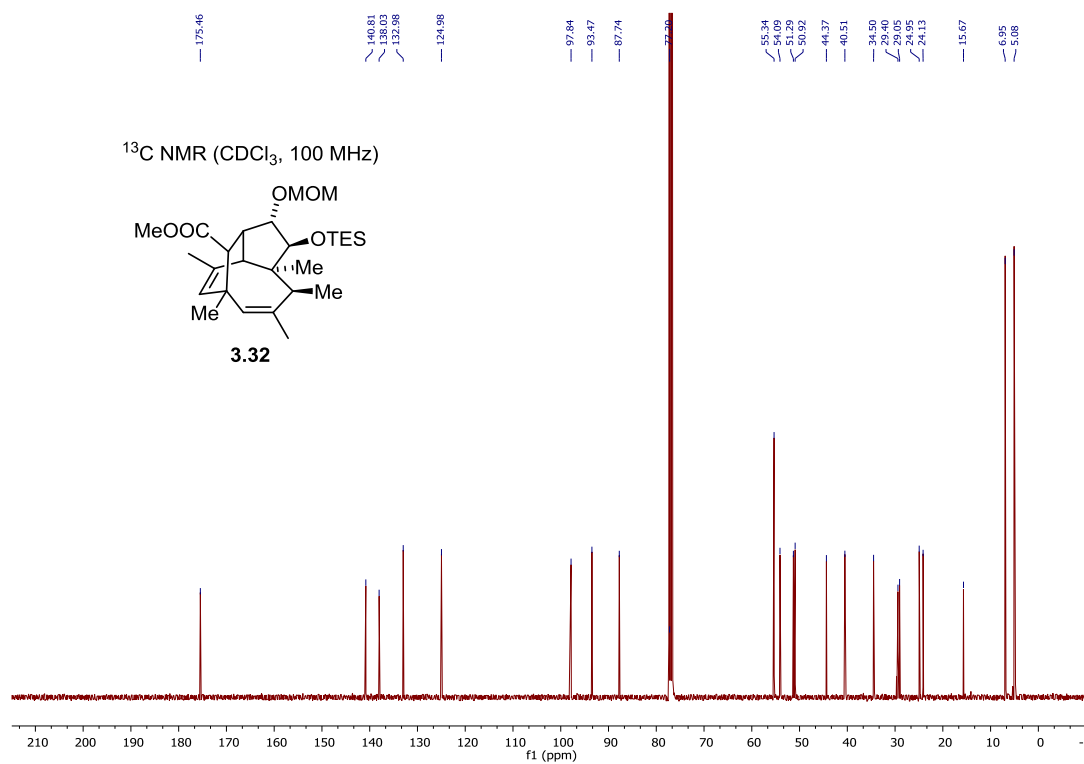
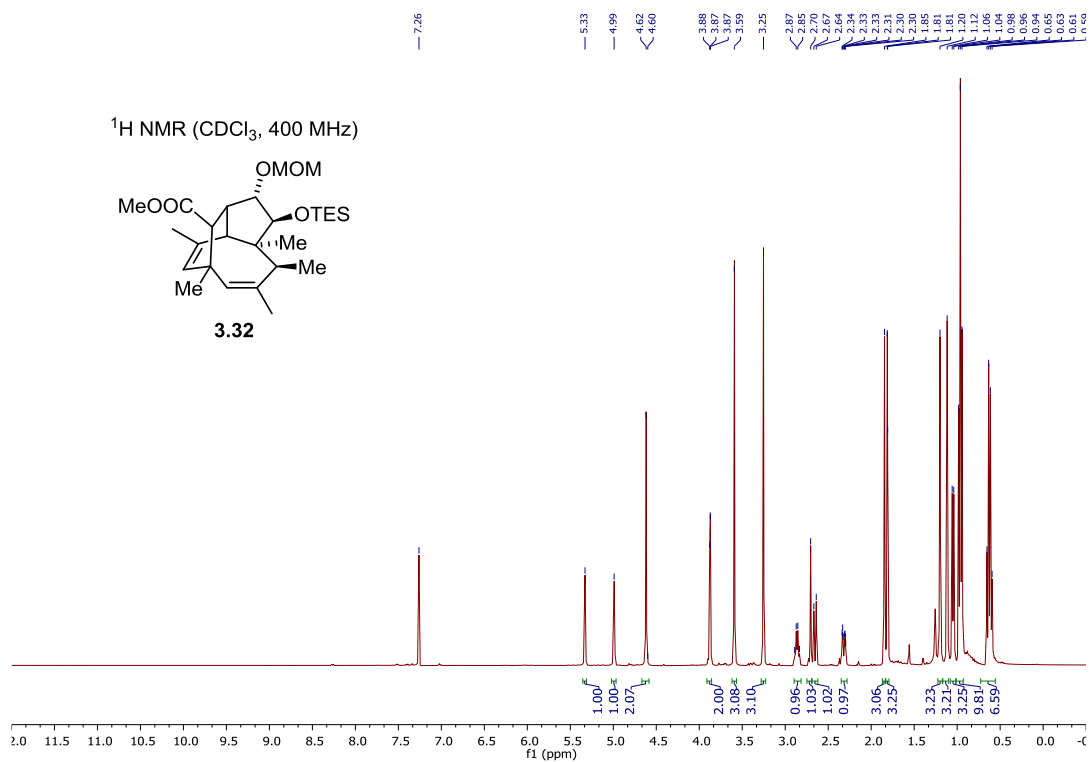


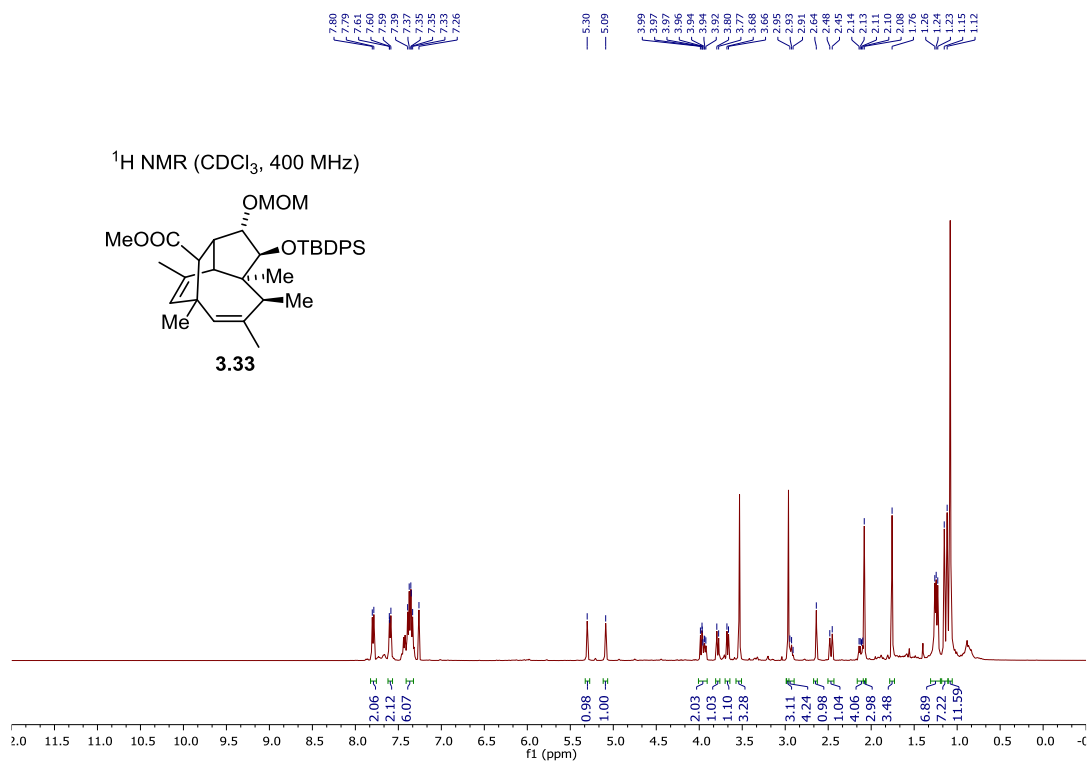
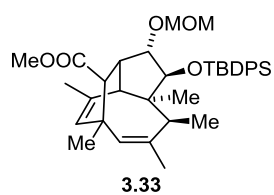
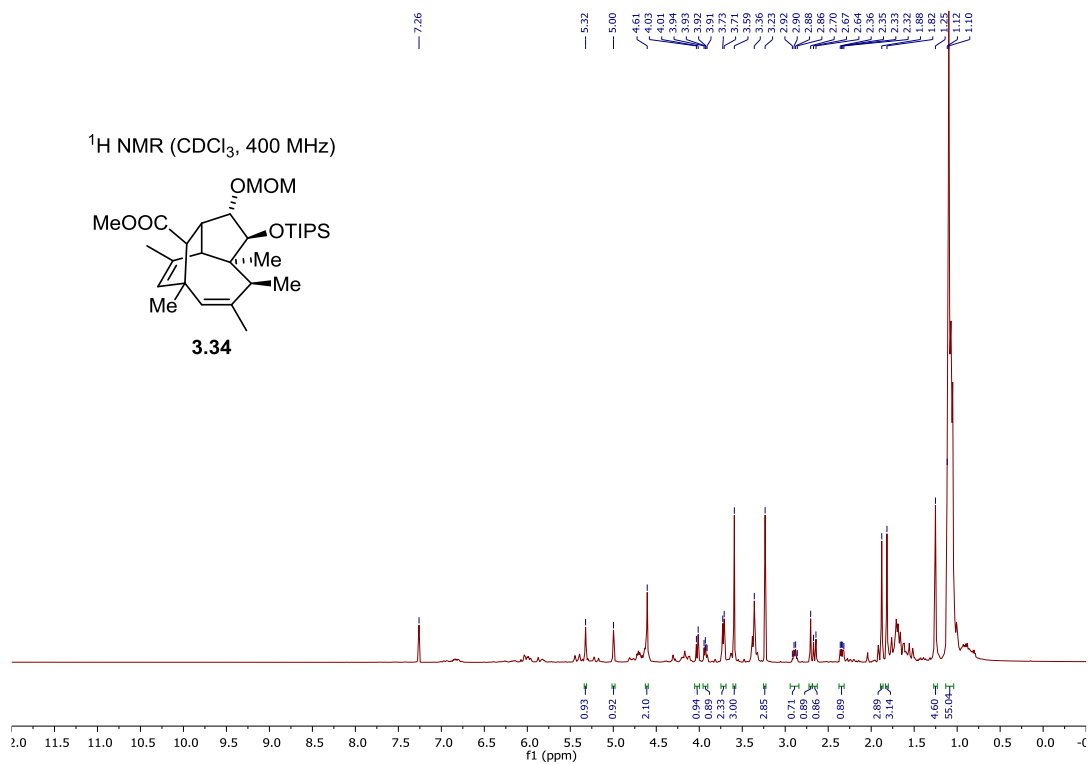
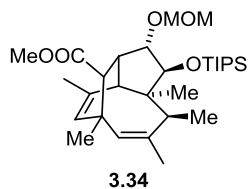


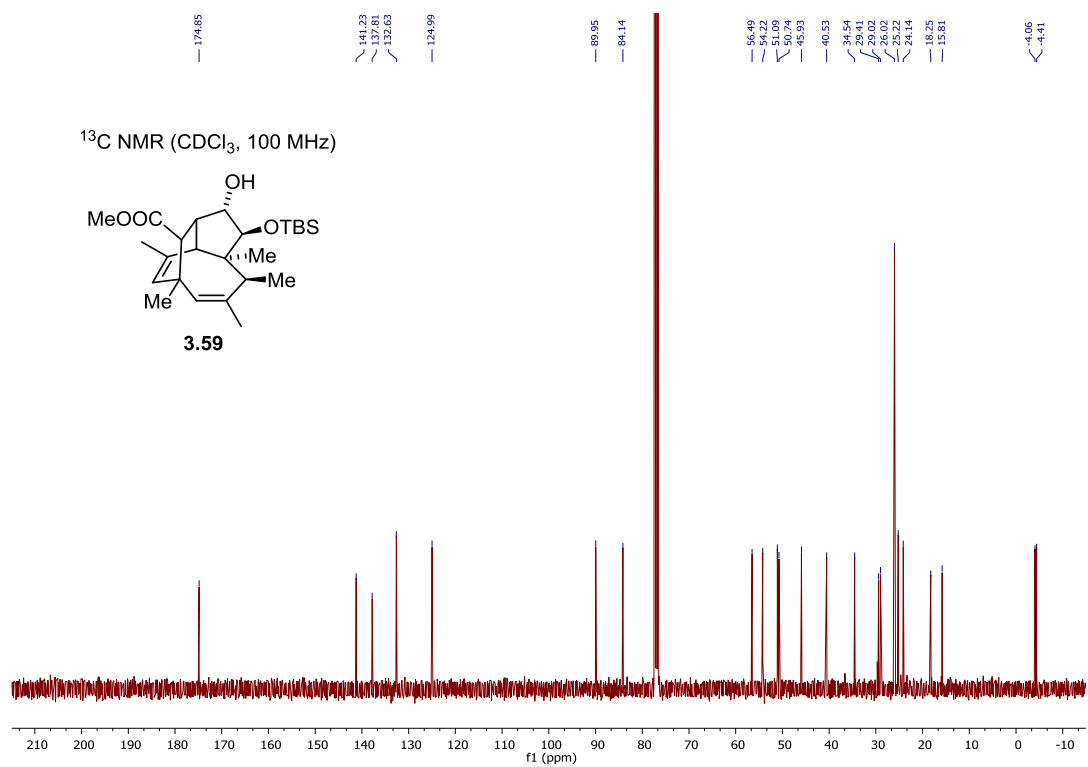
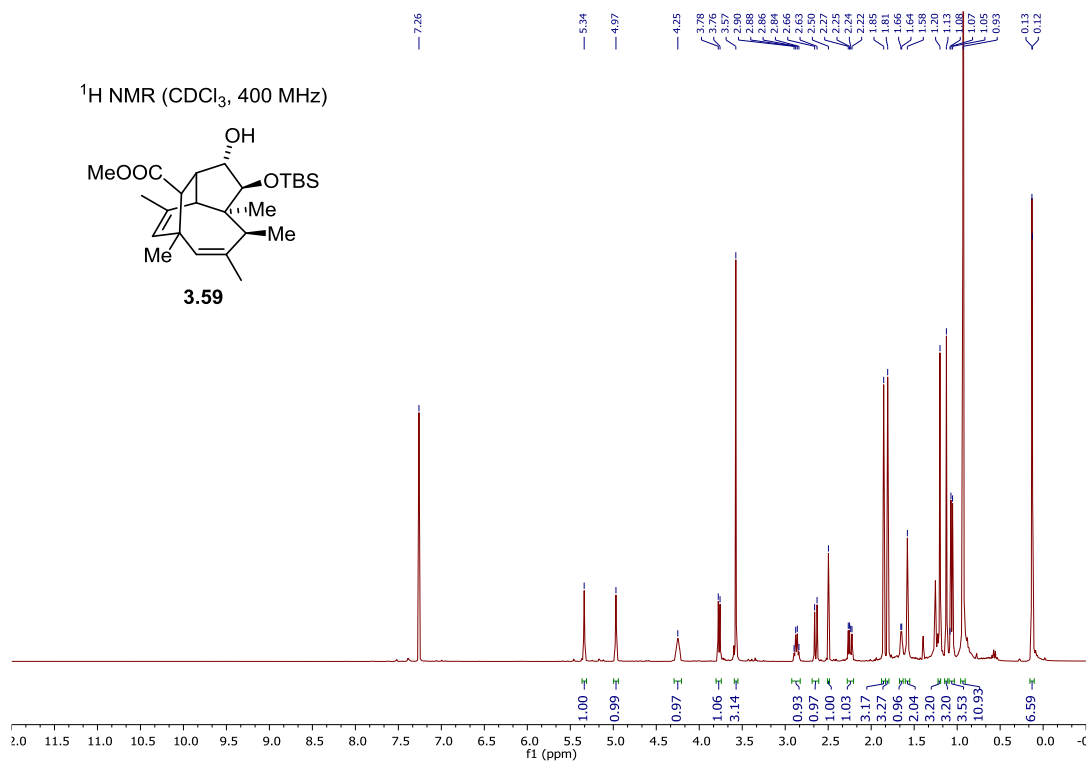


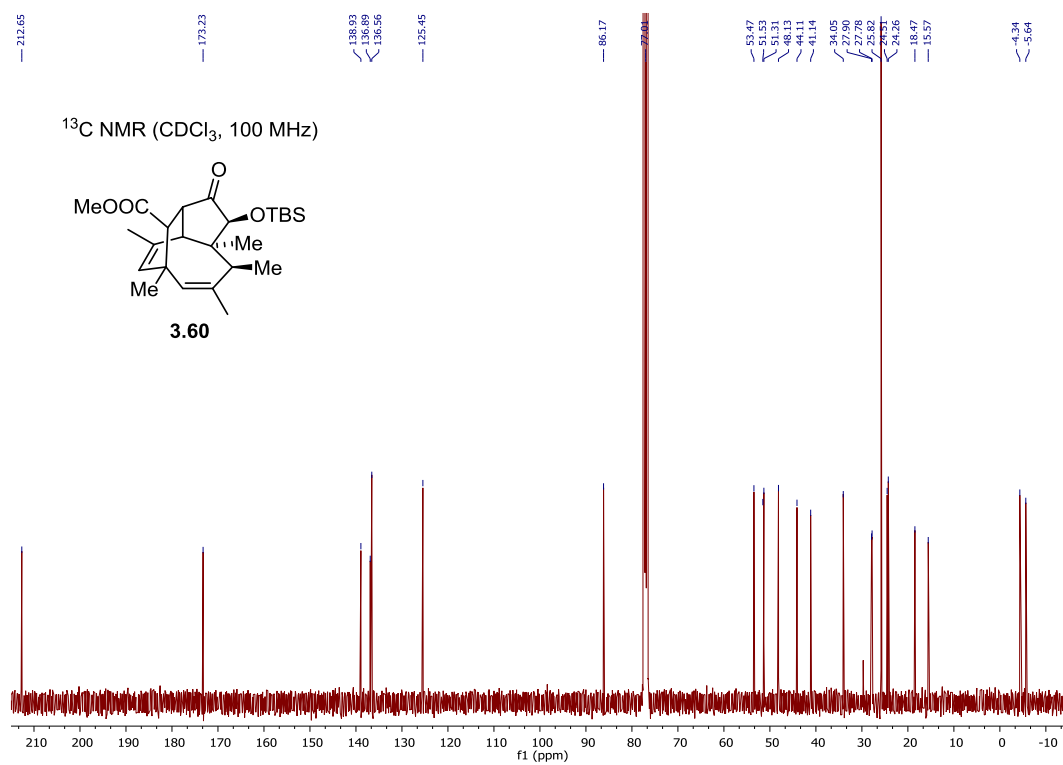
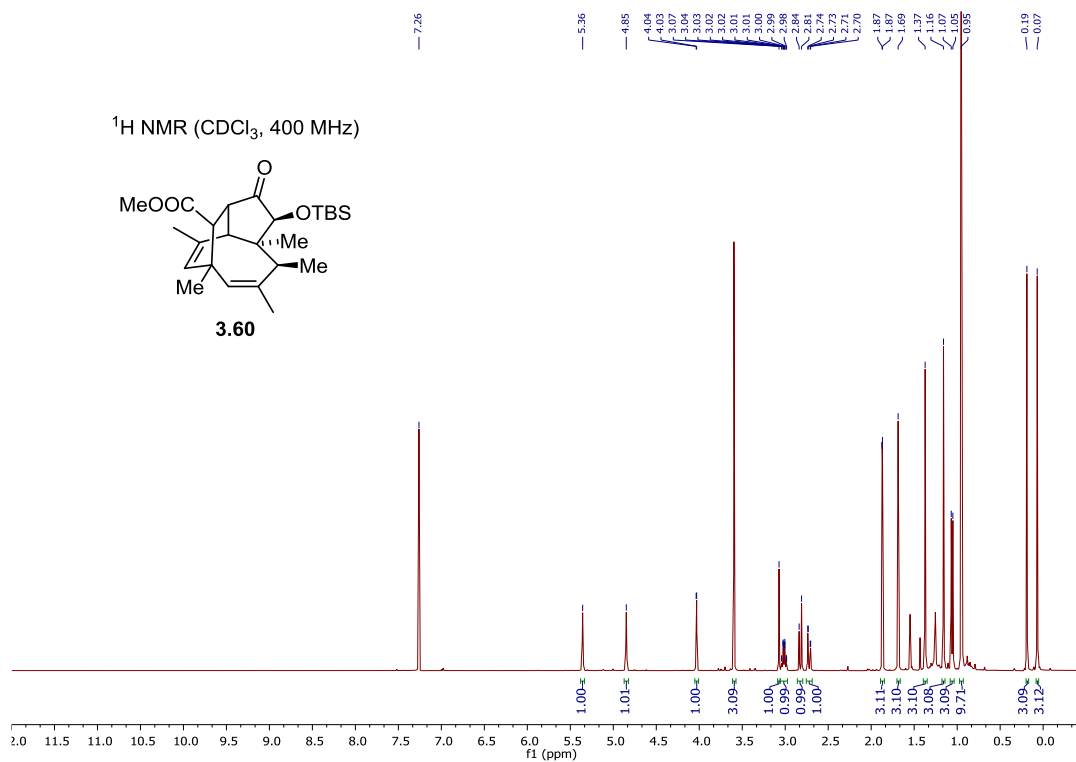


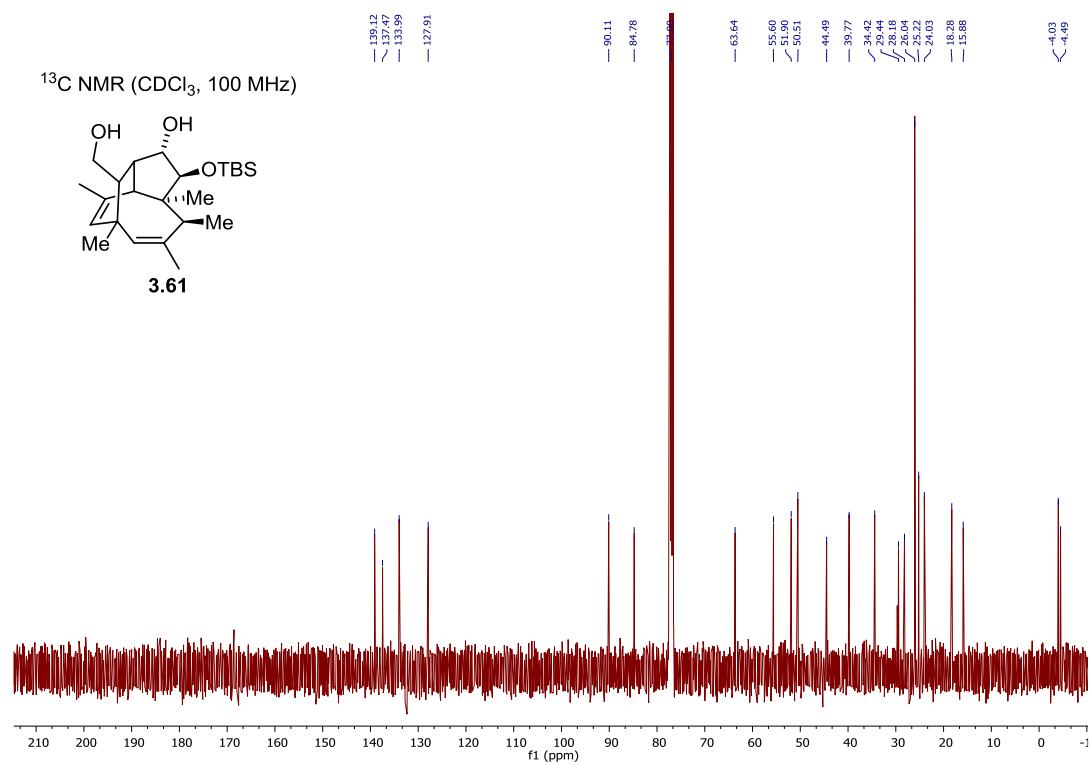
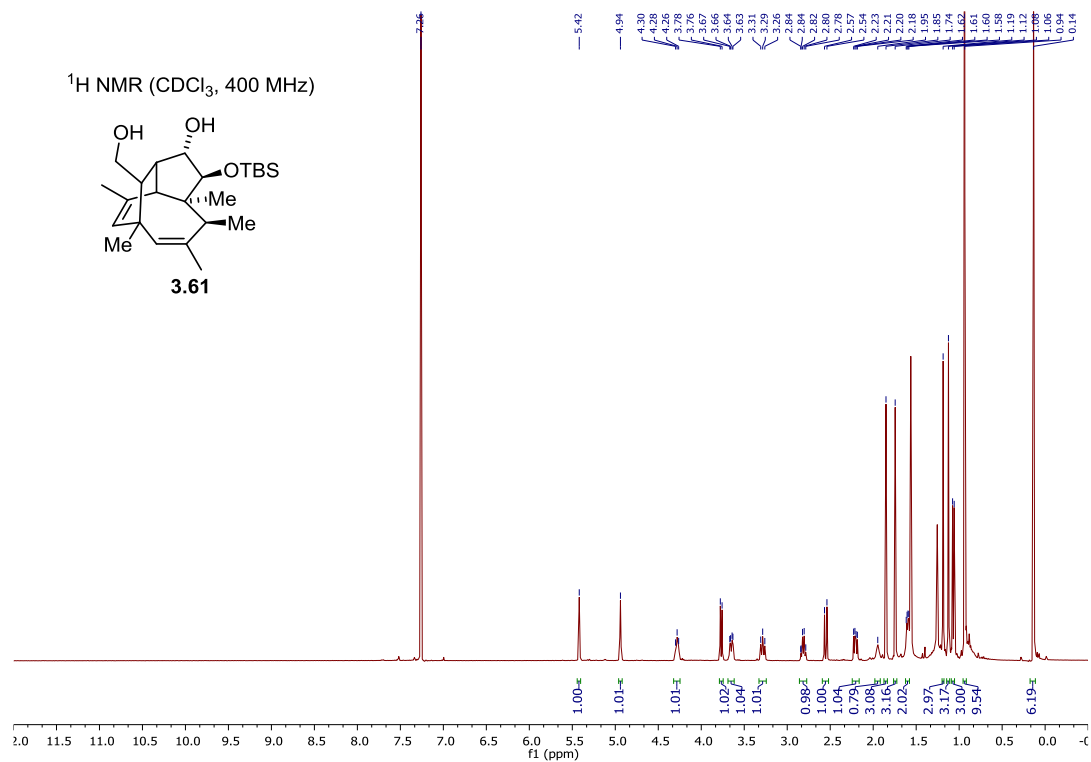


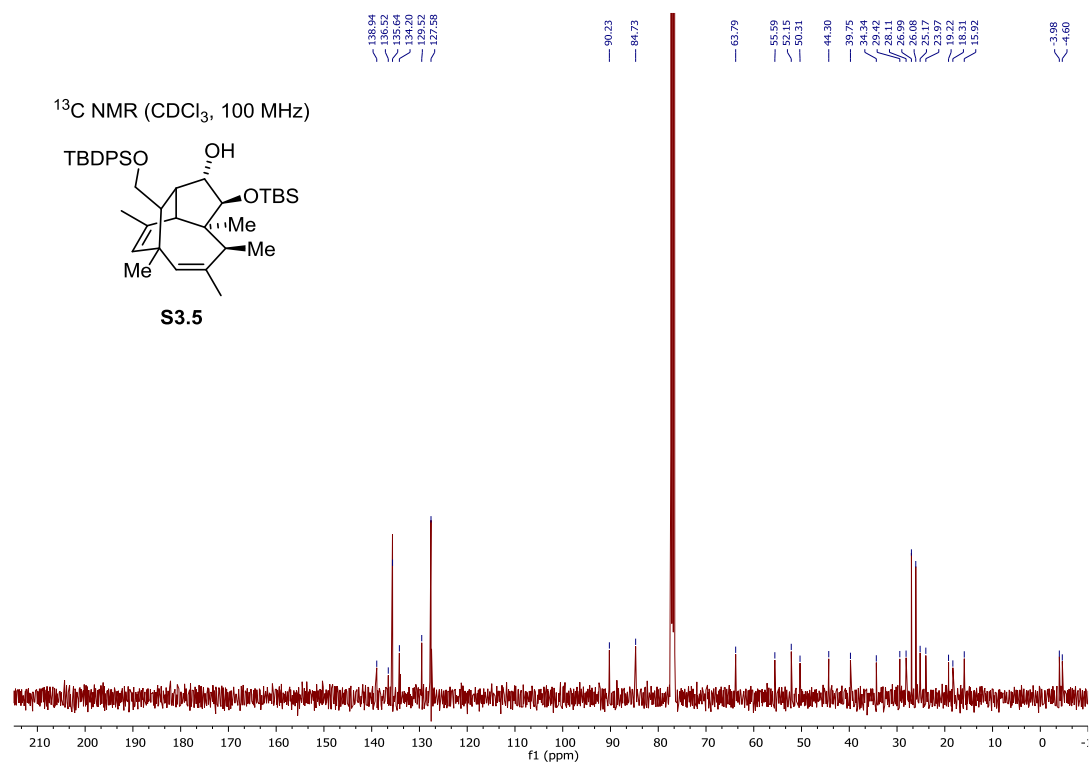
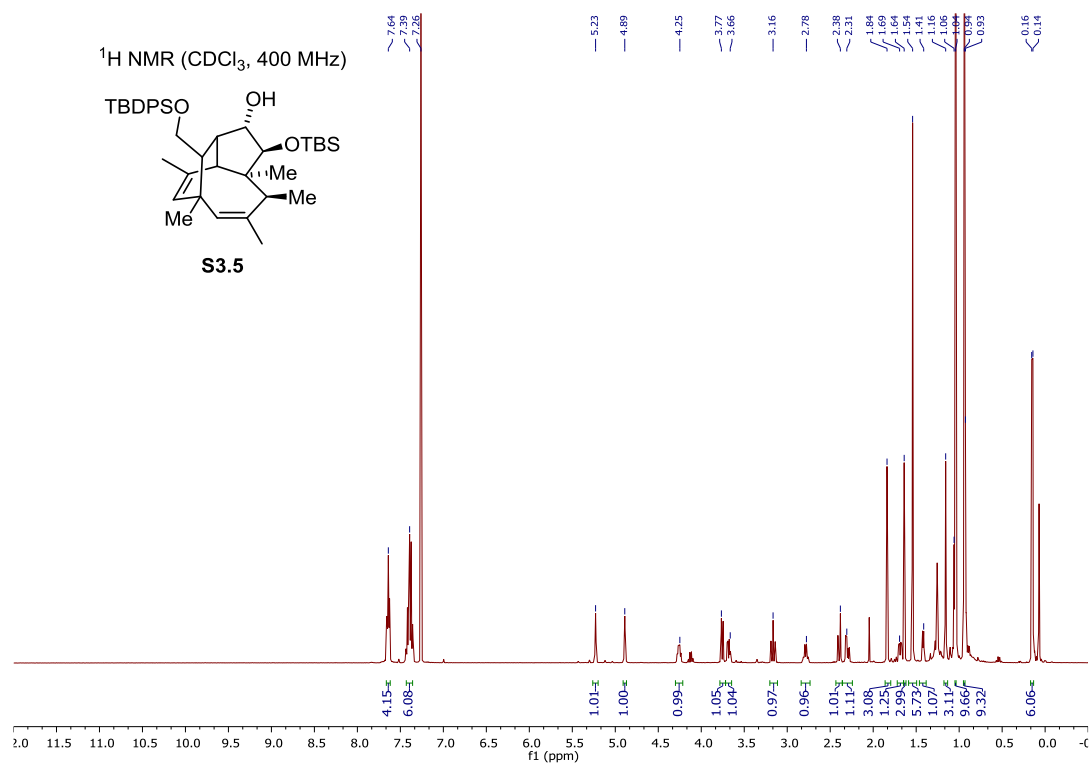


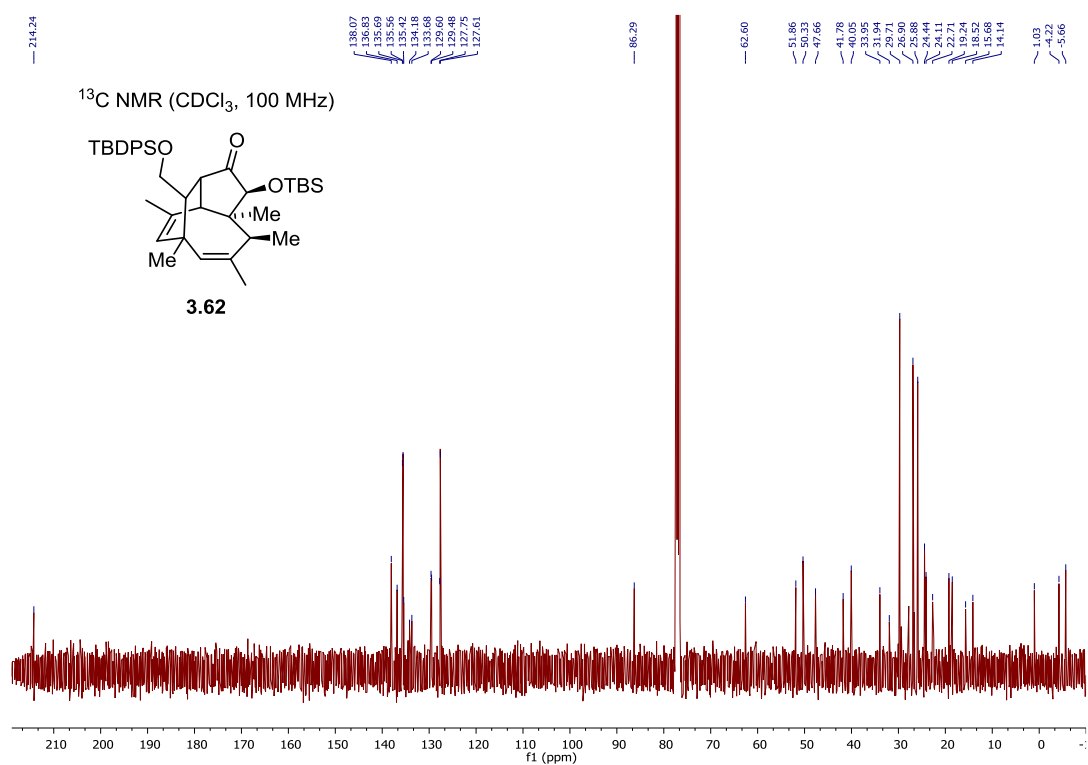
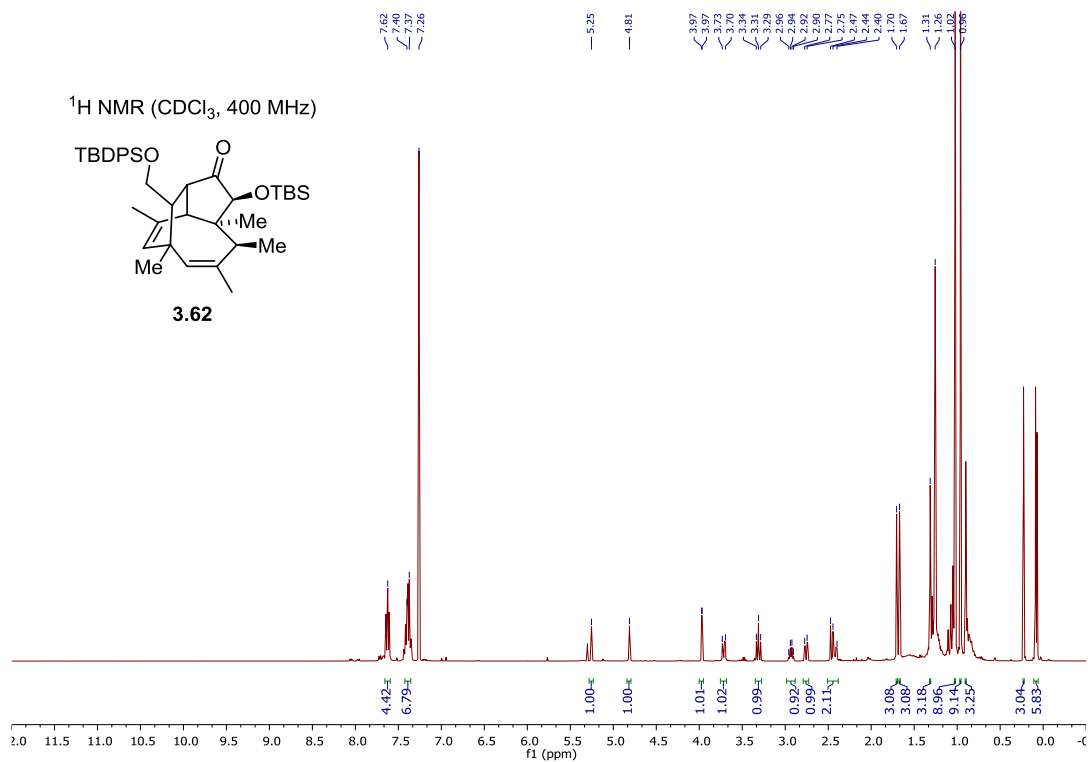
<sup>1</sup>H NMR (CDCl<sub>3</sub>, 400 MHz)<sup>1</sup>H NMR (CDCl<sub>3</sub>, 400 MHz)



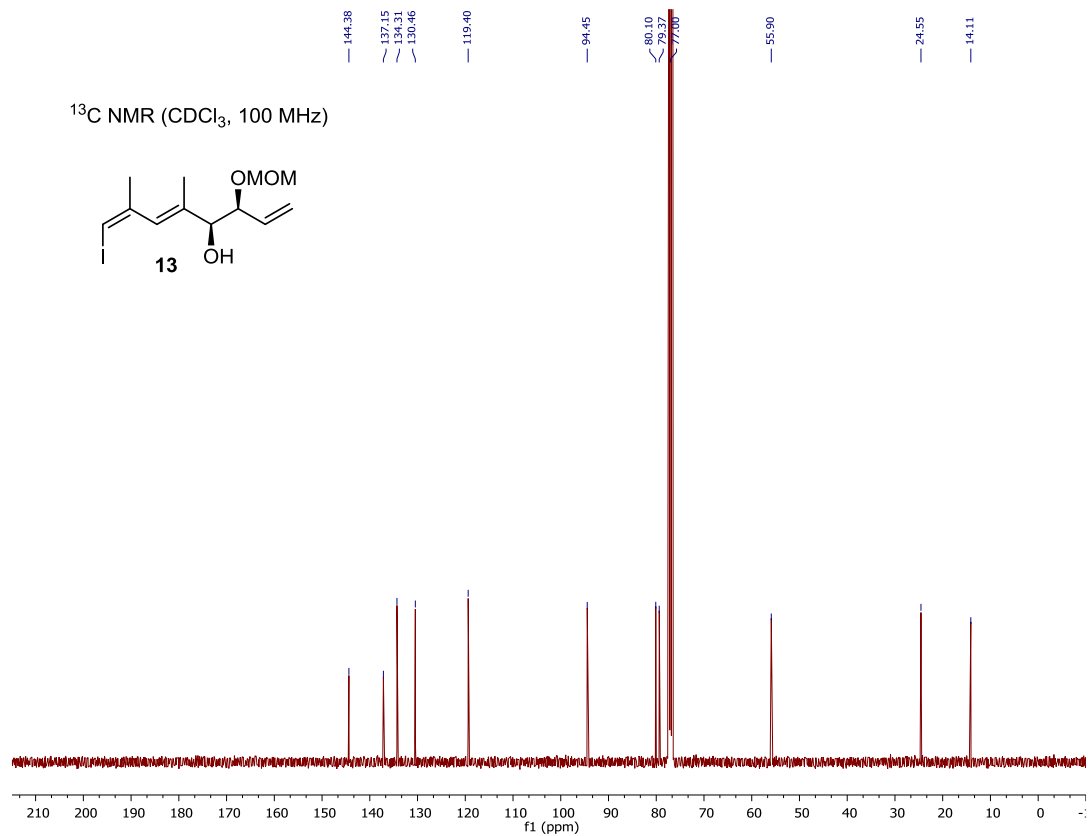
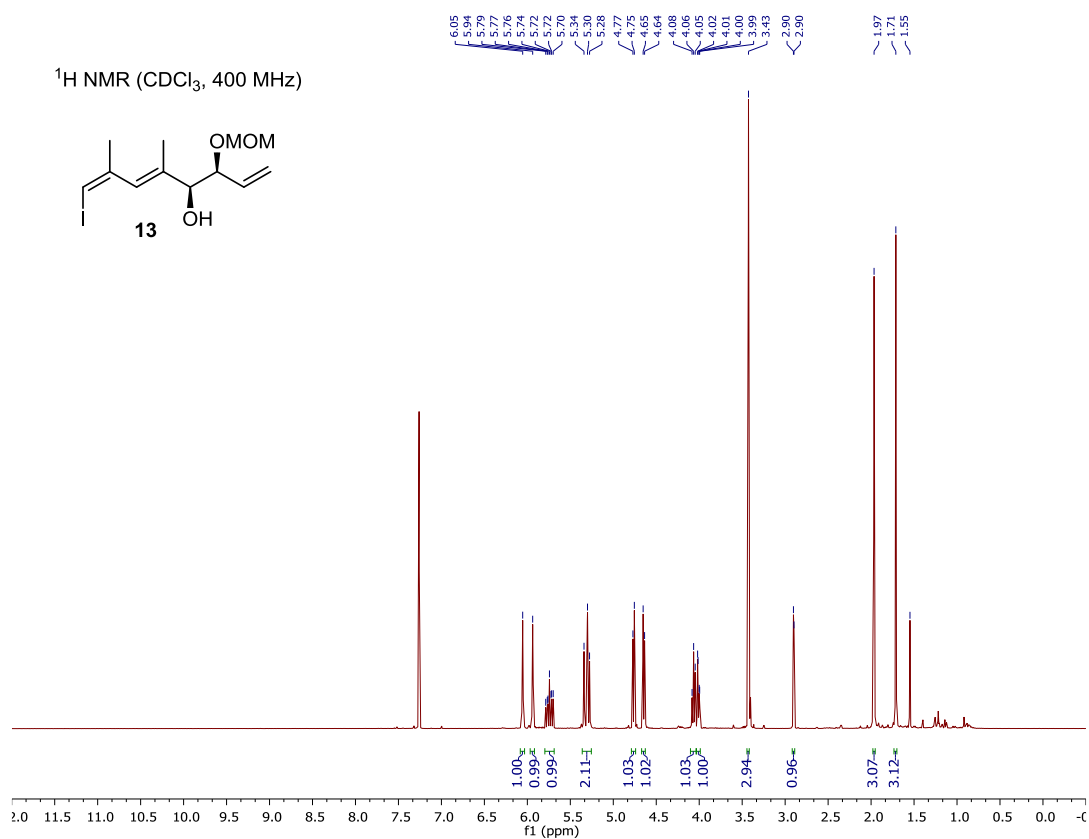




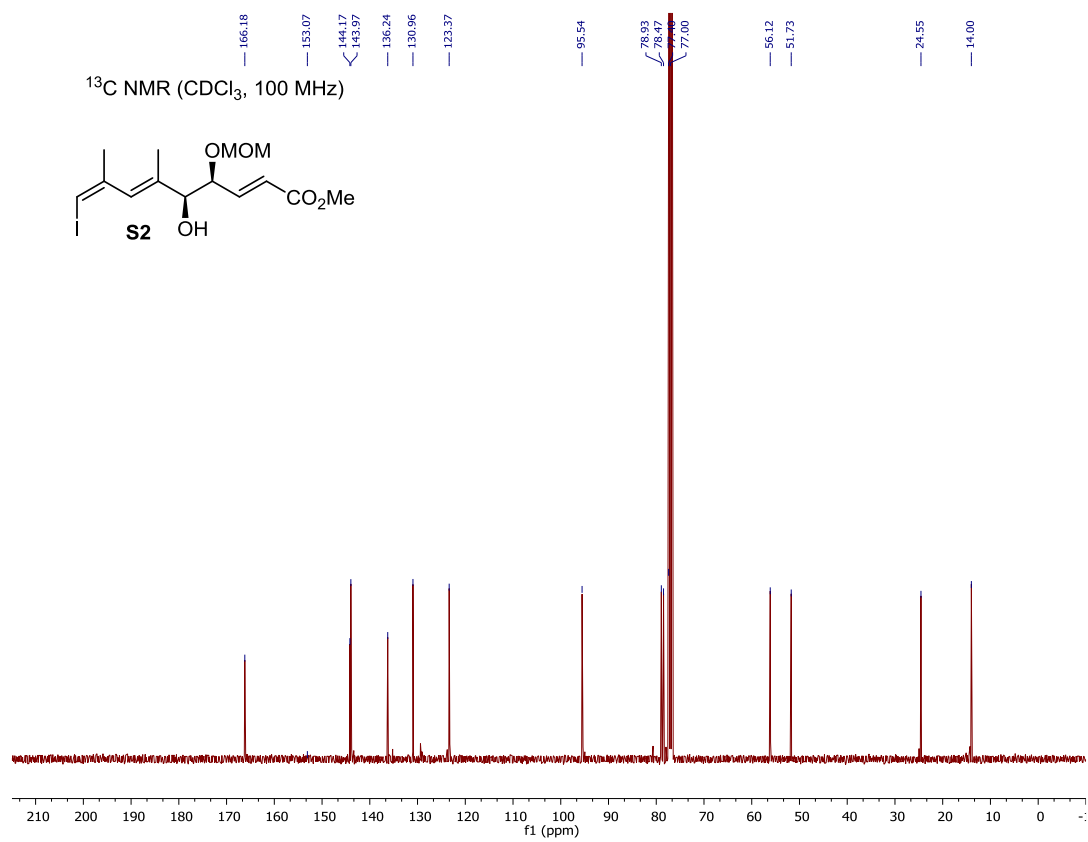
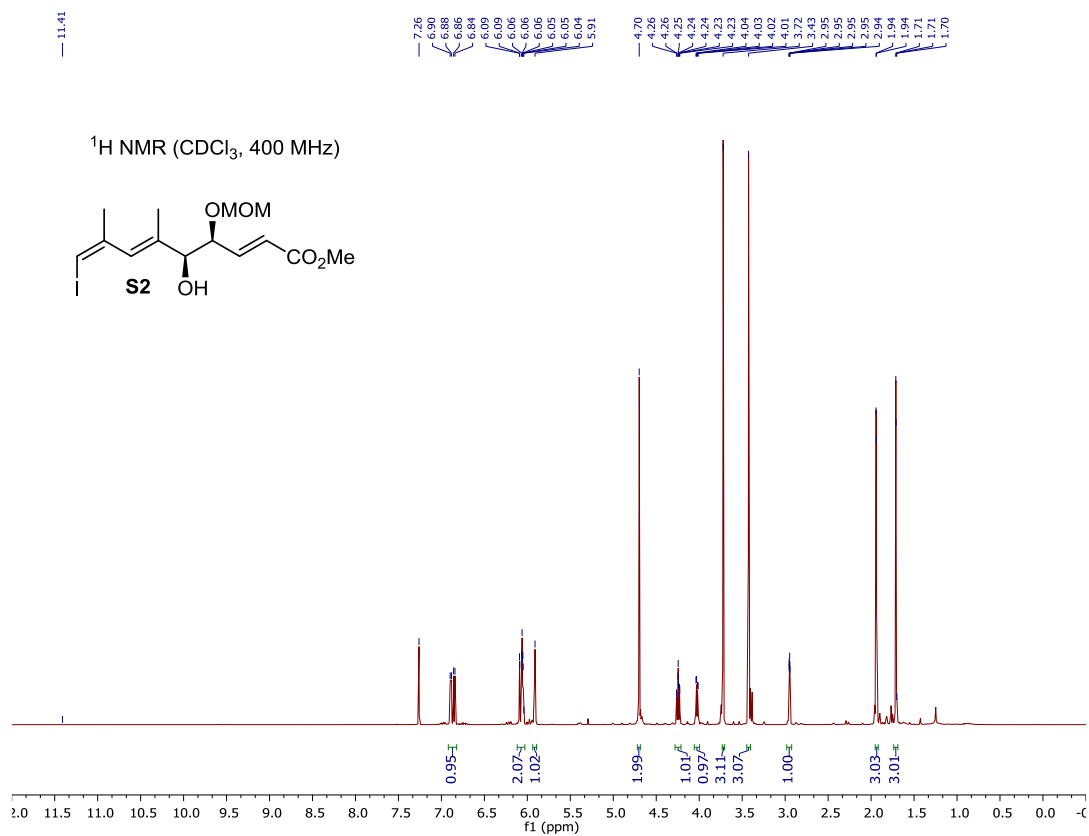


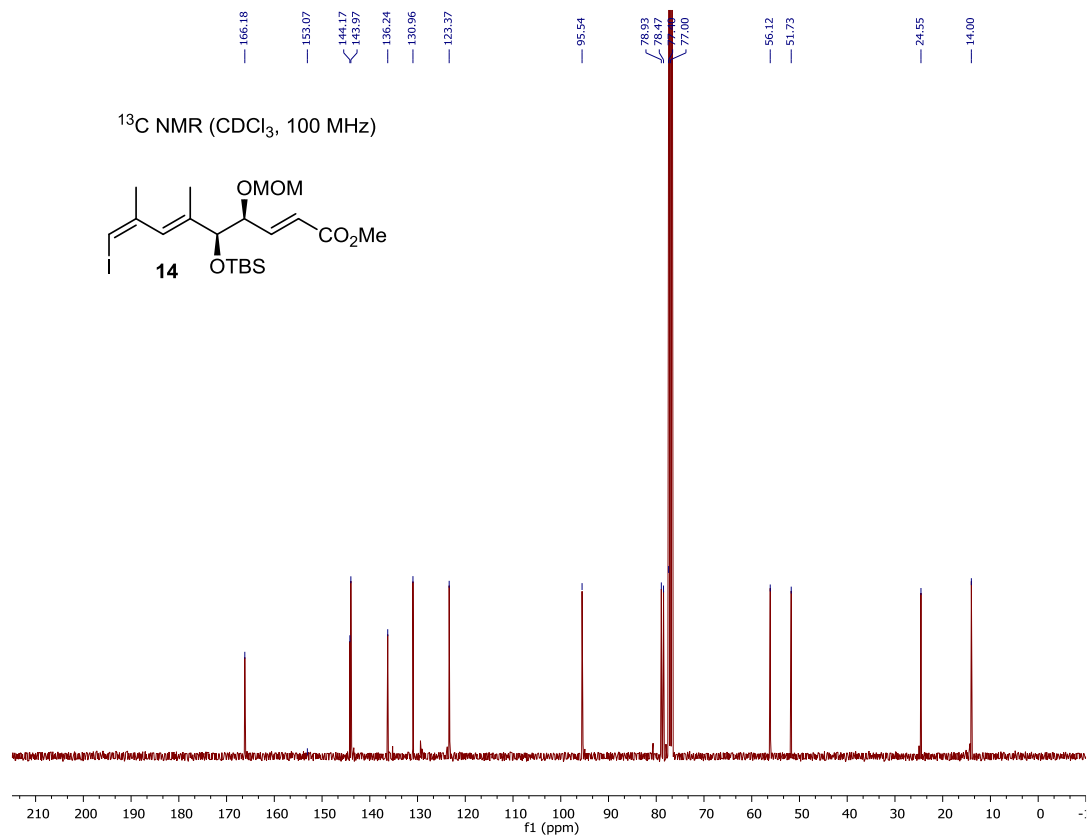
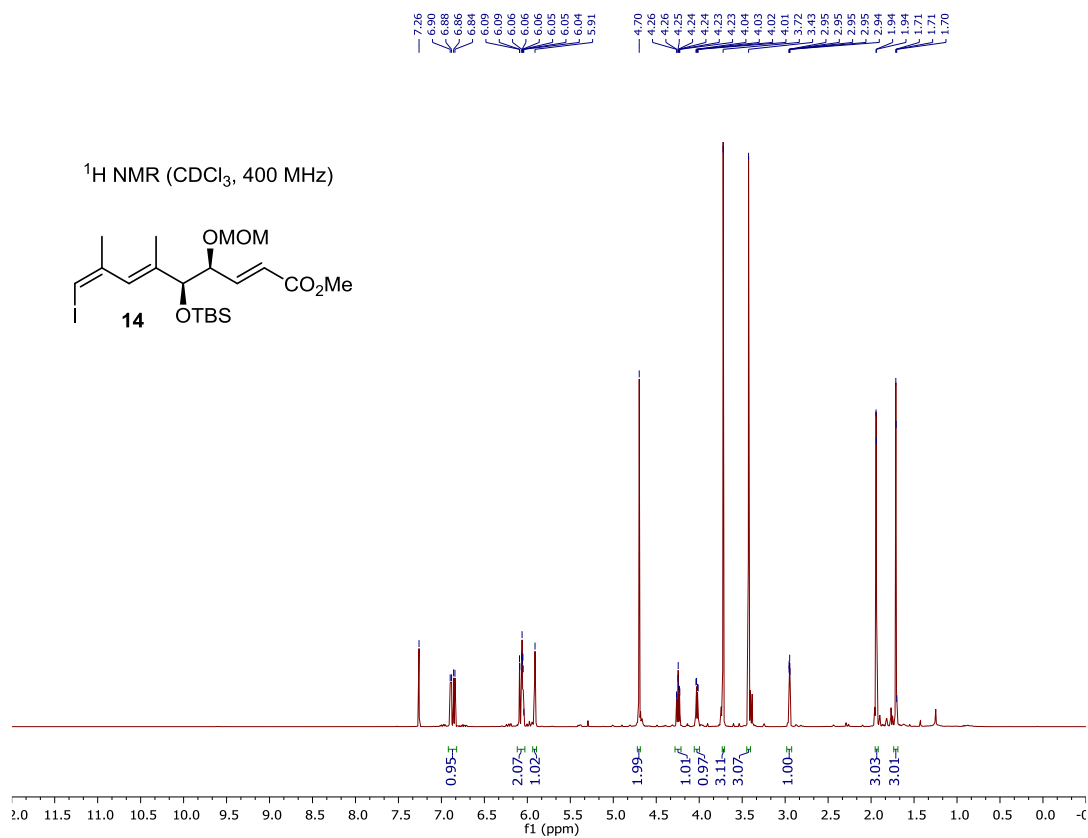


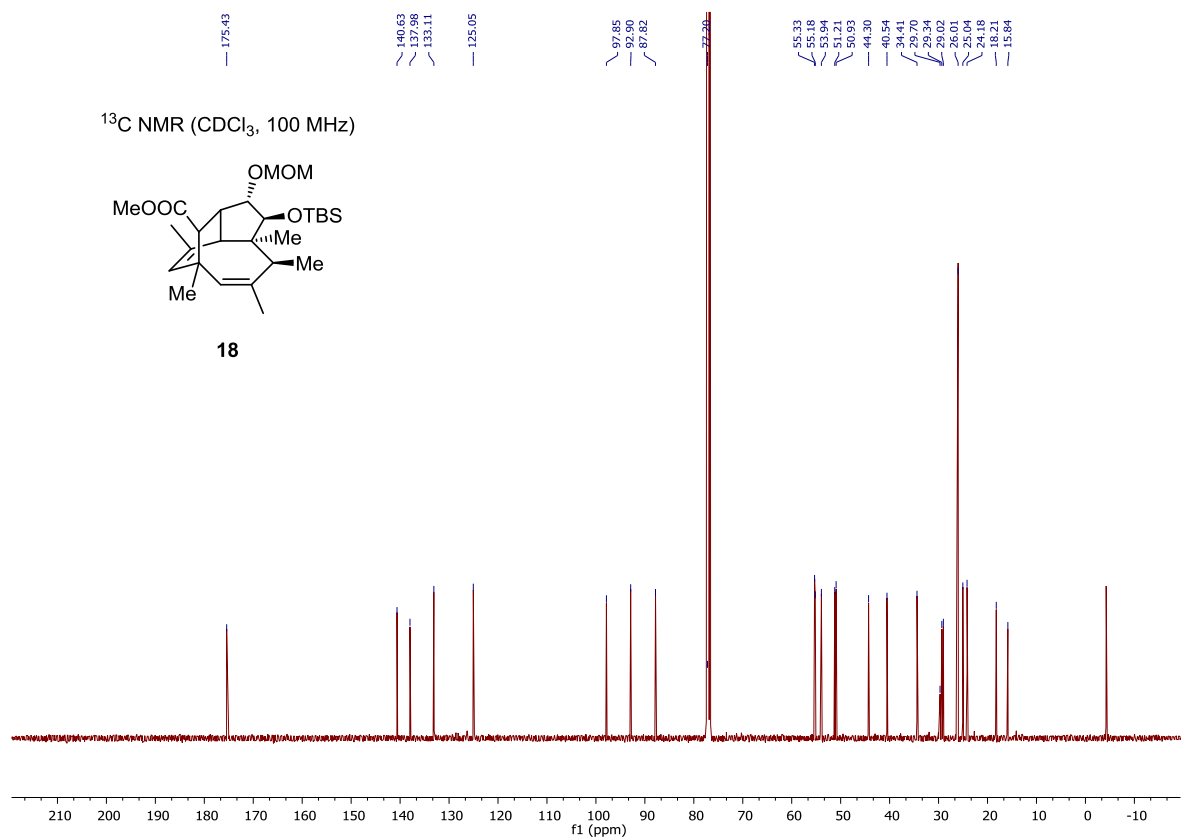
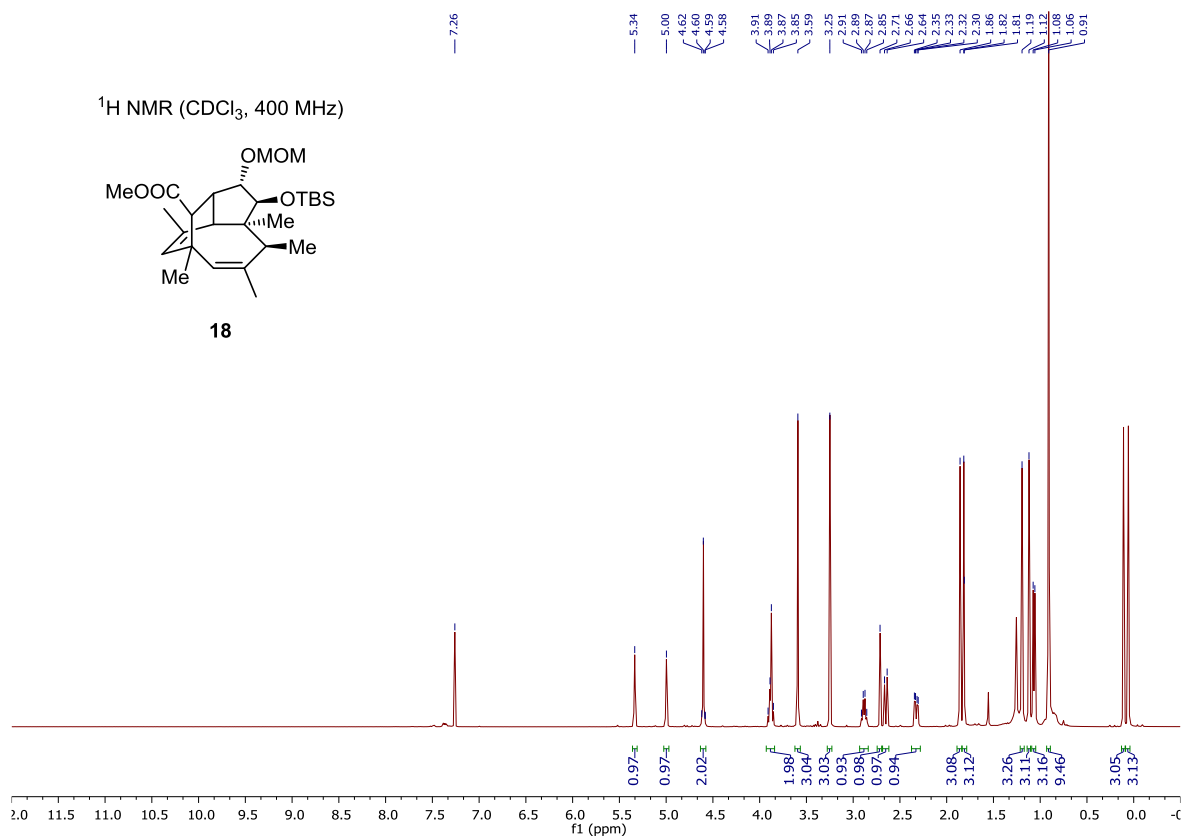
## 8.8.3 NMR Spectra for Chapter 3.3

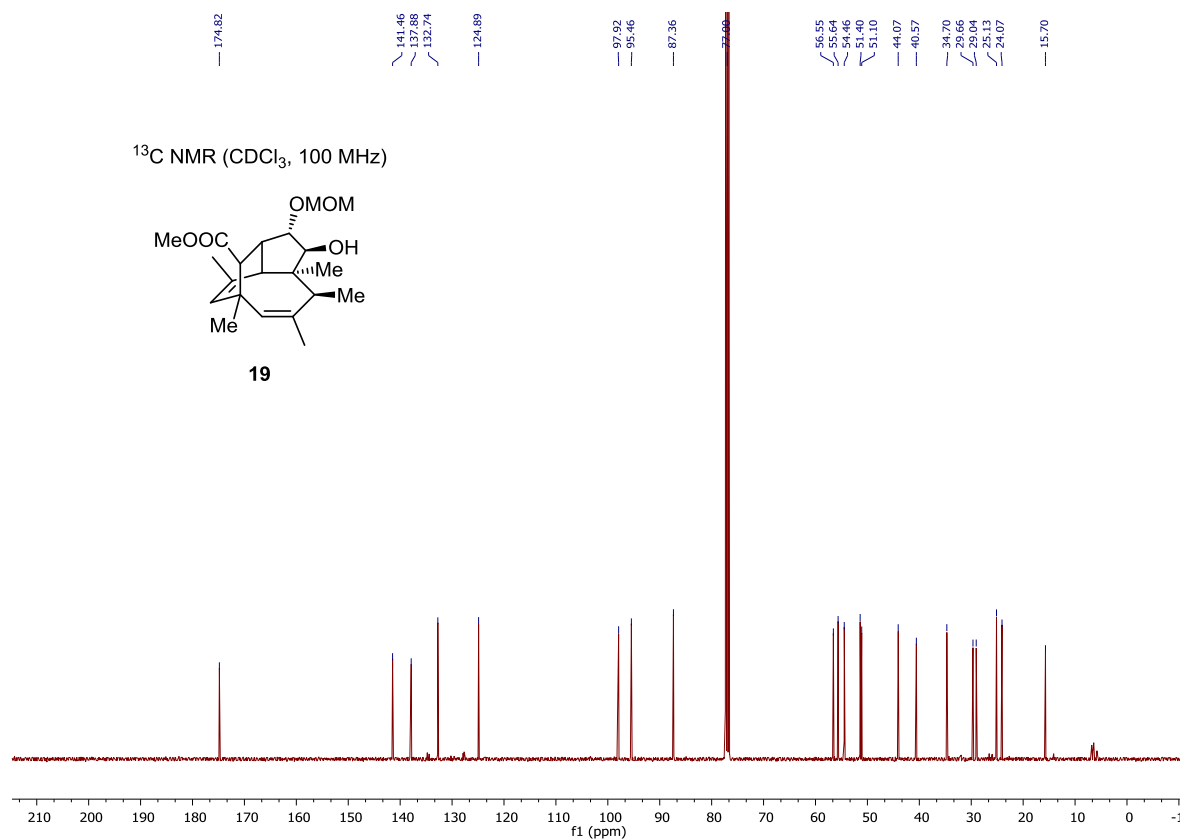
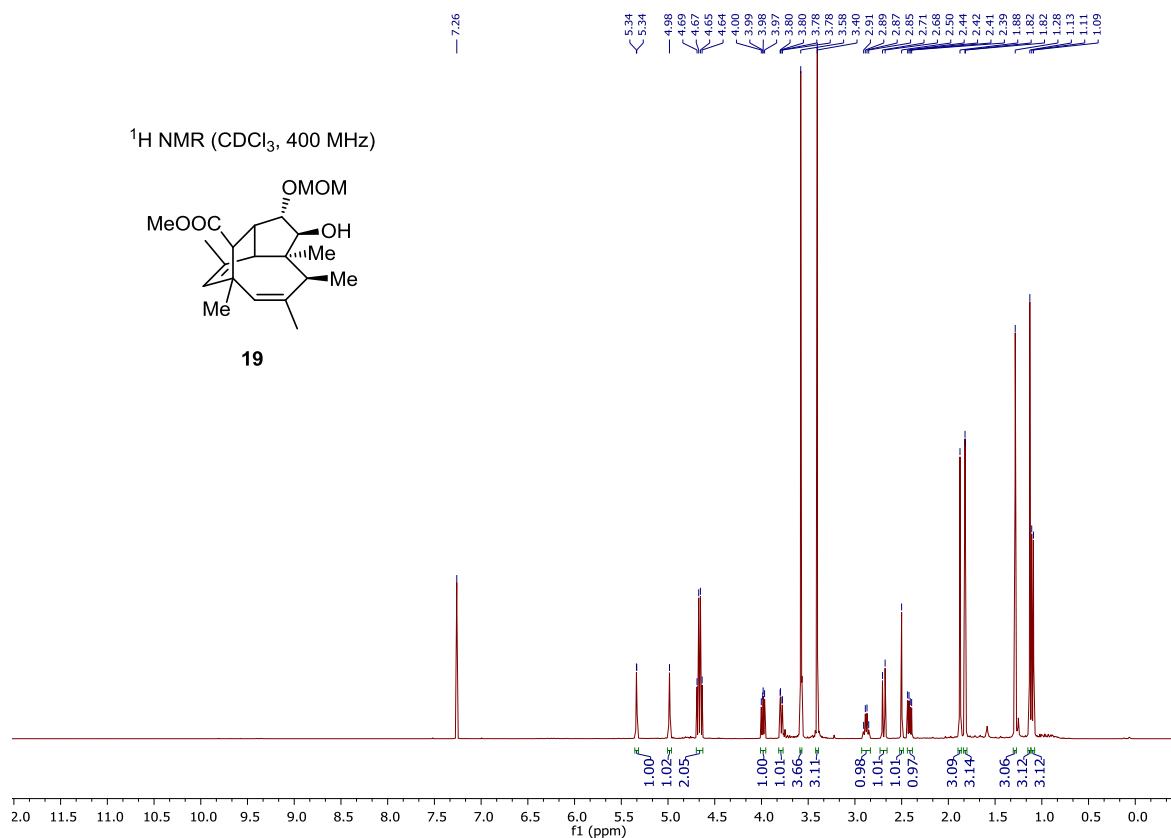


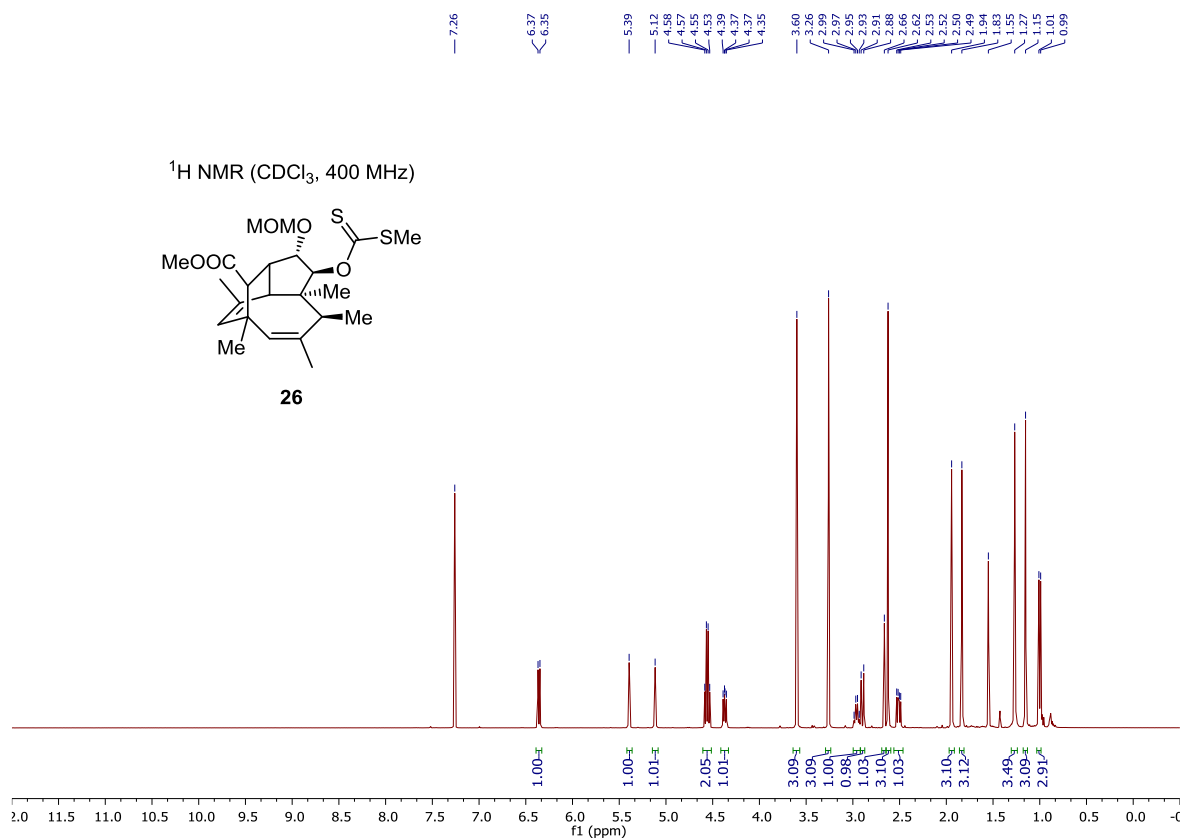
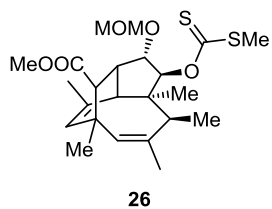
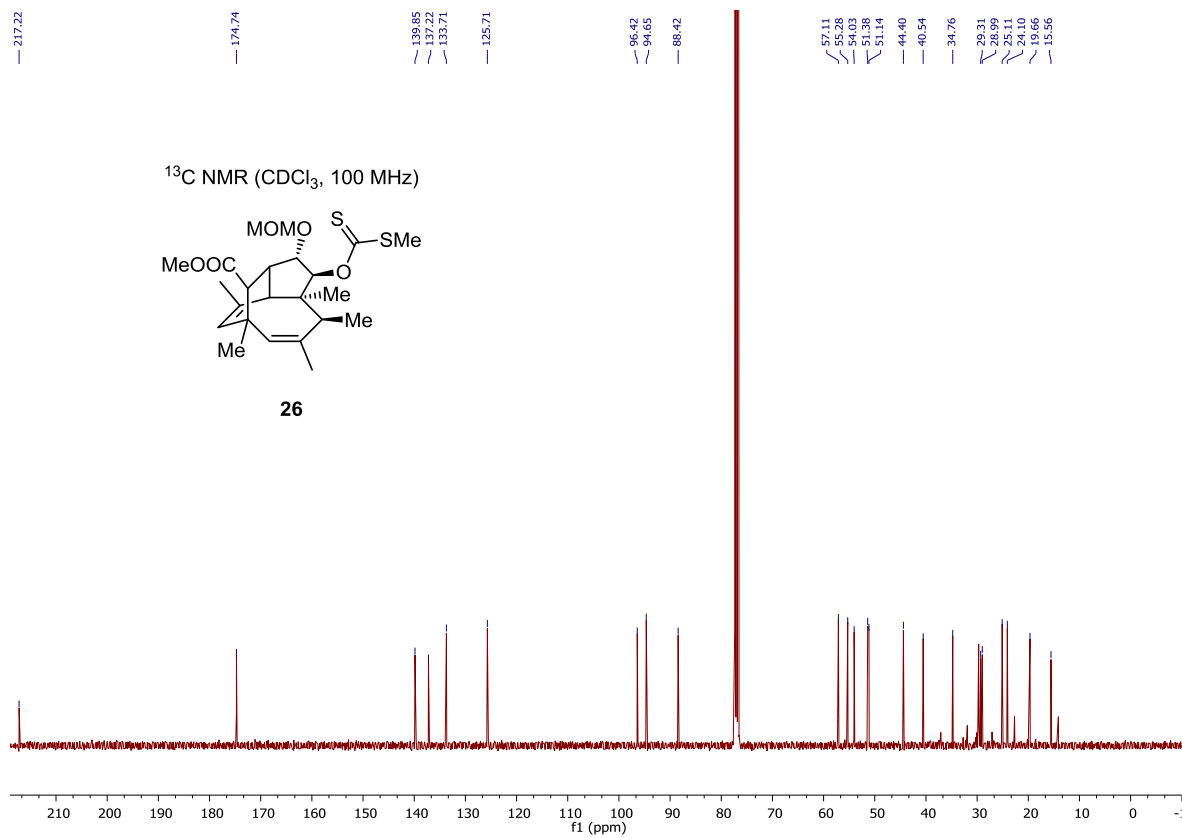
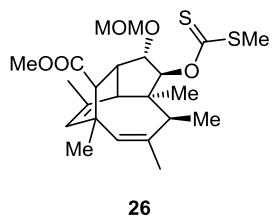


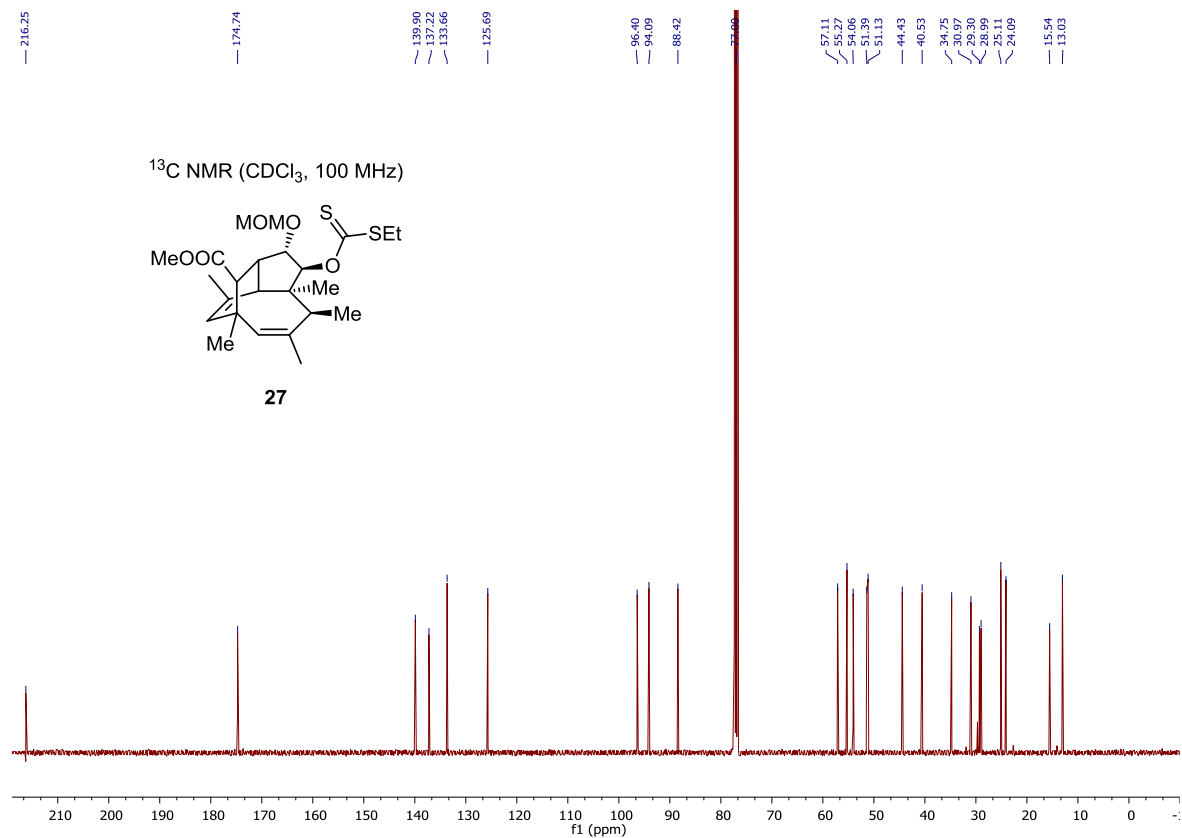


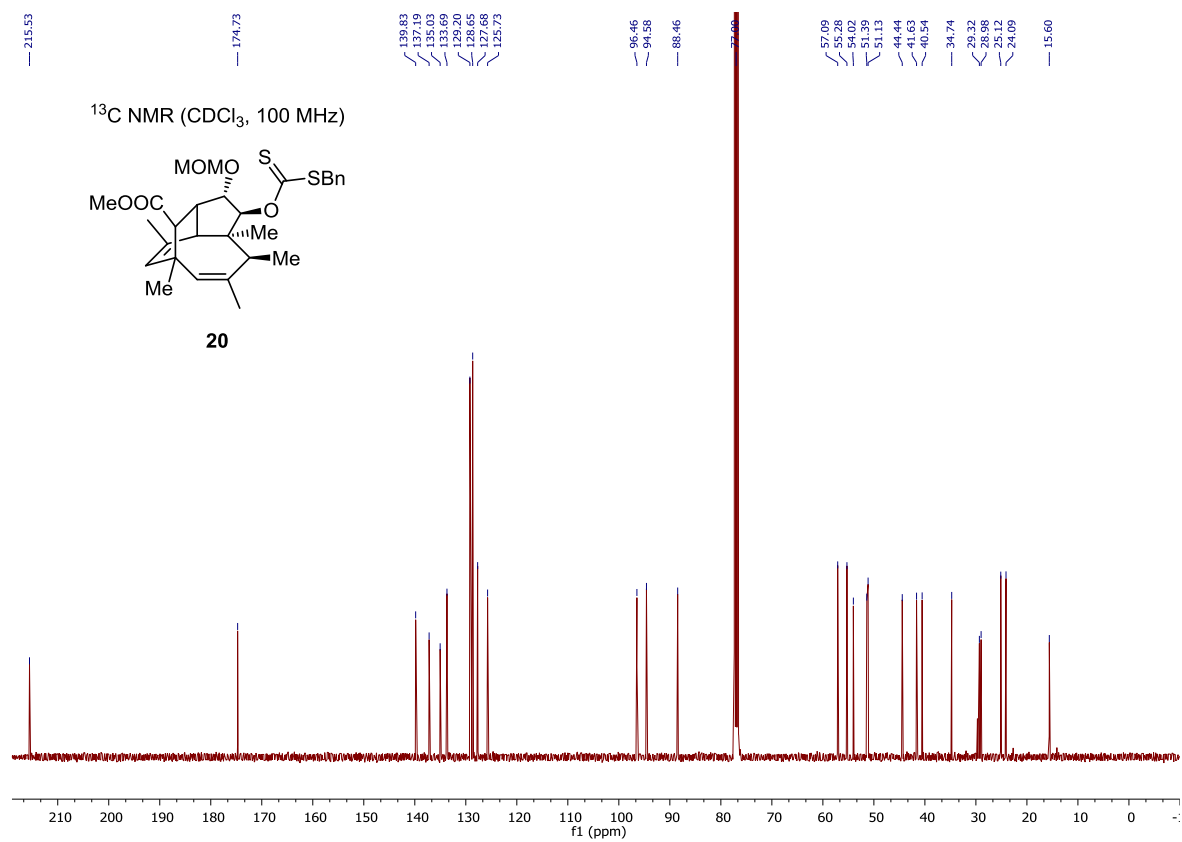
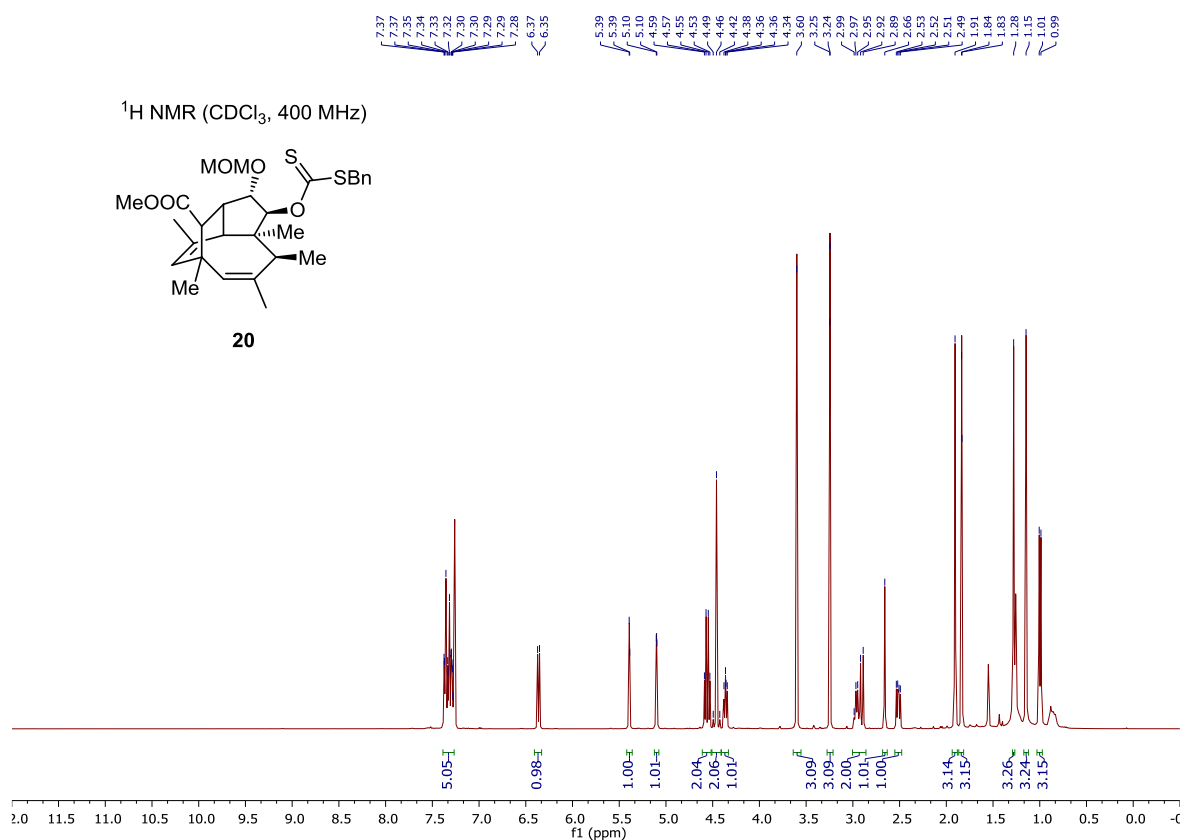


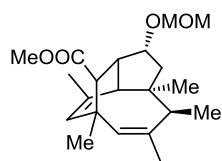
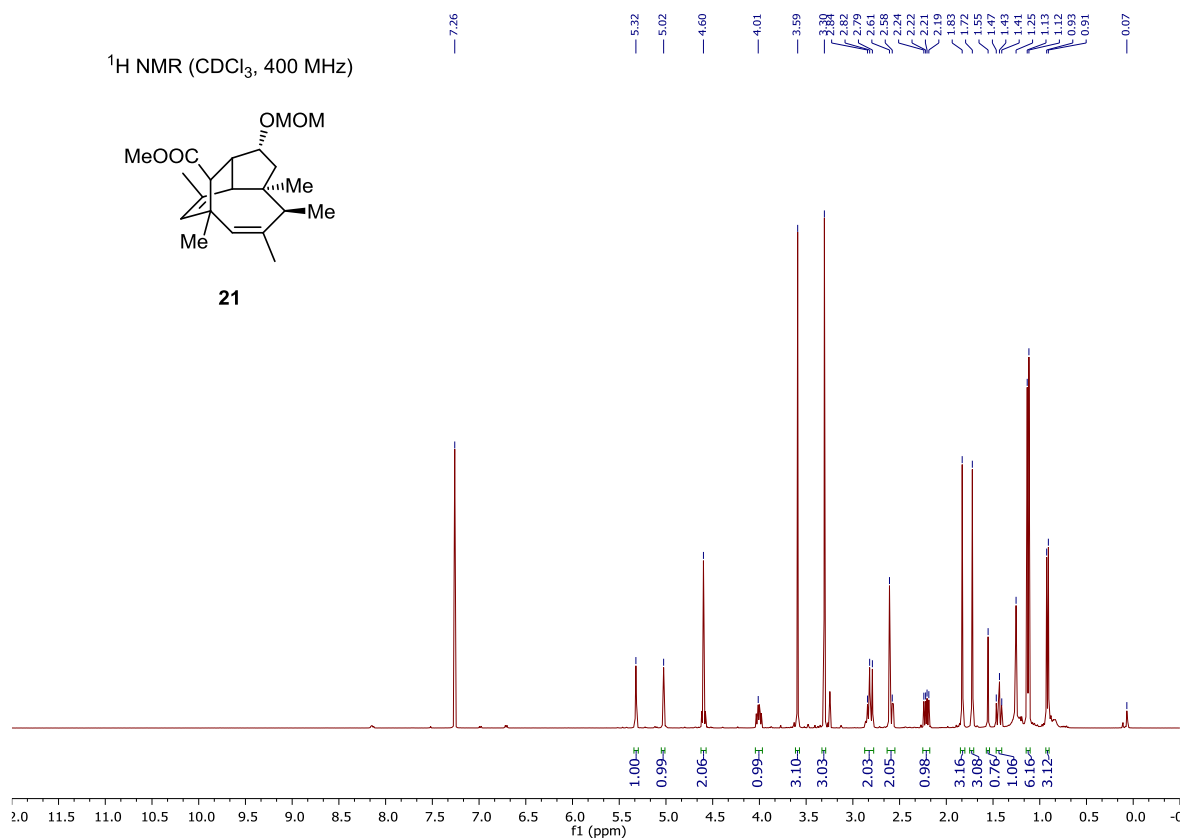
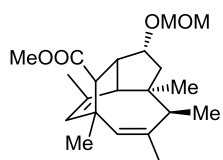
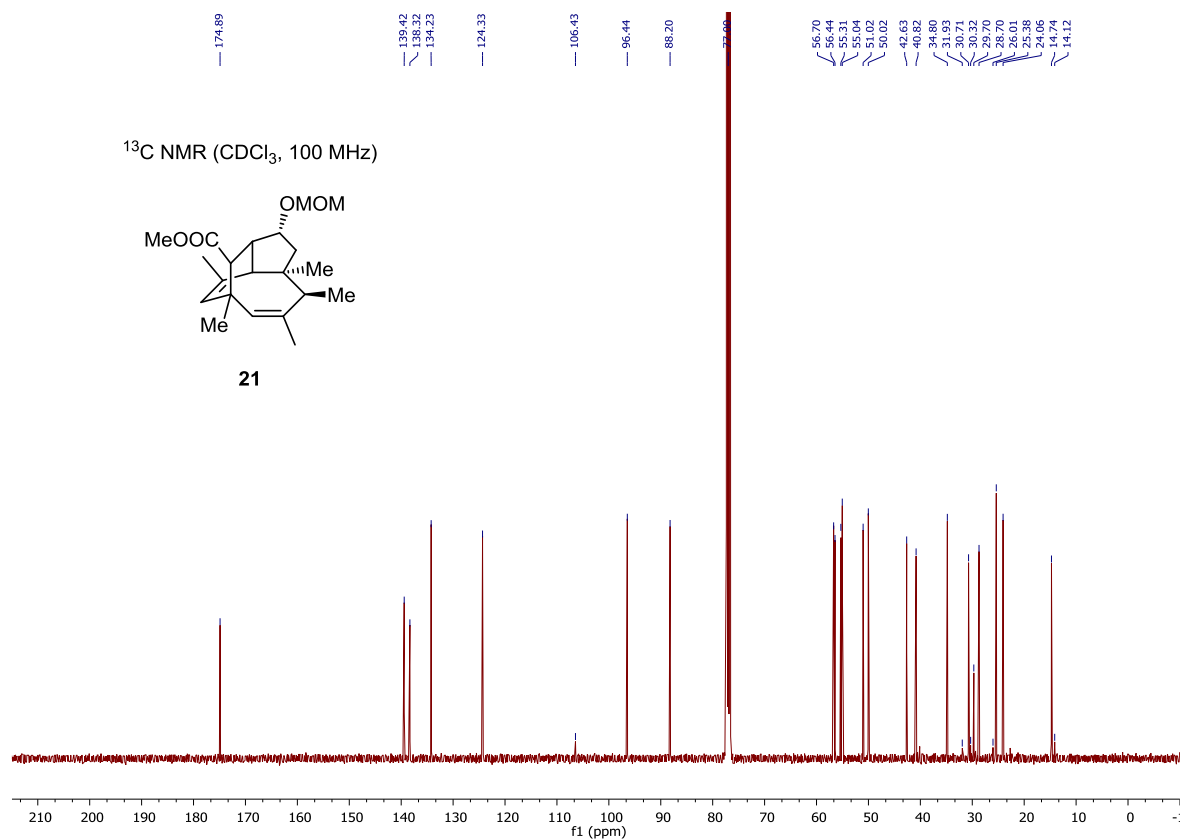




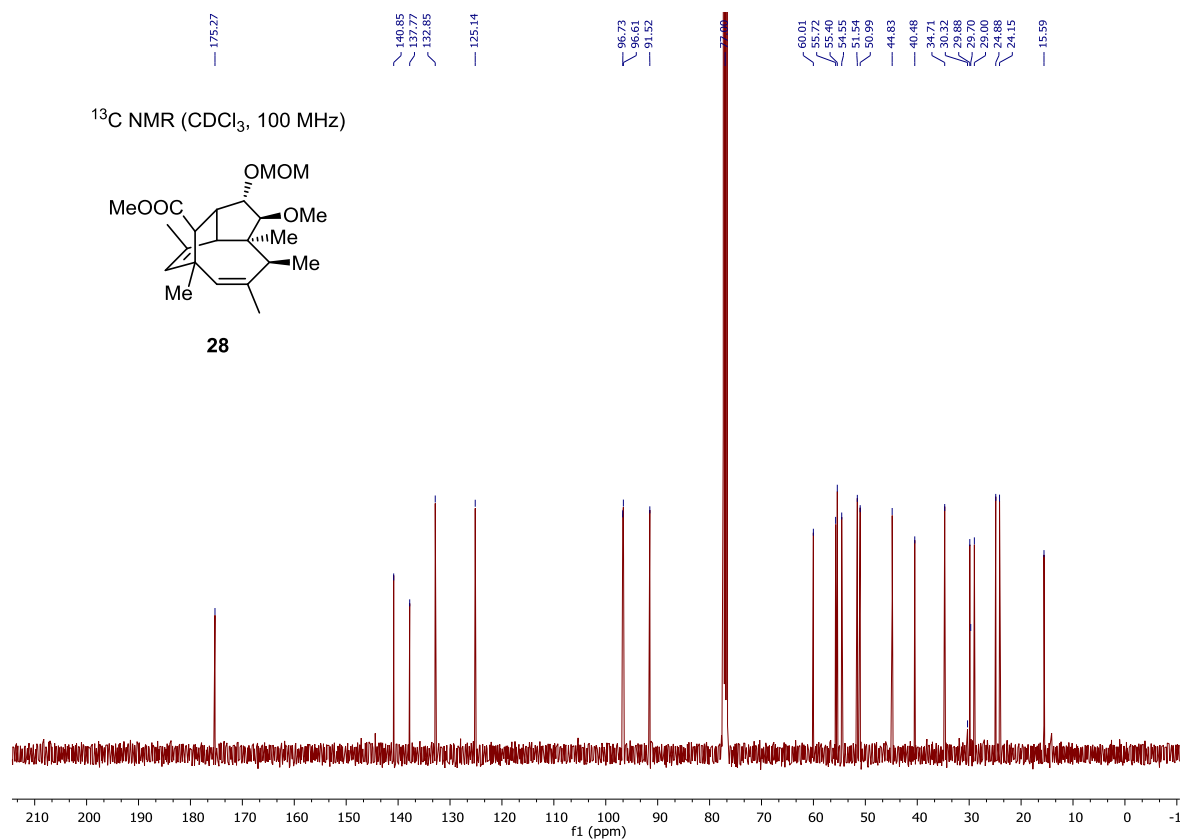
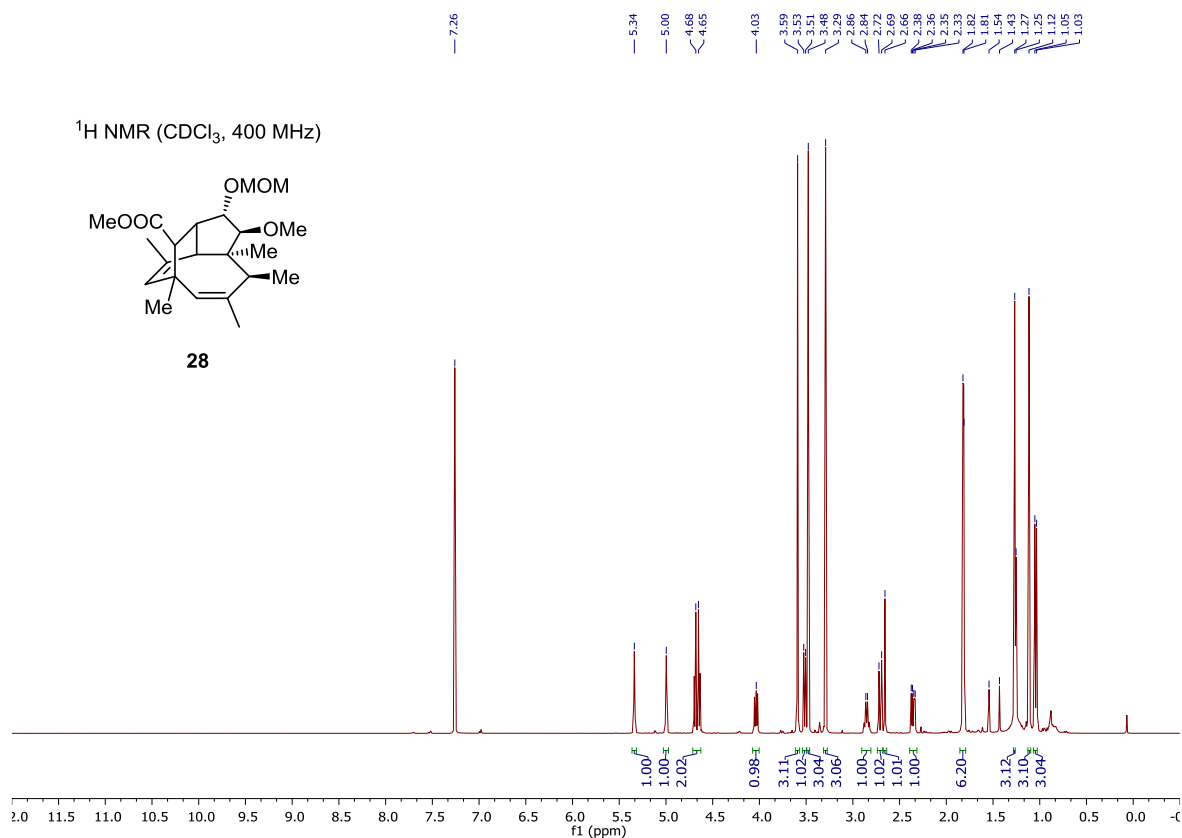
<sup>1</sup>H NMR (CDCl<sub>3</sub>, 400 MHz)<sup>13</sup>C NMR (CDCl<sub>3</sub>, 100 MHz)

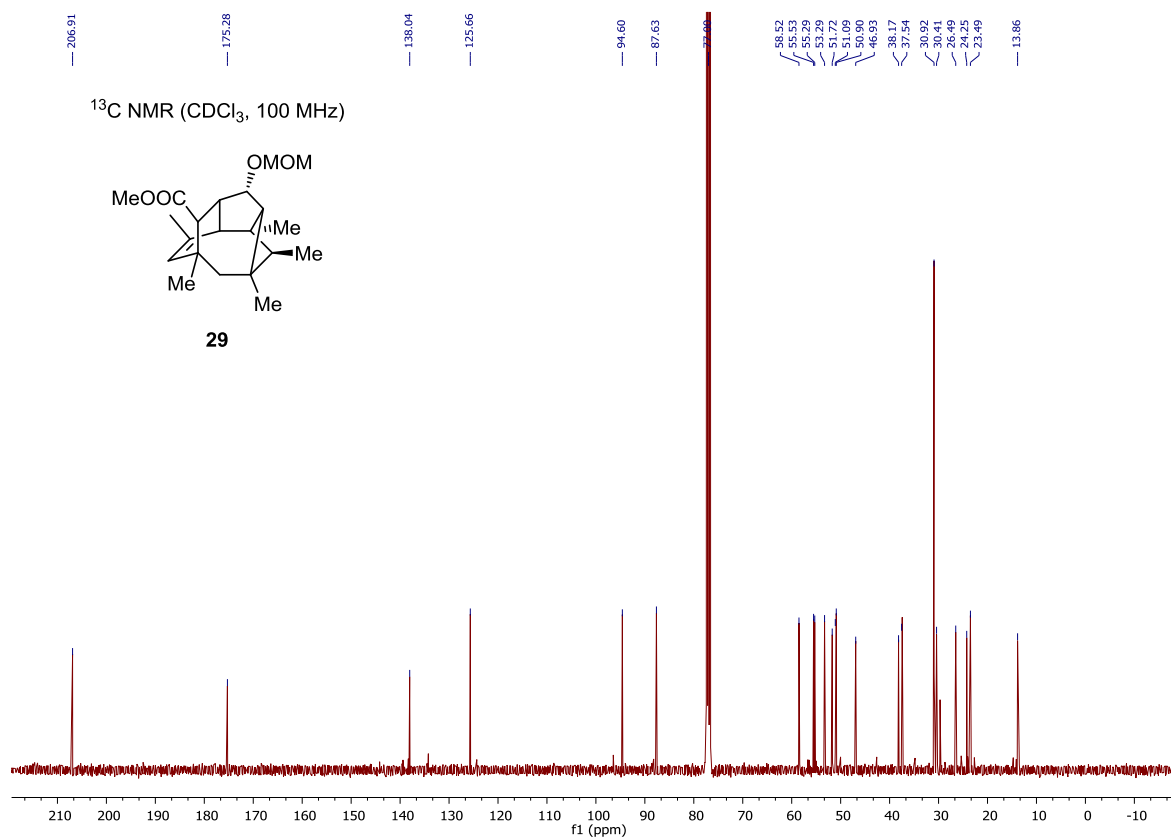
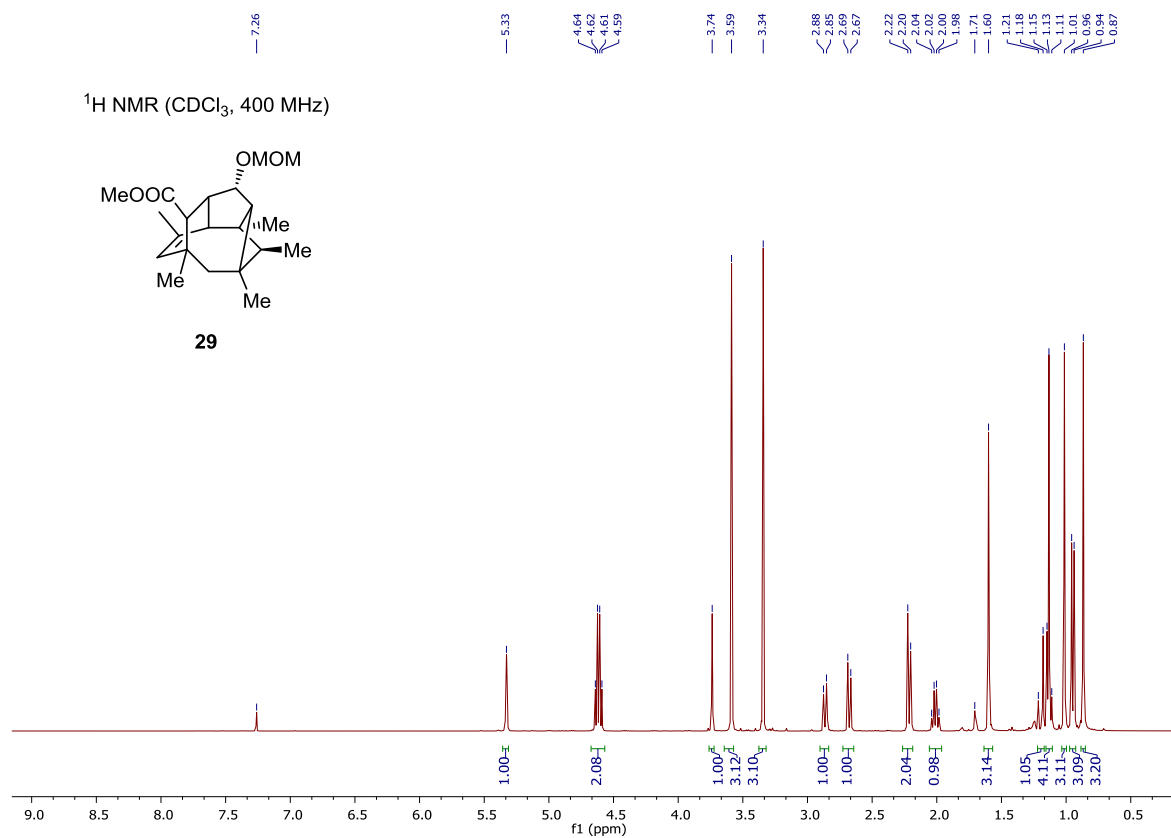


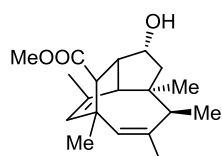
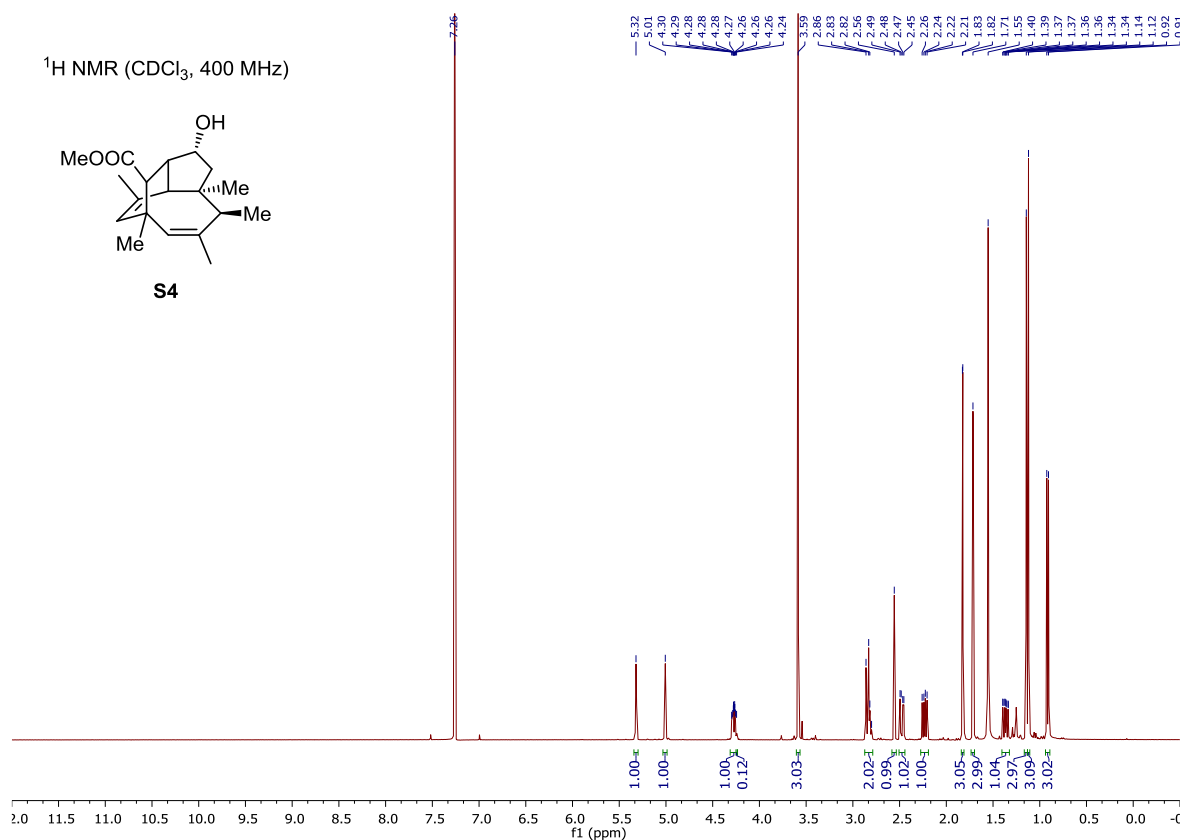
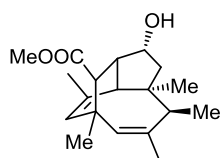
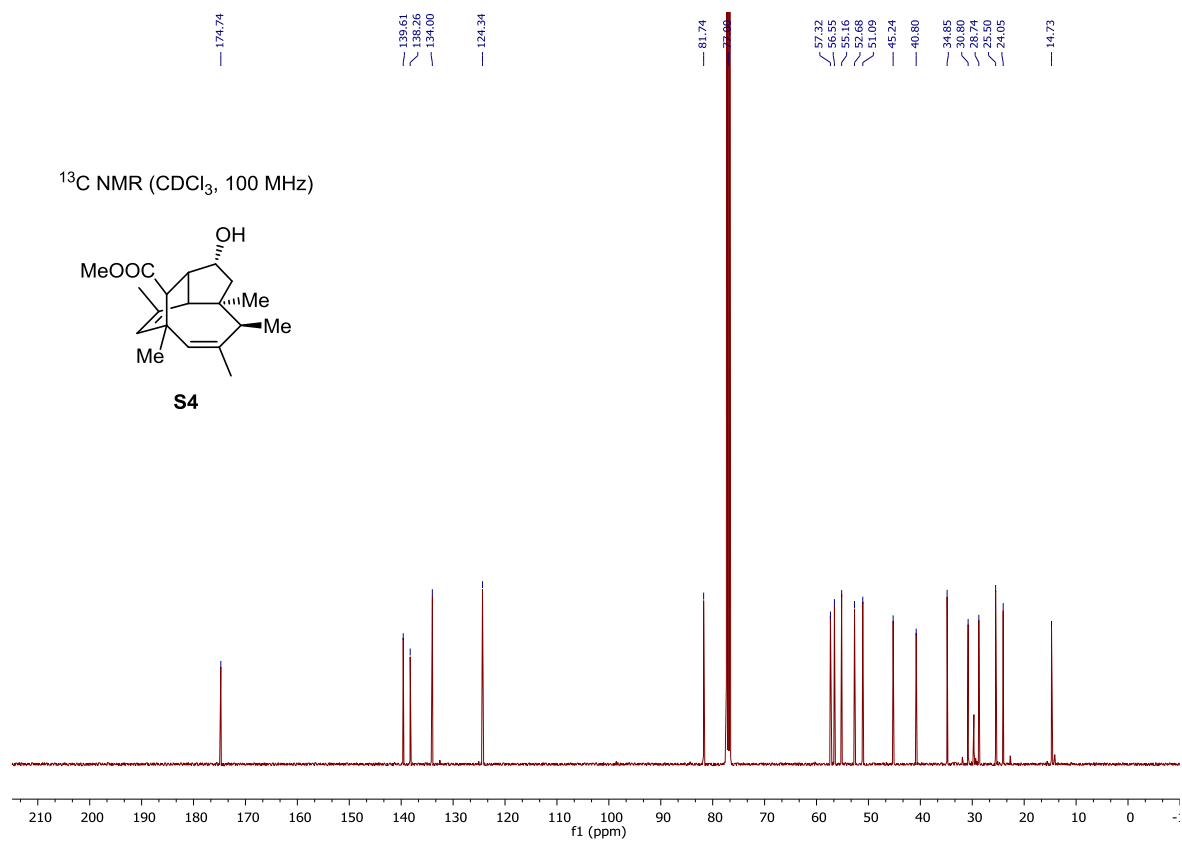


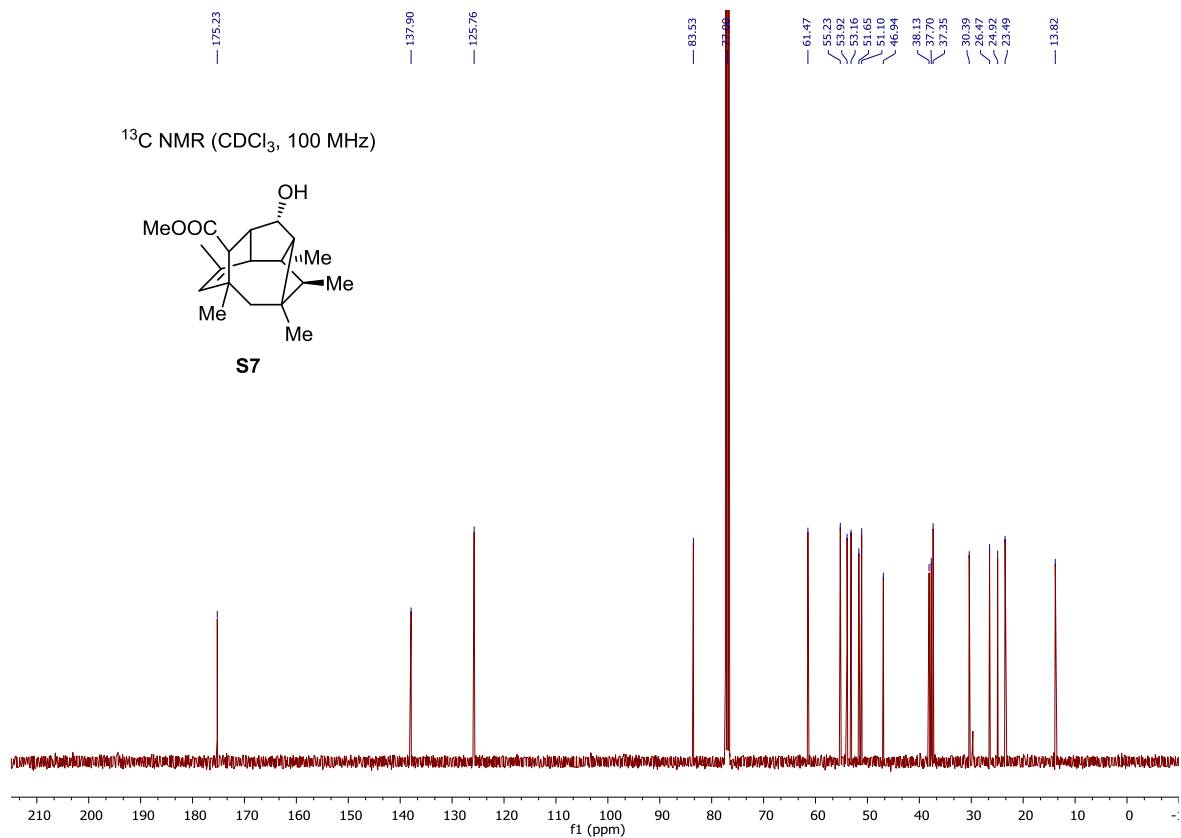
$^1\text{H}$  NMR ( $\text{CDCl}_3$ , 400 MHz)**21** $^{13}\text{C}$  NMR ( $\text{CDCl}_3$ , 100 MHz)**21**

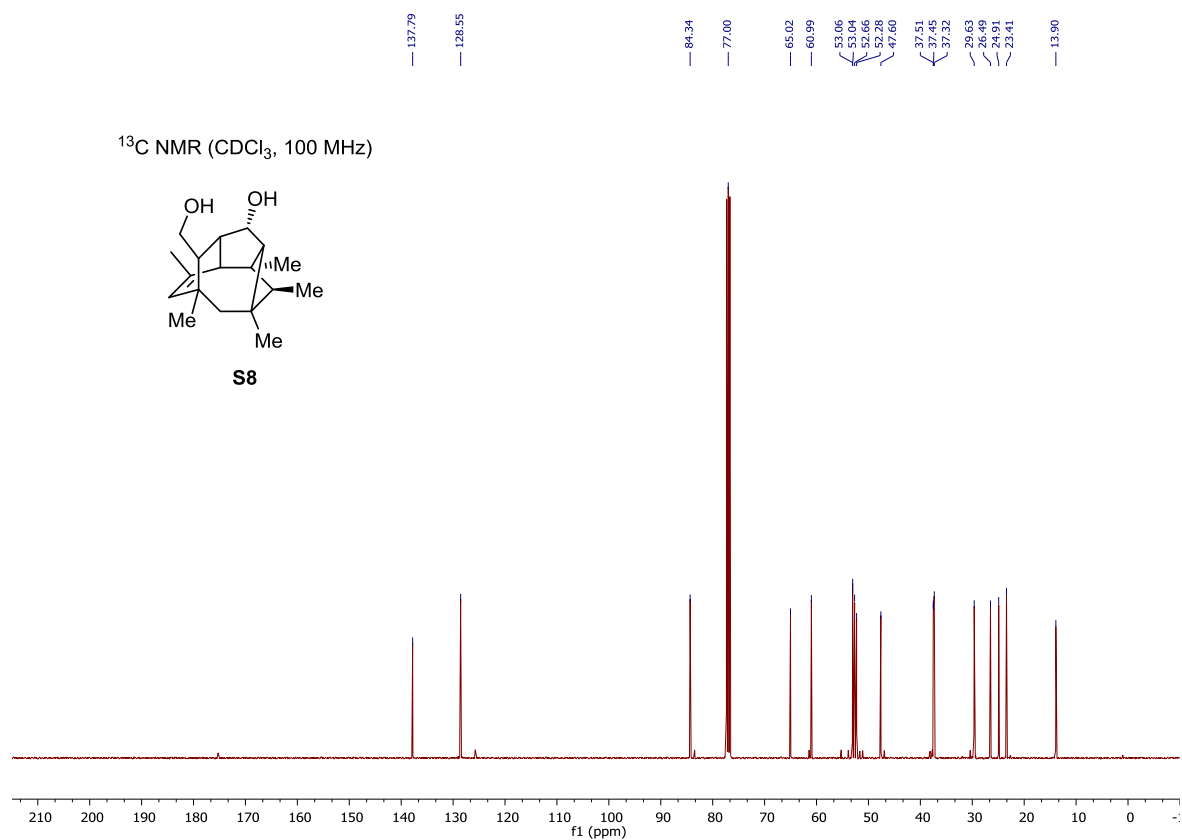
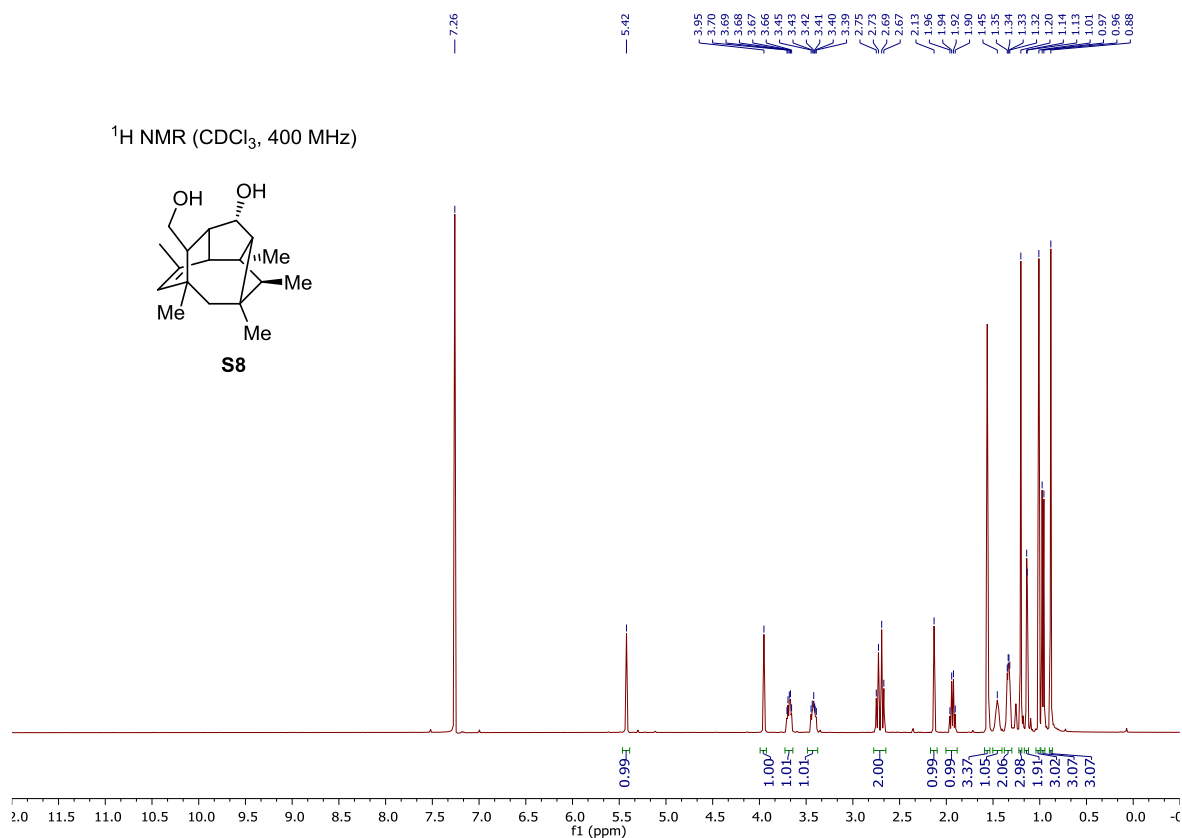


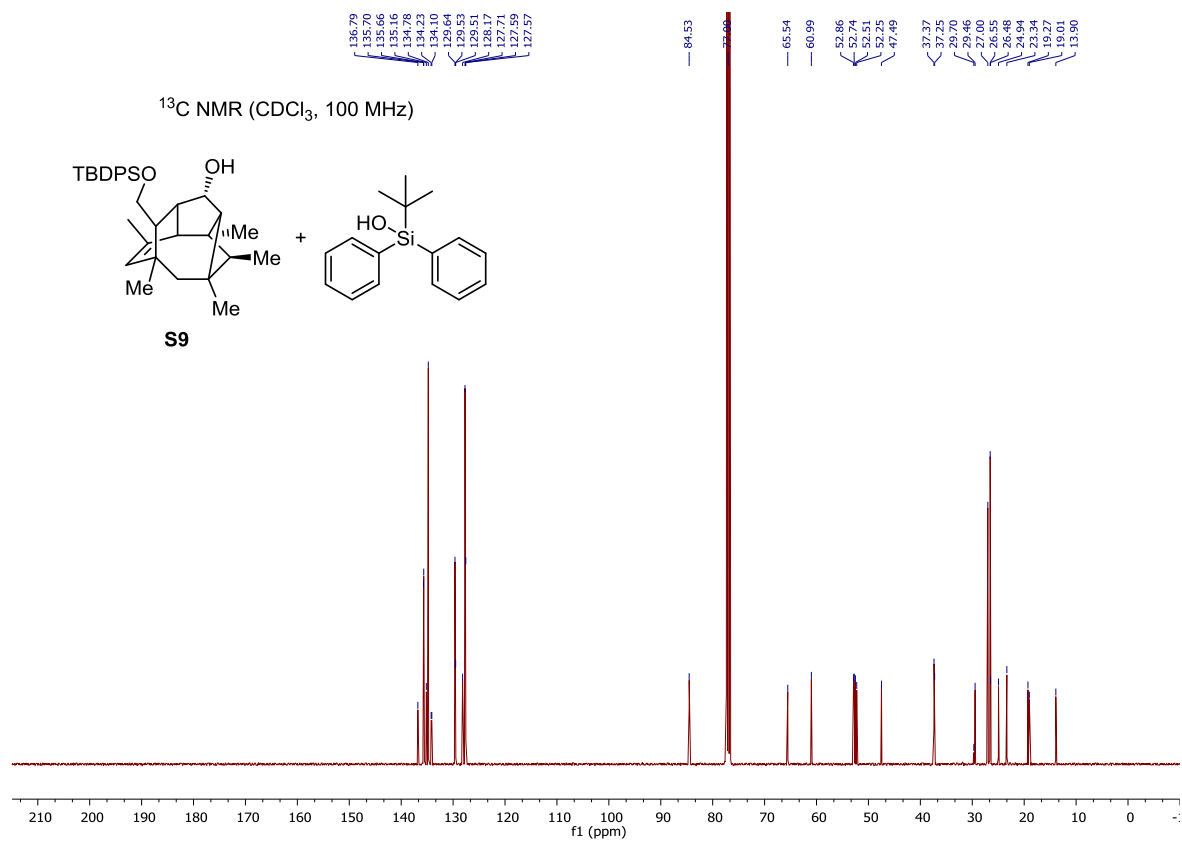
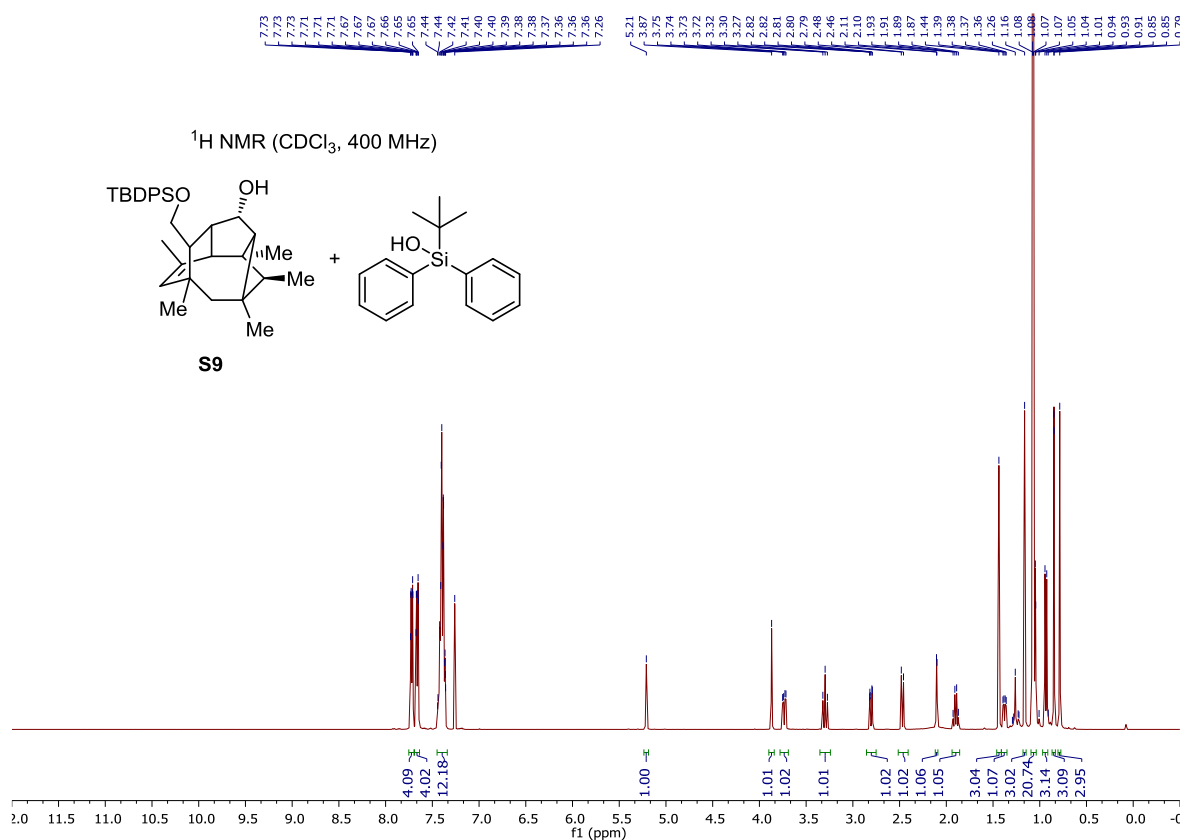


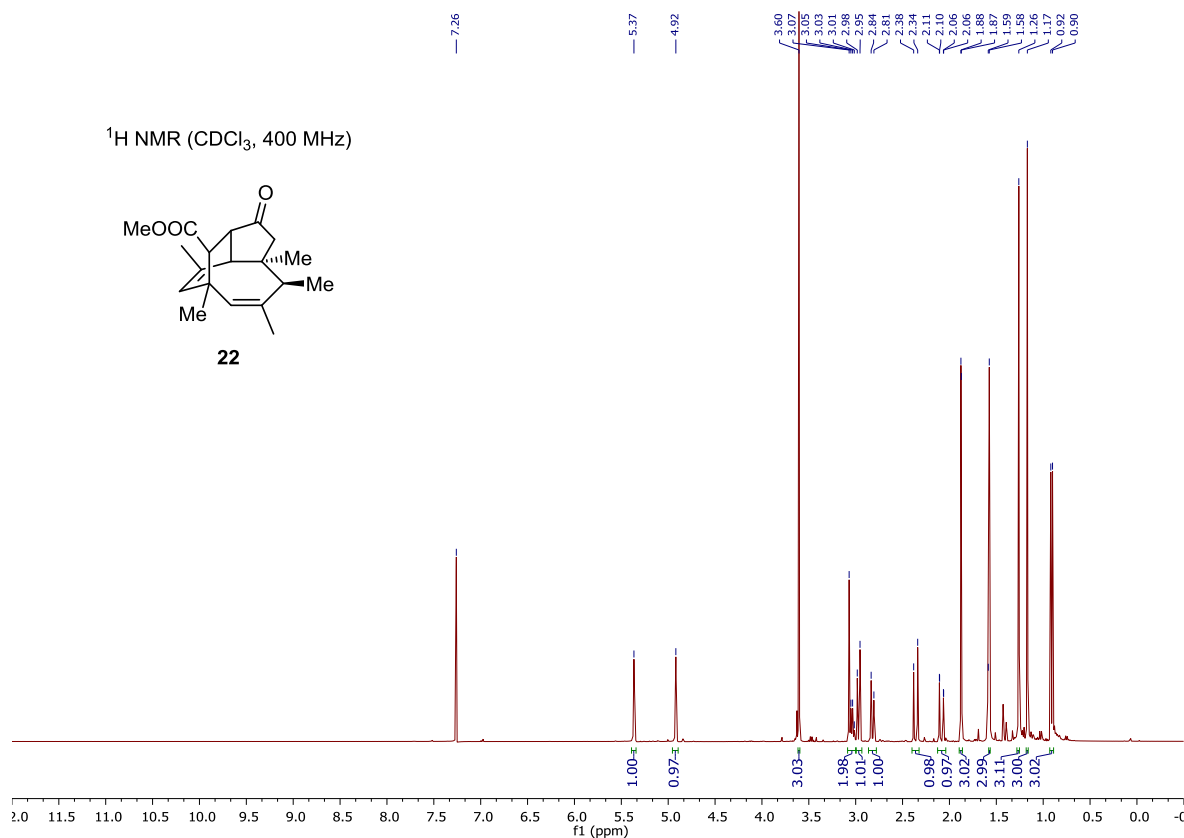
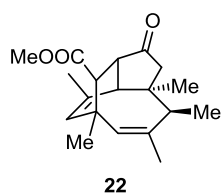
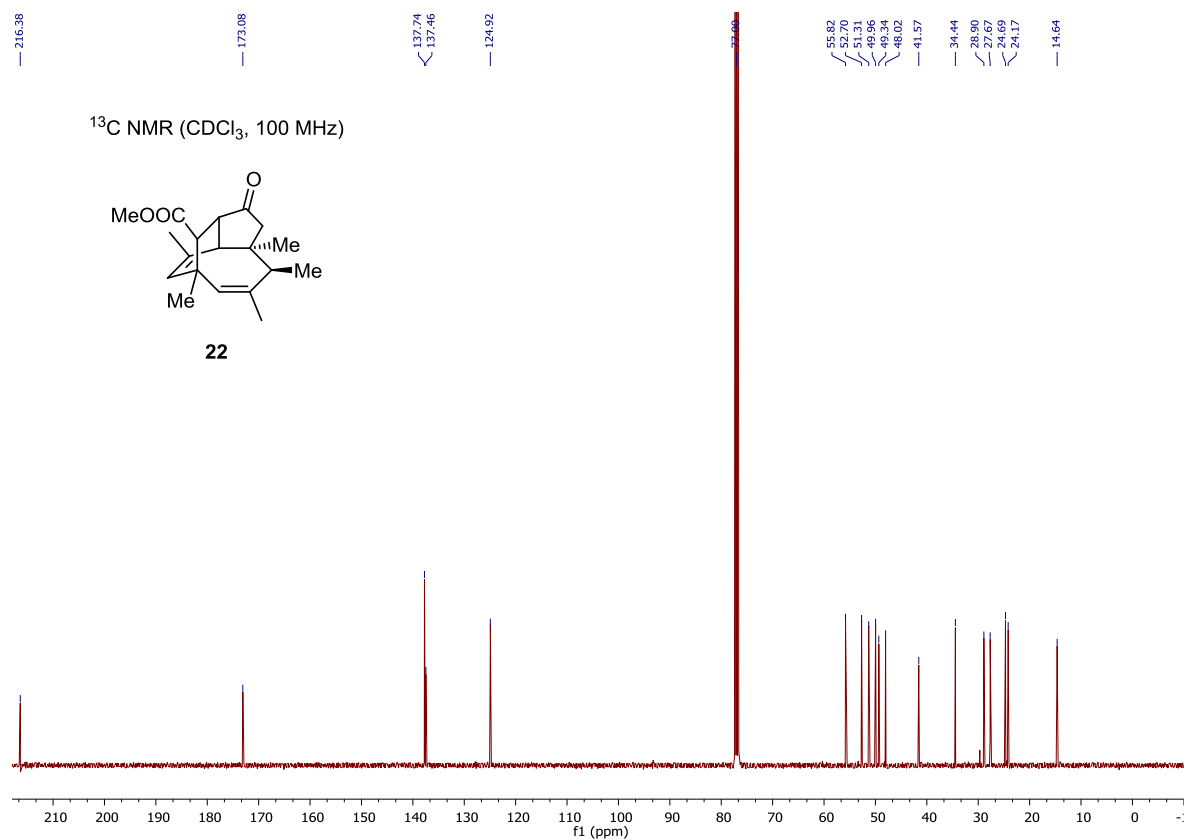
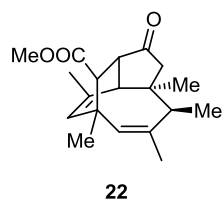


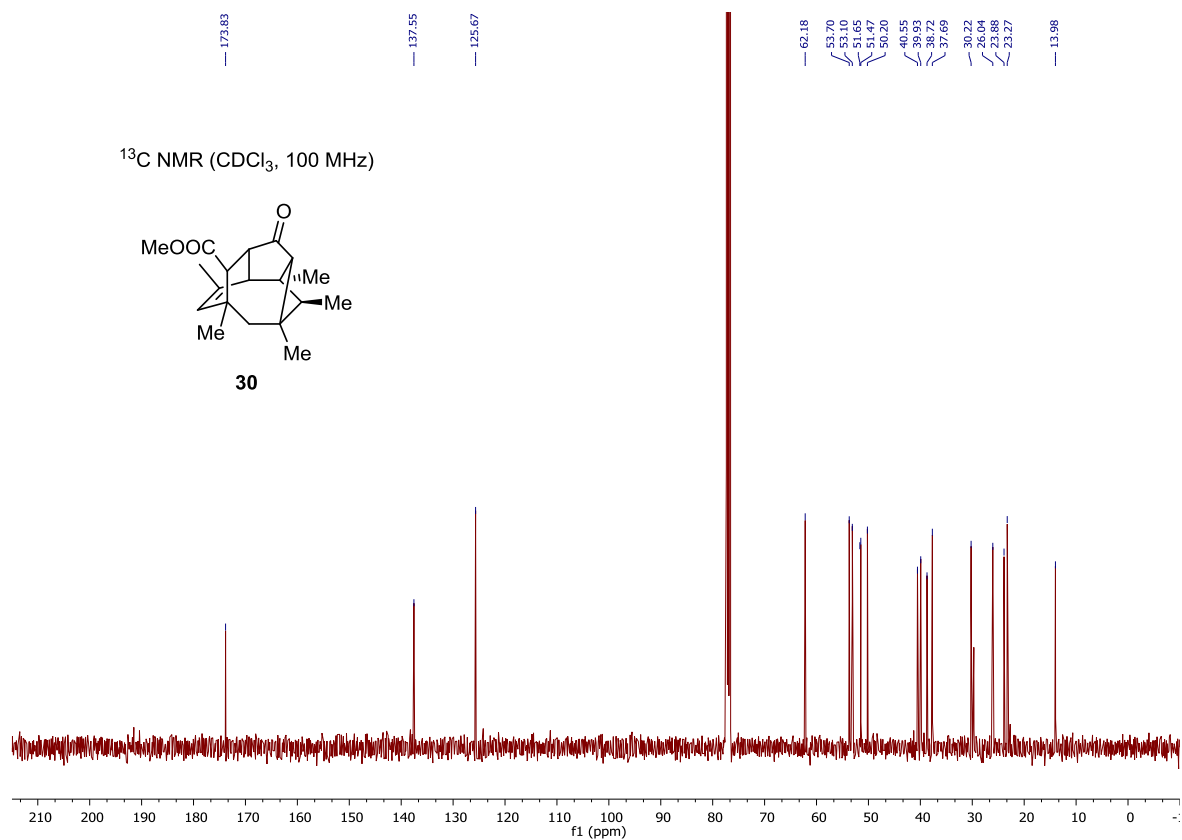
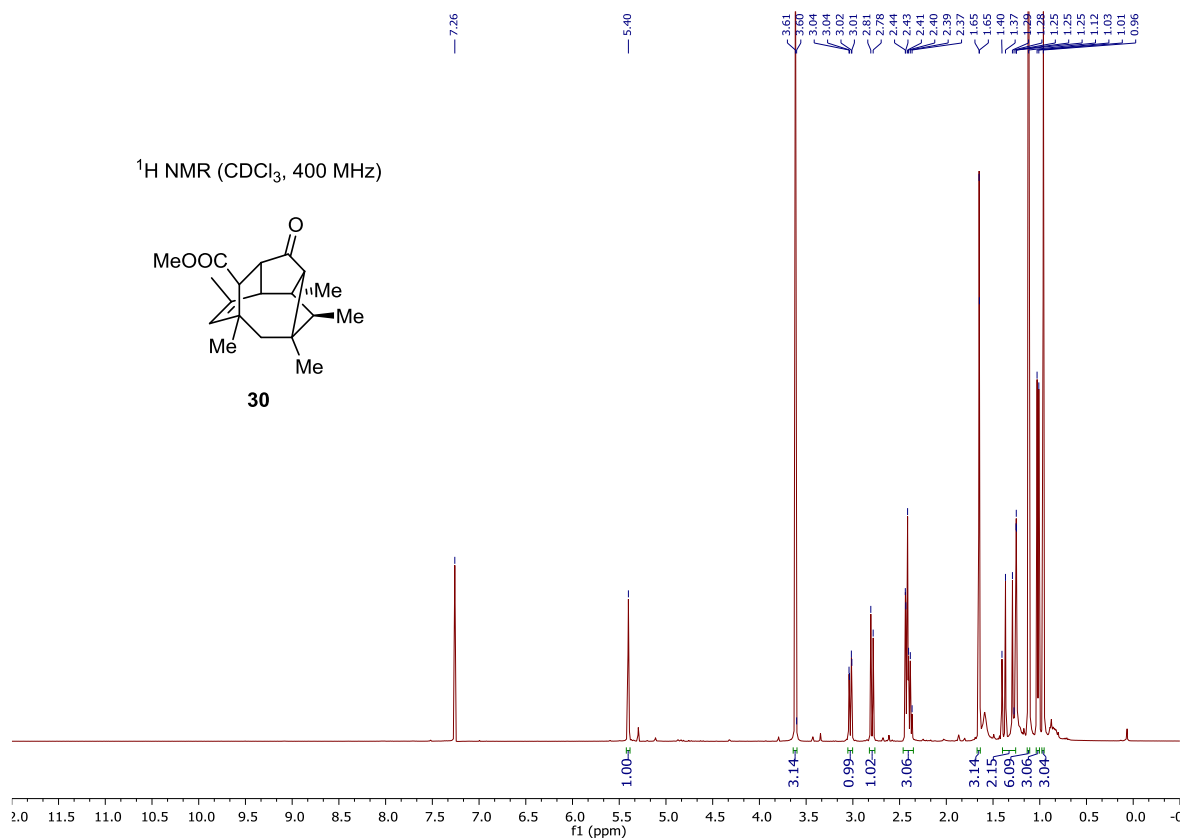
<sup>1</sup>H NMR (CDCl<sub>3</sub>, 400 MHz)**S4**<sup>13</sup>C NMR (CDCl<sub>3</sub>, 100 MHz)**S4**



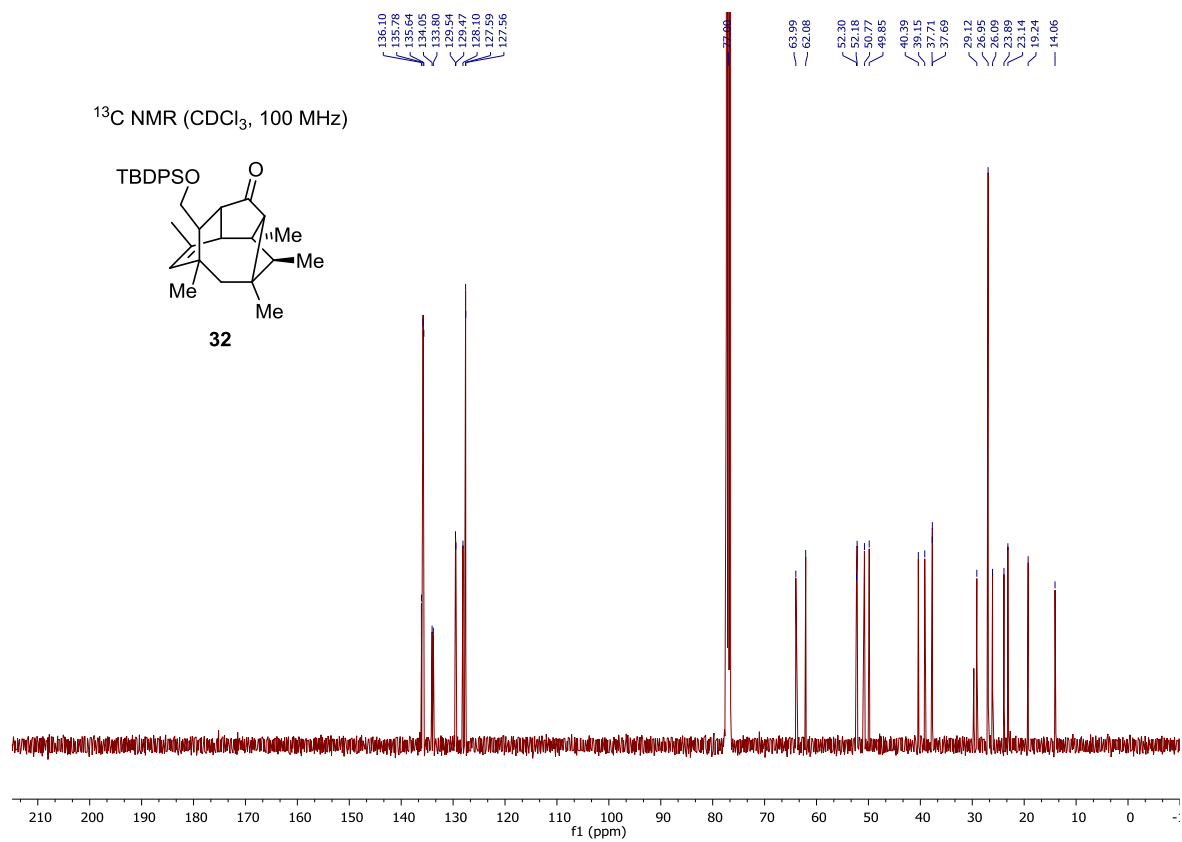
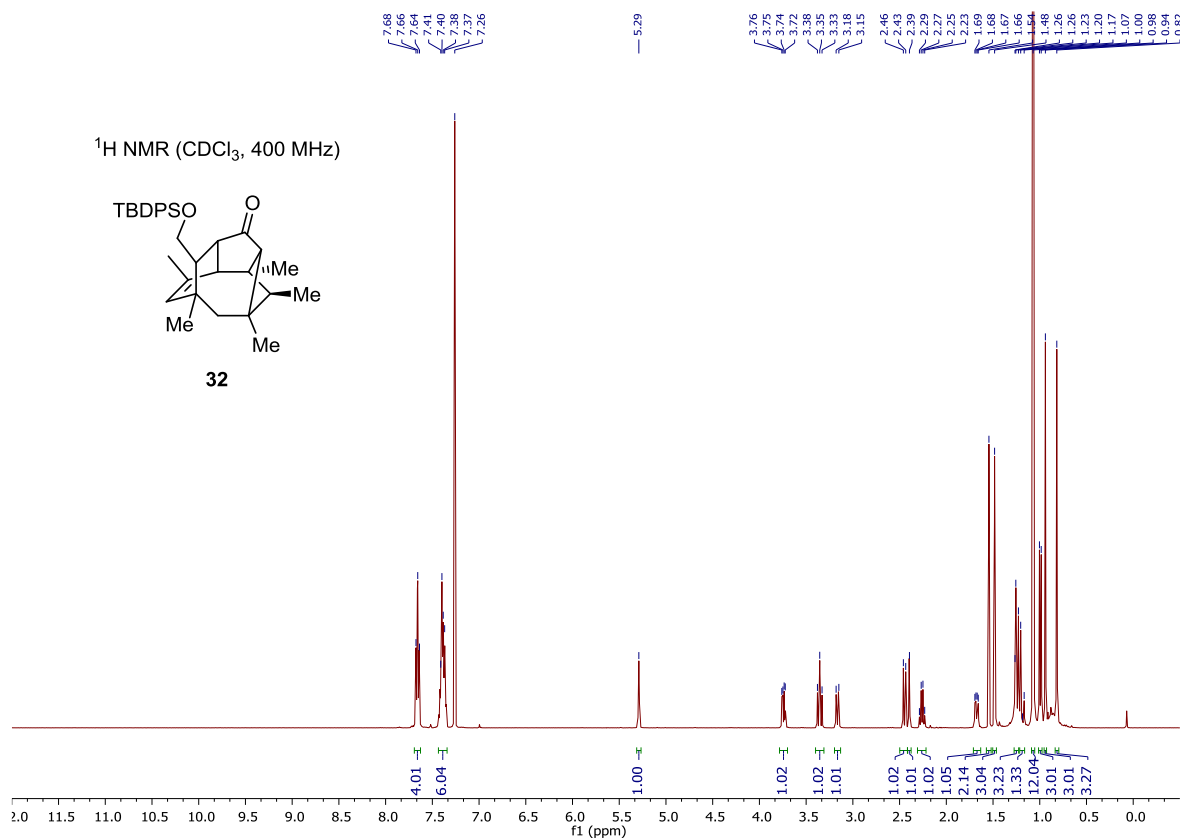


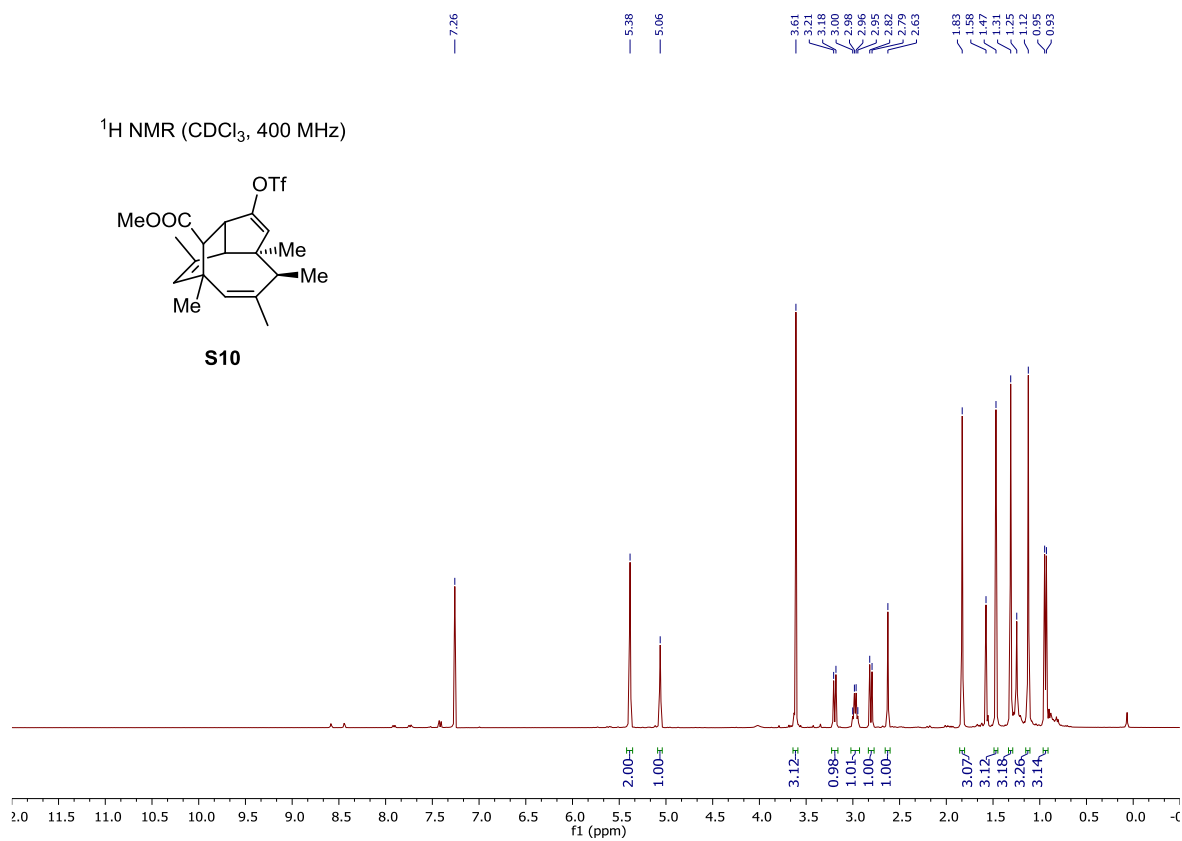
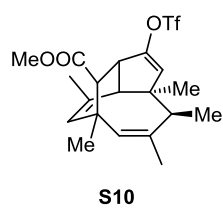
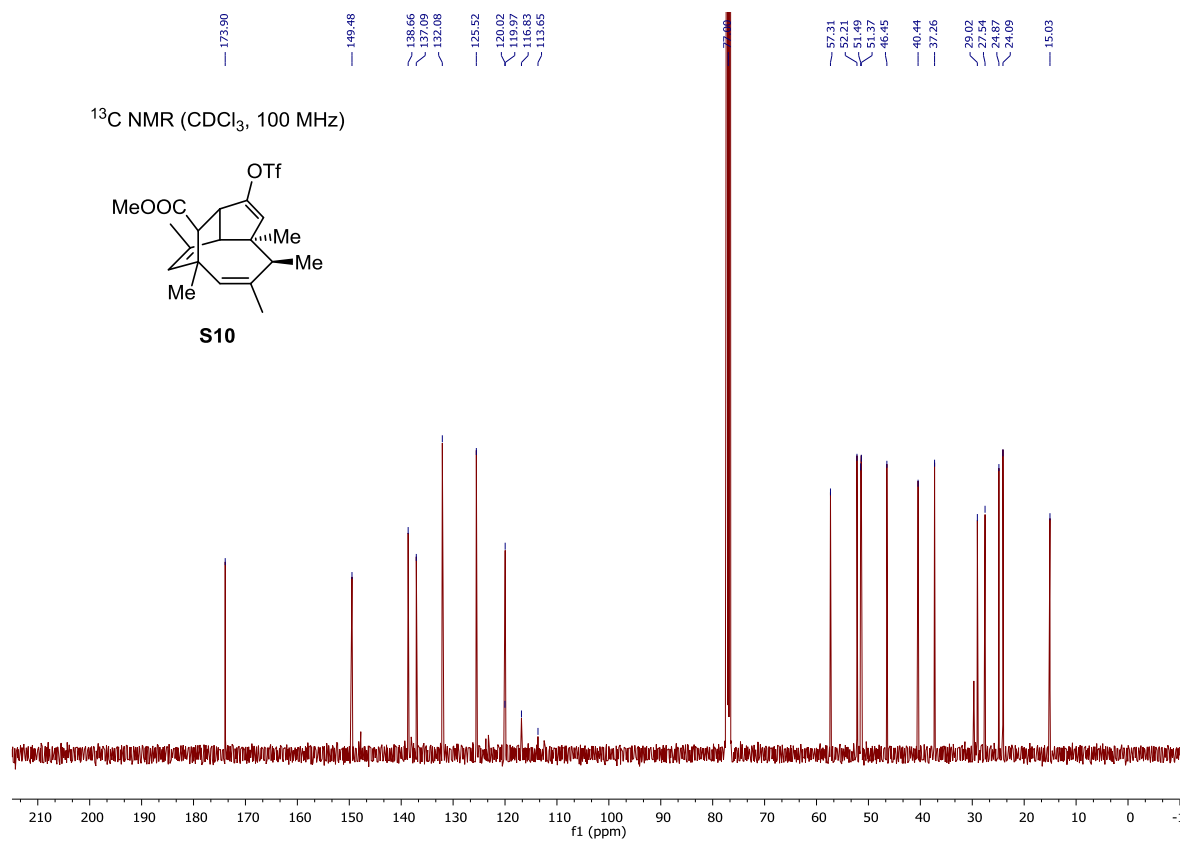
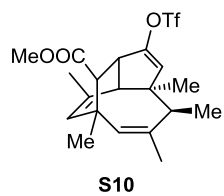


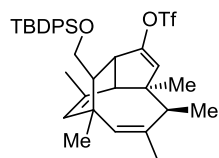
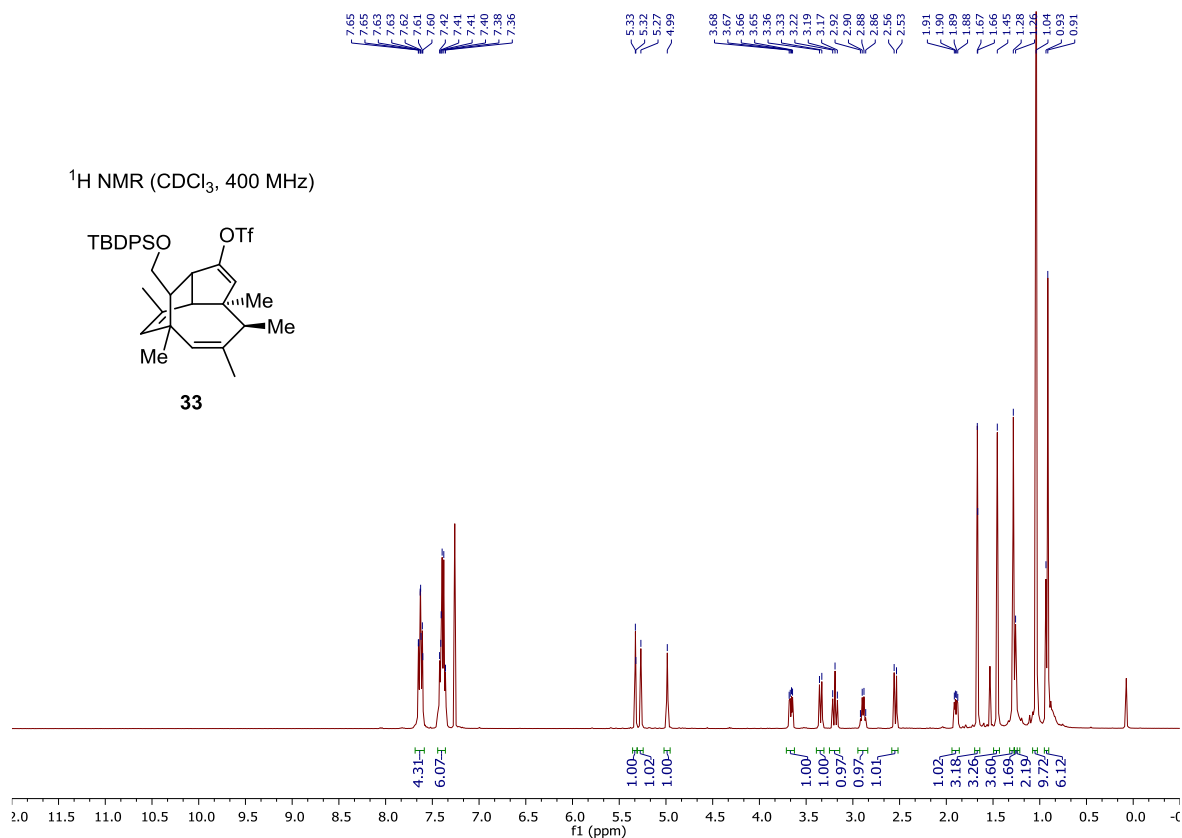
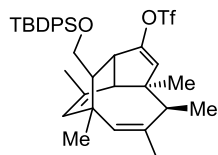
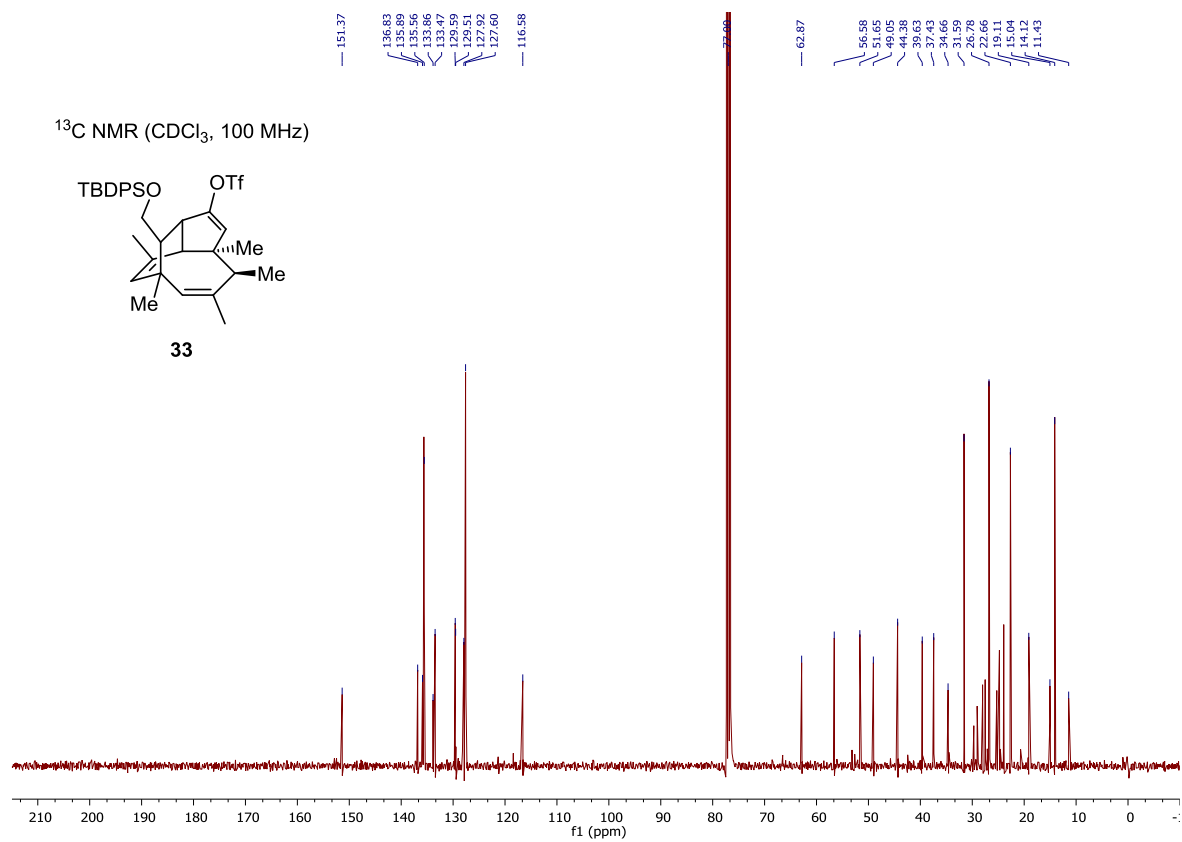
<sup>1</sup>H NMR (CDCl<sub>3</sub>, 400 MHz)<sup>13</sup>C NMR (CDCl<sub>3</sub>, 100 MHz)

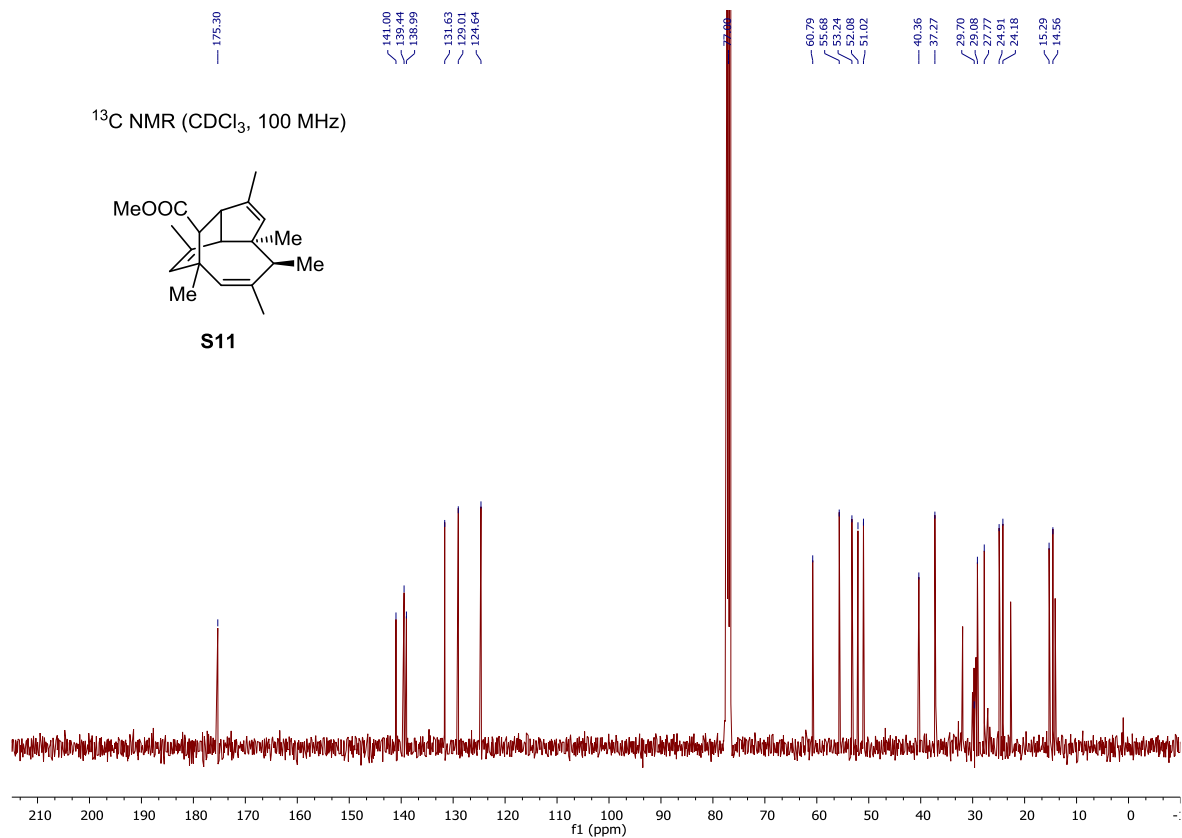


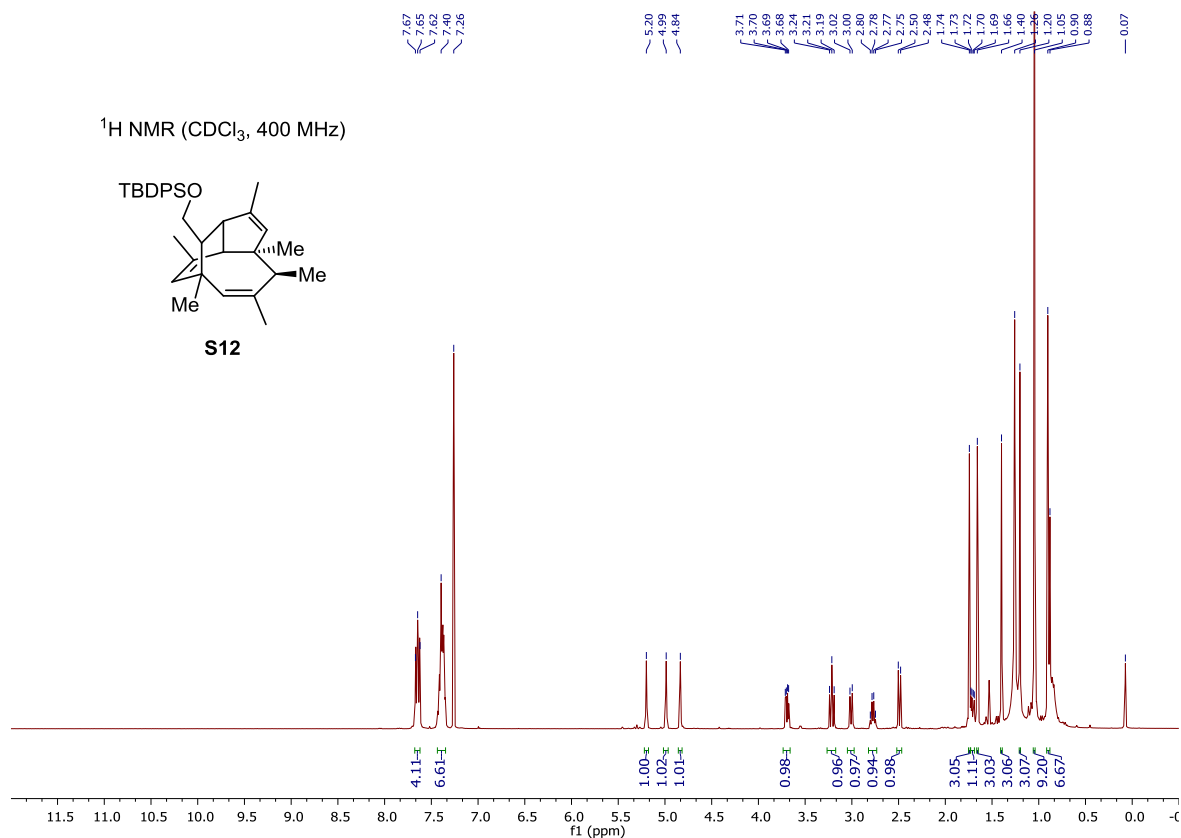
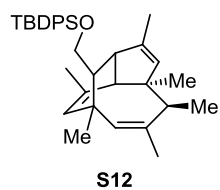
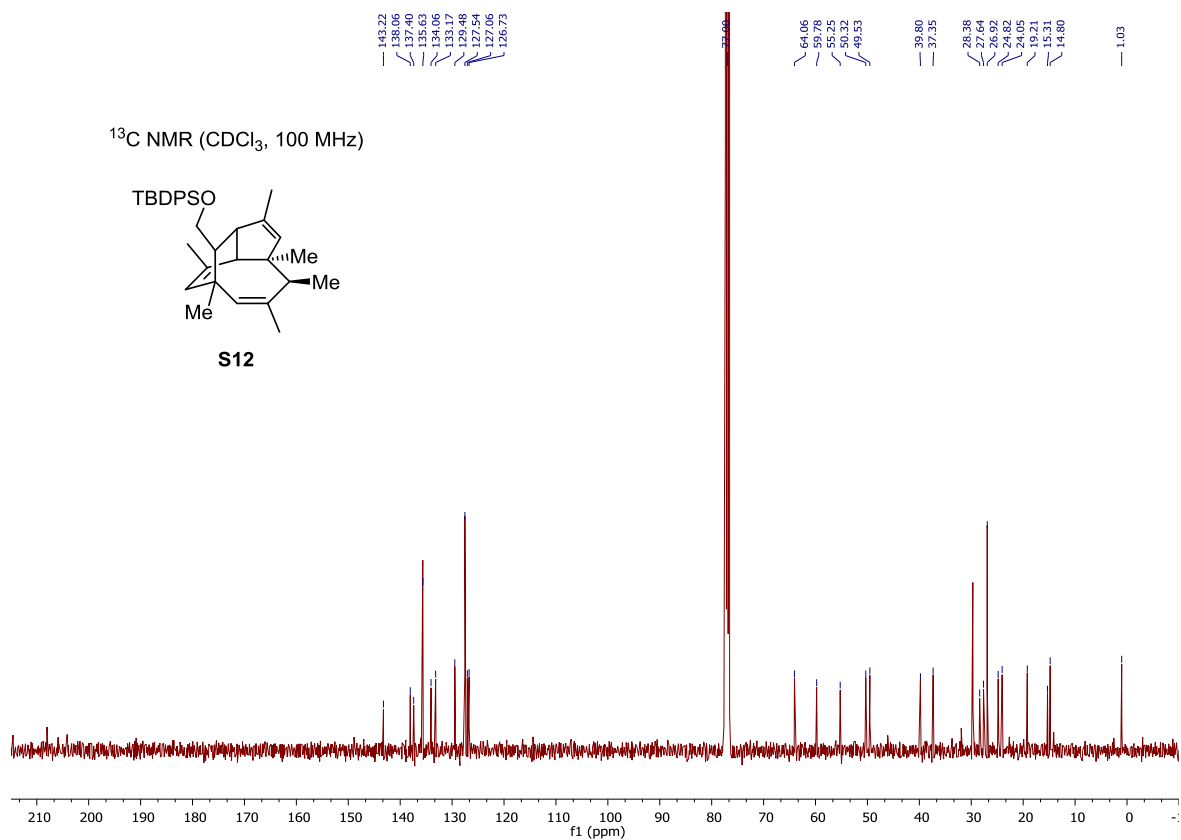
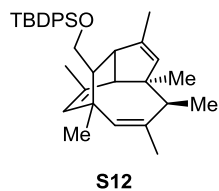




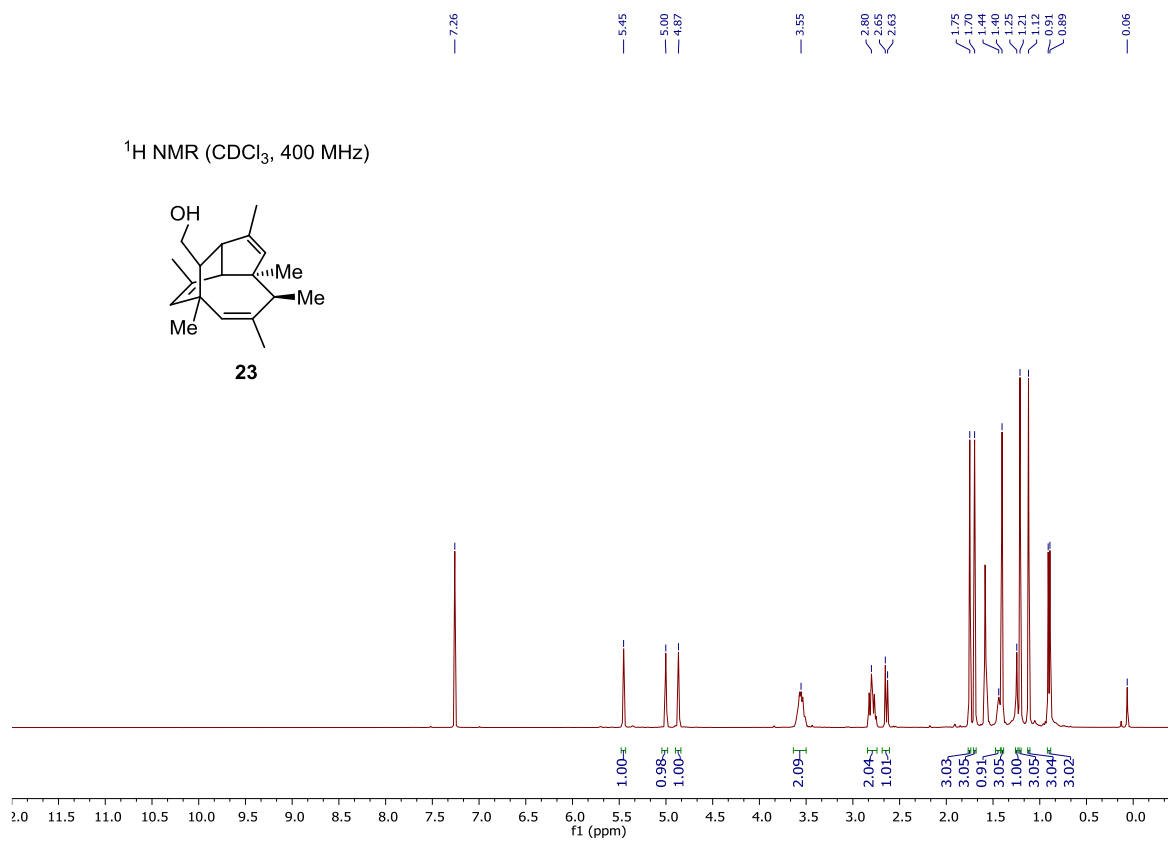
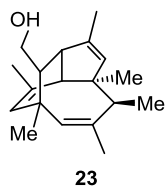
<sup>1</sup>H NMR (CDCl<sub>3</sub>, 400 MHz)<sup>13</sup>C NMR (CDCl<sub>3</sub>, 100 MHz)

<sup>1</sup>H NMR (CDCl<sub>3</sub>, 400 MHz)**33**<sup>13</sup>C NMR (CDCl<sub>3</sub>, 100 MHz)**33**

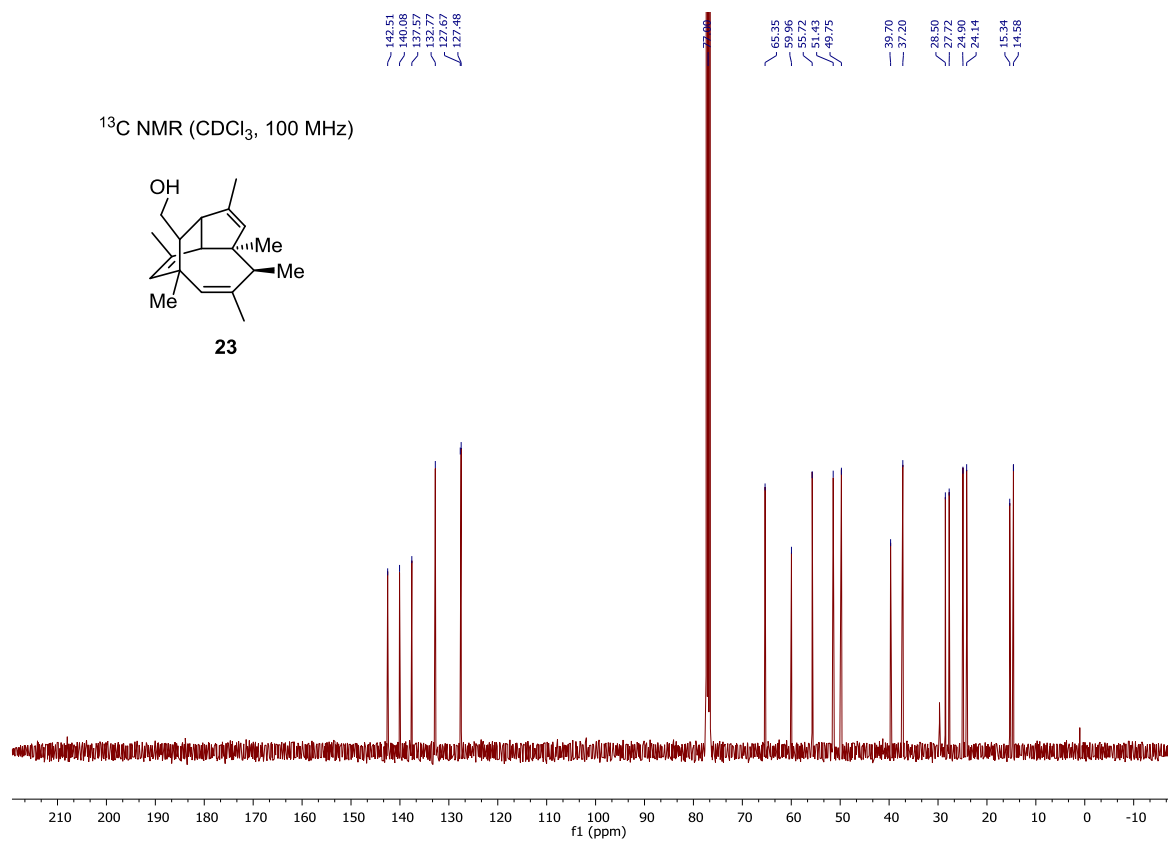
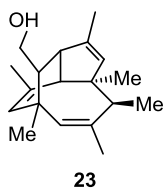


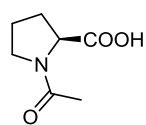
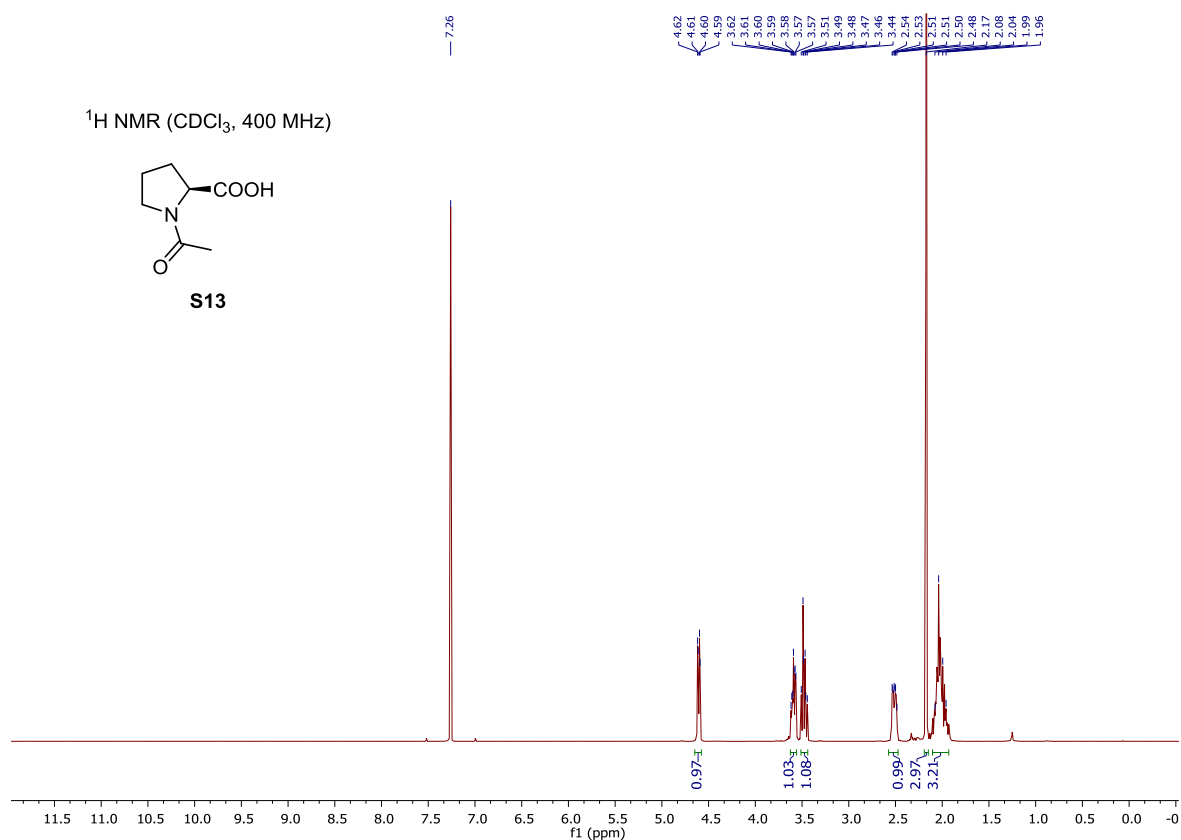
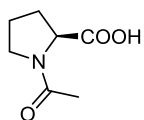
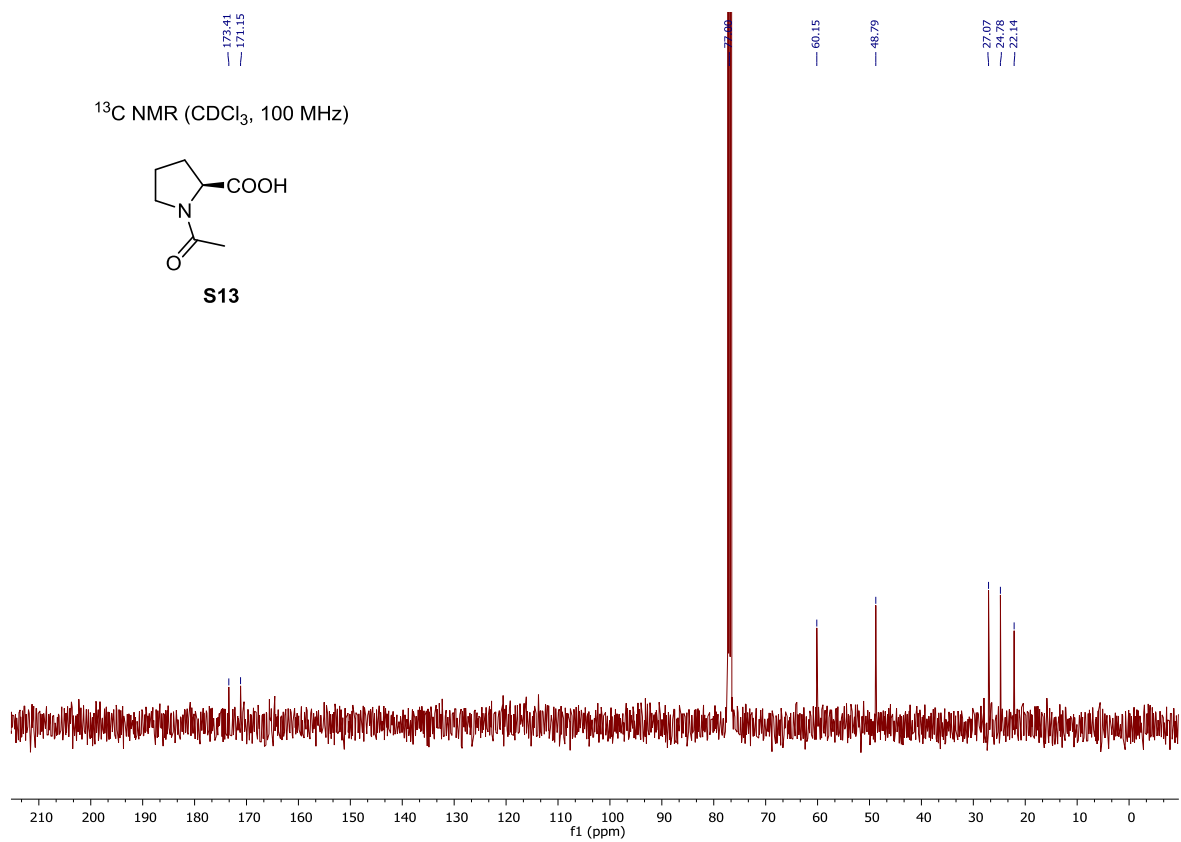
$^1\text{H}$  NMR ( $\text{CDCl}_3$ , 400 MHz) $^{13}\text{C}$  NMR ( $\text{CDCl}_3$ , 100 MHz)

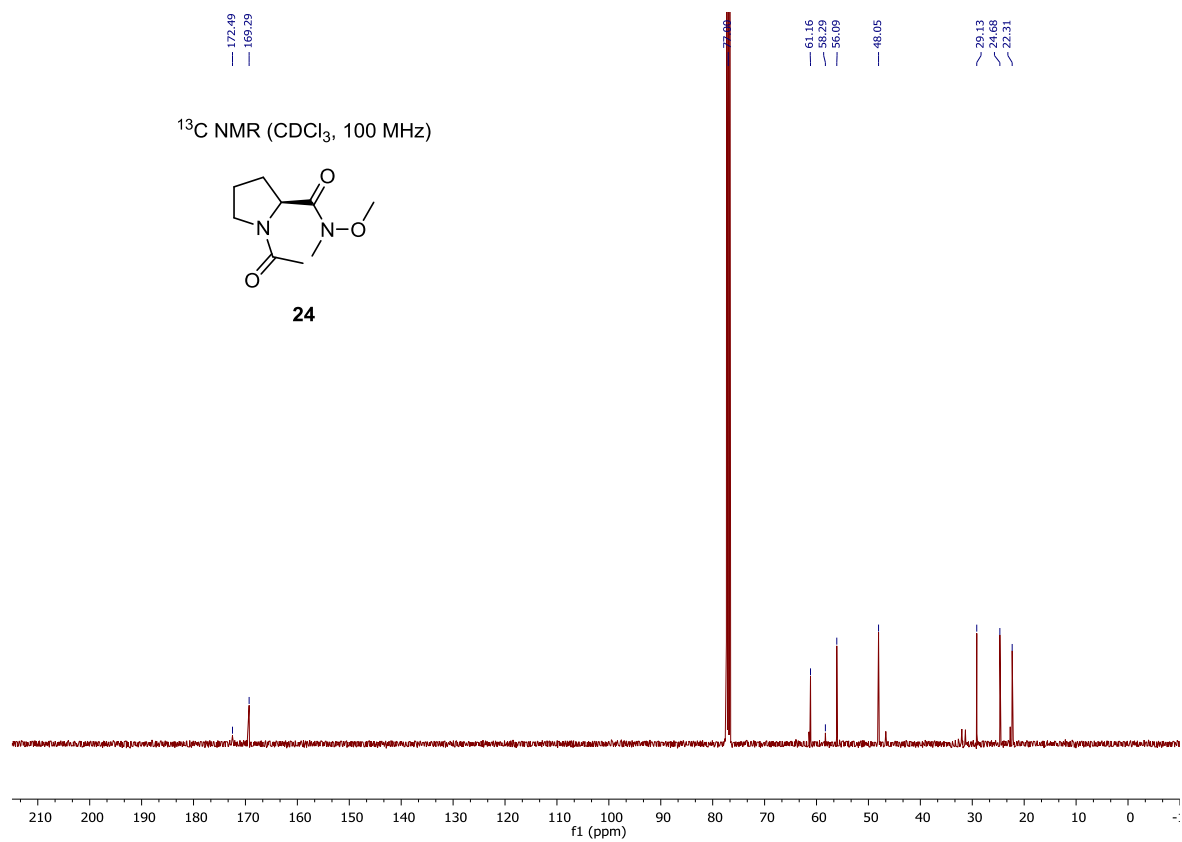
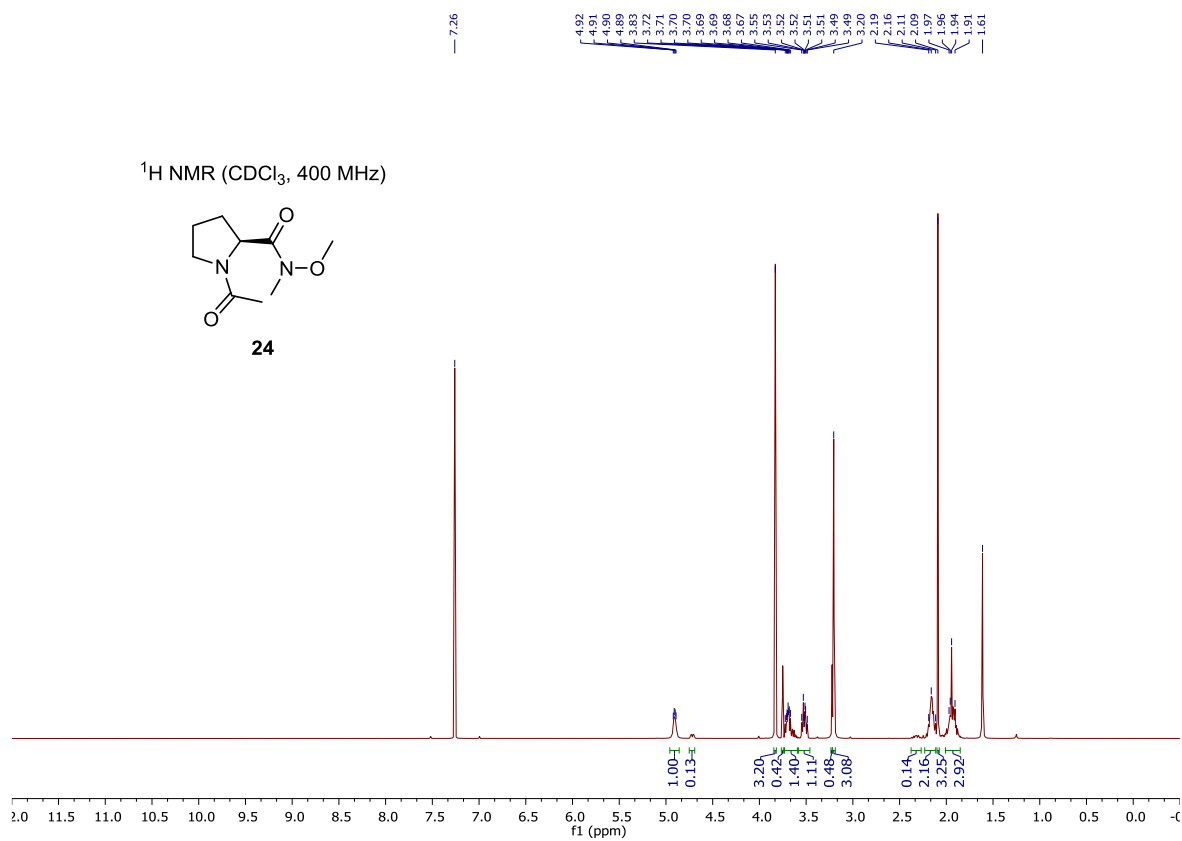
<sup>1</sup>H NMR (CDCl<sub>3</sub>, 400 MHz)



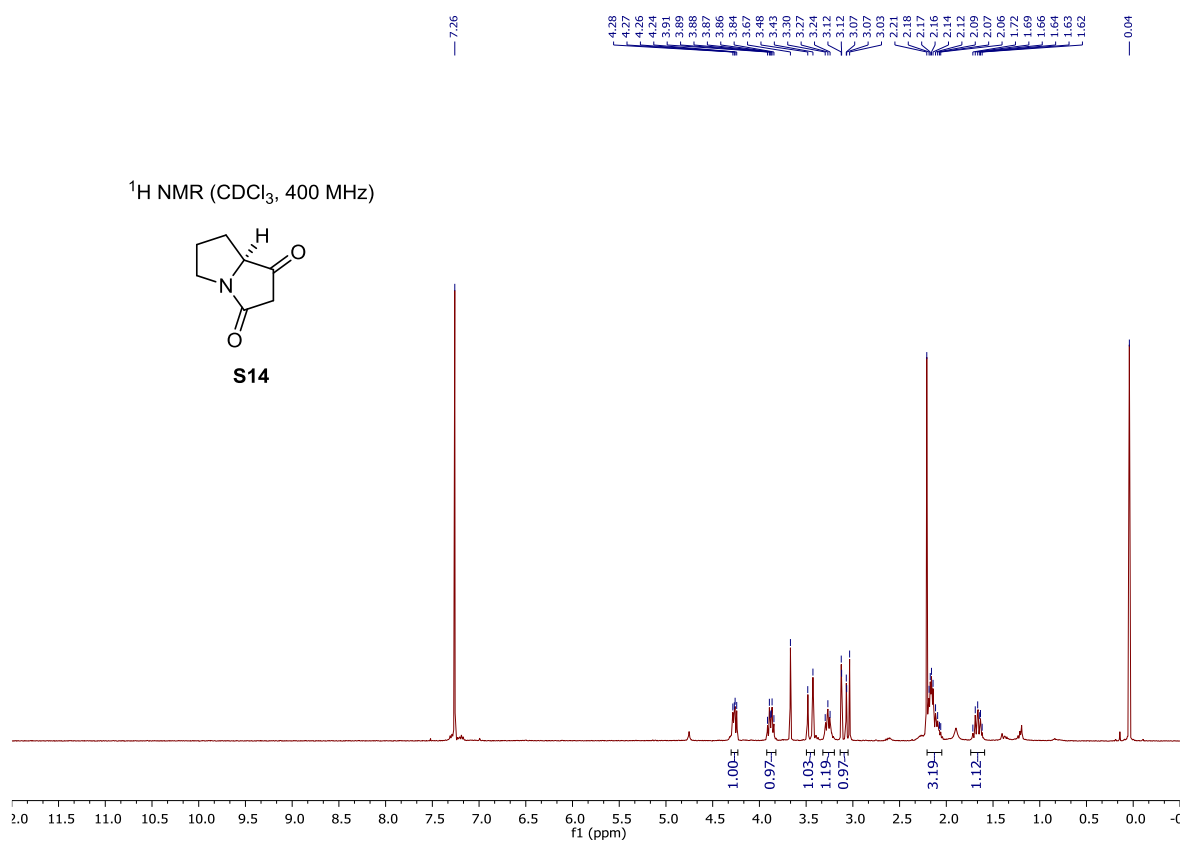
<sup>13</sup>C NMR (CDCl<sub>3</sub>, 100 MHz)

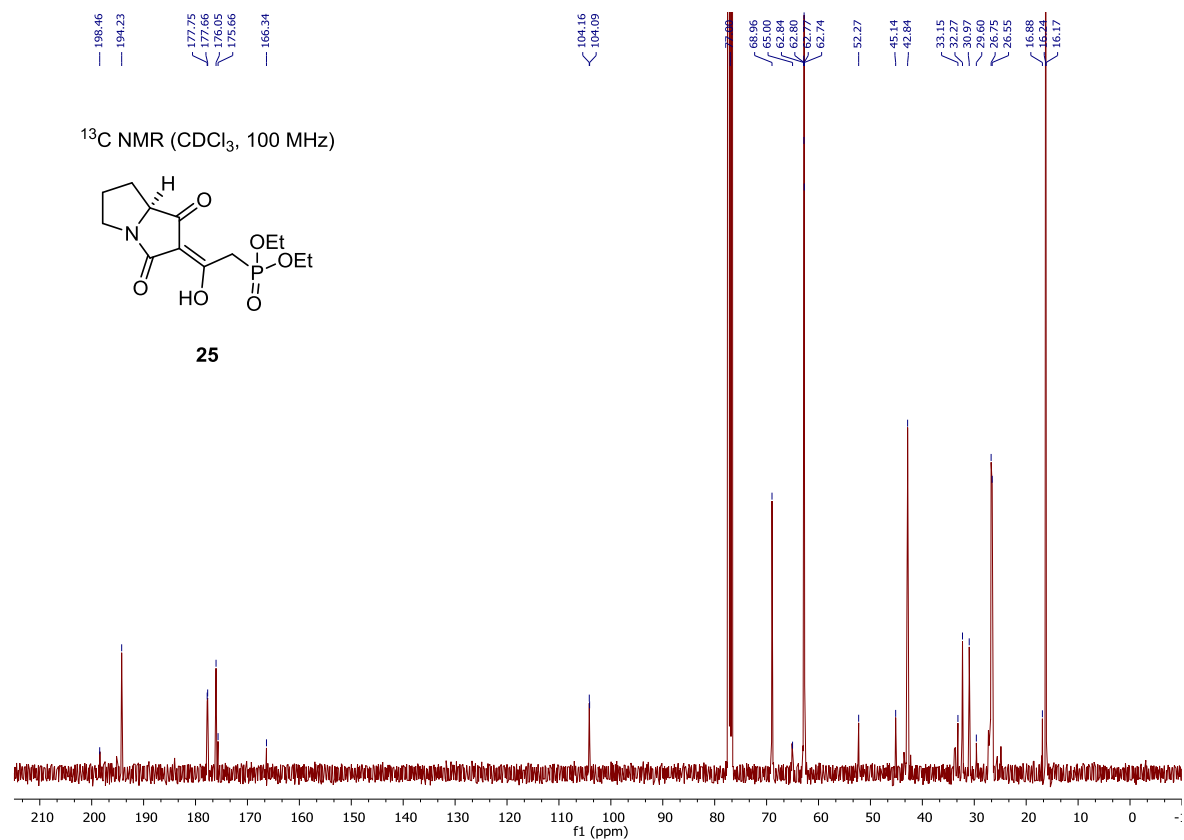
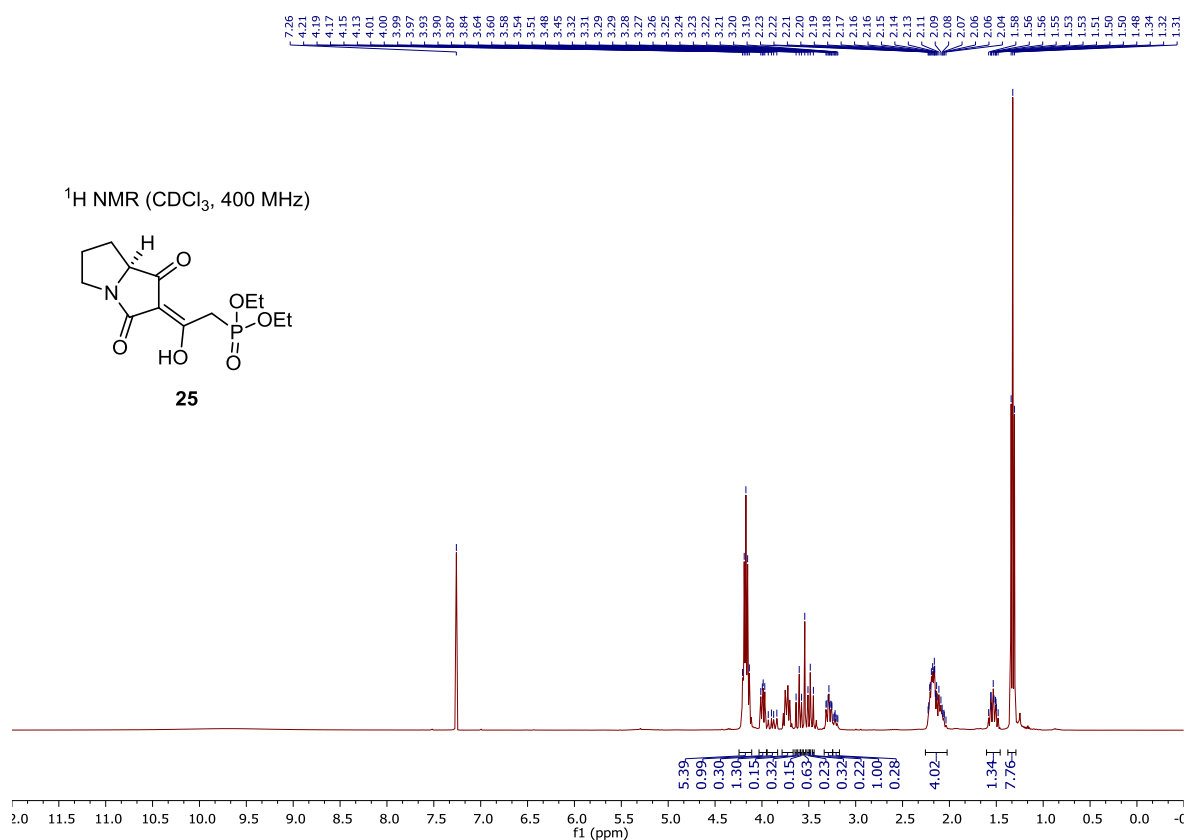


<sup>1</sup>H NMR (CDCl<sub>3</sub>, 400 MHz)**S13**<sup>13</sup>C NMR (CDCl<sub>3</sub>, 100 MHz)**S13**

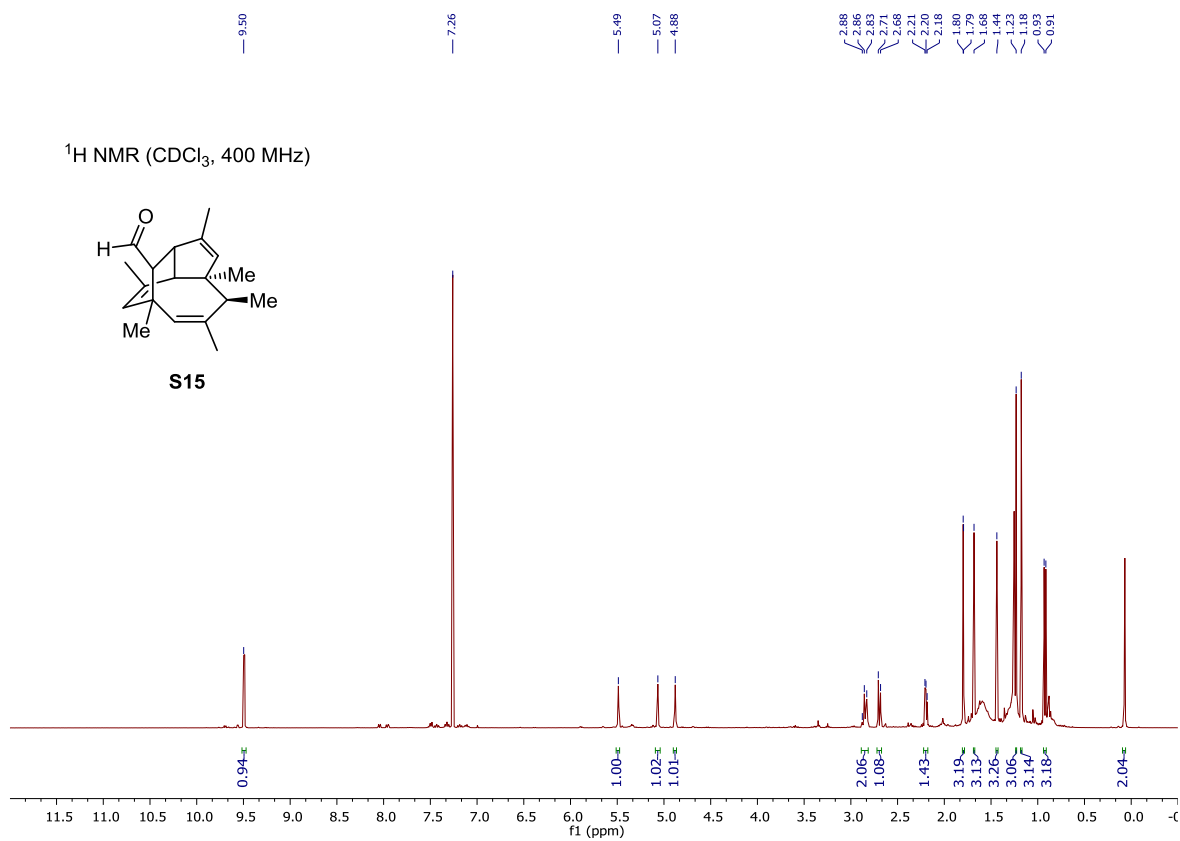




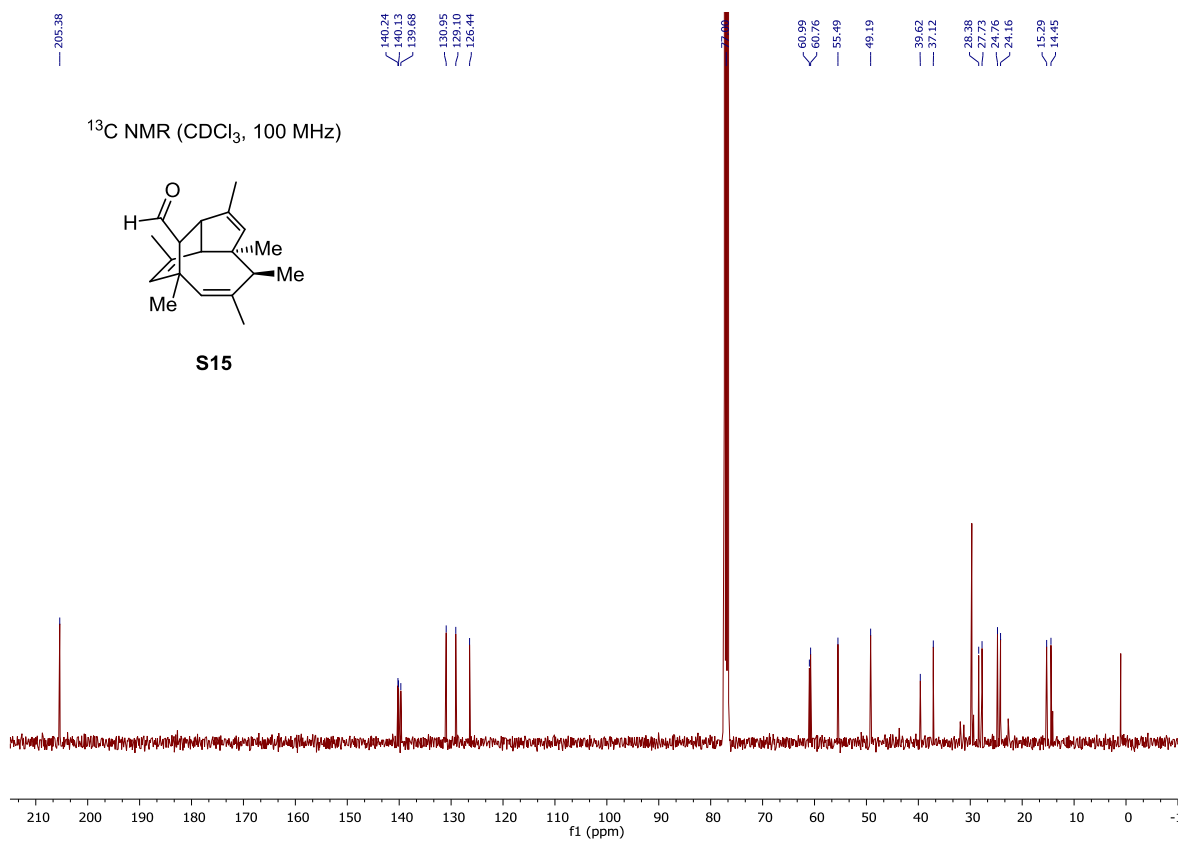


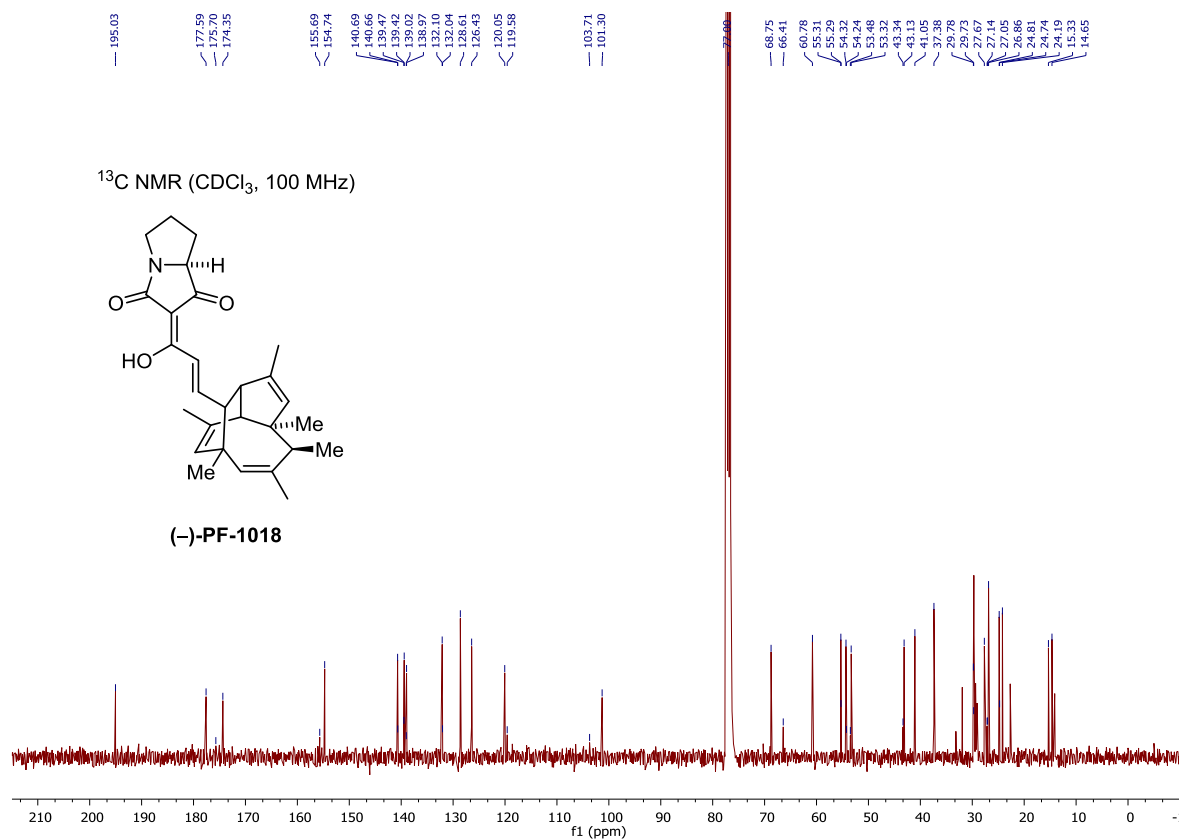
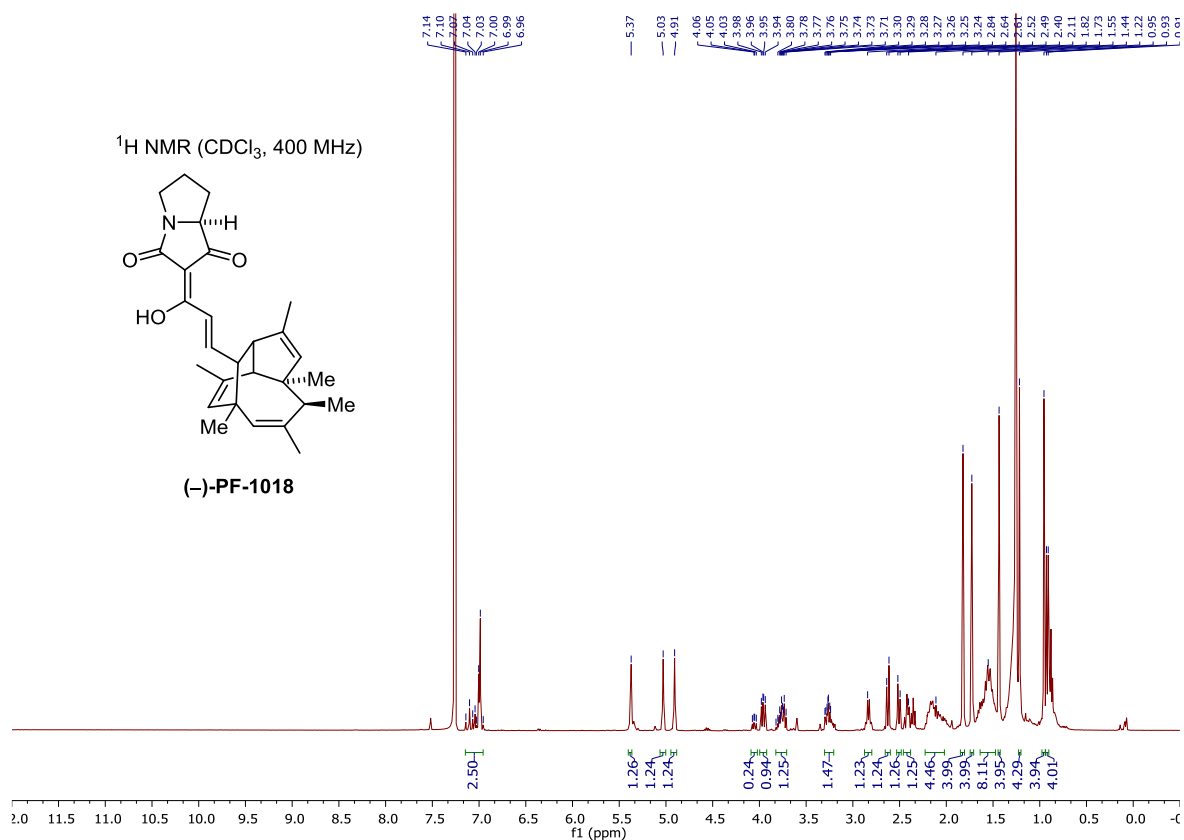


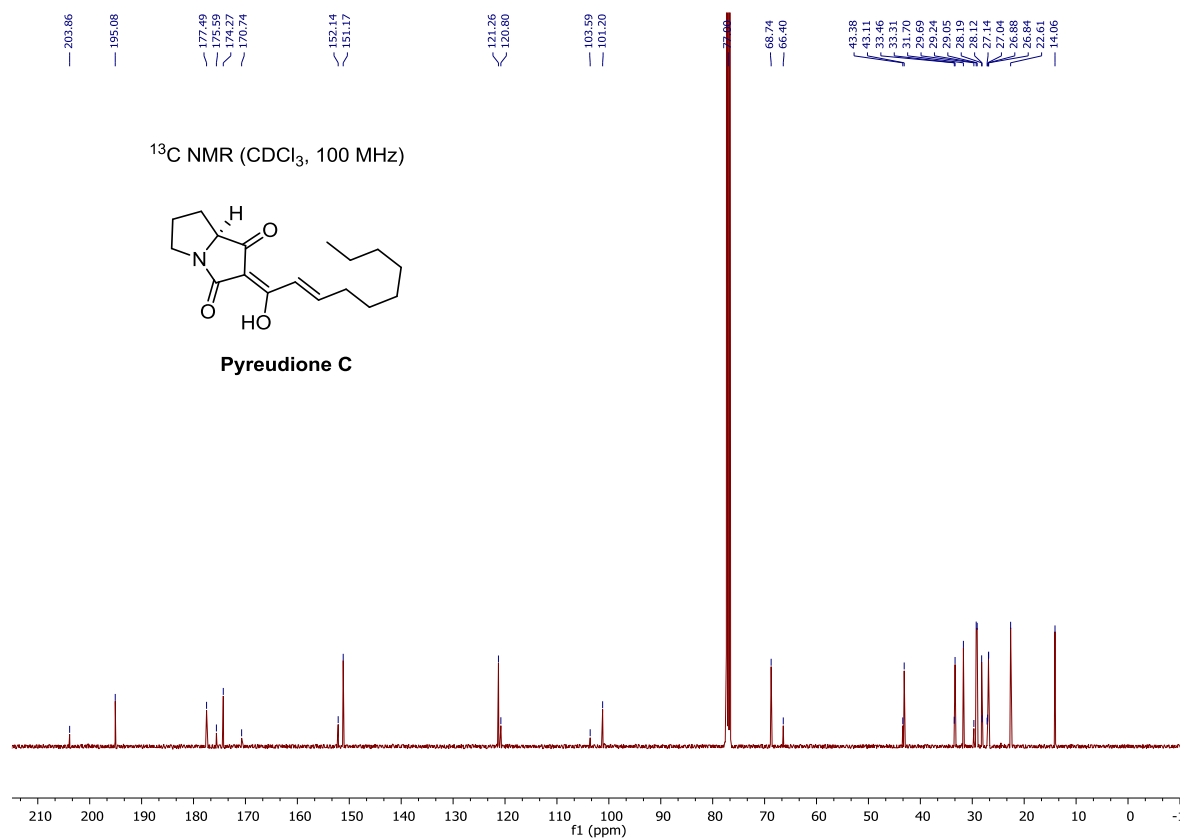
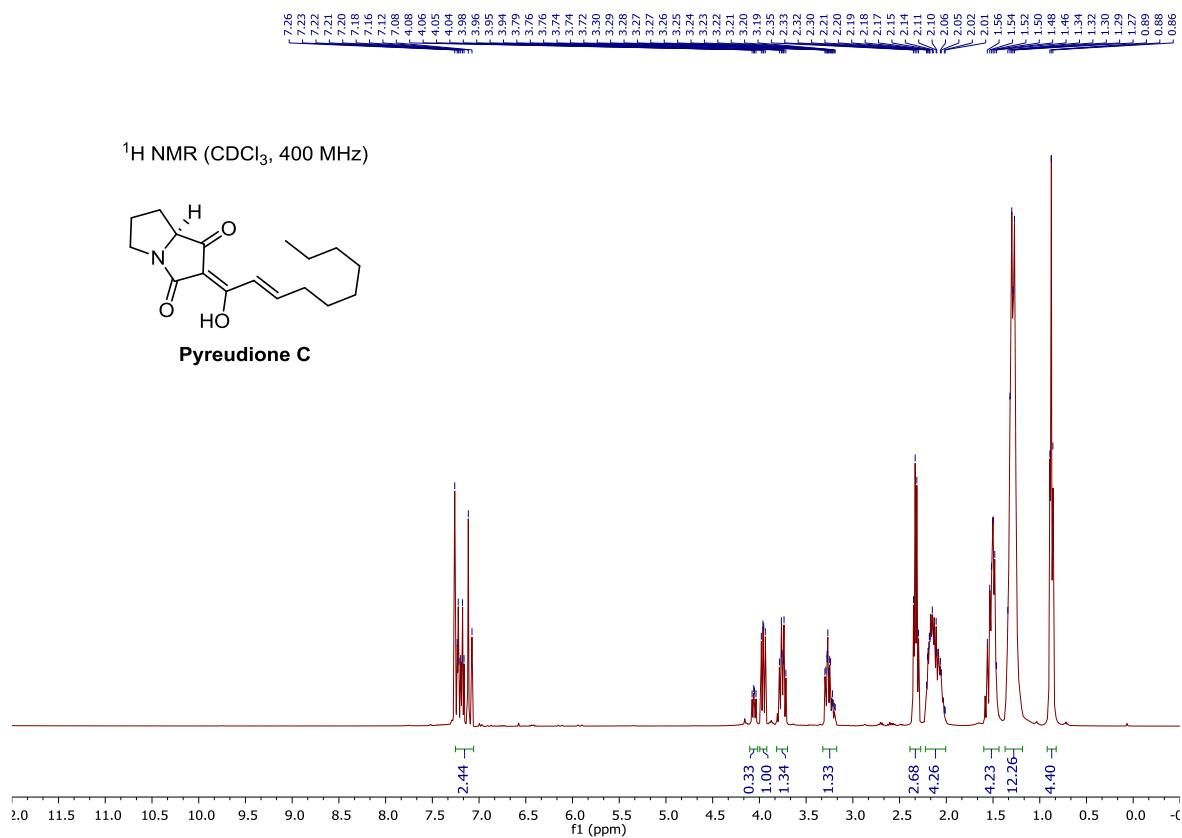
<sup>1</sup>H NMR (CDCl<sub>3</sub>, 400 MHz)

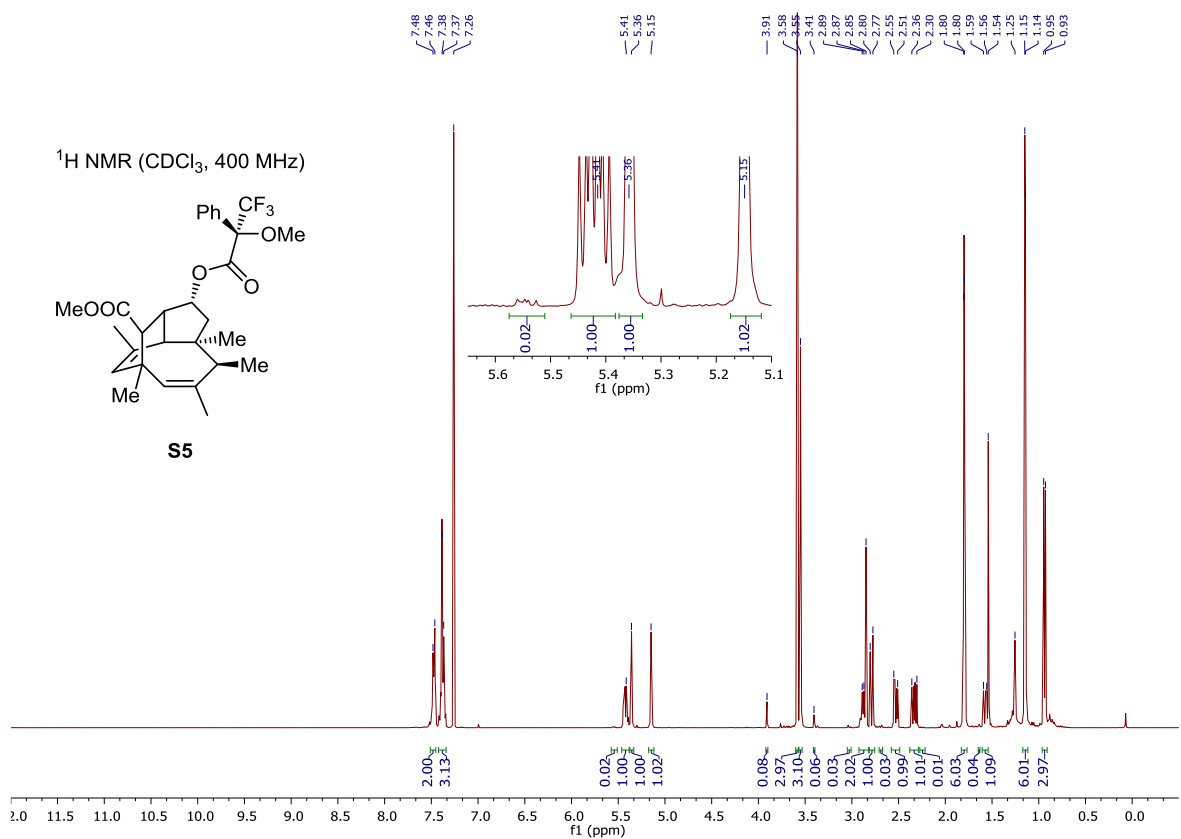
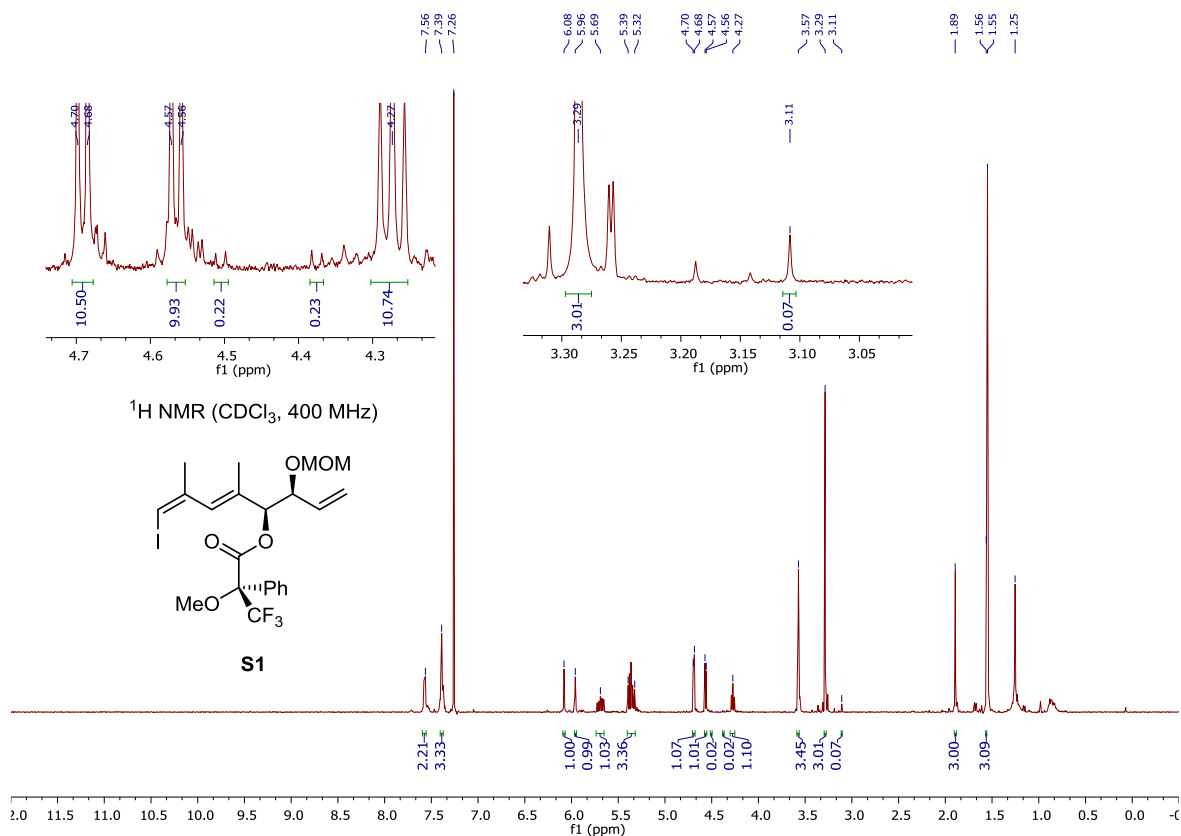


<sup>13</sup>C NMR (CDCl<sub>3</sub>, 100 MHz)

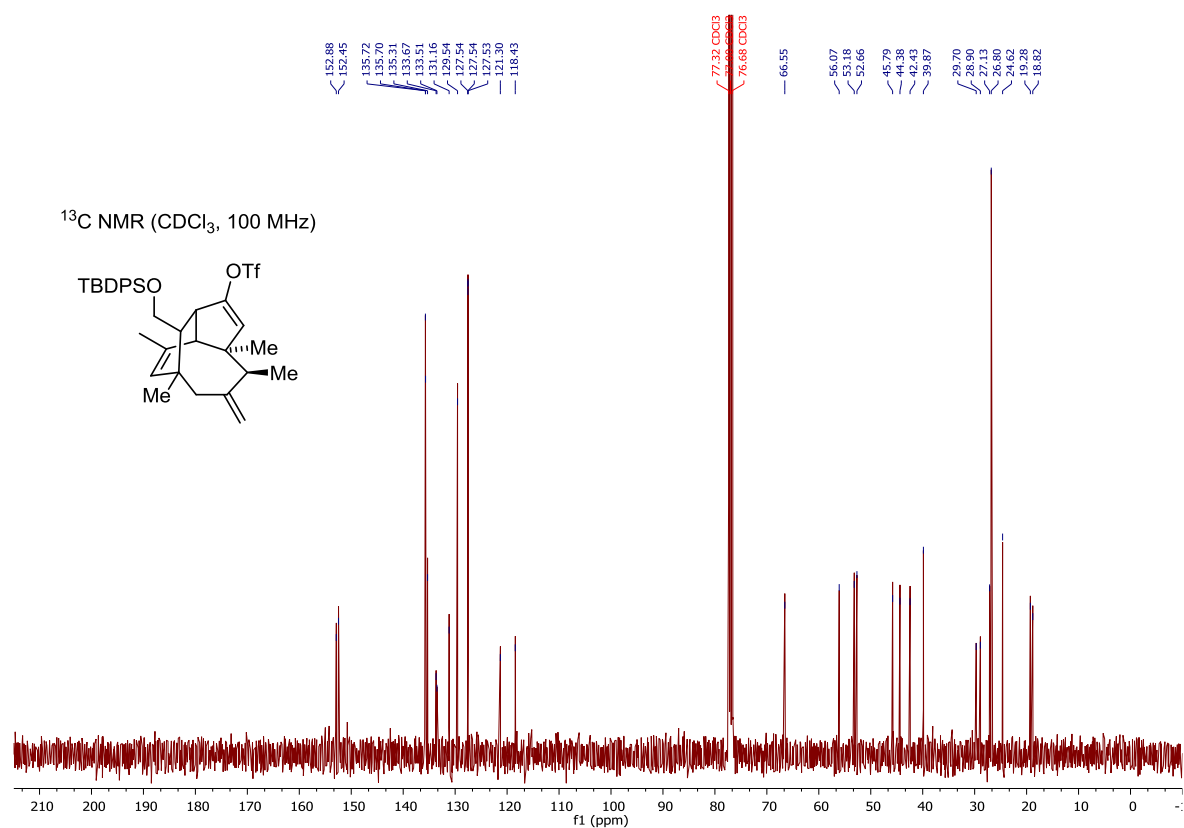
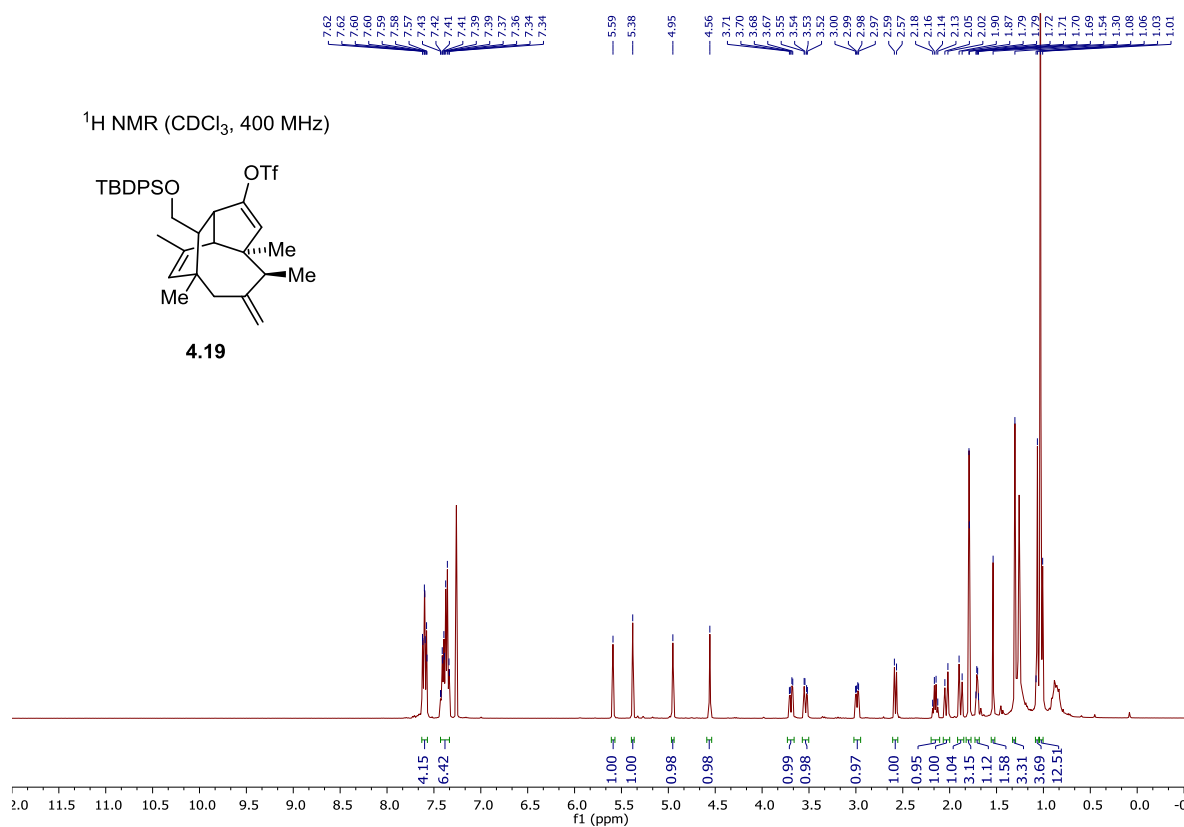


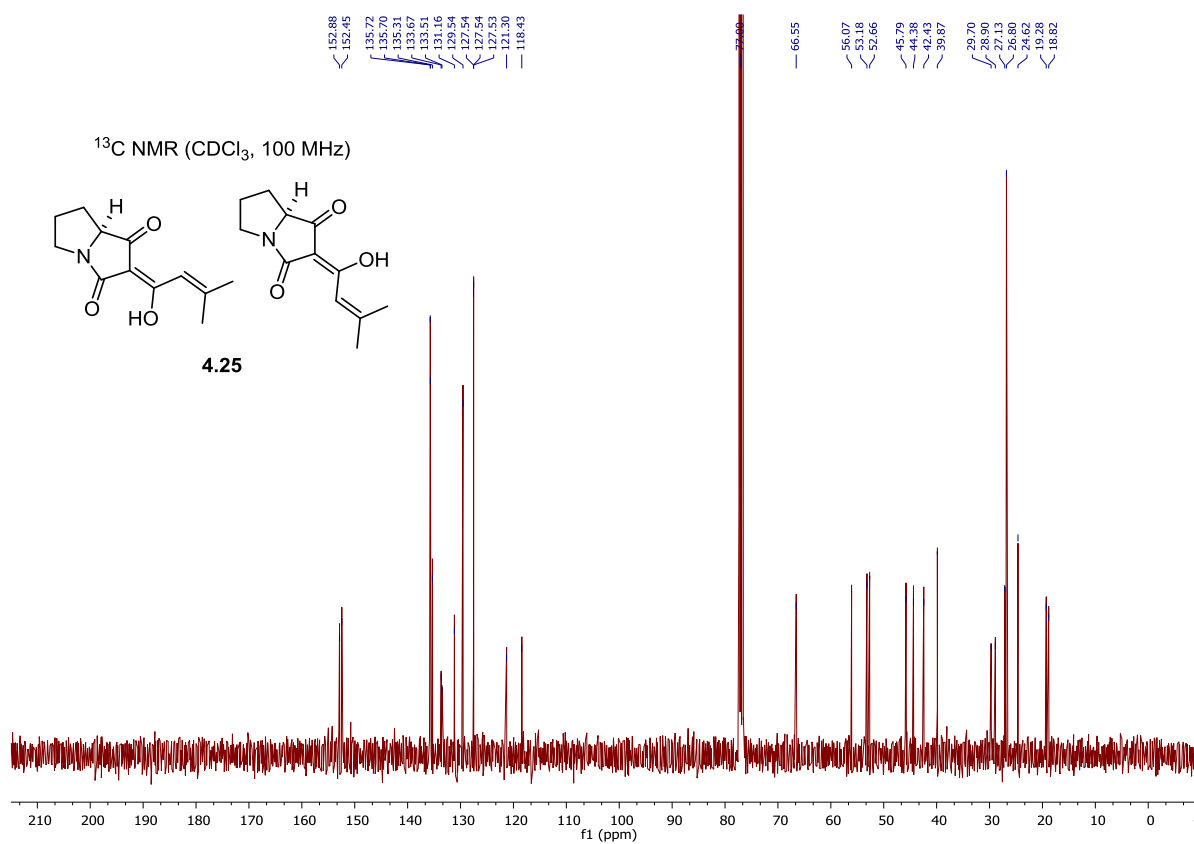
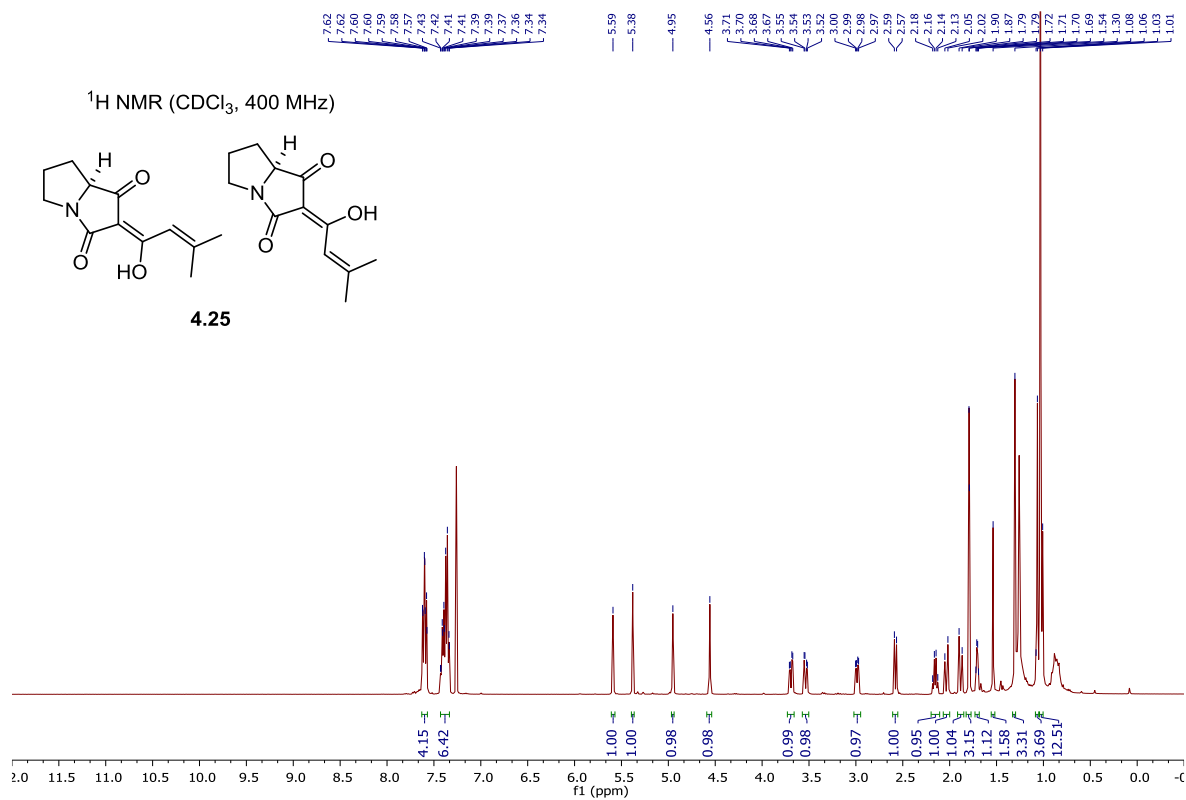




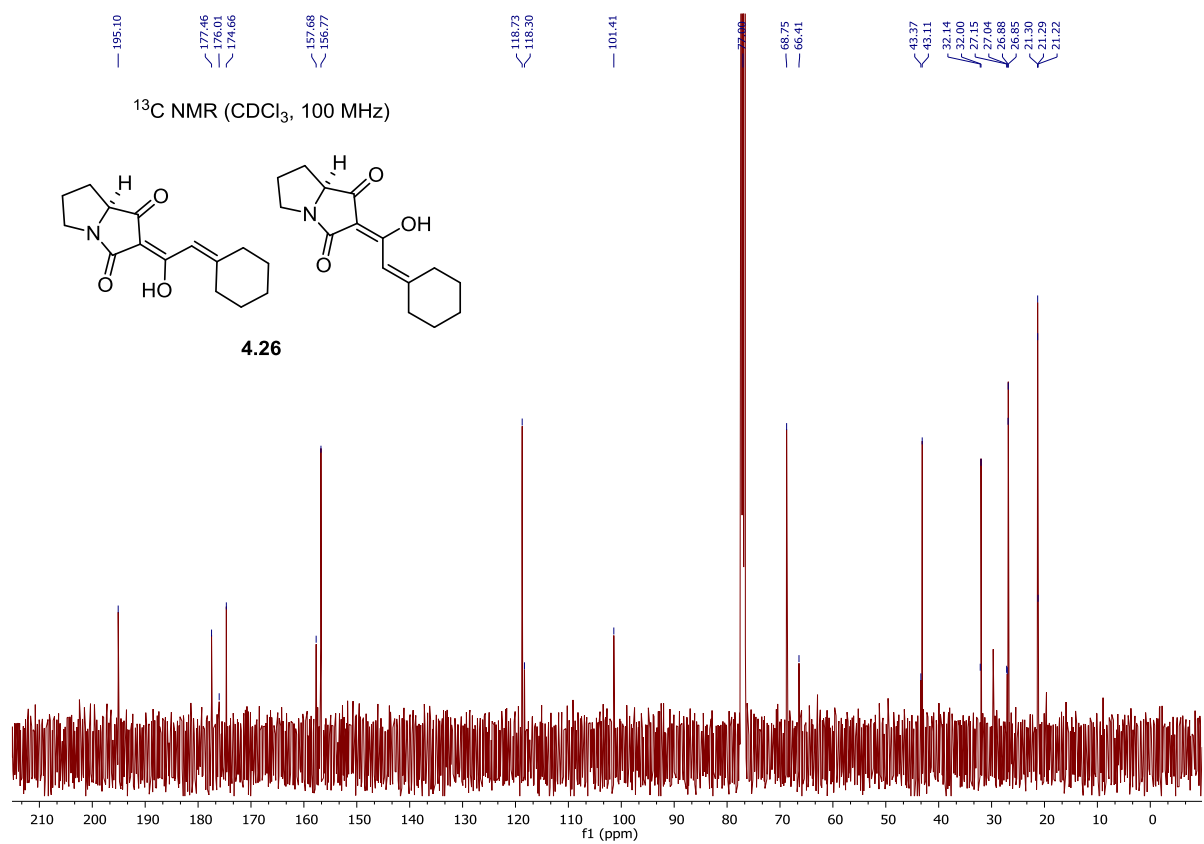
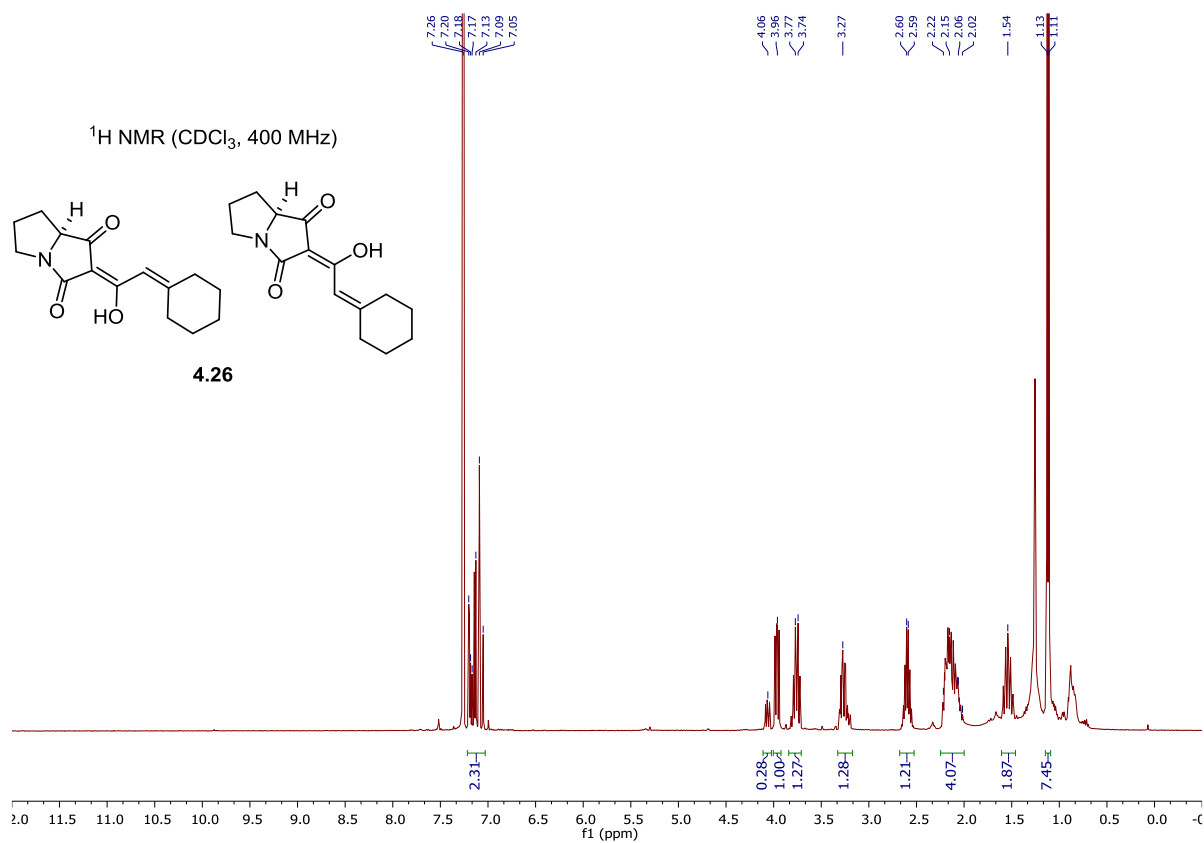


## 8.8.4 NMR Spectra for Chapter 3.4

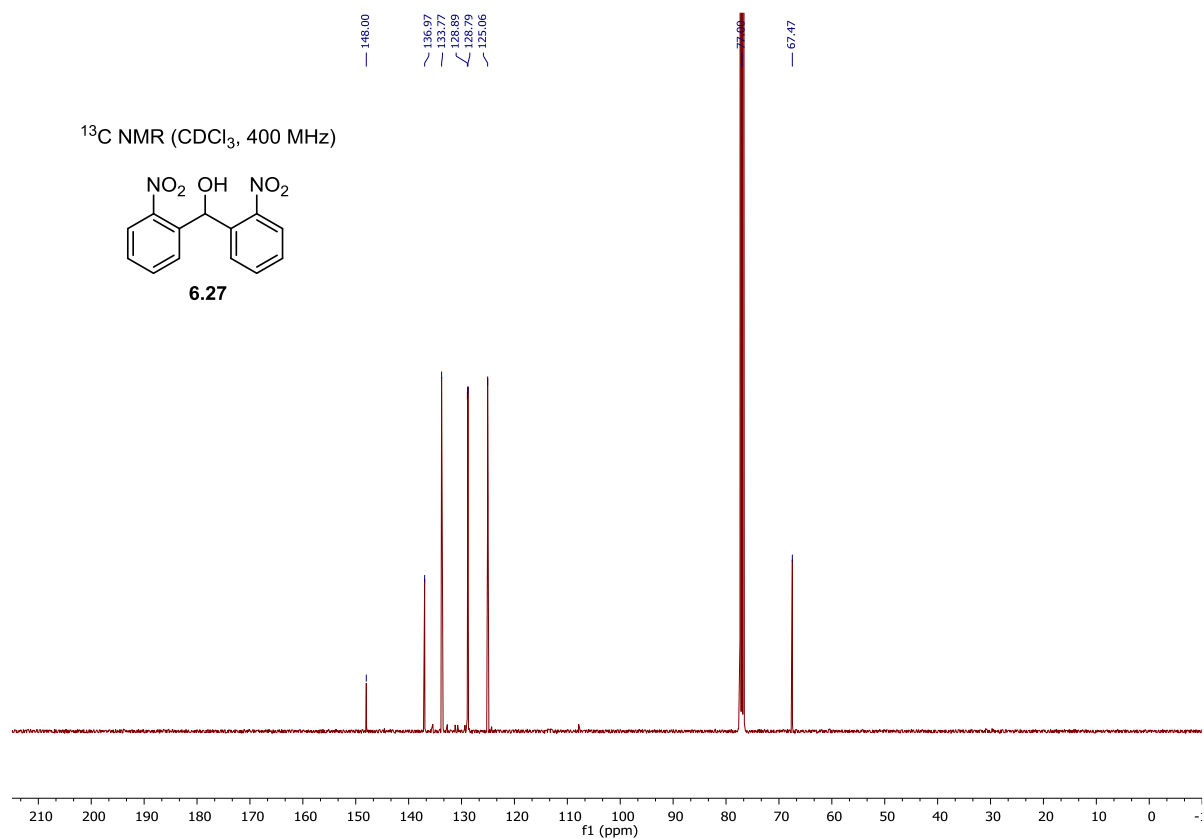
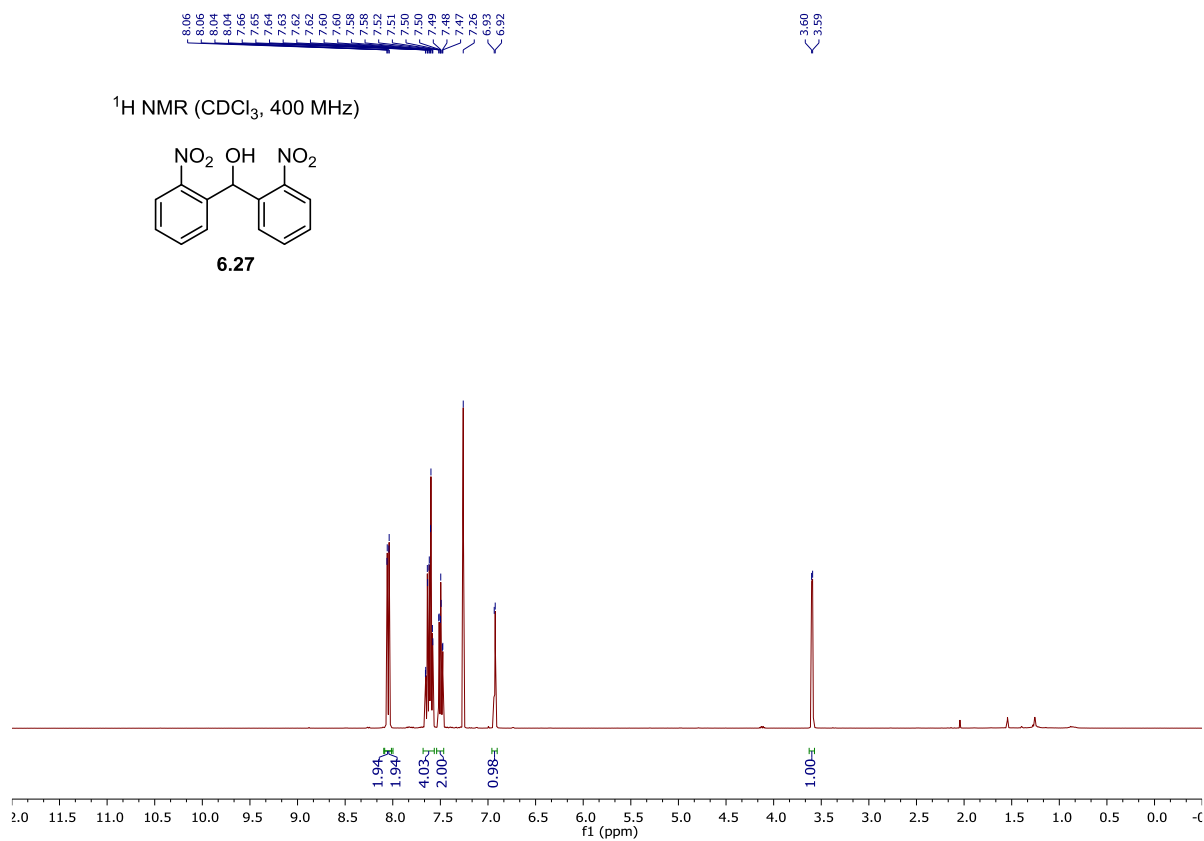






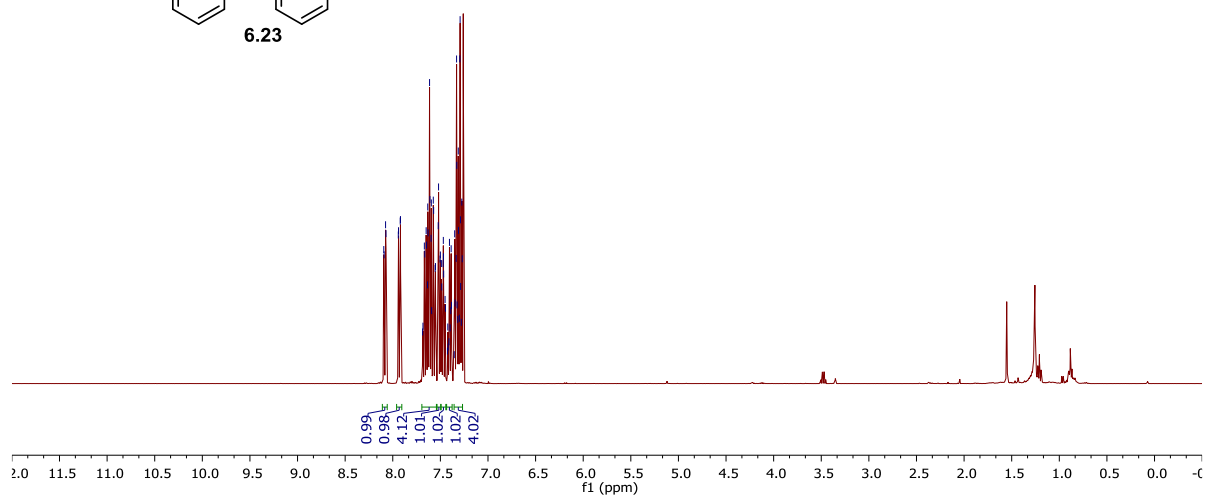


## 8.8.5 NMR Spectra for Chapter 6.1

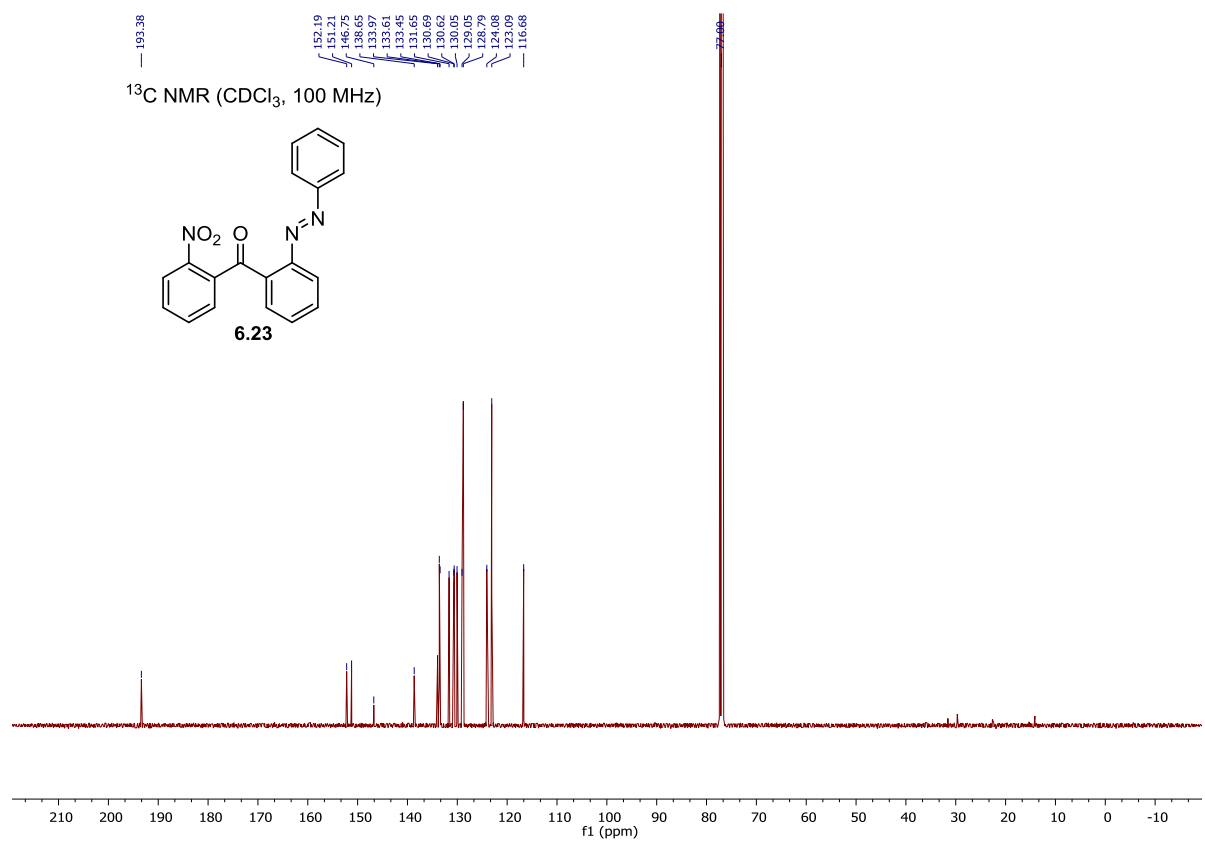


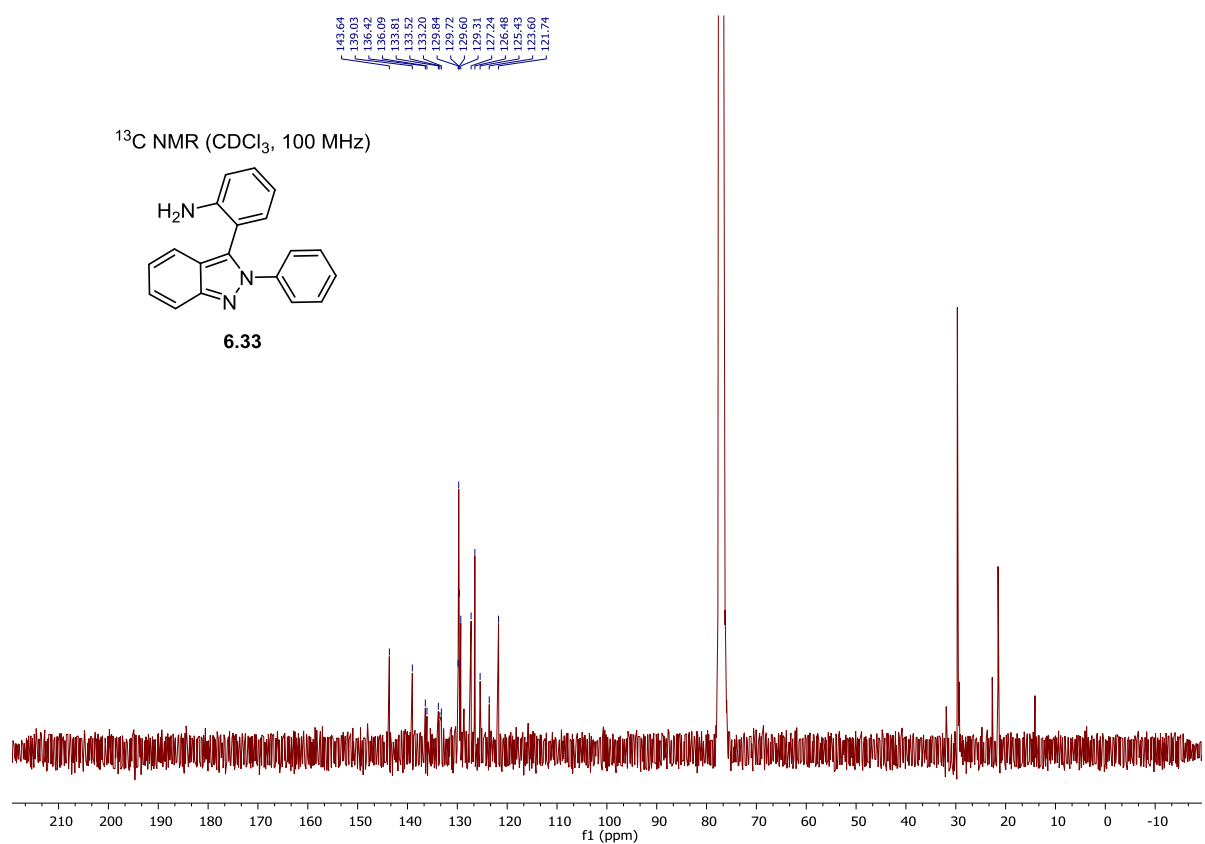
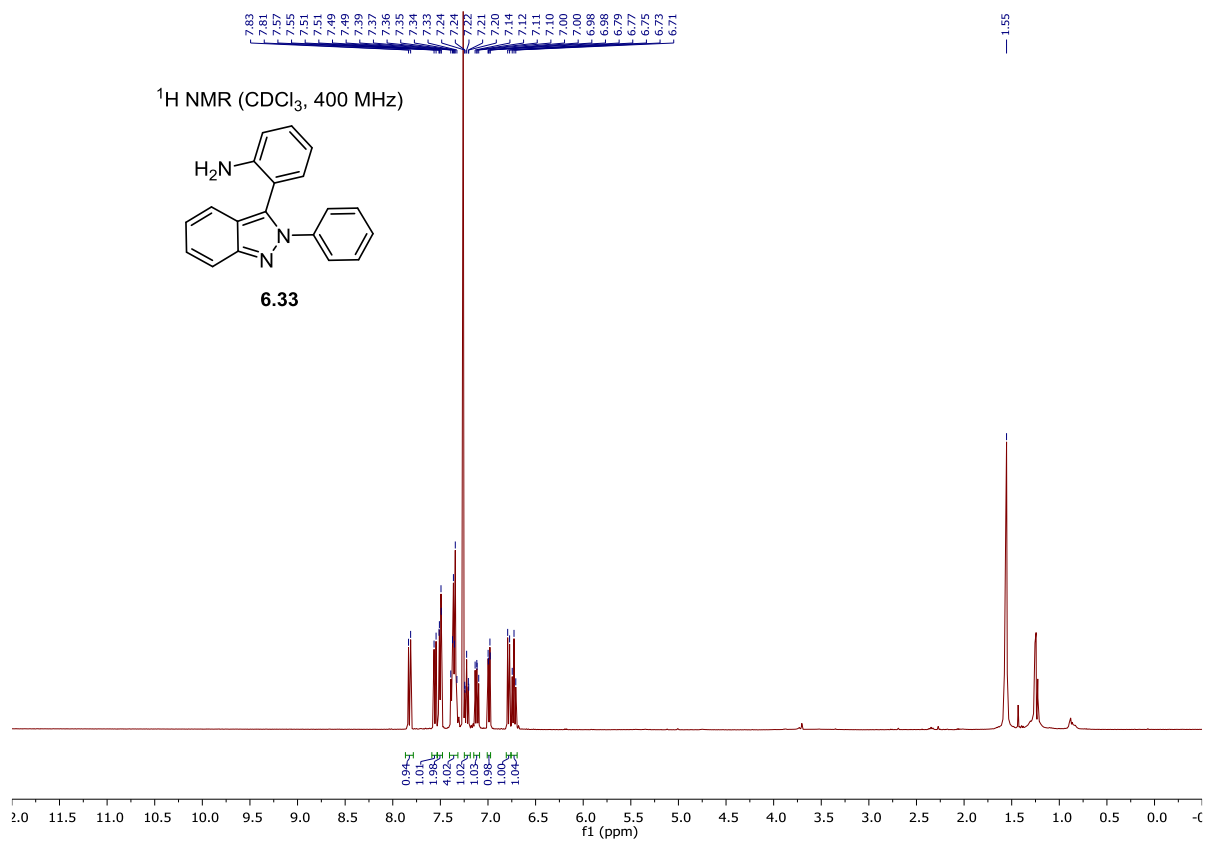
O=[N+]([O-])c1ccccc1C(=O)c2ccccc2N=Nc3ccccc3

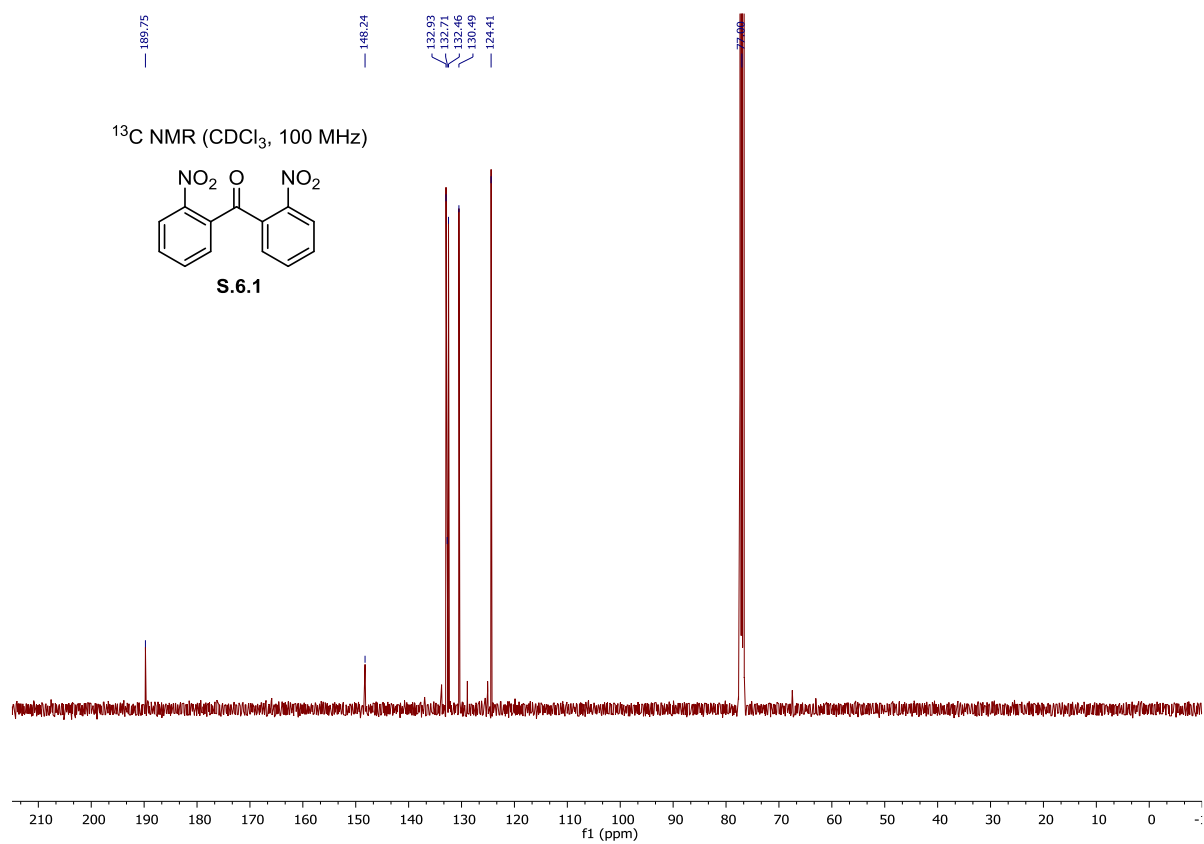
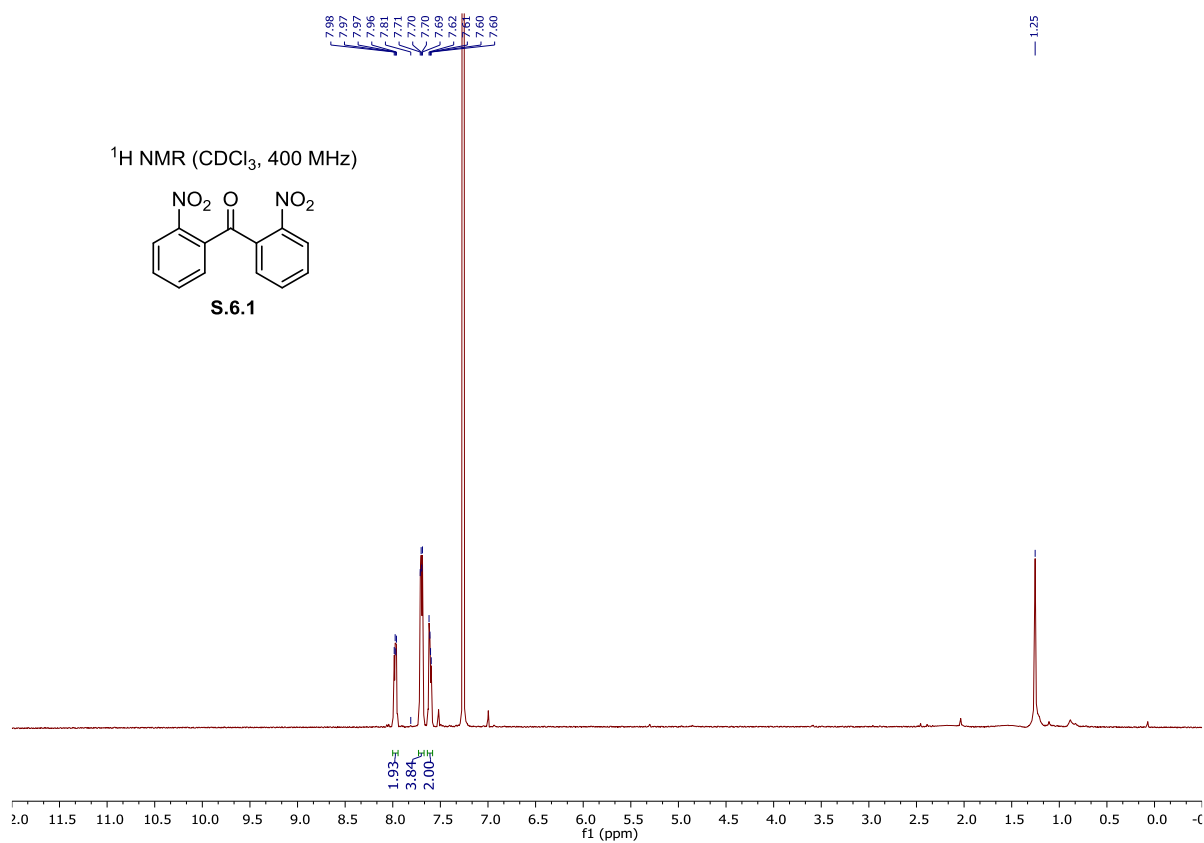
**6.23**

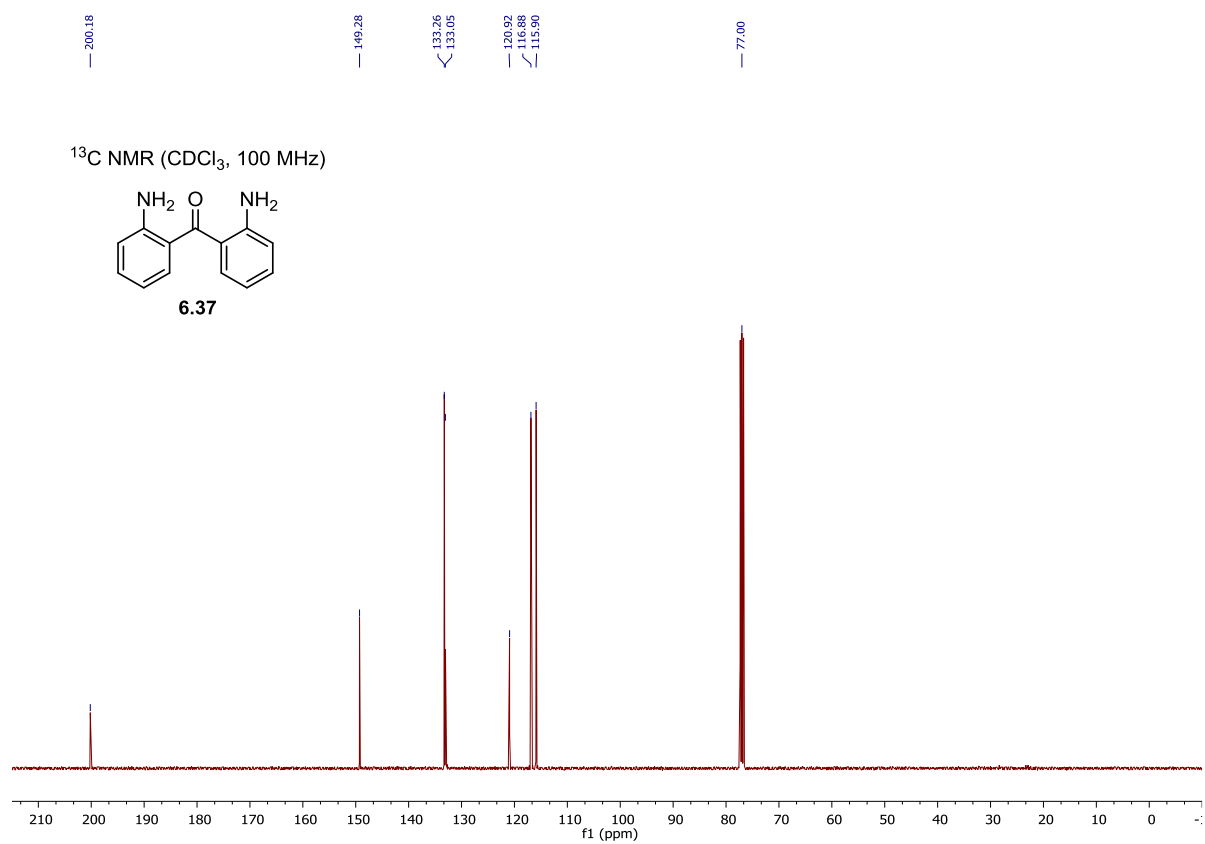
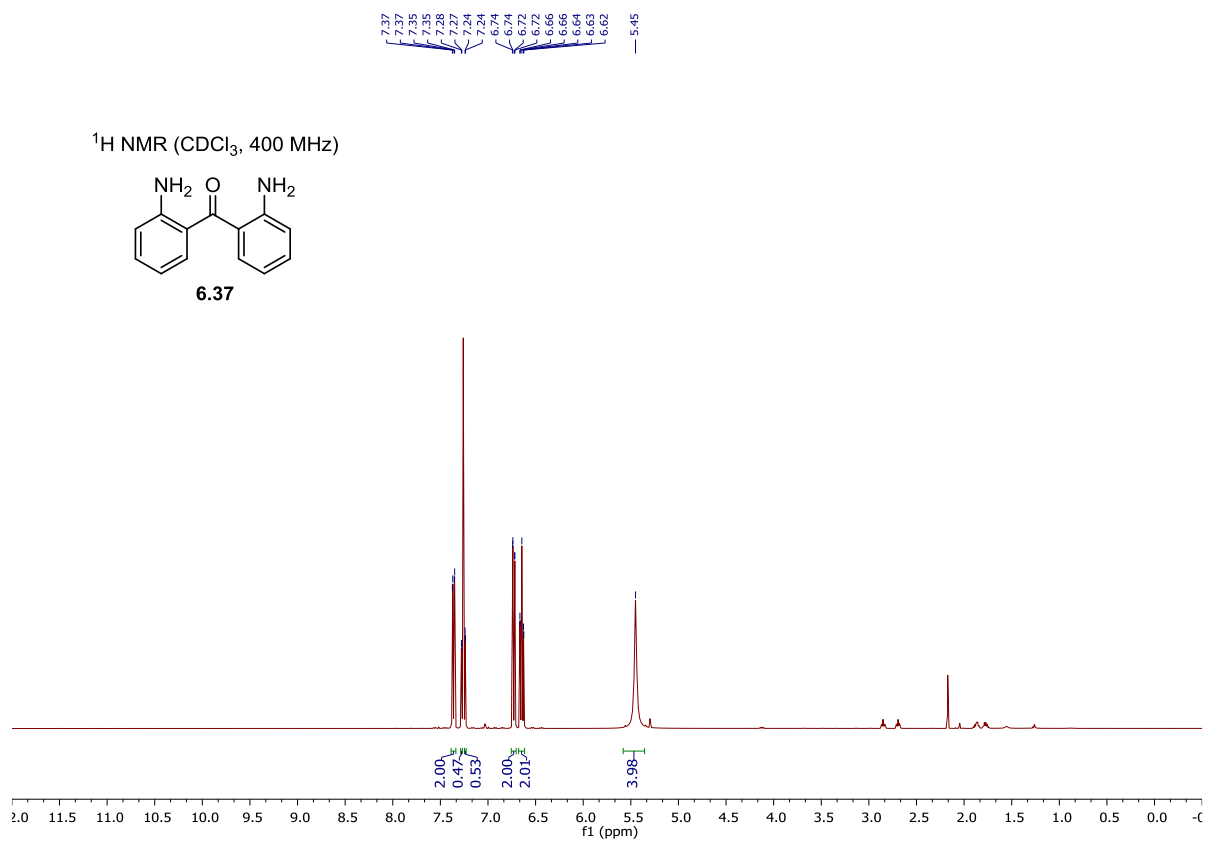
O=[N+]([O-])c1ccccc1C(=O)c2ccccc2/N=N/c3ccccc3

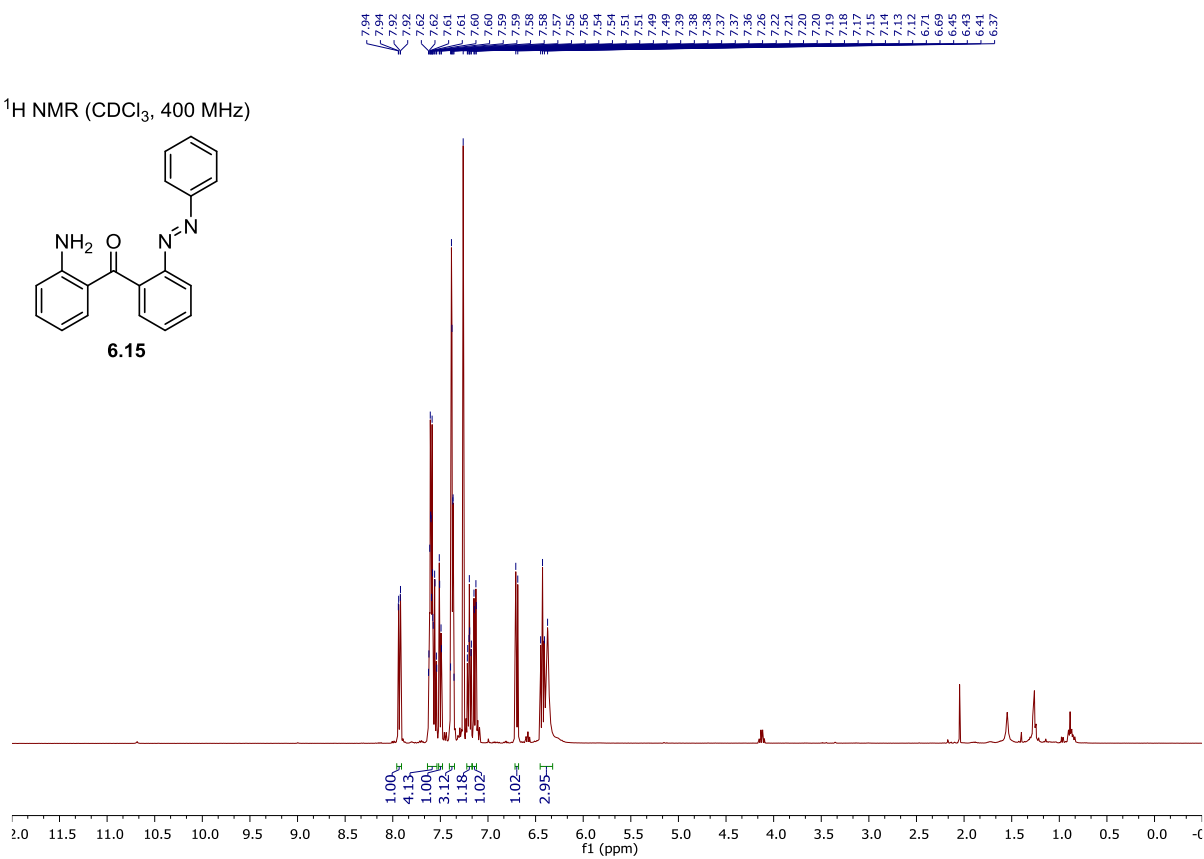
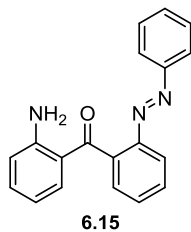
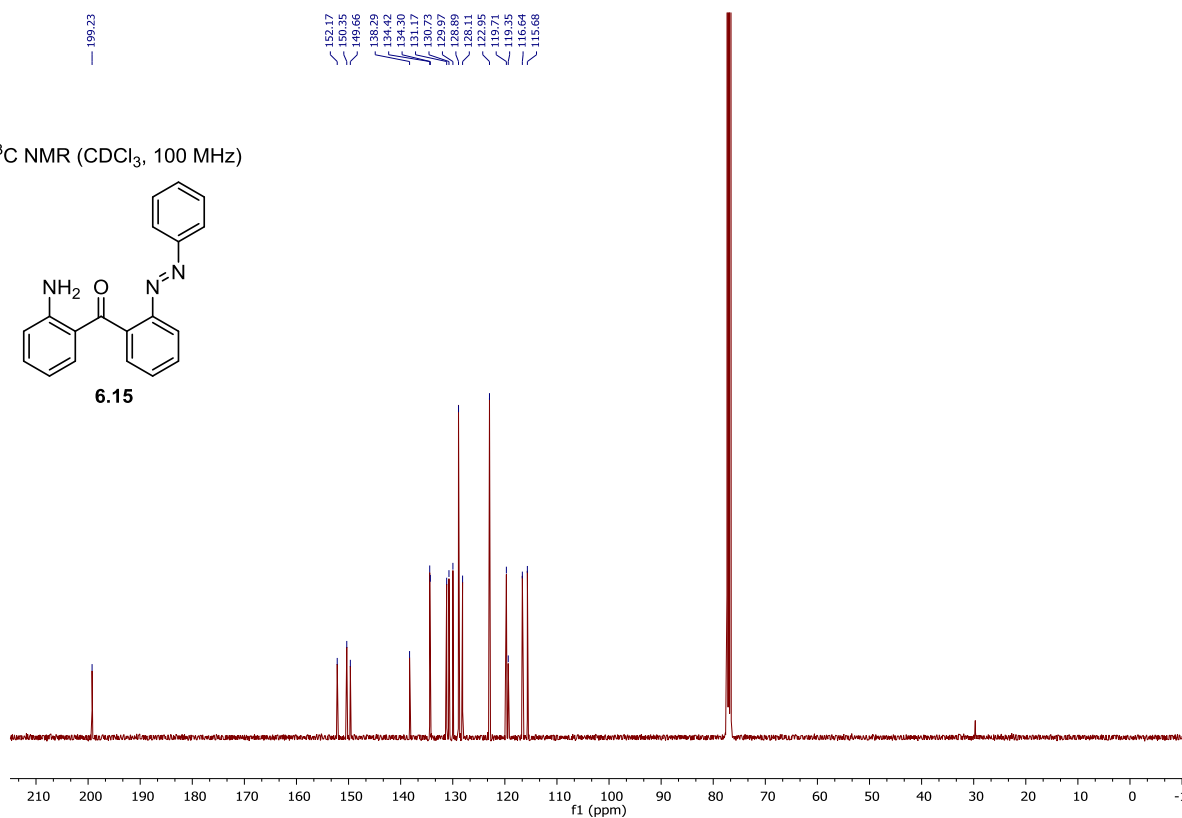
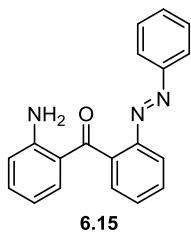
**6.23**

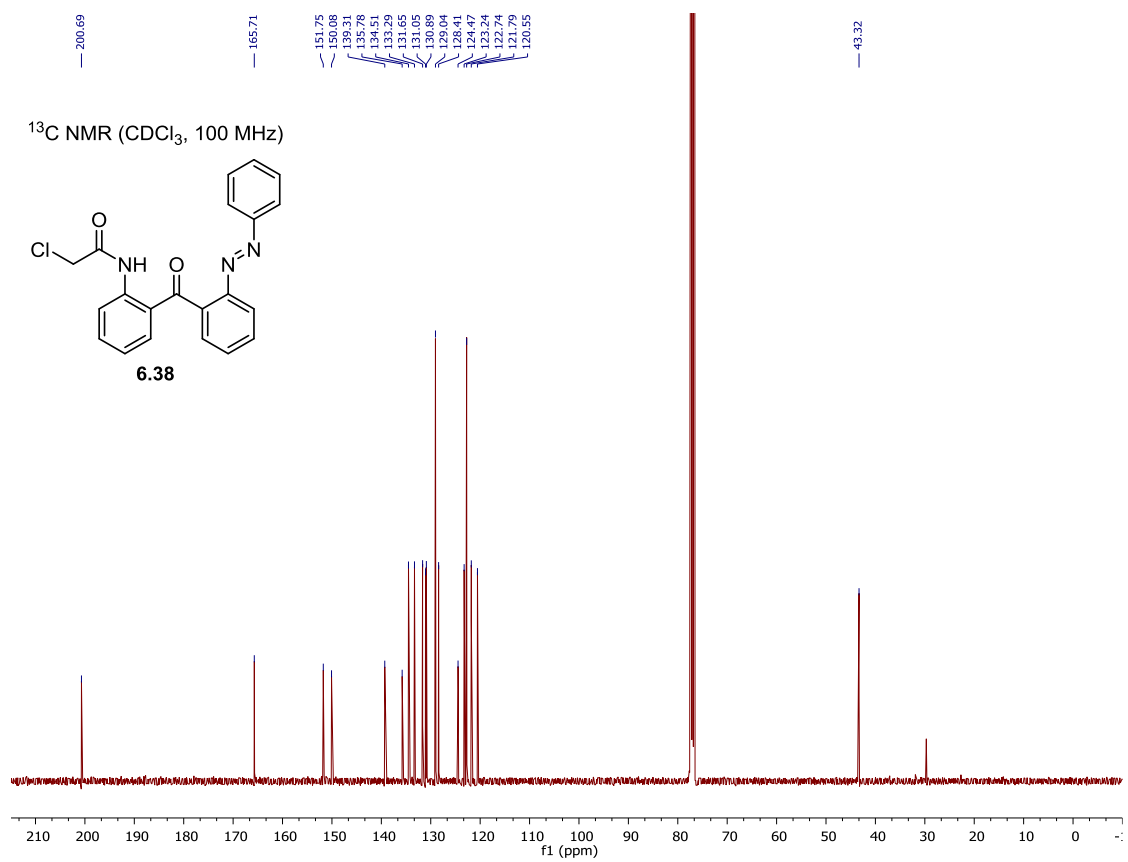
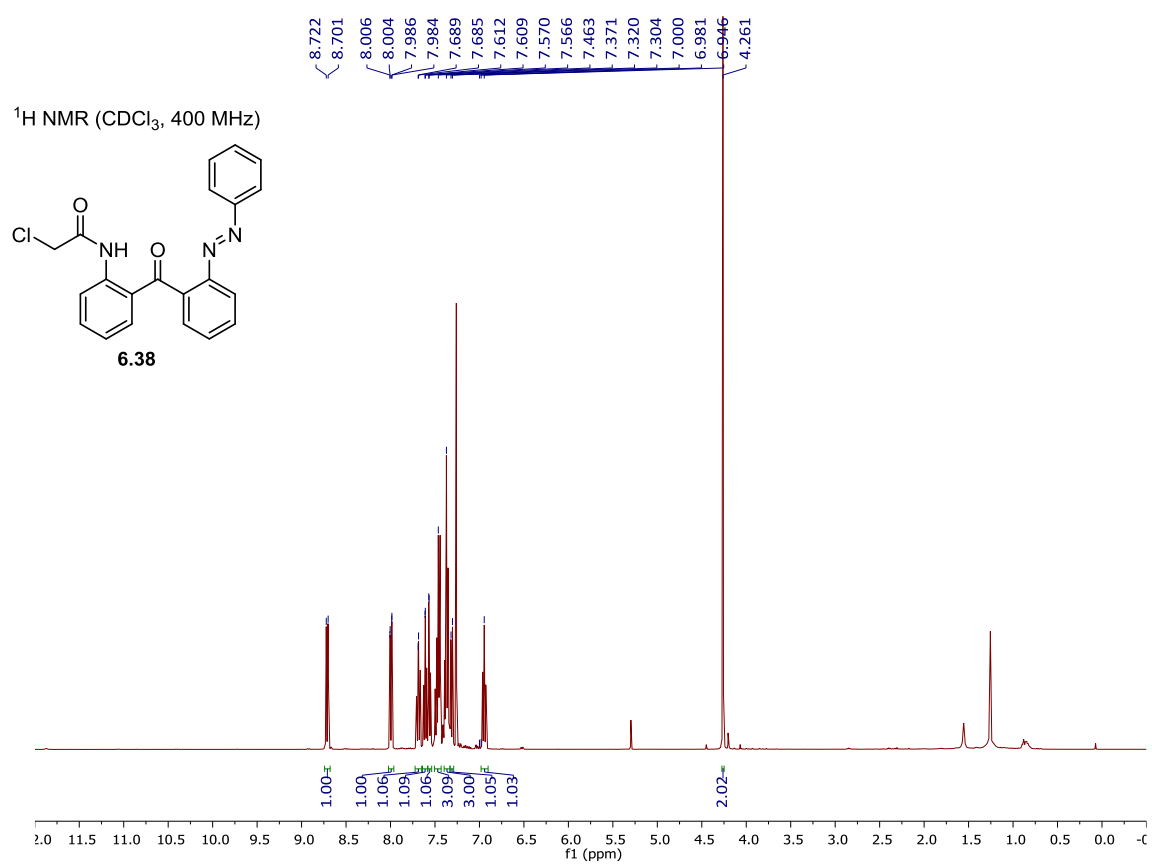




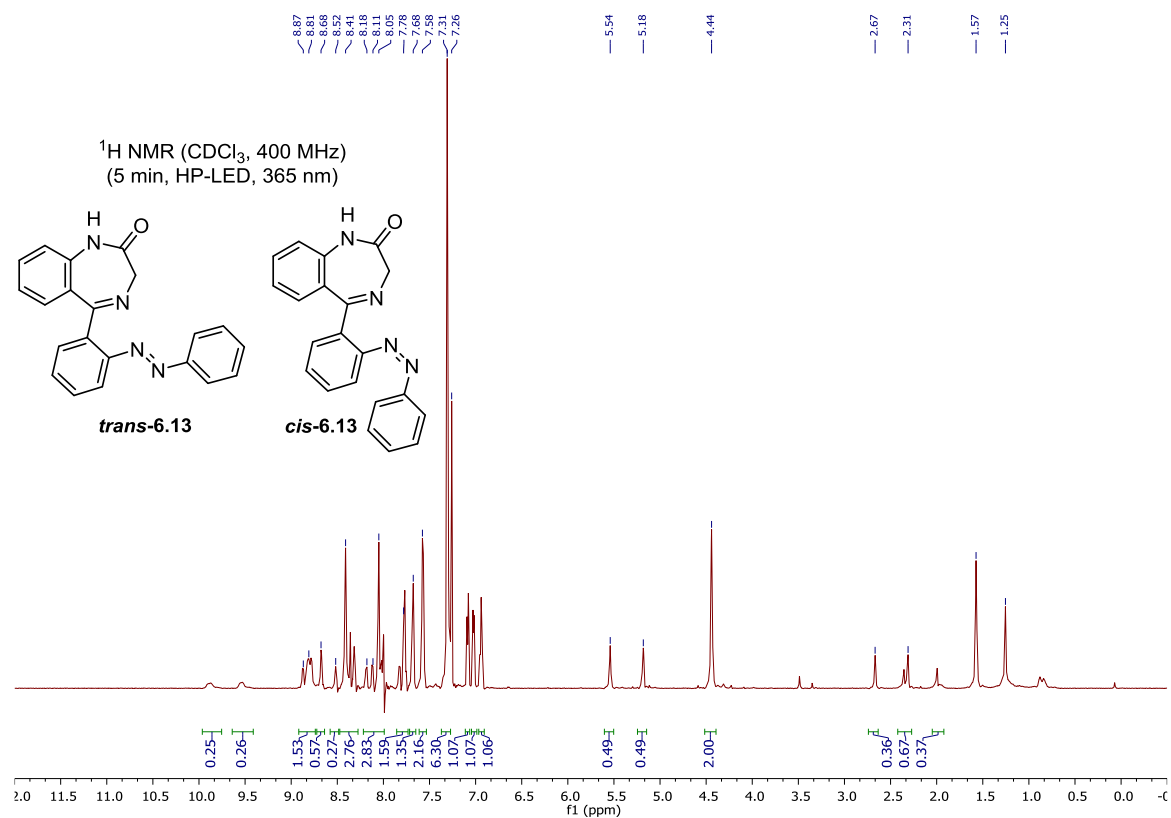
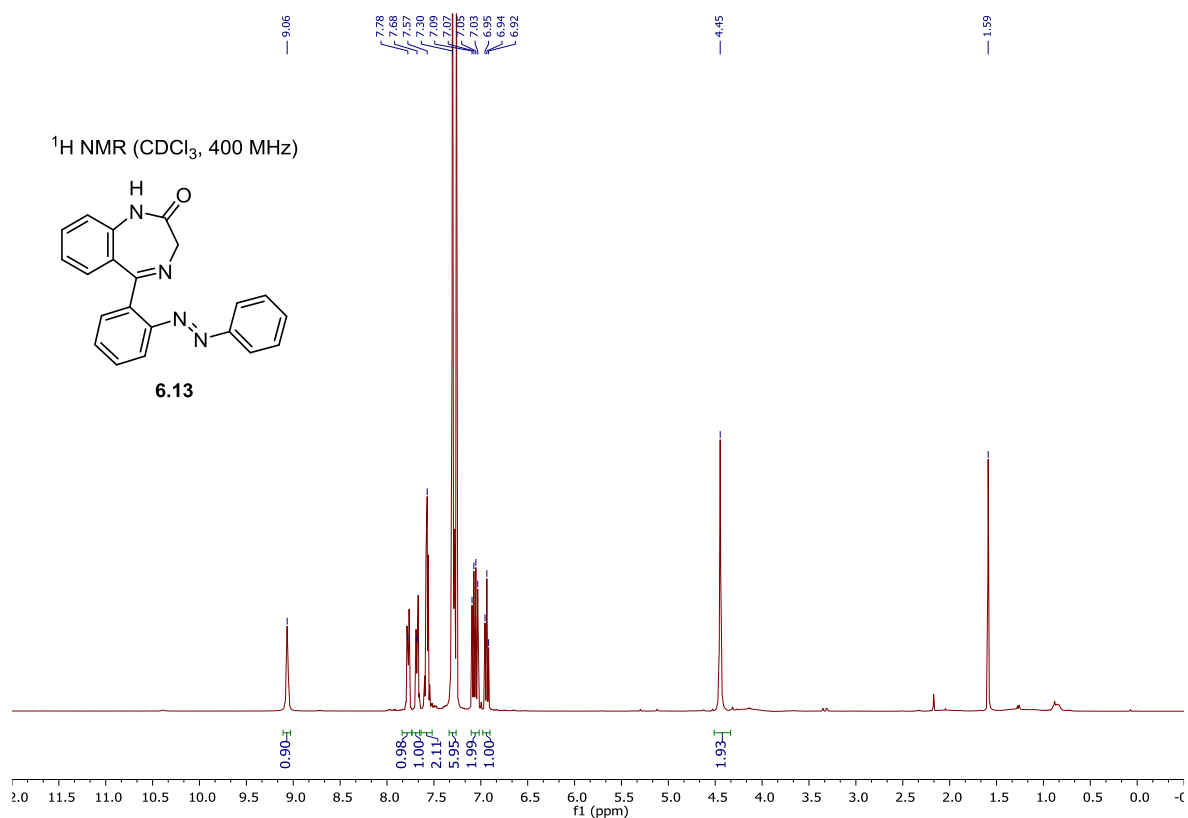


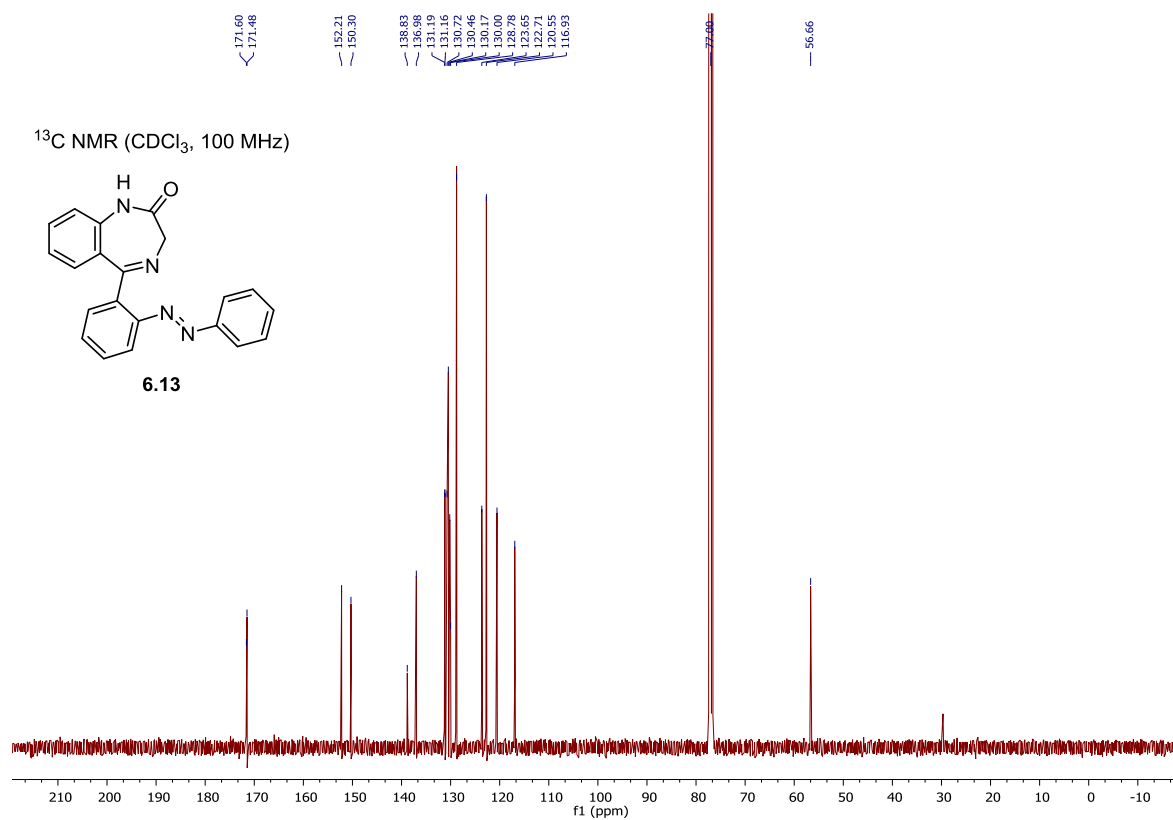


<sup>1</sup>H NMR (CDCl<sub>3</sub>, 400 MHz)<sup>13</sup>C NMR (CDCl<sub>3</sub>, 100 MHz)

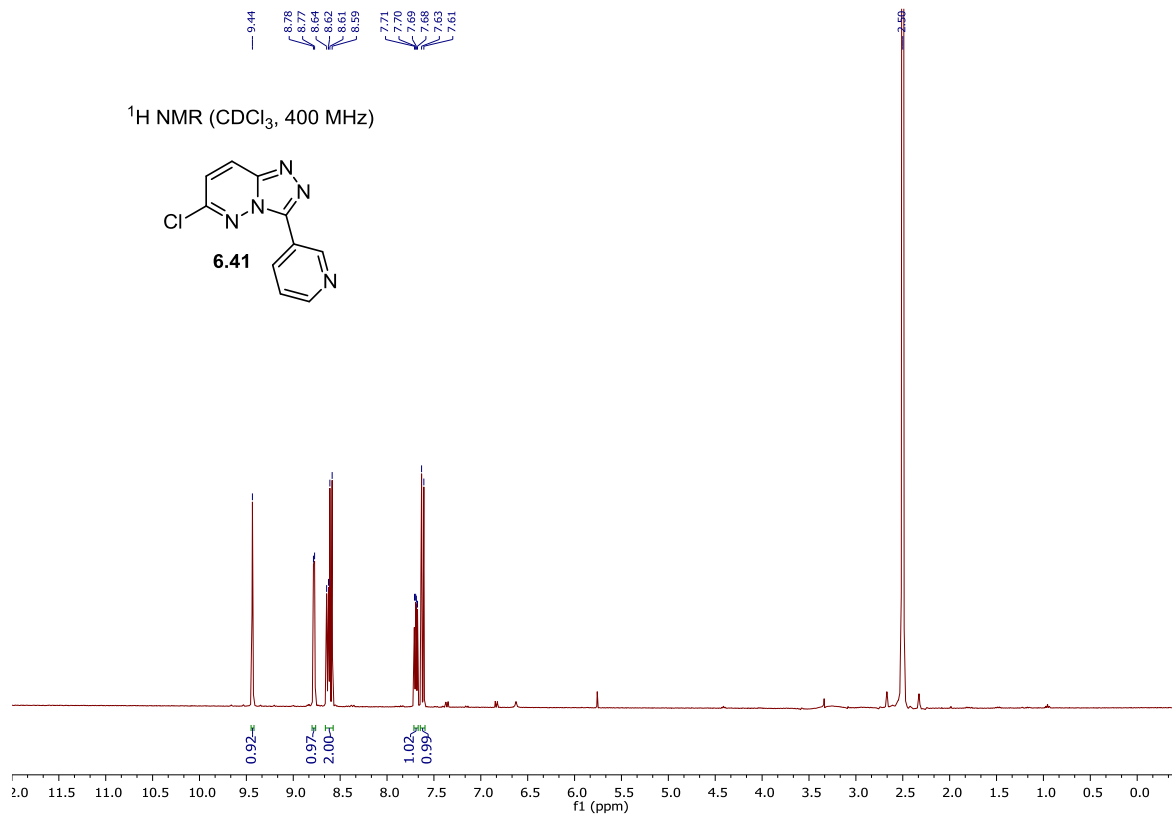
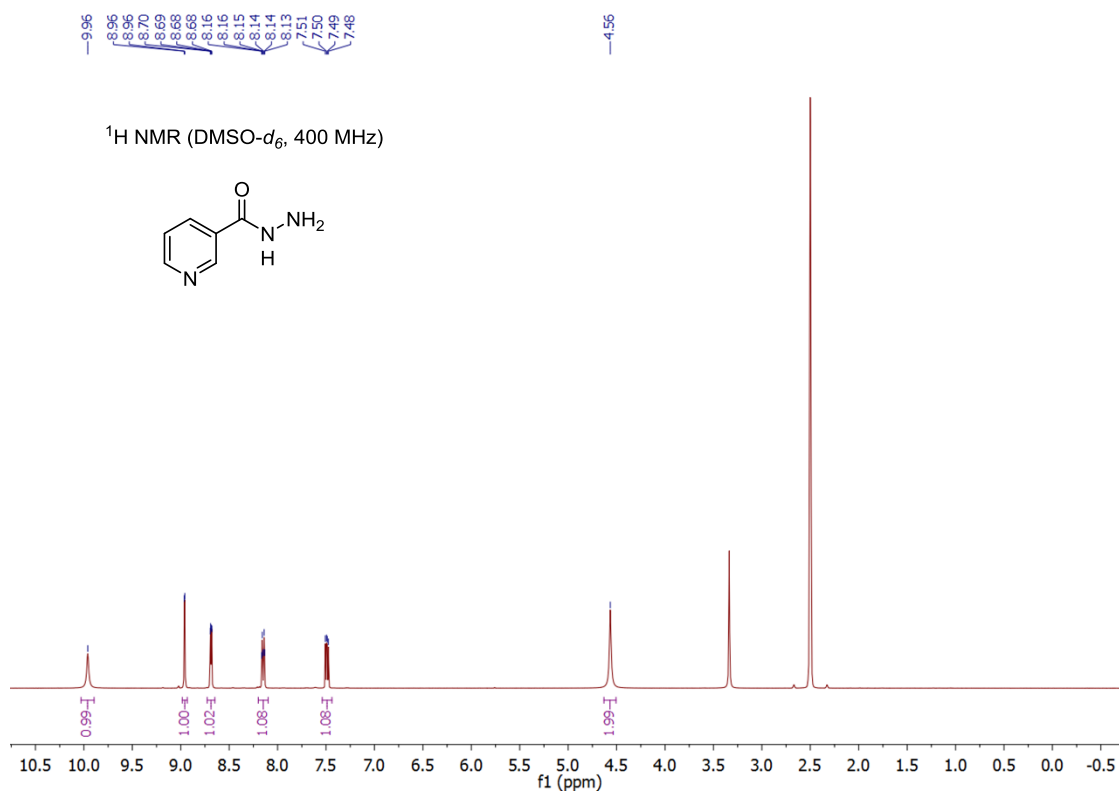


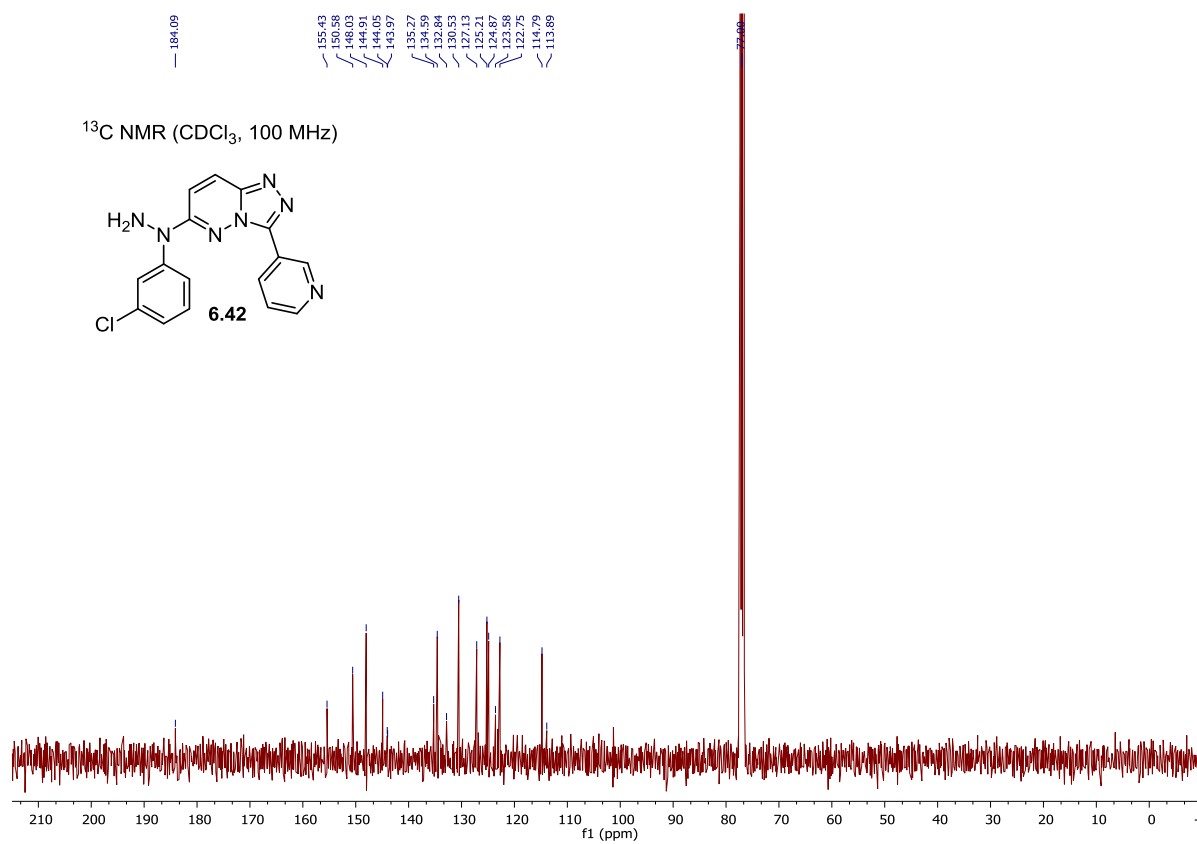
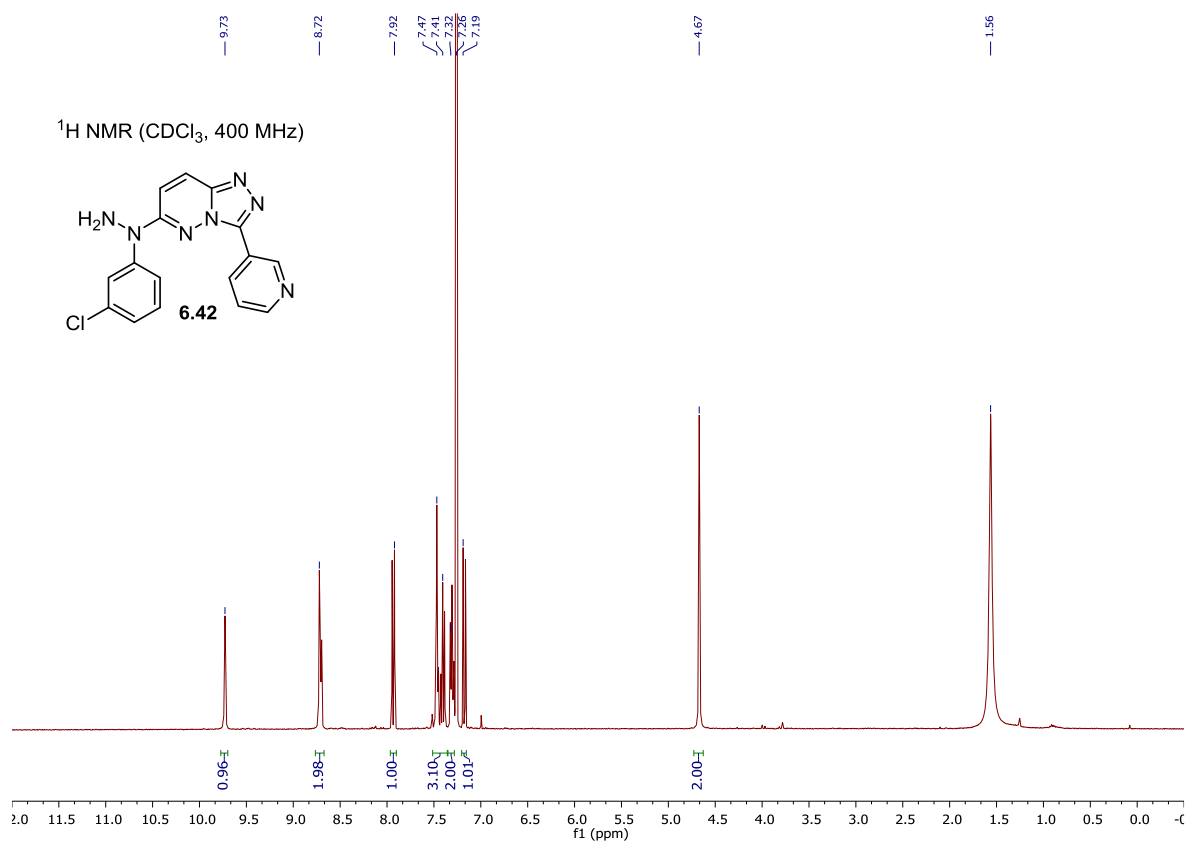


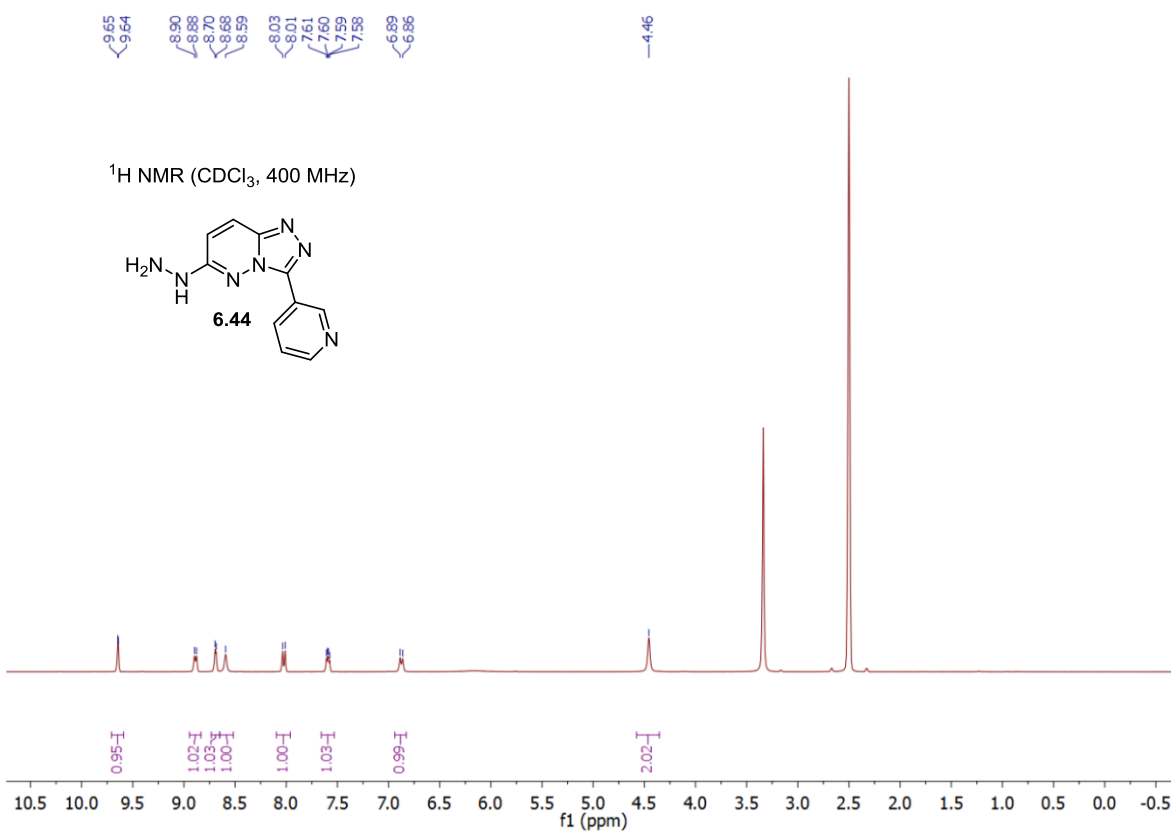
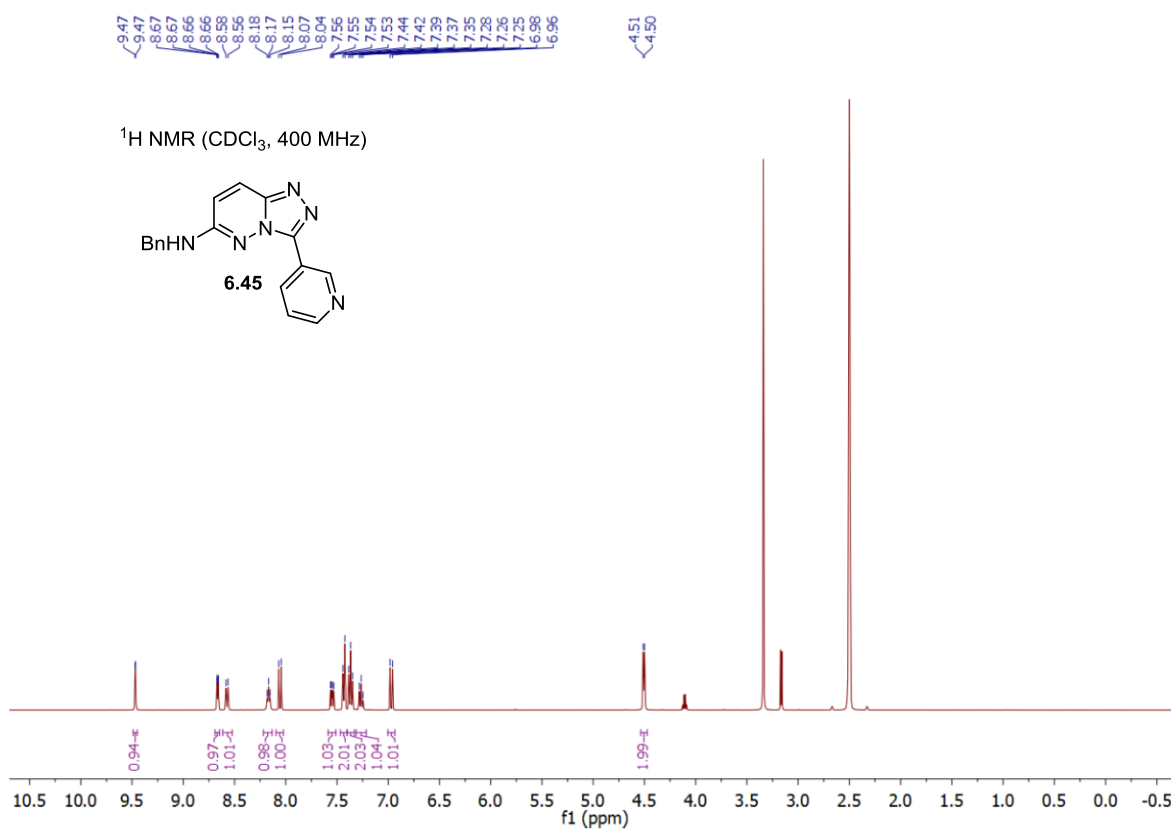


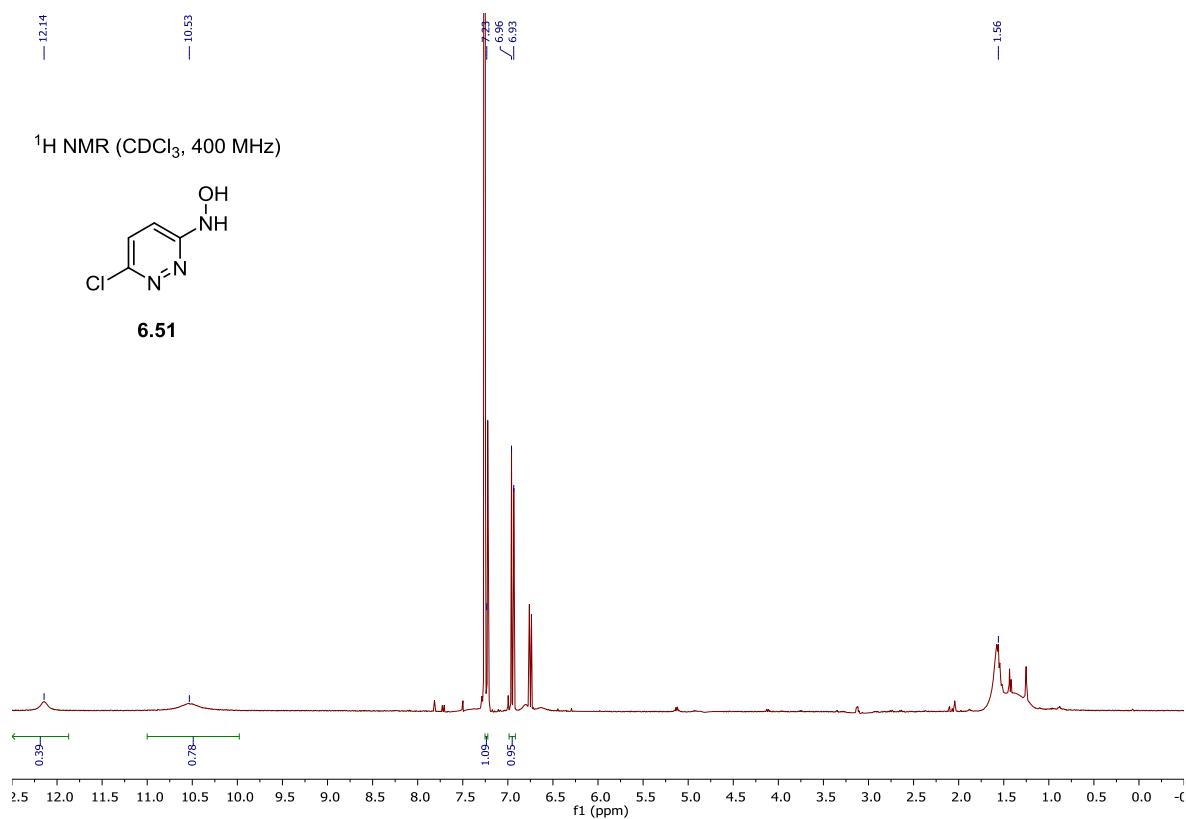
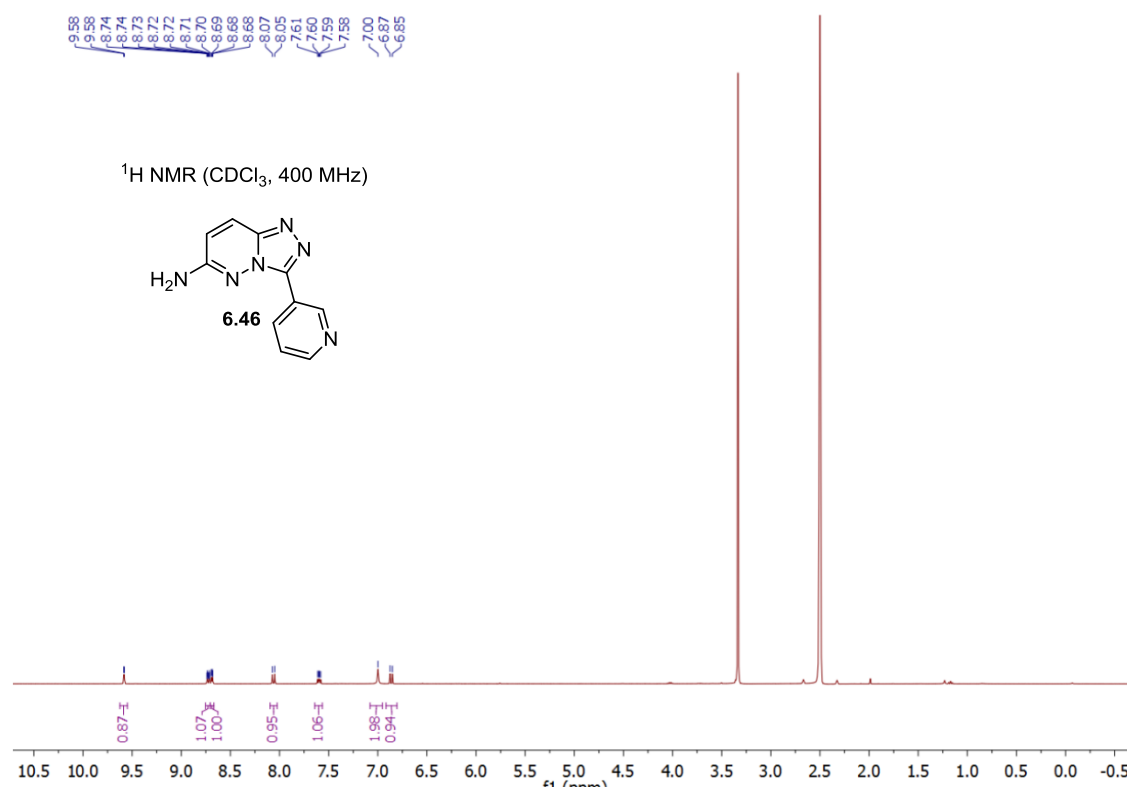


## 8.8.6 NMR Spectra for Chapter 6.2

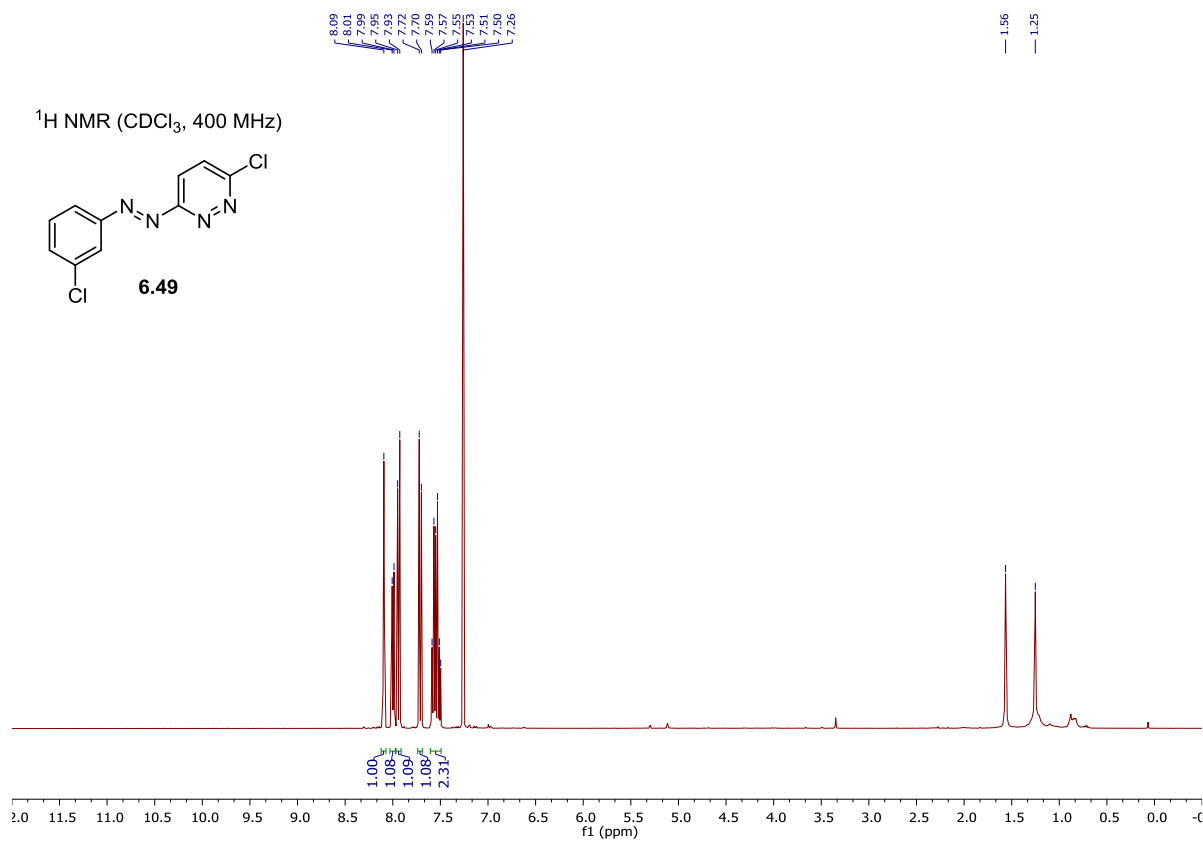
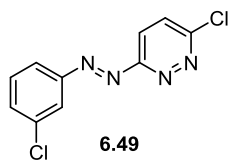




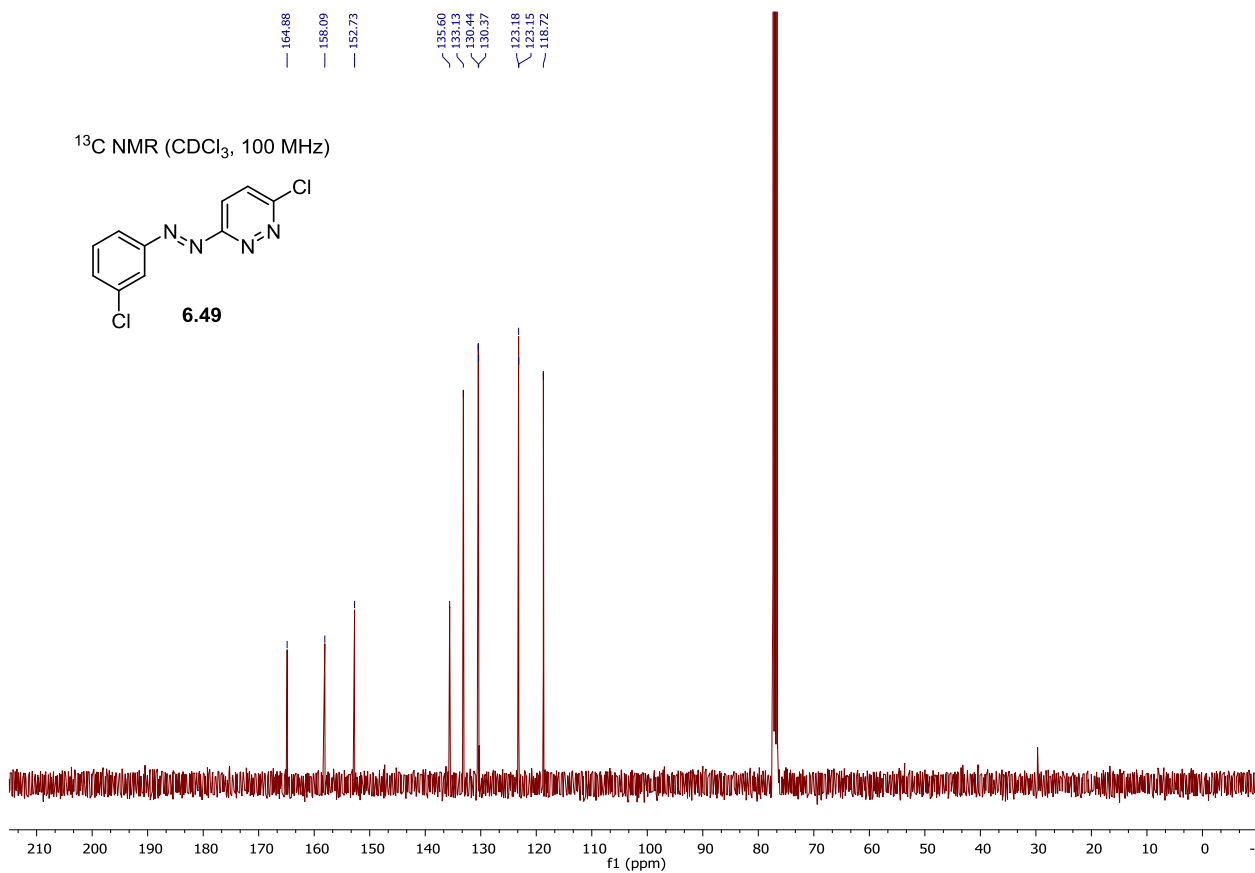
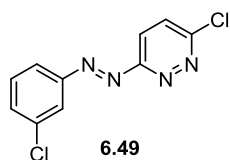


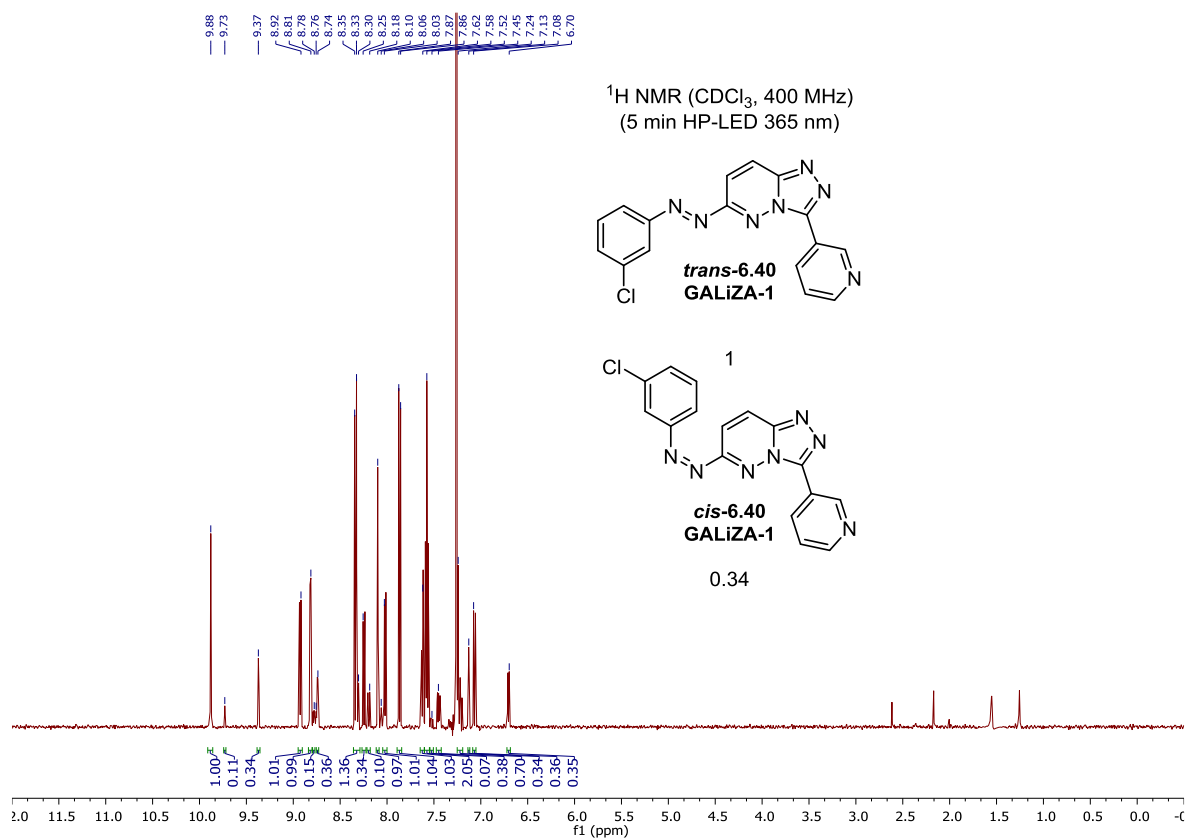
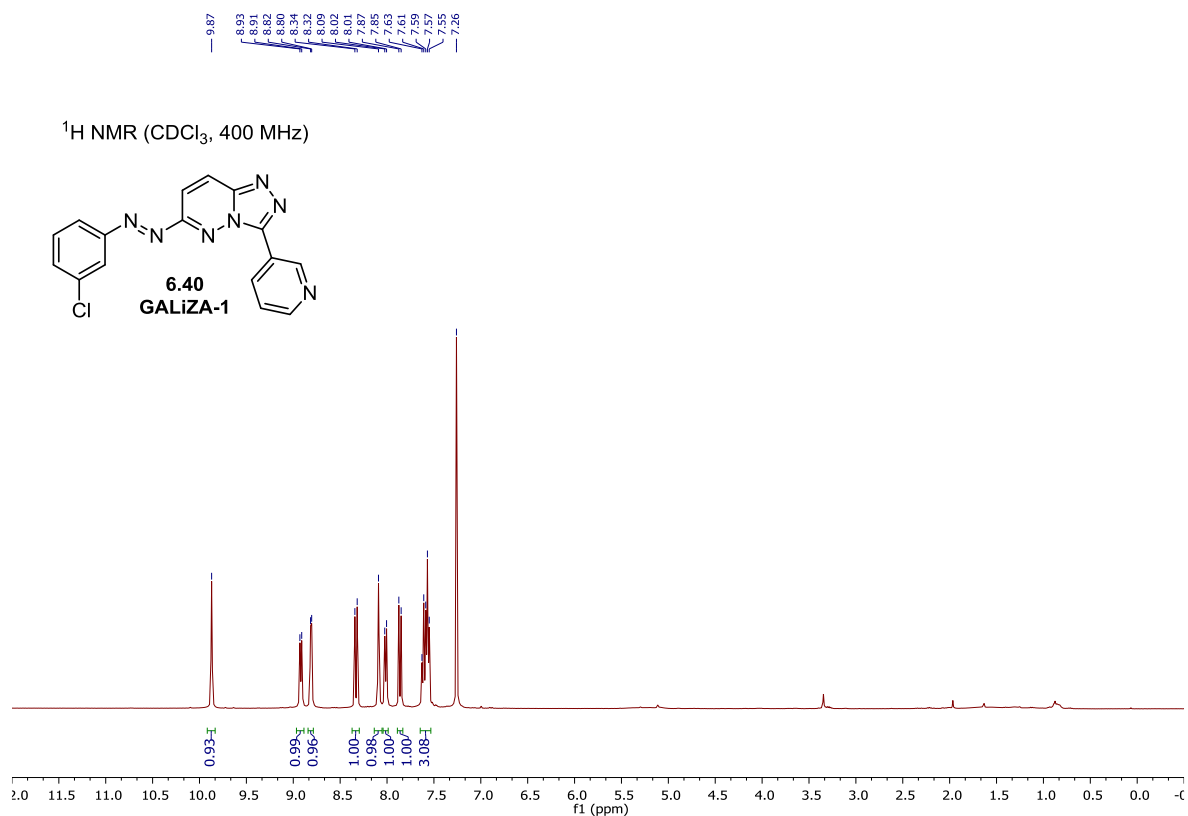


<sup>1</sup>H NMR (CDCl<sub>3</sub>, 400 MHz)

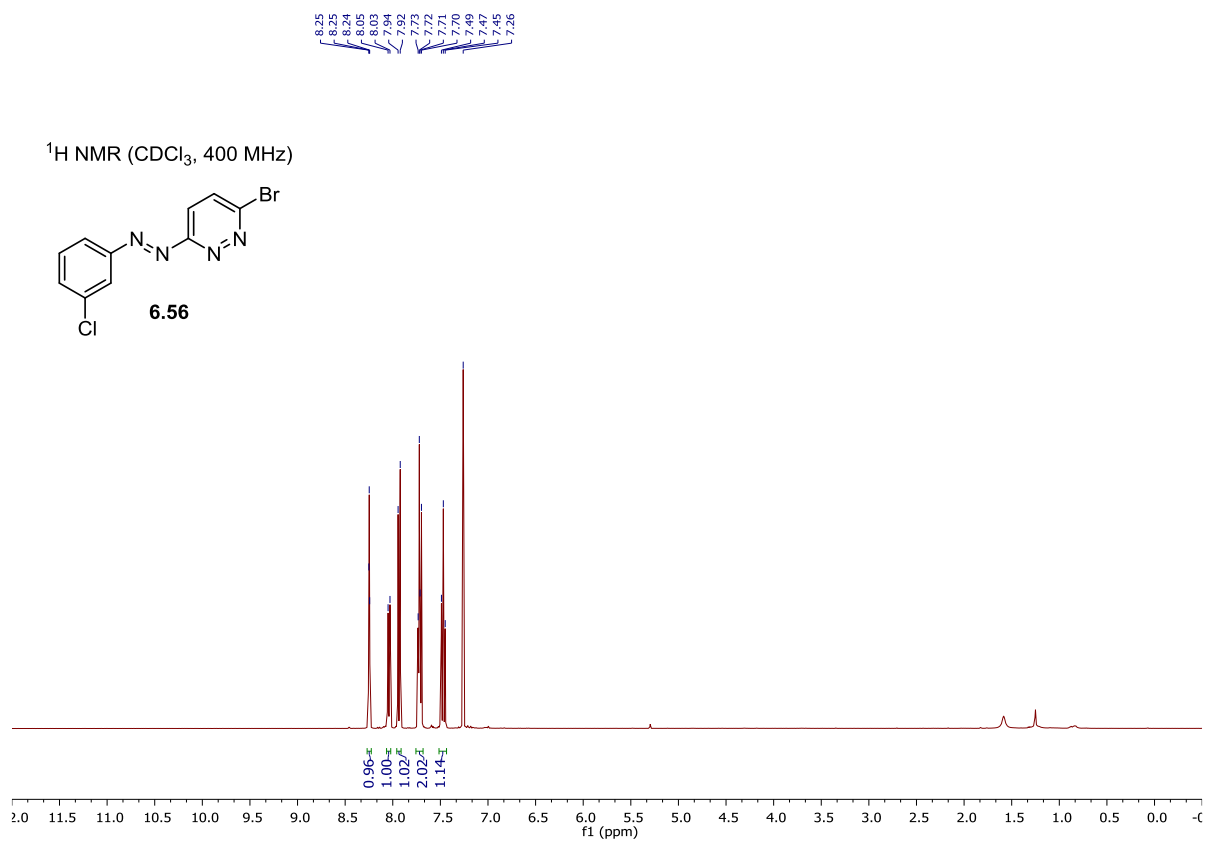
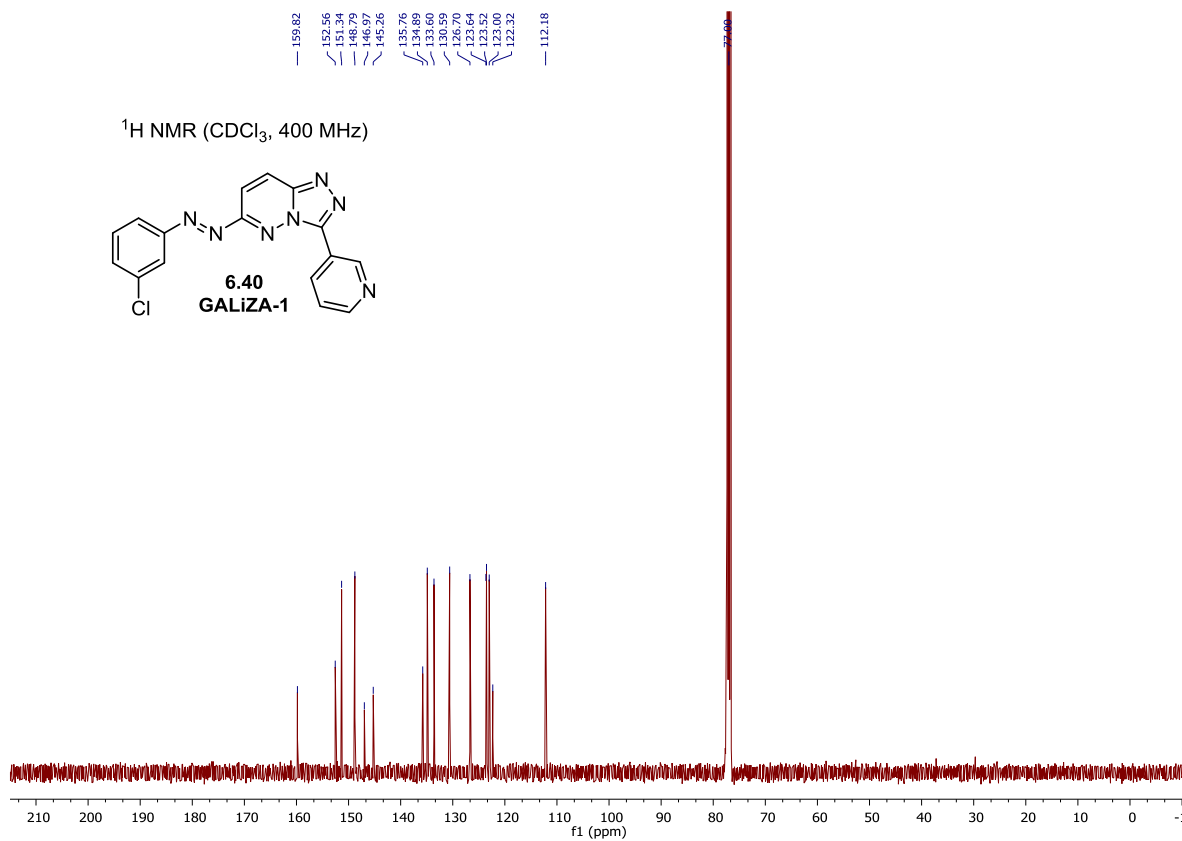


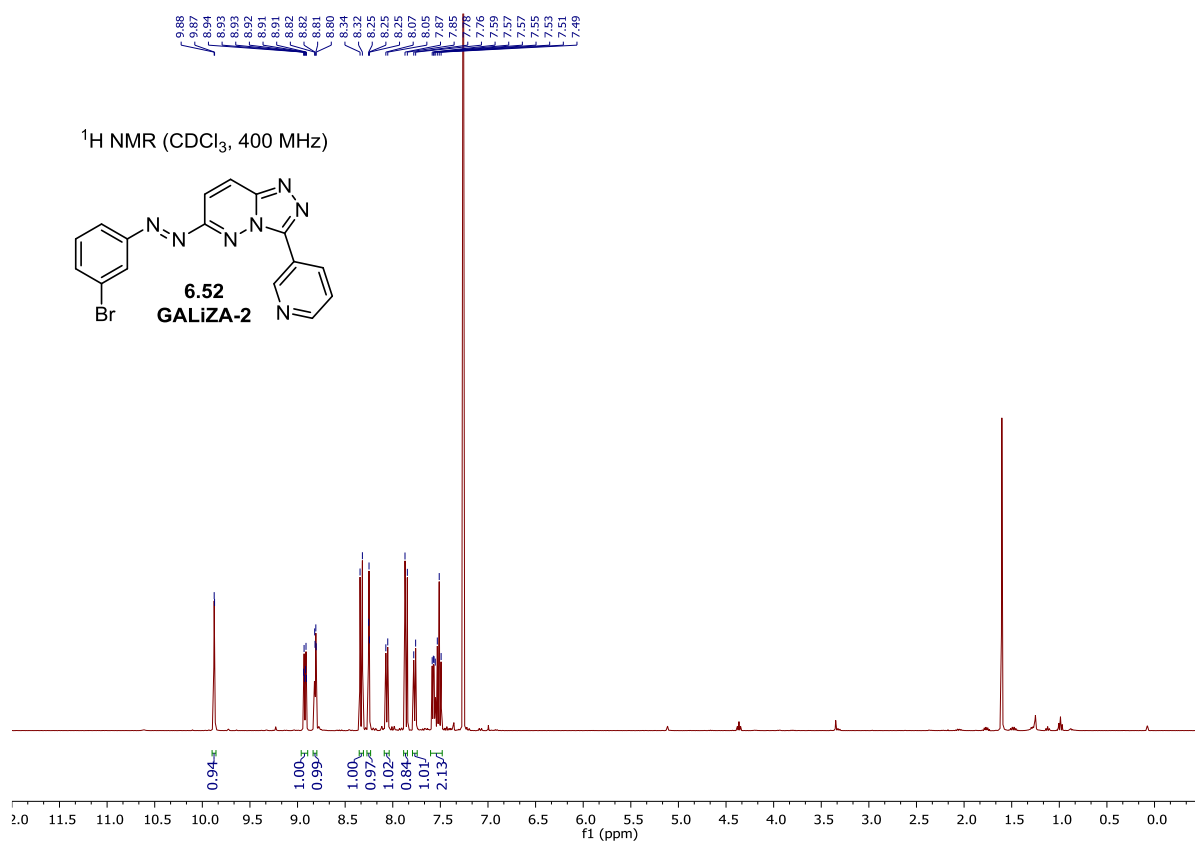
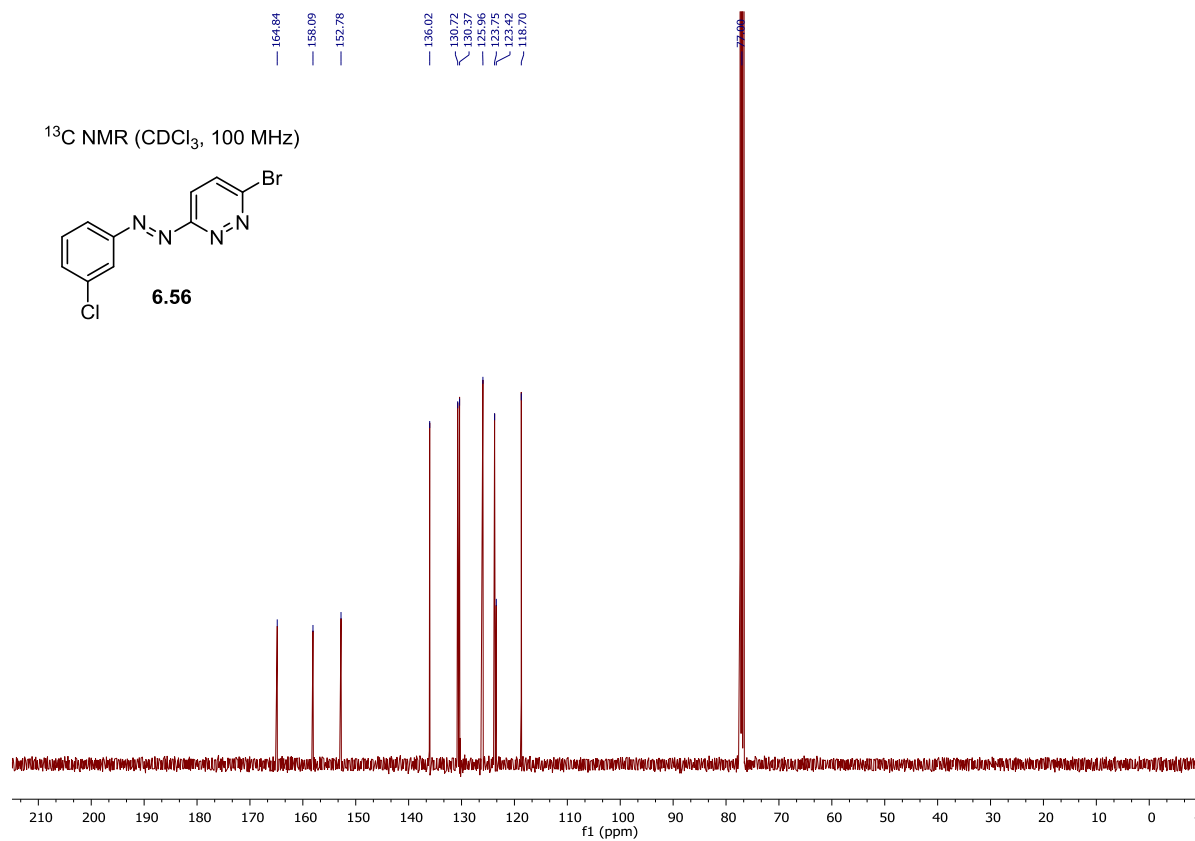
<sup>13</sup>C NMR (CDCl<sub>3</sub>, 100 MHz)

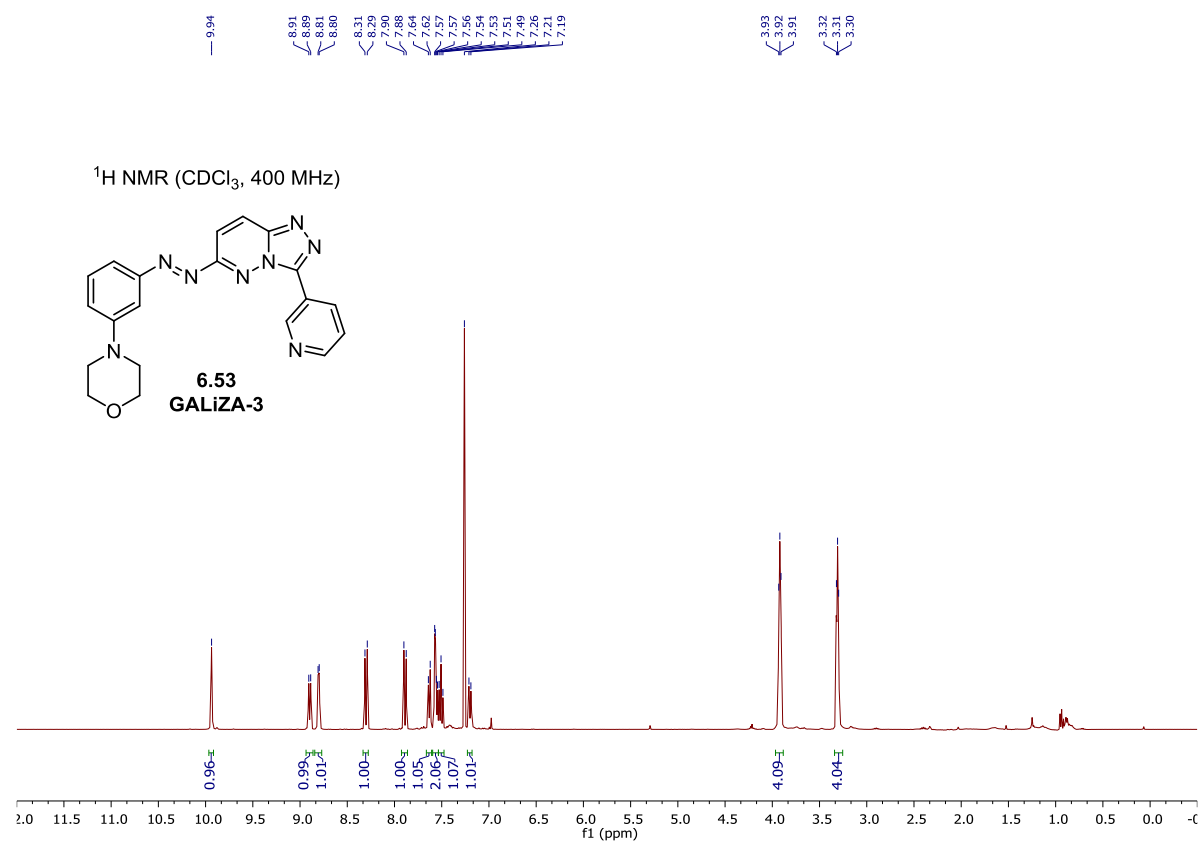
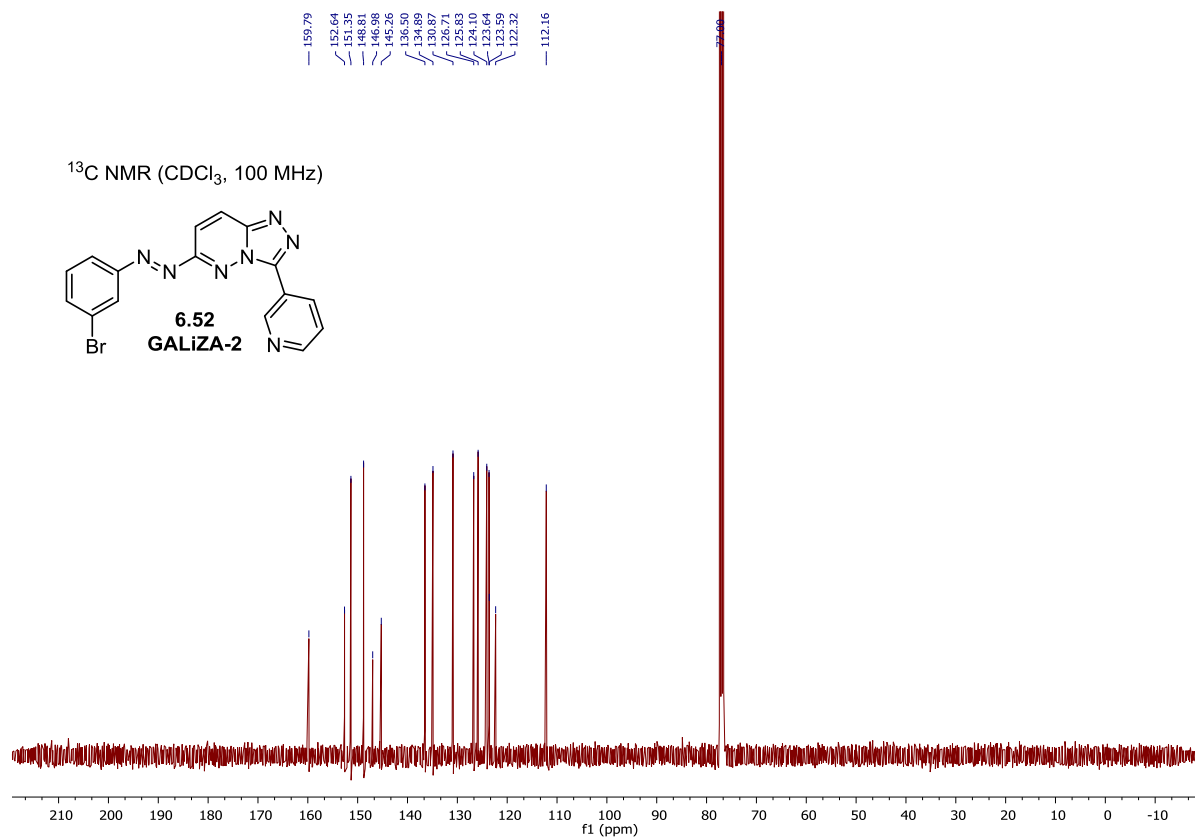


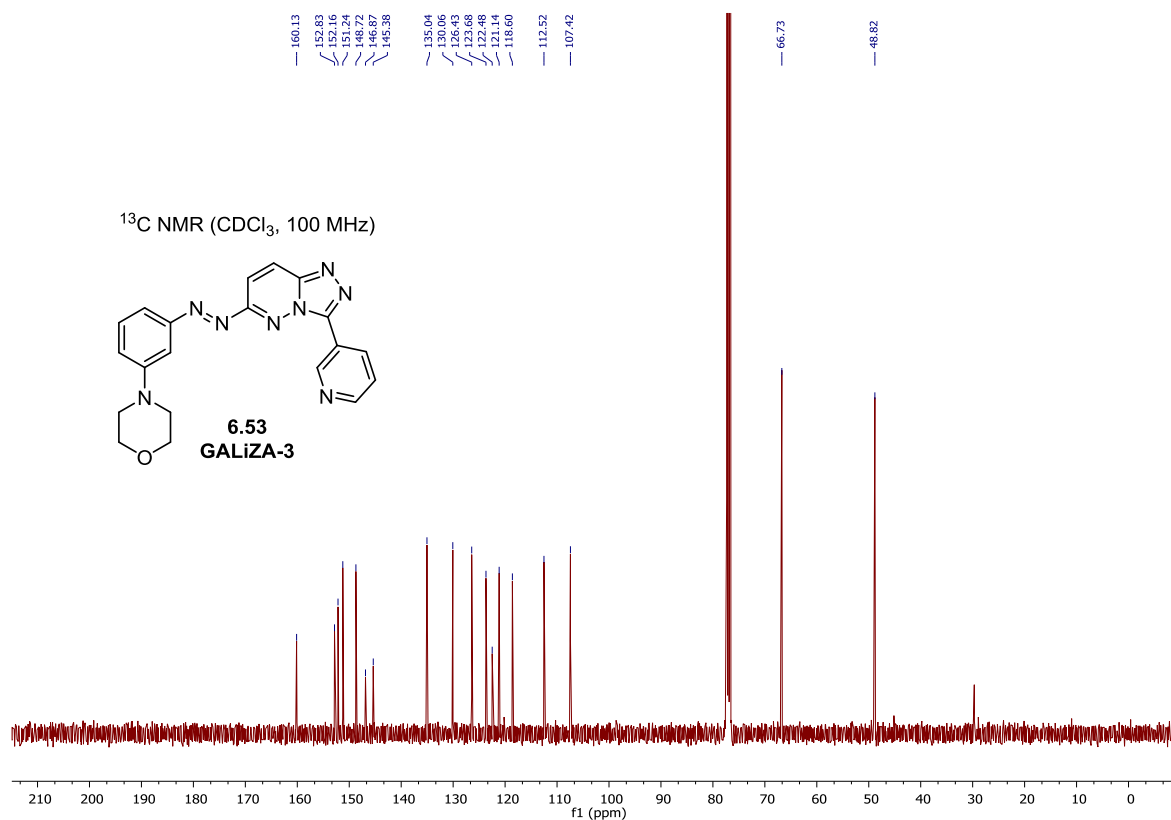
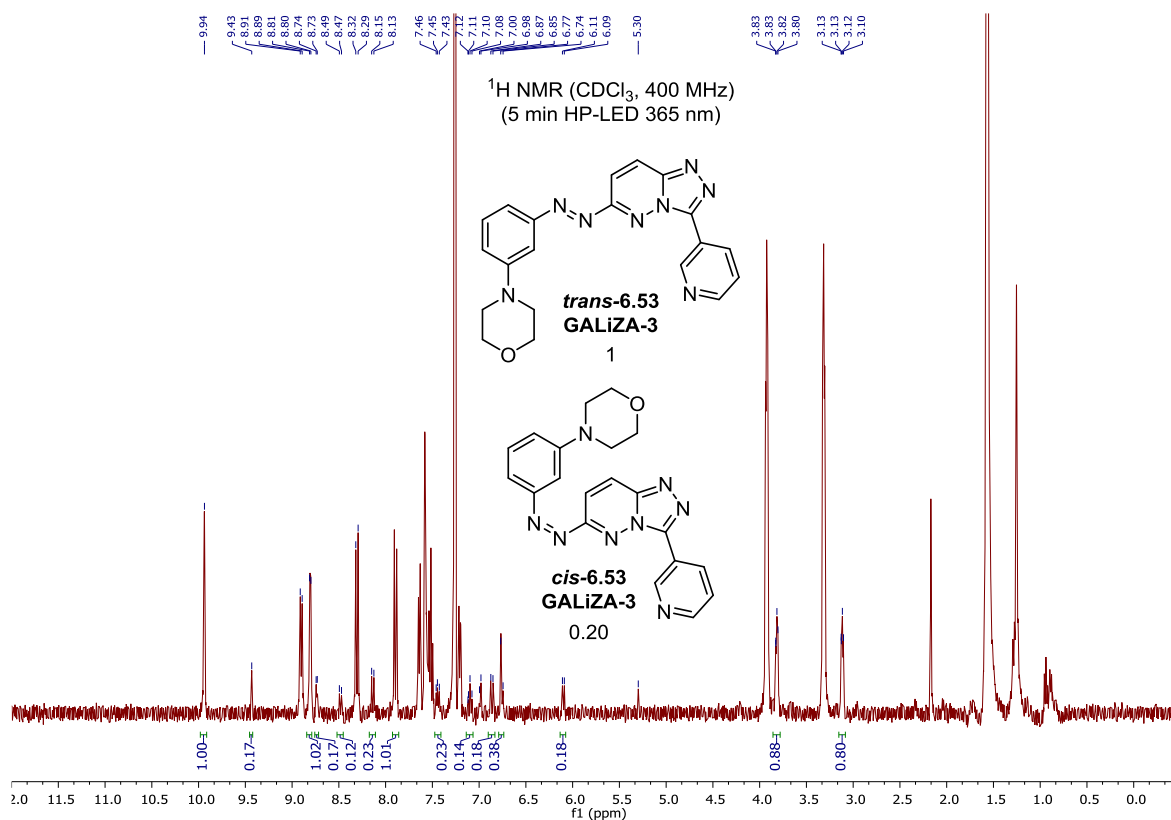


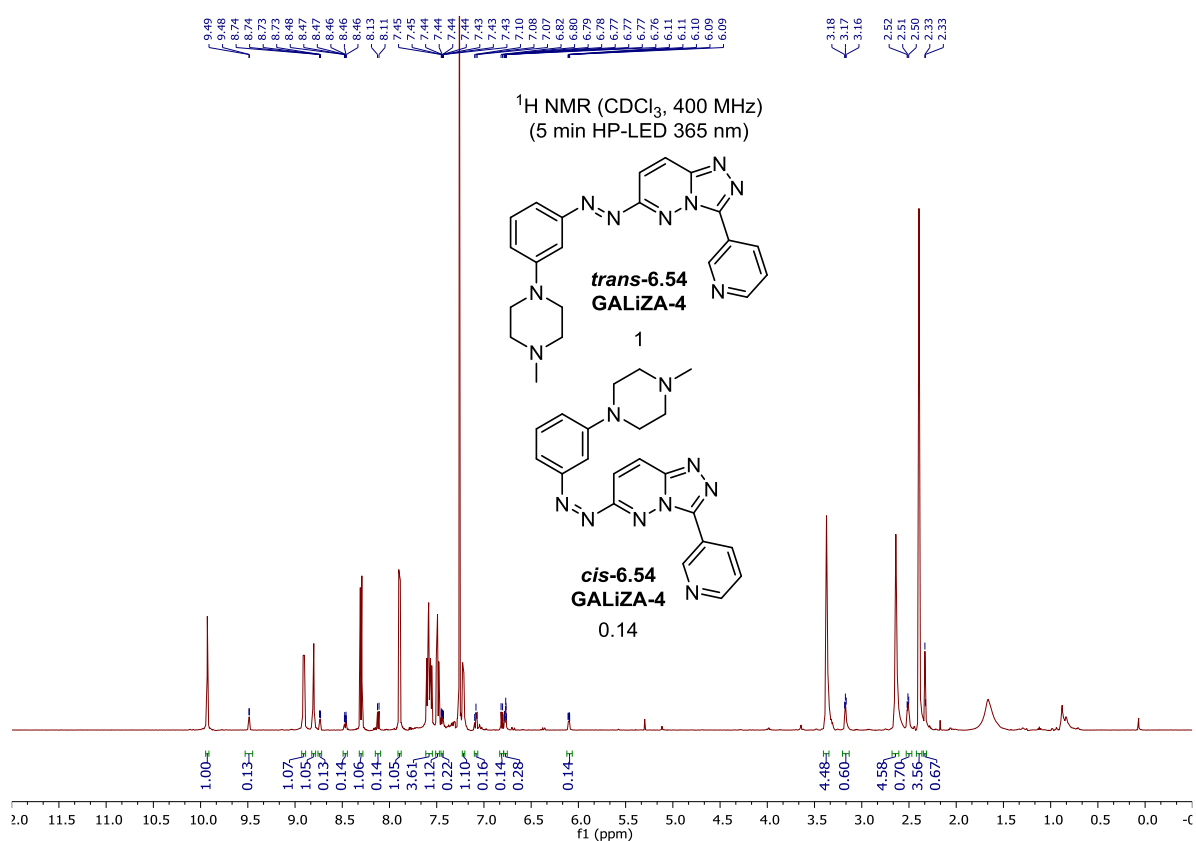
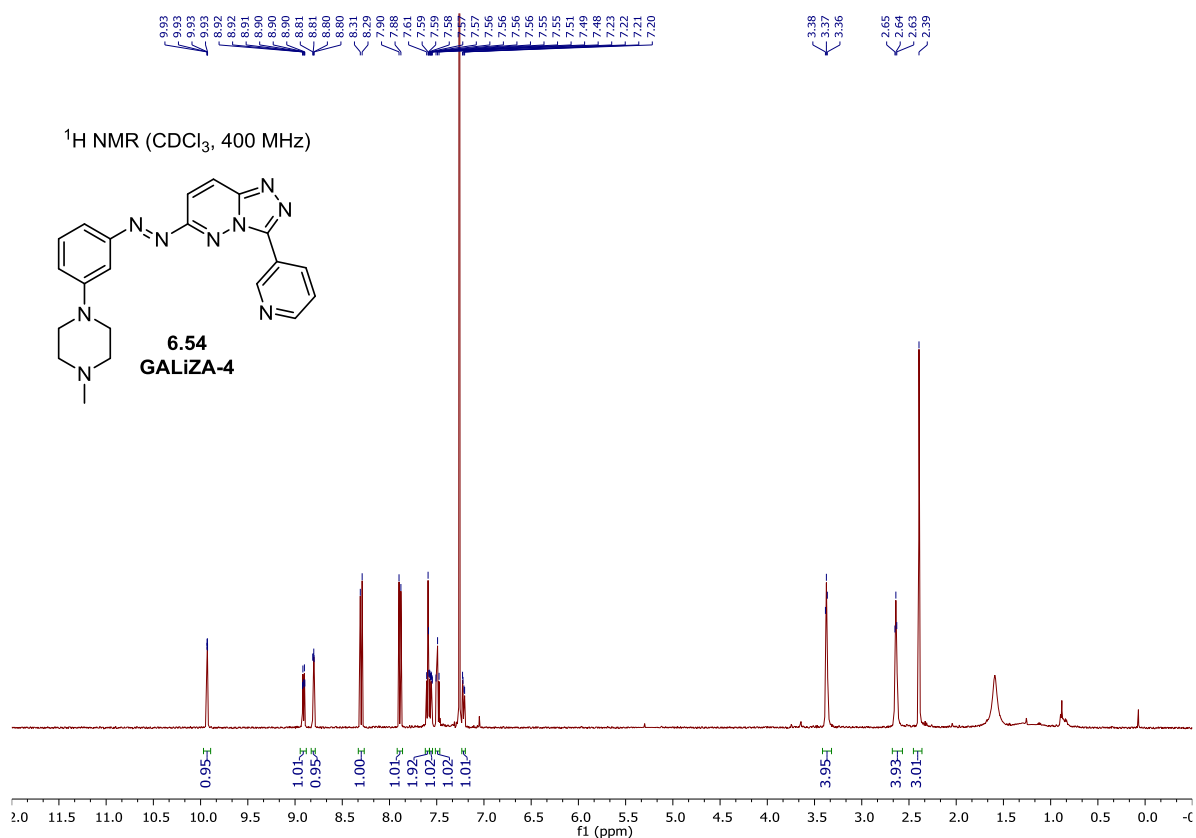


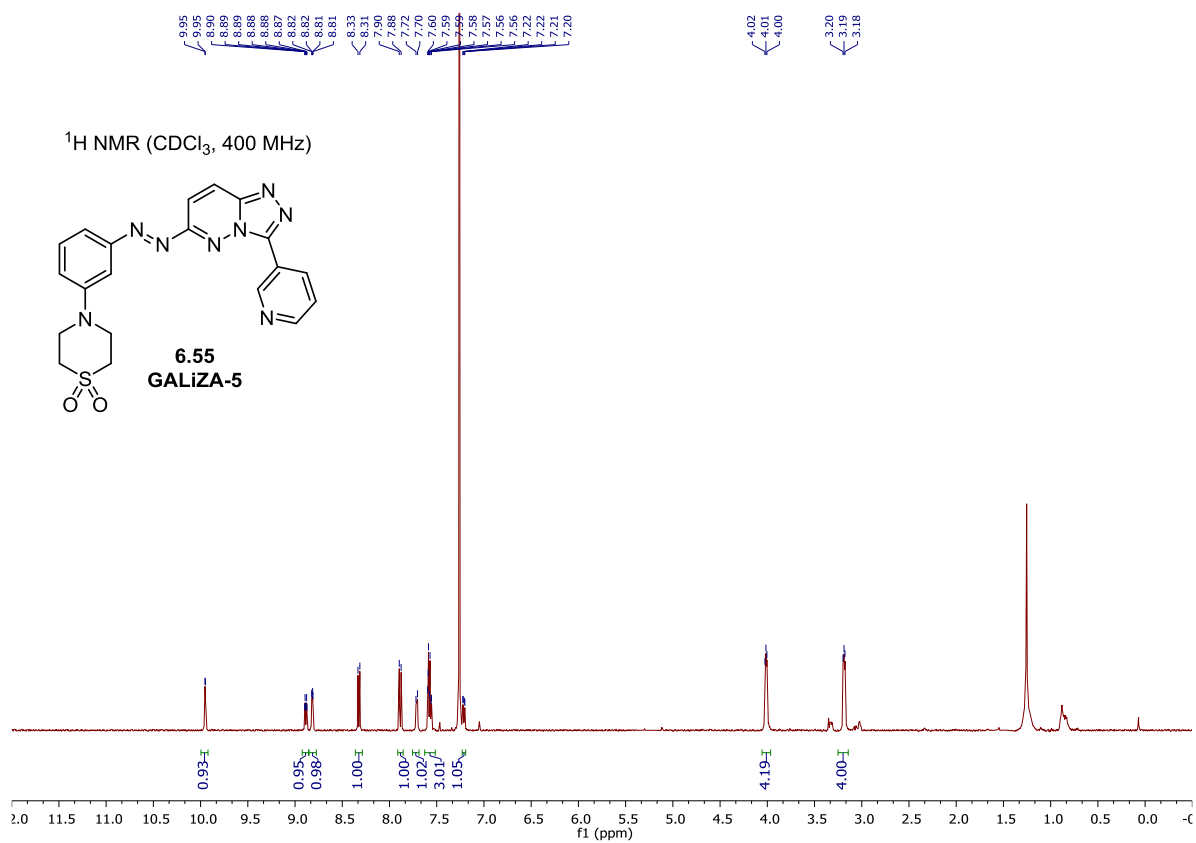
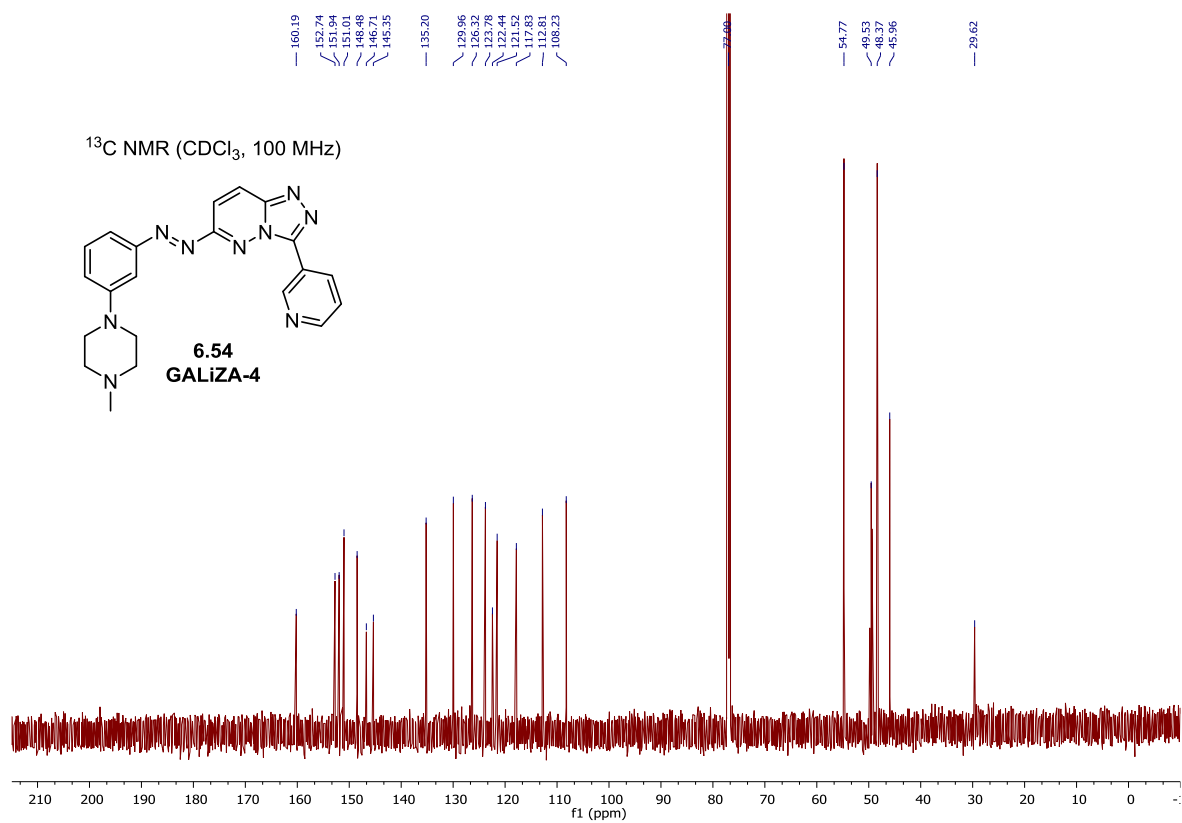


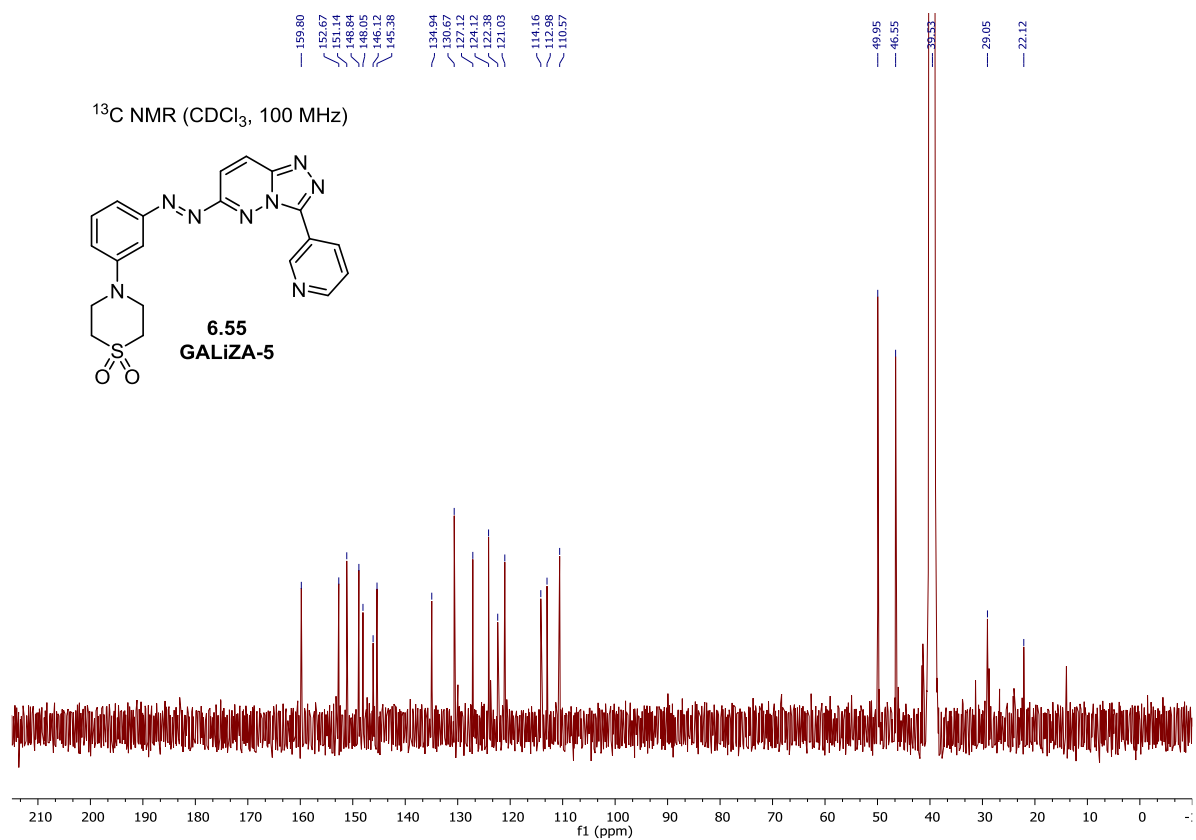
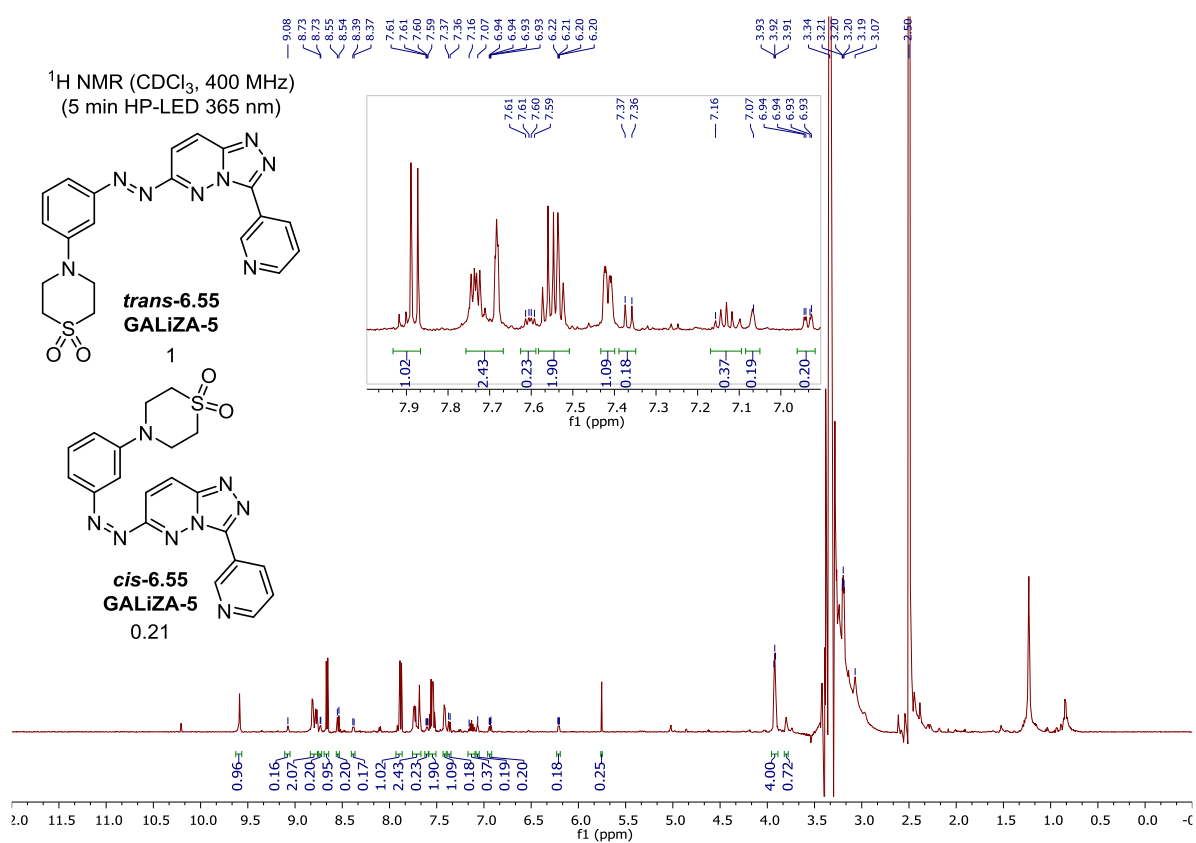












## 9. Bibliography

- [1] R. Willstätter, H. Veraguth, *Berichte Dtsch. Chem. Ges.* **1905**, 38, 1975–1984.
- [2] J. R. VINCENT, A. F. THOMPSON, L. IRVIN. SMITH, *J. Org. Chem.* **1939**, 3, 603–610.
- [3] Seymore. Goldwasser, H. S. Taylor, *J. Am. Chem. Soc.* **1939**, 61, 1260–1263.
- [4] C. D. Hurd, L. R. Drake, *J. Am. Chem. Soc.* **1939**, 61, 1943–1945.
- [5] W. Baker, *J. Chem. Soc. Resumed* **1945**, 258–267.
- [6] A. C. Cope, C. G. Overberger, *J. Am. Chem. Soc.* **1948**, 70, 1433–1437.
- [7] W. Reppe, O. Schlichting, K. Klager, T. Toepel, *Justus Liebigs Ann. Chem.* **1948**, 560, 1–92.
- [8] A. C. Cope, F. A. Hochstein, *J. Am. Chem. Soc.* **1950**, 72, 2515–2520.
- [9] W. Ziegenbein, *Chem. Ber.* **1965**, 98, 1427–1430.
- [10] H. Meister, *Chem. Ber.* **1963**, 96, 1688–1696.
- [11] A. C. Cope, A. C. Haven, F. L. Ramp, E. R. Trumbull, *J. Am. Chem. Soc.* **1952**, 74, 4867–4871.
- [12] W. Sanne, O. Schlichting, *Angew. Chem.* **1963**, 75, 156–161.
- [13] E. N. Marvell, Juergen. Seubert, *J. Am. Chem. Soc.* **1967**, 89, 3377–3378.
- [14] Rolf. Huisgen, Alexander. Dahmen, Helmut. Huber, *J. Am. Chem. Soc.* **1967**, 89, 7130–7131.
- [15] R. Huisgen, W. E. Konz, G. E. Gream, *J. Am. Chem. Soc.* **1970**, 92, 4105–4106.
- [16] R. Huisgen, F. Mietzsch, *Angew. Chem. Int. Ed. Engl.* **1964**, 3, 83–85.
- [17] R. Huisgen, A. Dahmen, H. Huber, *Tetrahedron Lett.* **1969**, 10, 1461–1464.
- [18] R. Huisgen, G. Boche, A. Dahmen, W. Hechtel, *Tetrahedron Lett.* **1968**, 9, 5215–5219.
- [19] A. Dahmen, R. Huisgen, *Tetrahedron Lett.* **1969**, 10, 1465–1469.
- [20] A. Patel, K. N. Houk, *J. Org. Chem.* **2014**, 79, 11370–11377.
- [21] B. E. Thomas, J. D. Evanseck, K. N. Houk, *J. Am. Chem. Soc.* **1993**, 115, 4165–4169.
- [22] B. E. Thomas, J. D. Evanseck, K. N. Houk, *Isr. J. Chem.* **1993**, 33, 287–293.
- [23] K. N. Houk, Y. Li, J. D. Evanseck, *Angew. Chem. Int. Ed. Engl.* **1992**, 31, 682–708.
- [24] A. de Meijere, S. Blechert, Eds., *Strain and Its Implications in Organic Chemistry: Organic Stress and Reactivity*, Springer Netherlands, **1989**.
- [25] A. B. Buda, Y. Wang, K. N. Houk, *J. Org. Chem.* **1989**, 54, 2264–2266.
- [26] N. G. Rondan, K. N. Houk, *J. Am. Chem. Soc.* **1985**, 107, 2099–2111.
- [27] B. Lecea, A. Arrieta, F. P. Cossío, *J. Org. Chem.* **2005**, 70, 1035–1041.
- [28] A. K. Miller, D. Trauner, *ChemInform* **2006**, 37, DOI 10.1002/chin.200647263.
- [29] J. E. Moses, J. E. Baldwin, S. Brückner, S. J. Eade, R. M. Adlington, *Org. Biomol. Chem.* **2003**, 1, 3670–3684.
- [30] I. Škorić, M. Šmehil, Ž. Marinić, K. Molčanov, B. Kojić-Prodić, M. Šindler-Kulyk, *J. Photochem. Photobiol. Chem.* **2009**, 207, 190–196.
- [31] A. K. Miller, D. Trauner, *Angew. Chem. Int. Ed.* **2003**, 42, 549–552.
- [32] J. E. Moses, R. M. Adlington, R. Rodriguez, S. J. Eade, J. E. Baldwin, *Chem. Commun.* **2005**, 1687–1689.
- [33] A. K. Miller, D. Trauner, *Angew. Chem. Int. Ed.* **2005**, 44, 4602–4606.
- [34] C. M. Beaudry, D. Trauner, *Org. Lett.* **2002**, 4, 2221–2224.
- [35] W. M. Bandaranayake, J. E. Banfield, D. S. C. Black, G. D. Fallon, B. M. Gatehouse, *J. Chem. Soc. Chem. Commun.* **1980**, 162–163.



- [36] W. M. Bandaranayake, J. E. Banfield, D. S. C. Black, *J. Chem. Soc. Chem. Commun.* **1980**, 902–903.
- [37] J. E. Banfield, D. S. C. Black, S. R. Johns, R. I. Willing, *Aust. J. Chem.* **1982**, *35*, 2247–2256.
- [38] J. E. Banfield, D. S. C. Black, G. D. Fallon, B. M. Gatehouse, *Aust. J. Chem.* **1983**, *36*, 627–632.
- [39] H. Goossens, J. M. Winne, S. Wouters, L. Hermosilla, P. J. De Clercq, M. Waroquier, V. Van Speybroeck, S. Catak, *J. Org. Chem.* **2015**, *80*, 2609–2620.
- [40] K. C. Nicolaou, N. A. Petasis, R. E. Zipkin, J. Uenishi, *J. Am. Chem. Soc.* **1982**, *104*, 5555–5557.
- [41] K. C. Nicolaou, N. A. Petasis, J. Uenishi, R. E. Zipkin, *J. Am. Chem. Soc.* **1982**, *104*, 5557–5558.
- [42] K. C. Nicolaou, R. E. Zipkin, N. A. Petasis, *J. Am. Chem. Soc.* **1982**, *104*, 5558–5560.
- [43] K. C. Nicolaou, N. A. Petasis, R. E. Zipkin, *J. Am. Chem. Soc.* **1982**, *104*, 5560–5562.
- [44] K. A. Parker, Y.-H. Lim, *J. Am. Chem. Soc.* **2004**, *126*, 15968–15969.
- [45] K. Kurosawa, K. Takahashi, E. Tsuda, *J. Antibiot. (Tokyo)* **2001**, *54*, 541–547.
- [46] K. Takahashi, E. Tsuda, K. Kurosawa, *J. Antibiot. (Tokyo)* **n.d.**, 6.
- [47] K. Kurosawa, K. Takahashi, N. Fujise, Y. Yamashita, N. Washida, E. Tsuda, *J. Antibiot. (Tokyo)* **2002**, *55*, 71–77.
- [48] M. Turks, S. Laclef, P. Vogel, in *Ster. Synth. Drugs Nat. Prod.*, American Cancer Society, **2013**, pp. 1–48.
- [49] J. E. Moses, J. E. Baldwin, R. Marquez, R. M. Adlington, A. R. Cowley, *Org. Lett.* **2002**, *4*, 3731–3734.
- [50] K. Kakinuma, C. A. Hanson, K. L. Rinehart, *Tetrahedron* **1976**, *32*, 217–222.
- [51] K. A. Parker, Y.-H. Lim, *Org. Lett.* **2004**, *6*, 161–164.
- [52] C. M. Beaudry, D. Trauner, *Org. Lett.* **2005**, *7*, 4475–4477.
- [53] S. P. H. Mee, V. Lee, J. E. Baldwin, *Angew. Chem. Int. Ed.* **2004**, *43*, 1132–1136.
- [54] M. F. Jacobsen, J. E. Moses, R. M. Adlington, J. E. Baldwin, *Tetrahedron* **2006**, *62*, 1675–1689.
- [55] M. Müller, B. Kusebauch, G. Liang, C. M. Beaudry, D. Trauner, C. Hertweck, *Angew. Chem. Int. Ed.* **2006**, *45*, 7835–7838.
- [56] G. Liang, I. B. Seiple, D. Trauner, *Org. Lett.* **2005**, *7*, 2837–2839.
- [57] B. M. Trost, S. Sharma, T. Schmidt, *J. Am. Chem. Soc.* **1992**, *114*, 7903–7904.
- [58] J. E. Barbarow, A. K. Miller, D. Trauner, *Org. Lett.* **2005**, *7*, 2901–2903.
- [59] M. Cueto, L. D’Croz, J. L. Maté, A. San-Martín, J. Darias, *Org. Lett.* **2005**, *7*, 415–418.
- [60] R. K. Trench, R. W. Greene, B. G. Bystrom, *J. Cell Biol.* **1969**, *42*, 404–417.
- [61] G. Stork, K. Zhao, *Tetrahedron Lett.* **1989**, *30*, 2173–2174.
- [62] M. Suzuki, H. Ohtake, Y. Kameya, N. Hamanaka, R. Noyori, *J. Org. Chem.* **1989**, *54*, 5292–5302.
- [63] E. Manzo, M. L. Ciavatta, M. Gavagnin, E. Mollo, S. Wahidulla, G. Cimino, *Tetrahedron Lett.* **2005**, *46*, 465–468.
- [64] M. Kobayashi, H. Wei, T. Itoh, N. Kotoku, *HETEROCYCLES* **2006**, *68*, 111.
- [65] H. Wei, T. Itoh, M. Kinoshita, N. Kotoku, S. Aoki, M. Kobayashi, *Tetrahedron* **2005**, *61*, 8054–8058.
- [66] V. Sofiyev, G. Navarro, D. Trauner, *Org. Lett.* **2008**, *10*, 149–152.
- [67] A. Leverrier, M. E. T. H. Dau, P. Retailleau, K. Awang, F. Guéritte, M. Litaudon, *Org. Lett.* **2010**, *12*, 3638–3641.
- [68] P. Sharma, D. J. Ritson, J. Burnley, J. E. Moses, *Chem. Commun.* **2011**, *47*, 10605–10607.
- [69] A. Leverrier, K. Awang, F. Guéritte, M. Litaudon, *Phytochemistry* **2011**, *72*, 1443–1452.
- [70] H. N. Lim, K. A. Parker, *J. Org. Chem.* **2014**, *79*, 919–926.

- [71] S. E. Nigenda, D. M. Schleich, S. C. Narang, T. Keumi, *J. Electrochem. Soc.* **1987**, *134*, 2465–2470.
- [72] J. C. Moore, E. S. Davies, D. A. Walsh, P. Sharma, J. E. Moses, *Chem. Commun.* **2014**, *50*, 12523–12525.
- [73] S. L. Drew, A. L. Lawrence, M. S. Sherburn, *Angew. Chem. Int. Ed.* **2013**, *52*, 4221–4224.
- [74] S. L. Drew, A. L. Lawrence, M. S. Sherburn, *Chem. Sci.* **2015**, *6*, 3886–3890.
- [75] Y. Nishihara, K. Ikegashira, K. Hirabayashi, J. Ando, A. Mori, T. Hiyama, *J. Org. Chem.* **2000**, *65*, 1780–1787.
- [76] K. A. Parker, H. N. Lim, in *Strateg. Tactics Org. Synth.* (Ed.: M. Harmata), Academic Press, **2014**, pp. 51–78.
- [77] A.-K. C. Schmidt, C. B. W. Stark, *Org. Lett.* **2011**, *13*, 4164–4167.
- [78] S. Lin, M. A. Ischay, C. G. Fry, T. P. Yoon, *J. Am. Chem. Soc.* **2011**, *133*, 19350–19353.
- [79] L. A. Paquette, L. H. Kuo, A. T. Hamme, R. Kreuzholz, J. Doyon, *J. Org. Chem.* **1997**, *62*, 1730–1736.
- [80] L. A. Paquette, J. Tae, *J. Org. Chem.* **1998**, *63*, 2022–2030.
- [81] J. Negri, T. Morwick, J. Doyon, P. D. Wilson, E. R. Hickey, L. A. Paquette, *J. Am. Chem. Soc.* **1993**, *115*, 12189–12190.
- [82] F. Geng, J. Liu, L. A. Paquette, *Org. Lett.* **2002**, *4*, 71–73.
- [83] L. A. Paquette, F. Geng, *J. Am. Chem. Soc.* **2002**, *124*, 9199–9203.
- [84] E. M. de Souza-Fagundes, B. B. Cota, L. H. Rosa, A. J. Romanha, R. Corrêa-Oliveira, C. A. Rosa, C. L. Zani, A. Teixeira-Carvalho, O. A. Martins-Filho, *Braz. J. Med. Biol. Res. Rev. Bras. Pesqui. Medicas E Biol.* **2010**, *43*, 1054–1061.
- [85] J. Kupka, T. Anke, B.-M. Giannetti, W. Steglich, *Arch. Microbiol.* **1981**, *130*, 223–227.
- [86] S. Takahashi, H. Iinuma, T. Takita, K. Maeda, H. Umezawa, *Tetrahedron Lett.* **1969**, *10*, 4663–4666.
- [87] H.-P. Hanssen, W.-R. Abraham, *Tetrahedron* **1988**, *44*, 2175–2180.
- [88] C. Baralotto, M. Chanon, M. Julliard, *J. Org. Chem.* **1996**, *61*, 3576–3577.
- [89] T. L. Fevig, R. L. Elliott, D. P. Curran, *J. Am. Chem. Soc.* **1988**, *110*, 5064–5067.
- [90] S. Danishefsky, R. Zamboni, M. Kahn, S. J. Etheredge, *J. Am. Chem. Soc.* **1980**, *102*, 2097–2098.
- [91] K. Weinges, R. Braum, U. Huber-Patz, H. Irngartinger, *Liebigs Ann. Chem.* **1993**, *1993*, 1133–1140.
- [92] L. Van Hijfte, R. D. Little, J. L. Petersen, K. D. Moeller, *J. Org. Chem.* **1987**, *52*, 4647–4661.
- [93] S. Gomi, K.-I. Imamura, T. Yaguchi, Y. Kodama, N. Minowa, M. Koyama, *J. Antibiot. (Tokyo)* **1994**, *47*, 571–580.
- [94] P. S. Steyn, P. L. Wessels, *Tetrahedron Lett.* **1978**, *19*, 4707–4710.
- [95] M. J. Nolte, P. S. Steyn, P. L. Wessels, *J. Chem. Soc. Perkin 1* **1980**, 1057–1065.
- [96] S. Dutta, J. R. Whicher, D. A. Hansen, W. A. Hale, J. A. Chemler, G. R. Congdon, A. R. H. Narayan, K. Håkansson, D. H. Sherman, J. L. Smith, et al., *Nature* **2014**, *510*, 512–517.
- [97] Y. A. Chan, A. M. Podevels, B. M. Kevany, M. G. Thomas, *Nat. Prod. Rep.* **2008**, *26*, 90–114.
- [98] M. Klapper, S. Götz, R. Barnett, K. Willing, P. Stallforth, *Angew. Chem. Int. Ed.* **2016**, *55*, 8944–8947.
- [99] M. Klapper, D. Braga, G. Lackner, R. Herbst, P. Stallforth, *Cell Chem. Biol.* **2018**, *25*, 659–665.e9.
- [100] H. Li, C. L. M. Gilchrist, H. J. Lacey, A. Crombie, D. Vuong, J. I. Pitt, E. Lacey, Y.-H. Chooi, A. M. Piggott, *Org. Lett.* **2019**, *21*, 1287–1291.
- [101] D. Boettger, C. Hertweck, *ChemBioChem* **2013**, *14*, 28–42.
- [102] K. M. Fisch, *RSC Adv.* **2013**, *3*, 18228–18247.

- 
- [103] D. Tan, C. S. Jamieson, M. Ohashi, M.-C. Tang, K. N. Houk, Y. Tang, *J. Am. Chem. Soc.* **2019**, *141*, 769–773.
- [104] N. Kato, T. Nogawa, H. Hirota, J.-H. Jang, S. Takahashi, J. S. Ahn, H. Osada, *Biochem. Biophys. Res. Commun.* **2015**, *460*, 210–215.
- [105] K.-I. C. M. S. K. L. Imamura, S. C. M. S. K. L. Gomi, M. C. M. S. K. L. Iwata, S. C. M. S. K. L. Miyadoh, M. C. M. S. K. L. Shimura, T. C. M. S. K. L. Shomura, M. C. M. S. K. L. Sezaki, S. C. M. S. K. L. Inoye, *Novel Compound Having Insecticidal Activity and Process for Producing the Same*, **1990**, EP0368331A2.
- [106] V. C. Santos, H. de Siqueira, J. da Silva, M. de Farias, *Neotrop. Entomol.* **2011**, *40*, 264–270.
- [107] T. Jiang, S. Wu, T. Yang, C. Zhu, C. Gao, *Fla. Entomol.* **2015**, *98*, 65–73.
- [108] R. B. Mohamad, Mohd. Y. Ismail, *Int. J. Trop. Insect Sci.* **1988**, *9*, 109–112.
- [109] C. Ayra-Pardo, B. Raymond, A. Gulzar, L. Rodríguez-Cabrera, I. Morán-Bertot, N. Crickmore, D. J. Wright, *Insect Mol. Biol.* **2015**, *24*, 589–600.
- [110] C. G. Sawant, C. S. Patil, *Int. J. Curr. Microbiol. Appl. Sci.* **2018**, *7*, 2986–2998.
- [111] “Efficacy of Different Insecticides Against *Plutella xylostella* under Field Conditions - SciAlert Responsive Version,” DOI 10.3923/pjbs.2004.10.13 can be found under <https://scialert.net/fulltextmobile/?doi=pjbs.2004.10.13>, **n.d.**
- [112] Dept. of Entomology, Agricultural College, Naira, ANGRAU, Andhra Pradesh (532 185), India, G. Harika, S. Dhurua, Dept. of Entomology, Agricultural College, Naira, ANGRAU, Andhra Pradesh (532 185), India, M. Suresh, Dept. of Entomology, Agricultural College, Naira, ANGRAU, Andhra Pradesh (532 185), India, N. Sreesandhya, Dept. of Entomology, Agricultural College, Naira, ANGRAU, Andhra Pradesh (532 185), India, *Int. J. Bio-Resour. Stress Manag.* **2019**, *10*, 070–076.
- [113] M. P. Zalucki, A. Shabbir, R. Silva, D. Adamson, L. Shu-Sheng, M. J. Furlong, *J. Econ. Entomol.* **2012**, *105*, 1115–1129.
- [114] R. Webster, B. Gaspar, P. Mayer, D. Trauner, *Org. Lett.* **2013**, *15*, 1866–1869.
- [115] J. W. Phillips, M. A. Goetz, S. K. Smith, D. L. Zink, J. Polishook, R. Onishi, S. Salowe, J. Wiltsie, J. Allocco, J. Sigmund, et al., *Chem. Biol.* **2011**, *18*, 955–965.
- [116] S. Suzuki, T. Hosoe, K. Nozawa, K. Kawai, T. Yaguchi, S. Udagawa, *J. Nat. Prod.* **2000**, *63*, 768–772.
- [117] N. U. Sata, S. Wada, S. Matsunaga, S. Watabe, R. W. M. van Soest, N. Fusetani, *J. Org. Chem.* **1999**, *64*, 2331–2339.
- [118] S. B. Singh, D. L. Zink, B. Heimbach, O. Genilloud, A. Teran, K. C. Silverman, R. B. Lingham, P. Felock, D. J. Hazuda, *Org. Lett.* **2002**, *4*, 1123–1126.
- [119] X. Mo, Q. Li, J. Ju, *RSC Adv.* **2014**, *4*, 50566–50593.
- [120] E. L. Ghisalberti, in *Stud. Nat. Prod. Chem.* (Ed.: A. Rahman), Elsevier, **2003**, pp. 109–163.
- [121] N. X. Chin, H. C. Neu, *Eur. J. Clin. Microbiol. Infect. Dis.* **1992**, *11*, 755–757.
- [122] G. Höfle, K. Gerth, H. Reichenbach, B. Kunze, F. Sasse, E. Forche, E. V. Prusov, *Chem. – Eur. J.* **2012**, *18*, 11362–11370.
- [123] K. Hiroya, K. Takuma, K. Inamoto, T. Sakamoto, *HETEROCYCLES* **2009**, *77*, 493.
- [124] J. G. Duboudin, B. Jousseau, A. Saux, *J. Organomet. Chem.* **1979**, *168*, 1–11.
- [125] M. B. Andrus, E. J. Hicken, E. L. Meredith, in *Strateg. Tactics Org. Synth.* (Ed.: M. Harmata), Academic Press, **2005**, pp. 38–70.
- [126] T. Engesser, R. Brückner, *Eur. J. Org. Chem.* **2017**, *2017*, 5789–5794.
- [127] G. V. M. Sharma, G. R. Cherukupalli, *Tetrahedron Asymmetry* **2006**, *17*, 1081–1088.
- [128] C. M. Burnett, R. M. Williams, *Tetrahedron Lett.* **2009**, *50*, 5449–5451.
- [129] I. Paterson, E. A. Anderson, S. M. Dalby, J. H. Lim, P. Maltas, O. Loiseleur, J. Genovino, C. Moessner, *Org. Biomol. Chem.* **2012**, *10*, 5861–5872.

- [130] O. Miyata, T. Shinada, T. Naito, I. Ninomiya, T. Date, K. Okamura, *Tetrahedron* **1993**, *49*, 8119–8128.
- [131] P. Stallforth, A. Adibekian, P. H. Seeberger, *Org. Lett.* **2008**, *10*, 1573–1576.
- [132] H. C. Brown, P. K. Jadhav, K. S. Bhat, *J. Am. Chem. Soc.* **1988**, *110*, 1535–1538.
- [133] M. T. Crimmins, M. W. Haley, E. A. O'Bryan, *Org. Lett.* **2011**, *13*, 4712–4715.
- [134] C. Hertweck, W. Boland, *J. Für Prakt. Chem.* **1999**, *341*, 83–87.
- [135] J. A. Dale, H. S. Mosher, *J. Am. Chem. Soc.* **1973**, *95*, 512–519.
- [136] A. K. Chatterjee, T.-L. Choi, D. P. Sanders, R. H. Grubbs, *J. Am. Chem. Soc.* **2003**, *125*, 11360–11370.
- [137] G. S. Forman, A. E. McConnell, R. P. Tooze, W. Janse van Rensburg, W. H. Meyer, M. M. Kirk, C. L. Dwyer, D. W. Serfontein, *Organometallics* **2005**, *24*, 4528–4542.
- [138] B. Schmidt, S. Hauke, *Org. Biomol. Chem.* **2013**, *11*, 4194–4206.
- [139] A. G. Santos, G. A. Bailey, E. N. dos Santos, D. E. Fogg, *ACS Catal.* **2017**, *7*, 3181–3189.
- [140] G. D. Allred, L. S. Liebeskind, *J. Am. Chem. Soc.* **1996**, *118*, 2748–2749.
- [141] S. Zhang, D. Zhang, L. S. Liebeskind, *J. Org. Chem.* **1997**, *62*, 2312–2313.
- [142] A. L. Casado, P. Espinet, *Organometallics* **2003**, *22*, 1305–1309.
- [143] P. Espinet, A. M. Echavarren, *Angew. Chem. Int. Ed.* **2004**, *43*, 4704–4734.
- [144] M. Wang, Z. Lin, *Organometallics* **2010**, *29*, 3077–3084.
- [145] A. Abad, C. Agulló, M. Arnó, A. C. Cuñat, M. T. García, Ramón. J. Zaragoza, *J. Org. Chem.* **1996**, *61*, 5916–5919.
- [146] Y. Mori, K. Yaegashi, H. Furukawa, *J. Am. Chem. Soc.* **1997**, *119*, 4557–4558.
- [147] Y. Wu, C. Dockendorff, *J. Org. Chem.* **2019**, *84*, 5292–5304.
- [148] J. B. Schwarz, A. I. Meyers, *J. Org. Chem.* **1995**, *60*, 6511–6514.
- [149] H. Schostarez, L. A. Paquette, *Tetrahedron* **1981**, *37*, 4431–4435.
- [150] S. W. M. Crossley, F. Barabé, R. A. Shenvi, *J. Am. Chem. Soc.* **2014**, *136*, 16788–16791.
- [151] S. Chiba, M. Kitamura, K. Narasaka, *J. Am. Chem. Soc.* **2006**, *128*, 6931–6937.
- [152] Q. Liu, G. Yue, N. Wu, G. Lin, Y. Li, J. Quan, C. Li, G. Wang, Z. Yang, *Angew. Chem. Int. Ed.* **2012**, *51*, 12072–12076.
- [153] M. Hatano, T. Matsumura, K. Ishihara, *Org. Lett.* **2005**, *7*, 573–576.
- [154] M. Hatano, S. Suzuki, K. Ishihara, *J. Am. Chem. Soc.* **2006**, *128*, 9998–9999.
- [155] R. K. Boeckman, J. C. Potenza, *Tetrahedron Lett.* **1985**, *26*, 1411–1414.
- [156] L. A. Paquette, Z. Gao, Z. Ni, G. F. Smith, *Tetrahedron Lett.* **1997**, *38*, 1271–1274.
- [157] R. Kaul, Y. Brouillette, Z. Sajjadi, K. A. Hansford, W. D. Lubell, *J. Org. Chem.* **2004**, *69*, 6131–6133.
- [158] J. H. Han, Y. E. Kwon, J.-H. Sohn, D. H. Ryu, *Tetrahedron* **2010**, *66*, 1673–1677.
- [159] H. Cheng, F.-H. Zeng, X. Yang, Y.-J. Meng, L. Xu, F.-P. Wang, *Angew. Chem. Int. Ed.* **2016**, *55*, 392–396.
- [160] H. Fujioka, Y. Sawama, N. Murata, T. Okitsu, O. Kubo, S. Matsuda, Y. Kita, *J. Am. Chem. Soc.* **2004**, *126*, 11800–11801.
- [161] H. Fujioka, T. Okitsu, Y. Sawama, N. Murata, R. Li, Y. Kita, *J. Am. Chem. Soc.* **2006**, *128*, 5930–5938.
- [162] H. Fujioka, O. Kubo, K. Senami, Y. Minamitsuji, T. Maegawa, *Chem. Commun.* **2009**, 4429–4431.
- [163] E. A. Colby, K. C. O'Brie, T. F. Jamison, *J. Am. Chem. Soc.* **2005**, *127*, 4297–4307.
- [164] D. A. Evans, S. W. Kaldor, T. K. Jones, J. Clardy, T. J. Stout, *J. Am. Chem. Soc.* **1990**, *112*, 7001–7031.
- [165] K. A. Scheidt, H. Chen, B. C. Follows, S. R. Chemler, D. S. Coffey, W. R. Roush, *J. Org. Chem.* **1998**, *63*, 6436–6437.
- [166] T. Kang, S. B. Song, W.-Y. Kim, B. G. Kim, H.-Y. Lee, *J. Am. Chem. Soc.* **2014**, *136*, 10274–10276.

- 
- [167] J. Esteve, C. Jiménez, J. Nebot, J. Velasco, P. Romea, F. Urpí, *Tetrahedron* **2011**, 67, 6045–6056.
- [168] C. Lagisetti, M. Urbansky, R. M. Coates, *J. Org. Chem.* **2007**, 72, 9886–9895.
- [169] L. Fitjer, H.-J. Scheuermann, D. Wehle, *Tetrahedron Lett.* **1984**, 25, 2329–2332.
- [170] M. T. Reetz, S. H. Kyung, M. Hüllmann, *Tetrahedron* **1986**, 42, 2931–2935.
- [171] S. Berger, W. Bock, G. Frenking, V. Jonas, F. Mueller, *J. Am. Chem. Soc.* **1995**, 117, 3820–3829.
- [172] M. T. Reetz, R. Steinbach, J. Westermann, R. Peter, *Angew. Chem.* **1980**, 92, 1044–1045.
- [173] M. T. Reetz, J. Westermann, R. Steinbach, B. Wenderoth, R. Peter, R. Ostarek, S. Maus, *Chem. Ber.* **1985**, 118, 1421–1440.
- [174] H. R. Diéguez, A. López, V. Domingo, J. F. Arteaga, J. A. Dobado, M. M. Herrador, J. F. Quílez del Moral, A. F. Barrero, *J. Am. Chem. Soc.* **2010**, 132, 254–259.
- [175] D. H. R. Barton, S. W. McCombie, *J. Chem. Soc. Perkin I* **1975**, 1574–1585.
- [176] S. W. McCombie, W. B. Motherwell, M. J. Tozer, in *Org. React.*, American Cancer Society, **2012**, pp. 161–432.
- [177] C. S. Bensasson, S. J. Cornforth, M.-H. Du, J. R. Hanson, *Chem. Commun.* **1997**, 1509–1510.
- [178] Binkley, Edith, R., Binkley, Roger, W., *Radical Reactions of Carbohydrates*, **2013**.
- [179] D. H. R. Barton, D. Crich, A. Löbberding, S. Z. Zard, *Tetrahedron* **1986**, 42, 2329–2338.
- [180] D. H. R. Barton, D. Crich, A. Löbberding, S. Z. Zard, *J. Chem. Soc. Chem. Commun.* **1985**, 646–647.
- [181] C. Chatgililoglu, C. Ferreri, M. Lucarini, *J. Org. Chem.* **1993**, 58, 249–251.
- [182] S. G. Sethofer, S. T. Staben, O. Y. Hung, F. D. Toste, *Org. Lett.* **2008**, 10, 4315–4318.
- [183] M. Newcomb, S.-Y. Choi, J. H. Horner, *J. Org. Chem.* **1999**, 64, 1225–1231.
- [184] D. Crich, Q. Yao, *J. Org. Chem.* **1995**, 60, 84–88.
- [185] C. A. Grob, *Angew. Chem. Int. Ed. Engl.* **1969**, 8, 535–546.
- [186] F. Effenberger, E. Sohn, G. Epple, *Chem. Ber.* **1983**, 116, 1195–1208.
- [187] M. E. Wright, S. R. Pulley, *J. Org. Chem.* **1989**, 54, 2886–2889.
- [188] M. Wallner, A. K. Lindemeyer, R. W. Olsen, *Oxf. Handb. Neuronal Ion Channels* **2018**, DOI 10.1093/oxfordhb/9780190669164.013.6.
- [189] T. F. Haydar, F. Wang, M. L. Schwartz, P. Rakic, *J. Neurosci.* **2000**, 20, 5764–5774.
- [190] G. Barbin, H. Pollard, J. L. Gaïarsa, Y. Ben-Ari, *Neurosci. Lett.* **1993**, 152, 150–154.
- [191] A. Schousboe, D. A. Redburn, *J. Neurosci. Res.* **1995**, 41, 1–7.
- [192] C. F. Burgos, G. E. Yévenes, L. G. Aguayo, *Mol. Pharmacol.* **2016**, 90, 318–325.
- [193] D. Debanne, G. Daoudal, V. Sourdet, M. Russier, *J. Physiol.-Paris* **2003**, 97, 403–414.
- [194] Y. S. Kim, B.-E. Yoon, *Exp. Neurobiol.* **2017**, 26, 122–131.
- [195] S. H. Fatemi, T. J. Reutiman, T. D. Folsom, P. D. Thuras, *J. Autism Dev. Disord.* **2008**, 39, 223.
- [196] M. Mele, R. O. Costa, C. B. Duarte, *Front. Cell. Neurosci.* **2019**, 13, DOI 10.3389/fncel.2019.00077.
- [197] M. Chebib, G. A. R. Johnston, *Clin. Exp. Pharmacol. Physiol.* **1999**, 26, 937–940.
- [198] K. R. Tovar, G. L. Westbrook, in *Cell Physiol. Source Book Fourth Ed.* (Ed.: N. Sperelakis), Academic Press, San Diego, **2012**, pp. 549–562.
- [199] Martin Ian, L., Bowery, Norman G., Dunn, Susan, M. J., “Tocris scientific reviews, GABA Receptors,” **n.d.**
- [200] G. A. R. Johnston, M. Chebib, R. K. Duke, K. N. Mewett, A. D. Mitrovic, R. J. Vandenberg, *Drug Dev. Res.* **1999**, 46, 255–260.
- [201] S. J. Farrar, P. J. Whiting, T. P. Bonnert, R. M. McKernan, *J. Biol. Chem.* **1999**, 274, 10100–10104.
- [202] E. Engin, R. S. Benham, U. Rudolph, *Trends Pharmacol. Sci.* **2018**, 39, 710–732.

- 
- [203] T. C. Jacob, S. J. Moss, R. Jurd, *Nat. Rev. Neurosci.* **2008**, 9, 331–343.
- [204] S. Kowalczyk, A. Winkelmann, B. Smolinsky, B. Förster, I. Neundorff, G. Schwarz, J. C. Meier, *Eur. J. Neurosci.* **2013**, 37, 544–554.
- [205] H.-M. Maric, J. Mukherjee, V. Tretter, S. J. Moss, H. Schindelin, *J. Biol. Chem.* **2011**, 286, 42105–42114.
- [206] M. J. J. and J. Vlainic, *Curr. Pharm. Des.* **2015**, 21, 4943–4959.
- [207] N. Karim, P. Wellendorph, N. Absalom, L. H. Bang, M. L. Jensen, M. M. Hansen, H. J. Lee, G. A. R. Johnston, J. R. Hanrahan, M. Chebib, *Biochem. Pharmacol.* **2012**, 84, 549–557.
- [208] S. Zhu, C. M. Noviello, J. Teng, R. M. Walsh, J. J. Kim, R. E. Hibbs, *Nature* **2018**, 559, 67–72.
- [209] S. Masiulis, R. Desai, T. Uchański, I. S. Martin, D. Lavery, D. Karia, T. Malinauskas, J. Zivanov, E. Pardon, A. Kotecha, et al., *Nature* **2019**, 565, 454–459.
- [210] S. W. Baumann, R. Baur, E. Sigel, *J. Neurosci.* **2003**, 23, 11158–11166.
- [211] D. A. Wagner, C. Czajkowski, *J. Neurosci.* **2001**, 21, 67–74.
- [212] Image of 6HUP from the RCSB PDB Database, P. S. Miller, A. R. Aricescu, *Nature* 2014, 512, 270–275. Created with PyMOL Version 2.3.2, Schrodinger LLC., **n.d.**
- [213] Image of 6D6US from the RCSB PDB Database, Zhu, C. M. Noviello, J. Teng, R. M. Walsh, J. J. Kim, R. E. Hibbs, *Nature* 2018, 559, 67–72. Created with PyMOL Version 2.3.2, Schrodinger LLC., **n.d.**
- [214] G. A. R. Johnston, *Neurochem. Res.* **2014**, 39, 1942–1947.
- [215] M. Mortensen, B. Ebert, K. Wafford, T. G. Smart, *J. Physiol.* **2010**, 588, 1251–1268.
- [216] G. A. R. Johnston, *Trends Pharmacol. Sci.* **1996**, 17, 319–323.
- [217] N. R. Gleason, G. Gallos, Y. Zhang, C. W. Emala, *J. Appl. Physiol.* **2009**, 106, 1257–1263.
- [218] P. Meera, M. Wallner, T. S. Otis, *J. Neurophysiol.* **2011**, 106, 2057–2064.
- [219] T. Roth, C. Lines, K. Vandormael, P. Ceesay, D. Anderson, D. Snively, *J. Clin. Sleep Med.* **2010**, 06, 30–40.
- [220] “Results From Phase 3 Trial of Gaboxadol in Insomnia Does Not Support Further Development,” can be found under <https://www.ptcommunity.com/news/20070329/results-phase-3-trial-gaboxadol-insomnia-does-not-support-further-development>, **2007**.
- [221] G. A. Johnston, *Br. J. Pharmacol.* **2013**, 169, 328–336.
- [222] P. M. Beart, G. A. R. Johnston, *Brain Res.* **1972**, 38, 226–227.
- [223] R. W. Olsen, M. Ban, T. Miller, G. A. R. Johnston, *Brain Res.* **1975**, 98, 383–387.
- [224] V. Seutin, S. W. Johnson, *Trends Pharmacol. Sci.* **1999**, 20, 268–270.
- [225] T. Hinton, G. A. R. Johnston, *GABA Glutamate - New Dev. Neurotransmission Res.* **2018**, DOI 10.5772/intechopen.72678.
- [226] H. J. Lee, N. L. Absalom, J. R. Hanrahan, P. van Nieuwenhuijzen, P. K. Ahring, M. Chebib, *Brain Res.* **2016**, 1644, 222–230.
- [227] M. Chebib, T. Hinton, K. L. Schmid, D. Brinkworth, H. Qian, S. Matos, H.-L. Kim, H. Abdel-Halim, R. J. Kumar, G. A. R. Johnston, et al., *J. Pharmacol. Exp. Ther.* **2009**, 328, 448–457.
- [228] E. J. Corey, H. L. Pearce, *J. Am. Chem. Soc.* **1979**, 101, 5841–5843.
- [229] S. W. M. Crossley, G. Tong, M. J. Lambrecht, H. E. Burdge, R. Shenvi, **2019**, DOI 10.26434/chemrxiv.9275318.v1.
- [230] R. E. Hibbs, E. Gouaux, *Nature* **2011**, 474, 54–60.
- [231] N. Unwin, *J. Mol. Biol.* **2005**, 346, 967–989.
- [232] R. J. C. Hilf, R. Dutzler, *Nature* **2008**, 452, 375–379.
- [233] P. S. Miller, A. R. Aricescu, *Nature* **2014**, 512, 270–275.
- [234] D. Lavery, P. Thomas, M. Field, O. J. Andersen, M. G. Gold, P. C. Biggin, M. Gielen, T. G. Smart, *Nat. Struct. Mol. Biol.* **2017**, 24, 977–985.

- 
- [235] G. Akk, D. F. Covey, A. S. Evers, J. H. Steinbach, C. F. Zorumski, S. Mennerick, *Pharmacol. Ther.* **2007**, *116*, 35–57.
- [236] Z.-W. Chen, J. R. Bracamontes, M. M. Budelier, A. L. Germann, D. J. Shin, K. Kathiresan, M.-X. Qian, B. Manion, W. W. L. Cheng, D. E. Reichert, et al., *PLOS Biol.* **2019**, *17*, e3000157.
- [237] R. Siegwart, R. Jurd, U. Rudolph, *J. Neurochem.* **2002**, *80*, 140–148.
- [238] D. J. Shin, A. L. Germann, A. D. Johnson, S. A. Forman, J. H. Steinbach, G. Akk, *Mol. Pharmacol.* **2018**, *93*, 178–189.
- [239] G. M. S. Yip, Z.-W. Chen, C. J. Edge, E. H. Smith, R. Dickinson, E. Hohenester, R. R. Townsend, K. Fuchs, W. Sieghart, A. S. Evers, et al., *Nat. Chem. Biol.* **2013**, *9*, 715–720.
- [240] V. R. Solomon, V. J. Tallapragada, M. Chebib, G. A. R. Johnston, J. R. Hanrahan, *Eur. J. Med. Chem.* **2019**, *171*, 434–461.
- [241] D. Belelli, J. J. Lambert, J. A. Peters, K. Wafford, P. J. Whiting, *Proc. Natl. Acad. Sci.* **1997**, *94*, 11031–11036.
- [242] V. Campagna-Slater, D. F. Weaver, *Neurosci. Lett.* **2007**, *418*, 28–33.
- [243] P. S. Garcia, S. E. Kolesky, A. Jenkins, *Curr. Neuropharmacol.* **2010**, *8*, 2.
- [244] M. J. Brodie, P. Kwan, *Epilepsia* **2012**, *53*, 40–46.
- [245] S. A. Thompson, P. J. Whiting, K. A. Wafford, *Br. J. Pharmacol.* **1996**, *117*, 521–527.
- [246] D. C. Chiara, S. S. Jayakar, X. Zhou, X. Zhang, P. Y. Savechenkov, K. S. Bruzik, K. W. Miller, J. B. Cohen, *J. Biol. Chem.* **2013**, *288*, 19343–19357.
- [247] A. Rosen, M. Bali, J. Horenstein, M. H. Akabas, *Biophys. J.* **2007**, *92*, 3130–3139.
- [248] H. J. Hanchar, P. Chutsrinopkun, P. Meera, P. Supavilai, W. Sieghart, M. Wallner, R. W. Olsen, *Proc. Natl. Acad. Sci.* **2006**, *103*, 8546–8551.
- [249] A. L. Morrow, M. J. VanDoren, S. N. Penland, D. B. Matthews, *Brain Res. Brain Res. Rev.* **2001**, *37*, 98–109.
- [250] J. Wick, *Consult. Pharm.* **2013**, *9*, 538–548.
- [251] H. Valerie Curran, *Psychopharmacology (Berl.)* **1991**, *105*, 1–8.
- [252] H. Ashton, *Curr. Opin. Psychiatry* **2005**, *18*, 249.
- [253] E. Sigel, M. E. Steinmann, *J. Biol. Chem.* **2012**, *287*, 40224–40231.
- [254] R. W. Olsen, *Neuropharmacology* **2018**, *136*, 10–22.
- [255] E. Sigel, M. Ernst, *Trends Pharmacol. Sci.* **2018**, *39*, 659–671.
- [256] C. Campo-Soria, Y. Chang, D. S. Weiss, *Br. J. Pharmacol.* **2006**, *148*, 984–990.
- [257] O. Malminiemi, E. R. Korpi, *Eur. J. Pharmacol.* **1989**, *169*, 53–60.
- [258] P. B. Wingrove, P. Safo, L. Wheat, S. A. Thompson, K. A. Wafford, P. J. Whiting, *Eur. J. Pharmacol.* **2002**, *437*, 31–39.
- [259] D. B. Pritchett, H. Sontheimer, B. D. Shivers, S. Ymer, H. Kettenmann, P. R. Schofield, P. H. Seeburg, *Nature* **1989**, *338*, 582–585.
- [260] K. R. Tan, U. Rudolph, C. Lüschner, *Trends Neurosci.* **2011**, *34*, 188–197.
- [261] R. M. McKernan, T. W. Rosahl, D. S. Reynolds, C. Sur, K. A. Wafford, J. R. Atack, S. Farrar, J. Myers, G. Cook, P. Ferris, et al., *Nat. Neurosci.* **2000**, *3*, 587–592.
- [262] F. Crestani, K. Löw, R. Keist, M.-J. Mandelli, H. Möhler, U. Rudolph, *Mol. Pharmacol.* **2001**, *59*, 442–445.
- [263] N. Collinson, F. M. Kuenzi, W. Jarolimek, K. A. Maubach, R. Cothliff, C. Sur, A. Smith, F. M. Otu, O. Howell, J. R. Atack, et al., *J. Neurosci.* **2002**, *22*, 5572–5580.
- [264] K. M. G. and A. A. Grace, *Curr. Pharm. Des.* **2014**, *20*, 5069–5076.
- [265] J. R. Atack, in *Behav. Neurobiol. Anxiety Its Treat.* (Eds.: M.B. Stein, T. Steckler), Springer Berlin Heidelberg, Berlin, Heidelberg, **2010**, pp. 331–360.
- [266] W. Sieghart, *J. Psychiatry Neurosci.* **1994**, *19*, 24–29.
- [267] R. Baur, K. R. Tan, B. P. Lüschner, A. Gonthier, M. Goeldner, E. Sigel, *J. Neurochem.* **2008**, *106*, 2353–2363.

- [268] M. C. Maldifassi, R. Baur, E. Sigel, *J. Neurochem.* **2016**, *138*, 722–730.
- [269] B. Antkowiak, U. Rudolph, *Curr. Opin. Anaesthesiol.* **2016**, *29*, 447–453.
- [270] U. Rudolph, F. Knoflach, *Nat. Rev. Drug Discov.* **2011**, *10*, 685–697.
- [271] T. T. Stamenić, M. M. Poe, S. Rehman, A. Santrač, B. Divović, P. Scholze, M. Ernst, J. M. Cook, M. M. Savić, *Eur. J. Pharmacol.* **2016**, *791*, 433–443.
- [272] N. W. Gilman, P. Rosen, J. V. Earley, C. Cook, L. J. Todaro, *J. Am. Chem. Soc.* **1990**, *112*, 3969–3978.
- [273] H. Mohler, T. Okada, *Science* **1977**, *198*, 849–851.
- [274] M. Simonyi, G. Maksay, I. Kovács, Z. Tegye, L. Párkányi, A. Kálmán, L. Ötvös, *Bioorganic Chem.* **1990**, *18*, 1–12.
- [275] L. Richter, C. de Graaf, W. Sieghart, Z. Varagic, M. Mörzinger, I. J. P. de Esch, G. F. Ecker, M. Ernst, *Nat. Chem. Biol.* **2012**, *8*, 455–464.
- [276] A. A. Elgarf, D. C. B. Siebert, F. Steudle, A. Draxler, G. Li, S. Huang, J. M. Cook, M. Ernst, P. Scholze, *ACS Chem. Biol.* **2018**, *13*, 2033–2039.
- [277] S. J. Middendorp, R. Puthenkalam, R. Baur, M. Ernst, E. Sigel, *ACS Chem. Biol.* **2014**, *9*, 1854–1859.
- [278] D. C. B. Siebert, K. Bampali, R. Puthenkalam, Z. Varagic, I. Sarto-Jackson, P. Scholze, W. Sieghart, M. D. Mihovilovic, M. Schnürch, M. Ernst, *ACS Chem. Biol.* **2018**, *13*, 2040–2047.
- [279] E. Sigel, *Nature* **2018**, *559*, 37–38.
- [280] T. Atkin, S. Comai, G. Gobbi, *Pharmacol. Rev.* **2018**, *70*, 197–245.
- [281] D. J. Nutt, S. M. Stahl, *J. Psychopharmacol. (Oxf.)* **2010**, *24*, 1601–1612.
- [282] D. J. Nutt, *J. Psychopharmacol. (Oxf.)* **2005**, *19*, 125–127.
- [283] J. Montplaisir, R. Hawa, H. Moller, C. Morin, M. Fortin, J. Matte, L. Reinish, C. M. Shapiro, *Hum. Psychopharmacol. Clin. Exp.* **2003**, *18*, 29–38.
- [284] F. López-Muñoz, R. Ucha-Udabe, C. Alamo, *Neuropsychiatr. Dis. Treat.* **2005**, *1*, 329–343.
- [285] O. Babii, S. Afonin, M. Berditsch, S. Reißer, P. K. Mykhailiuk, V. S. Kubyshev, T. Steinbrecher, A. S. Ulrich, I. V. Komarov, *Angew. Chem. Int. Ed.* **2014**, *53*, 3392–3395.
- [286] W. J. Deal, B. F. Erlanger, D. Nachmansohn, *Proc. Natl. Acad. Sci. U. S. A.* **1969**, *64*, 1230–1234.
- [287] E. Bartels, N. H. Wassermann, B. F. Erlanger, *Proc. Natl. Acad. Sci.* **1971**, *68*, 1820–1823.
- [288] W. Szymański, J. M. Beierle, H. A. V. Kistemaker, W. A. Velema, B. L. Feringa, *Chem. Rev.* **2013**, *113*, 6114–6178.
- [289] M. M. Lerch, M. J. Hansen, G. M. van Dam, W. Szymanski, B. L. Feringa, *Angew. Chem. Int. Ed.* **2016**, *55*, 10978–10999.
- [290] K. Hüll, J. Morstein, D. Trauner, *Chem. Rev.* **2018**, *118*, 10710–10747.
- [291] P. Klán, T. Šolomek, C. G. Bochet, A. Blanc, R. Givens, M. Rubina, V. Popik, A. Kostikov, J. Wirz, *Chem. Rev.* **2013**, *113*, 119–191.
- [292] P. Leippe, J. Koehler, D. Trauner, *Biochemistry* **2017**, *56*, 5214–5220.
- [293] M. Irie, *Chem. Rev.* **2000**, *100*, 1685–1716.
- [294] R. Klajn, *Chem. Soc. Rev.* **2014**, *43*, 148–184.
- [295] C. Brieke, A. Heckel, *Chem. Weinh. Bergstr. Ger.* **2013**, *19*, 15726–15734.
- [296] S. Wiedbrauk, H. Dube, *Tetrahedron Lett.* **2015**, *56*, 4266–4274.
- [297] D. J. van Dijken, P. Kovaříček, S. P. Ihrig, S. Hecht, *J. Am. Chem. Soc.* **2015**, *137*, 14982–14991.
- [298] H. K. Cammenga, V. N. Emel'yanenko, S. P. Verevkin, *Ind. Eng. Chem. Res.* **2009**, *48*, 10120–10128.
- [299] “Colorants Industry History,” can be found under <http://www.colorantshistory.org/>, **n.d.**
- [300] F. M. D. Chequer, D. J. Dorta, D. P. de Oliveira, *Adv. Treat. Text. Effl.* **2011**, DOI 10.5772/19872.



- [301] J. Morstein, M. Awale, J.-L. Reymond, D. Trauner, *ACS Cent. Sci.* **2019**, *5*, 607–618.
- [302] J. F. Zeidner, J. E. Karp, *Leuk. Res.* **2015**, *39*, 1312–1318.
- [303] J. I. Trujillo, J. R. Kiefer, W. Huang, A. Thorarensen, L. Xing, N. L. Caspers, J. E. Day, K. J. Mathis, K. K. Kretzmer, B. A. Reitz, et al., *Bioorg. Med. Chem. Lett.* **2009**, *19*, 908–911.
- [304] M. Borowiak, W. Nahaboo, M. Reynders, K. Nekolla, P. Jalinot, J. Hasserodt, M. Rehberg, M. Delattre, S. Zahler, A. Vollmar, et al., *Cell* **2015**, *162*, 403–411.
- [305] M. Stein, A. Breit, T. Fehrentz, T. Gudermann, D. Trauner, *Angew. Chem. Int. Ed.* **2013**, *52*, 9845–9848.
- [306] M. W. H. Hoorens, W. Szymanski, *Trends Biochem. Sci.* **2018**, *43*, 567–575.
- [307] R. Siewertsen, H. Neumann, B. Buchheim-Stehn, R. Herges, C. Näther, F. Renth, F. Temps, *J. Am. Chem. Soc.* **2009**, *131*, 15594–15595.
- [308] M. Hammerich, C. Schütt, C. Stähler, P. Lentès, F. Röhricht, R. Höppner, R. Herges, *J. Am. Chem. Soc.* **2016**, *138*, 13111–13114.
- [309] R. Siewertsen, J. B. Schönborn, B. Hartke, F. Renth, F. Temps, *Phys. Chem. Chem. Phys.* **2010**, *13*, 1054–1063.
- [310] E. R. Thapaliya, J. Zhao, G. C. R. Ellis-Davies, *ACS Chem. Neurosci.* **2019**, *10*, 2481–2488.
- [311] J. Trads, K. Hüll, B. Matsuura, L. Laprell, T. Fehrentz, N. Görldt, K. A. Kozek, D. Weaver, N. Klöcker, D. Barber, et al., **2019**, DOI 10.26434/chemrxiv.8014580.v1.
- [312] D. M. Barber, M. Schönberger, J. Burgstaller, J. Levitz, C. D. Weaver, E. Y. Isacoff, H. Baier, D. Trauner, *Chem. Sci.* **2016**, *7*, 2347–2352.
- [313] M. Volgraf, P. Gorostiza, S. Szobota, M. R. Helix, E. Y. Isacoff, D. Trauner, *J. Am. Chem. Soc.* **2007**, *129*, 260–261.
- [314] I. H. Greger, J. F. Watson, S. G. Cull-Candy, *Neuron* **2017**, *94*, 713–730.
- [315] D. M. Barber, S.-A. Liu, K. Gottschling, M. Sumser, M. Hollmann, D. Trauner, *Chem. Sci.* **2016**, *8*, 611–615.
- [316] M. Stein, S. J. Middendorp, V. Carta, E. Pejo, D. E. Raines, S. A. Forman, E. Sigel, D. Trauner, *Angew. Chem. Int. Ed.* **2012**, *51*, 10500–10504.
- [317] D. S. Stewart, P. Y. Savechenkov, Z. Dostalova, D. C. Chiara, R. Ge, D. E. Raines, J. B. Cohen, S. A. Forman, K. S. Bruzik, K. W. Miller, *J. Med. Chem.* **2011**, *54*, 8124–8135.
- [318] D. Hadjipavlou-Litina, C. Hansch, *Chem. Rev.* **1994**, *94*, 1483–1505.
- [319] Q. Huang, X. He, C. Ma, R. Liu, S. Yu, C. A. Dayer, G. R. Wenger, R. McKernan, J. M. Cook, *J. Med. Chem.* **2000**, *43*, 71–95.
- [320] A. W. Sobańska, G. Żydek, P. Włodno, E. Brzezińska, *Eur. J. Med. Chem.* **2015**, *89*, 147–155.
- [321] P. Bregestovski, G. Maleeva, P. Gorostiza, *Br. J. Pharmacol.* **2018**, *175*, 1892–1902.
- [322] M. Anzini, S. Valenti, C. Braile, A. Cappelli, S. Vomero, S. Alcaro, F. Ortuso, L. Marinelli, V. Limongelli, E. Novellino, et al., *J. Med. Chem.* **2011**, *54*, 5694–5711.
- [323] H. Song, D. Chen, C. Pi, X. Cui, Y. Wu, *J. Org. Chem.* **2014**, *79*, 2955–2962.
- [324] F. Szabó, D. Simkó, Z. Novák, *RSC Adv.* **2013**, *4*, 3883–3886.
- [325] I. Sapountzis, P. Knochel, *Angew. Chem. Int. Ed.* **2002**, *41*, 1610–1611.
- [326] W. B. Dickinson, *J. Am. Chem. Soc.* **1964**, *86*, 3580–3581.
- [327] S. Kim, S. S. Friedrich, L. J. Andrews, R. M. Keefer, *J. Am. Chem. Soc.* **1970**, *92*, 5452–5456.
- [328] O. J. Cope, R. K. Brown, *Can. J. Chem.* **1961**, *39*, 1695–1710.
- [329] H. Li, P. Li, L. Wang, *Org. Lett.* **2013**, *15*, 620–623.
- [330] P. Carré, *Ann. Chim. Phys.* **1910**, 220–222.
- [331] G. Lukács, M. Porcs-Makkay, G. Simig, *Eur. J. Org. Chem.* **2004**, 2004, 4130–4140.
- [332] K. M. Nicholas, D. K. O'Dell, *HETEROCYCLES* **2004**, *63*, 373.

- 
- [333] S. Kumar, D. P. Matharasi, S. Gopi, S. Sivakumar, S. Narasimhan, *J. Asian Nat. Prod. Res.* **2010**, *12*, 360–370.
- [334] L. H. Sternbach, R. I. Fryer, O. Keller, W. Metlesics, G. Sach, N. Steiger, *J. Med. Chem.* **1963**, *6*, 261–265.
- [335] H. A. Hassan, M. Abdel-Aziz, G. E.-D. A. A. Abuo-Rahma, H. H. Farag, *Bioorg. Med. Chem.* **2009**, *17*, 1681–1692.
- [336] García, A., Pastor, J., Blanco, C., Rodríguez, A., Hernando, J. I., Ramos, F. Hernández, A. I., *WO 2011/080510 A1*, **n.d.**
- [337] L. Wang, A. Ishida, Y. Hashidoko, M. Hashimoto, *Angew. Chem. Int. Ed.* **2017**, *56*, 870–873.
- [338] *Arkivoc* **2013**, *2013*, 165.
- [339] B. Maji, H. Yamamoto, *J. Am. Chem. Soc.* **2015**, *137*, 15957–15963.
- [340] N. R. Ayyangar, S. N. Naik, K. V. Srinivasan, *Tetrahedron Lett.* **1989**, *30*, 7253–7256.
- [341] E. P. QU, J., Rivero, R., Sanchez, R., Tedesco, R., **n.d.**
- [342] R. Rodriguez, R. M. Adlington, S. J. Eade, M. W. Walter, J. E. Baldwin, J. E. Moses, *Tetrahedron* **2007**, *63*, 4500–4509.
- [343] L. Guillade, A. B. González-Pérez, Á. R. de Lera, *Org. Biomol. Chem.* **2017**, *15*, 7430–7438.
- [344] H. Yu, C. E. Ballard, P. D. Boyle, B. Wang, *Tetrahedron* **2002**, *58*, 7663–7679.
- [345] G. Solladié, M. Adamy, F. Colobert, *J. Org. Chem.* **1996**, *61*, 4369–4373.
- [346] D. Askin, R. A. Reamer, D. Joe, R. P. Volante, I. Shinkai, *Tetrahedron Lett.* **1989**, *30*, 6121–6124.
- [347] V. Kubyshkin, P. Durkin, N. Budisa, *New J. Chem.* **2016**, *40*, 5209–5220.
- [348] K. Hori, M. Arai, K. Nomura, E. Yoshii, *Chem. Pharm. Bull. (Tokyo)* **1987**, *35*, 4368–4371.
- [349] S. Grimme, C. Bannwarth, S. Dohm, A. Hansen, J. Pisarek, P. Pracht, J. Seibert, F. Neese, *Angew. Chem. Int. Ed.* **2017**, *56*, 14763–14769.
- [350] S. Grimme, *J. Chem. Theory Comput.* **2019**, *15*, 2847–2862.
- [351] S. Grimme, C. Bannwarth, P. Shushkov, *J. Chem. Theory Comput.* **2017**, *13*, 1989–2009.
- [352] C. Bannwarth, S. Ehlert, S. Grimme, *J. Chem. Theory Comput.* **2019**, *15*, 1652–1671.
- [353] P. Pracht, E. Caldeweyher, S. Ehlert, S. Grimme, **2019**, DOI 10.26434/chemrxiv.8326202.v1.
- [354] M. J. Frisch, et al., *Gaussian 16 Revision A.03*. 2016., **n.d.**
- [355] V. A. Rassolov, J. A. Pople, M. A. Ratner, T. L. Windus, *J. Chem. Phys.* **1998**, *109*, 1223–1229.
- [356] A. V. Marenich, C. J. Cramer, D. G. Truhlar, *J. Phys. Chem. B* **2009**, *113*, 6378–6396.
- [357] J. D. Dill, J. A. Pople, *J. Chem. Phys.* **1975**, *62*, 2921–2923.
- [358] M. M. Francl, W. J. Pietro, W. J. Hehre, J. S. Binkley, M. S. Gordon, D. J. DeFrees, J. A. Pople, *J. Chem. Phys.* **1982**, *77*, 3654–3665.
- [359] J.-D. Chai, M. Head-Gordon, *Phys. Chem. Chem. Phys.* **2008**, *10*, 6615–6620.
- [360] J.-P. Blaudeau, M. P. McGrath, L. A. Curtiss, L. Radom, *J. Chem. Phys.* **1997**, *107*, 5016–5021.
- [361] M. Linder, T. Brinck, *Phys. Chem. Chem. Phys.* **2013**, *15*, 5108–5114.
- [362] A. Schäfer, C. Huber, R. Ahlrichs, *J. Chem. Phys.* **1994**, *100*, 5829–5835.
- [363] F. Weigend, R. Ahlrichs, *Phys. Chem. Chem. Phys.* **2005**, *7*, 3297–3305.
- [364] J.-D. Chai, M. Head-Gordon, *Phys. Chem. Chem. Phys.* **2008**, *10*, 6615–6620.
- [365] Paton Lab, Jaime Rodríguez-Guerra, JingTao Chen, IFunes, *Bobbypaton/GoodVibes: GoodVibes v3.0.0*, Zenodo, **2019**.
- [366] S. Grimme, *Chem. – Eur. J.* **2012**, *18*, 9955–9964.

- [367] Y.-P. Li, J. Gomes, S. Mallikarjun Sharada, A. T. Bell, M. Head-Gordon, *J. Phys. Chem. C* **2015**, *119*, 1840–1850.
- [368] A. K. Miller, D. Trauner, *Synlett* **2006**, *2006*, 2295–2316.